

**Characterising mismatch negativity biomarker
signatures in preclinical models relevant to
schizophrenia**

A thesis submitted to

The Department of Biomedical Engineering

University of Strathclyde

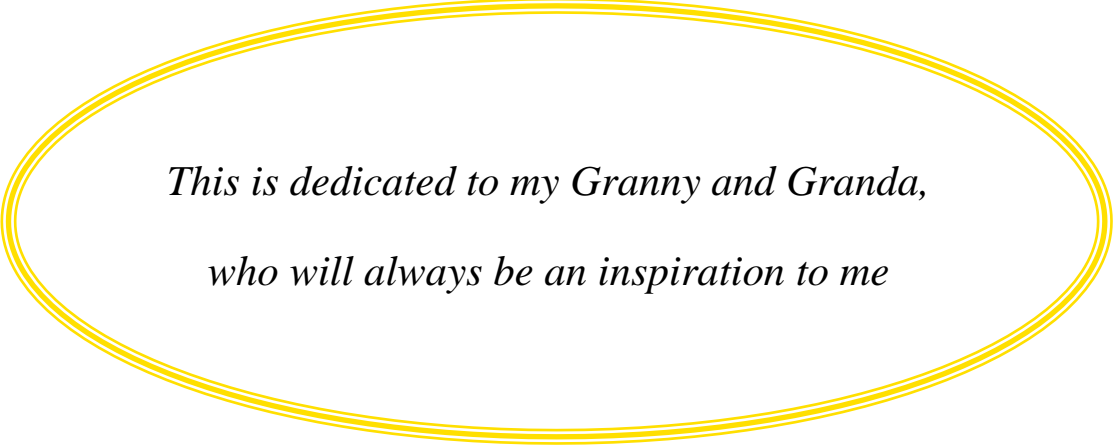
for the degree of

Doctor of Engineering

by

Jamie Alexander O'Reilly

2017



*This is dedicated to my Granny and Granda,
who will always be an inspiration to me*

Declaration of Author's Rights

This thesis is the result of the author's original research. It has been composed by the author and has not been previously submitted for examination which has led to the award of a degree.

The copyright of this thesis belongs to the author under the terms of the United Kingdom Copyright Acts as qualified by University of Strathclyde Regulation 3.50. Due acknowledgement must always be made of the use of any material contained in, or derived from, this thesis.

Signed:

Date:

Acknowledgements

First and foremost, I thank God for everything, and my family who have always supported me. I am grateful to my supervisors Judith Pratt and Bernard Conway for their efforts in guiding me throughout this study. Judy has been a constant source of support, encouragement and invaluable feedback. Bernie has been there when called upon, more so in the later stages, with a calm and considered approach. Both have a great deal of my gratitude for proof-reading this thesis and helping me to achieve my goal. John Dempster was an adviser for part of my time working on this project. I am thankful for the discussions we had about technology, analytical methods and statistics, and for his support in taking a pragmatic approach to completing this course. Shuzo Sakata allowed me to work in his lab to complete the final experiment in this study. He was instrumental in this element of the thesis, making available specialised equipment, providing knowledgeable input for experimental design, analyses and interpretation of results. Mark Thomson has been a friend and mentor since beginning this research. He provided training on behavioural neuroscience, animal welfare, *in-vivo* techniques and stereotactic surgery, and has always been there for scientific and non-scientific discussions. Most of all I thank Mark for introducing me to the game of squash, which provided a much needed outlet for excess energy during stressful times. Thanks are also due to Campbell Reid for teaching me about mismatch negativity research techniques using electroencephalography in humans, providing advice on matlab programming and being available for regular progress meetings at the outset of the project. I am indebted to fellow students Rebecca Openshaw, for genotyping and maintaining the experimental animals used in this study, and Vladimir Visokis, for providing training on aseptic surgical technique, critical to completing the practical aspects of this research. Josue Garcia Yague provided guidance for performing *in-vivo* electrophysiology experiments with multi-channel silicon probes. I'm sincerely grateful to these three people without whom this work would not have been possible. Thanks also to Morag Farquhar for demonstrating stereotactic surgery in rats, and to Richard Pinnell who handed-over his surgical equipment and expertise. I also thank all the staff in the BPU who assisted in caring for animals bred for this study, including Kevin, Carol, Lee, Peter, Stevie, George and Linda. I appreciate the unique person qualities of each of my colleagues from the Biomedical Engineering Department, Neurophysiology Lab; Alejandra Aranceta Garza, Ange Tano, Bilal Nassir, Chi-Hsu Wu, Sibani Mohanty, Lijo Varughese Chacko and Syahrull Hifisyambinahmadjamil (Hi-Fi). I'm glad we were able to share our journeys, and wish everyone good fortune in their future endeavours. I am grateful for the professionalism and support of the staff involved in the EPSRC Centre for Doctoral Training in Medical Devices and Healthcare Technologies who facilitate the program which enabled me to complete this course of study. In particular, Carol McInness, Richard Black and Heba Lakany were always there with practical assistance, support and encouragement. I'm pleased to have been welcomed into the Neuroscience Research Group at Strathclyde Institute of Pharmacy and Biomedical Sciences (SIPBS), having had the pleasure of attending and participating in seminars across a broad depth of this fascinating area of scientific research. Meeting and getting to know some of the other researchers there was great. Interaction with the wider community at University of Strathclyde, including those at the Centre for Sport and Recreation, Researcher Development Programme, and Strathclyde Entrepreneurial Network also enhanced my experience and skill base during this study, and I'm thankful for all those who I was lucky enough to have met. Last but not least, I'm grateful for my wee deer Amonrat (Molly) Khayungarnnawee and for her love and support.

Abstract

Mismatch negativity (MMN) has been hailed as a “break-through biomarker in predicting psychosis onset” (Naatanen 2015). This is because deficits have been found in clinical populations diagnosed with psychotic syndromes such as schizophrenia. MMN is an auditory evoked potential (AEP) difference waveform produced by subtracting standard from deviant stimuli AEPs elicited by an oddball paradigm; purportedly arising from any discriminable change in auditory stimulation.

Despite nearly four decades of basic research into MMN the underlying mechanisms are not fully understood. Although popular theories suggest that it reflects a sensory-memory trace disruption and/or differential adaptation of responses to standard and deviant/oddball stimuli, there remains considerable debate over the neural mechanism and its interpretation.

Nevertheless, associations made between N-methyl-d-aspartate (NMDA) receptors in schizophrenia and findings showing that NMDA receptor antagonists (e.g. ketamine) induce MMN deficits in healthy volunteers suggests abnormal MMNs share common traits and support its use as a biomarker from an electrophysiological perspective. However, this is still speculative and there is great impetus on developing reliable preclinical models of MMN in order to examine the underpinning neurophysiology and therefore its reliance on NMDA receptors as a test of pathology in schizophrenia. A question this thesis aims to address is whether a mismatch response (MMR) exists in rodents which is analogous to the human MMN, and whether its modification by NMDA receptor antagonists or as a result of schizophrenia-related genetic modification sheds light on its utility as a biomarker in disease models of schizophrenia.

This thesis describes three experiments performed using mitogen activated protein kinase kinase 7 heterozygous (*Map2k7^{+/-}*) mice and their wild-type littermates, incorporating NMDA receptor antagonism with ketamine (10 mg/kg i.p.). The *MAP2K7* gene is associated with schizophrenia and codes for a post-synaptic intracellular signalling enzyme which is activated following glutamatergic excitation, for instance via NMDA receptors. The MMR to stimuli duration, frequency and intensity changes in oddball paradigms are characterised in urethane-anaesthetised and conscious animals, followed by an examination of laminar auditory cortex activity in response to these physical changes. Data recorded throughout this series of experiments includes cortical electroencephalography (EEG), video footage, and intra-cortical spiking information. These data were then analysed using various time, frequency and time-frequency domain techniques; although mainly focussing on the event-related potential (ERP) approach.

Recordings demonstrated substantial differences in the AEP waveform evoked from urethane-anaesthetised and conscious animals, with the latter displaying considerably more dynamic responses, although onset and offset of auditory stimuli induced comparable waveform features in both states. Effects of varying physical properties of stimuli in oddball and control paradigms have been identified as key determinants of the AEP and correspondingly the MMR difference waveform amplitudes. The finding that NMDA receptor disruption in conscious animals by ketamine acutely diminishes a specific AEP feature ($\approx 20-50$ ms post stimulus onset) which may impact the resulting MMR tentatively links this study in mice with findings from humans noted above. Ketamine was also found to enhance animal movement and increase EEG spectral power in the 50-70 Hz (gamma-band) frequency range, observed for approximately 10 minutes following drug administration. Both anaesthetised and conscious cohorts of *Map2k7*^{+/-} mice displayed a significantly enhanced onset response ($\approx 0-20$ ms) in the AEP. Interestingly, ketamine did not appear to have a differential effect on *Map2k7*^{+/-} mice compared with the wild-type group, suggesting that NMDA receptor-mediated neurotransmission is unimpaired in this genetic model relevant to schizophrenia.

Overall, the findings suggest that the MMR in mice is fundamentally influenced by the physical properties of stimuli employed; ketamine causes an acute, specific alteration to the AEP in conscious mice in addition to other electrophysiological and behavioural changes; and *Map2k7* gene disruption causes a specific and replicable change in AEP amplitude. Overall this study indicates that mouse models are useful for exploring the effects of different pharmacological and genetic manipulations on the auditory evoked response; however, MMN data in clinical cohorts still needs to be interpreted with care. In order to address whether the rodent MMR is analogous to human MMN, it would be necessary to probe how influencing factors revealed in the rodent studies impact on the human response. Whilst the rodent MMR and human MMN show some degree of translation, their potential as schizophrenia biomarkers requires further characterisation and validation.

Contents

DECLARATION OF AUTHOR'S RIGHTS	I
ACKNOWLEDGEMENTS	II
ABSTRACT	III
CONTENTS	V
LIST OF FIGURES	XIII
LIST OF TABLES	XIX
LIST OF ABBREVIATIONS AND SYMBOLS	XX
Chapter 1. Introduction	1
1.1 Schizophrenia	2
1.1.1 Epidemiology	2
1.1.2 Symptomatology	2
1.1.3 Genetic and environmental risk factors	3
1.1.4 Neurobiology.....	4
1.1.5 Electrophysiological deficits	8
1.1.6 Preclinical research.....	12
1.2 Mismatch negativity (MMN) in humans	13
1.2.1 MMN in schizophrenia and other neuropsychiatric disorders	19
1.2.1.1 Duration mismatch negativity (dMMN)	21
1.2.1.2 Frequency mismatch negativity (fMMN)	21
1.2.1.3 Intensity mismatch negativity (iMMN)	22
1.2.2 Neurobiology of auditory processing	23
1.2.2.1 Sound and hearing	23
1.2.2.2 Auditory pathway	25
1.2.2.3 Topography of the auditory cortex	27
1.2.2.4 Laminar structure of the auditory cortex	29
1.2.2.5 Auditory cortex in schizophrenia.....	32
1.2.2.6 Stimulus specific adaptation	32
1.2.3 Theoretical models of MMN	33
1.3 Mismatch response (MMR) in animals.....	36
1.3.1.1 Control paradigms in animal MMR studies	42
1.4 Mouse models in this study	44
1.4.1 Mitogen activated protein kinase kinase 7 (<i>Map2k7^{+/-}</i>)	44
1.4.2 NMDA receptor antagonist	45
1.5 Hypotheses and experiment outline	47

Chapter 2. General methods	48
2.1 Introduction	49
2.2 Statement of ethical practice	49
2.3 Study overview	49
2.3.1 Experiment I overview	50
2.3.2 Experiment II overview	50
2.3.3 Experiment III overview	50
2.4 Animal details	51
2.4.1 <i>Map2k7</i> ^{+/-} gene disruption	51
2.4.2 Ketamine NMDA receptor antagonism	51
2.4.3 Experiment I animal details	52
2.4.4 Experiment II animal details	52
2.4.5 Experiment III animal details	53
2.4.6 Animal husbandry	53
2.5 Surgical techniques	54
2.5.1 Experiment I: non-recovery	54
2.5.2 Experiment II: aseptic	56
2.5.3 Experiment III: multichannel probe implantation	58
2.6 Electrophysiological recording setups	59
2.6.1 Recording Chamber A	59
2.6.1.1 Experiment I configuration	60
2.6.1.2 Experiment II configuration	60
2.6.2 Recording Chamber B	62
2.6.2.1 Frequency response screening	64
2.6.2.2 Auditory paradigm configuration	64
2.7 Auditory paradigms	65
2.7.1 Oddball paradigm: designed to elicit a mismatch response	65
2.7.2 Consecutive-repetition paradigm: control for adaptation	66
2.7.3 Deviant-alone paradigm: control for sensory-memory disruption	67
2.7.4 Many-standards paradigm: control for stimuli presentation rate with unpredictable sensory-memory trace	68
2.8 Auditory stimuli parameters	69
2.8.1 Experiment I specifications	69
2.8.2 Experiment II specifications	71
2.8.3 Experiment III specifications	75
2.9 Experimental protocols	77
2.9.1 Experiment I protocol	78
2.9.2 Experiment II protocol	79
2.9.3 Experiment III protocol	80

2.10	Data Analyses	81
2.10.1	Auditory evoked potentials	81
2.10.1.1	Peak amplitude	82
2.10.1.2	Peak latency	83
2.10.1.3	Rectified Area	83
2.10.2	Spectral analyses	84
2.10.2.1	Power spectrum	84
2.10.2.2	Event-related spectral perturbation	84
2.10.3	Video footage	85
2.10.4	Local field potentials	85
2.10.5	Current source density	86
2.10.6	Spike activity	87
2.10.7	Frequency response area	88
2.10.8	Statistics	88

Chapter 3. Experiment I: evaluation of multivariate auditory paradigms in urethane-anaesthetised wild-type and *Map2k7*^{+/-} mice exposed to ketamine..... 89

3.1	Introduction	90
3.1.1	Previous MMR studies in anaesthetised rodents	90
3.1.1.1	Duration	90
3.1.1.2	Frequency	92
3.1.1.3	Intensity	93
3.1.2	Urethane anaesthetised condition	94
3.1.3	Experiment I aims	95
3.2	Methods	96
3.2.1	Animal details	96
3.2.2	Surgery	96
3.2.3	Electrophysiological recordings	96
3.2.4	Auditory paradigms	96
3.2.5	Stimuli properties	96
3.2.6	Experimental protocol	97
3.2.7	Artifact rejection	97
3.2.8	Auditory evoked potential computations	97
3.2.8.1	Mismatch response calculation	98
3.2.8.2	Removing offset responses	99
3.2.8.3	Custom baseline correction	99
3.2.9	Auditory evoked potential measurements	100
3.2.9.1	Stimulus onset potential (N1)	100
3.2.9.2	Stimulus offset potential (P_{offset})	100

3.2.9.3	Deviant evoked activity (DEA)	100
3.3	Results	101
3.3.1	Duration paradigms in urethane-anaesthetised mice	101
3.3.1.1	<i>Map2k7^{+/-}</i> mice display increased stimulus onset response.....	101
3.3.1.2	Duration mismatch response in urethane-anaesthetised mice is generated by stimulus offset potentials	104
3.3.1.3	Auditory evoked potentials from duration consecutive-repetition, oddball and many- standards paradigms are qualitatively similar	107
3.3.1.4	Duration many-standards control paradigm reveals offset responses and a slow biphasic waveform in <i>Map2k7^{+/-}</i> mice.....	109
3.3.1.5	Duration deviant-alone paradigm elicits extended latency response which is attenuated following ketamine.....	111
3.3.2	Frequency paradigms in urethane-anaesthetised mice.....	114
3.3.2.1	Stimulus frequency influences auditory evoked potentials.....	114
3.3.2.2	Ascending and descending frequency oddballs elicit mismatch responses	118
3.3.2.3	Auditory evoked potentials from frequency consecutive-repetition, oddball and many-standards paradigms suggest context-specific response	123
3.3.2.4	Frequency deviant-alone paradigm stimuli elicit extended latency potentials which correlate with frequency mismatch responses	126
3.3.3	Intensity paradigms in urethane-anaesthetised mice	129
3.3.3.1	Stimulus intensity influences auditory evoked potentials.....	129
3.3.3.2	Increasing intensity oddball elicits a mismatch response	132
3.3.3.3	Auditory evoked potentials from intensity consecutive-repetition, oddball and many- standards paradigms suggest context-specific response	137
3.3.3.4	Intensity deviant-alone paradigm elicits extended latency potentials which correlate with mismatch response of increasing intensity oddball stimuli	140
3.3.4	Auditory evoked potential changes throughout Experiment I	143
3.3.4.1	Stimulus onset potential.....	144
3.3.4.2	Stimulus offset potential	145
3.3.4.3	Deviant evoked activity	146
3.3.5	Spectral analyses	147
3.3.6	Results Summary.....	150
3.4	Discussion.....	153
3.4.1	Effects of stimuli duration, frequency and intensity on auditory evoked potentials in urethane-anaesthetised mice	154
3.4.2	Mismatch responses in urethane-anaesthetised mice.....	156
3.4.3	<i>Map2k7^{+/-}</i> gene disruption in urethane-anaesthetised mice.....	157
3.4.4	Ketamine, confounds and longitudinal analyses	159
3.4.5	Recommendations for Experiment II	160

Chapter 4. Experiment II: evaluation of multivariate auditory paradigms in conscious wild-type and *Map2k7*^{+/-} mice exposed to ketamine 161

4.1	Introduction	162
4.1.1	Previous studies in conscious rodents	162
4.1.1.1	Duration	162
4.1.1.2	Frequency	164
4.1.1.3	Intensity	165
4.1.2	Challenges and opportunities of using conscious rodents	166
4.1.3	Experiment II aims	167
4.2	Methods	168
4.2.1	Animal details	168
4.2.2	Surgery	168
4.2.3	Electrophysiological recordings	168
4.2.4	Auditory paradigms	168
4.2.5	Stimuli properties	168
4.2.6	Experimental protocol	169
4.2.7	Artifact rejection.....	169
4.2.8	Auditory evoked potential computations.....	171
4.2.9	Auditory evoked potential measurements	171
4.2.9.1	Primary onset potential (N1)	171
4.2.9.2	Secondary potential (P2).....	171
4.2.9.3	Subsequent peaks (N3, P4, N5 and P6)	171
4.2.9.4	Offset response (P _{offset} and N _{offset})	172
4.2.10	Video footage analysis	172
4.3	Results	173
4.3.1	Duration paradigms in conscious mice.....	173
4.3.1.1	<i>Map2k7</i> ^{+/-} mice display increased stimulus onset response.....	173
4.3.1.2	Inter-stimulus interval influences auditory evoked potentials	176
4.3.1.3	Stimuli offset responses are observed in conscious mice	178
4.3.1.4	Duration mismatch response in conscious mice is influenced by stimuli offset potentials.....	182
4.3.1.5	Inter-stimulus interval mismatch response in conscious mice	185
4.3.1.6	Context-specific effects of varying inter-stimulus interval stimuli in oddball and control paradigms	185
4.3.1.7	Comparison of auditory-evoked potential waveforms from identical stimuli presented in duration paradigms throughout Experiment II	187
4.3.2	Frequency paradigms in conscious mice	192
4.3.2.1	Stimulus frequency influences auditory evoked potentials.....	192

4.3.2.2	Frequency mismatch response in conscious mice.....	194
4.3.2.3	Context-specific effects of varying frequency stimuli in oddball and control paradigms	196
4.3.2.4	Acute effect of ketamine on conscious mouse auditory evoked potentials.....	199
4.3.3	Intensity paradigms in conscious mice.....	202
4.3.3.1	Stimulus intensity influences auditory evoked potentials.....	202
4.3.3.2	Intensity mismatch response in conscious mice	205
4.3.3.3	Comparison of deviant-alone vs. consecutive-repetition paradigm auditory evoked potentials with extended inter-stimulus interval	207
4.3.3.4	Auditory evoked potential changes throughout Experiment II.....	212
4.3.4	Spectral analyses	216
4.3.5	Video footage analysis	219
4.3.6	Results Summary.....	223
4.4	Discussion.....	225
4.4.1	Effects of inter-stimulus interval, duration, frequency and intensity on auditory evoked potentials in conscious mice.....	226
4.4.2	Mismatch responses in conscious mice	227
4.4.3	<i>Map2k7^{+/-}</i> gene disruption in conscious mice	228
4.4.4	Ketamine effects in conscious mice	230
4.4.5	Summary of findings from Experiment II	232
4.4.6	Recommendations for Experiment III.....	233

Chapter 5. Experiment III: laminar auditory cortex mismatch response investigation in urethane-anaesthetised wild-type and *Map2k7^{+/-}* mice exposed to ketamine..... 234

5.1	Introduction	235
5.1.1	Laminar investigations of the auditory cortex	235
5.1.2	Duration-tuned neurons	236
5.1.3	Frequency-tuned neurons	237
5.1.4	Intensity tuned neurons	237
5.1.5	Stimulus specific adaptation and mismatch responses	238
5.1.6	Experiment III aims.....	239
5.2	Methods	240
5.2.1	Animal details	240
5.2.2	Surgery	240
5.2.3	Multichannel probe implantation	240
5.2.4	Electrophysiological recordings	242
5.2.5	Auditory paradigms.....	243

5.2.6	Stimuli properties	243
5.2.7	Experimental protocol	246
5.2.8	Current source density analysis	246
5.3	Results	249
5.3.1	Duration paradigms and laminar responses in urethane-anaesthetised mice	249
5.3.1.1	Offset responses vary with channel depth	249
5.3.1.2	Re-referencing to deep channels reveals slow positive amplitude response in superficial channels underlying the offset response	255
5.3.1.3	Group analysis reveals little evidence of multi-unit activity correlates of stimuli onset and offset responses	257
5.3.2	Frequency paradigms and laminar response in urethane-anaesthetised mice	259
5.3.2.1	Frequency effect in modified consecutive-repetition paradigm	259
5.3.2.2	Frequency effect in the many-standards paradigm	263
5.3.2.3	Frequency mismatch responses observed in multichannel electrodes	266
5.3.2.4	Frequency deviant-alone paradigm control waveforms	275
5.3.2.5	Comparison of auditory evoked potentials and multi-unit activity from frequency deviant-alone stimuli	282
5.3.3	Intensity paradigms and laminar response in urethane-anaesthetised mice	284
5.3.3.1	Effect of stimulus intensity on grand-average auditory evoked potential across electrodes of multichannel probe	284
5.3.3.2	Comparison of auditory evoked potentials and multi-unit activity in response to different intensity stimuli	288
5.3.4	Spike analyses	290
5.3.4.1	Examples of spike waveforms	291
5.3.5	Results summary	294
5.3.5.1	Stimuli duration effects	294
5.3.5.2	Stimuli frequency effects	294
5.3.5.3	Stimuli intensity effects	295
5.3.5.4	Ketamine and spiking activity	295
5.3.5.5	<i>Map2k7</i> ^{+/-} gene disruption	295
5.4	Discussion	296
5.4.1	Effects of stimuli duration, frequency and intensity on laminar auditory evoked potentials in urethane-anaesthetised mice	296
5.4.2	Frequency mismatch response laminar profile in urethane-anaesthetised mice	298
5.4.3	The effect of ketamine on spike activity in urethane-anaesthetised mice	299
5.4.4	Success rate/recording issues and suggestions for improvement	299

Chapter 6. General discussion	301
6.1 Discussion of main findings	302
6.1.1 Anaesthetised and conscious states	302
6.1.2 Mismatch responses in mice.....	303
6.1.3 The <i>Map2k7^{+/-}</i> model.....	305
6.1.4 The NMDA antagonist model	306
6.2 Suggestions for further work	307
6.2.1 Technical improvements	307
6.2.2 Component characterisation	307
6.2.3 Translational validity.....	308
6.3 Conclusions	309
References	310
Appendices	336
Appendix A - Experiment I animal details	337
Appendix B - Experiment II animal details	338
Appendix C - Experiment III animal details	339
Appendix D - Multichannel probe datasheet	340
Appendix E - Matlab scripts	341
Research output.....	388

List of Figures

Figure 1.1 - The post-synaptic intracellular JNK signalling pathway with genes/proteins implicated in schizophrenia.....	6
Figure 1.2 - The proposed mechanism of gamma synchrony dysregulation in schizophrenia	9
Figure 1.3 - Example of human auditory evoked potential components	11
Figure 1.4 - The ear.....	24
Figure 1.5 - The central auditory pathway.....	25
Figure 1.6 - The human auditory cortex	28
Figure 1.7 - The mouse auditory cortex.....	29
Figure 1.8 - The six-layered structure of the auditory cortex	31
Figure 1.9 - Predictive coding model of mismatch negativity	34
Figure 1.10 - Oddball and control paradigms used in rodent mismatch response studies	43
Figure 2.1 - Experiment I electrode implantation surgery	56
Figure 2.2 - Experiment II electrode implantation surgery.....	57
Figure 2.3 - Experiment III electrode implantation surgery	58
Figure 2.4 - Recording Chamber A: configuration for Experiment I.....	60
Figure 2.5 - Recording Chamber A: configuration for Experiment II	61
Figure 2.6 - Multichannel probe geometry	63
Figure 2.7 - Recording Chamber B: configuration for Experiment III	64
Figure 2.8 - Oddball (OD) paradigm representation.....	66
Figure 2.9 - Consecutive-repetition (CR) paradigm representation.....	66
Figure 2.10 - Deviant-alone (DA) paradigm representation	68
Figure 2.11 - Many-standards (MS) paradigm representation	69
Figure 2.12 - Stimulus onset asynchrony (SOA) and inter-stimulus interval (ISI) trade-off.	72
Figure 2.13 - Frequency response screening procedure in Experiment III	76
Figure 2.14 - General paradigm sequence for Experiment I and Experiment II.....	78
Figure 2.15 - Recording and auditory stimulation protocol for Experiment I	78
Figure 2.16 - Order of test sessions in Experiment II	79
Figure 2.17 - Recording and auditory stimulation protocol for Experiment III.....	80
Figure 3.1 - Traditional and extended epoch mismatch response calculations.....	98
Figure 3.2 - Custom baseline correction used in this study	99
Figure 3.3 - Comparison of urethane-anaesthetised control and <i>Map2k7^{+/-}</i> grand-average auditory evoked potential waveforms	103
Figure 3.4 - Decreased duration (-50 ms) oddball mismatch response in urethane-anaesthetised mice.....	104
Figure 3.5 - Increased duration (+50 ms) oddball mismatch response in urethane-anaesthetised mice.....	105

Figure 3.6 - Quantification of decreased (-50 ms) and increased (+50 ms) duration oddball mismatch responses in urethane-anaesthetised mice.....	106
Figure 3.7 - Auditory evoked potentials from urethane-anaesthetised mice to different duration stimuli presented in oddball and control paradigms.....	108
Figure 3.8 - Auditory evoked potentials to duration many-standards paradigm stimuli in urethane-anaesthetised mice.....	110
Figure 3.9 - Extended latency auditory evoked potentials to duration deviant-alone paradigm stimuli in urethane-anaesthetised mice.....	112
Figure 3.10 - Quantification of extended latency auditory evoked potentials to duration deviant-alone paradigm stimuli in urethane-anaesthetised mice.....	113
Figure 3.11 - Effect of tone frequency on the auditory onset response in urethane-anaesthetised mice.....	115
Figure 3.12 - Effect of tone frequency on the auditory offset response in urethane-anaesthetised mice.....	117
Figure 3.13 - Descending frequency (-2.5 kHz) oddball mismatch response in urethane-anaesthetised mice.....	119
Figure 3.14 - Ascending frequency (+2.5 kHz) oddball mismatch response in urethane-anaesthetised mice.....	120
Figure 3.15 - Quantification of frequency mismatch responses in urethane-anaesthetised control, <i>Map2k7^{+/-}</i> and NMDA receptor antagonism models	122
Figure 3.16 - Auditory evoked potentials from urethane-anaesthetised mice to different frequency stimuli presented in oddball and control paradigms.....	124
Figure 3.17 - Quantification of deviant evoked activity from urethane-anaesthetised mice to different frequency stimuli presented in oddball and control paradigms	125
Figure 3.18 - Extended latency auditory evoked potentials to frequency deviant-alone paradigm stimuli in urethane-anaesthetised mice.....	127
Figure 3.19 - Comparison of frequency mismatch response and deviant-alone paradigm extended latency evoked potentials from urethane-anaesthetised mice	128
Figure 3.20 - Effect of sound pressure level on auditory onset response in urethane-anaesthetised mice.....	130
Figure 3.21 - Effect of sound pressure level on auditory offset response in urethane-anaesthetised mice.....	131
Figure 3.22 - Quieter intensity (-10 dB) oddball mismatch response in urethane-anaesthetised mice.....	133
Figure 3.23 - Louder intensity (+10 dB) oddball mismatch response in urethane-anaesthetised mice.....	134
Figure 3.24 - Quantification of intensity mismatch responses in urethane-anaesthetised control, <i>Map2k7^{+/-}</i> and NMDA receptor antagonism models	136
Figure 3.25 - Auditory evoked potentials from urethane-anaesthetised mice to different intensity stimuli presented in oddball and control paradigms	138
Figure 3.26 - Quantification of deviant evoked activity from urethane-anaesthetised mice to different intensity stimuli presented in oddball and control paradigms	139

Figure 3.27 - Extended latency auditory evoked potentials to intensity deviant-alone paradigm stimuli in urethane-anaesthetised mice.....	141
Figure 3.28 - Comparison of intensity mismatch response and deviant-alone paradigm extended latency evoked potentials from urethane-anaesthetised mice	142
Figure 3.29 - Auditory stimulus onset response peak amplitudes from physically identical stimuli presented throughout Experiment I.....	144
Figure 3.30 - Auditory stimulus offset response peak amplitudes from identical physical stimuli presented throughout Experiment I.....	145
Figure 3.31 - Deviant evoked activity measured from deviant-alone paradigm stimuli presented throughout Experiment I.....	146
Figure 3.32 - EEG power spectra from urethane-anaesthetised mice exposed to ketamine	148
Figure 3.33 - Auditory event-related spectral perturbation (ERSP) from urethane-anaesthetised mice exposed to ketamine	149
Figure 3.34 - Illustration of auditory evoked potential features observed from urethane-anaesthetised mice.....	153
Figure 4.1 - Examples of accepted and rejected data for auditory evoked potential analyses	170
Figure 4.2 - Comparison of conscious wild-type and <i>Map2k7^{+/-}</i> grand-average auditory evoked potential waveforms.....	175
Figure 4.3 - Effect of inter-stimulus interval on primary and secondary auditory responses in conscious wild-type and <i>Map2k7^{+/-}</i> mice.....	177
Figure 4.4 - Quantification of inter-stimulus interval effect on auditory evoked potentials in conscious wild-type and <i>Map2k7^{+/-}</i> mice.....	178
Figure 4.5 - Effect of stimulus duration on auditory offset response in conscious mice	180
Figure 4.6 - Characterising the auditory stimulus offset response in conscious mice	181
Figure 4.7 - Increasing (+50 ms) and decreasing (-50 ms) duration oddball mismatch responses in conscious mice.....	183
Figure 4.8 - Quantification of decreased (-50 ms) and increased (+50 ms) duration oddball mismatch responses in conscious mice	184
Figure 4.9 - Inter-stimulus interval oddball mismatch responses in conscious wild-type and <i>Map2k7^{+/-}</i> mice receiving ketamine	186
Figure 4.10 - Context-specific analysis of primary and secondary auditory evoked features from inter-stimulus interval oddball and control paradigms	187
Figure 4.11 - Auditory evoked potentials from conscious control animals throughout an Experiment II test session.....	189
Figure 4.12 - Auditory evoked potentials from conscious <i>Map2k7^{+/-}</i> animals throughout an Experiment II test session.....	190
Figure 4.13 - Effect of tone frequency on primary and secondary auditory responses in conscious wild-type and <i>Map2k7^{+/-}</i> mice.....	192
Figure 4.14 - Quantification of tone frequency effects on auditory evoked potentials in conscious wild-type and <i>Map2k7^{+/-}</i> mice.....	193

Figure 4.15 - Frequency mismatch responses in conscious wild-type and <i>Map2k7^{+/-}</i> mice receiving ketamine	195
Figure 4.16 - Context-specific analysis of primary and secondary auditory evoked features from frequency oddball and control paradigms conscious wild-type and <i>Map2k7^{+/-}</i> mice	198
Figure 4.17 - Acute effects of 10 mg/kg i.p. ketamine on auditory evoked potentials in conscious wild-type and <i>Map2k7^{+/-}</i> mice.....	200
Figure 4.18 - Quantification of the acute effects of 10 mg/kg i.p. ketamine on auditory evoked potential features in conscious wild-type and <i>Map2k7^{+/-}</i> mice.....	201
Figure 4.19 - Effect of sound pressure level on primary and secondary auditory responses in conscious wild-type and <i>Map2k7^{+/-}</i> mice.....	203
Figure 4.20 - Quantification of sound pressure level effects on auditory evoked potentials in conscious wild-type and <i>Map2k7^{+/-}</i> mice.....	204
Figure 4.21 - Intensity mismatch responses in conscious wild-type and <i>Map2k7^{+/-}</i> mice receiving ketamine	206
Figure 4.22 - Intensity mismatch response- <i>like</i> waveforms from intensity consecutive-repetition paradigm in conscious wild-type and <i>Map2k7^{+/-}</i> mice following 10 mg/kg i.p. ketamine	207
Figure 4.23 - Auditory evoked potentials from deviant-alone paradigm stimuli in conscious wild-type and <i>Map2k7^{+/-}</i> mice receiving ketamine	209
Figure 4.24 - Auditory evoked potentials from consecutive-repetition paradigm with extended inter-stimulus interval in conscious wild-type and <i>Map2k7^{+/-}</i> mice receiving ketamine	210
Figure 4.25 - Quantification of deviant-alone and consecutive-repetition paradigms with extended inter-stimulus interval in conscious wild-type and <i>Map2k7^{+/-}</i> mice receiving ketamine	211
Figure 4.26 - Longitudinal examination of six peak amplitudes from conscious mice throughout Experiment II	214
Figure 4.27 - Longitudinal examination of six peak latencies from conscious mice throughout Experiment II	215
Figure 4.28 - EEG power spectra from conscious mice exposed to ketamine.....	217
Figure 4.29 - Auditory event-related spectral perturbation (ERSP) from conscious mice exposed to ketamine	218
Figure 4.30 - Example of video frames used in a block-matching algorithm to estimate motion of conscious mice in Experiment II	220
Figure 4.31 - Gross motion data output from the block-matching algorithm	221
Figure 4.32 - Time-binned comparisons of gross motion from conscious mice in Experiment II	222
Figure 4.33 - Illustration of auditory evoked potential features observed from conscious mice	225
Figure 5.1 – Illustration of multichannel probe implantation axes and potential misalignments.....	241
Figure 5.2 - Channel averaging used to analyse laminar auditory evoked responses	243

Figure 5.3 - Frequency Response Area plots from Experiment III subjects	245
Figure 5.4 - Example of current source density estimate of electrode depth from Subject 75 (HET, male).....	248
Figure 5.5 - Grand-average auditory evoked potentials to different duration stimuli across multichannel probe electrodes Ch1-16 (Shank A)	250
Figure 5.6 - Grand-average auditory evoked potentials to different duration stimuli across multichannel probe electrodes Ch17-32 (Shank B).....	251
Figure 5.7 - Channel-averaged grand-average auditory evoked potentials to different duration stimuli in Experiment III	253
Figure 5.8 - Quantification of onset and offset responses to different duration stimuli from wild-type and <i>Map2k7^{+/-}</i> mice in Experiment III.....	254
Figure 5.9 - Difference between proximal/superficial and distal/deep channel auditory evoked potentials to different duration stimuli.....	256
Figure 5.10 - The effects of stimulus duration on auditory evoked potentials and multi-unit activity in Experiment III	258
Figure 5.11 - Grand-average auditory evoked potentials to different frequency stimuli across multichannel probe electrodes Ch1-16 (Shank A)	260
Figure 5.12 - Grand-average auditory evoked potentials to different frequency stimuli across multichannel probe electrodes Ch17-32 (Shank B).....	261
Figure 5.13 - Quantification of onset and offset responses to different frequency stimuli from wild-type and <i>Map2k7^{+/-}</i> mice in Experiment III.....	262
Figure 5.14 - Grand-average auditory evoked potential analysis from frequency many-standards paradigm stimuli.....	264
Figure 5.15 - Individual subjects' absolute auditory evoked potential responses to stimuli from the frequency many-standards paradigm.....	265
Figure 5.16 - Frequency mismatch response in Subject 36 (WT, female) before ketamine	267
Figure 5.17 - Frequency mismatch response in Subject 36 (WT, female) following 10 mg/kg i.p. ketamine	268
Figure 5.18 - Frequency mismatch response in Subject 74 (HET, male) before ketamine..	269
Figure 5.19 - Frequency mismatch response in Subject 74 (HET, male) following 10 mg/kg i.p. ketamine	270
Figure 5.20 - Frequency mismatch response in Subject 76 (WT, male) before ketamine ...	271
Figure 5.21 - Frequency mismatch response in Subject 76 (WT, male) following 10 mg/kg i.p. ketamine	272
Figure 5.22 - Frequency mismatch response in Subject 77 (HET, female) before ketamine	273
Figure 5.23 - Frequency mismatch response in Subject 77 (HET, female) following 10 mg/kg i.p. ketamine	274
Figure 5.24 - Frequency mismatch response in Subject 75 (HET, male)	276
Figure 5.25 - Frequency deviant-alone control waveforms in Subject 36 (WT, female).....	277
Figure 5.26 - Frequency deviant-alone control waveforms in Subject 74 (HET, male)	278

Figure 5.27 - Frequency deviant-alone control waveforms in Subject 75 (HET, male)	279
Figure 5.28 - Frequency deviant-alone control waveforms in Subject 76 (WT, male).....	280
Figure 5.29 - Frequency deviant-alone control waveforms in Subject 77 (HET, female) ...	281
Figure 5.30 - Comparison of frequency deviant-alone auditory evoked potentials and multi-unit activity from Subject 75 (HET, male).....	283
Figure 5.31 - Grand-average auditory evoked potentials to different intensity stimuli across multichannel probe electrodes Ch1-16 (Shank A)	285
Figure 5.32 - Grand-average auditory evoked potentials to different intensity stimuli across multichannel probe electrodes Ch17-32 (Shank B).....	286
Figure 5.33 - Quantification of onset and offset responses to different intensity stimuli from wild-type and <i>Map2k7^{+/-}</i> mice in Experiment III.....	287
Figure 5.34 - Analysis of auditory evoked potential and multi-unit activity responses to different intensity stimuli in Subject 75 (HET, male)	289
Figure 5.35 - Overview of multi-unit activity from all subjects in Experiment III.....	290
Figure 5.36 - Contrasting effects of 10 mg/kg i.p. ketamine on multi-unit activity in different subjects	292
Figure 5.37 - Example spike waveforms	293

List of Tables

Table 1.1 - 'Optimal' oddball paradigm for eliciting mismatch negativity in humans.....	15
Table 1.2 - Summary of mismatch response studies in rodents	39
Table 1.3 - Overview of the current study	47
Table 2.1 - Overview of study methods	49
Table 2.2 - Parameters for oddball (OD), consecutive-repetition (CR) and deviant-alone (DA) paradigm stimuli in Experiment I	70
Table 2.3 - Parameters for many-standards (MS) paradigm stimuli in Experiment I.....	71
Table 2.4 - Parameters for oddball (OD), consecutive-repetition (CR) and deviant-alone (DA) paradigm stimuli in Experiment II.....	73
Table 2.5 - Parameters for many-standards (MS) paradigm stimuli in Experiment II.....	74
Table 2.6 - Parameters for modified consecutive-repetition (CR) paradigm stimuli in Experiment III	77
Table 3.1 - Summary of auditory evoked potential features observed from urethane-anaesthetised mice.....	150
Table 3.2 - Summary of urethane-anaesthetised mouse auditory evoked potential sensitivities to stimuli duration, frequency and intensity variations	150
Table 3.3 - Summary of urethane-anaesthetised <i>Map2k7^{+/-}</i> and 10 mg/kg i.p. ketamine model effects on auditory evoked potential features.....	151
Table 3.4 - Paradigm-specific observations from stimuli duration, frequency and intensity manipulations in urethane-anaesthetised mice	152
Table 4.1 - Summary of auditory evoked potential features observed from conscious mice	223
Table 4.2 - Summary of conscious mouse auditory evoked potential sensitivities to stimuli duration, frequency and intensity variations	224
Table 4.3 - Summary of conscious <i>Map2k7^{+/-}</i> and 10 mg/kg i.p. ketamine model effects on auditory evoked potential features and video analysis	224
Table 5.1 - Auditory stimuli frequencies determined for Experiment III subjects	244
Table 5.2 - Main current sink and source channels from current source density analysis of urethane-anaesthetised mice in Experiment III	246

List of Abbreviations and Symbols

<	Less than
≠	Not equal to
>	More than
≈	Approximately equal to
≤	Less than or equal to
≥	More than or equal to
↑	Increase
↓	Decrease
μ	Micro ($\times 10^{-6}$)
μm	Micrometre
μV	Micro-volts
2-DG	2-deoxyglucose
5-CSRTT	Five choice serial reaction time task
5-HT	Serotonin/5-hydroxytryptamine
A/R	Anterior/rostral
A1	Primary auditory cortex
A2	Secondary auditory cortex
AAF	Anterior auditory field
AC	Auditory cortex
ACh	Acetylcholine
AEP	Auditory Evoked Potential
AERP	Auditory Event Related Potential
AMPA	α -amino-3-hydroxy-5-methyl-4-isoxazolepropionic acid
AMPK	AMP-activated protein kinase
AP5	D-(-)-2-amino-5-phosphonopentanoic acid
ARS	Acute restraint stress
ASSR	Auditory steady-state response
BF	Best frequency
BPU	University of Strathclyde Biological Procedures Unit
C57BL/6J	Laboratory mouse strain
Ca ²⁺	Calcium
CA3	CA3 region of the hippocampus
CF	Characteristic frequency
cm	Centimetre
CNV	Copy number variants
CR	Consecutive Repetition Paradigm
CSD	Current source density
d	Duration

D ₂	Dopamine receptor type 2
DA	Deviant Alone Paradigm
DC	Direct current
dCR	Duration-varying consecutive repetition paradigm
dDA	Duration-varying deviant-alone paradigm
DEA	Deviant evoked activity
DFT	Discrete Fourier transform
dMS	Duration-varying many-standards paradigm
dOD	Duration-varying oddball paradigm
DP	Dorsoposterior field
DP	Descending auditory pathway
DUSP14	Dual-specificity phosphatase 14
EEG	Electroencephalography
EEG	Electroencephalogram
EMG	Electromyography
ERBB4	Receptor tyrosine kinase
ERP	Event Related Potential
ERSP	Event Related Spectral Perturbation
f	Frequency
FC	Frontal cortex
fCR	Frequency-varying consecutive repetition paradigm
fDA	Frequency-varying deviant-alone paradigm
fMRI	Functional magnetic resonance imaging
fMS	Frequency-varying many-standards paradigm
fOD	Frequency-varying oddball paradigm
FR	Frequency response
FRA	Frequency response area
Fz	Fronto-central scalp location for human EEG montage
GABA	γ-amino butyric acid
GluN1- GluN3	NMDA receptor subtypes (previously NR1, NR2 and NR3)
HET	Heterozygous (<i>Map2k7^{+/-}</i>)
Hz	Hertz/cycles per second
i	Intensity
I/V	Inferior/ventral
IC	Inferior colliculus
iCR	Intensity-varying consecutive repetition paradigm
iDA	Intensity-varying deviant-alone paradigm
iMS	Intensity-varying many-standards paradigm
iOD	Intensity-varying oddball paradigm
ISI	Inter-stimulus interval

JIP1	JNK-interacting protein 1
JNK	c-Jun N-terminal kinase
k	Kilo ($\times 10^3$)
K ⁺	Potassium
Ket	Ketamine
LDAEP	Loudness dependence of the auditory evoked potential
LFP	Local Field Potential
LFP	Local field potential
LI-VI	Cortical layers 1-6
LLR	Long-latency response
LRP1B	low-density lipoprotein receptor-related protein 1B
LTD	Long term depression
LTP	long term potentiation
m	Metre
MAP2K7	Mitogen activated protein kinase kinase 7
MEG	Magnetoencephalography
MERTK	Type 1 transmembrane tyrosine kinase
MG	Medial geniculate nucleus (auditory thalamus)
mGluR1-8	Metabotropic glutamate receptors 1-8
MK-801	Dizocilpine
MLR	Middle-latency response
mm	Millimetre
MMN	Mismatch Negativity
MMNm	Magnetic mismatch negativity
MMP	Mismatch positivity
MMR	Mismatch Response
MOF	Mean optical flow
MS	Many Standards Paradigm
MUA	Multi-Unit Activity
N100	Negative peak in human AEP occurring at ≈ 100 ms
N200	Negative peak in human AEP occurring at ≈ 200 ms
NCK1	Non-catalytic region of tyrosine kinase adaptor protein 1
NIMH	National Institute of Mental Health (US)
NMDA	N-methyl-d-aspartate
NMDAr	N-methyl-D-aspartate receptor
NR1-3	NMDA receptor subtypes (now notated GluN1-3)
NRG	Nuregulin
NRGN4	Neuroigin 4
OD	Oddball Paradigm
Odb	Oddball Stimulus

P/C	Posterior/caudal
P200	Positive peak in human AEP occurring at \approx 200 ms
P300	Positive peak in human AEP occurring at \approx 300 ms
P50	Positive peak in human AEP occurring at \approx 50 ms
PCP	Phencyclidine
PDZ-GEF	PDZ-domain guanine exchange factor
PET	Positron emission tomography
PIL	UK Home Office personal licence
PPEF2	Protein phosphatase with EF-hand motif
PPL	UK Home Office project licence
PSD95	Scaffolding postsynaptic density protein
PSTH	Peri-stimulus time histogram
PV	Parvalbumin
Rap2	Member of the Ras family of GTPases
RDoC	Research Domain Criteria
RGB	Red-green-blue
s	Second
S	Sample
S/D	Superior/dorsal
SA	Signed Area
Sal	Saline
SNP	Single nucleotide polymorphism
SNR	Signal-to-noise ratio
SOA	Stimulus onset asynchrony
SPL	Sound pressure level
SSA	Stimulus specific adaptation
Std	Standard Stimulus
STK11	Serine/threonine kinase 11
SUA	Single-Unit Activity
TAK1	Transforming-growth-factor-beta activated kinase 1
TAOK	Thousand-and-one amino acids protein kinase
UF	Ultrasonic field
V	Volts
VEP	Visual evoked potential
VRK2	Vaccinia Related Kinase 2
VSSR	Visual steady-state response
WT	Wild-type control (<i>Map2k7^{+/+}</i>)
Ω	Ohms (impedance)

Chapter 1. Introduction

1.1 Schizophrenia

1.1.1 Epidemiology

The diagnosis of schizophrenia is given to approximately 0.5-1 % of the global population. This incidence remains relatively constant over geographical, ethnic, social and demographic groups, although it is highly heterogeneous in its phenotypic and genetic presentation (Weinberger and Harrison, 2010). Disease onset tends to occur earlier in males (age 15-25) than females (age 20-30), although both sexes are impacted equally overall (van der Werf et al., 2014). According to London School of Economics, the annual expense per patient with schizophrenia in England, through direct healthcare costs and indirect societal costs, is estimated at approximately £96,000 (Schizophrenia Commission, 2012), providing significant economic impetus to improve treatment of this disorder.

1.1.2 Symptomatology

Schizophrenia is a debilitating neuropsychiatric condition which causes marked social or occupational dysfunction. It is characterised by the presentation of positive and negative symptoms with cognitive and emotional impairment. The positive symptom class describes sensations which are additional to those experienced by healthy persons; for example, delusions, hallucinations (predominantly auditory), disorganised thinking/speech and catatonia. Negative symptoms refer to normal functions which are blunted in comparison with healthy persons; such as affective flattening, poverty of speech/alogia, anhedonia, and avolition. Cognitive deficits include impaired working memory and attention. Presentation of a mixture of these symptoms over a sustained period (6 months) sufficient to cause significant social or occupational dysfunction will generally be diagnosed as schizophrenia. There were previously five subtypes defined based on the particular manifestation of symptoms and stage of disease progression; these were named paranoid, disorganised, catatonic, undifferentiated or residual (APA 2000).

More recently, in the fifth edition of the American Psychiatric Association's Diagnostic and Statistical Manual of Mental Disorders (2013), these subtypes have been removed and schizophrenia is recognised as a spectrum including other psychotic disorders. The interpretation of schizophrenia as a spectrum is supported by evidence linking it with bipolar and psychotic mood disorders (Craddock and Owen, 2010, Lake, 2012). This has led the National Institute of Mental Health (NIMH) in the United States to initiate the Research Domain Criteria (RDoC) project (Insel et al., 2010), which aims to inform the future classification of psychiatric disorders based on objective neurobiological and behavioural measurements. This movement aims to fundamentally shift treatment strategies from a one-

size-fits-all model to a targeted, ‘precision medicine’ approach, which is hoped will be more successful (Cuthbert and Insel, 2013). Thus far the RDoC project has determined several domains: negative and positive valence systems, cognitive systems, systems for social processes, arousal and regulatory systems. Various quantifiable neurophysiological and behavioural constructs, or pathologies, common to multiple DSM-V diagnoses are categorised according to these domains. Over a course of time this project may lead to a future where cross-diagnostic diseases are treated based on specific pathophysiological mechanisms with predicted therapeutic outcomes (Insel et al., 2010). Key to these aims is the identification and validation of objective biomarkers which can detect onset, track progression and predict treatment of these cross-diagnostic constructs.

1.1.3 Genetic and environmental risk factors

The statistical probability of developing schizophrenia is influenced by genetic and environmental risk factors; moreover, a combination of these factors may further increase the likelihood of developing a schizophrenia spectrum disorder. Environmental factors associated with increased risk include prenatal nutrition, prenatal infection, pregnancy and birth complications, paternal age, drug abuse (amphetamine, methamphetamine and cannabis), urban birth/upbringing, migration and traumatic life events (Weinberger and Harrison, 2010). These environmental risks may interact with the following genetic risk factors to compound the potential for developing a schizophrenia syndrome.

Familial and twin studies have provided convincing evidence that there is a substantial, complex genetic contribution towards the risk of developing schizophrenia. This polygenic disorder arises from heterogeneous combinations of single nucleotide polymorphisms (SNPs) and copy number variants (CNVs); where common SNPs convey less relative risk than rarer CNVs (Winchester et al., 2014). Many of these high penetrance CNVs are also implicated in autism, mental retardation, epilepsy and other neurodevelopment disorders; to be considered during the RDoC efforts to reclassify neuropsychiatric diseases discussed above (Doherty et al., 2012). Interestingly, many of these identified mutations tend to localize at chromosomal regions which encode functionally associated proteins acting at the glutamate synapse (Ripke et al., 2014, Morris and Pratt, 2014). For example, a number of genes implicated in the intracellular *c-Jun N-terminal kinase* (JNK) signalling pathway (discussed in Section 1.3.1.1), activated in the post-synaptic neuron following glutamate binding (see Figure 1.1), have been associated with schizophrenia and other neuropsychiatric diseases.

1.1.4 Neurobiology

The pathophysiology underlying schizophrenia spectrum disorders is highly complex, reflecting an elaborate interplay between genetic and environmental factors which combine to produce neurodevelopmental abnormalities in brain circuits that are not fully understood. The multifactorial and heterogeneous nature of this condition may suggest the involvement of equally diverse biological mechanisms. It may then come as little surprise that there are multiple hypotheses of the pathogenesis of schizophrenia.

The long-standing dopamine hypothesis is principally supported by the finding that positive symptoms (e.g. hallucination, delusions) are ameliorated by therapeutics which block D₂ receptors (Seeman, 1987, Van Rossum, 1966). Generally, dopamine D₂ receptor antagonists act as antipsychotics whereas indirect agonists (which enhance dopamine release) such as amphetamine are psycho-stimulant, capable of inducing psychotic symptoms in healthy subjects and exacerbating positive symptoms in schizophrenia patients (reviewed by Lieberman et al., 1987). This hypothesis has developed to the current understanding that excessive striatal dopamine underlies psychosis in schizophrenia. However, this physiological situation is considered to be a final common pathway that can be reached by different means, evidenced by findings that disease models ranging from brain lesions to social isolation and gene deletions induce excess striatal dopamine (Seeman, 2011, Howes and Kapur, 2009). The negative and cognitive symptoms are not as well accounted for by dopamine functions, and it is suggested that dopamine collaborates with other dysfunction neurotransmitter systems such as glutamate signalling to encompass full blown schizophrenia (Lau et al., 2013).

Glutamate is the primary excitatory neurotransmitter acting throughout the nervous system. It binds to ionotropic α -amino-3-hydroxy-5-methyl-4-isoxazolepropionic acid (AMPA), N-methyl-D-aspartate (NMDA) and kainate receptors, and eight different types of metabotropic receptor (mGluR1-8). Gereau and Swanson (2008) provides a comprehensive discussion of these receptors. Each of the ionotropic receptors is composed of up to five subunits which combine in different formations to produce distinct physiological properties. The NMDA receptor subunits GluN1, GluN2 and GluN3 (previously NR1, NR2 and NR3) are further subdivided into different variants; GluN1, GluN2A-D and GluN3A-B. Every NMDA receptor incorporates an obligatory GluN1 subunit combined with three other subunits which determine the behaviour of the channel. Furthermore, these are plastic, changing throughout development (reviewed by Paoletti et al., 2013). AMPA receptors are involved in the fastest transmission of neural excitation throughout the brain. NMDA receptors require binding of

both glutamate and glycine to become active and enable calcium (Ca^{2+}) and sodium (Na^+) influx into the post-synaptic neuron. Once the cell becomes sufficiently depolarised, a divalent magnesium cation (Mg^{2+}) will clog the channel, preventing further Ca^{2+} and Na^+ entry and allowing the cell to repolarise, thus NMDA receptor channels are known to be voltage-sensitive. Kainate receptors are more diverse and play a role in modulating synaptic excitation and inhibition. There are findings of each of these ionotropic receptor classes being down-regulated and implicated in the pathophysiology of schizophrenia (reviewed by Meador-Woodruff and Healy, 2000).

The glutamate hypothesis of schizophrenia arose from observations that non-competitive NMDA receptor channel antagonists such as ketamine, phencyclidine (PCP) and dizocilpine (MK-801) induce psychotomimetic effects (reviewed by Ellison, 1995). These substances induce psychotic symptoms in healthy volunteers and exacerbate those in schizophrenia spectrum sufferers, somewhat similar to dopaminergic agonists. In contrast with dopamine manipulations however, NMDA receptor antagonists also model some of the negative and cognitive symptoms of schizophrenia; e.g. working memory deficits, affecting flattening and disordered thought (Goff and Coyle, 2001, Jentsch and Roth, 1999). Further information on the NMDA receptor antagonist model employed in this study is provided in Section 1.4.2. Additionally, NMDA receptor antagonists increase dopamine release, indicating how neuropathology of one system can have a knock-on effect on the other, linking these two hypotheses of schizophrenia (Bowers Jr et al., 1987, Deutch et al., 1987, Verma and Moghaddam, 1996).

Neuroimaging techniques have also shown reduced hippocampal NMDA receptor activity in schizophrenia patients not receiving antipsychotic treatment compared with healthy controls; whereas this difference was not significant in patients receiving treatment (Pilowsky et al., 2006, Egerton and Stone, 2012). Glutamate is the most abundant neurotransmitter and is inextricably tied to γ -aminobutyric acid (GABA), the primary inhibitory neurotransmitter, which acts to modulate glutamatergic signalling via various intercellular feedback mechanisms, and both are associated with neuropathology in schizophrenia (Rowland et al., 2012, Cherlyn et al., 2010). Moreover, NMDA receptors are fundamentally involved in long term potentiation (LTP) and long term depression (LTD), forms of neural plasticity serving key functions in neural circuit development; and impaired LTP/LTD have been linked with multiple neuropsychiatric disorders including schizophrenia (Citri and Malenka, 2008). In simple terms, LTP may be thought of as an enhancement of synaptic connectivity, whereas LTD is the opposite, a weakening of synaptic strength; or in a more abstract sense, each of these processes may be considered as a form of synaptic memory which ‘remembers’

previous neural inputs. Additionally, genetic research has predominantly found that genes implicated in NMDA receptor signalling are mutated in patients diagnosed on the schizophrenia spectrum. Figure 1.1 displays cellular machinery interacting in the post-synaptic neuron of a glutamatergic synapse, including *mitogen activated protein kinase kinase 7* (MAP2K7), as part of the JNK pathway which has become linked genetically with schizophrenia (reviewed by Morris and Pratt, 2014; discussed further in Section 1.4.1). Glutamate binding to NMDA receptors activates downstream signalling cascades which regulate synaptic strength, as noted above. Proteomic analysis has shown that these intracellular signalling mechanisms involve MAPK pathway components (Husi et al., 2000), suggesting that this MAP2K7-JNK pathway may be involved in NMDA receptor-mediated signalling regulation.

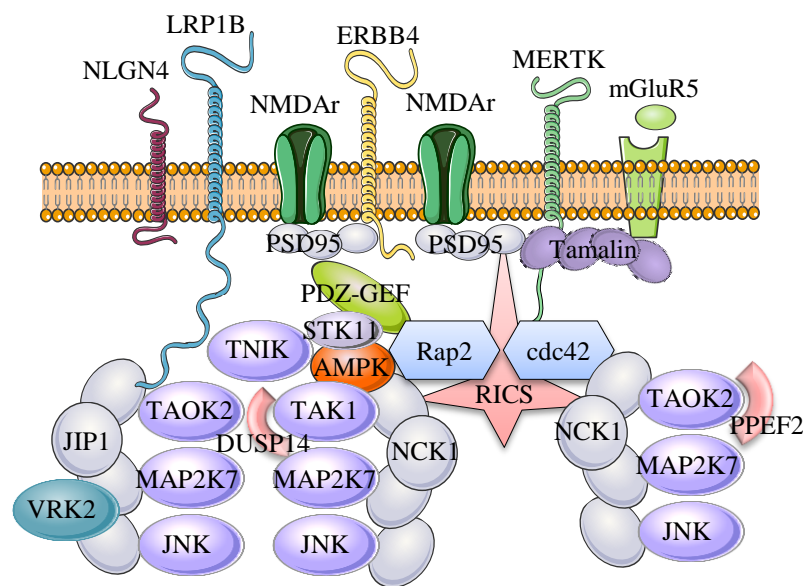


Figure 1.1 - The post-synaptic intracellular JNK signalling pathway with genes/proteins implicated in schizophrenia Each of these elements has been linked with schizophrenia through genetic studies. NRG4 (neuroligin 4; trans-synaptic binding protein for neuroligin 1); LRP1B (low-density lipoprotein receptor-related protein 1B); NMDAr (N-methyl-D-aspartate receptor); ERBB4 (receptor tyrosine kinase; binds with neuregulin); MERTK (type 1 transmembrane tyrosine kinase, can activate ERK and JNK pathways); mGluR5 (metabotropic glutamate receptor 5); PSD95 (scaffolding postsynaptic density protein); PDZ-GEF (PDZ-domain guanine exchange factor); STK11 (serine/threonine kinase 11); AMPK (AMP-activated protein kinase); Rap2 (member of the Ras family of GTPases); cdc42 (cell division control protein 42); TAOK2 (thousand-and-one amino acids protein kinase 2); TAK1 (transforming-growth-factor-beta activated kinase 1); RICS (brain-specific rho GTPase-activating protein); TAOK (thousand-and-one amino acids protein kinase); JIP1 (JNK-interacting protein 1); DUSP14 (dual-specificity phosphatase 14); NCK1 (non-catalytic region of tyrosine kinase adaptor protein 1); PPEF2 (protein phosphatase with EF-hand motif); VRK2 (vaccinia Related Kinase 2); MAP2K7 (mitogen activated protein kinase kinase 7); JNK (c-Jun N-terminal kinase). A full description of each of their functions exceeds the scope of this thesis. Adapted from the review by Morris and Pratt (2014).

Another hypothesis of schizophrenia concerning adenosine has arisen which aims to integrate the two previous models (Lara et al., 2006). This neuromodulator acts upstream from both dopamine and glutamate pathways, thus offering an attractive potential target for pharmacological intervention to treat both positive and negative symptoms. Furthermore, adenosine is considered to play an important role in neurodevelopment, which may explain this component of the pathogenesis of schizophrenia spectrum disorders. However promising, this model is in its relative infancy and targeted therapeutics are still under development (Boison et al., 2012).

Hayashi-Takagi and Sawa (2010) succinctly describe research linking genetic risk and neurodevelopmental factors which contribute toward schizophrenia. This review highlights genetic evidence suggestive of prenatal (centrosome and neuregulin pathways) and postnatal (D-serine and post-synaptic pathways; see Figure 1.1 for an example of the latter) defects that can alter the normal trajectory of glutamate synapse expression, morphology and function; emphasising synaptic reorganisation in adolescence may be impinged by these genetic factors. With regards to the post-synapse pathway, it is suggested that via interactions with the postsynaptic density scaffolding protein, *PSD95*, NMDA receptor behaviour may be modulated by downstream signalling proteins. It would not therefore be unreasonable to think that some of the molecules depicted in Figure 1.1 may be able to regulate NMDA receptor activity. As noted, the molecule under investigation in this thesis is MAP2K7, and the experiments described herein aim to establish whether NMDA receptor mediated signalling may be modified by this enzyme.

This is far from an exhaustive discussion of the proposed pathophysiological mechanisms underlying schizophrenia spectrum disorders. In truth, the precise mechanisms of pathogenesis are yet to be fully elucidated, thus this remains an active area of research. This thesis does not contribute significantly to these efforts; the information provided here shall simply allow the reader to glean the biological complexity of this condition. The attention of this study is focussed on examining glutamatergic contributions via genetic (*Map2k7*^{+/-}; Section 1.3.1.1) and pharmacological (ketamine induced NMDA receptor antagonism; Section 1.4.2) mouse models relevant to schizophrenia.

1.1.5 *Electrophysiological deficits*

The electroencephalogram (EEG) is predominantly generated by synchronous post-synaptic potentials with similar orientation, measured from the scalp through volume-conduction. This recording technique reflects neuronal processes en masse with high temporal precision but poor spatial localisation. The EEG signal may be deconstructed into multiple frequency bands which are considered to reflect distinct psychophysiological processes (reviewed by Ward, 2003). These are typically referred to as *delta* (0-4 Hz; seen in deep sleep), *theta* (5-8 Hz; involved in memory formation), *alpha* (9-12 Hz; associated with increased cognitive processing), *beta* (13-30 Hz; linked with motor coordination) and *gamma* (31-100 Hz; implicated in multiple higher cognitive processes including attention and working memory). Normal functioning of these neural oscillations is generally required for healthy brain function. Furthermore, due to the temporal precision of EEG it is useful for analysing neural responses to discrete experimental events, such as sensory stimulation or subject responses. This is generally achieved by applying the event-related potential (ERP) technique, where EEG segments recorded during repeated experimental events are averaged together, effectively removing non-event-related activity and leaving the prototypical ERP in response to a particular experimental event (Luck, 2014). Significant frequency band and ERP deficits have been found in schizophrenia patients compared with healthy controls, as discussed in the two following paragraphs.

Schizophrenia spectrum patients and their relatives have widely been found to display altered gamma band power, generally summarised as increased during passive/resting states and decreased during active/cognitive states, relative to healthy controls (Andreou et al., 2015, Gallinat et al., 2004, Sun et al., 2011, Symond et al., 2005). These deficits may reflect inefficient or dysfunctional regulation of neural activity; seen in both first-episode (Andreou et al., 2015, Gallinat et al., 2004, Minzenberg et al., 2010) and chronic patients (Spencer et al., 2008, Tsuchimoto et al., 2011), with evidence suggesting they are not perturbed by antipsychotic treatment (Minzenberg et al., 2010). This is comparable with findings from cognitive and negative symptom domains which are not well treated by current dopaminergic or glutamatergic antipsychotics (Buchanan et al., 2007); leading some to consider gamma band EEG power as an attractive candidate biomarker for these symptoms (Gandal et al., 2012). Moreover, because gamma oscillations can be observed from non-human species, including rodents, animal models could help decipher the underlying pathophysiological mechanisms responsible for these abnormalities.

There are several proposed mechanisms of gamma wave generation that could go awry in schizophrenia, reviewed by Sun et al. (2011). Among these are fast-spiking parvalbumin (PV; calcium-binding protein) containing GABAergic interneurons that act in phase to synchronise other neurons. These PV-containing cells express dendritic NMDA receptors, which are widely implicated in schizophrenia. In short, dysfunctional NMDA receptors expressed on PV cells impairs their normal behaviour, disinhibiting cortical pyramidal neurons, causing a state of over-excitation, increased glutamate availability, and altering gamma-band regulation. This mechanism has been convincingly demonstrated in mice with a specific deficit of NMDA receptors in fast-spiking PV-containing neurons (Carlen et al., 2012). A simple example of this is illustrated in Figure 1.2. In both human and animal studies, administration of ketamine in sub-anaesthetic doses has been found to enhance gamma synchrony and diminish low frequency (delta/theta) band power (Hong et al., 2009, Lazarewicz et al., 2010, Pinault, 2008). It has been suggested that this excess of oscillatory gamma frequency activity obstructs conscious integration, as experienced by users of these dissociative substances, as well as patients with psychosis. This is a highly complex phenomena, characterised by increased localised cortical gamma power and decreased overall global synchronisation. It remains to be seen whether the MAP2K7-JNK signalling pathway (Figure 1.1; see Section 1.3.1.1) is involved in gamma band oscillations, although its role downstream from NMDA receptors in the post-synaptic neuron suggests it might be; data presented in this thesis provide the first examination of this question.

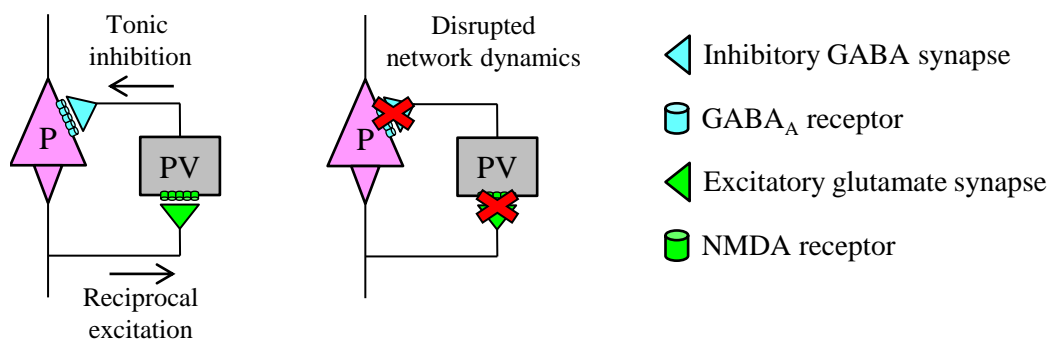


Figure 1.2 - The proposed mechanism of gamma synchrony dysregulation in schizophrenia Dysfunctional dendritic NMDA receptors on parvalbumin-containing (PV) fast-spiking GABAergic interneurons diminish their firing rates, decreasing release of inhibitory neurotransmitter, producing a state of cortical disinhibition. This would in turn over-excite, or disinhibit, large pyramidal (P) neurons, and increase extracellular glutamate availability, potentially contributing to the dysregulation of gamma synchrony in schizophrenia. Adapted from Gonzalez-Burgos and Lewis (2012)

Visual and auditory steady-state evoked responses (VSSR and ASSR) are also impaired in patients with schizophrenia (reviewed by Brenner et al., 2009). These measure the entrainment of sensory neurophysiological processes to a stimulating frequency. For example, a visual stimulus flashing at 12 Hz will induce neural activity that generates a 12 Hz repetitive pattern in EEG recordings from the visual cortex in the occipital lobe. Similarly, an auditory stimulus clicking at 12 Hz will entrain neural activity in the auditory cortex (Section 1.2.2.3), generating a repetitive pattern with the same frequency. In schizophrenia patients, impaired ASSR to 40 Hz stimuli is a particularly robust finding, as noted in a recent meta-analysis (Thuné et al., 2016). This may be tentatively linked to gamma-band oscillations and the same dysregulated mechanisms found in schizophrenia by the fact that both phenomena occur within the same frequency range; however a conclusive link of the underlying mechanisms is yet to be proven.

Several ERP/auditory evoked potential (AEP) components have been studied in schizophrenia patients. An AEP is essentially an ERP elicited by an auditory stimulus, thus these terms are used interchangeably throughout this thesis. The following abnormalities in AEP components have been observed from patients with schizophrenia and their first-degree relatives. Arranged by latency, these features of the human AEP include attenuated P50 sensory gating (Patterson et al., 2008), reduced N100 (sometimes called N1) amplitude (Rosburg et al., 2008), deficits in amplitude and latency of mismatch negativity (MMN; reviewed by Näätänen et al., 2012) and P300 (Turetsky et al., 2015). Earlier components (P50 and N100) are thought to involve mainly sensory processes, while later features (MMN and P300) are believed to reflect aspects of cognition (Pratt et al., 2011). P50 and N100 fall into the categories of middle-latency and long-latency responses (MLR and LLR), respectively. The P50 component is believed to originate from afferent subcortical structures and primary auditory cortices (Korzyukov et al., 2007, Polyakov and Pratt, 1994, Polyakov and Pratt, 1995); while N100 generators are predominantly found in areas of the primary auditory cortex known as Heschl's gyrus and planum temporale, both described in Section 1.2.2.3 below (Godey et al., 2001). In many publications the y-axis of AEP plots (amplitude, or potential, in microvolts) is inverted; however throughout this thesis the usual Cartesian convention with positive values going upwards is applied.

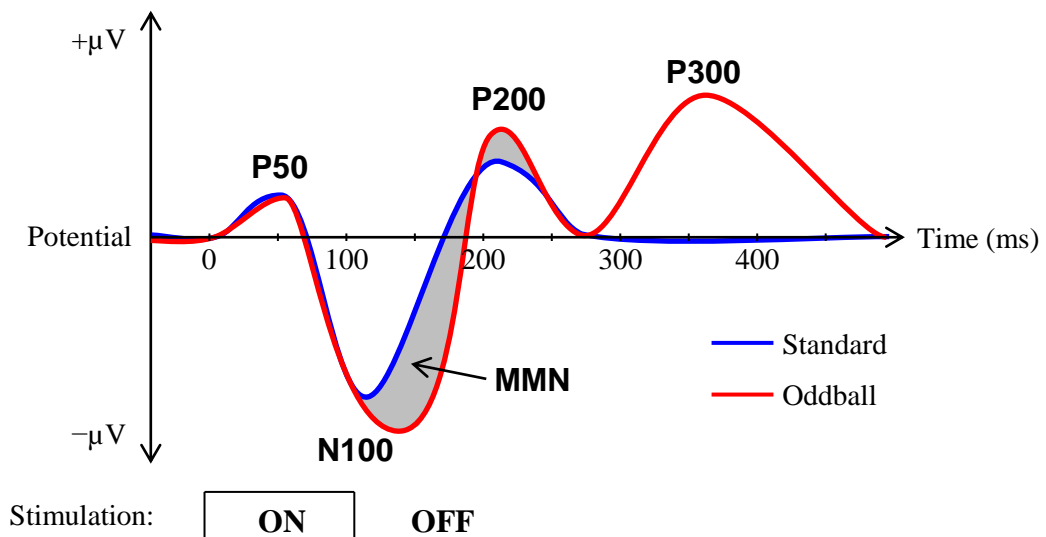


Figure 1.3 - Example of human auditory evoked potential components This is an example of AEP waveforms evoked by an oddball paradigm, where subjects are required to count the number of oddball stimuli. P50, N100 and P200 are obligatory sensory components of the AEP. Mismatch negativity (MMN) is the difference between standard and oddball stimuli, shaded in grey. P300 is only generated if the subject consciously attends to stimuli, for instance by counting or button-pressing each time they detect an oddball stimulus. The presence of these components may vary quite considerably at different electrode sites on the skull; this example shows a typical vertex response measured from a fronto-central scalp electrode location.

Both MMN and P300 are suggested to involve cognitive processes, with the potential to be used as diagnostic tools for related disorders, such as schizophrenia, cognitive decline, mood disorders and dementia, among others (Duncan et al., 2009). MMN is elicited without the subject paying attention whereas P300 requires the subject to attend to specific stimuli for its generation; this is an attractive property for the clinical application of MMN with patients who may struggle to perform certain tasks, and furthermore, for use as a preclinical tool in animal research to uncover the underlying neurophysiological mechanisms. MMN is the most extensively studied of these ERP components, and there is a large body of literature (over 200 publications; Michie et al., 2016) which reports to find abnormalities in schizophrenia spectrum patients. Henceforth, replication of this response in mouse models would assist in determining any correspondence between genetic, behavioural and neurophysiological factors with the observed electrophysiological deficit. The question of whether genetic and pharmacological mouse models relevant to schizophrenia can accurately replicate electrophysiological deficits associated with this disease is explored in this thesis, and accordingly MMN in humans is discussed at length in Section 1.2.

1.1.6 *Preclinical research*

Animal models have been widely utilised in preclinical schizophrenia research. Rodents are the most commonly used non-human species in this arena. They have been instrumental in furthering our understanding of how brain systems coordinate behaviour. It is infeasible to produce an all-encompassing animal model of schizophrenia, due to the vast heterogeneity and diversity of possible symptoms in this syndrome. Instead certain manipulations are performed to examine specific relevant behaviours and neurophysiology individually. Broadly speaking, these models may be classified as either neurodevelopmental, pharmacological or genetic, depending on the method of inducing schizophrenia-like symptoms.

Neurodevelopmental techniques involve enacting a perinatal insult, e.g. an infection or a lesion, to the developing organism's brain then investigating the effects in adulthood. These methods have reportedly been successful in producing a broad selection of behavioural and cellular abnormalities considered somewhat comparable with those seen in schizophrenia patients (Lipska, 2004). Pharmacological models typically target dopaminergic (e.g. apomorphine; Hoffman and Donovan, 1994) or glutamatergic/NMDA receptor (e.g. PCP, ketamine; reviewed by Bickel and Javitt, 2009) neurotransmitter systems; although these may also be aimed at modulating 5-hydroxytryptamine (5-HT, serotonin) and GABA systems (reviewed by Marcotte et al., 2001). Genetic models are generated by causing mutations (typically in mice) in chromosomal regions associated with schizophrenia patient groups; both common SNP and rare CNV mutations (Arguello and Gogos, 2011).

Various schizophrenia-relevant behavioural and physiological endpoints may be quantified from these models. Examples of clinically translatable behavioural tests include pre-pulse inhibition (PPI) of the startle reflex/sensorimotor gating (Geyer et al., 2001), 5 choice serial reaction time task (5-CSRTT) of cognitive performance (Thomson et al., 2011), and locomotor tests associated with psychotic symptoms (van den Buuse, 2010). In addition, functional neuroimaging techniques, along with electrophysiological approaches, may offer potentially translatable *in vivo* biomarker utility (Luck et al., 2011, Pratt et al., 2012).

1.2 Mismatch negativity (MMN) in humans

The term *mismatch negativity* (MMN) was first coined by Näätänen et al. (1978) to define the observation that infrequent auditory stimuli (*oddballs*) produce a differential scalp-recorded EEG response than frequent repeated stimuli (*standards*). This was actually a reinterpretation of findings from others investigating auditory attention using ERPs (Picton et al., 1971, Hillyard et al., 1973), which itself was an extension of the *orientation reaction* literature. Orienting response studies generally monitor all physiological systems for reactions to changes in environmental stimuli, the most accessible of which were traditionally the galvanic skin response, pupillary dilation and eye movements (reviewed by Barham and Boersma, 1975). This concept of the body's ability to detect and automatically adjust to environmentally salient stimuli logically led to the examination of the central nervous system, which presumably initiates these reactions. The precise temporal sequence of physiological events underlying these systemic changes in bodily function must occur fairly rapidly, thus EEG recordings are a powerful neuroimaging technique for probing the cortical origins of this response. Furthermore, this is likely to be a cross-species phenomenon, presenting an opportunity to perform *in vivo* neurophysiological research in order to gain a greater understanding of this response.

MMN is a component of the ERP evoked in response to an auditory oddball paradigm; illustrated in Figure 1.3 (reviewed by Näätänen et al., 2007, Näätänen et al., 2012). There is also evidence for visual (reviewed by Pazo-Alvarez et al., 2003), somatosensory (Akatsuka et al., 2005) and olfactory (reviewed by Pause and Krauel, 2000) equivalents; although the MMN is foremost considered in terms of the auditory sense and this thesis does not directly concern the other sensory modalities. In the oddball paradigm a series of regular, high-probability, physically identical 'standard' stimuli are presented with pseudo-randomly interspersed irregular, low-probability 'deviant' (or *oddball*) stimuli which differ physically from the standard; these are typically presented with a constant inter-stimulus interval (ISI). EEG signals are recorded throughout the oddball paradigm and AEPs computed post-hoc. MMN is produced by subtracting the AEP in response to standard stimuli from the AEP in response to deviant/oddball stimuli. In humans, this difference waveform characteristically displays a negative peak amplitude component at $\approx 150\text{-}250$ ms from change onset, indicated by the name "Mismatch Negativity", with peak amplitude measured from the frontocentral scalp location (Fz site in the standard 10-20 electrode positioning system). This is typically recorded with nose or mastoid electrode referencing; mastoid referencing results in greater amplitude at Fz, whereas nose referencing produces an inverted polarity MMN (or 'mismatch positivity'; MMP) measured from mastoid electrodes (Pakarinen et al., 2007).

In order for the MMN to be elicited, the standard stimulus must be repeated multiple times before the presentation of an oddball stimulus. Using the same terminology as Näätänen et al. (1978), this is required for the formation of a ‘template’ of the standard stimulus’ features in memory. When the oddball features deviate from this template the MMN component is produced. Therefore in oddball paradigms there are typically a large number of repetitions of the standard before any oddballs, and subsequently there are a predefined minimum number of standards between each oddball; although the precise sequence of stimuli in oddball paradigms varies between different studies. Additionally, it is suggested that this template is held in memory for a limited period of time, because the MMN response disappears when ISI is increased beyond 10 s (Bottcher-Gandor and Ullsperger, 1992). Furthermore, the probability of deviant/oddball stimuli being presented inversely affects the MMN magnitude, with lower probability oddballs resulting in greater MMN amplitude (Sabri and Campbell, 2001); and the magnitude of difference between standards and oddballs also significantly alters the MMN response (Näätänen, 1992, Näätänen and Kreegipuu, 2012).

The MMN is referred to as a pre-attentive process, meaning that it is generated without the subject paying attention to the incoming sequence of stimuli. Subjects are generally asked to watch a silent film to distract their attention from the auditory sequence; specifically to avoid anticipation/expectancy effects that can influence the resulting ERP (Brunia et al., 2012). Furthermore, MMN is said to result from any discriminable change in auditory stimulation. It is observed in response to oddball changes in frequency or pitch, duration, sound energy level or intensity, and perceived sound-source location (Pakarinen et al., 2007); which may all be recorded in the so-called ‘optimal paradigm’ introduced by Näätänen et al. (2004). The parameters of this optimal paradigm are displayed in Table 1.1. In addition, MMN has also been reported to occur in response to more complex multi-feature physical changes in stimuli, for example, in musical compositions when an out-of-tune sound is presented (Tervaniemi and Brattico, 2004), and vocalisation sounds (Szymanski et al., 1999).

Parameter	Comment
<i>I. Stimulus factors</i>	
A. Optimal Paradigm	One frequent standard, five rare deviant tones
Standard	Harmonic stimulus comprising 3 sinusoidal partials of 500, 1000, and 1500 Hz, with intensity of second and third partials 3 and 6 dB lower than the first partial.
Duration	75 ms, 5 ms rise/fall
Intensity	80 dB SPL
Interstimulus interval	1000 ms (fixed)
Location	Midline (binaural)
Deviants	
Duration	25 ms, 5 ms rise/fall
Frequency	Half of frequency deviants are 10% higher partials, half are 10% lower partials.
Intensity	Half of intensity deviants are 10 dB higher, half are 10 dB lower.
Location	Half of location deviants are perceived as having a spatial location 90° to the right and half 90° to the left of the midline by introducing an interaural time difference of 800 μ s.
Gap	Silent gap of 7 ms (including 1 ms rise/fall) in the middle of a 75-ms stimulus.
Probabilities	.50 (standard), .10 (each of the deviants), one standard between each deviant
<i>II. Participant and task</i>	
Position	Seated
Eyes	Open
Active or passive task	Participants are asked to watch a familiar muted video.
<i>III. Electrophysiological recording</i>	
Electrode sites	32 scalp electrodes (Cz, C3, C4, T7, T8, FC2, FC3, FC4, FT7, FT8, CPz, CP3, CP4, TP7, TP8, Fz, F3, F4, F7, F8, Pz, P3, P4, P7, P8, O2, O1, Oz, FP1, FP2) and left and right mastoid electrodes (M1 and M2).
Reference	Average mastoid
Ground	AFz
Bandpass of amplifiers	DC, 0-500 Hz
Digitization rate	2000 Hz
Epoch length	1000 ms; with 100-ms pre-stimulus baseline only for the filtered data
Artifact reduction	Vertical and Horizontal EOG rejection or correction; ± 50 μ V for all EEG channels
Minimum # trials	150 of each deviant
Digital filtering	1–50 Hz
<i>IV. Quantification</i>	
Average ERPs	Average ERP waveforms and difference waveforms are presented for each condition.
Difference waveform	Deviant average ERP minus Standard average ERP
Latency	120–250 ms
Amplitude	Peak amplitude in a latency window in difference waveforms.
Scalp distribution	Maximal at Fz;

Table 1.1 - 'Optimal' oddball paradigm for eliciting mismatch negativity in humans

This table outlines the parameters used to elicit mismatch negativity from duration, frequency, intensity, source location and mid-stimulus silent gap in a single oddball paradigm. Reproduced with permission from Mohanty (2011); originally adapted from Näätänen et al. (2004).

The concept of perceiving an auditory object has many facets; physical dimensions (e.g. temporal structure, frequency structure, sound energy and source location), associations (e.g. crying baby, familiar voices, words, animal calls and natural sounds) and contexts (e.g. acoustic environment, recent history of auditory stimulation, and neurological\behavioural state). Each of these factors may alter the auditory response hence MMN experiments must be well controlled. As noted in Table 1.1, subjects are typically asked to watch a silent film while calmly remaining still to decrease movement artifacts which can interfere with EEG data quality. This broadly controls the behavioural state of the subject. Audio stimulation may be delivered to both ears with noise-cancelling headphones in a quiet room, decreasing background acoustic noise. The stimuli employed are generally inconspicuous, either pure-tones or a simple combination of harmonics (as in Table 1.1), which avoids associations; although more complex stimuli are occasionally used. Physical properties may be controlled for by using a balanced oddball paradigm, which incorporates physical changes in both directions; e.g. increasing and decreasing duration, ascending and descending frequency, louder and quieter intensity, left-shift and right-shift source location, etc. Additionally, control protocols/paradigms aim to verify interpretations of MMN by disproving alternative explanations for the observed electrophysiological activity.

Since its founding, MMN was computed, and often still is, by subtracting the standard stimulus AEP from the oddball stimulus AEP produced from EEG data recorded during an oddball paradigm. To control for differences in obligatory AEP components caused by the physical characteristics of stimuli themselves, a ‘flip-flop’ control may be used. In this protocol two oddball paradigms are presented that use the same two physically distinct stimuli, only their roles are reversed. For example, the stimulus used as the standard in one paradigm will be the oddball in the other paradigm, and vice versa. Thereafter, the MMN may be produced by subtracting the standard AEP from the oddball AEP elicited by the same physical stimulus (Näätänen and Kreegipuu, 2012). There is also the ‘roving stimulus’ paradigm in which many (e.g. 30) standards are repeated consecutively before a single oddball is presented; this oddball then becomes the standard and is repeated multiple times before another oddball is presented. In this manner, physical levels of standard and oddball stimuli can be varied but there remains a change to induce the MMN. Additionally this paradigm may utilise a combination of physical changes. For example, if the first oddball varies in duration and is followed immediately by a different frequency stimulus that provides the next standard, followed by another duration oddball. This sequence should elicit an MMN in response to changes in duration and frequency (Baldeweg et al., 2002, Baldeweg and Hirsch, 2015).

MMN has been interpreted as the electrophysiological manifestation of a change-detection mechanism, which prepares conscious attention to shift towards attending potentially salient environmental stimuli; reflecting the violation of an auditory sensory-memory (or echoic-memory) trace (Näätänen et al., 1978, Näätänen et al., 1989). In other words, when an auditory stimulus is repeated often it ceases to divert attention, whereas a rare auditory stimulus presented infrequently attracts attention involuntarily. The MMN component is suggested to reflect this process of detecting irregularities in auditory stimuli and automatically redirecting attention, believed to be a distant evolutionary trait.

Some authors argue against this sensory-memory disruption concept, instead suggesting that fresh afferent neurons activated by the deviant/oddball stimulus modulate N1/N100 latency and amplitude (see Figure 1.3) resulting in MMN produced by ERP subtraction (reviewed by May and Tiitinen, 2010). This is supported by a growing body of research which identifies stimulus specific adaptation (SSA) as a potential single-neuron correlate of MMN (Klein et al., 2014, Nelken, 2014, Nelken and Ulanovsky, 2007). SSA describes the property of neurons to reduce their firing rates in response to frequently repeated stimuli, sometimes called habituation or repetition suppression. This interpretation follows that the MMN arises from differences in the level of adaptation of discrete neural units which respond preferentially towards standard and oddball stimuli. Neurons responsive to the standard which is repeated often undergo more adaptation than those tuned towards the oddball, thus the response to oddball stimuli will be greater; revealed in a difference waveform as the MMN. The SSA literature is discussed in more detail in Section 1.2.2.6, and both theoretical models developed to account for MMN generation are discussed further in Section 1.2.3.

In contrast, the memory-based model is not currently supported by neurophysiological evidence, and relies more on interpretation of the underlying mechanisms from a psychological perspective. Nevertheless, proponents of the memory-based theory of MMN strongly refute this adaptation hypothesis, claiming that MMN is “based on separate memory-related deviance-detection neurons” (Näätänen et al., 2005); although evidence for such neurons is lacking. According to this theory, subcortical structures, including the thalamus and hippocampus, are suggested to play a key role in MMN generation, although evidence of this from animal models is inconclusive (Näätänen et al., 2007). Additionally, studies using more complex phonetic stimuli have found it difficult to interpret their findings within this framework, stating that “MMN generation is much more complex than a simple preattentive detection of physical deviance” (Szymanski et al., 1999). Therefore the precise mechanisms underlying these electrophysiological observations are still debated.

Both sides of this debate may be making a similar error by prematurely generalising potentially separable phenomena. There is evidence that MMN responses caused by different physical features of auditory deviance are dissociable (discussed below); and although SSA appears to be robustly observed in response to changes in stimulus frequency (see Section 1.2.2.6), few studies address changes in other physical properties of sound. This thesis treats different physical properties of sound apart to establish their influence over AEP waveforms. This approach will help to identify electrophysiological responses which are common and distinct between basic physical features of sound; in doing so providing insight into the underlying neurophysiology of MMN(s), which may translate into clinically useful knowledge.

Interestingly, MMN and N100 have reportedly been observed from patients in comatose states and shown utility for predicting their return to consciousness (Fischer et al., 1999, Fischer et al., 2000, Kane et al., 1996). Heinke et al. (2004) found that although the MMN was present during different stages of propofol sedation, it then disappeared when subjects were fully unconscious. State of consciousness can dramatically alter the perception of sound in very obvious ways, e.g. during deep sleep sound is not perceived. It can equally alter the experience of sound in more subtle ways, e.g. under the effects of amphetamine music is reported to relay an emotional tone and recreational drug users often report being able to “feel the music”. This effect of brain state on the perception of sound is well recognised, however the extent to which auditory processing is altered during these states is less well understood. This aspect of MMN research is intriguing, and may provide insights as to where and when auditory information and perception interact within the brain. Furthermore, the fact that these responses are observed from humans in anaesthetised and comatose states lends support for using anaesthetised animal models to study these phenomena.

Using magnetoencephalography (MEG), the magnetic counterpart of the EEG recording technique, the magnetic mismatch negativity equivalent (MMNm) can be elicited (Alho, 1995, Hari et al., 1984). Other neuroimaging modalities have also been applied to investigate processes underlying the MMN; e.g. functional magnetic resonance imaging (fMRI; Celsis et al., 1999, Opitz et al., 2002, Schall et al., 2003, Molholm et al., 2005), positron emission tomography (PET; Tervaniemi et al., 2000, Müller et al., 2002), intracranial recordings (Halgren et al., 1995, Kropotov et al., 2000) and optical imaging techniques (Rinne et al., 1999, Tse et al., 2006). Each of these neuroimaging modalities have reportedly been able to detect differences between standard and oddball evoked activity, but with variable temporal resolutions, and different methods of determining the source of this neural activity have been applied.

Source localisation studies have thus far reported two separate generators of MMN; a bilateral temporal generator located in the primary auditory cortex, said to be responsible for discriminating auditory objects (Hari et al., 1984, Scherg et al., 1989), and a frontal generator, associated with involuntary redirection of attention (Deouell et al., 1998, Giard et al., 1990, Jemel et al., 2002). The temporal generators are generally well established throughout the literature, although the existence of frontal generators is not wholly accepted due to a mix of positive and negative findings from various neuroimaging modalities; furthermore, there is a lack of direct evidence to substantiate the distinct functional interpretations of these proposed generators (reviewed by Deouell, 2007).

There are data which indicates that the temporal source generators responding to changes in stimuli duration, frequency and intensity are located in slightly different areas of the auditory cortex; suggested to stress the importance of feature analysis in MMN generation (Frodal-Bauch et al., 1997, Molholm et al., 2005, Rosburg, 2003). Equally, this may indicate that different physical features of auditory stimuli are processed through distinct neural mechanisms, hence by different neural generators. This is critical when considering that different physical features of oddball stimuli elicit MMN waveforms which are suggested to provide specific information about neuropsychiatric disorders, including schizophrenia, discussed in Section 1.2.1 below.

1.2.1 MMN in schizophrenia and other neuropsychiatric disorders

Since the first published investigation of MMN in schizophrenia patients by Shelley et al. (1991) showing significantly lower MMN amplitude in patients compared with healthy controls, there has been deluge of studies in this area. Reduced amplitude and increased latency are observed in patients with schizophrenia and their first-degree relatives (Jessen et al., 2001); although there are significant differences between first-episode and chronic patients, with the latter exhibiting greater MMN deficits in a frequency oddball paradigm (Salisbury et al., 2002). The extent of this amplitude reduction reportedly correlates with functional impairments (Javitt et al., 1995, Baldeweg et al., 2004, Light and Braff, 2005). MMN deficits observed from schizophrenia patients are suggested to reflect NMDA receptor pathology because of the finding that healthy volunteers administered ketamine, a non-selective NMDA receptor antagonist, display reduced MMN amplitude relative to controls (Umbricht et al., 2002). Subsequently the authors suggest that measurement of the MMN may provide a non-invasive biomarker for NMDA receptor function.

There have been several studies investigating various pharmacological manipulations and their effect on MMN in humans (reviewed in Todd et al., 2013). For the most part, NMDA

receptor antagonists diminish MMN amplitude; in contrast, several studies showed nicotinic agonists enhance MMN amplitude. This may correlate with evidence that schizophrenia patients are more likely to be heavy tobacco smokers, according to the nicotine self-medication hypothesis (Kumari and Postma, 2005). Dopaminergic, serotonergic and other pharmacological challenges have had inconsistent or negligible effect on MMN.

Umbricht and Krljes (2005) conducted a meta-analysis of reports linking schizophrenia with MMN deficits, confirming that this is a robust finding in chronic schizophrenia patients; furthermore, they found that the duration MMN was more impaired than frequency MMN, although frequency MMN deficits correlated with duration of illness, therefore may indicate disease progression. This highlights that specific physical features of deviant stimuli may elicit distinct neural responses reflected by the MMN. This may involve different neural circuits and neurochemistry. Following up, Todd et al. (2008) examined the response to duration, frequency and intensity oddball paradigms in schizophrenia patients and healthy controls; concluding that these different properties may offer 'complimentary' information about onset (duration, intensity) and progression (frequency) of the disorder. Published studies of duration, frequency and intensity MMN are reviewed in Section 1.2.1.1, Section 1.2.1.2 and Section 1.2.1.3, respectively.

Considering this evidence, it may be a shortcoming to persist in applying the general term of MMN when referring to these potentially separable phenomena; to distinguish between them, duration, frequency and intensity MMN will be abbreviated to dMMN, fMMN and iMMN, respectively, throughout this thesis. Furthermore, in relation to research in animal models (discussed in Section 1.3) the term mismatch response (MMR) is applied interchangeably for MMN, for reasons discussed below.

A large body of research now indicates that deficits in MMN may not be specific to schizophrenia alone, and are seen in a host of different neuropsychiatric (e.g. bipolar disorder, schizophrenia), neurological (e.g. Alzheimer's, Parkinson's) and neurodevelopmental (e.g. autism, dyslexia) disorders, substance intoxications (e.g. alcohol, opioids), as well as in normal aging (see Table 1 in Näätänen et al., 2012). This is suggested to reflect abnormalities in NMDA receptor function which broadly occur in these conditions. Although some have found deficits in MMN that are specific to schizophrenia patients (Baldeweg and Hirsch, 2015). That said, the development of MMN as a biomarker for NMDA receptor function may be highly beneficial for stratifying patients and selecting appropriate therapies based on known underlying neuropathology. In order to achieve this the MMN and its various manifestations must be better understood (Michie et al., 2016).

1.2.1.1 Duration mismatch negativity (dMMN)

A change in stimulus duration in an oddball paradigm produces dMMN which varies depending on the direction (shortened vs. lengthened) and size of the change (Colin et al., 2009, Shelley et al., 1991, Takegata et al., 2008). Two of these studies found that shorter duration oddballs generate a more pronounced dMMN (Colin et al., 2009, Takegata et al., 2008), whereas one found longer oddballs elicit a larger dMMN (Shelley et al., 1991). Changes in stimuli duration can alter the inter-stimulus interval (ISI) if stimulus onset-to-onset time is held constant, which can affect the AEP and induce an MMN response (Martin et al., 2009, Näätänen et al., 1993). A decrease in stimulus duration will increase ISI, thus enlarging AEP features in response to the stimulus following the longer ISI. Depending on how stimuli sequences are structured this could result in an enlarged oddball AEP, if for example the longer ISI is incorporated before the oddball stimulus. It is unclear whether this is the case for the above studies, as this is typically not reported. The finding that dMMN amplitude is reduced during prodromal phases of psychotic disorders highlight it for further research aimed at identifying a biomarker capable of predicting disease onset and prescribing early intervention (Atkinson et al., 2012, Todd et al., 2008, Michie et al., 2000). Moreover, a longitudinal study of test-retest reliability found dMMN to be more replicable than fMMN or iMMN (Tervaniemi et al., 1999). Although the majority of MMN studies found group differences between schizophrenia patients and healthy controls, a considerable amount of variability exists between subjects. The physiological processes which give rise to this response must be considered if it is to prove effective as a biomarker. Modelling the dMMN in animals may provide a valuable tool for probing the underlying neurophysiological mechanisms and how these may respond to pharmacological treatment.

1.2.1.2 Frequency mismatch negativity (fMMN)

Changes in sound frequency or pitch in an oddball paradigm is used to generate fMMN. As mentioned, this may offer a potential objective measure for tracking the progression of schizophrenia, because its amplitude is reported to decrease with duration of illness (Todd et al., 2008, Umbricht and Krljes, 2005). This may also be used for gauging treatment efficacy on underlying neuropathology. However, in order to be applied effectively, the responsible mechanisms and neurochemistry would be fully elucidated. Similar to the dMMN, the degree of frequency separation between standards and oddballs influences the fMMN (May et al., 1999). The auditory system is discussed in Section 1.2.2 below, wherein frequency sensitivity is both anatomically and physiologically fundamental. This presents a framework for our current understanding of sound frequency processing in the brain. Stimulus-specific

adaptation (SSA; described in Section 1.2.2.6) of frequency-specific neurons may underlie the fMMR, addressed in Section 1.2.3.

1.2.1.3 Intensity mismatch negativity (iMMN)

Similarly to the dMMN, deficits in iMMN have been found early in the time course of schizophrenia, in contrast with the fMMN (Todd et al., 2008). Earlier studies also suggested that fMMN and iMMN responses rely on functionally different neural mechanisms; the former being insensitive to ISI and intensity variations, whereas the latter was greater at longer ISI intervals and higher intensity (Schröger, 1996). However both ISI and intensity are known to alter obligatory AEP components (Beagley and Knight, 1967, Hari et al., 1982). Interestingly, a study using different intensity tone-pairs as stimuli in an oddball paradigm found that the iMMN to a quieter tone-pair was absent whereas it was present when using a louder tone-pair (Schröger et al., 1996). It has been suggested that intensity-tuned neurons (discussed below) may be responsible for the iMMN, such that neurons which respond specifically to standard and oddball stimuli intensities may be in different refractory states, resulting in a differential AEP; however, data have been produced with an equiprobable, or ‘many-standards’, control condition which reject this hypothesis and support the concept of a pre-attentive memory-based comparison underlying the MMN (Jacobsen et al., 2003). Jacobsen et al. (2003) state that although varying intensity alters N1/N100 and P2 deflections, with greater sound energy producing larger amplitudes (Beagley and Knight, 1967), both softer and louder oddball stimuli elicit comparable iMMN amplitudes, taken as evidence that iMMN reflects a change detection mechanism and not simply differences in sound energy. Nevertheless, the underlying neurophysiological mechanisms remain to be fully explained and therefore development of an animal model of iMMR should be a useful tool for answering further questions on this subject.

In order to begin attempting to understand the neurophysiological mechanisms behind these MMN responses and how they may be altered in neuropsychiatric conditions it is important to review the auditory system, introduced in Section 1.2.2. Stimulus specific adaptation is discussed in Section 1.2.2.6. Further hypothetical models developed to consolidate MMN research and its psychophysiological interpretations with neurophysiological evidence are expanded upon in Section 1.2.3. The development of reliable animal models of MMN has been highlighted as a key step towards fully understanding its neurobiology and presentation in human subjects/patients (Luck et al., 2011), and published studies addressing these efforts are reviewed in Section 1.3. The specific genetic (Section 1.3.1.1) and pharmacological (Section 1.4.2) models relevant to schizophrenia which are the subjects of this thesis and then introduced, followed by the hypothesis and aims driving this research in Section 1.5.

1.2.2 *Neurobiology of auditory processing*

1.2.2.1 *Sound and hearing*

Plack (2013) provides an excellent discussion of the sense of hearing, from which the following overview has been partially informed. Sound is a pressure wave that propagates from its source through media. It usually reaches the human ear via the medium of air, although also travels through solid and liquid materials. The source is a moving or vibrating object which converts a source of potential energy (e.g. kinetic or chemical) into mechanical energy as sound pressure waves. When this pressure wave reaches the ear it is channelled through the outer ear, which performs some minor spectral filtering that helps to determine the relative location of its source. As sound enters the ear hole, or *concha*, it travels through the ear canal which terminates at the eardrum, or *tympanic membrane*. At the other side of the eardrum the three smallest bones in the body, the *ossicles*, interconnect to transmit air-mediated vibrations of the tympanic membrane to the fluid-filled *cochlea* of the inner ear; the ossicles form the middle ear along with the *eustachian tube*, which connects to the back of the throat and is involved in the ‘ear-popping’ feeling associated with pressure changes.

The cochlea is responsible for converting pressure waves into neural impulses which ultimately travel to the neocortex and enable us to perceive sound. It is a thin ovoid tube coiled in a ‘snail-shell’ spiral structure with roughly two and a half turns. This tube is ≈ 3.5 cm in length and varies in diameter from ≈ 2.28 mm at its broadest point, the *base*, to ≈ 1.08 mm at its most narrow, the *apex*, in a slightly conical fashion (Rask-Andersen et al., 2012). The cochlea contains an intricate biological system for converting mechanical vibration into electrical impulses. This is named the *organ of corti* and incorporates the *basilar membrane* which runs the length of the spiralled cochlea, and inner and outer *hair cells* which synaptically connect to neurons which form the *auditory nerve*. When sound waves are transmitted to the cochlea they cause the basilar membrane to vibrate; depending upon frequency of vibration (pitch), the basilar membrane will vibrate at a different specific point along its length. Near the base it resonates with higher frequencies in the range of hearing, while the apex is tuned towards lower frequencies, and each point along its length corresponds with a different *characteristic frequency*. Any individual sound may be composed of multiple frequency components, causing the membrane to vibrate at multiple points corresponding with those frequencies. This frequency sensitive, or *tonotopic*, organisation is an important and withstanding feature throughout the afferent auditory

system, and will be discussed further. The outer, middle and inner ear, and organ of corti are depicted in Figure 1.4.

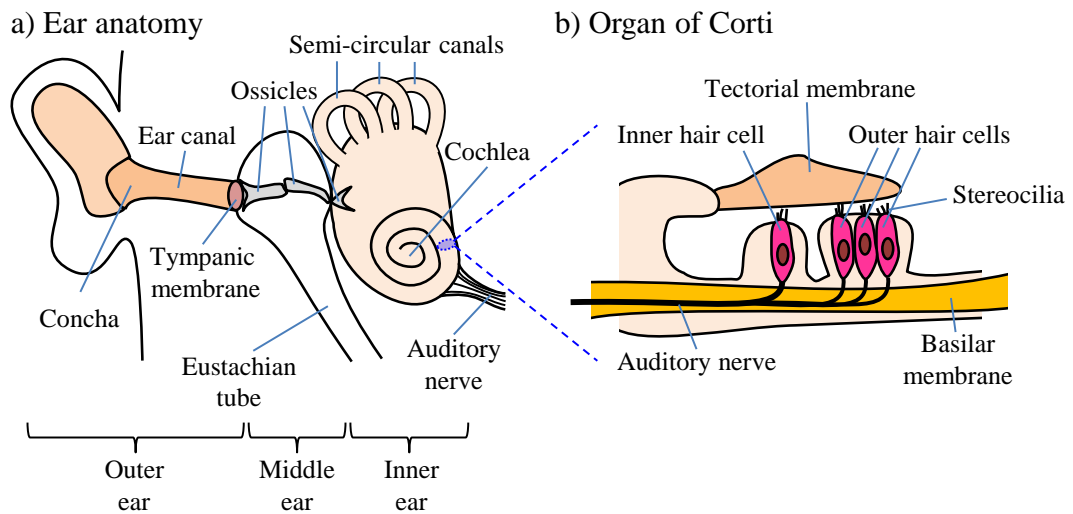


Figure 1.4 - The ear a) Simplified anatomy of the outer, middle and inner ear. Sound waves enter via the concha and travel through the ear canal causing the tympanic membrane to vibrate; this movement is transmitted to the fluid-filled cochlea by three tiny bones called the ossicles. The inner structures of the cochlea subsequently convert this into a neural signal that flows through the auditory nerve. Semi-circular canals are concerned with the vestibular sense. b) Components of the organ of corti, found inside the cochlea, which interact to convert mechanical vibration of the basilar membrane into bioelectric impulses. Movement of the basilar membrane causes stereocilia on inner and outer hair cells to shear against the tectorial membrane, exciting them to release neurotransmitter to their connecting auditory neuron, inducing an action potential which is transmitted through the CNS. This figure was adapted from Plack (2013).

When the basilar membrane vibrates at a particular point it causes the *stereocilia* (hairs) from hair cells to brush against the *tectorial membrane*. This tickling causes depolarisation of the inner hair cells which releases glutamate to the adjoining afferent auditory neuron (Oestreicher et al., 2002); the magnitude of hair displacement modifies the level of this depolarisation and thus the quantity of excitatory neurotransmitter released. Sufficient excitation of the afferent auditory neuron causes it to generate an action potential (*spike*), transmitting an electrical impulse through the auditory nerve. The auditory nerve in each hemisphere contains $\approx 30,000$ neurons or fibres in total, facilitating hearing of frequencies from ≈ 20 - $20,000$ Hz in humans.

1.2.2.2 Auditory pathway

The neuroanatomical connections information travels through in order to reach the auditory cortex are; firstly the ipsilateral *cochlear nucleus*, then bilaterally to the *superior olivary nucleus* of both the ipsilateral and contralateral hemispheres, from there travelling bilaterally to the *inferior colliculus* and also ipsilaterally to the *lateral lemniscus*, before being relayed bilaterally to the *medial geniculate nucleus* of the thalamus and subsequently onwards to the *auditory cortex*. Afferent neurons relay sensory signals upwards between stations in the pathway, and efferent neurons send regulatory signals back down through the pathway; this is represented by the signal flow diagram illustrated in Figure 1.5.

Bidirectional communication exists even at the earliest stages of this system, with efferent neurons from upper structures in the pathway descending into the cochlea, exerting regulatory feedback upon hair cells and their connecting auditory neurons (discussed extensively in Ryugo et al., 2010). Feedback regulation is a core feature of sensory systems, tuning the neural response to sensory information, enabling us to selectively attend to relevant stimuli by filtering that which is lower priority.

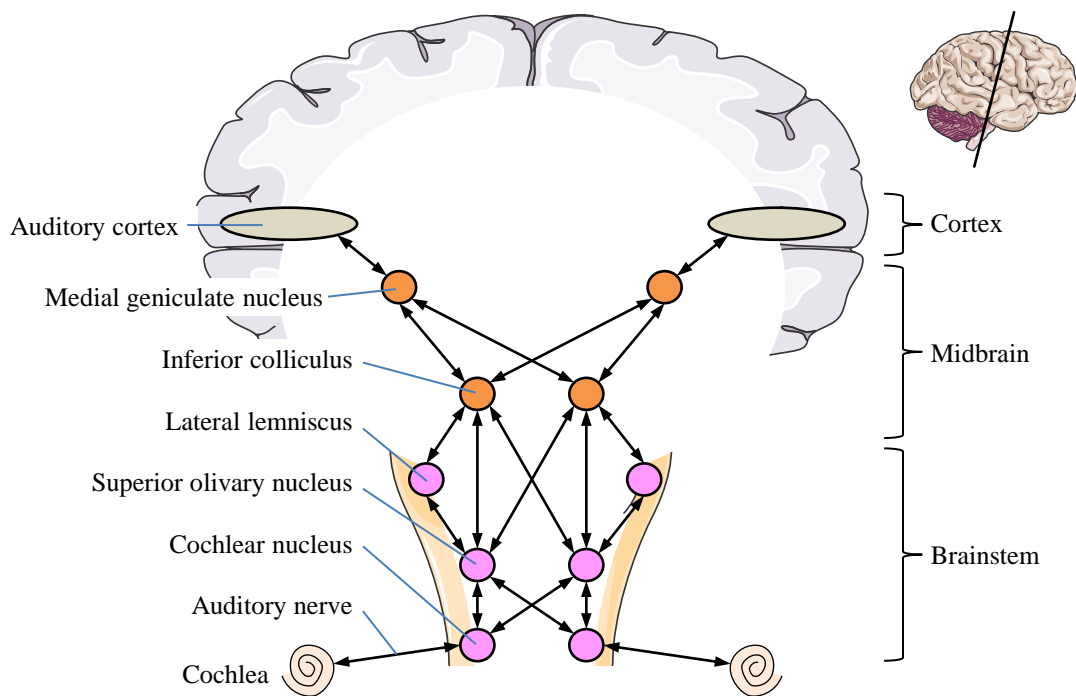


Figure 1.5 - The central auditory pathway Electrical impulses travel along neurons in the auditory nerve to the cochlear nucleus, and then up through the superior olivary nucleus, lateral lemniscus, inferior colliculus, medial geniculate nucleus and on to the auditory cortex. Double-ended arrows represent bidirectional neural communication by afferent and efferent neurons. The high degree of bilateral communication between both hemispheres is thought to be specialised for sound source localisation. This figure was adapted from Plack (2013).

Neurons at each substation along the central auditory pathway are found to display different response properties as a function of auditory stimulation. Some are narrowly tuned to a specific frequency, or *characteristic frequency*, such as afferent auditory nerve fibres. Others may be broadly tuned to fire in response to many different frequencies. There are neurons that fire at the onset of stimulation but then remain quiet, whereas others are found to fire preferentially at stimulation offset (Qin et al., 2007). Furthermore, there are duration-tuned neurons which may favourably respond at a particular time-window during stimulation, or *characteristic duration* (Brand et al., 2000); and intensity-tuned neurons which fire more with increasing sound energy level (monotonic), or increase until a *characteristic intensity* is reached then decrease firing with increasing intensity (non-monotonic) (Phillips and Irvine, 1981). It should be noted that while these observations were made from non-human species, it is generally accepted in principle that these biological properties are also expressed in humans.

These properties of neurons are found throughout the auditory system from brainstem and midbrain nuclei through to the auditory cortex. Subcortical structures are suggested to play an important role in analysing parameters of sound objects as information flows upwards towards the auditory cortex. The cochlear nucleus is the first processing stage, and separates signals from the auditory nerve into parallel streams of information related to different aspects of sound (e.g. frequency, intensity, onset/offset, duration, etc.). The superior olive is involved in determining differences between incident sound properties at each ear, called interaural differences, in latency and intensity, which are important components of sound source localisation (van Opstal, 2016). Although the precise function of the lateral lemniscus is not known, it is found to relay primarily feed-forward GABAergic inhibitory signals towards the inferior colliculus (Adams and Mugnaini, 1984). Each of these brainstem structures may be subdivided into multiple discrete compartments (typically dorsal and ventral nuclei, and sometimes more), executing various functions, although a full discussion of these is beyond the scope of this thesis.

The inferior colliculus of the midbrain has three components; central nucleus, dorsal cortex and external cortex. Ascending connections from various brainstem nuclei, including the lateral lemniscus and superior olivary nucleus, are integrated here before being relayed onwards to the thalamus and cortex. It is interconnected with the superior colliculus, a hub for processing sensory information, implicated in multisensory integration. Studies using fMRI imaging have shown that the human inferior colliculus has a tonotopic organisation (De Martino et al., 2013), confirming data from animal work, which is preserved throughout the afferent auditory pathway. The medial geniculate nucleus, also known as the auditory

thalamus, is the final midbrain structure encountered before sensory information reaches the cortex. The thalamus was previously considered to be a ‘simple relay’ that directs sensory information towards the appropriate specialised cortical area (Sherman, 2005). However, more recently it has become recognised as serving far more intricate functions, including coordinating communication between distant cortical regions, giving rise to synchronised network oscillations thought to be involved in cognitive processing and memory access (Ketz et al., 2015, Saalman and Kastner, 2011, Schmid et al., 2012, Sherman, 2007). Dysfunctional thalamo-cortical interactions are widely implicated in the neuropathology of schizophrenia (reviewed by Pratt et al., 2016), and may underlie cognitive deficits observed in this disorder.

1.2.2.3 *Topography of the auditory cortex*

Winer and Schreiner (2011) provide a thorough review of the auditory cortex, from which this discussion has been partially informed. The human auditory cortex is located in the temporal lobe, positioned underneath the large *Sylvian fissure*, rising into the *supratemporal gyrus* and round the *supratemporal sulcus* (Figure 1.6a). The *primary auditory cortex*, or *core*, receives input from the medial geniculate nucleus, and is surrounded by *belt* and *para-belt* regions of non-primary ‘association’ or *secondary auditory cortex* that are thought to be responsible for interpreting sounds (Figure 1.6b). Approximately this corresponds to Brodmann’s areas 41 and 42 (Brodmann, 2007). The core preserves a tonotopic organisation from the cochlea; moreover, the core, belt and para-belt areas may be subdivided into multiple smaller regions based on structural and functional differences (not represented in the figure), several of which may display tonotopy (Moerel et al., 2014). Additionally, there are specialised areas adjacent to the auditory cortex responsible for language comprehension (Wernicke’s area) and speech production (Broca’s area).

Heschl’s gyrus runs transversally from lateral to medial on the underside of the large Sylvian fissure, along the upper side of the supratemporal gyrus. It is also known as the transverse temporal gyrus, where the auditory cortex is located. Planum temporale is located posterior to Heschl’s gyrus and forms part of Wernicke’s area; this region exhibits pronounced hemispherical asymmetry, with the left hemisphere typically being larger (Galaburda et al., 1987). Interestingly, hemispheric asymmetry of the planum temporale is reduced in patients with schizophrenia (Rossi et al., 1994, Falkai et al., 1995, Barta et al., 1997, Oertel-Knöchel et al., 2013, Ratnanather et al., 2013, Atagün et al., 2015). This may be particularly relevant considering that some have identified this area as a potential source of neural generators underlying the MMN response (Godey et al., 2001).

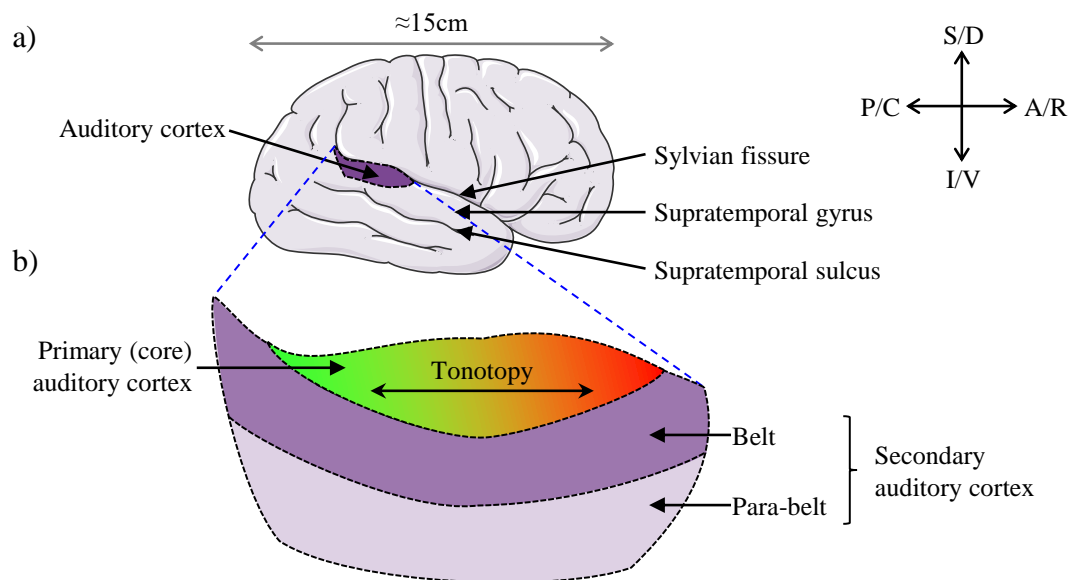


Figure 1.6 - The human auditory cortex a) Topographical location of the auditory cortex in the human brain. Anatomical coordinates given are anterior/rostral (A/R), posterior/caudal (P/C), superior/dorsal (S/D), and inferior/ventral (I/V). b) Primary and secondary subdivisions of the human auditory cortex. Frequency selectivity, or tonotopy, is observed along the A to P axis in the core; higher frequencies corresponding to the basal basilar membrane are shown in red and lower frequencies corresponding to the apical basilar membrane are green.

For comparison, diagrams of the mouse brain and auditory cortex are displayed in Figure 1.7. Both human and mouse auditory cortex representations here are greatly simplified, and their precise anatomy and physiology are subjects of continuous detailed scientific investigation; beyond the scope of this thesis, which is concerned with electrophysiological activity that is typically difficult to resolve spatially to such a degree. In humans the auditory cortex is ≈ 3 mm thick, whereas that of mice is ≈ 1 mm thick; additionally, the former is folded into gyri (ridges) and sulci (furrows), in contrast to the latter which is smooth (Sun and Hevner, 2014). This makes identifying regions analogous to various gyri (e.g. Heschl's gyrus, planum temporale) problematic. Furthermore, there is a high degree of topographic variability between species. This is unsurprising considering the vastly different hearing capacity possessed by different species; particularly between humans and mice, which can generally hear in the ranges of ≈ 0.02 -20 kHz and ≈ 1 -100 kHz, respectively (Heffner and Heffner, 2007).

The ultrasonic field (UF), as one may expect, is concerned with processing ultrasonic frequencies, typically above 45 kHz; the anterior auditory field (AAF) and primary auditory cortex (A1) display mirrored tonotopic organisation about the highest audible frequency representation below the UF range; the dorsoposterior field (DP) and secondary auditory cortex (A2) are less well characterised by frequency responses, and are thought to be similar to association areas in humans (Linden et al., 2003, Stiebler et al., 1997).

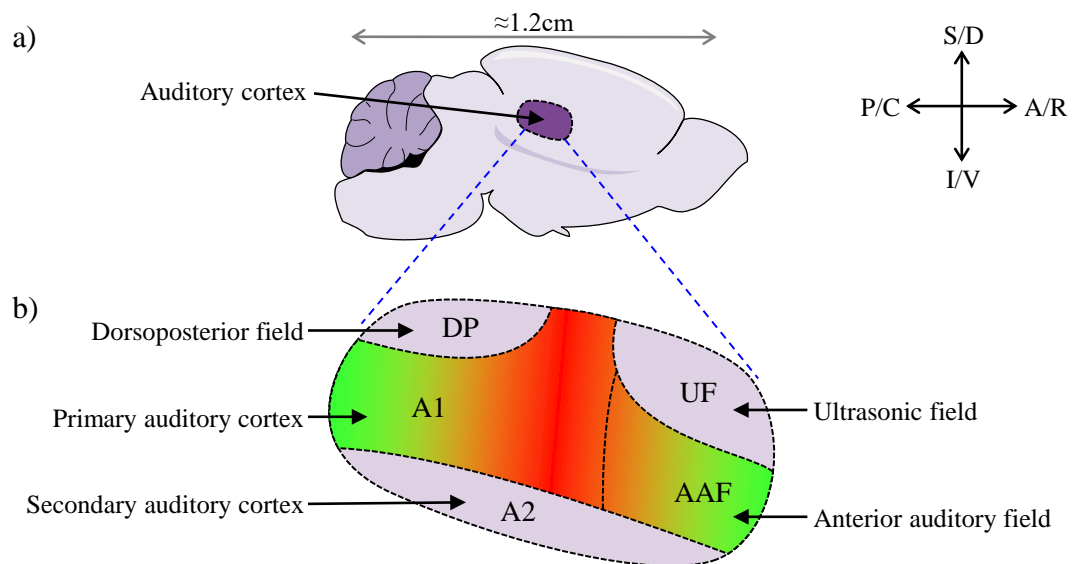


Figure 1.7 - The mouse auditory cortex a) Topographical location of the auditory cortex in the mouse brain. Anatomical coordinates given are anterior/rostral (A/R), posterior/caudal (P/C), superior/dorsal (S/D), and inferior/ventral (I/V). b) Subdivisions of the mouse auditory cortex. Primary and secondary auditory cortices (A1 and A2), dorsoposterior field (DP), ultrasonic field (UF) and anterior auditory field (AAF) are shown; adapted from Linden et al. (2003). A1 and AAF display reversed tonotopy, with higher frequencies represented by red and lower by green.

1.2.2.4 Laminar structure of the auditory cortex

The cortex is a six-layered structure (LI-VI), with each layer having a distinct, complex cellular and neurotransmitter composition, and connections developed to perform specific functions (Figure 1.8). These are sometimes broadly referred to as supragranular (LI-III), granular (LIV), and infragranular (LV-VI) layers; named in relation to the small cell-body, ‘granule’ like stellate cells which are prominent in LIV. These layers are different thicknesses, with deeper layers generally being thicker. There are also topographical variations, with some regions of cortex displaying more or less well defined layers. For example, the supratemporal gyrus where the auditory cortex resides has pronounced granule cells in LII and LIV (Snell, 2001). Some are difficult to distinguish from each other visually, particularly LII and LIII which are often grouped together. Interestingly, this six-layered structure is shared by mammalian species, and is conserved in mice. It is described in terms of cortical columns which are found to contain predominantly vertically communicating cells. Along the tonotopic gradient of the auditory cortex each column spaced over 100 μm apart will respond preferentially to a specific pure-tone frequency (Rothschild et al., 2010). A cortical column with volume $\approx 0.29 \text{ mm}^3$ contains $\approx 31,000$ neurons, each of which may be classified into one of 55 morphologically distinct layer-specific groups, and further into 207 specific electrophysiological classes; these form a dense interconnected network of ≈ 8 million cell-to-cell connections via ≈ 32 million synapses (Markram et al., 2015). This

incredibly complex biological system is the focus of many an investigation in modern neuroscience.

Neuron types found in the cortex include pyramidal, stellate, fusiform, and horizontal cells, among others (Snell, 2001). There is a dense network of nerve fibres arranged horizontally in LI, with lower numbers of cell bodies compared to deeper layers. These fibres arise mainly from apical dendrites of deep pyramidal cells, long thalamo-cortical afferents, and horizontal neurons (Snell, 2001, Watson et al., 2010, Winer and Schreiner, 2011). Over 90% of the cell bodies found in LI are reportedly GABAergic interneurons (Winer and Larue, 1989). LII contains more cell bodies. These include small glutamatergic pyramidal and stellate cells, which project dendrites up to LI and axons down to deeper layers. LIII is a thick layer containing mostly glutamatergic pyramidal cells with dendrites growing upwards towards LI and axons involved in cortical-cortical communication (Thomas and López, 2003). This layer also receives a lot of glutamatergic thalamic inputs to non-pyramidal neurons from the medial geniculate nucleus.

Maximal thalamo-cortical glutamatergic input is received by non-pyramidal cells of LIV. This is a highly granular layer in the auditory cortex, with many well-developed stellate cells; there are also a large number of horizontal GABAergic interneurons in LIV. It has been suggested that this horizontal intra-cortical signal transmission, from a cortical column intimately tuned to the stimulating sound frequency outwards towards distantly tuned columns, may underlie broad spectral integration in auditory processing (Kaur et al., 2005). The fifth layer is the thickest and comprises many large and medium sized pyramidal cells, among stellate, horizontal and other diverse cell types. Efferent projections providing cortical feedback to areas outside of the auditory cortex originate in LV and transmit signals to the medial geniculate nucleus and inferior colliculus (Winer and Schreiner, 2011). Furthermore, there is also reportedly a lower relative concentration of GABAergic cells in this layer (Prieto and Winer, 1999). LVI contains the lowest proportion of inhibitory GABAergic neurons, and many small pyramidal cells which mainly provide glutamatergic projections down to the medial geniculate nucleus of the thalamus, producing a thalamo-cortical feedback loop (Prieto and Winer, 1999, Watson et al., 2010, Winer and Schreiner, 2011).

As seen from Figure 1.8, the primary auditory cortex receives dense thalamo-cortical afferents in a layer-specific fashion. Inputs to the auditory cortex may be summarised as approximately 15% thalamic in origin, 15% from the contralateral hemisphere, and 70% from the ipsilateral cortex (Lee et al., 2004a, Lee et al., 2004b, Winer and Schreiner, 2011).

The primary auditory cortex is therefore highly interconnected with other areas of cortex as well as subcortical structures. Efferent connections from the cortex are predominantly directed towards the auditory thalamus, inferior colliculus, and down to earlier structures in the auditory pathway (shown in Figure 1.5). Cortico-cortical communication directed towards other areas of primary auditory cortex and nearby association cortices is believed to be responsible for interpreting the meaning of different sounds (Winer and Schreiner, 2011).

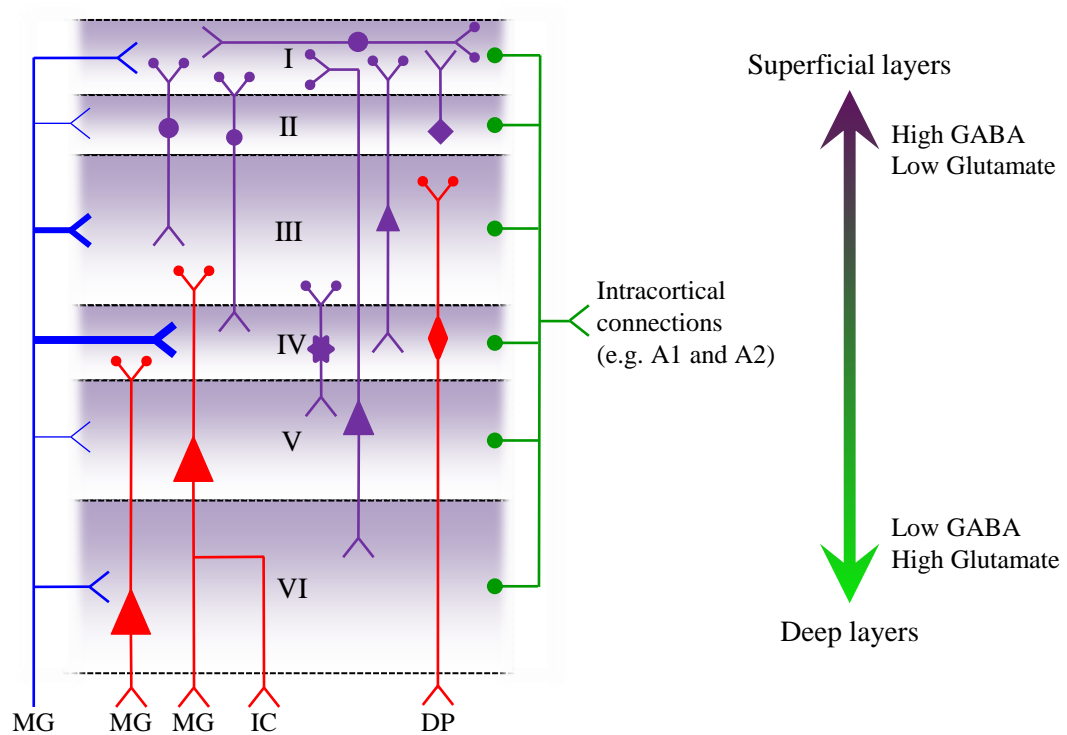


Figure 1.8 - The six-layered structure of the auditory cortex This simplified diagram illustrates the six-layered structure of the auditory cortex, the relative thickness, and some of the cell types and connections associated with each layer. Afferent fibres from the medial geniculate nucleus (MG) are labelled in blue, with line thickness and length indicating the degree of connectivity and lateral projections, respectively; efferent fibres to the MG, inferior colliculus (IC), and descending pathway (DP, which includes superior olive and cochlear nuclei) in red; within-column interneurons in purple; and intracortical connections to other primary (A1) and secondary auditory cortices (A2) in green. The balance of excitation and inhibition dominance varies across layers, generally with higher levels of inhibitory GABA cells in more superficial layers. Adapted from Khodai (2014) and Winer and Schreiner (2011).

1.2.2.5 *Auditory cortex in schizophrenia*

Baldeweg and Hirsch (2015) highlight that post-mortem schizophrenia brains display pathological reductions in the density of synaptic connections (dendritic spines) on LII/III pyramidal neurons in the supratemporal cortex (Garey et al., 1998), dorsolateral prefrontal cortex (Garey et al., 1998, Glantz and Lewis, 2000, Kolluri et al., 2005) and hippocampus (Harrison and Eastwood, 1998). These dendritic spines normally express glutamatergic receptors (e.g. AMPA and NMDA receptors) and are implicated in synaptic plasticity, including LTD and LTP mentioned in Section 1.1.4 (Sala and Segal, 2014). Interestingly, as Baldeweg and Hirsch also point out, intracranial electrophysiological recordings in monkeys suggest that generators of MMN are located in LII/III of the primary auditory cortex and rely on intact NMDA receptor function (Javitt et al., 1996). These converging lines of evidence hold promise for using MMN as a surrogate measure of NMDA receptor neuropathology associated with schizophrenia. In Chapter 5, laminar activity of the auditory cortex during oddball paradigms in mouse models relevant to schizophrenia is examined, which aims to contribute towards this discussion.

1.2.2.6 *Stimulus specific adaptation*

As referenced above, SSA refers to the property of neurons to modify their firing patterns in response to repeated identical stimuli. This phenomenon may also be referred to as *repetition suppression*, *habituation* or *sensory gating*. It occurs in cells from all sensory modalities, but for clarity these discussions relate to neurons of the auditory system. SSA is suggested to represent a possible single-neuron correlate of MMN, serving some cellular form of sensory-memory function (Nelken and Ulanovsky, 2007, Ulanovsky et al., 2003, Ulanovsky et al., 2004). It has been observed from neurons at multiple stages throughout the auditory pathway, including the inferior colliculus (Zhao et al., 2011, Duque et al., 2012), medial geniculate nucleus of the thalamus (Anderson et al., 2009, Antunes et al., 2010), and primary auditory cortex (Ulanovsky et al., 2003, Ulanovsky et al., 2004, Taaseh et al., 2011). Subcortical and cortical SSA is thought to be a precursor to the cortical MMN, interacting in a hierarchically organised system designed to detect deviance in the auditory environment (Grimm and Escera, 2012). The degree of adaptation at stations throughout the auditory system may be one mechanism by which switching between alternative neural circuitry for processing repetitive standard stimuli versus irregular oddball stimuli may occur, and as such perhaps invoking different downstream activity. Theoretical models of MMN generation are discussed in Section 1.2.3.

In a review of the literature, Grill-Spector et al. (2006) propose different models that may explain SSA. Mechanisms they set forth include *fatigue* and *sharpening* models. The fatigue

model describes a situation where neurons intrinsically diminish firing rates with stimulus repetitions, potentially due to increased intracellular potassium (K^+) concentration or reduced neurotransmitter availability. The sharpening model suggests that neurons originally responding weakly will cease to fire while fewer ‘more specific’ neurons will respond more strongly with stimulus repetitions; this would decrease overall neural activity but increase firing of few neurons, essentially improving the efficiency of neuronal representations of stimuli.

This phenomenon is typically discussed in relation to stimuli frequencies, thus the term “stimulus-specific” may be an over-generalisation. Frequency-selective habituation may more accurately describe the findings from these studies, which all employed frequency-varying oddball paradigms derived from those used by Ulanovsky et al. (2003). One recent study measuring responses in the primary auditory cortex to word-like and white-noise-token oddball paradigms illustrated that SSA is apparent between spectrally similar stimuli presented at different probabilities, thus supporting the use of SSA as the appropriate term to describe these phenomena (Nelken et al., 2013). However, to the author’s knowledge there are no reports of SSA in response to duration or intensity specificity, thus this remains to be proven.

1.2.3 *Theoretical models of MMN*

As introduced above, there are competing theories of what exactly the MMN component of the AEP represents. The original and widely cited theory states that the MMN arises from a sensory-memory trace disruption that initiates pre-attentive attention switching towards an oddball/deviant stimulus which differs from recent auditory stimuli (Näätänen et al., 1978). This is known as the *model adjustment hypothesis*, and interprets MMN as an error signal used to update an internal neural representation (sensory memory) of the auditory scene (Winkler et al., 1996). This is based on there being two main generators, located in auditory and prefrontal cortices, which form a network responsible for integrating current auditory inputs with expectations based on previous auditory inputs; where a mismatch between current and previous auditory inputs produces the MMN component which updates sensory memory expectations.

An alternative explanation also mentioned above proposes that fresh afferent neurons transmit information about the oddball/deviant stimulus, whereas those which convey information about the standard are in a refractory state having undergone SSA. This *adaptation hypothesis* states that MMN is simply a modification of the obligatory N1 component (slight increase in amplitude and latency) that occurs in response to a rare

stimulus relative to that of a frequent stimulus, and is localised to the auditory cortex (Jääskeläinen et al., 2004). The argument over memory-based versus adaptation-based interpretations of MMN has been reviewed by several authors, without reaching an absolute consensus (Baldeweg, 2007, Garrido et al., 2009, May and Tiitinen, 2010, Näätänen et al., 2005).

Garrido et al. (2009) propose a unifying theory based on *predictive coding* which purports to account for both the model adjustment and adaptation hypotheses. Predictive coding or hierarchical inference is based on the principle of higher structures relaying top-down predictions about expected inputs to lower structures, which in turn attempt to integrate and consolidate actual inputs with these predictions and return a bottom-up prediction error, which is the difference between these two entities. This agrees well with the model adjustment theory, in which MMN is suggested to reflect this prediction error signal. Additionally, hierarchical inference relies on optimising lower structures to minimise the prediction error, which accounts for adaptation observed along the auditory pathway. The predictive coding model is portrayed as a control system diagram in Figure 1.9; this may be described as a process of perceptual learning, and provides a framework for understanding sensory-memory disruption and adaptation elements of MMN.

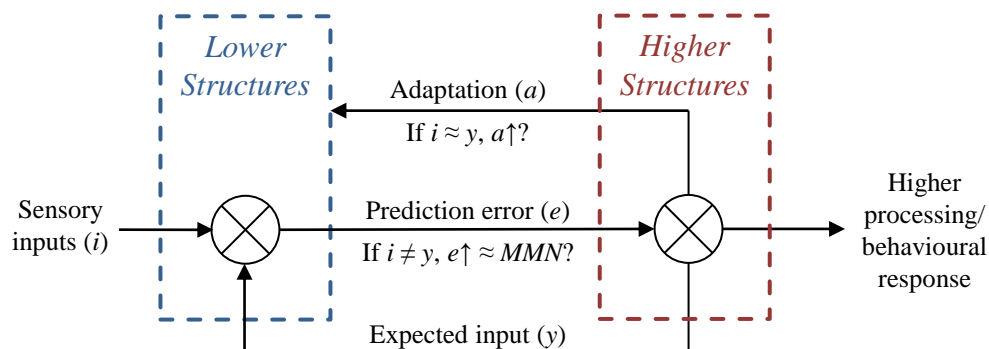


Figure 1.9 - Predictive coding model of mismatch negativity This theoretical model is represented here as a comparative control system. Sensory inputs reaching lower structures (auditory cortex) are compared with an expected input derived from higher structures (prefrontal cortex); when there is a mismatch the prediction error signal is large, causing higher structures to update the expected input to feedback into lower structures. If the prediction error is small higher structures may initiate adaptation in lower structures to improve efficiency of neural activity. It should be noted that this is a theoretical model and there is no consensus on its validity.

Baldeweg and Hirsch (2015), interpreting their findings in terms of the predictive coding theory, suggest that supragranular layers (LI-III) play an important computational role in generating the prediction error. According to the proposed microcircuitry by Bastos et al. (2012), pyramidal neurons in LII/III encode predictive errors with modulation from inhibitory interneurons, which are sent towards higher structures/cortical areas. It may be

this system that becomes disrupted by neuropathology in schizophrenia, diminishes patients' ability to generate this response, and resulting in decreased MMN amplitude.

This is an attractive model, but it does not address differences between responses elicited by different physical properties of sound, which as discussed may reflect separate neurophysiological processes. The predictive coding theory of MMN may assume that all physical parameters of stimuli are already represented by sensory inputs reaching lower structures (from the afferent auditory pathway), although this is not clarified. Again, this model may be guilty of generalising the observed phenomena and neglecting to recognise the potentially important contributions that different physical properties of sound may have on electrophysiological recordings of central auditory processing. As noted, this thesis aims to investigate different basic physical properties of sound separately with adequate control paradigms (discussed in Section 2.7) to interpret the findings with respect to each of the discussed models.

1.3 Mismatch response (MMR) in animals

Identifying an MMR in animals analogous to MMN in humans is a key objective in this field of research. Development of reliable animal MMR models will provide an unparalleled resource for investigating the underlying neurophysiology of MMN by more invasive methods than usually possible with human subjects. Different pharmacological manipulations may be applied to dissect the neurotransmitter systems responsible for generating this MMR, and contributions of genetics and other environmental factors which can be controlled. Thus far, evidence for an equivalent signal has been found from several different animal species, including; macaque monkeys (e.g. Javitt et al., 1992, Steinschneider et al., 1992, Sobotka and Ringo, 1994, Javitt et al., 1996, Javitt et al., 2000, Fishman and Steinschneider, 2012), cats (e.g. Csépe et al., 1987, Csépe, 1995, Pincze et al., 2001, Pincze et al., 2002, Ulanovsky et al., 2004, Ulanovsky et al., 2003), rabbits (e.g. Ruusuvirta et al., 1995, Astikainen et al., 2001), pigeons (e.g. Schall et al., 2015), rats (e.g. Ruusuvirta et al., 1998, Astikainen et al., 2006, Astikainen et al., 2011, Nakamura et al., 2011, Harms et al., 2014), guinea pigs (e.g. Christianson et al., 2014, Kraus et al., 1994, Okazaki et al., 2006) and mice (e.g. Umbricht et al., 2005, Ehrlichman et al., 2008, Ehrlichman et al., 2009, Featherstone et al., 2015). Although each may be useful for studying MMN, the rest of this discussion focusses primarily on rodents, and specifically mice, which are a preferred model species due to their relatively low associated costs of housing and feed. In addition, the availability of advanced techniques for modelling human genetic deficits and selectively controlling neuronal activity via optogenetics (Boyden et al., 2005) are attractive aspects of using mouse models for neurophysiology research.

Published research articles that aimed to model human MMN in mice and rats are summarised in Table 1.2. The majority of the 22 studies cited have been performed in rats with only four studies using mice. Similar reviews have been performed in the literature (Harms, 2016, Nakamura et al., 2011, Nelken and Ulanovsky, 2007, Todd et al., 2013). Note there are several other publications addressing AEP responses in rodents that may be relevant even though they do not directly probe the MMR; these are omitted from the table for brevity, but discussed in the relevant chapters which follow. In relation to mice, studies have suggested strain plays an important role in AEP morphology (Ehlers and Somes, 2002, Siegel et al., 2003), and in influencing the response to NMDA receptor antagonists (Connolly et al., 2004). This is important considering that different mouse strains have been used in MMR studies (Table 1.2); potentially accounting for some of the variability in results. Furthermore, it may be noted that the majority of work in mice has been performed by the research group of Professor S. J. Siegel (University of Pennsylvania, United States);

these results are yet to be replicated by independent groups. In fact, other authors have reported negative findings from frequency oddball paradigms in mice (Umbricht et al., 2005). This could perhaps be due to differences in animal details, electrophysiology recording protocol, oddball paradigm parameters, and interpretation in comparison with control waveforms. Overall, it may be said that there is inconclusive evidence of an MMR in mice analogous to the human MMN. The current thesis aims to contribute towards this discussion.

It can be seen from Table 1.2 that results from rats have also been variable. Following an initial positive finding (Ruusuvirta et al., 1998), a couple of negative findings were published in which an MMR was not observed from rats (Lazar and Metherate, 2003, Eriksson and Villa, 2005); however each of these studies used different breeds, states of consciousness, variations of the oddball paradigm, controls, and relatively low sample numbers. Each of these factors could potentially have contributed to this variability in results. Subsequent reports were mainly positive, although not entirely consistent regarding the polarity or latency range of the MMR. Differences in polarity observed across different studies has been speculated by some to be an effect of anaesthesia (Shiramatsu et al., 2013); although as seen several different anaesthetic agents have been employed. This proposal is examined in this thesis by investigating the responses of urethane-anaesthetised (Chapter 3 and Chapter 5) and conscious (Chapter 4) cohorts of mice. It may also be noted that a majority of studies investigating rats have been published by a Finnish collaboration (Universities of Jyväskylä and Turku, Finland); however other groups have also reported positive findings.

There are a limited number of published studies investigating genetic risk factors for schizophrenia and their effect on the mismatch response in rodents. Neuregulin heterozygous (*Nrg^{+/-}*) mice have reportedly shown diminished negative amplitude fMMR over 50-75 ms post stimuli onset (Ehrlichman et al., 2009). Mice heterozygous for the GluN1 (previously NR1) NMDA receptor subunit (*NR1^{+/-}*) gene also show reduced fMMR amplitude measured over 50-100 ms (Featherstone et al., 2015). These are interesting findings, and the authors suggest that these genetic mouse models relevant to schizophrenia exhibit fMMR deficits comparable with the human fMMN. However, the waveform shapes and methods of quantifying the fMMR varied between these two publications, and neither employed any control paradigms. In order to verify both of these findings they should be replicated with appropriate controls to avoid any misinterpretation.

Additionally, there is a lack of systematic investigations using multiple physical features of sound to elicit the MMR from rodents. The majority of studies have used variants of the frequency oddball paradigm. As discussed in the subsections of Section 1.2.1 above, duration, frequency and intensity changes may elicit different neurophysiological mechanisms in the human MMN, suggested to reveal different aspects and time-course of schizophrenia neuropathology. In mice, frequency and duration oddball paradigms have been used to examine any corresponding mismatch responses, with inconclusive results (Umbricht et al., 2005). None of the published studies have employed duration, frequency and intensity manipulations in mice while incorporating multiple control paradigms (see Section 1.3.1.1 below). Throughout this thesis these different physical parameters are systematically examined, and their potential for eliciting an MMR in mice comparable with the human MMN is explored.

In a discussion about modelling mismatch responses in rodents, Harms et al. (Harms et al., 2015) highlight that differences in neuroanatomical orientation, brain morphology and electrophysiology recording setups make it unlikely to attain a carbon copy of the human MMN in animals. These factors may account for differences in latency range and polarity of the rodent MMR compared with human MMN, which are considered superfluous to the underlying generative mechanisms. Important features that should be modelled in an equivalent rodent MMR are the reliance on a sensory-memory disruption effect (according to the predictive coding model in Figure 1.9) and not an adaptation effect (e.g. SSA, discussed in Section 1.2.2.6). Dissociation of these two mechanisms requires the use of control paradigms designed to invoke these separate processes, several of which are outlined in Section 1.3.1.1 below. Rodent MMR and AEP literature are discussed in greater detail in the relevant chapters which follow.

Reference	Animal details	Recording configuration	Oddball feature(s)	Control paradigm(s)	Schizophrenia-related model	Results
Umbricht et al. (2005)	Conscious, freely-moving mice (128Sv/B6; n=21); 64-68 weeks	Epidural EEG above AC; frontal reference	Frequency, duration	Flip-flop, Deviant-alone	-	dMMR: -ve, \approx 50 ms after deviance onset. No fMMR
Ehrlichman et al. (2008)	Conscious, freely-moving mice (DBA/2Hsd; n=27); 10-13 weeks	LFP in CA3; frontal reference	Frequency	-	Ketamine	fMMR: -ve, 25-75 ms; reduced by ketamine
Ehrlichman et al. (2009)	Conscious, freely-moving mice (<i>NRG</i> ^{+/-} on C57BL/6/129 hybrid background; n=28); 16-18 weeks	LFP in CA3; frontal reference	Frequency	-	<i>Nrg</i> ^{+/-} heterozygote model	fMMR: -ve, 50-75 ms; reduced in <i>NRG</i> ^{+/-} mice
Featherstone et al. (2014)	Conscious, freely-moving mice (<i>NRG</i> ^{+/-} on C57BL/6NH1a background; n=24); 9-10 weeks	LFP in CA3; frontal reference	Frequency	-	<i>NR1</i> ^{+/-} heterozygote model	fMMR: -ve, 50-100 ms; reduced in <i>NRG</i> ^{+/-} mice
Ruusuvirta et al. (1998)	Urethane anaesthetised Wistar rats (n=9)	Epidural EEG above AC; cerebellar reference	Frequency	Flip-flop, Deviant-alone	-	fMMR: +ve, 63-196 ms
Lazar and Metherate (2003)	Urethane-xylazine anaesthetised Sprague-Dawley rats (n=7)	Epidural EEG above AC; cerebellar reference	Frequency	Standard-like response	-	No MMR
Eriksson and Villa (2005)	Conscious freely moving Long Evans rats (n=6)	Epidural EEG above AC; cerebellar reference	Synthesised vowels	Flip-flop, Deviant-alone	-	No MMR

Table 1.2 - Summary of mismatch response studies in rodents Studies in mice and rats are listed chronologically, separated with a double-line; results given include polarity and latency range of MMR. AC = auditory cortex, CA3 = region of the hippocampus, LFP = local field potential.

Reference	Animal details	Recording configuration	Oddball feature(s)	Control paradigm(s)	Schizophrenia-related model	Results
Astikainen et al. (2006)	Urethane anaesthetised Wistar rats	Epidural EEG above AC; nasal reference	Frequency, frequency-intensity	Flip-flop	-	fMMR: +ve, 76-108 ms
Ruusuvirta et al. (2007)	Urethane anaesthetised Wistar rats (n=14)	Epidural EEG above AC; nasal reference	Melodic contours	Flip-flop	-	MMR: +ve and -ve, 106-136 ms
Tikhonravov et al. (2008)	Pentobarbital sodium anaesthetised Hannover Wistar rats (n=30)	Epidural EEG above AC; posterior reference	Frequency	Flip-flop, Deviant-alone	MK-801	fMMR: +ve, 150-180 ms; reduced by MK-801
Roger et al. (2009)	Conscious freely moving Long Evans rats (n=10)	Epidural EEG above AC, parietal cortex, ACC; bregma/posterior reference	Duration	-	-	dMMR; -ve, 25-75 ms after deviance onset
Tikhonravov et al. (2010)	Pentobarbital sodium anaesthetised Hannover Wistar rats (n=24)	Epidural EEG above AC; posterior reference	Frequency	Flip-flop, Deviant-alone	Memantine	fMMR: +ve, 91-180 ms; reduced by memantine
Ahmed et al. (2011)	Urethane-anaesthetised Sprague-Dawley rats (n=9)	Epidural EEG above AC; cerebellar reference	Speech sounds	Many-standards	-	MMR: +ve, 30-80 ms
Astikainen et al. (2011)	Urethane-anaesthetised Sprague-Dawley rats (n=33)	Epidural EEG above AC; cerebellar reference	Frequency	Many-standards	-	fMMR: +ve, 60-100 ms (only higher frequency oddballs)
Nakamura et al. (2011)	Awake and fentanyl-medetomidine anaesthetised Wistar rats (n=7)	Epidural EEG above AC; posterior reference	Frequency, duration	Flip-flop, many-standards	-	MMR: -ve (awake) and +ve (anaesthetised), 67-100 ms (frequency and duration pooled together)

Table 1.2 - Continued ACC = anterior cingulate cortex

Reference	Animal details	Recording configuration	Oddball feature(s)	Control paradigm(s)	Schizophrenia-related model	Results
Jung et al. (2013)	Conscious freely moving Black Hooded rats (n=16)	Epidural EEG above AC; frontal reference	Band-passed noise/frequency	Flip-flop, many-standards	-	fMMR: biphasic, 22-81 ms
Ruusuvirta et al. (2013)	Urethane-anaesthetised Sprague-Dawley rats (n=10)	Epidural EEG above AC and LFP from hippocampus; cerebellar reference	Duration	-	-	dMMR: +ve (AC) and -ve (hippocampus), 51-89 ms
Shiramatsu et al. (2013)	Isoflurane anaesthetised Wistar rats (n=18)	Surface microelectrode array EEG on AC	Frequency	Flip-flop, many-standards	AP5	fMMR: -ve, 53-110 ms; reduced by AP5
Harms et al. (2014)	Conscious freely moving Wistar rats (n=27)	Epidural EEG above AC, FC; cerebellar reference	Frequency	Flip-flop, many-standards, cascade	-	fMMR: +ve, 60-80 ms (only higher frequency oddballs)
Sivarao et al. (2014)	Conscious freely moving Sprague-Dawley rats (n=16)	Epidural EEG above FC and vertex;	Frequency	Flip-flop, many-standards	Ketamine, CP-101,606 (GluN2B antagonist)	fMMR: +ve, 30-60 ms; reduced by ketamine and CP-101,606
Witten et al. (2014)	Conscious freely moving Lister-Hooded rats (n=26)	Epidural EEG above PC and LFP in CA3; frontal reference	Frequency	Balanced	Social isolation model	fMMR: -ve, 30-80 ms; social isolation reduced cortical fMMR
Ruusuvirta et al. (2015)	Urethane-anaesthetised Sprague-Dawley rats (n=11)	Epidural EEG above AC and LFP from hippocampus; cerebellar reference	Frequency	Balanced, many-standards,	-	fMMR: 75-125 ms; may be explained by stimulus frequency effects

Table 1.2 – Continued AP5 = D-(-)-2-amino-5-phosphonopentanoic acid; FC = frontal cortex; PC = parietal cortex.

1.3.1.1 Control paradigms in animal MMR studies

The *flip-flop* control involves switching the roles of standard and oddball stimuli, such that in one paradigm stimulus X is the standard and stimulus Y is the oddball, then in the ‘flipped’ paradigm stimulus Y is the standard and stimulus X is the oddball (Figure 1.10a); AEP responses from the oddball/deviant condition may then be compared with the standard condition using physically identical stimuli.

The *standard-like* control used by Lazar and Metherate (2003) was produced by presenting a consecutive train of stimuli identical to the oddball before and after the oddball paradigm (Figure 1.10b); generating an AEP that reflects the build-up, but not violation, of a sensory-memory trace (i.e. adaptation), akin to the standard in an oddball paradigm. This may also be referred to as a *consecutive-repetition* control.

The *balanced* control is an oddball paradigm which includes deviant stimuli that vary in both directions from the standard (Figure 1.10c); enabling comparisons of increasing and decreasing oddball effects, controlling for stimulus levels.

The *many-standards* control, also known as an equi-probable condition, is a situation where oddball stimuli are presented along with multiple different ‘standard’ stimuli pseudo-randomly at the same probability as the deviant/oddball in the oddball paradigm (Figure 1.10d); thus retaining the same stimulus probability while lacking regularity of previous stimuli, controlling for stimulation rate without a reliable sensory-memory trace.

The *deviant-alone* paradigm has been widely applied to control for different stimulation rates of the deviant/oddball, although without the sensory-memory trace formation of the standard (Figure 1.10e); this involves presenting the same sequence as in the oddball paradigm with silent standards, thus retaining the same inter-deviant interval. However, this paradigm may be reinterpreted as a positive control for sensory-memory disruption, on the basis that a sensory-memory trace of relative silence may be more drastically violated.

The *cascade* control is similar to the many-standards in that multiple stimuli are presented with the same probability as the deviant/oddball in the oddball paradigm, although these are presented in a structured sequence (Figure 1.10f); controlling for stimulation rate within a predictable pattern of auditory stimulation, although in implementing this approach Harms et al (2014) have suggested it holds no clear advantages over the many-standards control. The control paradigms implemented in this study and their rationale are discussed further in Chapter 2.

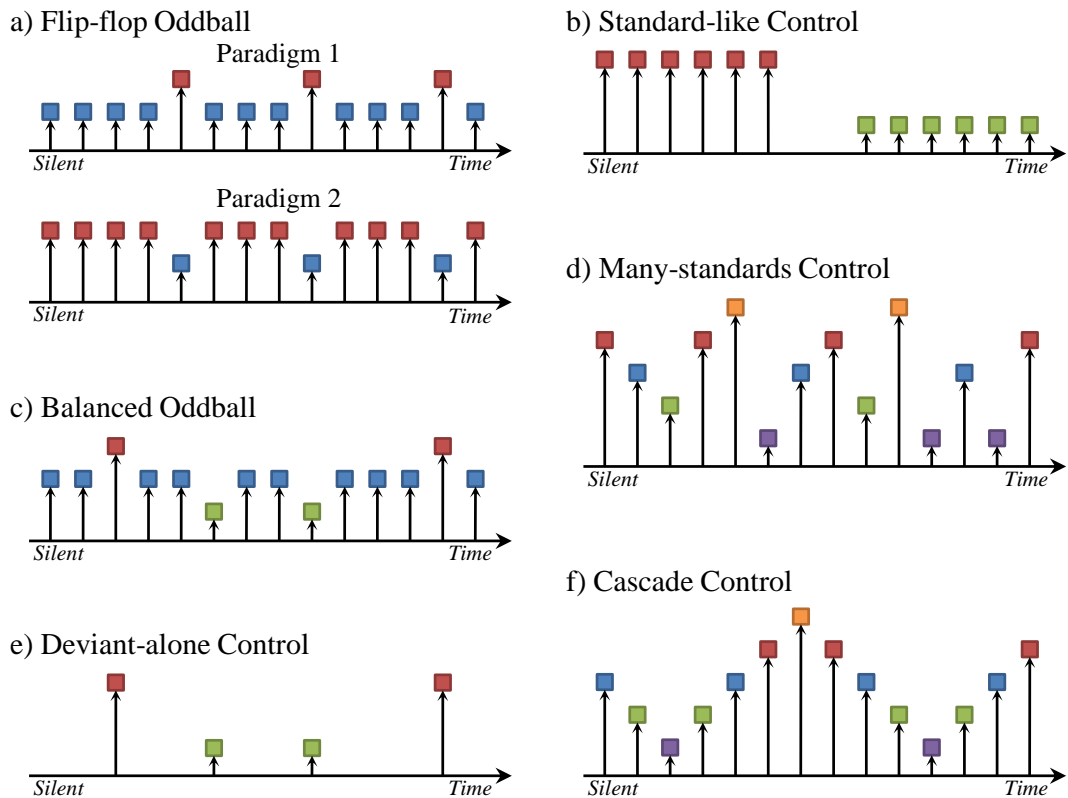


Figure 1.10 - Oddball and control paradigms used in rodent mismatch response studies

This figure illustrates some of the auditory paradigms used in rodent MMR studies. a) The flip-flop design involves switching the identity of oddball (red) and standard (blue) stimuli in two different paradigms. b) The standard-like control entails repeating oddball stimuli (red or green) in an unbroken stream. c) The balanced oddball paradigm incorporates increasing (red) and decreasing (green) oddball stimuli. d) The many-standards control uses many equally-probable stimuli presented at the same probability as oddballs in the oddball paradigm. e) The deviant-alone control is the same as the oddball paradigm without any standards. f) The cascade control involves presenting an ascending and descending sequence of stimuli, each with the same probability as the oddball in the oddball paradigm. Black lines with rising vertical arrows illustrate the point of reference for each transition into an auditory stimulus, which is relative silence. Adapted from Harms et al. (2014).

1.4 Mouse models in this study

1.4.1 Mitogen activated protein kinase kinase 7 (*Map2k7*^{+/-})

As illustrated in Figure 1.1, the MAP2K7-JNK pathway is implicated in schizophrenia. This link has been established through genome-wide association and gene expression studies, which have identified two separate SNPs of the *MAP2K7* gene conveying increased risk of disease (Pergadia, 2012, Winchester et al., 2012). MAP2K7 is an intracellular signalling enzyme activated downstream from glutamate binding to N-Methyl-D-Aspartate (NMDA) receptors in the post-synaptic neuron. Upon activation, MAP2K7 phosphorylates the stress-activated protein kinase c-Jun-N-terminal kinase (JNK). This supports a vast body of evidence suggesting glutamatergic neurotransmission is aberrant in schizophrenia and also implicates the MAP2K7-JNK signalling cascade in these dysregulated processes.

Heterozygote *Map2k7*^{+/-} (HET) mice have been generated to facilitate the study of this pathway; complete deletion of both chromosomal copies of this gene results in mortality (Kishimoto et al., 2003, Sasaki et al., 2001). It is unclear exactly how well this mutant replicates genetic deficits observed in humans; although it can be said with certainty that *Map2k7* protein expression is reduced in this model, as confirmed by western blotting. Through a collaborative research effort headed up by Professors Judith Pratt (University of Strathclyde, Glasgow, UK) and Brian Morris (University of Glasgow, Glasgow, UK), these HET mice have been assessed with a battery of behavioural and molecular tests (Openshaw et al., 2016, Thompson, 2013, Winchester et al., 2012); this work is ongoing, and the current thesis forms part of this effort.

Initial behavioural assessments identified a working memory deficit in HET mice compared with wild-type (WT; *Map2k7*^{+/+}) control animals, and dissociated this from the potential confound of any locomotive abnormalities. Additionally, in-situ hybridisation revealed that *Map2k7* expression is reduced in the PFC and hippocampus of HET mice relative to WT controls, paralleling observations from post-mortem tissue of schizophrenia patients (Thompson, 2013, Winchester et al., 2012).

More recently, Openshaw et al. (2016) found that *Map2k7*^{+/-} mice exhibit an impairment in attention during the five-choice serial reaction time task (5-CSRTT). This behavioural task involves paying attention to five different potential response choices (nose-poke holes) for an indicator (light flash), then selecting the appropriate choice for nose-poking, and subsequently collecting a food reward for correct responses. In this study HET mice omitted more trials than WT controls, although they were able to learn the task and achieve comparable performance, which is thought to reflect lapses in attention. This is suggested to

indicate a decrease in *Map2k7* protein expression in the prefrontal cortex and hippocampus (although other regions were not tested), considering that the prefrontal cortex is involved in 5-CSRTT performance (reviewed in Robbins, 2002).

There is a close association between abnormal MMN responses in humans with schizophrenia and altered NMDA receptor function, as discussed in Section 1.2.1. Deficits in the MAP2K7 gene are linked with schizophrenia (discussed in Section 1.1.4) and it is suggested that this post-synaptic signalling molecule may be involved in exerting modulatory action on NMDA receptors (Hayashi-Takagi and Sawa, 2010). Considering this it is reasonable to hypothesise that *Map2k7* gene disruption may feasibly alter auditory processing activity and the MMR in mice through its involvement in a post-glutamatergic signalling cascade. This question is explored throughout this thesis.

1.4.2 NMDA receptor antagonist

NMDA receptor antagonists are widely used to model symptoms of schizophrenia in animal models. Commonly used agents include ketamine, PCP, and MK-801 which induce what is referred to as NMDA receptor hypo-function by blocking these channels; translating into a set of behavioural and physiological deficits relevant to schizophrenia, including measures of working-memory, attention and electrophysiology (reviewed by Neill et al., 2010). These are non-competitive NMDA channel blockers, meaning they functionally disable the channel when bound. The precise neurobiology underpinning the emergence of these behavioural deficits is yet to be fully elucidated. However some authors have recently argued that a prominent contribution may come from PV-containing GABAergic interneurons, as suggested in Section 0 and Figure 1.2 (Cohen et al., 2015, Nakazawa et al., 2012).

As discussed throughout this introductory chapter, NMDA receptor abnormalities implicated in schizophrenia are associated with deficits in human MMN. Previous studies have examined the effects of NMDA receptor antagonists in rodents (see Table 1.2). AP5 (Shiramatsu et al., 2013), CP101-606 (Sivarao et al., 2014), ketamine (Ehrlichman et al., 2008, Sivarao et al., 2014), memantine (Tikhonravov et al., 2010) and MK-801 (Tikhonravov et al., 2008) have all been reported to diminish a rodent MMR; although the exact features (e.g. polarity and latency) of these MMR waveforms are not consistent. In a study using mice, Ehrlichman et al. (2008) demonstrated that administering 10 mg/kg i.p. ketamine significantly reduced a fMMR in the region of 25-75 ms. This forms an initial point of reference to begin dissecting the role of non-specific NMDA receptor disruption on mouse mismatch responses. This thesis emulates the NMDA antagonism model implemented by Ehrlichman et al. (2008), applying it in WT and HET mice to confirm whether this

diminishes the MMR to different physical properties of sound deviance (i.e. duration, frequency and intensity), and probe the existence of any differential response between these two genotypes.

1.5 Hypotheses and experiment outline

The initial hypothesis of this thesis is that mice exhibit a mismatch response (MMR) comparable with the human mismatch negativity (MMN), that this MMR varies with different physical properties of sound (duration, frequency and intensity) and relies on intact NMDA receptor function. Furthermore, this response may be viewed from anaesthetised or conscious animals, and potentially relies on an intracortical generator located in the auditory cortex. Additionally, it is hypothesised that the heterozygote *Map2k7*^{+/-} (HET) gene disruption model relevant to schizophrenia displays electrophysiological deficits, including diminished MMR, consistent with those found in patients with schizophrenia syndrome. Thus three experiments were performed in this study that aimed to test these hypotheses, as outlined in Table 1.3 below.

Experiment	Overview
I (Chapter 3)	Record epidural EEG from the auditory cortex of urethane-anaesthetised WT and HET mice in response to oddball and control paradigms varying in stimuli duration, frequency and intensity following saline and 10 mg/kg i.p. ketamine injections.
II (Chapter 4)	Replicate Experiment I using conscious animals, additionally including auditory paradigms varying in inter-stimulus interval.
III (Chapter 5)	Record laminar electrophysiological activity from the auditory cortex of urethane-anaesthetised WT and HET mice in response to stimuli duration, frequency and intensity variations, and to frequency oddball and control paradigms before and after 10 mg/kg i.p. ketamine administration.

Table 1.3 - Overview of the current study This table provides an overview of three experiments performed as part of the investigations into mismatch response signatures in mouse models relevant to schizophrenia detailed in this thesis.

Chapter 2. General methods

2.1 Introduction

This chapter contains a description of the materials and methods applied throughout this study. The animal models, surgeries, electrophysiological techniques and data analyses used are explained.

2.2 Statement of ethical practice

All procedures were approved by the Animal Welfare and Ethical Review Body at University of Strathclyde and performed in accordance with the UK Animals (Scientific Procedures) Act 1986. At time of writing the author/experimenter possesses a Home Office Personal Licence (PIL) 60/13734. Experiments were conducted under two Home Office Project Licences (PPL); 60/4463 and 60/4217, with remits to investigate schizophrenia-like phenotypes and altered auditory processing in rodent models, respectively. The experimenter personally took every available precaution to minimise pain and suffering to animals used for this study.

2.3 Study overview

Three different experiments were performed in this thesis to investigate the mismatch response (MMR) to multiple features of auditory oddball stimuli in mouse models relevant to schizophrenia. The following three subsections outline the approaches taken in each of these experiments which are also summarised in Table 2.1 below. Detailed descriptions of the methods applied are provided throughout this chapter.

Exp.	Model	State	Oddball	Recordings	Data Analyses
I	<i>Map2k7</i> ^{+/-} , Ketamine	Urethane Anaesthesia	Duration, Frequency, Intensity	Cortical EEG	AEP, MMR, power spectra
II	<i>Map2k7</i> ^{+/-} , Ketamine	Conscious	Duration, Frequency, Intensity	Cortical EEG	AEP, MMR, power spectra, motion
III	<i>Map2k7</i> ^{+/-} , Ketamine	Urethane Anaesthesia	Frequency	LFP, spikes	AEP, MMR, MUA

Table 2.1 - Overview of study methods This table outlines the disease models, conscious state, oddball conditions, and data analyses used in the three experiments performed in this study.

2.3.1 *Experiment I overview*

Experiment I involved recording cortical electroencephalography (EEG) from the auditory cortex of anaesthetised mice while presenting auditory stimulation paradigms designed to evoke an MMR similar to the human mismatch negativity (MMN) and various control paradigms. Two groups of animals were used; a schizophrenia-related genetically altered *Map2k7^{+/-}* heterozygous (HET) model and a wild-type (WT) control group. Paradigms with auditory stimuli varying in duration, frequency and intensity (sound pressure level; SPL) were explored both in the presence and absence of the NMDA receptor antagonist and psychomimetic drug ketamine which is also used to model aspects of schizophrenia.

The experimental procedure involved firstly anaesthetising the mice, performing surgery to implant recording electrodes into the skull and administering saline before presenting a predetermined sequence of auditory paradigms with stimuli varying in duration, frequency then intensity (in that order) while recording cortical EEG from the auditory cortex, then administering ketamine before repeating the sequence.

2.3.2 *Experiment II overview*

Experiment II was essentially a repetition of Experiment I using conscious animals to investigate the effects of state on the resulting auditory evoked potential (AEP) and MMR waveforms observed. This involved performing aseptic surgery to implant recording electrodes inside the skull and allowing animals to fully recover over five days before making electrophysiological recordings.

In this experiment auditory paradigms with stimuli varying in duration, frequency, and intensity were also explored. One feature of sound was manipulated on each test day after recovery from surgery, presented following physiological saline control and then immediately following ketamine administrations. Mice were given at least 24 hour rest intervals between test days.

2.3.3 *Experiment III overview*

In Experiment III a multichannel silicon probe was acutely implanted into the auditory cortex of anaesthetised mice to record the local field potential (LFP) and neuronal spiking response of regionally located neurons during presentation of auditory stimulation paradigms designed to evoke an MMR and various control paradigms. WT and HET mice were also examined in this experiment. The 32-channel probe comprised two shanks each with 16 linearly spaced electrodes, facilitating recording through layers of the auditory cortex in two spatially discrete cortical columns.

Auditory paradigms in Experiment III mainly investigated the effects of frequency variance and the resulting fMMR; although some paradigms were included to study the effects of stimuli duration and intensity manipulations. Paradigms were presented following physiological saline and ketamine administrations, as in Experiment I and Experiment II, to investigate the effects of NMDA receptor blockade.

2.4 Animal details

Two genetically heterogeneous groups of mice were employed during this research, the details of which follow. Specific group sizes, genders, weights and ages plus additional details are provided in the appropriate subsection for each experiment. Ketamine concentration per administration was also constant, although dosing regimes varied as explained below.

2.4.1 *Map2k7^{+/-} gene disruption*

Map2k7^{+/-} heterozygous (HET) mice and *Map2k7^{+/+}* wild-type (WT) littermates of both sexes were used in this study. The originating colony came from the lab of Professor. J. Penninger (Institute of Molecular Biology of the Austrian Academy of Science, Vienna, Austria) and were bred at the University of Strathclyde Biological Procedures Unit (BPU) on an established back-cross of C57BL/6J. Homozygous knock-out of this gene (*Map2k7^{-/-}*) induces complete pre-weaning mortality, thus the HET gene disruption model is used to study its effects on whole-organism physiology. The colony breeding programme and genotypic characterisation was managed by Rebecca Louise Openshaw, candidate for PhD at University of Glasgow in collaboration with University of Strathclyde under the supervision of Professors Brian Morris and Judith Pratt.

2.4.2 *Ketamine NMDA receptor antagonism*

Mice were administered ketamine to induce NMDA receptor antagonism. This non-selective NMDA receptor antagonist is commonly used in human and animal studies to induce a psychotic state which models some symptomatology of schizophrenia (Section 1.4.2). Here this model was employed to study the effects of acute NMDA receptor blockade on auditory evoked activity and the MMR in mice, and additionally to examine any potential differences between induced electrophysiological changes in HET and WT mice.

Ketamine was administered by the intraperitoneal route at a concentration of 10 mg/kg in solution with sterile saline. This concentration was selected based on published findings showing a significant effect on auditory responses in mice (Connolly et al., 2004, Ehrlichman et al., 2008). In Experiment I and Experiment II the overall solution volume was

2 ml/kg and injected through a 1 ml syringe; thus the volume of physiological saline control administration was also 2 ml/kg. In Experiment III the solution volume was 10 ml/kg, delivered by a flexible plastic tube injector inserted into the intraperitoneal cavity before implanting the multichannel electrode; hence the saline control volume was 10 ml/kg.

Experiment I and Experiment III mice which were under terminal anaesthetic received a single administration of ketamine which followed the saline control session. Experiment II mice received a total of five ketamine administrations, each following a saline control session, with at least one non-test day between each.

The precise neuropharmacology of ketamine during urethane anaesthesia is presently unclear. In a small number of cases combining these two substances with anaesthetic properties did produce adverse depressive effects on respiratory and cardiovascular function resulting in a loss of mice from the study; details of which are provided below.

2.4.3 Experiment I animal details

There were 21 animals originally allocated for use in Experiment I. Four died during surgery leaving a cohort of 17 mice for the experiment; seven HET (three female) and ten WT (five female) aged between 14-17 weeks (mean 15.4). The males weighed from 24.9-32.4g (mean 27.8g) and females weighed from 20.6-22.4g (mean 24.4g). There were no significant differences in age or weight between groups. Following ketamine administration a further three mice were lost from the experiment; one HET female and two WT (one female). Full animal details for Experiment I are provided in Appendix A.

2.4.4 Experiment II animal details

A total of 24 animals were assigned for use in Experiment II and one was lost during surgery resulting in a cohort size of 23; 12 HET (six female) and 11 WT (six female) aged between 29-37 weeks (mean 32.4). The males weighed from 27.4-35g (mean 32.1g) and females weighed from 22.6-25.9g (mean 24g). There were no significant differences in age or weight between groups. A total of four test sessions were performed on all mice in this experiment except from three which only underwent three test sessions; one male WT (pilot) and two females (one HET) which encountered head-mount dislodgement and were immediately euthanized. Legible auditory evoked potentials (AEPs) failed to be elicited from three subjects who were therefore removed from electrophysiological analyses; one WT (male; pilot) and two HET females, leaving two groups of ten animals. Full animal details for Experiment II are provided in Appendix B.

2.4.5 *Experiment III animal details*

In Experiment III 23 mice were initially allocated, two of which were lost during surgery, thus resulting in a cohort size of 21; 12 HET (nine female) and 9 WT (six female) aged between 15-19 weeks (mean 17.1). The males weighed from 25.8-32.5g (mean 29.4g) and females weighed from 15.1-26.6g (mean 23.7g). Again there were no significant differences in age or weight between groups. Five subjects from this cohort were deemed to have clear AEP (two WT and three HET) responses and were used for further analysis. Low conversion rate from animals used to useful data obtained indicates that methodological improvements are needed, as suggested with the concluding remarks in Chapter 5. Full animal details for Experiment III are provided in Appendix C.

2.4.6 *Animal husbandry*

The daily treatment and care of animals in this study conformed to best practice as advised by the UK Home Office. The physiological state and development of an animal is fundamentally influenced by its stress levels. Rodents exposed to psychological stress may produce unexpected variability in their physiology, potentially interfering with the neurophysiological processes under investigation. Reasonable precautions were therefore taken to minimise unnecessary stress by applying current best-practice husbandry guidelines throughout the lifetime of these animals, as described below.

All mice were housed in a well-ventilated atmospherically controlled holding room at 21 °C (± 1 °C), 55 % relative humidity (± 10 %) with a 12 hour light cycle from 0700 to 1900. Standard pelleted rodent chow (CRM; Special Diets Services, Essex, UK) and water were freely available in each home cage. Cages were environmentally enriched with the provision of straw bedding and coloured plastic shelters. Males and females were housed separately and kept within compatible litter groups. Before experiments they were all habituated to the experimenter by handling.

Experiment I and Experiment III mice were housed in groups of two or more in appropriately sized enclosures; at least 24 cm³ for an individual plus 12 cm³ for each additional mouse in the group. For each experiment a mouse was taken from their home cage and underwent surgical and electrophysiological recording procedures, after which they were humanely euthanized by cervical dislocation.

Experiment II mice were housed in pairs inside high-top cages. They were paired up several days before undergoing surgery and placed in these cages specifically to mitigate post-surgical insults from head-mount catching. During recording sessions each mouse was

placed inside a Plexiglas holding tube (10 x 4.4 cm; length x diameter) similar to procedures used in acoustic startle tasks (e.g. Sandner and Canal, 2007). They were introduced to this holding tube over three habituation sessions before beginning recording test sessions which each lasted approximately 90 minutes. Each mouse underwent five recording sessions in total with at least one non-test day between each. This may have inadvertently induced some degree of acute restraint stress (ARS). However the length of exposure, aperture and degree of free movement within the holding tube was considerably less restrictive than in direct models of ARS (Maestroni et al., 1988, Poleszak et al., 2006). The presence of auditory stimulation may also have reduced any associated stress (Sugimoto et al., 2015). Experiment II mice received a chocolate treat (Heinz 4 Month Mum's Own Banana & Chocolate Dessert; H.J. Heinz Foods UK Ltd, Middlesex, UK) following each recording session as a method of positive reinforcement and to counteract this moderately severe treatment.

2.5 Surgical techniques

Stereotactic surgery was performed on all animals in this study to implant recording electrodes. Experiment I and Experiment III surgeries were non-recovery procedures, thus aseptic technique was not essential. However good hygiene practices, clean instruments and drapes etc., were used. Experiment II did require proper aseptic technique because animals were recovered after surgery. The following three subsections provide a detailed description of the surgical procedures conducted in each experiment. It should be noted that there is a degree of crossover between experiments (e.g. Experiment I and Experiment II employed the same electrode configurations, whereas Experiment I and Experiment III used the same anaesthesia protocol) which is highlighted in the text as applicable.

2.5.1 Experiment I: non-recovery

Urethane anaesthesia was used in the non-recovery experiments. Its advantages are that it produces relatively stable cardiorespiratory performance over extended periods (up to eight hours). Its mechanism of action is suggested to “involve multiple neurotransmitter systems in a complex, imprecise manner” (Hara and Harris, 2002). Studies have shown that urethane anaesthesia can alter cortical auditory processing activity (Capsius and Leppelsack, 1996). Nevertheless it has longstanding acceptance and successful widespread application in sensory neurophysiology research using small animals and remains the preferred veterinary anaesthetic for these experiments (Sakata and Harris, 2009, Schumacher et al., 2011, Turner et al., 2005).

Mice received three intra-peritoneal injections of urethane totalling 1.5g/kg in circa 20 minute intervals to induce anaesthesia, with supplementary concentrations of 0.2g/kg given as required to reach the desired state of unconscious. Anaesthetic depth was verified by absent response to painful stimuli (tail and toe pinch) and corneal reflex. When suitably anaesthetised, animals were transferred into a stereotactic frame for rodents (Model 900; David Kopf Instruments, CA, USA) and attached by their incisors to a mouse head-holder adapter (Model 923-B; David Kopf Instruments, CA, USA). Their heads were clamped laterally with non-rupture zygoma ear cups (Model 921; David Kopf Instruments, CA, USA) to secure their skulls whilst avoiding damage to the auditory organs. They were placed on an isothermal heating pad (approx. 35°C) to maintain body temperature during surgery. Their craniums were shaven and hair removal cream (Nair; Church & Dwight Ltd., Kent, UK) was applied to remove any excess fur.

Lidocaine (2 %, 0.1-0.2 ml/kg) was injected subcutaneously beneath the scalp to provide local analgesia at the incision site. This was allowed to take effect over five minutes before invasive surgery began. A scalp incision from rostral to caudal exposed the skull. The wound was held open by retracting the skin laterally using forceps to ensure an unobstructed working view of the skull. Membranous tissue above the skull was removed by scraping with a blunt scalpel before cleaning with 70 % ethanol and drying with compressed air (Dust Remover; RS Components Ltd., Corby, UK).

Cortical EEG electrode implantation sites were mapped out bilaterally above the primary auditory cortices (2.2 mm caudal and 3.8 mm lateral relative to Bregma) on the exposed skull using a stereotactic manipulator. These coordinates were obtained from a standardised C57 mouse brain atlas. Shallow burr holes were then drilled at these sites and skull screw electrodes (1 mm diameter; Royem Scientific Ltd., Luton, UK) implanted, including a single reference placed above the cerebellum aligned to the midline. This protocol will record 'global' activity from a combination of fields in the mouse auditory cortex (Figure 1.7). Trailing electrode wires connected to electrophysiological recording equipment.

Figure 2.1 represents the layout of the skull following completion of this surgery. After surgery Experiment I mice were administered an intraperitoneal injection of physiological saline (2 ml/kg) and moved to Recording Chamber A (Experiment I configuration; Figure 2.4) to commence the recording phase of the experiment.

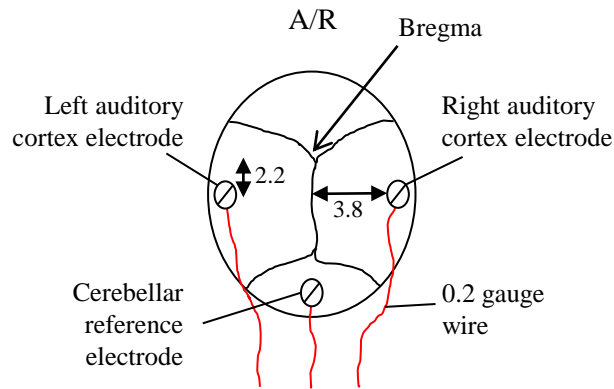


Figure 2.1 - Experiment I electrode implantation surgery This bird's eye representation illustrates skull screw electrodes implanted bilaterally above the primary auditory cortices and a single reference electrode above the cerebellum. Trailing electrode wires were connected to the Intan Technologies electrophysiological recording system.

2.5.2 *Experiment II: aseptic*

Experiment II mice participated in a chronic experiment requiring recovery after-surgery. In order to minimise the potential for post-surgical infection the principles of aseptic technique were strictly adhered to. All instrumentation and surfaces within the surgery room were sterilised and a sterile gown, gloves and face mask were worn by the experimenter.

Isoflurane anaesthesia was used for this procedure, delivered by a vaporizer (Neptune 3; A E Services & Supplies Ltd., Keighley, UK). This provided rapid induction and well-controlled anaesthesia throughout the procedure in addition to a quick post-surgical recovery. Excess anaesthetic gas was scavenged with a Fluovac system (Harvard Apparatus, MA, USA) and charcoal absorber (Cardiff Aldasorber; Pioneer Veterinary Products, Kent, UK).

Anaesthesia was induced by placing mice inside a sealed chamber supplied with 5l/min isoflurane and 1l/min oxygen. When the animal's locomotive behaviour stopped isoflurane concentration was reduced to 2l/min, after which they remained in the induction chamber under constant visual inspection for a further five minutes. They were then transferred to the same stereotactic frame used in Experiment I, with the gas mixture (1l/min O₂: 2l/min isoflurane) delivered via a face mask to maintain anaesthesia. Anaesthetic depth was verified intermittently throughout the procedure in the same manner as Experiment I. Sterile eye ointment (Lacri-lube; Allergan Ltd., Buckinghamshire, UK) was applied to prevent the eyes drying out during surgery. In these recovery experiments additional precautions included cleansing of the surgical area with iodine (Tamodine; Vetark Ltd., Winchester, UK) with subsequent sterile saline rinse and a hydrogen peroxide wash of the open wounds for antisepsis. Surgical implantation of electrodes was performed similarly to Experiment I, although electrode wires were attached to the pins of a 4-way socket connector (SDL-12-G-

10, Samtec, IN, USA) which was positioned centrally on top of the skull. After approximately 30 minutes of anaesthesia the flow rate of isoflurane was reduced to 1.5l/min. Following electrode implantation the attached connector was cemented to the skull using dental acrylic (Simplex Rapid; Associated Dental Products Ltd, Swindon, UK). The implanted electrodes acted as anchor points to effectively glue this connector to the skull. This head-mount provided the interface to electrophysiological recording equipment. Figure 2.2 illustrates the skull configuration following this procedure.

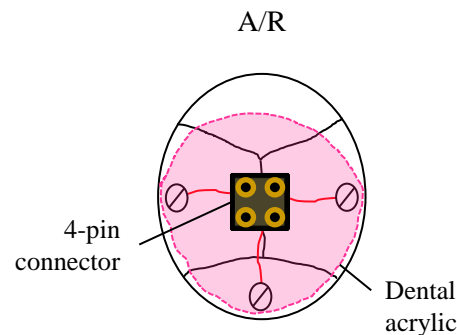


Figure 2.2 - Experiment II electrode implantation surgery Applied dental acrylic covered the implanted electrodes and cemented a 4-pin connector to the skull, with electrodes providing anchorage. A custom adapter interfaced between the head-mounted connector and the Intan Technologies electrophysiological recording system. Animals were left to recover without suturing.

Once the headstage connector was securely fixed to the skull, Carprofen 5 mg/kg was injected subcutaneously in the lateral inferior abdomen for postoperative systemic analgesia and rehydration therapy. The wound was cleaned again with iodine and rinsed with sterile saline before allowing the mouse to recover from anaesthesia. No sutures were inserted and the wound healed without any further interventions.

Appropriate measures were taken throughout this procedure to follow aseptic technique and mice were monitored during recovery for at least five days post-surgery before electrophysiological recordings were made. No postoperative complications were observed. On the contrary, mice displayed remarkable recovery rates, returning to normal behaviours within hours following surgery. Mice were allowed to recover for 5 full days before beginning recordings which also took place in Recording Chamber A (Experiment II configuration; Figure 2.5).

2.5.3 Experiment III: multichannel probe implantation

The anaesthetic and surgical procedure for Experiment III follows the description provided for Experiment I but differs with respect to electrode implantation. The region above the left auditory cortex was plotted (2.2 mm caudal and 4 mm lateral relative to Bregma) using the stereotactic manipulator and an identifying mark was scored on the skull with a pencil. A cerebellar referencing electrode was implanted aligned to the midline, as performed in Experiment I and Experiment II.

The reference electrode was covered with dental acrylic which was used to attach two stacked M2.5 hexagonal nuts which formed an anchor point for the head-fixing assembly. Care was taken not to obstruct the auditory cortex during this part of the procedure. After cementing the head-fixing nut in place a 2x2 mm craniotomy was performed in the dorsolateral direction from the mark identifying the auditory cortex. The exposed cortical tissue was bathed in sterile saline and mice were transferred to Recording Chamber B (Figure 2.7) where a multichannel silicon probe (A2x16-10 mm-50-500-177-A32; NeuroNexus Technologies Inc., MI, USA) was inserted. A description of this chamber follows below. Figure 2.3 represents the condition of the skull following completion of this procedure and illustrates the direction from which the multichannel probe was implanted. The probe implantation procedure is described in Section 2.6.2.

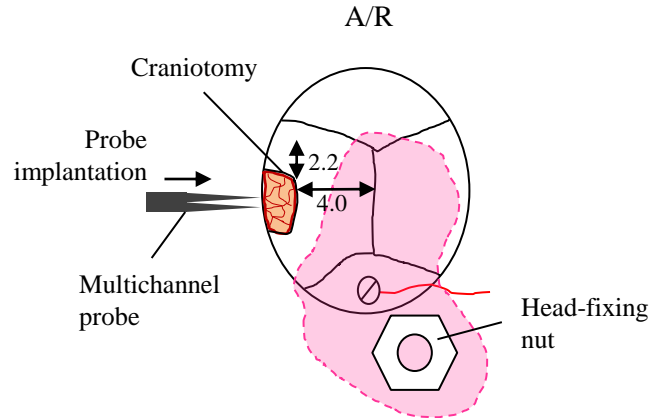


Figure 2.3 - Experiment III electrode implantation surgery A cerebellar referencing electrode was implanted beneath dental acrylic which provided a platform for cementing a head-fixing nut in place for subsequently clamping the head still during recordings. A craniotomy above the left auditory cortex exposed the target tissue for multichannel probe implantation using a motorised stereotactic manipulator.

2.6 Electrophysiological recording setups

Experiments designed to measure electrophysiological responses to auditory stimulation must take place in a precisely controlled environment. Electromagnetic interference (EMI) and background acoustic noise levels within the recording room/chamber must be controlled and ideally kept to a minimum. Visual or olfactory stimulation present which may potentially influence animal behaviour should also be taken into consideration. The following two subsections describe the recording chambers designed to satisfy these criteria and specific configurations for implementing each experiment. The electrophysiological data acquisition systems and key recording parameters are also specified here.

2.6.1 *Recording Chamber A*

A standard acoustic startle sound attenuating cubicle (Med Associates Inc., VT, USA) was retrofitted with EMI shielding and additional soundproofing (Paulstra Snc., Paris, France) to construct a custom recording chamber for Experiment I and Experiment II. An infrared digital video recorder was positioned inside the chamber ceiling to capture behaviour and enable real-time visual observation during experiments. There were no illuminated visible light sources or active olfactory stimulation within the chamber. Off-the-shelf computer speakers (HK19.5; Harman International, CT, USA) with a specified frequency response of 80-20,000 Hz were used to play auditory stimuli. These speakers were calibrated in sound pressure level (SPL) with a digital sound meter (Model 33-2055, Radioshack, TX, USA). Background acoustic noise levels were maintained below 55 dB.

The skull screw electrodes were connected to an amplifier board (RHD2132; Intan Technologies, CA, USA) using a custom adapter. Cortical EEG signals were digitized (1 kS/s) and band-pass filtered (0.1-500 Hz) by the amplifier board before transmission via a serial peripheral interface (SPI) cable to a USB interface board (RHD Evaluation System; Intan Technologies, CA, USA) for acquisition and storage on computer memory. Further filtering and signal processing operations were performed offline as described in Section 2.10. Electrophysiology data and synchronisation signals were viewed in real-time and stored for post hoc analyses using Open Ephys GUI software (open-ephys.org).

Auditory stimulation and synchronisation pulses were generated in Matlab (Mathworks Inc., MA, USA) using custom scripts and output via a USB input/output device (USB-6255; National Instruments, TX, USA). The scripts for performing Experiment I and Experiment II are provided in Appendix E. The synchronisation line was connected to an additional analogue input port on the Intan Technologies USB interface board and sampled simultaneously with electrophysiological data. The auditory stimuli signal line was

connected as audio input to the speaker(s). When sounds were played the synchronisation pulse instantaneously changed state, providing an accurate time-stamp event for analyses.

Specific configurations and additional apparatus used for Experiment I and Experiment II are provided in the appropriate subsection below.

2.6.1.1 Experiment I configuration

Recording Chamber A was configured for Experiment I as illustrated in Figure 2.4. Immediately after surgery mice were placed inside the chamber on an isothermal silicon warming mat. This heat-pad was maintained at approximately 35°C to maintain normal temperature levels throughout the experiment. A single loudspeaker directed auditory stimuli towards the mouse from a front-facing location. This speaker was calibrated at the position of the animal's head. The orientation of the anaesthetised mice relative to the speaker remained constant throughout the recording session.

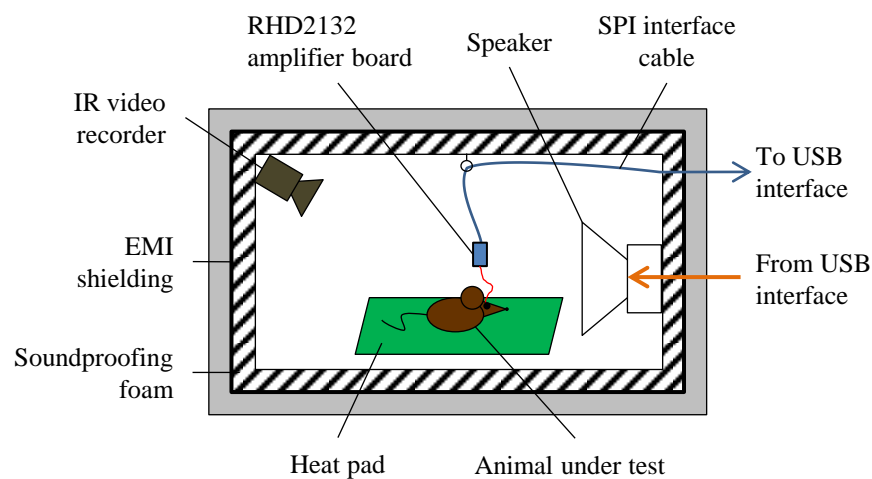


Figure 2.4 - Recording Chamber A: configuration for Experiment I Mice were placed on an isothermal heat pad and received auditory stimulation from a front-facing speaker. Animals were immobile for this experiment thus no additional measures were taken to reduce movement artifacts.

2.6.1.2 Experiment II configuration

Experiment II mice were conscious which presented several additional challenges. Firstly, connecting the amplifier board to the head-mount distresses the animals, potentially inducing physiological changes that may alter auditory processing. This is very difficult to avoid entirely without sedating the animal, which will unequivocally alter its neurophysiology. A firm but gentle approach was taken to mate the amplifier board with the head-mounted connector on conscious mice. The experimenter clasped the scruff of the animal's neck and applied enough downward pressure to hold the head still while attaching the two connectors. This understandably caused some distress, however after release mice appeared to resume

normal behaviour. The same technique was applied to all animals and therefore should not have introduced biases within the study groups.

Performing this experiment in conscious animals also introduced challenges in terms of additional EMI produced by muscular bioelectric sources as well as controlling relative stimuli source location, which itself alters the auditory response. In order to mitigate both of these extraneous movement artifacts a novel approach using a containment tube was developed.

Mice were habituated to a perforated Plexiglas containment tube (10 x 4.4 cm; *length x diameter*) for three consecutive sessions lasting five, fifteen and thirty minutes over three days. They were placed therein and within the recording chamber during test sessions, substantially restricting their movement. Two speakers positioned facing either end of the tube directed audio output in opposite directions. The inclusion of an additional speaker effectively minimised the effect of animal orientation within the tube on the incident stimulus properties; because mice generally orient themselves longitudinally within the tube they will have a noise source from the front and the rear. This method controlled relative stimuli source location without fully head-fixing the animal and also reduced movement-associated EMI.

The average of two speaker calibrations, performed with the sound meter facing either direction, was taken for the overall speaker calibration. Figure 2.5 illustrates the Recording Chamber A setup for Experiment II.

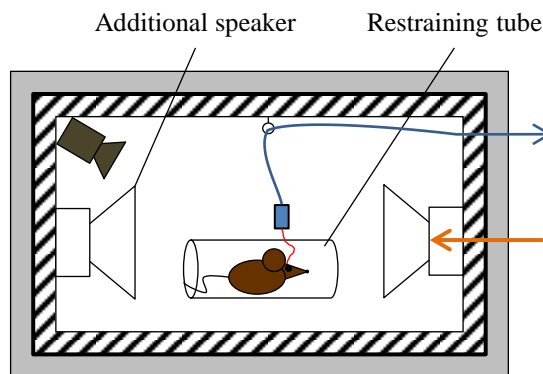


Figure 2.5 - Recording Chamber A: configuration for Experiment II Mice were placed within a containment tube and received simultaneous auditory stimulation symmetrically from front and rear to limit the effect of animal orientation within the tube on the incident stimulus properties. This novel approach was designed to reduce gross movement artifacts observed in conscious freely moving mice.

2.6.2 *Recording Chamber B*

Experiment III mice were immediately placed on top of an isothermal heat-mat inside of a mini acoustical chamber (MAC 3; IAC Acoustics Ltd., Hampshire, UK). They were attached to a head-fixing post with an M2.5 bolt tightened into the head-fixing nut assembly cemented to the skull during surgery. This fixed the head securely in position during the experiment, limiting the potential for cardiorespiratory movements to impose motion artifacts or damage the implanted silicon probe.

Prior to beginning electrophysiological measurements a flexible microtube needle was inserted into the peritoneal cavity to allow ketamine administration midway through the experiment.

A 32-channel dual-shank linear silicon probe (A2x16-10 mm-50-500-177-A32; NeuroNexus Technologies Inc., MI, USA) was implanted at 40° into the cortical surface exposed at the craniotomy site using a motorised stereotactic manipulator (DMA-1511; Narishige Scientific Instrument Lab., Tokyo, Japan). This procedure was carried out in view of a dissection microscope (SZ51 stereo microscope; Olympus Medical, Essex, UK). Probe geometry is provided in the schematic diagram in Figure 2.6; for datasheet specifications see Appendix D. It was slowly advanced (approx. 0.5 µm/s) to a penetration depth of 1 mm below the cortical surface. Mouse cerebral cortex typically reaches a maximum thickness of up to 1.2 mm (Sun and Hevner, 2014) therefore this probe implantation strategy was designed to provide a conductive path through the layered structure of the auditory cortex (Figure 1.8) in two separate cortical columns. Shanks A and B shown in Figure 2.7 were oriented horizontally along the sagittal plane spaced 0.5 mm apart.

A 32-channel amplification system (Headstage J; Plexon Inc., TX, USA) was connected to the multichannel probe via an adapter board and interfaced with a customised data acquisition system (PXI-6255; National Instruments, TX, USA). Wide-band signals from 32 data channels were digitised (20 kS/s), visualised and stored in real-time using custom LabVIEW software (National Instruments, TX, USA). No on-line filtering was performed thus there was an effective bandwidth of 10 kHz.

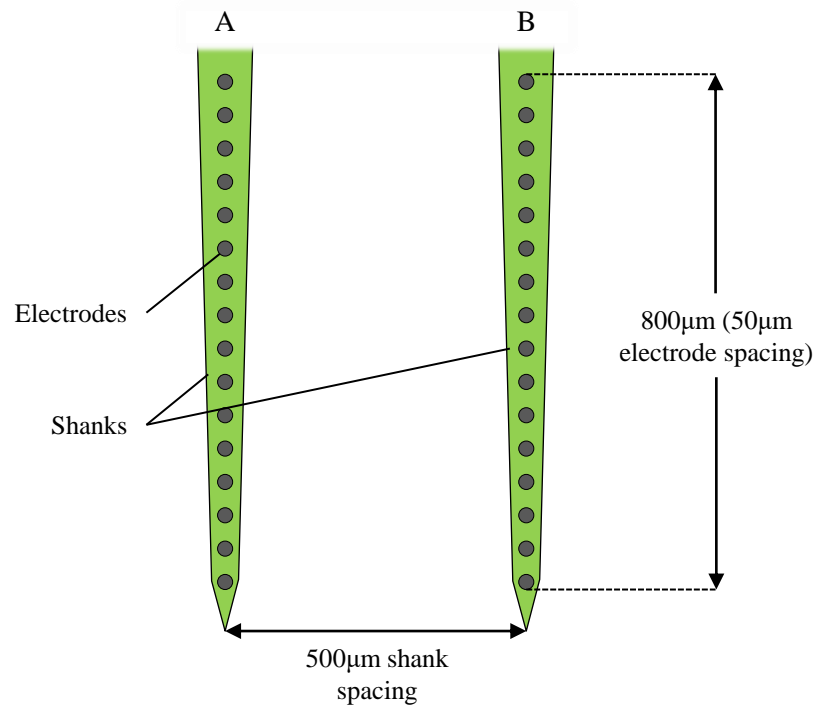


Figure 2.6 - Multichannel probe geometry This 32 channel silicon probe consists of shank A and shank B spaced 500 μm apart, each with 16 linearly spaced electrodes with a separation of 50 μm. This design could effectively measure neural responses across layers of the auditory cortex in two discrete columns. See datasheet excerpt in Appendix D.

Vibration resistant aluminium optical breadboard (973/579-7227; Thorlabs Inc., NJ, USA) provided a base plate for arranging equipment within Recording Chamber B. A real-time auditory processing system (System 3; Tucker Davis Technologies Inc., FL, USA) was used to output auditory stimuli which were generated by one of two methods; 1) for frequency response screening, and 2) for presenting auditory stimuli paradigms. Both of these methods are described in the following subsections.

A free-field electrostatic speaker (ES1; Tucker Davis Technologies Inc., FL, USA) with specified frequency response of 4-110 kHz emitted auditory stimuli. It was calibrated in SPL for pure-tone frequencies of 4-32 kHz at intensities ranging from 0-80 dB using a pressure microphone (PS9200 KIT-1/4, ACO Pacific Inc., CA, USA) positioned in the approximate location of the right ear of the mouse. Figure 2.7 illustrates the Recording Chamber B arrangement for Experiment III.

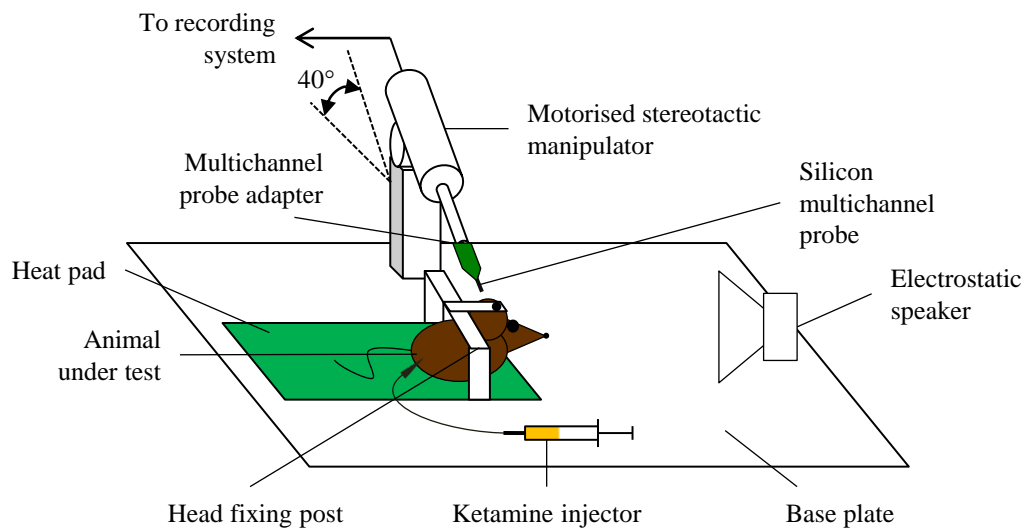


Figure 2.7 - Recording Chamber B: configuration for Experiment III Mice were placed on top of an isothermal heat pad and head-fixed while the multichannel silicon probe was implanted using a motorised stereotactic manipulator. During the experiment ketamine was administered via a syringe with flexible microtube needle inserted before implantation. A front-facing electrostatic speaker directed auditory stimulation towards the ear contralateral to the electrode implantation site. All equipment was securely fastened and grounded to the base plate.

2.6.2.1 Frequency response screening

Frequency response (FR) screening was performed in Experiment III to effectively calibrate the stimuli frequencies used in auditory paradigms to the neural response observed at the electrode recording sites; designed to account for tonotopy, discussed in Section 1.2.2. Various frequency tones were presented and the optimum frequency for eliciting neural activity was determined. This informed the choice of standard frequency to use in the auditory paradigms, from which all other stimuli frequencies were based on predetermined variances. This procedure is described in detail in Section 2.8.3.

For this procedure, stimuli were generated digitally using custom LabVIEW software and a real-time auditory processor (RP2.1; Tucker Davis Technologies Inc., FL, USA) with sampling rate of 96kS/s. Stimuli were then output via a speaker driver (ED1; Tucker Davis Technologies Inc., FL, USA) to the electrostatic speaker positioned inside Recording Chamber B.

2.6.2.2 Auditory paradigm configuration

Auditory paradigm stimuli were generated in Matlab using custom scripts (as in Experiment I and Experiment II) and transmitted via an input/output device (PXI-6221; National Instruments, TX, USA) to the driver and electrostatic speaker positioned inside Recording Chamber B. These scripts are provided in Appendix E.

2.7 Auditory paradigms

The various auditory paradigms (sequences of auditory stimulation) utilised throughout these experiments are described in the following four subsections. Their intended evoked responses are discussed briefly alongside a technical description. Each paradigm was implemented multiple times with stimuli varying specifically in one feature of sound at a time; either in duration, frequency or intensity/SPL. Specific stimulus parameters for the auditory paradigms used in each experiment are provided further on in this chapter (Section 2.8).

2.7.1 *Oddball paradigm: designed to elicit a mismatch response*

The oddball (OD) paradigm was introduced in Chapter 1. It is designed to elicit a mismatch response (MMR) by repeatedly presenting identical *standard* stimuli, forming an echoic sensory-memory trace, which is intermittently interrupted by an infrequent deviant, or *oddball*, stimulus that differs in some physical characteristic. Interpretations of the underlying neurophysiological mechanisms probed by the OD paradigm are discussed at some length in Section 1.2; here it is sufficient to say that the auditory evoked response to standard and oddball stimuli are expected to differ, thereby producing an MMR when the standard and oddball AEP responses are subtracted.

Throughout this study all of the OD paradigms comprised 1000 total stimuli presentations; consisting of 800 standards, 100 increasing-deviant (i.e. either extended duration, ascending frequency or louder intensity) and 100 decreasing-deviant (i.e. either shortened duration, descending frequency or quieter intensity) oddball stimuli with an inter-stimulus interval (ISI) of 450 ms. Therefore this may be referred to as a balanced oddball paradigm (Figure 1.10c). An initial sequence of 20 standards was followed by pseudo-random presentation of either deviant/oddball stimulus, with at least three intervening standards between each. Figure 2.8 illustrates a short segment from the OD paradigm where the deviant/oddball stimulus varies by positive or negative changes either in duration ($\pm\Delta d$), frequency ($\pm\Delta f$) or intensity ($\pm\Delta i$). This is similar to several other paradigms reported in the literature to elicit an MMR in rodents (Nakamura et al., 2011, Ruusuvirta et al., 2007, Umbricht et al., 2005).

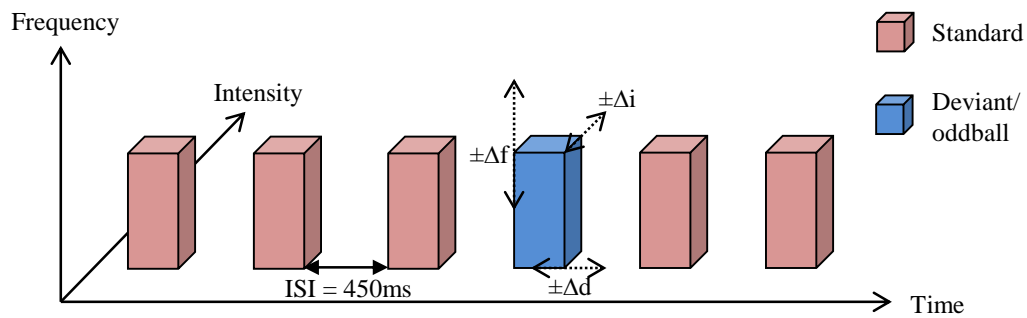


Figure 2.8 - Oddball (OD) paradigm representation This illustration represents a segment from the OD paradigm sequence where a train of identical standard stimuli are interspersed with deviant/oddball stimuli which vary by positive or negative changes either in duration, frequency or intensity.

2.7.2 Consecutive-repetition paradigm: control for adaptation

The consecutive-repetition (CR) paradigm is a sequence designed to generate an un-violated echoic sensory-memory trace to a specific stimulus. The same physical stimuli from the OD paradigm are each repeated 100 times consecutively, with an ISI of 450 ms, followed by a 5s silent period. In this manner, the standard, increasing- and decreasing-deviant oddball stimuli from the OD paradigm are presented 100 times each, sequentially. The CR paradigm is represented diagrammatically in Figure 2.9. The auditory evoked potential (AEP) produced by each stimulus may be thought of as standard-like (Figure 1.10b) because stimulus-specific adaptation/repetition suppression should occur without the presence of an oddball to disrupt the auditory sensory-memory trace.

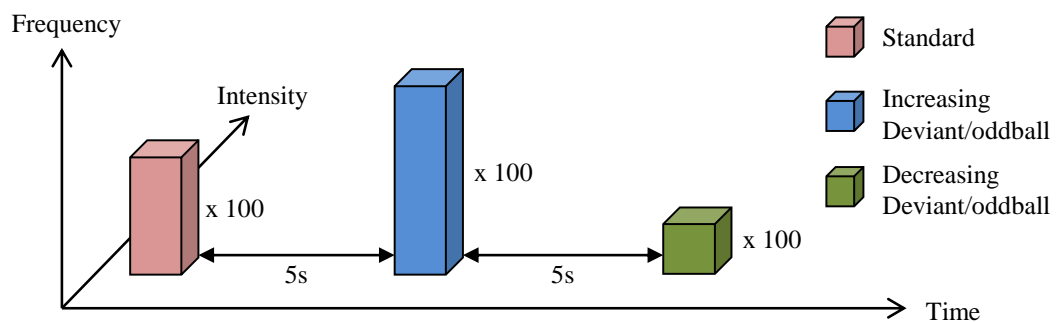


Figure 2.9 - Consecutive-repetition (CR) paradigm representation This example illustration shows the standard followed by an increasing-frequency then decreasing-frequency stimulus. Each are presented 100 times consecutively followed by a five second quiet period. Stimuli varied either in duration, frequency or intensity. Variations of this paradigm were implemented in each experiment.

In Experiment II, after analysing the results from Experiment I, two additional sequences of 100 consecutive stimuli were included at the end of the CR paradigm. Both deviant/oddball stimuli were presented 100 times each consecutively with an ISI of 2s. This addition to the sequence was introduced to investigate the effects of an extended ISI on the resulting AEP waveforms.

In Experiment III another modified version of the CR paradigm was included. This experiment focused mainly on characterising the frequency-deviant induced MMR; however, to observe the effects of altering stimuli duration, frequency and intensity in an abbreviated format, an extended version of the CR paradigm was added to the experimental protocol. This included seven different auditory stimuli which are specified in Table 2.6.

2.7.3 Deviant-alone paradigm: control for sensory-memory disruption

The deviant-alone (DA) paradigm incorporates exactly the same sequence of stimuli as the OD paradigm, with the fundamental difference that standards are silent. Therefore in total 200 stimuli were presented (100 of each deviance-direction oddball) with an inherent minimum ISI greater than 1.8s; i.e. more than four times that used in the OD paradigm because of the three intervening standards criteria mentioned in Section 2.7.1.

DA paradigms emerged in the earliest reports of rodent MMN studies (Ruusuvirta et al., 1998) with the rationale of controlling for tone repetition rate (Tikhonravov et al., 2008); i.e. assuming that neurons exhibit stimulus-selective firing patterns which are tempered by repetitive presentation of the activating stimulus, known as stimulus-specific adaptation/repetition suppression. The DA paradigm presents deviant/oddball stimuli at the same rate as in the OD paradigm, with the intention of dissociating the effect of differing stimulation rates between standard and oddball stimuli from the presence of a true sensory-memory disruption effect. This approach has been criticised for its inherently lengthened ISI and reduced overall stimulation rates which may significantly alter the resulting auditory evoked activity (Nelken and Ulanovsky, 2007). Figure 2.10 illustrates a segment from the duration-varying DA paradigm.

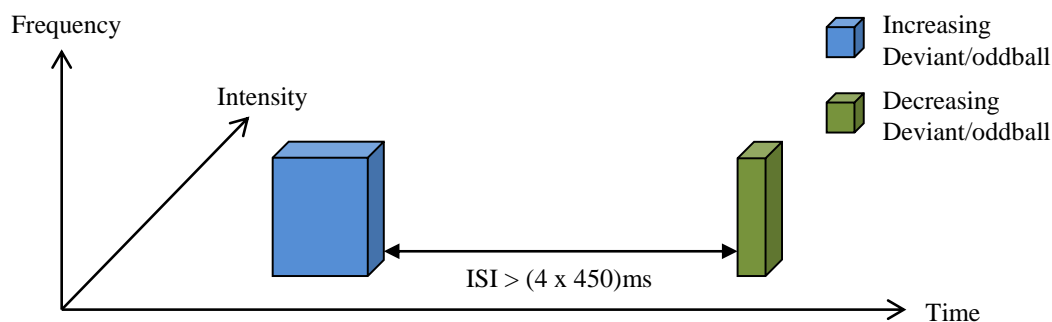


Figure 2.10 - Deviant-alone (DA) paradigm representation This diagram illustrates a pair of deviant/oddball stimuli which alternate between increasing-duration and decreasing-duration, thus this is an example from the duration-varying DA paradigm. The ISI is inherently over four times that of the OD paradigm due to the absence of standard stimuli and the three-intervening-standards rule.

The DA paradigm may alternatively be interpreted as an exaggerated oddball condition. For example, if an MMR occurs due to disruption of auditory sensory-memory then a stimulus presented against a background of relative silence should cause a more pronounced violation of sensory-memory than if preceded by a series of stimuli varying slightly in some physical characteristic. Therefore one may expect to see similar evoked components from oddball and deviant-alone stimuli, although the latter may be of greater magnitude.

2.7.4 *Many-standards paradigm: control for stimuli presentation rate with unpredictable sensory-memory trace*

The many standards (MS) control paradigm was introduced by Jacobsen and Schröger (2001). In this sequence multiple stimuli varying in a single feature of sound (the same property changed in deviant/oddball stimuli) are presented with the same probabilities in random order, without any consecutive repetitions. These stimuli include the standard and both deviant/oddball stimuli from the OD paradigm, presented at the same rate as oddball stimuli. This paradigm presents deviant/oddball stimuli at the same rate as in the OD paradigm, with the same overall stimulation rate, however without a predictable pattern of background stimuli. The MS paradigm is therefore considered to be a more appropriate control than the DA because overall stimuli presentation rate is the same, but there is no reliable auditory sensory-memory trace; therefore perhaps more effectively dissociating these two potential mechanisms of MMR generation.

In this study the MS paradigm comprised 10 different stimuli presented 100 times each with an ISI of 450 ms. This paradigm effectively enabled an assessment of changes to the AEP waveform caused by incremental differences in a single physical property of auditory stimuli, therefore providing insight into neural processing of various physical features of sound. Figure 2.11 illustrates a segment from the frequency-varying MS paradigm, with

shading used to identify each consecutive stimulus frequency as different from its neighbours.

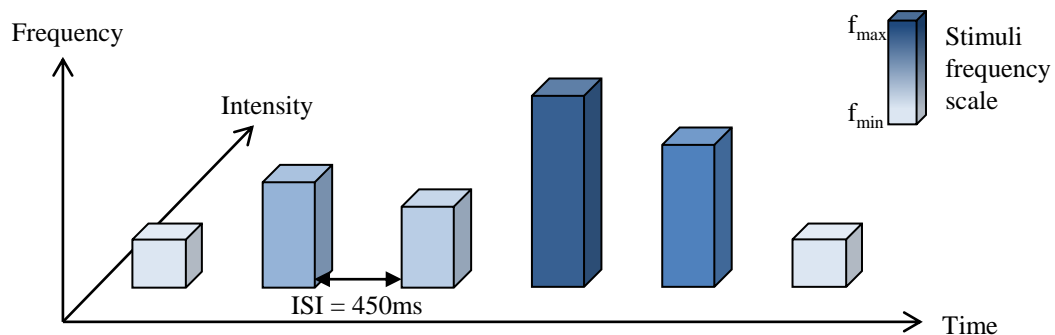


Figure 2.11 - Many-standards (MS) paradigm representation This diagram illustrates a sequence of continually alternating stimuli varying in frequency (along the y-axis) with an ISI equivalent to the OD paradigm. Stimuli physically identical to standards and deviants/oddballs are included in the MS paradigm; presented in an equally-probable context to control for varying stimulation rates, without a reliable pattern of preceding stimuli.

2.8 Auditory stimuli parameters

Auditory stimuli were monophonic pure tones. As mentioned already, paradigms were implemented with stimuli varying in duration, frequency and intensity. Section 2.8.1 and Section 2.8.2 outline the stimulus parameters used in Experiment I and Experiment II, respectively. The frequency response (FR) screening procedure for selecting stimuli frequencies in Experiment III and subsequently updating paradigms is described in Section 2.8.3.

The C57BL/6J laboratory mouse strain is known to exhibit age-related hearing loss, becoming hard of hearing to the frequencies used at ≈ 40 weeks (Ison et al., 2007). All of the standard and deviant/oddball stimuli employed in these experiments are predicted to exceed the audible threshold of mice used in this study, which may be thought of as young to middle-aged adults. Some stimuli in the frequency- and intensity-varying MS paradigms were reaching the boundary of these hearing thresholds and where applicable this is highlighted in the results. The ages of mice used are provided in Section 2.4.3 for Experiment I, Section 2.4.4 for Experiment II and Section 2.4.5 for Experiment III.

2.8.1 Experiment I specifications

To the best of the author's knowledge, Experiment I was the first of its kind to investigate MMR waveforms in urethane-anaesthetised mice. Thus it was exploratory in nature and stimulus parameters were selected based on published studies in rats and conscious mice (Umbricht et al., 2005).

The standard stimulus was constant throughout all paradigms in Experiment I; a 100 ms, 10 kHz, 80 dB sinusoid tone ‘beep’. Deviant/oddball stimuli differed only in the specific feature of sound variance being investigated in a particular paradigm; e.g. in duration-varying paradigms the increasing-deviant oddball stimulus was a 150 ms, 10 kHz, 80 dB tone while the decreasing-deviant oddball stimulus was a 50 ms, 10 kHz, 80 dB tone. All stimuli in Experiment I and Experiment II had instantaneous rise/fall times. The standard stimulus parameters and oddball deviances in either direction for duration, frequency and intensity paradigms are specified in Table 2.2.

Standard	100 ms	10 kHz	80 dB
	Duration	Frequency	Intensity
Oddball Deviance	±50 ms	±2.5 kHz	±10 dB

Table 2.2 - Parameters for oddball (OD), consecutive-repetition (CR) and deviant-alone (DA) paradigm stimuli in Experiment I Parameters for the standard stimulus are given on the top row. For duration, frequency and intensity varying paradigms only said feature of sound is altered in deviant/oddball stimuli; the other two remain identical to the standard.

The same standard, increasing-deviant and decreasing-deviant oddball stimuli parameters were applied throughout OD, CR and DA paradigms, as discussed. They also featured in MS paradigms along with seven additional stimuli, which similarly varied only in a single physical feature of sound. For example, in the frequency-varying MS paradigm there were 10 different frequency stimuli varying from 1.25 kHz to 12.5 kHz in 1.25 kHz increments; this included the 10 kHz standard, 7.5 kHz (lower frequency) oddball and the 12.5 kHz (higher frequency) oddball stimuli, albeit in a different context. Table 2.3 specifies the appropriate variable property of sound for duration-, frequency- and intensity-varying MS paradigm stimuli in Experiment I; other parameters were identical to the standard stimulus.

Stimulus	Duration MS	Frequency MS	Intensity MS
1	50 ms ^{-Odb}	1.25 kHz	60 dB
2	75 ms	2.5 kHz	65 dB
3	100 ms ^{Std}	3.75 kHz	70 dB ^{-Odb}
4	125 ms	5 kHz	75 dB
5	150 ms ^{+Odb}	6.25 kHz	80 dB ^{Std}
6	175 ms	7.5 kHz ^{-Odb}	85 dB
7	200 ms	8.75 kHz	90 dB ^{+Odb}
8	225 ms	10 kHz ^{Std}	95 dB
9	250 ms	11.25 kHz	100 dB
10	275 ms	12.5 kHz ^{+Odb}	105 dB

Table 2.3 - Parameters for many-standards (MS) paradigm stimuli in Experiment I For each version of the MS paradigm stimuli 1-10 vary explicitly in a single feature of sound. Parameters are given in respective columns for stimuli used in each version of the MS paradigm, varying either in duration, frequency or intensity. For each stimulus the other two features of sound were equivalent to the standard parameters (Table 2.2). Standard (Std), increasing (+Odb) and decreasing-deviant oddball (-Odb) stimuli from other paradigms are noted in superscript.

2.8.2 Experiment II specifications

Experiment II stimuli were altered slightly as a result of the findings from Experiment I. Frequency- and intensity-varying paradigms stimuli were reduced to 50 ms duration. This was intended to enable greater visibility of deviance-induced components observed in AEP waveforms from Experiment I. Duration-varying paradigms' stimuli durations remained the same as in Experiment I. Frequency deviant/oddball separation was reduced to ± 2 kHz, decreased from ± 2.5 kHz in Experiment I, for reasons noted below. Stimuli parameters for Experiment II OD, CR and DA paradigms are provided in Table 2.4.

Although duration-varying paradigm stimuli durations were the same, stimulus onset asynchrony (SOA) and ISI parameters were altered. SOA is the time between successive stimuli onsets, whereas ISI is the silent gap between offset of one stimulus and onset of the next. In paradigms using duration varying stimuli there is a trade-off between these two

parameters. A constant SOA condition results in a variable ISI condition, and vice versa. This problem is conceptualised in Figure 2.12.

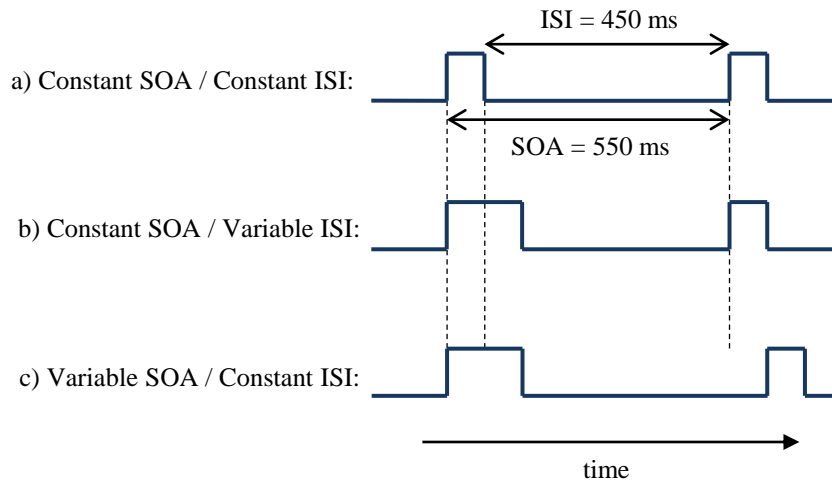


Figure 2.12 - Stimulus onset asynchrony (SOA) and inter-stimulus interval (ISI) trade-off Both SOA and ISI cannot remain constant when employing duration-varying stimuli. Two sets of duration varying paradigms were therefore devised, one with constant SOA (b) and another with constant ISI (c); this additionally facilitated an analysis of varying ISI on evoked auditory activity.

Experiment I duration-varying paradigm data was gathered under a constant ISI scenario.

The results from this initially suggested a constant SOA may be more advantageous for analysing the resulting waveforms which was therefore implemented in Experiment II.

However this introduced effects attributed to the variable ISI (see Section 4.3.1.2). After preliminary analysis of Experiment II duration-varying paradigm data, with a constant SOA condition, an additional iteration of these paradigms with a constant ISI was included.

Therefore in Experiment II there were two versions of duration-varying paradigms; one with a constant SOA of 550 ms and another with constant ISI of 450 ms, illustrated in Figure 2.16.

Standard Duration:	100 ms	50 ms	
Standard Frequency:	10 kHz		
Standard Intensity:	80 dB		
	Duration Paradigms	Frequency Paradigms	Intensity Paradigms
Oddball Deviance	±50 ms	±2 kHz	±10 dB

Table 2.4 - Parameters for oddball (OD), consecutive-repetition (CR) and deviant-alone (DA) paradigm stimuli in Experiment II Standard stimulus duration was reduced to 50 ms for frequency- and intensity-varying paradigms in response to findings from Experiment I. The frequency oddball separation was also reduced to 2 kHz, resulting from narrowing the overall frequency range of stimuli used (see Table 2.5).

Experiment II frequency-varying MS paradigm stimuli ranged from 8-12.5 kHz in 500 Hz increments. This change was made because lower frequency stimuli in Experiment I elicited only a small AEP response, presumably because they were nearing the lower audible frequency range of these mice. Intensity-varying MS paradigm stimuli were also adjusted, ranging from 70-92.5 dB in 2.5 dB increments. This change was made to avoid playing excessively loud noises which may inadvertently damage the auditory organs and cause further distress to conscious animals. Parameters for duration-, frequency- and intensity-varying MS paradigm stimuli are given in Table 2.5.

Stimulus	Duration MS	Frequency MS	Intensity MS
1	50 ms ^{-Odb}	8 kHz ^{-Odb}	70 dB ^{-Odb}
2	75 ms	8.5 kHz	72.5 dB
3	100 ms ^{Std}	9 kHz	75 dB
4	125 ms	9.5 kHz	77.5 dB
5	150 ms ^{+Odb}	10 kHz ^{Std}	80 dB ^{Std}
6	175 ms	10.5 kHz	82.5 dB
7	200 ms	11 kHz	85 dB
8	225 ms	11.5 kHz	87.5 dB
9	250 ms	12 kHz ^{+Odb}	90 dB ^{+Odb}
10	275 ms	12.5 kHz	92.5 dB

Table 2.5 - Parameters for many-standards (MS) paradigm stimuli in Experiment II
Duration MS stimuli parameters were unchanged from Experiment I. The span of frequency stimuli was reduced to remove tones at the lower boundary of the mouse hearing range. The intensity range was also decreased to avoid both damagingly loud and nearing inaudible stimuli. These adjustments were made in light of the results from Experiment I.

2.8.3 *Experiment III specifications*

In Experiment III neural responses were measured at a much finer scale. Unlike Experiment I and Experiment II where the activity of many thousands of neurons was observed in cortical EEG, here the multichannel probe enabled recording signals from individual neurons. Topological frequency-selective maps in the auditory cortex occur at this micro-scale, as discussed in Chapter 1. To address this, a frequency response (FR) screening procedure was conducted after implanting the probe to identify the best frequency (BF) of neurons at the probe electrode sites. The neural response observed at the recording location was then used to determine the stimulus frequencies selected for subsequent auditory paradigms. This experimental approach resembles that taken by Farley et al (2010).

FR screening (Figure 2.13) involved presenting 9 different frequency pure tone auditory stimuli each 50 ms in duration with an ISI of 450 ms. Tones ranging from 2-32 kHz in 4 kHz increments were presented sequentially at 40, 50, 60 and 70 dB. This sequence was repeated 10 times, totalling 360 stimulus presentations. FR screening was repeated three times per animal to confirm the best frequency (BF) and test for reliability. Full details of how the frequency response area (FRA) was calculated are provided in Section 2.10.7. Once determined, the BF was applied to the standard stimulus which also had 50 ms duration and 70 dB intensity. All stimuli in Experiment III had 5 ms cosine ramp rise/fall envelope functions. Frequency OD and DA paradigm deviant/oddball stimuli varied from the standard by ± 3 kHz, whereas stimuli in the MS paradigm ranged from -4 to $+5$ kHz about the BF in 1 kHz increments.

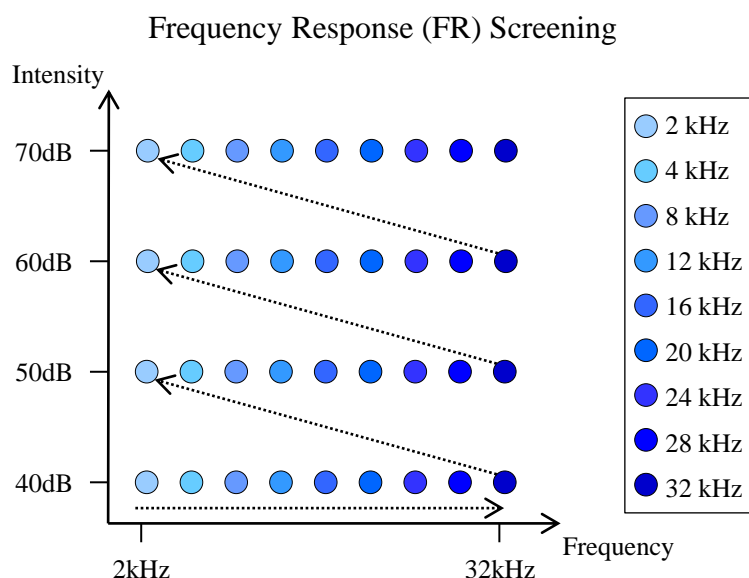


Figure 2.13 - Frequency response screening procedure in Experiment III Nine tones ranging from 2-32 kHz in 4 kHz increments were presented sequentially at 40, 50, 60 then 70 dB. This sequence was repeated 10 times, equalling 360 total stimulus presentations. The neural response to each stimulus was analysed on-line to compute the frequency response area (FRA) and select the best frequency (BF) for use in subsequent paradigms.

Results from Experiment I raised concern over methodological issues surrounding urethane anaesthesia time course and the effect of prolonged exposure on the auditory evoked response (see Figure 3.29, Figure 3.30 and Figure 3.31). This led to focussing investigations on frequency-varying paradigms in Experiment III. However, a modified version of the CR paradigm incorporating 7 physically different stimuli was included to study the effects of stimuli duration-, frequency- and intensity-variations in an abbreviated manner to which was previously conducted. Stimuli parameters for this modified CR paradigm used in Experiment III are provided in Table 2.6. The duration-varying MS paradigm with a constant ISI was also included with the same stimuli parameters as in Experiment I and Experiment II, shown in Table 2.3 and Table 2.5 respectively.

Stimulus	Duration	Frequency	Intensity
1	100 ms	BF	70 dB
2	150 ms	BF	70 dB
3	50 ms	BF	70 dB
4	50 ms	BF+3 kHz	70 dB
5	50 ms	BF-3 kHz	70 dB
6	50 ms	BF	80 dB
7	50 ms	BF	60 dB

Table 2.6 - Parameters for modified consecutive-repetition (CR) paradigm stimuli in Experiment III Stimuli 1-7 listed were each repeated 100 times consecutively, with an ISI of 450 ms, and 5s silence between each. This paradigm enabled an analysis of positive and negative changes in stimuli duration, frequency and intensity.

2.9 Experimental protocols

Paradigms were presented in specific sequences during each experiment. Throughout Experiment I and Experiment III the entire experimental protocol was identical for each animal. In Experiment II, however, the particular feature of sound being varied in paradigms on each test day was counterbalanced; with the exception of the final test session which was the additional set of duration-varying paradigms with constant ISI, as discussed.

Experiment I and Experiment II employed the same paradigm presentation sequence consisting of CR, OD, DA and MS paradigms presented in consecutive order; this sequence is illustrated in Figure 2.14. This paradigm presentation sequence was replicated for stimuli varying in duration, frequency and intensity, as discussed, both in the presence and absence of ketamine. The experimental protocols for Experiment I and Experiment II incorporating this paradigm presentation sequence are described in Section 2.9.1 and Section 2.9.2, respectively. Experiment III utilised a variation of this paradigm sequence, described in Section 2.9.3.

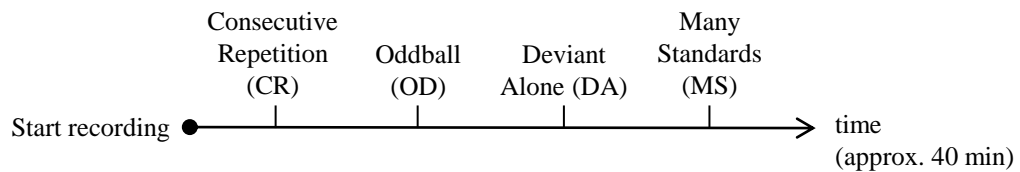


Figure 2.14 - General paradigm sequence for Experiment I and Experiment II This fixed sequence was repeated for stimuli varying in duration, frequency and intensity, following saline and ketamine administrations. Thus each animal was exposed to a minimum of six repetitions of this sequence.

2.9.1 Experiment I protocol

The entire recording protocol and paradigm sequence implemented in Experiment I is shown in Figure 2.15. This remained constant for all animals making cross-group comparisons valid. This assumption would not hold true if the *Map2k7* gene mutation altered the physiological action of urethane; although currently there is no data indicating that this may be the case. The strict ordering of paradigms across subjects also enables a longitudinal examination of the resulting auditory evoked activity.

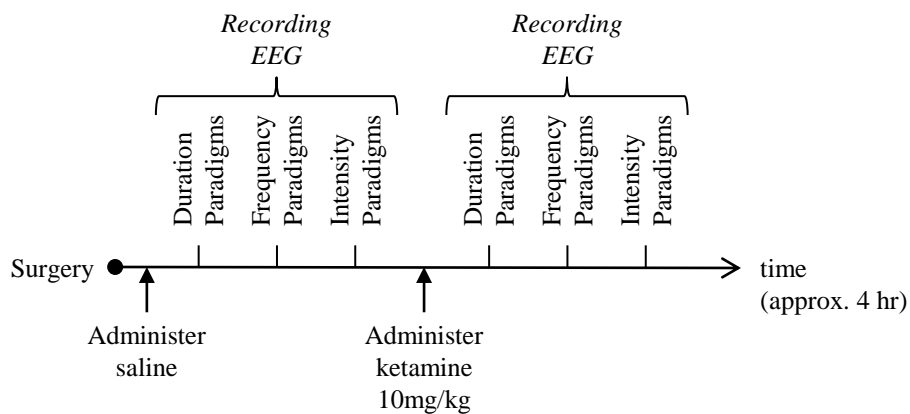


Figure 2.15 - Recording and auditory stimulation protocol for Experiment I The general paradigm sequence (Figure 2.14) was presented with stimuli varying in duration, frequency then intensity; first after a saline control injection and then again after administering ketamine. The entire recording protocol lasted approximately four hours, during which animals were continuously under urethane anaesthesia.

The precise pharmacodynamics of ketamine during urethane anaesthesia are unclear. The usual time-course of behavioural and neurophysiological changes attributed to ketamine may potentially be altered during this state. As mentioned in Section 2.4.2, combining these two anaesthetic agents did have adverse effects, resulting in loss of mice from Experiment I and Experiment III; highlighted in the Section 2.4.3 and Section 2.4.5, respectively.

2.9.2 Experiment II protocol

Experiment II mice recovered for five days post-surgery before recording sessions began. A single physical feature of sound was investigated on each test day. Paradigm sequences (Figure 2.14) were presented twice for the property of sound being varied, firstly after saline and then following ketamine injections. Mice rested for at least 24 hours between recording sessions.

Duration- (with constant SOA), frequency- and intensity-varying paradigms were counter-balanced over test days 6-10 after surgery. This sequence is represented in Figure 2.16.

Duration-varying paradigms with constant ISI, as implemented in Experiment I, were presented after preliminary analysis revealed the effect of maintaining a static SOA, which inherently altered the ISI (Figure 2.12). These results are discussed in Chapter 4.

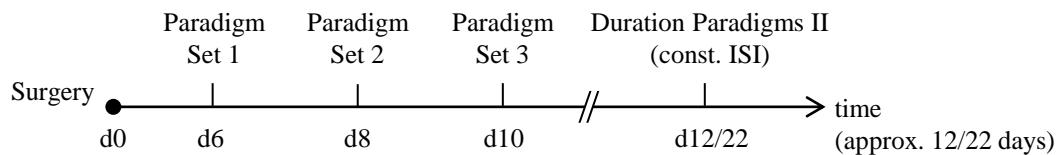


Figure 2.16 - Order of test sessions in Experiment II Paradigm sets 1-3 comprised the general paradigm sequence (Figure 2.14) presented with stimuli varying either in duration with constant stimulus onset asynchrony (SOA), frequency or intensity, firstly after saline and then after ketamine administrations. The feature of sound being varied in each paradigm set was counter-balanced across animals. The final paradigm set, Duration Paradigms II, applied variable stimuli durations with a constant inter-stimulus interval (ISI).

Mice underwent surgery and the first three test sessions in two groups, thus duration paradigms with a constant ISI were presented either on day 22 or 12 for the first or second surgery group, respectively. This occurred due to the initially unplanned inclusion of the final paradigm set.

2.9.3 Experiment III protocol

The experimental protocol and sequence of paradigms presented in Experiment III is illustrated in Figure 2.17. This began with a modified version of the CR paradigm which included the standard stimulus, plus frequency (± 3 kHz), duration (± 50 ms) and intensity (± 10 dB) varying stimulus pairs. Thus in the modified CR paradigm of Experiment III there were 7 different stimuli (Table 2.6), each presented 100 times, with an ISI of 450 ms.

This was carried out to study the effects of altering these features of sound in an uninterrupted sequence of identical stimuli. The duration MS paradigm implemented with a constant ISI, as in Experiment I and at the end of Experiment II, was then presented to investigate the effects of graded stimulus duration changes on laminar neural activity. Frequency OD, DA and MS paradigms were then presented in sequential order before and after administering ketamine and repeating.

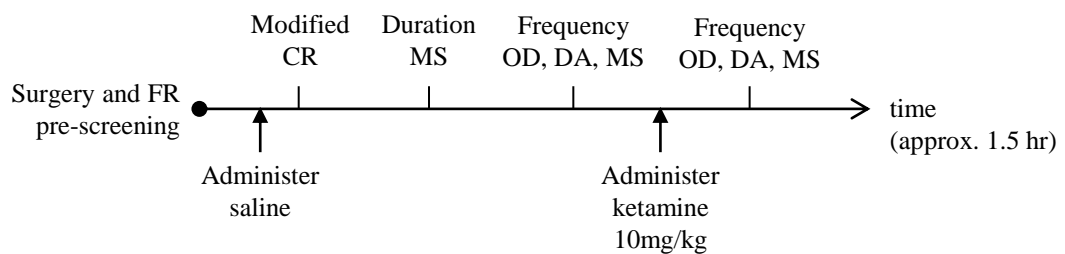


Figure 2.17 - Recording and auditory stimulation protocol for Experiment III Following multichannel electrode implantation and frequency response (FR) screening, animals were administered saline and presented with the modified CR and duration MS paradigms. Then an abbreviated set of frequency-varying paradigms (excluding CR) were presented before and after injecting ketamine. Throughout this protocol animals were continuously under urethane anaesthesia.

2.10 Data Analyses

Several methods of data analysis were applied throughout this study. Cortical EEG recorded from the primary auditory cortices during Experiment I and Experiment II and inter-laminar local field potential (LFP) and neural spike recordings from Experiment III were analysed. Electrophysiological data were characterised with time, frequency and time-frequency domain measures. Video footage of conscious animals in Experiment II was also analysed to quantify movement within the recording chamber during test sessions. The remainder of this chapter is dedicated to presenting these analytical methods, with further details provided in the relevant sections of Chapter 3, Chapter 4 and Chapter 5.

2.10.1 Auditory evoked potentials

The event-related potential (ERP) technique was applied to compute the auditory-evoked potential (AEP) generated by each stimulus type in the various auditory paradigms and compare features of interest. This is a well-established method for extracting information from human EEG recordings, which typically have a very small signal-to-noise ratio (SNR). The book by Steven J. Luck (2014) describes this technique in detail. The EEG response that is time-locked to the auditory stimulus is effectively isolated from non-phase-locked activity through a process of averaging. Data recorded during each stimulus presentation are segmented with respect to a trigger event (e.g. stimulus onset), then averaged together after removing artifacts. This method was implemented with the open-source Matlab toolbox, EEGLab (Delorme and Makeig, 2004), and its associated plug-in, ERPLab (Lopez-Calderon and Luck, 2014).

In general, cortical EEG or LFP data were segmented into epochs ranging from 100 ms pre-stimulus to 450 ms post-stimulus onset. Pre-stimulus baseline correction was applied to remove non-stimulus related amplitude offsets. For certain stimulus types (e.g. deviant-alone paradigm stimuli in Experiment I), epoch duration was increased up to 1000 ms post-stimulus onset to analyse extended latency activity; this is clear from figures where extended epochs are analysed.

Data segments containing non-physiological artifacts exceeding amplitude thresholds of $\pm 500 \mu\text{V}$ were automatically discarded. Specific artifact rejection rates for Experiment I and Experiment II are provided in the methods sections of Chapter 3 and Chapter 4, respectively. Artifact rejection was not performed on LFP recordings from Experiment III, as explained in the methods section of Chapter 5. The remaining segments were then averaged together to produce the AEP. This method was applied to generate the AEP from each animal subject to each of the auditory stimuli presented in each paradigm.

The *Map2k7^{+/+}* (WT) and *Map2k7^{+/-}* (HET) group grand-average AEPs were then computed to identify and compare features of interest. A zero-phase 8th order low-pass Butterworth filter with cut-off frequency of 100 Hz was typically applied to remove high-frequency interference. Slow-wave potentials, or extended-latency waveforms, were filtered with a 30 Hz corner frequency; this is indicated in the applicable figures.

In analysis of oddball (OD) paradigm data only standard stimuli presented immediately before deviant/oddball stimuli were included in the standard AEP computation, balancing the overall standard-to-oddball ratio. In other paradigms (CR, DA and MS) all stimuli presented were included in the generation of their respective AEP waveforms. Various computations were performed on AEPs from different paradigms (e.g. subtracting standard from deviant/oddball AEPs to generate the MMR) which are explained in the appropriate methods sections of Chapter 3, Chapter 4 and Chapter 5.

2.10.1.1 Peak amplitude

Peak amplitude measurements are one of the fundamental tools for characterising AEP waveforms. This reflects the magnitude of synchronised electrophysiological activity in the recorded EEG/LFP; depending largely upon the orientation and topographic location of underlying neural generators in relation to recording and reference electrodes.

Specific features of the AEP were visually identified from grand-averages, and suitable measurement windows selected for analysis. The peak amplitude within a defined measurement window was taken from each individual animal's AEP. These were then compared using statistical tests, as described in Section 2.10.8, to quantify any effect of genotype, gender, ketamine administration, stimulus type, etc.

In some instances mean amplitude over an extended measurement window was used to quantify AEP features of interest. This was typically applied to measure slow amplitude changes. Mean amplitude is less susceptible to distortion from transient peaks, and is therefore more suitable than peak amplitude for measuring slow wave activity (Luck, 2014). Specific AEP features and the parameters applied to quantify their amplitude are described in the relevant methods and results sections of Chapter 3, Chapter 4 and Chapter 5.

2.10.1.2 Peak latency

Time to peak, referred to as peak latency, is another fundamental metric used to characterise AEP waveforms. This measurement may be used to assess pathway conduction and elements related to the speed of gross neurological processing. However, the latency of a peak visible in the AEP may be arbitrary; e.g. when multiple components/generators interact to produce a peak. Differences in peak latency between groups or conditions may infer altered speed of processing; however, caution is warranted against misinterpreting this information (Luck, 2014). Measurement windows were also applied when quantifying peak latencies, as described in the applicable methods and results sections of Chapter 3, Chapter 4 and Chapter 5.

2.10.1.3 Rectified Area

Rectified area (RA) is the numerical integration of a time-varying signal over time, which effectively quantifies the 'area under the curve'. This is useful for comparing response magnitudes, regardless of polarity. This method of quantification was applied to MMR waveforms observed from Experiment II, detailed in Chapter 4.

2.10.2 Spectral analyses

To quantify any neural oscillations in EEG recordings made throughout this study, these time-domain signals were converted into the frequency- and time-frequency domains for analysis. Power spectra were computed to quantify frequency-domain properties of electrophysiology data, while event-related spectral perturbation (ERSP) was computed to investigate the evoked time-frequency domain response. Both of these analyses were supported by the EEGLab toolbox for analysing electrophysiological data (Delorme and Makeig, 2004) within the MATLAB programming environment.

2.10.2.1 Power spectrum

Power spectra were computed with the fast Fourier transform method (Welch, 1967). This was performed on EEG data segmented from 100 ms pre-stimulus to 450 ms post-stimulus, therefore may also be termed the evoked EEG power spectrum. Plotted as power in decibels (dB), i.e. $10 \cdot \text{Log}_{10}(\mu\text{V}^2)$, calculated from 2-100 Hz with 2 Hz spectral resolution, this frequency-domain analysis is used to assess the effects of genotype and ketamine in urethane-anaesthetised (Section 3.3.5) and conscious mice (Section 4.3.4).

2.10.2.2 Event-related spectral perturbation

The event-related spectral perturbation (ERSP) technique developed by Makeig (1993) was used to analyse the spectral dynamics of EEG recorded in response to, but not necessarily phase-locked to auditory stimuli. Analysing the change in time-frequency components of these signals provides more information than otherwise available through time-domain measures alone and may potentially aid our understanding of the underlying neural generators.

The following formula from Delorme and Makeig (2004) describes how ERSP is calculated:

$$ERSP(f, t) = \frac{1}{n} \sum_{k=1}^n |F_k(f, t)|^2 \quad (1)$$

Where n is the number of trials, k is the current trial, and $F_k(f, t)$ is the spectral estimate of trial k at frequency f and time t . The discrete Fourier transform (DFT) method was used to calculate spectral estimate over linearly spaced frequencies from 2-500 Hz in 2 Hz increments across each stimulus trial in overlapping time windows, relative to a 100 ms pre-stimulus baseline. These are then averaged together to produce the ERSP, plotted with time on the x-axis, frequency on the y-axis and each pixel displaying the power in decibels (dB). This analysis was performed on data from urethane-anaesthetised (Figure 3.33) and conscious mice (Figure 4.29) during saline and 10 mg/kg i.p. ketamine trials.

2.10.3 Video footage

Conscious animals were used in Experiment II, presenting additional challenges arising from their motor activity. The behaviour of mice inside Recording Chamber A was captured in real-time using an infrared video camera positioned inside the ceiling of the chamber. This allowed the experimenter to check the status of mice during test sessions and also enabled a post-hoc analysis of movement within the chamber. Video footage was captured at 7.5 frames per second in a 160 by 120 pixel RGB (red/green/blue) colour format. These films were not synchronised to auditory stimuli so stimulus-locked movement artifacts were not directly quantified. The videos were deconstructed into a series of grey-scale images representing each frame. Gross motion over time was approximated using a block-matching algorithm with exhaustive search which compared consecutive images in the film for changes in 5 by 5 pixel block locations and returned the optical flow matrix. The average value from each of these 160 by 120 matrices was taken as the mean optical flow (MOF), providing an estimation of motion over time. This analysis was performed using the computer vision system toolbox in Matlab. Movement detected using these parameters could only have been generated by the animal being observed within the recording chamber. Gross motion data averaged across 5 min bins were used to explore ketamine, genotype and gender effects.

By analysing the frequency content in raw gross motion data an attempt was made to infer the presence of auditory stimuli-induced movement artifacts. In CR, OD and MS paradigms stimuli were presented at approximately 2 Hz therefore increased motion vectors occurring at the same frequency may reasonably be assumed to result from the presentation of stimuli. This is a relatively crude method of analysing auditory stimuli-induced movement artifacts and proved inconclusive. Preferable video footage will have been synchronised with neural recordings and electromyography (EMG) from the head of each mouse; this approach is recommended as a potential development for future studies in Chapter 6.

2.10.4 Local field potentials

The local field potential (LFP) is an electric field measured in the extracellular space of neural tissue by an implanted microelectrode. These are generally dominated by postsynaptic potentials of nearby synapses, although all ionic current flows in the extracellular space are thought to contribute to the superposition of the LFP (Buzsáki et al., 2012). The LFP frequency range is typically the same as EEG, with observed oscillations of up to approximately 500 Hz (Einevoll et al., 2013).

LFPs were recorded from the 32 channel two-shank multichannel probe in Experiment III. The ERP technique was applied to LFP recordings to compute and analyse the AEP, as described in Section 2.10.1 above. This approach enabled a comparison of deep/distal and superficial/proximal layer/channel auditory evoked responses in the LFP (e.g. Figure 5.9).

2.10.5 Current source density

The current source density (CSD) technique defined by Nicholson and Freeman (1975) was applied to depth electrode recordings from Experiment III (Section 5.2.4). Current sources are generated by an efflux of ionic current from within a neuron into the extracellular space, whereas a current sink is the opposite, an influx of ionic current from the extracellular space into a cell. The synchronised activity of these current sources and sinks generate net potential differences between regions of the extracellular space, measured in the LFP. This analysis was performed on each 16-channel shank of the multichannel probe separately. First LFP recordings were spatially filtered, meaning neighbouring channels were averaged together and smoothed to remove spatial noise, which effectively reduces the number of channels by two by removing the first and last electrodes on each shank:

$$\varphi(r) = \frac{1}{4}(\varphi(r+h) + 2\varphi(r) + \varphi(r-h)) \quad (2)$$

Where $\varphi(r)$ is the LFP at depth r , and h is the distance between electrodes, which was 50 μm . The second derivative of (2) is then taken to calculate the CSD estimate between each pair of channels, where positive values are considered to reflect current sinks and negative values are considered to reflect current sources:

$$CSD = \frac{1}{h^2}(\varphi(r+h) - 2\varphi(r) + \varphi(r-h)) \quad (3)$$

CSD analysis is widely applied in *in-vivo* neurophysiology experiments to estimate the depth of recording electrodes implanted into the rodent auditory cortex (Sakata and Harris, 2009, Szymanski et al., 2009, Sakata, 2016). During auditory stimulation the approximate depth of the main thalamic recipient layer (LIII/IV) is obtained by determining the maximum sink channel. This provides a reference point for estimating individual channel depths in relation to the layered cortical structure. Using this method, recordings from multiple animals can theoretically be aligned to a common reference point, enabling an analysis of group laminar-specific effects. CSD analysis was applied to data from Experiment III; however, mixed results prevented a confident alignment of data (Table 5.1), for which possible reasons are explored in Section 5.4.4.

2.10.6 Spike activity

The term spike refers to an extracellular recording of neural action potential. These were extracted from multichannel probe data sampled at 20 kS/s in Experiment III. Automatic spike detection and classification was performed with the Python-based Klusta (<http://klusta-team.github.io/>) suite of programs, which are specifically designed for electrophysiological data acquired with multichannel electrode arrays (Rossant et al., 2016).

Broadband signals were filtered with a 500 Hz cut-off frequency high-pass filter and an anti-aliasing low-pass filter with a 9.5 kHz cut-off frequency; both 3rd order Butterworth zero-phase shift frequency response digital filters. This removed the lower frequency LFP signal. A double-threshold is applied to detect spikes, with an upper threshold equal to 4 times and lower threshold equal to 2 times the standard deviation of the filtered signal. This is combined with geometric information about the probe and electrode connections to classify spikes which occur in spatially discrete locations, but may overlap temporally. This method is said to reduce the potential for misclassification of noise artifacts as spikes.

Following threshold spike detection individual spike waveforms are aligned at a common time point and characterised by a three feature principle component analysis (PCA), referred to as a feature vector. A feature mask is then produced using peak amplitude information from each channel. These feature vectors and feature masks are then used in clustering, in which spike waveforms with shared features are automatically classified. Finally, using a graphical user-interface the investigator manually checked output from the algorithm to remove any misclassified noise artifacts. These algorithms are described in detail in the paper by Rossant et al. (2016).

Single-unit activity (SUA) refers to spikes measured from an individual cell, classified by the measured waveform shape and spatiotemporal relationship with recording electrodes. SUA may be used to characterise the function of individual neurons under experimental conditions. Multi-unit activity (MUA) is the term which describes gross spiking activity from a group of recorded cells. MUA therefore provides an overview of neural activity, whereas SUA provides information about the function of a single cell, during the experiment. An analysis of spiking activity from Experiment III is provided in Section 5.3.4.

2.10.7 Frequency response area

Frequency response area (FRA) is a metric for analysing the frequency sensitivity of auditory neurons at a particular recording site. The FRA is typically derived from a situation where multiple frequency tones are presented at multiple intensities (e.g. Figure 2.13). The average gross neural spike rate (i.e. multi-unit activity; MUA) is calculated for each stimuli and a three-dimensional plot generated with frequency on the x-axis, intensity on the y-axis and a colour-coded scale representing the mean spike rate at each frequency and intensity coordinate.

Electrophysiology data recorded during the FR screening procedure (Section 2.8.3) was first band-pass filtered between 500-9500 Hz to remove any LFP oscillations. MUA during each stimulus presentation was approximated by applying a $-150 \mu\text{V}$ amplitude threshold criterion. Spikes exceeding this threshold during stimulus presentation counted towards the mean spike rate for computing the FRA. Tone frequencies eliciting greatest overall firing rates across all sound intensities were then calculated.

FRA was computed separately for each 16-channel shank, with the expectation that cortical tonotopy may introduce variation between them (500 μm separation). However, the whole-probe FRA was used to select the best frequency (BF) that was subsequently applied as the standard frequency in auditory paradigms. Examples of FRA plots obtained from multichannel silicon probes in Experiment III are provided in Figure 5.3.

2.10.8 Statistics

IBM SPSS Statistics 22 software was used to perform statistical analysis of ERP measures. Amplitude or latency measurements were taken from one or more AEP waveforms of each individual subject and inserted into a database including their gender and genotype. Repeated measures analysis of variance (ANOVA) was generally performed on a particular measure, with *genotype* and *gender* as between-subjects factors and *stimulus type* and *ketamine treatment* as within-subjects factors. Specific details of tests applied are described in the appropriate results sections. The statistics and machine learning toolbox in Matlab was also used to perform t-tests on data (Figure 5.9), and statistical tests were also performed using EEGLab. Bonferroni adjustment of the alpha value was used to correct for multiple comparisons; noted in the respective results sections where this applies.

Chapter 3. Experiment I: evaluation of multivariate auditory paradigms in urethane-anaesthetised wild-type and *Map2k7*^{+/-} mice exposed to ketamine

3.1 Introduction

Experiment I fundamentally aims to determine the existence and characteristics of the mismatch response (MMR) to different physical features of auditory stimuli (duration, frequency and intensity) in urethane-anaesthetised mice. To the best of the Author's knowledge there are no current publications of such studies in urethane-anaesthetised mice, although there are several involving other rodent species; these are reviewed below. According to the aims of this thesis outlined in Section 1.5, both genetic (*Map2k7^{+/-}*) and pharmacological (ketamine) mouse models relevant to schizophrenia were examined for any alterations in the resulting auditory evoked potential (AEP) waveforms and MMR compared with controls. This is the first in a series of experiments discussed throughout this thesis and provides an initial evidence base (in addition to the reviewed literature) upon which subsequent experiments seek to elaborate.

3.1.1 Previous MMR studies in anaesthetised rodents

The body of literature addressing animal mismatch responses (e.g. see mouse and rat studies in Table 1.2) is somewhat smaller than that of the human mismatch negativity (MMN) reviewed in Section 1.2. Nevertheless, research publications pertaining to the search for an analogous mismatch negativity-like (MMN-like), or more directly an MMR, in rodent models are summarised below in three subsections; individually addressing duration, frequency, and intensity. The majority of MMN research in anaesthetised rodents has focussed on rats and reviewing the literature revealed a lack of studies in anaesthetised mice, thus the following introduction mainly concerns findings from anaesthetised rats.

3.1.1.1 Duration

There have been a small number of published research articles investigating duration oddball paradigms in anaesthetised animals, specifically in guinea pigs (Okazaki et al., 2006) and rats (Nakamura et al., 2011, Ruusuvirta et al., 2013). There have also been studies in conscious animals which will be discussed in Chapter 4 (Experiment II). In each of these investigations different anaesthetic substances were used; for instance, sevoflurane (Okazaki et al., 2006), fentanyl/medetomidine (Nakamura et al., 2011), and urethane (Ruusuvirta et al., 2013). These may feasibly alter the auditory system in different respects, for instance through their complex actions on different neurotransmitter systems which may be involved in sensory-cognitive processes (Rojas et al., 2006, Cederholm et al., 2012), obscuring direct comparisons of results. In all of these experiments epidural EEG recordings were made from the primary auditory cortex with a reference electrode placed above the contralateral

cerebellar cortex. However, different variations of the oddball paradigm were applied in each, again confounding interpretation of cross-study comparisons.

Okazaki et al. (2006) demonstrated that oddball stimuli varying in duration generally elicit a different AEP than that of standard duration stimuli. The authors suggest that this may reflect change detection in the brain, implying the involvement of cognitive functions.

Unfortunately, there were insufficient control paradigms to dissociate this proposed sensory-memory/cognitive aspect of MMR generation from normal processing of two physically distinct auditory stimuli. Various controls have since been developed in more recent studies which aim to dissociate between ordinary processing (without a prominent sensory-memory/cognitive component) of auditory stimulation and a true sensory-memory disruption response (Harms et al., 2014). In an attempt to avoid this situation and clarify the oddball effect, consecutive-repetition (Section 2.7.2), deviant-alone (Section 2.7.3), and many-standards (Section 2.7.4) control paradigms introduced in Section 1.3.1.1 are used throughout this thesis. Additionally, both increasing and decreasing duration oddball stimuli are incorporated into a 'balanced' oddball paradigm. In their discussions, Okazaki et al. (2006) emphasise the need to address mismatch responses to different physical features of sound individually to gain a better understanding of the underlying neurophysiology, as these may rely upon separate, combined, or a mixture of neuronal mechanisms. This is an insightful recommendation considering that the rat auditory cortex is now known to be anatomically and functionally specialised for processing different physical properties of sound, with distinct regions have been associated with duration, frequency and intensity tuning by Polley et al. (2007).

In the study by Nakamura et al. (2011) offset potentials were observed from anaesthetised rats but not when they were conscious. Termination of stimuli elicited positive amplitude deflections of opposite polarity to the negative amplitude onset response. This finding may point towards a feature of the AEP which could potentially influence the traditional duration mismatch response; i.e. the difference between AEPs from standard and oddball stimuli of different durations. However, these features are not quantified in this paper, and in its concluding analysis both frequency and duration oddball AEPs are averaged together and measured as a single entity. This is in contrast to previous recommendations which stated the need to treat mismatch responses arising from variations in different physical features of sound separately (Okazaki et al., 2006). Hence throughout this thesis duration, frequency and intensity effects are each addressed individually.

3.1.1.2 Frequency

Tone frequency is by far the most widely studied elicitor of mismatch responses in anaesthetised rodents, with several studies publishing evidence of a fMMR to frequency oddball paradigms (Ruusuvirta et al., 1998, Tikhonravov et al., 2008, Tikhonravov et al., 2010, Astikainen et al., 2011, Nakamura et al., 2011, Shiramatsu et al., 2013, Ruusuvirta et al., 2015). These papers all reported to show an MMN-like response of some description from anaesthetised rats.

Two publications reported negative findings; i.e. no evidence of MMN-like responses (Lazar and Metherate, 2003, Eriksson and Villa, 2005). Eriksson and Villa (2005) used a mixture of ketamine and xylazine hydrochloride to anaesthetise two rats in their study. However, the human MMN is attenuated following NMDA receptor blockade (as discussed in Section 1.2) and therefore the absence of an MMR may be explained by the administration of ketamine as an anaesthetic. Lazar and Metherate (2003), on the other hand, used a constant frequency oddball stimulus of 10 kHz and applied different standard frequency stimuli of 9.75/9.5/9/5/2.5/1.25 kHz in six separate oddball paradigms. Standard frequencies close to the oddball (9.75/9.5/9 kHz) were found to diminish the oddball AEP, while more distant standard frequencies caused the oddball AEP to be greater. These paradigms are unbalanced, because the oddball is always of higher frequency than the standard, therefore perhaps not sufficiently controlled. The authors conclude that no real MMR was found, and question the interpretation of Ruusuvirta et al. (1998), highlighting that a negative-polarity MMR in rats is yet to be demonstrated. However, the larger portion of literature in this field tends to support the hypothesis that there may be a rodent MMR/MMN-like response which is analogous with the human MMN (Ruusuvirta et al., 1998, Tikhonravov et al., 2008, Tikhonravov et al., 2010, Astikainen et al., 2011, Nakamura et al., 2011, Shiramatsu et al., 2013).

Aside from electrode placement generally within the primary auditory cortex (in addition to other structures in some cases), there were multiple methodological differences between these ‘successful’ studies that reported to find an MMN-like response to frequency oddball paradigms in anaesthetised rats. Frequencies, control paradigms and anaesthetics used, and occasionally electrode/reference placement varied. This may explain variability in the results from these studies, for although they were all ‘positive’, they were not entirely consistent in their findings, which may present cause for concern; see Section 1.3 and Table 1.2 for review. Overall, there seems to be some congruence on an approximate latency range of 50-180 ms for the rat fMMR. Several of these papers investigated the effects of various NMDA receptor antagonists on this response, including phencyclidine/MK-801 (Tikhonravov et al.,

2008), memantine (Tikhonravov et al., 2010), and AP5 (Shiramatsu et al., 2013), which all reportedly attenuated this fMMR in rats anaesthetised with urethane.

In one of the more recent studies, however, Ruusuvirta et al. (2015) reported findings which appear to contradict much of their preceding work in this field. Their main finding was that the so-called MMN-like response in rats may be explained by differences in stimuli frequencies, with larger frequencies typically producing a greater auditory response as also indicated by (Heffner et al., 1994), rather than being dependent on the oddball condition. This implies that the proposed sensory-memory aspect of MMN (Section 1.2.3) might not be modelled in the rat. The authors emphasise the need to control for differences in physical properties of stimuli used in animal MMN studies. Based upon these findings it can be concluded that the question of whether rodents exhibit an MMR analogous to the human MMN still remains to be established.

3.1.1.3 Intensity

There are virtually no published research articles investigating the intensity MMR in anaesthetised (or conscious) rodents. Two studies used combined frequency-intensity combination stimuli (Astikainen et al., 2006, Astikainen et al., 2014), with both concluding that the presence of an MMR from 75-125 ms provides evidence that anaesthetised rats are capable of categorising auditory objects. However, the controls for this experiment cannot determine the relative contributions of stimuli intensity and frequency to the overall AEP, hence this result should be treated with caution. Additionally, it is argued that mismatch responses to different physical features of sound should be treated separately (Okazaki et al., 2006) and adequate controls for physical properties of stimuli implemented (Harms et al., 2014, Harms et al., 2015, Ruusuvirta et al., 2015). This thesis therefore aims to investigate intensity MMR using a more systematic approach.

3.1.2 Urethane anaesthetised condition

As discussed in Section 1.2, the human MMN is reportedly observed from patients in various stages of sedation, anaesthesia and comatose states (Fischer et al., 1999, Fischer et al., 2000, Heinke et al., 2004, Kane et al., 1996). One may logically predict that if an analogous MMR signal exists in rodents then it would be present under similar conditions.

Urethane anaesthesia is typically used for terminal neuroscience/physiology experiments in small animals, and has been applied in several studies investigating the rat MMR (Ruusuvirta et al., 1998, Astikainen et al., 2006, Ruusuvirta et al., 2007, Ahmed et al., 2011, Astikainen et al., 2011, Nakamura et al., 2011, Ruusuvirta et al., 2013, Astikainen et al., 2014, Ruusuvirta et al., 2015). Urethane is only recommended for acute, non-recovery experiments, rather than recovering animals following surgery, because of its carcinogenic properties (Salaman and Roe, 1953). The main reason urethane is prevalent in neurophysiology research is that while obtaining long-lasting anaesthetic and analgesic effects suitable for performing extensive surgery and experimentation (Field et al., 1993), it is considered to have a relatively unobtrusive effect on subcortical and peripheral neurotransmission (Maggi and Meli, 1986). However, these merits remain controversial (Koblin, 2002) and it should be presumed that urethane by definition of being an anaesthetic does alter electrophysiological activity. Nevertheless, it is an ‘anaesthetic of choice’ for auditory neuroscience research (Sakata and Harris, 2009, Sakata and Harris, 2012) and thus was selected for use in experiments of anaesthetised animals throughout this thesis. By studying the AEP and MMR from urethane-anaesthetised (Chapter 3: Experiment I and Chapter 5: Experiment III) and conscious (Chapter 4: Experiment II) animals, this thesis examines potential effects of urethane on the electrophysiology of cortical auditory processing.

3.1.3 *Experiment I aims*

In this experiment, the hypothesis that an MMR is present in the auditory cortex of urethane-anaesthetised mice is tested. Duration, frequency and intensity manipulations in oddball and control paradigms are systematically investigated; aiming to overcome the limitations of previous work in anaesthetised rodents, which did not adequately control for physical factors that could confound the conclusions that an MMN-like response is present. In addition, the hypotheses that genetic (*Map2k7*^{+/-}) and pharmacological (NMDA antagonism by ketamine) models relevant to schizophrenia display changes to this MMR are examined. Furthermore, this experiment sought to question whether *Map2k7* gene disruption alters the electrophysiological response to ketamine; thereby determining whether this post-synaptic kinase influences NMDA receptor-mediated signalling.

Hence the five principle aims of Experiment I are to:

1. Determine the effects of auditory stimulus duration on the AEP and characterise the duration mismatch response (dMMR) from urethane-anaesthetised mice.
2. Determine the effects of auditory stimulus frequency on the AEP and characterise the frequency mismatch response (fMMR) from urethane-anaesthetised mice.
3. Determine the effects of auditory stimulus intensity on the AEP and characterise the intensity mismatch response (iMMR) from urethane-anaesthetised mice.
4. Examine any differences in respective AEP and MMR waveforms from urethane-anaesthetised wild-type control (WT) and *Map2k7*^{+/-} (HET) mice.
5. Investigate the effects of 10 mg/kg i.p. ketamine on the AEP in urethane-anaesthetised mice and whether this is altered in HET mice.

3.2 Methods

The materials and methods for Experiment I are summarised below. Detailed descriptions of these methodologies are provided in Chapter 2.

3.2.1 *Animal details*

Wild-type control (WT; n = 10) and *Map2k7*^{+/-} schizophrenia-related gene disruption model (HET; n = 7) mouse groups were used in this experiment. In the second electrophysiology recording session following a single dose of 10 mg/kg i.p. ketamine these group numbers were reduced to 8 and 6 for WT and HET mice, respectively. For full details see Section 2.4.3 and Appendix A.

3.2.2 *Surgery*

Stereotactic surgery was performed to implant epidural EEG recording electrodes bilaterally above the primary auditory cortices of each subject, with a reference placed above the cerebellum. Electrophysiological recordings were made immediately following surgery whilst animals remained in a urethane-anaesthetised state. A description of the entire surgical procedure is given in Section 2.5.1.

3.2.3 *Electrophysiological recordings*

Cortical EEG was acquired during a series of auditory stimulation sequences inside a customised soundproof recording chamber (Figure 2.4) using an Intan Technologies RHD Evaluation System, sampled at 1 kS/s with a bandwidth of 1-500 Hz, as described in Section 2.6.1.

3.2.4 *Auditory paradigms*

Experiment I incorporated the oddball (OD) paradigm plus consecutive-repetition (CR), deviant-alone (DA) and many-standards (MS) control paradigms. Descriptions and rationale for these are provided in Section 2.7. Each was presented separately with stimuli varying in duration (dOD/dCR/dDA/dMS), frequency (fOD/fCR/fDA/fMS) and intensity (iOD/iCR/iDA/iMS), firstly after physiological saline and then following 10 mg/kg i.p. ketamine administrations. Thus there were 24 paradigm presentations in total; i.e. 4 paradigms x 3 physical features of sound variance x 2 injections. This sequence is explained in Section 2.7.

3.2.5 *Stimuli properties*

Parameters of the auditory stimuli used are detailed in Section 2.8.1. The standard stimulus applied in all OD paradigms was 100 ms, 10 kHz, and 80 dB, with an inter-stimulus interval

(ISI) of 450 ms; duration oddball stimuli varied by ± 50 ms, frequency oddball stimuli varied by ± 2.5 kHz, and intensity oddball stimuli varied by ± 10 dB. Stimuli were monophonic pure tone sinusoids with instantaneous rise/fall times. ISI remained constant at 450 ms throughout all paradigms except from the deviant-alone control which was effectively ≥ 2.1 s. Ten dMS paradigm stimuli varied from 50-275 ms in 25 ms increments, fMS stimuli varied from 1.25-12.5 kHz in 1.25 kHz increments, and iMS stimuli varied from 60-105 dB in 5 dB increments. Levels of stimuli responsible for inducing AEP waveforms presented in the results section are clearly labelled in figure legends.

3.2.6 *Experimental protocol*

The experimental protocol and paradigm presentation sequence for Experiment I is described in Section 2.9.1. To summarise here, following surgery urethane-anaesthetised mice were placed inside Recording Chamber A (Figure 2.4), administered 2 ml/kg i.p. physiological saline, and EEG was recorded during presentation of dCR, dOD, dDA, dMS paradigms, followed by fCR, fOD, fDA, fMS, then iCR, iOD, iDA and iMS paradigms. They were then administered 10 mg/kg i.p. ketamine in a 2 ml/kg volume and this sequence was repeated. The total recording session time was approximately four hours, after which animals were euthanized by cervical dislocation.

3.2.7 *Artifact rejection*

As described in Section 2.10.1, a ± 500 μ V threshold artifact rejection criterion was applied to all datasets. This prevented data segments containing large amplitude non-physiological EMI sources from contributing to the AEP from each individual animal. The average overall artifact rejection rate was 0.229% (sd $\pm 1.289\%$) with no significant effects of genotype, gender, session or paradigm, thus none of these datasets were considered to be overtly distorted by extraneous noise.

3.2.8 *Auditory evoked potential computations*

Basic algebraic operations such as addition, subtraction, multiplication and division may be performed on the AEP. For example, the MMR is fundamentally a difference waveform between the standard and oddball AEP from the OD paradigm, hence a subtraction is performed. Slightly more complex computations such as custom baseline correction and data shifting may also be conducted provided there is sound justification for doing so.

Computations described below were generally applied to isolate and analyse specific AEP features of interest; with rationale for their implementation provided where applicable.

3.2.8.1 Mismatch response calculation

Traditionally the MMR is generated by subtracting the standard stimulus AEP from the oddball/deviant stimulus AEP. This method, illustrated in Figure 3.1a, was applied to duration oddball (dOD) paradigm data in Figure 3.4 and Figure 3.5. With this approach epoch length is limited to the duration of the shortest stimulus plus the ISI, which may be sufficient in most cases to observe the resulting MMR features over tens to hundreds of milliseconds. However, in frequency and intensity oddball (fOD and iOD) paradigms this was not the case, where MMR trajectories varied beyond the latency range imposed by this traditional method.

The novel paired AEP subtraction (extended epoch) method illustrated in Figure 3.1b was developed to overcome this limitation. Here a sequential standard-standard pair (two preceding oddball presentation) is subtracted from an oddball-standard pair to view the resulting MMR trajectory over an extended epoch, double the duration of that achieved by the traditional method. Practical application of this paired subtraction method to Experiment I fOD and iOD paradigm data was effective in isolating waveform features of interest (e.g. see Figure 3.19 and Figure 3.28).

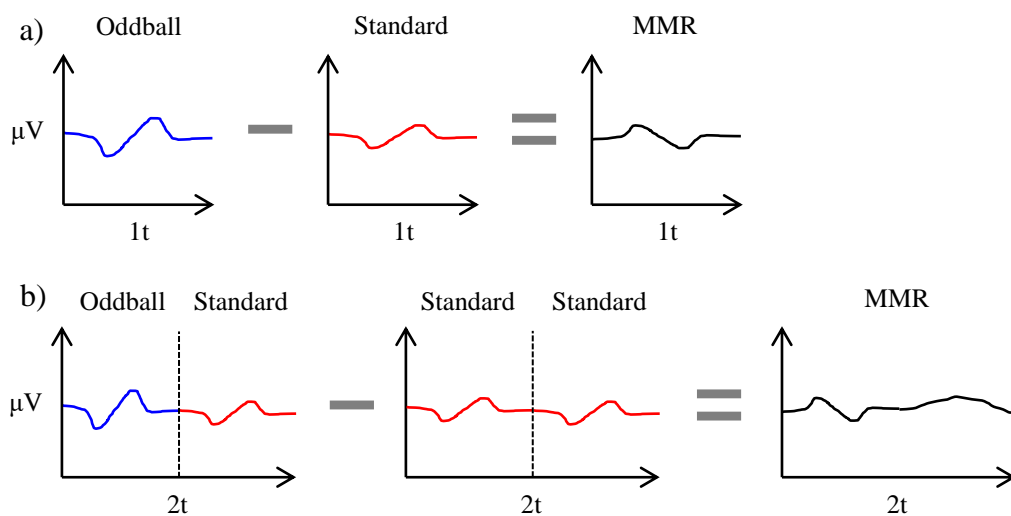


Figure 3.1 - Traditional and extended epoch mismatch response calculations a) Traditional method of subtracting the standard from the oddball auditory evoked potential (AEP). Here the viewing epoch is limited to $1t$; equal to the duration of the shortest stimulus plus the inter-stimulus interval (e.g. 100 ms + 450 ms). b) Paired AEP subtraction method where a standard-standard pair is subtracted from an oddball-standard pair. The desired effect is that the two additional conjoining standards cancel each other out, revealing the oddball-induced MMR over an extended epoch of duration $2t$.

3.2.8.2 Removing offset responses

Duration many-standards (dMS) paradigm stimuli offset responses were observed protruding from the underlying waveform shape (Figure 3.8a-b). To remove these offset responses and isolate the underlying waveform for analysis the average AEP from all 10 dMS paradigm stimuli was computed, effectively averaging-out individual stimuli offset responses. The resulting mean AEP waveforms from WT and HET mice are shown in Figure 3.8c.

3.2.8.3 Custom baseline correction

Amplitude measurements from the AEP are always taken relative to a baseline voltage. Unless otherwise stated this is the 100 ms pre-onset mean amplitude subtracted from the whole epoch when computing each AEP, as described in Section 2.10.1. However, in order to observe particular features from the waveform custom baseline correction may be performed. For example, to observe a stimulus offset response it may be desirable to adjust the baseline level to the amplitude immediately preceding stimulus offset, as illustrated in Figure 3.2.

Pre-offset baseline correction was performed to frequency and intensity many-standards (fMS and iMS) paradigm waveforms to observe the resulting stimuli offset responses, shown in Figure 3.12 and Figure 3.21, respectively. Practically, performing this kind of baseline correction at time point X and measuring the amplitude at point Y (Figure 3.2b) is equivalent to measuring the peak-to-peak amplitude between X and Y in Figure 3.2a. However, plotted figures with many AEPs are more readily interpreted when all of the waveforms begin from the same baseline voltage, justifying the application of custom baseline correction.

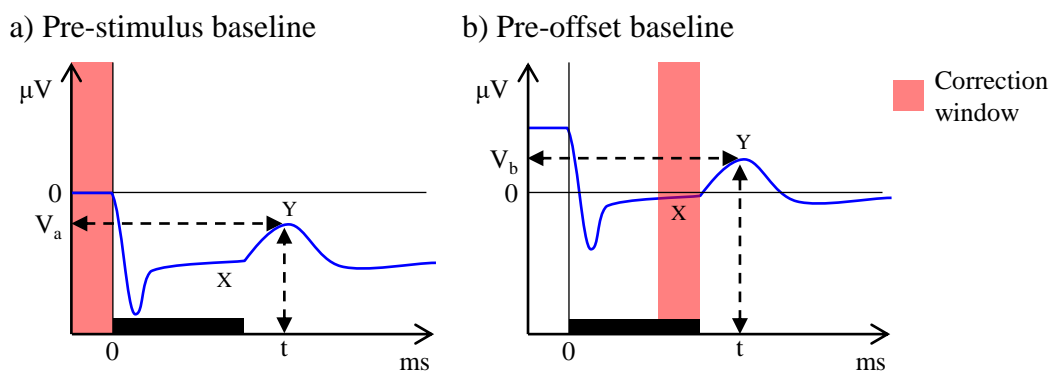


Figure 3.2 - Custom baseline correction used in this study a) Pre-onset baseline correction, applied by default to every AEP. b) Pre-offset baseline correction applied to analyse stimulus offset responses (e.g. see Figure 3.12 and Figure 3.21). The resulting amplitude measurements V_a and V_b at time point t are different due to the baseline correction window applied. Auditory stimulation is illustrated by a solid black bar beginning at 0 ms. In b) the baseline correction window covers time point X, and in this situation measuring the amplitude at Y is equivalent to measuring the peak-to-peak amplitude from X to Y in a).

3.2.9 *Auditory evoked potential measurements*

Electrophysiological features of the AEP elicited by various stimulation conditions in Experiment I are generally classified and quantified as outlined below. Aside from these, additional ad hoc analytical methods presented in the results are introduced in their respective sections as applicable.

3.2.9.1 *Stimulus onset potential (N1)*

Onset potential (N1) peak amplitude and latency measurements were made from a 0-50 ms post stimulus onset window on 100 Hz low-pass filtered, 100 ms pre-onset baseline corrected AEP waveforms from each subject. The greatest negative value over five samples (5 ms) supplied the peak amplitude measure and its sample position provided the latency measurement.

3.2.9.2 *Stimulus offset potential (P_{offset})*

Offset potential (P_{offset}) peak amplitude and latency measurements were made from a 0-50 ms post stimulus offset window from 100 Hz low-pass filtered, 10-0 ms pre-offset baseline corrected (explained in Section 3.2.8.3 above) AEP waveforms from each subject. The highest amplitude value over 5 ms was taken as the peak and its latency was provided by the corresponding sample number divided by the sampling frequency (1000 kS/s).

3.2.9.3 *Deviant evoked activity (DEA)*

The term deviant evoked activity (DEA) is introduced here to describe relatively large amplitude slow-wave responses observed from deviant-alone (DA) and both frequency and intensity oddball (fOD and iOD) paradigm waveforms. DEA is generally characterised by a series of large positive amplitude peaks followed by a slow negative deflection. Maxima were observed as the peak occurring between \approx 200-600 ms post stimulus onset. However, these extended latency waveform features were more appropriately quantified by mean amplitude measurements. After consideration and quantifying peak latencies (Figure 3.10) a standardised measurement window of 300-500 ms was determined to quantify the mean positive amplitude of DEA.

3.3 Results

Findings from Experiment I presented in this section are separated broadly into three categories reflecting the physical feature of sound manipulated in each respective set of auditory paradigms. Results from paradigms with auditory stimuli varying in duration are followed by those with stimuli varying in tone frequency, then intensity or sound pressure level. These are followed with an examination of auditory evoked potential changes observed throughout the entire recording protocol described in Section 2.9.1 and spectral analyses.

3.3.1 Duration paradigms in urethane-anaesthetised mice

Duration consecutive-repetition (dCR), oddball (dOD), deviant-alone (dDA) and many-standards (dMS) paradigms with auditory stimuli varying in duration were the first to be presented to urethane-anaesthetised mice, firstly after a physiological saline control and then following 10 mg/kg i.p. ketamine injections. Key findings from these recordings are provided below, including representative group AEP waveform differences, characterisation of the duration mismatch response observed, stimulus offset potentials and dDA paradigm waveform analyses.

3.3.1.1 *Map2k7*^{+/-} mice display increased stimulus onset response

The dCR control paradigm was presented first, providing an appropriate point to start presenting the results. Figure 3.3a illustrates both groups' grand-average AEP waveforms to the 100 ms, 10 kHz, 80 dB, 450 ms ISI stimulus in the dCR paradigm, presented during the saline session. Equivalent waveforms extracted from recordings made following 10 mg/kg i.p. ketamine administration are provided in Figure 3.3b. Note the slight differences between saline and ketamine session waveforms. Prominent AEP features elicited by the dCR paradigm in urethane-anaesthetised mice relate to stimulus onset and offset, labelled respectively as N1 and P_{offset} in Figure 3.3a.

The *Map2k7*^{+/-} heterozygous (HET) group appears to display a larger amplitude onset response (N1) compared with wild-type control mice. N1 peak amplitude is quantified in Figure 3.3c showing a significant effect of genotype [$F_{1,10} = 8.303$; $p = .016$] which was found by applying repeated measures analysis of variance (ANOVA) with genotype (WT/HET) and gender (female/male) as between-subjects factors and session (saline/ketamine) and stimulus duration (50 ms/100 ms/150 ms) as within-subjects factors. This within-subjects design included only subjects with complete saline and ketamine session recordings, such that there were eight WT and six HET mice. This analysis returned a statistically significant overall effect of ketamine [$F_{1,10} = 6.718$; $p = .027$] to reduce N1

peak amplitude; however, this may be ascribed to a general phenomenon presented in Section 3.3.4.1 which may not necessarily be dependent on the administration of ketamine *per se*. There were no significant differences between genders [$F_{1,10} = .066$; $p = .803$] or stimulus duration [$F_{2,9} = .383$; $p = .687$; Sphericity assumed] on N1 peak amplitude.

N1 peak latency is quantified in Figure 3.3d. Repeated measures ANOVA revealed no significant effects of genotype [$F_{1,10} = 1.577$; $p = .238$], gender [$F_{1,10} = .319$; $p = .584$], ketamine [$F_{1,10} = 1.215$; $p = .296$], or stimulus duration [$F_{2,9} = 1.054$; $p = .367$] on N1 peak latency, which occurs in urethane-anaesthetised mice at 15.5 ms (± 1.1 ms sem) post stimuli onset.

Visual inspection of the offset response (P_{offset}) in Figure 3.3b suggests WT and HET groups reach similar peak potentials. However, when pre-offset baseline correction is applied (described in Figure 3.2b) disparity may emerge between the two groups. Quantification of P_{offset} peak amplitude with a 10 ms pre-offset baseline correction window is presented in Figure 3.3e. There appears to be a contrasting effect of ketamine wherein the WT group exhibits a reduction and conversely the HET group displays an increase in peak amplitude. Nevertheless, repeated measures ANOVA of P_{offset} peak amplitude measured from each stimulus-evoked waveform with 10 ms pre-offset baseline correction revealed only a trend for an effect of genotype [$F_{1,10} = 4.298$; $p = .065$] and no other significant effects of gender [$F_{1,10} = .484$; $p = .503$], ketamine [$F_{1,10} = 3.841$; $p = .078$] or stimulus duration [$F_{2,9} = 1.505$; $p = .273$]. This trend towards increasing P_{offset} peak amplitude may reflect an underlying biphasic response in HET mice which goes negative from ≈ 50 -250 ms, altering their pre-offset baseline level compared with WT mice, discussed in Section 3.3.1.4.

Peak latency of the P_{offset} response is quantified in Figure 3.3e and occurs at 25.2 ms (± 1.2 ms sem) post stimuli offset. There were no significant effects of genotype [$F_{1,10} = .220$; $p = .649$], gender [$F_{1,10} = 3.302$; $p = .099$], ketamine [$F_{1,10} = .897$; $p = .366$] or stimulus duration [$F_{2,9} = 2.893$; $p = .107$] on this metric.

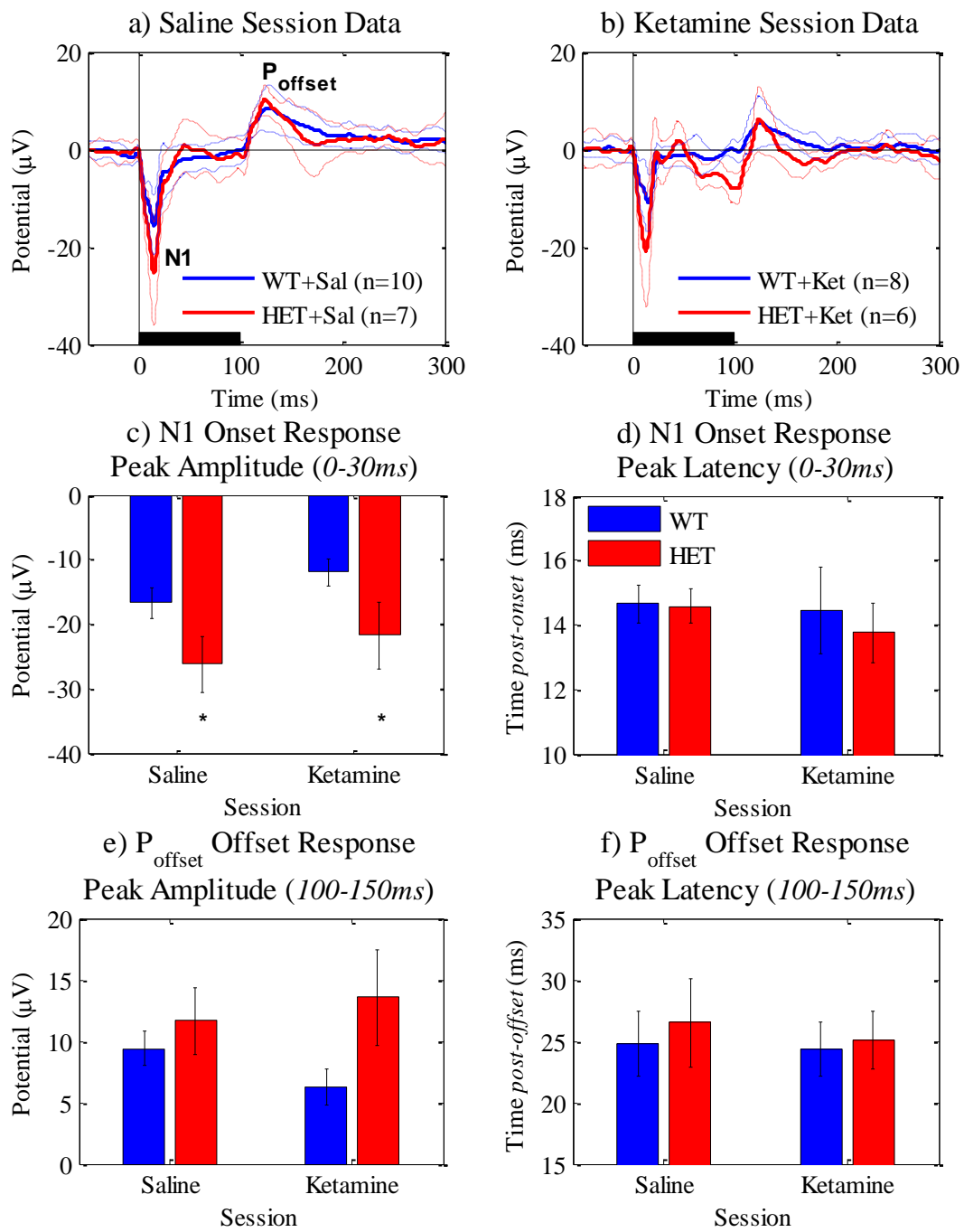


Figure 3.3 - Comparison of urethane-anaesthetised control and *Map2k7*^{+/-} grand-average auditory evoked potential waveforms Standard (100 ms, 10 kHz, 80 dB, 450 ms ISI) stimuli AEP responses from the duration consecutive-repetition (dCR) paradigm are shown for wild-type control (WT; blue) and *Map2k7*^{+/-} (HET; red) mice ± sem following a) injection of physiological saline (Sal), and b) 10 mg/kg i.p. ketamine (Ket). Auditory stimulation is indicated with a black rectangle and AEP peaks are annotated in (a). Quantification is provided in bar charts ± sem for: c) N1 peak amplitude, measured from 0-30 ms showing a significant ($p < .05$) effect of genotype; d) N1 peak latency; e) P_{offset} peak amplitude, measured from 100-150 ms with pre-offset baseline correction; and f) P_{offset} peak latency plotted relative to stimuli offset time.

3.3.1.2 Duration mismatch response in urethane-anaesthetised mice is generated by stimulus offset potentials

The dOD paradigm was designed to investigate the duration mismatch response of urethane-anaesthetised mice to oddball stimuli which vary by ± 50 ms from a 100 ms standard. Figure 3.4 presents the 100 ms standard and 50 ms (-50 ms) oddball stimuli AEPs, and the resulting dMMR computed by the traditional method described in Section 3.2.8.1. Figure 3.5 displays equivalent plots for the 150 ms ($+50$ ms) oddball.

Standard and oddball stimuli with different durations each evoke a P_{offset} response at different latencies, which respectively generate negative and positive deflections in the resulting dMMR waveforms. N1 responses to standard and oddball stimuli are generally equivocal, effectively cancelling each other out. Hence no distinctive features are evoked by duration oddball stimuli which are unique to the oddball condition.

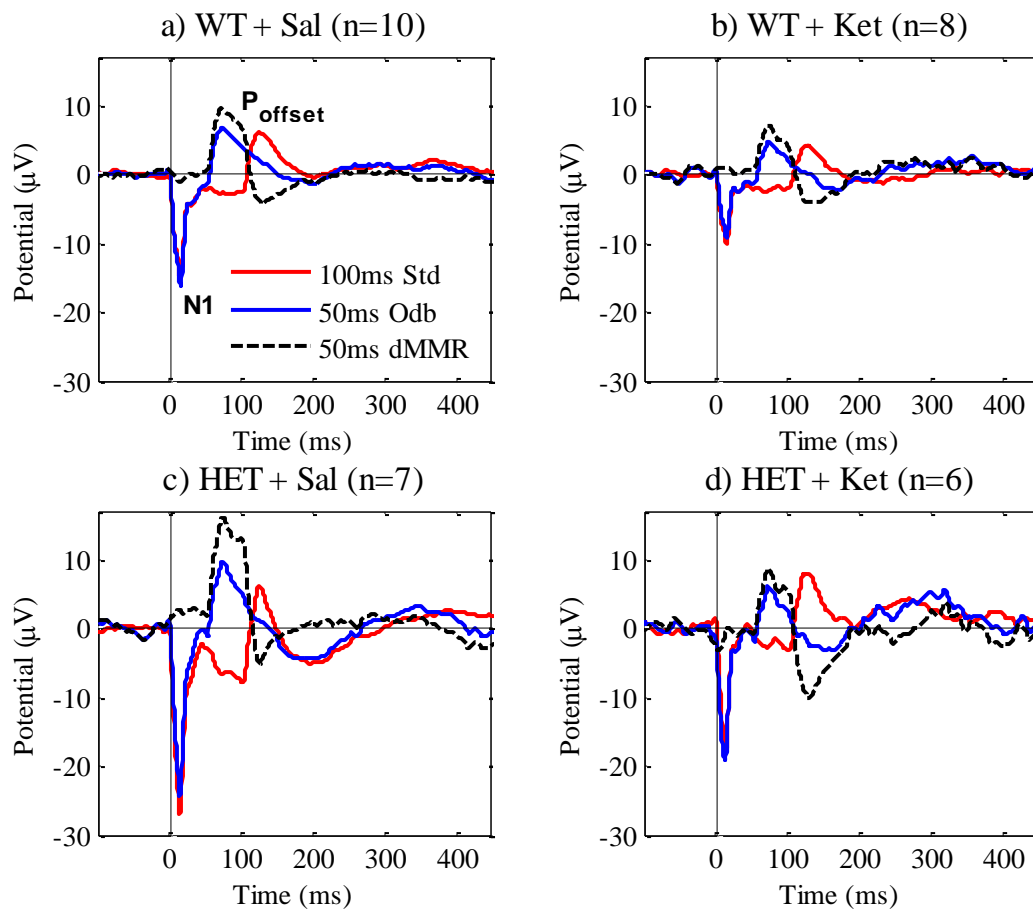


Figure 3.4 - Decreased duration (-50 ms) oddball mismatch response in urethane-anaesthetised mice The 100 ms standard (Std; red), 50 ms oddball (Odb; blue) and resulting duration mismatch response (dMMR; black dashed) auditory evoked potential waveforms are displayed for a) control (WT) mice during the saline session (Sal), b) WT mice following a 10 mg/kg i.p. ketamine injection (Ket), c) *Map2k7^{+/-}* (HET) mice during the saline session, and d) HET mice during the ketamine session. The traditional method of MMR computation (Figure 3.1a) has been applied to these waveforms. Onset (N1) and offset (P_{offset}) responses are annotated on (a).

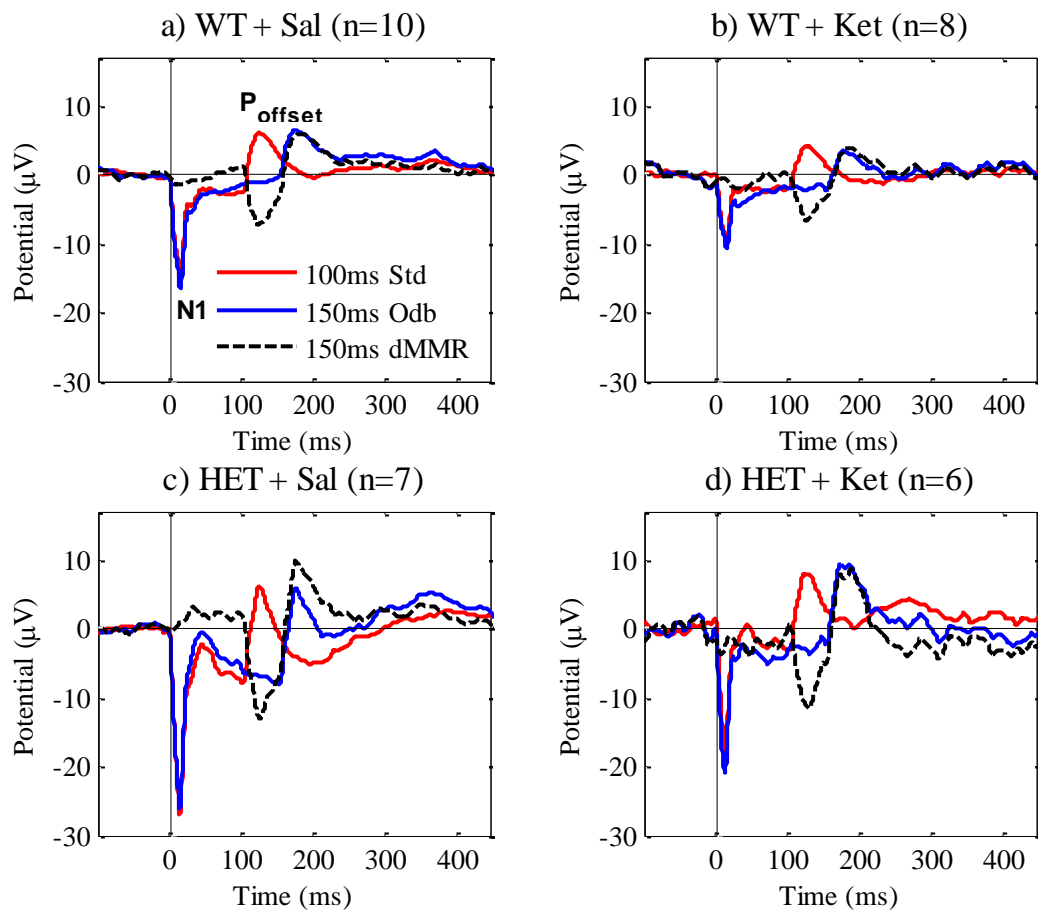


Figure 3.5 - Increased duration (+50 ms) oddball mismatch response in urethane-anesthetised mice The 100 ms standard (Std; red), 150 ms oddball (Odb; blue) and resulting duration mismatch response (dMMR; black dashed) auditory evoked potential waveforms are displayed for a) control (WT) mice during the saline session (Sal), b) WT mice following 10 mg/kg ketamine i.p. injection (Ket), c) *Map2k7*^{+/-} (HET) mice during the saline session, and d) HET mice during the ketamine session. The traditional method of MMR computation (Figure 3.1a) has been applied to these waveforms. Onset (N1) and offset (P_{offset}) responses are annotated on (a).

Stimulus onset responses in Figure 3.4 and Figure 3.5 are larger in HET mice compared with WT controls, and both appear reduced following 10 mg/kg i.p. ketamine administration (potentially due to factors other than ketamine action; see Figure 3.29), consistent with findings from dCR stimuli described in Section 3.3.1.1 above. Figure 3.4c and Figure 3.5c suggest HET mice display an underlying biphasic response not apparent in WT controls which goes negative from ≈ 50 -250 ms; analysis of this is provided in Figure 3.8c-d.

Quantification of 50 ms (-50 ms) and 150 ms ($+50$ ms) dMMR waveform positive and negative peak latencies and overall peak-to-peak amplitudes are provided in Figure 3.6. The difference between positive peak latencies is evidently due to the P_{offset} response from each respective oddball AEP. Negative peak latencies are comparable, and are obviously caused by the P_{offset} response of the 100 ms standard stimulus in both cases. The effect of genotype on peak-to-peak amplitude was approaching significance [$F_{1,10} = 4.564$; $p = .058$], and no

other significant effects of gender [$F_{1,10} = .033$; $p = .859$], ketamine [$F_{1,10} = 2.230$; $p = .166$] or stimulus duration [$F_{1,10} = .403$; $p = .540$].

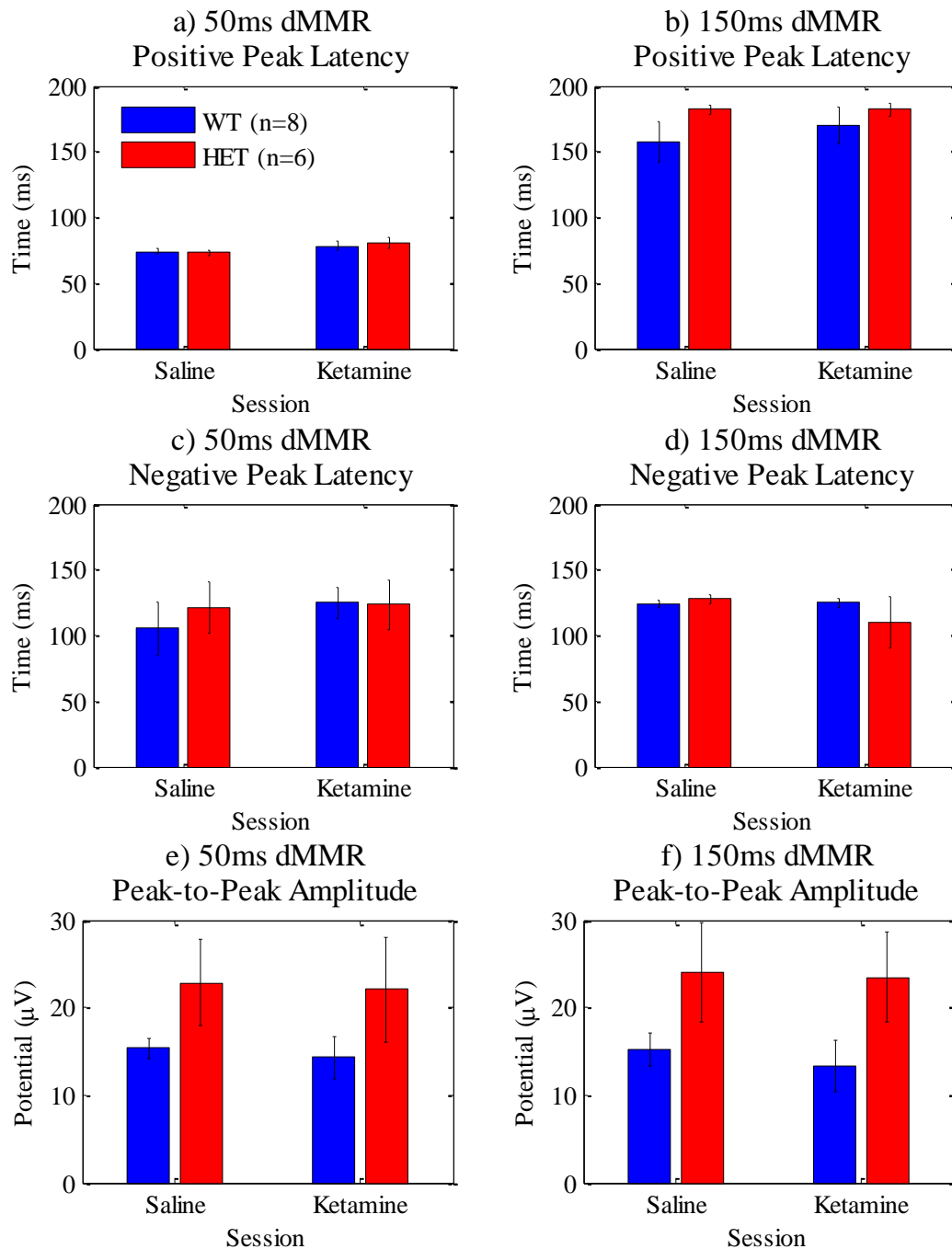


Figure 3.6 - Quantification of decreased (-50 ms) and increased ($+50$ ms) duration oddball mismatch responses in urethane-anesthetised mice Data are shown from control (WT) and *Map2k7*^{+/-} (HET) mice following saline and 10 mg/kg i.p. ketamine administrations \pm sem; positive peak latency from a) the 50 ms (-50 ms oddball) and b) the 150 ms ($+50$ ms oddball) duration mismatch response (dMMR); negative peak latency from c) the 50 ms and d) the 150 ms dMMR, and; peak-to-peak amplitude from e) the 50 ms and f) the 150 ms dMMR. No significant effects of session or genotype are observed in this analysis, although it is obvious that 50 ms and 150 ms dMMR waveforms display different positive peak latencies.

3.3.1.3 *Auditory evoked potentials from duration consecutive-repetition, oddball and many-standards paradigms are qualitatively similar*

To inspect any differences between the electrophysiological responses to physically identical auditory stimuli presented in different contexts, the AEP from each stimulus in dCR, dOD and dMS paradigms may be visually compared in Figure 3.7. These three paradigms are described in Section 2.7.

In the control group during the saline session (WT + Sal) there is little evidence of any context-specific activity in response to these duration-varying auditory paradigms. AEP waveforms evoked by identical stimuli presented in dCR, dOD and dMS paradigms appear qualitatively similar, each displaying onset and offset peaks of comparable amplitude and latency, without any obvious additional waveform features present.

In Figure 3.7d and Figure 3.7f the *Map2k7^{+/-}* group during the saline session (HET + Sal) group displays the emergence of an underlying slow biphasic response in AEPs from 100 ms and 150 ms duration stimuli in dOD and dMS paradigms which is not present in dCR paradigms, effectively resulting in greater negative potential from ≈ 50 -250 ms. To a lesser extent the WT response to 100 ms stimuli in the dCR paradigm is also higher amplitude than subsequently presented dOD and dMS paradigms, seen in Figure 3.7c. These observations may speculatively be considered effects of auditory stimulation rates which were far higher in OD and MS paradigms, or equally, may reflect adaptation to continued auditory stimulation given that CR, OD and MS paradigms were presented sequentially.

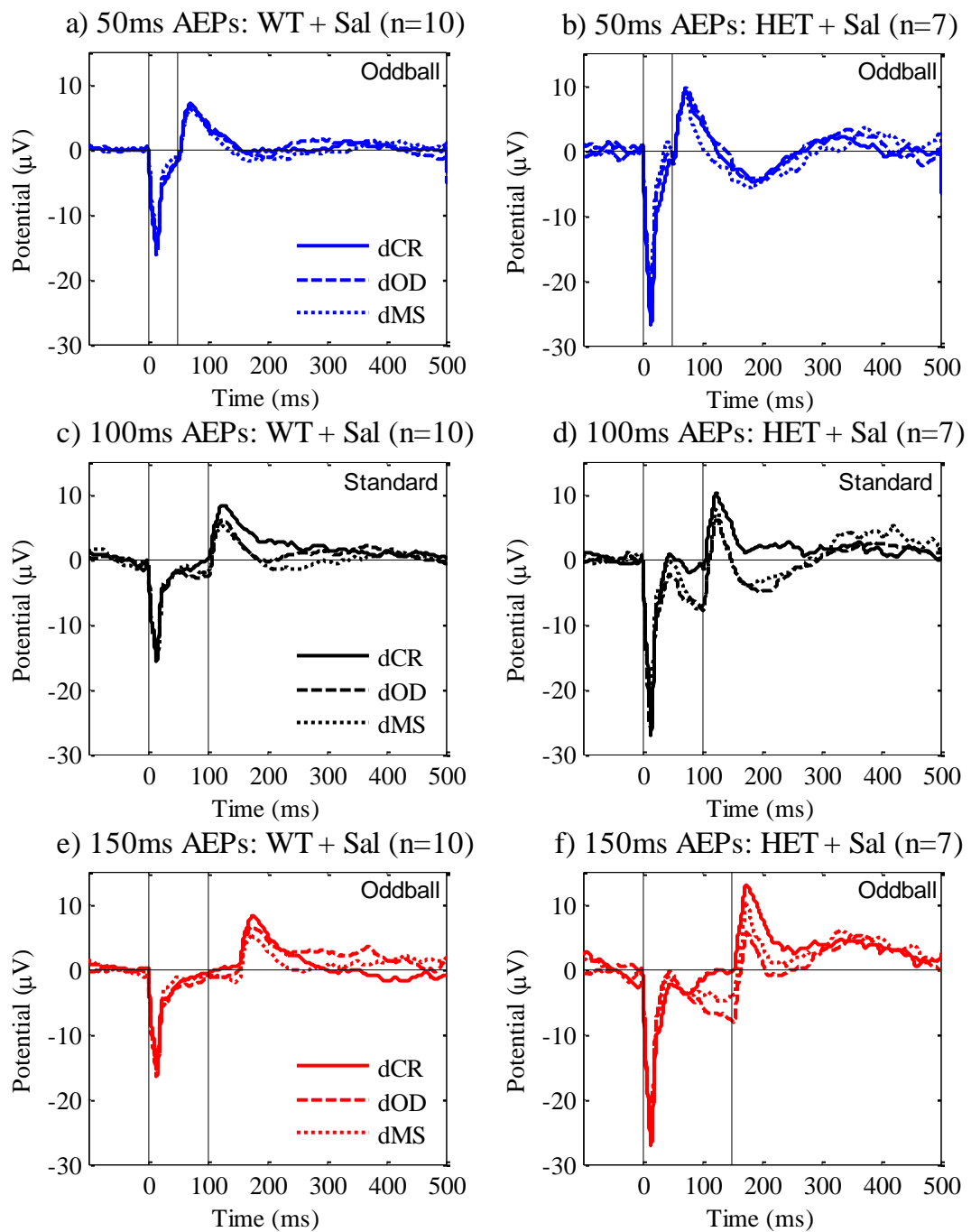


Figure 3.7 - Auditory evoked potentials from urethane-anaesthetised mice to different duration stimuli presented in oddball and control paradigms Control (WT) animal data are on the left and *Map2k7^{+/-}* (HET) data are on the right hand side plots, which each display evoked waveforms from physically identical stimuli in duration consecutive-repetition (dCR), oddball (dOD) and many-standards (dMS) paradigms which were presented sequentially throughout the saline (Sal) recording session. Waveforms plotted are 50 ms (-50 ms oddball) auditory evoked potentials (AEPs) from a) WT and b) HET mice, 100 ms (standard) AEPs from c) WT and d) HET mice, and 150 ms (+50 ms oddball) AEPs from e) WT and f) HET mice.

3.3.1.4 *Duration many-standards control paradigm reveals offset responses and a slow biphasic waveform in Map2k7^{+/-} mice*

The dMS paradigm AEP waveforms in response to ten different duration stimuli from urethane-anaesthetised WT control and HET mice in the saline recording session are shown in Figure 3.8a and Figure 3.8b, respectively. In these plots stimuli onset occurs at 0 ms and each stimulus offset times are marked by vertical dashed lines.

Offset of auditory stimulation evidently induces a robust, temporally dependant response characterised by a positive amplitude increase, peaking ≈ 25 ms post-offset and then steadily returning to baseline. This principle feature of the AEP from urethane-anaesthetised mice has already been viewed in dCR and dOD waveforms plotted above.

Consistent with these previous findings, HET grand-average AEPs display an onset response which reaches ≈ 10 μ V greater negative peak amplitude than the WT control group; whereas the offset response peak amplitude appears only marginally larger.

Additionally, these dMS paradigm waveforms plotted on the same graph reveal underlying activity upon which stimuli offset effects are superimposed. Specifically, a slow biphasic response is observed from HET mice which is less apparent in WT controls. Maximum negative potential of this feature is reached at ≈ 100 -200 ms, followed by a modest positive deflection which peaks at ≈ 300 -400 ms.

To analyse this AEP feature stimuli offset responses were effectively removed from the general waveform shape by averaging together all ten dMS stimuli AEPs (see Section 3.2.8.2). The resulting mean AEP waveforms from each group are shown in Figure 3.8c.

The presence of this slow biphasic amplitude deflection is quantified by measuring negative peak amplitude from 100-200 ms and positive peak amplitude from 300-400 ms, presented in Figure 3.8d. Statistically significant effects of genotype on 100-200 ms [$F_{1,10} = 6.540$; $p = .029$] and 300-400 ms [$F_{1,10} = 5.125$; $p = .049$] peak amplitudes were confirmed by repeated measures ANOVA with ketamine as a within-subjects factor, genotype and gender as between-subjects factors. There were no significant effects of gender on 100-200 ms [$F_{1,10} = .632$; $p = .445$] or 300-400 ms [$F_{1,10} = 2.214$; $p = .168$] peaks, and no significant effect of ketamine on 100-200 ms [$F_{1,10} = .003$; $p = .958$] or 300-400 ms [$F_{1,10} = 1.876$; $p = .201$] peaks.

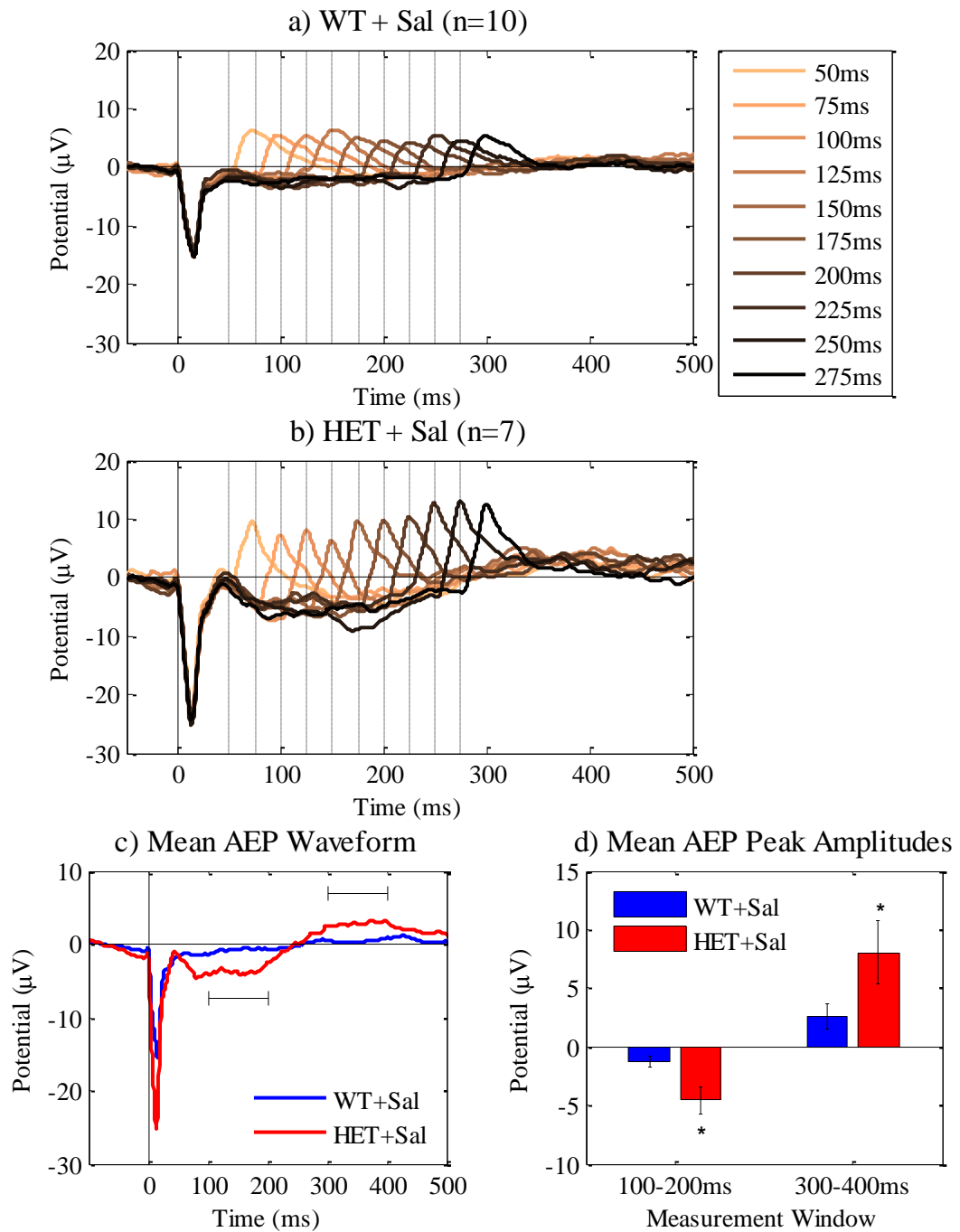


Figure 3.8 - Auditory evoked potentials to duration many-standards paradigm stimuli in urethane-anesthetised mice a) Control (WT), and b) *Map2k7^{+/-}* (HET) grand-average evoked potentials following administration of physiological saline (Sal). 25 ms linearly spaced stimuli offset times are marked with vertical dashed lines transecting the x-axis. c) Comparison of the mean AEP waveform from WT and HET groups, effectively without offset potentials. d) Quantification of peak amplitudes from 100-200 ms and 300-400 ms measurement windows illustrated in (c), showing significantly ($p < .05$) greater amplitudes in HET mice versus WT.

3.3.1.5 *Duration deviant-alone paradigm elicits extended latency response which is attenuated following ketamine*

The dDA paradigm AEPs from urethane-anaesthetised mice are presented in Figure 3.9. The saline recording session waveforms exhibit a series of large amplitude positive deflections at ≈ 200 -500 ms and a subsequent negative deflection peaking at ≈ 600 -700 ms which cannot readily be attributed to stimuli onset or offset effects previously observed in dCR, dOD and dMS paradigm AEPs. These additional waveform features will be referred to here as deviant evoked activity (DEA), introduced in Section 3.2.9.3.

Visually comparing DEA from 50 ms and 150 ms dDA stimuli may suggest that the initial sequence of additional positive deflections has an onset latency of ≈ 200 ms post stimulus onset. This is most evident in the 50 ms AEP, whereas it is partially obscured by the 150 ms stimulus' offset response, which may suggest that initiation of the DEA response is independent of stimulus duration.

There are clear differences between dDA waveforms from recordings made following physiological saline and 10 mg/kg i.p. ketamine injections. It appears as though ketamine diminishes the DEA potential, particularly in the HET group; however stimuli onset and offset responses also appear reduced between sessions.

Quantification of DEA from both 50 ms and 150 ms dDA stimuli is provided in Figure 3.10. Peak latency measured from 50 ms post stimulus offset to 600 ms post onset (data in Figure 3.10a and Figure 3.10c) indicates that DEA maxima occurs at 394.1 ms (± 23.3 ms sem) post stimuli onset. This was comparable for all DA paradigm stimuli AEPs, and there were no significant effects of genotype or ketamine.

To quantify the magnitude of DEA which was primarily manifested as a large positive amplitude deflection in the waveforms plotted in Figure 3.9, mean amplitude from 300-500 ms was measured, as shown in Figure 3.10b and Figure 3.10d for 50 ms and 150 ms dDA stimuli, respectively. This measurement window was selected post-hoc as a general method of quantifying DEA from all DA paradigm and frequency and intensity oddball (fOD and iOD) paradigm waveforms. Importantly here, offset responses from 150 ms dDA stimuli are avoided by selecting this measurement window.

Repeated measures ANOVA revealed a statistically significant overall effect of ketamine [$F_{1,10} = 9.260$; $p = .012$] to reduce DEA and no effects of stimulus duration, genotype or gender. Although it appears as though there may be a differential effect of ketamine in HET versus WT control groups, the interaction between genotype and ketamine is non-significant [$F_{1,10} = 3.407$; $p = .095$].

Average waveforms from all DA paradigms presented longitudinally throughout Experiment I are analysed in Section 3.3.4, shedding more light on this apparent effect of ketamine.

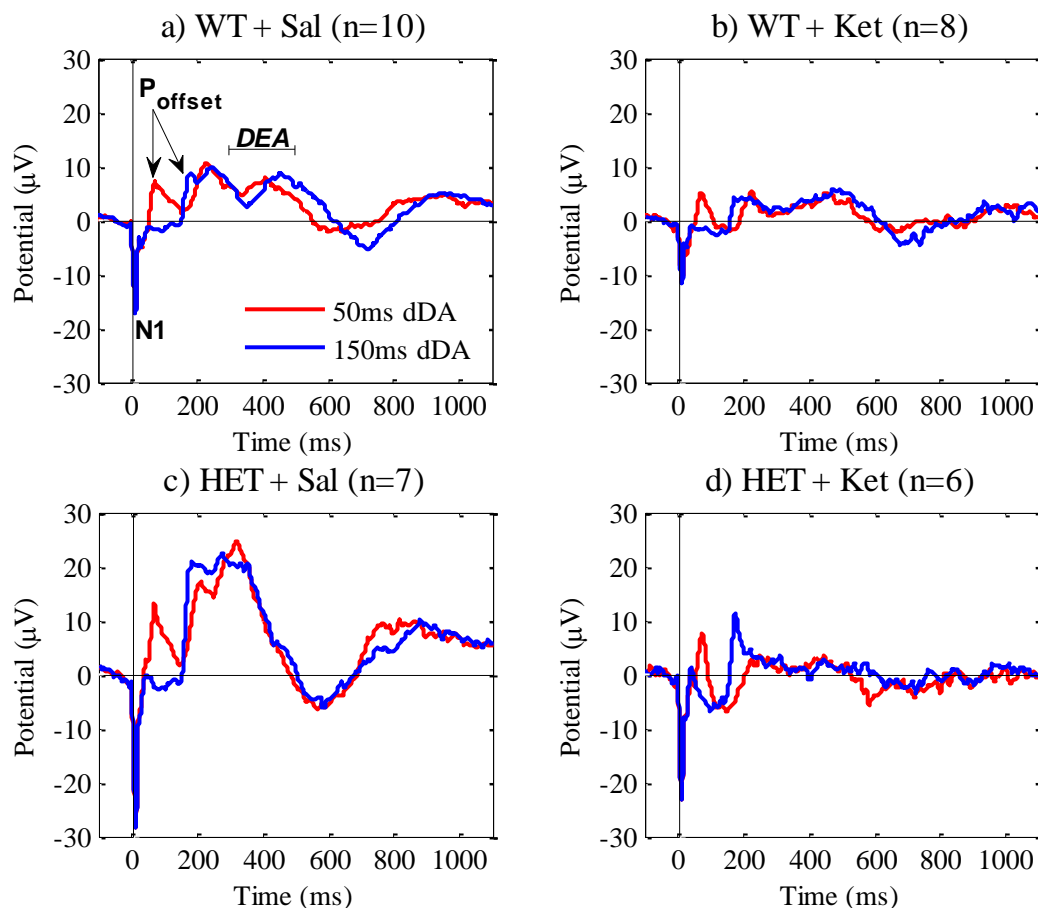


Figure 3.9 - Extended latency auditory evoked potentials to duration deviant-alone paradigm stimuli in urethane-anaesthetised mice The 50 ms (red) and 150 ms (blue) stimuli evoked waveforms are shown for a) control (WT) mice during the saline session (Sal), b) WT mice following 10 mg/kg i.p. ketamine injection (Ket), c) *Map2k7^{+/-}* (HET) mice during the saline session, and d) HET mice during the ketamine session. Onset (N1) and offset (P_{offset}) responses and deviant evoked activity (DEA) are annotated on (a). DEA peak latency and mean amplitude from 300-500 ms from these waveforms are quantified in Figure 3.10.

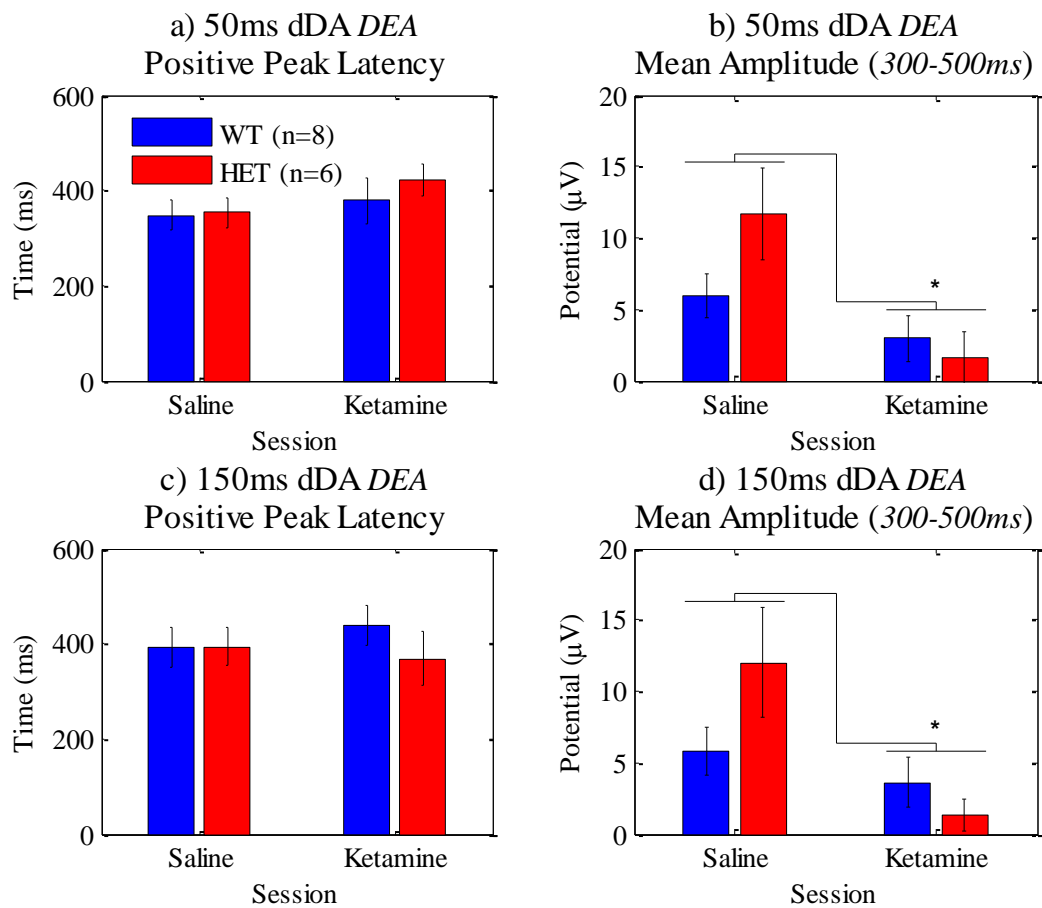


Figure 3.10 - Quantification of extended latency auditory evoked potentials to duration deviant-alone paradigm stimuli in urethane-anaesthetised mice Data from control (WT) and *Map2k7*^{+/-} (HET) mice following saline and 10 mg/kg i.p. ketamine injections are shown \pm sem. a) 50 ms duration deviant-alone (dDA) paradigm waveform deviant evoked activity (DEA) peak latency. b) 50 ms dDA waveform DEA mean amplitude from 300-500 ms showing a significant ($p < .05$) overall reduction following ketamine administration. c) 150 ms dDA waveform DEA peak latency. d) 150 ms dDA waveform DEA mean amplitude also exhibiting a significant effect of ketamine.

3.3.2 *Frequency paradigms in urethane-anaesthetised mice*

Findings from Experiment I frequency consecutive-repetition (fCR), oddball (fOD), deviant-alone (fDA) and many-standards (fMS) paradigms are presented in this section. The effect of tone frequency on AEP features, frequency mismatch responses and comparisons with control paradigms are covered. Observations already addressed in the duration-varying paradigms results section above are not repeated here, although bear in mind there are several consistencies.

3.3.2.1 *Stimulus frequency influences auditory evoked potentials*

Results from any of the frequency-varying paradigms may have been used to illustrate the relationship between tone frequency and the resulting stimuli N1 and P_{offset} potentials. However, this relationship is most effectively demonstrated by the fMS paradigm where ten different frequency tones were presented to urethane-anaesthetised control (WT) and *Map2k7^{+/-}* (HET) mice.

Analyses of stimuli onset responses from the fMS paradigm are provided in Figure 3.11. Waveforms plotted in Figure 3.11a-b illustrate that higher pitch auditory stimuli typically evoke larger N1 amplitudes. In Figure 3.11b it can be seen that the initial negative portion of the slow biphasic response observed from HET mice (Figure 3.8c-d) begins from ≈ 50 ms, whereas the WT group waveforms shown in Figure 3.11a remain closer to baseline during this period. Interestingly, lower frequency stimuli (≤ 6.5 kHz) generate a positive deflection immediately following the stimulus onset response which peaks at $\approx 20-30$ ms, perhaps indicating that these frequencies are towards the lower limit of the mouse hearing range.

N1 peak amplitudes from ten fMS paradigm evoked waveforms are quantified for WT and HET groups in Figure 3.11c and Figure 3.11d, respectively. Linear regressions and correlation coefficients highlight a strong inverse linear relationship (both $R^2 < -.9$) between tone frequency and N1 peak amplitude.

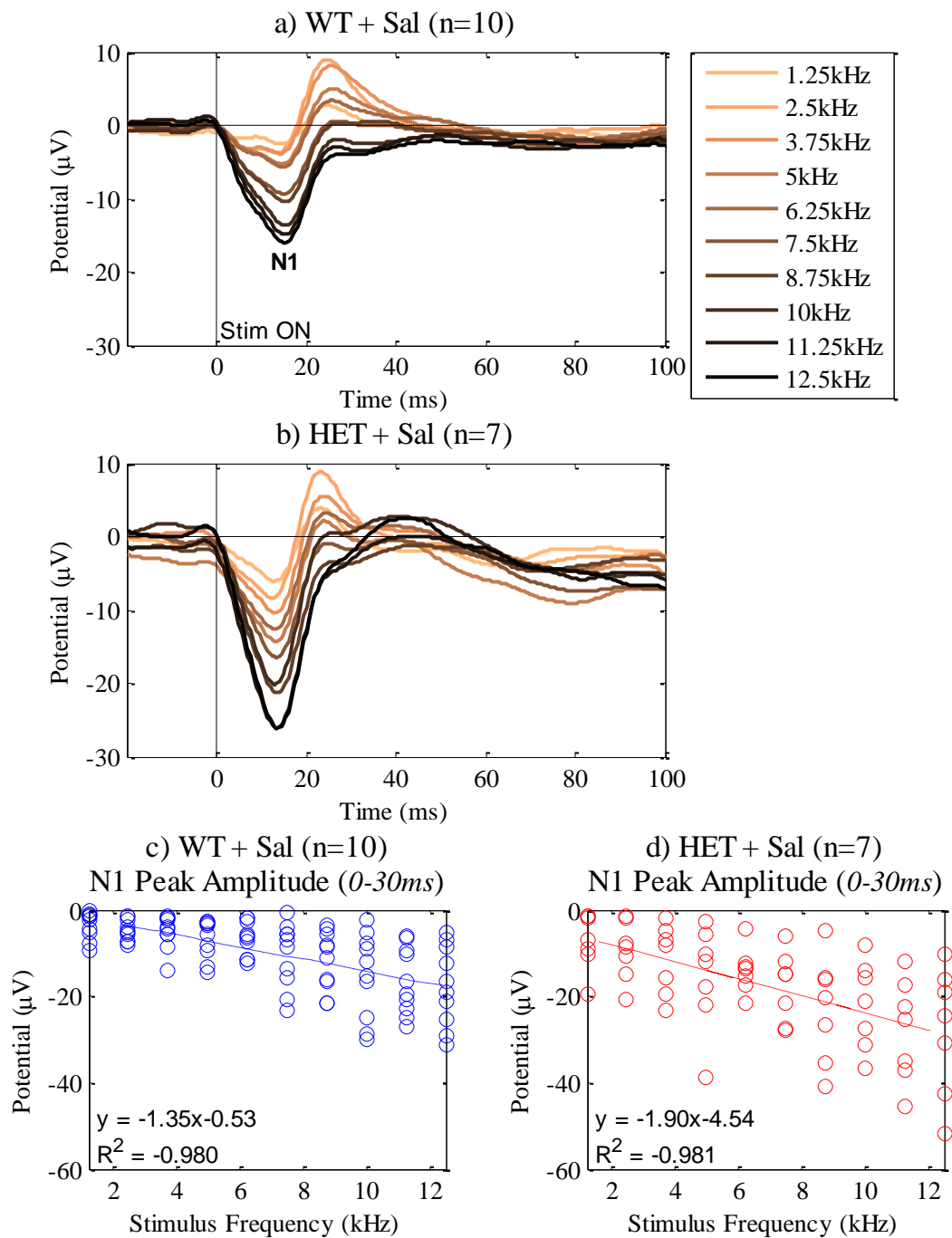


Figure 3.11 - Effect of tone frequency on the auditory onset response in urethane-anaesthetised mice This data was obtained from the frequency many-standards (fMS) paradigm presented during the saline recording session (Sal). a) Control (WT), and b) *Map2k7*^{+/-} (HET) group grand-average auditory evoked potential onset responses from ten fMS stimuli. c) WT and d) HET subject-wise quantification of onset response (N1) peak amplitude from different frequency stimuli with linear regression and correlation coefficients both showing highly linear inverse relationships ($R^2 < -.9$). Measurement windows are displayed *in brackets*.

Analysis of stimuli offset responses from the fMS paradigm waveforms are displayed in Figure 3.12. Pre-offset baseline correction is applied to the waveforms shown in Figure 3.12a-b. Here frequency sensitivity is more apparent in the WT group which visually exhibit greater peak amplitudes to higher frequency tones whereas offset responses from the HET group appear to be less clearly defined by stimulus frequency.

P_{offset} peak amplitude measurements were taken from 10 ms pre-offset baseline corrected waveforms, reported in Figure 3.12c and Figure 3.12d for WT and HET groups, respectively. Correlation coefficients from each group support the visual observation that WT mice waveforms are generally more correlated ($R^2 = .936$) than HET ($R^2 = .712$). HET group offset potential amplitude may be influenced by the negative half-cycle (≈ 50 - 250 ms) of the slow biphasic response previously identified (Figure 3.8b-d).

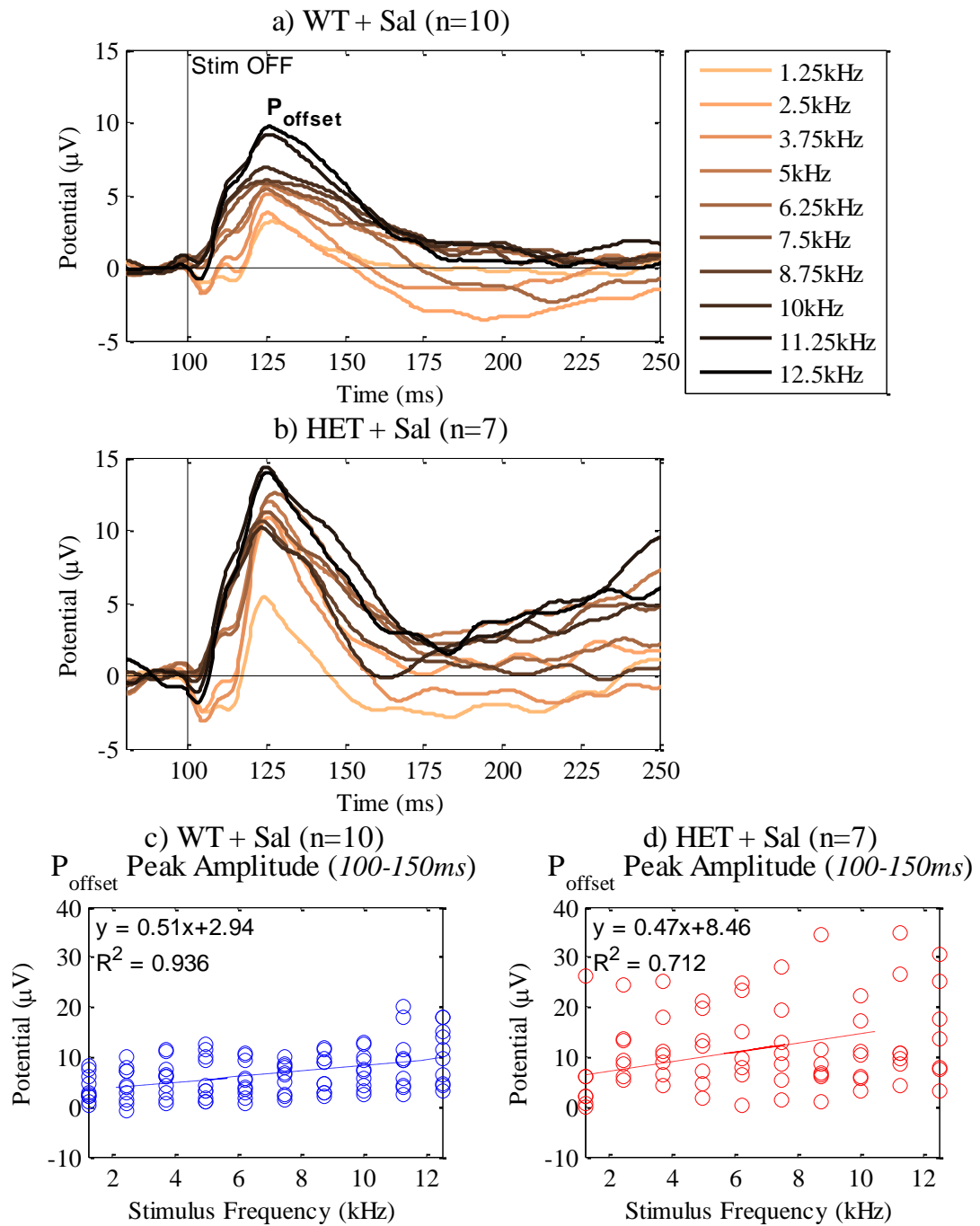


Figure 3.12 - Effect of tone frequency on the auditory offset response in urethane-anaesthetised mice This data was obtained from the frequency many-standards (fMS) paradigm after injecting physiological saline (Sal). a) Control (WT), and b) *Map2k7*^{+/-} (HET) group grand-average auditory evoked potential offset responses with 10 ms pre-offset baseline correction applied (e.g. see Figure 3.2). c) WT and d) HET subject-wise quantification of offset response (P_{offset}) peak amplitudes to different frequency stimuli with linear regression and correlation coefficients. Measurement windows are displayed *in brackets*.

3.3.2.2 Ascending and descending frequency oddballs elicit mismatch responses

The fOD in Experiment I was designed to investigate the frequency mismatch response (fMMR) of urethane-anaesthetised mice to oddball stimuli which vary by ± 2.5 kHz from a 10 kHz standard. Evoked potentials from descending (7.5 kHz) and ascending (12.5 kHz) oddball stimuli, the standard, and each resulting fMMR are shown in Figure 3.13 and Figure 3.14, respectively.

The paired AEP subtraction method described in Section 3.2.8.1 was applied in both cases to reveal an fMMR in the WT control group which may be approximately characterised as going positive from ≈ 200 -600 ms then negative from ≈ 600 -900 ms. These difference waveforms are mainly influenced by AEP features elicited by the oddball stimulus, which are not evoked by the standard. Earlier fluctuations in fMMR amplitudes would appear to reflect frequency sensitivities of N1 and P_{offset} components of standard and oddball evoked waveforms, thus ascending and descending frequency deviations generate opposite polarity deflections at these latencies.

Interestingly, the *Map2k7*^{+/-} group displays a similar response with a positive amplitude deflection from ≈ 200 -600 ms then negative from ≈ 600 -900 ms to both standard and oddball stimuli, effectively resulting in a lower amplitude fMMR difference waveform because they cancel each other out. It appears as though the positive deflection observed from ≈ 200 -600 ms may reflect the positive portion of the slow biphasic response previously identified in the HET group (Figure 3.8b-d). In both groups the fMMR amplitudes appear to be reduced in the second recording session, which followed injection of 10 mg/kg i.p. ketamine.

There are noticeable differences in onset and offset response amplitudes between the first two stimuli in each AEP pair (i.e. the ascending or descending oddball and the standard AEP). However, as discussed in Section 3.3.2.1, these are influenced by tone frequency, thus the second two stimuli in each pair (both standards) evoke N1 and P_{offset} responses of comparable amplitude which are effectively nullified in the resulting fMMR waveforms.

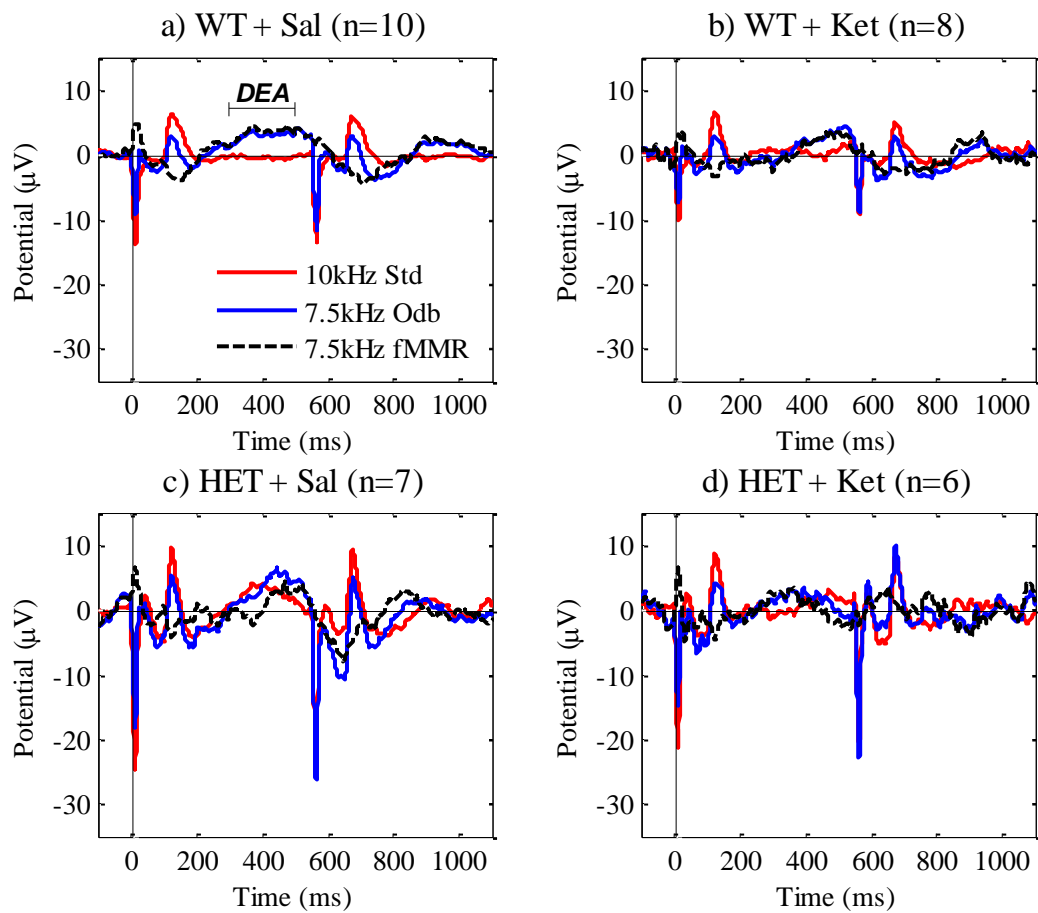


Figure 3.13 - Descending frequency (-2.5 kHz) oddball mismatch response in urethane-anesthetised mice The 10 kHz standard (Std; red), 7.5 kHz oddball (Odb; blue) and resulting frequency mismatch response (fMMR; black dashed) auditory evoked potential waveforms are displayed. a) Control (WT) mice during the saline session (Sal), b) WT mice following a single 10 mg/kg i.p. ketamine injection (Ket), c) *Map2k7^{+/-}* (HET) mice during the saline session, and d) HET mice during the ketamine session. The paired AEP subtraction method (Figure 3.1b) of computing the mismatch response has been applied in this analysis. Deviant evoked activity (DEA) is annotated on (a).

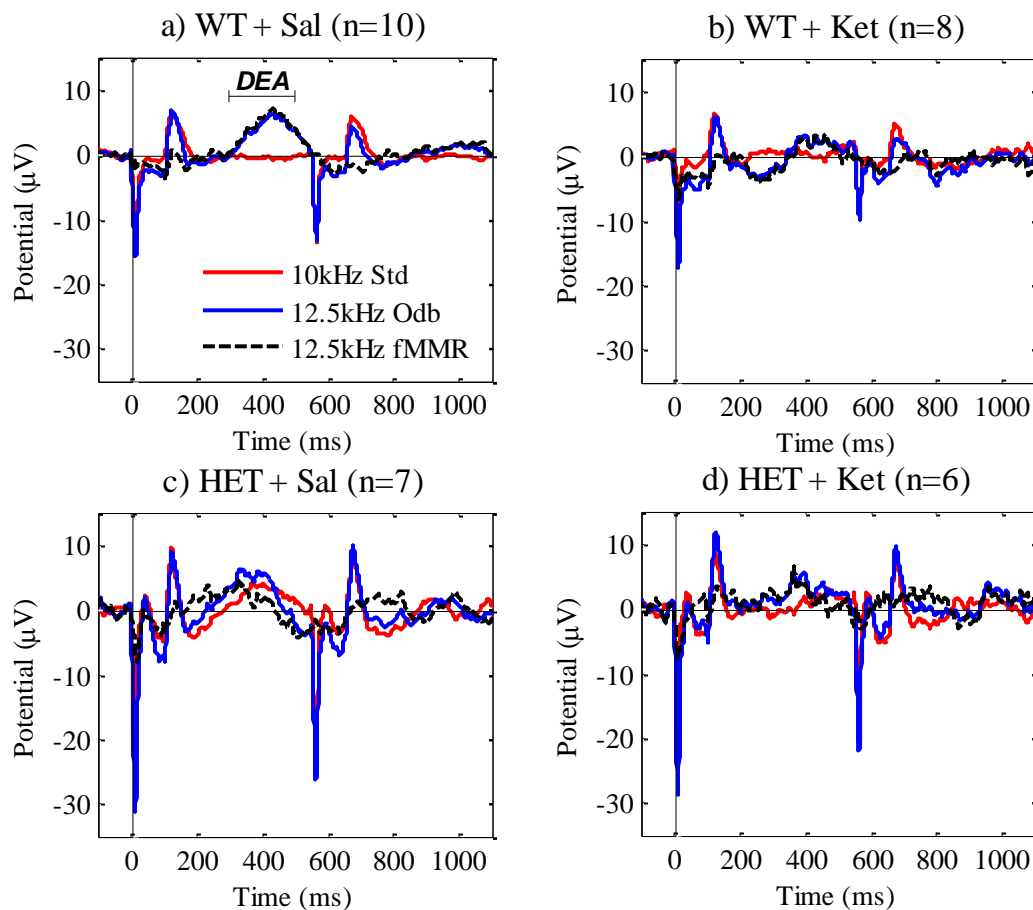


Figure 3.14 - Ascending frequency (+2.5 kHz) oddball mismatch response in urethane-anesthetised mice The 10 kHz standard (Std; red), 12.5 kHz oddball (Odb; blue) and resulting frequency mismatch response (fMMR; black dashed) auditory evoked potential waveforms are displayed for a) control (WT) mice during the saline session (Sal), b) WT mice following 10 mg/kg i.p. ketamine injection (Ket), c) *Map2k7^{+/-}* (HET) mice during the saline session, and d) HET mice during the ketamine session. The paired AEP subtraction method (Figure 3.1b) of computing the mismatch response has been applied in this analysis. Deviant evoked activity (DEA) is annotated on (a).

Control group grand-average data shown in Figure 3.13a and Figure 3.14a exhibit fMMR waveforms which reach maximum amplitude at 442.1 ms (± 16.3 ms sem). These amplitude changes are predominantly influenced by the oddball AEP, therefore may also be considered deviant evoked activity (DEA). The standardised measure of DEA mean amplitude from 300-500 ms used previously in dDA paradigm analysis (Figure 3.10) was applied here to quantify this response from WT and HET mice in the saline recording session and following 10 mg/kg i.p. ketamine administration. DEA from the 10 kHz standard are displayed in Figure 3.15a, ascending and descending (± 2.5 kHz) frequency oddballs are provided in Figure 3.15b, and the resulting fMMR difference waveforms are graphed in Figure 3.15c.

Figure 3.15a highlights that the genetic model displays increased DEA amplitude to the standard stimulus. One-way ANOVA comparing WT and HET group standard DEA mean amplitude from 300-500 ms measured from the saline recording session returned a significant effect of genotype [$F_{1,15} = 8.355$; $p = .011$], illustrating that the standard response is increased in this group, which in turn leads to a reduced fMMR shown in Figure 3.15c. Potentially this may reflect the positive half-cycle (≈ 250 -500 ms) of the underlying biphasic response observed in HET mice (Figure 3.8c-d).

From Figure 3.15b it can be seen that DEA measured from frequency oddball stimuli in both WT and HET mice are comparable. Interestingly, this amplitude was reduced following 10 mg/kg i.p. ketamine in WT mice. Oddball stimuli DEA measured from control mice were compared with a repeated measures ANOVA design with ketamine treatment as a within-subjects factor. This test confirmed that following ketamine administration DEA amplitudes were significantly lower [$F_{1,6} = 16.221$; $p = .007$], which therefore decreased the fMMR shown in Figure 3.14c.

The fMMR difference waveforms from 7.5 kHz and 12.5 kHz oddball AEPs minus the 10 kHz standard AEP are quantified in Figure 3.15c. Annotations indicate that control group (WT+Sal) DEA mean amplitudes are both significantly greater than zero (no-difference condition) [$F_{2,9} = 6.633$; $p = .030$; lower-bound adjustment], whereas HET+Sal [$F_{2,12} = .181$; $p = .837$; spherical distribution assumed], WT+Ket [$F_{2,7} = .568$; $p = .476$; lower-bound adjustment] and HET+Ket [$F_{2,8} = .551$; $p = .597$; spherical distribution assumed] group DEA measures are not significantly different from zero.

These data highlight a differential response to standard versus oddball stimuli in the WT+Sal group which results in a defined fMMR to both ascending and descending frequency oddballs. Following ketamine administration, the WT+Ket drug model displays reduced amplitude DEA to oddball stimuli, whereas the standard stimulus amplitude remains relatively similar to the saline session, thereby reducing the fMMR by a diminished oddball effect. In contrast, the HET+Sal genetic model displays oddball DEA mean amplitude comparable with the WT+Sal control group and significantly greater standard DEA, effectively reducing the fMMR by an increased response to the standard.

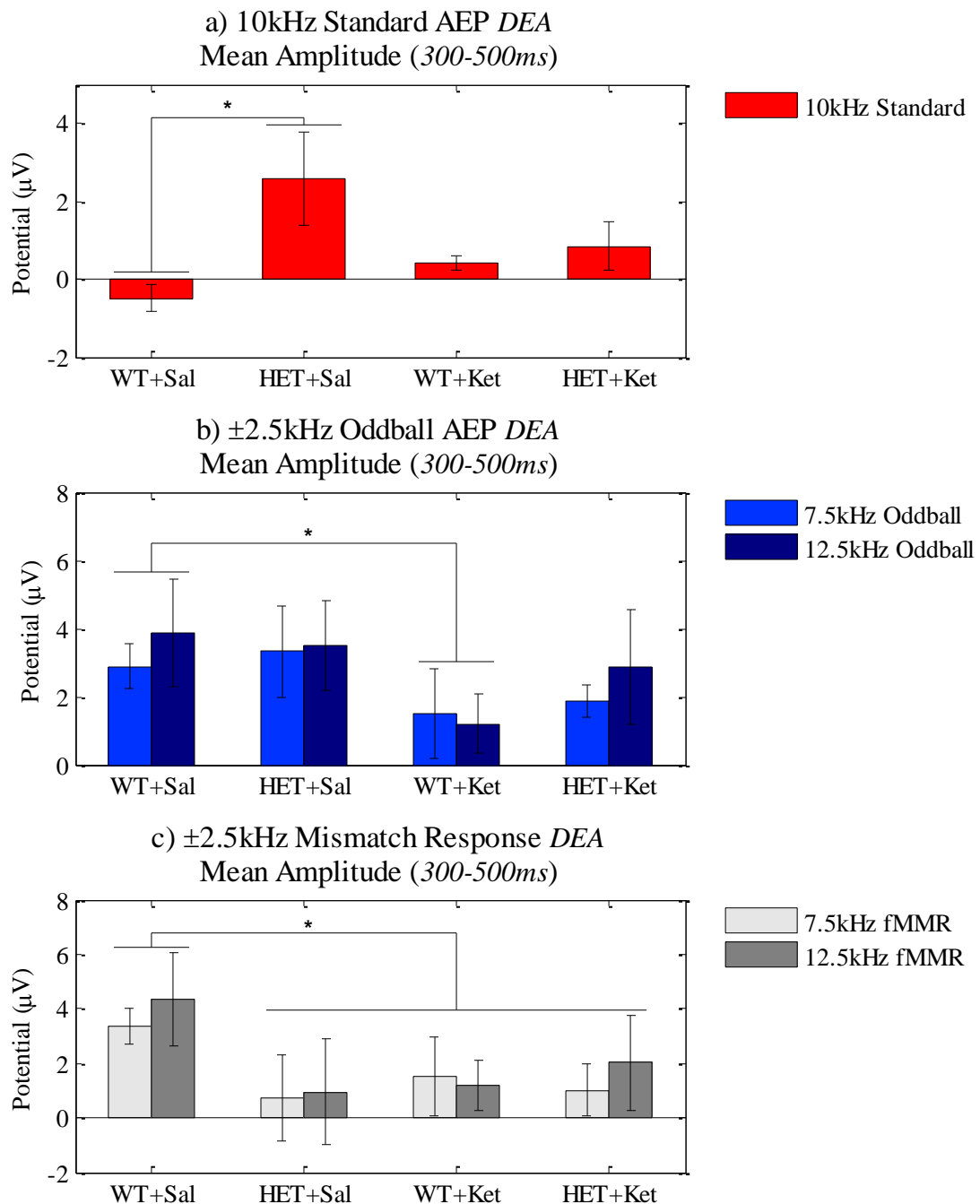


Figure 3.15 - Quantification of frequency mismatch responses in urethane-anaesthetised control, *Map2k7*^{+/-} and NMDA receptor antagonism models Deviant evoked activity (DEA), defined as mean amplitude from 300-500 ms, from control (WT) mice following saline injection (WT+Sal; control model; n = 10), *Map2k7*^{+/-} (HET) mice in the saline recording session (HET+Sal; genetic model; n = 7), WT mice following 10 mg/kg i.p. ketamine (WT+Ket; drug model; n = 8), and HET mice in the ketamine session (HET+Ket; combined genetic and drug model; n=6) is provided for: a) the 10 kHz standard stimulus auditory evoked potential (AEP), which shows a significant effect of the genetic model ($p < .05$); b) ascending (12.5 kHz) and descending (7.5 kHz) oddball stimuli AEPs showing a significant effect of the drug model ($p < .05$); and c) the resulting frequency mismatch response (fMMR) difference waves, illustrating the control group is the only one which displays amplitude significantly different from zero (no difference condition). Bar graphs represent group means \pm sem.

3.3.2.3 *Auditory evoked potentials from frequency consecutive-repetition, oddball and many-standards paradigms suggest context-specific response*

Evoked waveforms from physically identical stimuli presented in fCR, fOD and fMS paradigms are plotted alongside one another in Figure 3.16.

Data from WT animals displayed in the left hand side panels of Figure 3.16 may indicate context-specific activity in response to frequency oddball stimuli presented in the fOD paradigm. Close visual inspection of the waveforms plotted in Figure 3.16a and Figure 3.16e, from descending (7.5 kHz) and ascending (12.5 kHz) oddball stimuli, respectively, reveals a positive increase in amplitude from ≈ 300 -500 ms to these stimuli when presented in the fOD paradigm. In comparison, the standard frequency stimulus (10 kHz) AEP during the fOD paradigm in Figure 3.16c does not show this increase in potential, suggesting an amplitude increase in this period is specific to the frequency oddball condition in WT mice. The standard stimulus in the fCR paradigm may also evoke marginally higher amplitude over this latency range compared with fOD and fMS; perhaps this is because it was the first to be presented in the paradigm fCR which was played after several minutes of silence following the duration-varying auditory paradigms (see Section 2.9.1 for a description of the experimental protocol).

On the other hand, the *Map2k7*^{+/-} (HET) group grand-average waveforms plotted on the right hand side of Figure 3.16 exhibit increased potential from ≈ 300 -500 ms in response to oddball (shown in Figure 3.16b and Figure 3.16f for 7.5 kHz and 12.5 kHz stimuli, respectively) and standard frequency stimuli (Figure 3.16d); as described in Section 3.3.2.2 above. Concerning context-specific activity, it looks as though oddball stimuli in the fOD paradigm both generate amplitude that is more positive over ≈ 300 -500 ms compared with fCR and fMS paradigms. Based upon these visual observations further statistical analysis was conducted.

Deviant-evoked activity (DEA; defined in Section 3.2.9.3) mean amplitude from 300-500 ms was measured from each frequency stimulus' AEP in fCR, fOD and fMS paradigms to quantify whether visually observed context-specific amplitude changes were statistically significant. This analysis is presented in Figure 3.17a for the WT group and Figure 3.17b for the HET group during the first recording session immediately following an i.p. injection of physiological saline.

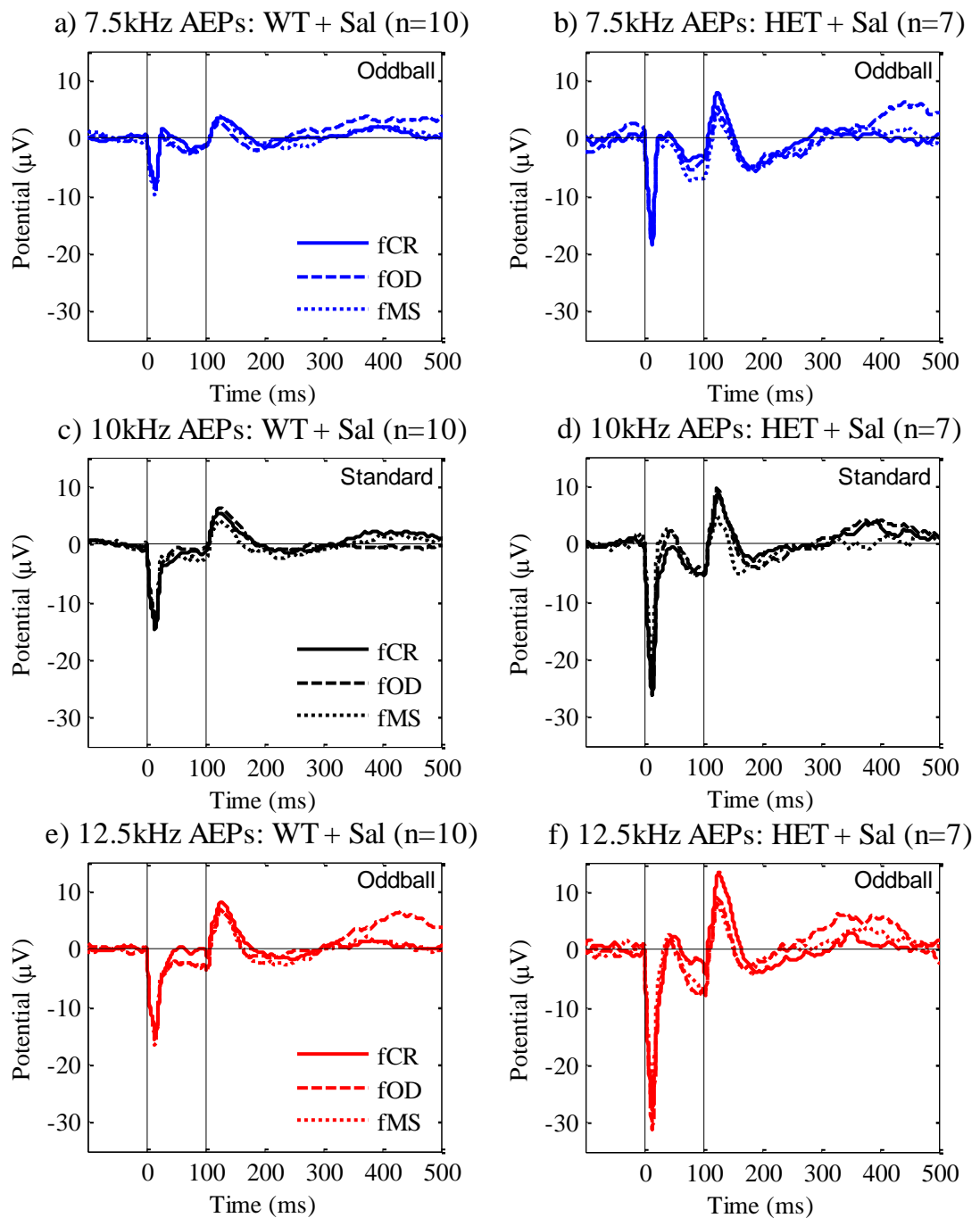


Figure 3.16 - Auditory evoked potentials from urethane-anaesthetised mice to different frequency stimuli presented in oddball and control paradigms Control (WT) animal data are on the left and *Map2k7^{+/-}* (HET) data are on the right hand side plots, which each display evoked waveforms from physically identical stimuli in frequency consecutive repetition (fCR), oddball (fOD) and many standards (fMS) paradigms presented sequentially throughout the saline recording session (Sal). Waveforms plotted are 7.5 kHz (-2.5 kHz oddball) auditory evoked potentials (AEPs) from a) WT and b) HET mice, 10 kHz (standard) AEPs from c) WT and d) HET mice, and 12.5 kHz (+2.5 kHz oddball) AEPs from e) WT and f) HET mice. There is a prominent biphasic response in the HET group waveforms which is negative from ≈ 50 -250 ms then positive from ≈ 250 -500 ms (e.g. see Figure 3.8c-d); the positive portion of this feature may correspond to the WT group frequency oddball AEP amplitude increase over approximately the same latency range.

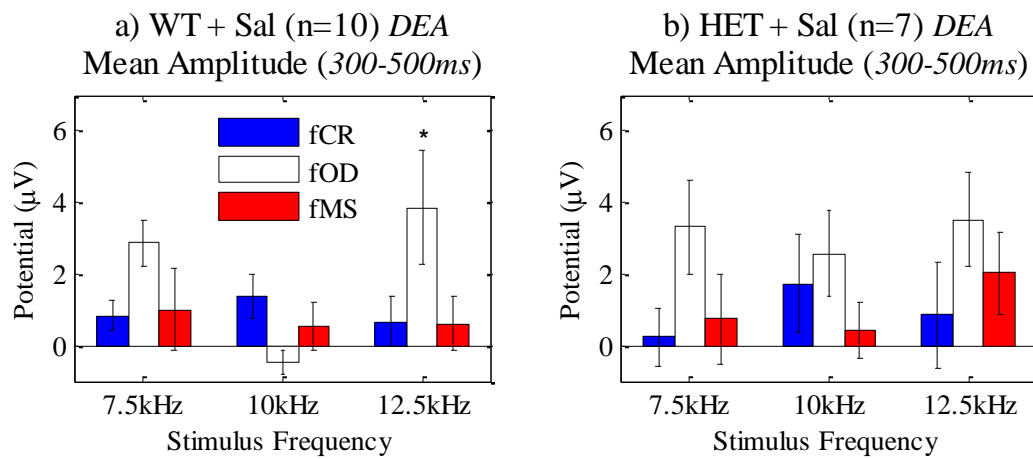


Figure 3.17 - Quantification of deviant evoked activity from urethane-anaesthetised mice to different frequency stimuli presented in oddball and control paradigms These plots display deviant evoked activity (DEA) mean amplitudes from 300-500 ms, as group means \pm sem, measured from 7.5 kHz (-2.5 kHz oddball), 10 kHz (standard) and 12.5 ($+2.5$ kHz oddball) evoked waveforms from the frequency oddball (fOD) paradigm and frequency consecutive-repetition (fCR) and many-standards (fMS) control paradigms presented during in the saline recording session (Sal). a) Control (WT) group measurements showing a significant effect of the ascending oddball presented in the fOD paradigm ($p < .05$). b) *Map2k7^{+/-}* (HET) group data.

Several other repeated measures ANOVA design tests were performed on WT and HET mice data from Figure 3.17 separately. These were conducted in three formats; 1) for each individual stimulus with paradigm as a within-subjects factor, 2) for each individual paradigm with stimulus as a within-subjects factor, and 3) taking both ascending and descending oddball stimuli and paradigm as within-subjects factors. In other words, stimuli presented in three different paradigms were compared, three physically distinct stimuli from the same auditory paradigm were compared, and oddball stimuli presented in three different paradigms were compared. For the HET group this yielded no significant results. The WT group analysis returned a significant effect of the fOD paradigm for the ascending frequency oddball (12.5 kHz) DEA [$F_{2,18} = 4.591$; $p = .024$; Mauchly's test $p > .05$], significantly lower amplitude response to the standard stimulus in the fOD paradigm [$F_{2,18} = 6.633$; $p = .030$; lower-bound because Mauchly's test $p < .05$], and a significant effect of paradigm for both oddball stimuli [$F_{2,18} = 5.118$; $p = .050$; lower-bound because Mauchly's test $p < .05$]. These findings reinforce the suggestion that urethane-anaesthetised WT control mice exhibit a context-specific fMMR that is not apparent in *Map2k7^{+/-}* mice.

3.3.2.4 *Frequency deviant-alone paradigm stimuli elicit extended latency potentials which correlate with frequency mismatch responses*

Similarly to the dDA paradigm discussed in Section 3.3.1.5, fDA paradigm evoked waveforms display relatively large amplitude deflections after stimulus onset and offset responses (see Figure 3.18). The cause of these features is not obviously linked to auditory stimulation *per se* because they occur well after stimuli offset. They also appear to be diminished in the second recording session after an injection of 10 mg/kg i.p. ketamine, as did the dDA paradigm waveforms shown in Figure 3.9. These observations from all DA paradigms in Experiment I are assessed in Section 3.3.4.3.

Quantification of these AEP features was performed by measuring DEA mean amplitude from 300-500 ms. This analysis is provided in Figure 3.18e and Figure 3.18f for 7.5 kHz and 12.5 kHz stimuli, respectively. Annotations in both of these plots indicate a significant overall reduction following 10 mg/kg i.p. ketamine administration [$F_{1,10} = 8.110$; $p = .017$]. This was determined by repeated measures ANOVA with stimulus frequency and session as within-subjects factors and gender and genotype as between-subjects factors. There were no significant effects of genotype [$F_{1,10} = .042$; $p = .842$], gender [$F_{1,10} = 2.253$; $p = .164$] or stimulus frequency [$F_{1,10} = .184$; $p = .677$].

Statistical analysis suggested a trend for an interaction effect between stimuli and genotype [$F_{1,10} = 4.098$; $p = .070$]. Visual comparison of the 7.5 kHz stimulus fDA data from the saline recording session in Figure 3.18e may suggest that there may be a difference between genotypes, and that following 10 mg/kg i.p. ketamine this response is abolished. To investigate further, a one-way ANOVA was performed on the 7.5 kHz fDA paradigm DEA from the saline recording session which revealed a significant effect of genotype [$F_{1,13} = 4.664$; $p = .050$], perhaps indicating that HET mice are more sensitive to the fDA condition. Notwithstanding, there was no significant interaction effect between genotype and ketamine [$F_{1,10} = .996$; $p = .342$] for the 7.5 kHz fDA stimulus DEA.

Interestingly, the shape and trajectory of fDA waveforms in Figure 3.18a-d bear some resemblance to fMMR difference waveforms in Figure 3.13 and Figure 3.14. Control group data from the saline recording session (WT+Sal) are sampled to compare these similarities, with descending (7.5 kHz) frequency stimuli plotted in Figure 3.19a and ascending (12.5 kHz) frequency stimuli in Figure 3.19b. The HET group are considered to have a potentially disrupted fMMR therefore are unsuitable for this analysis.

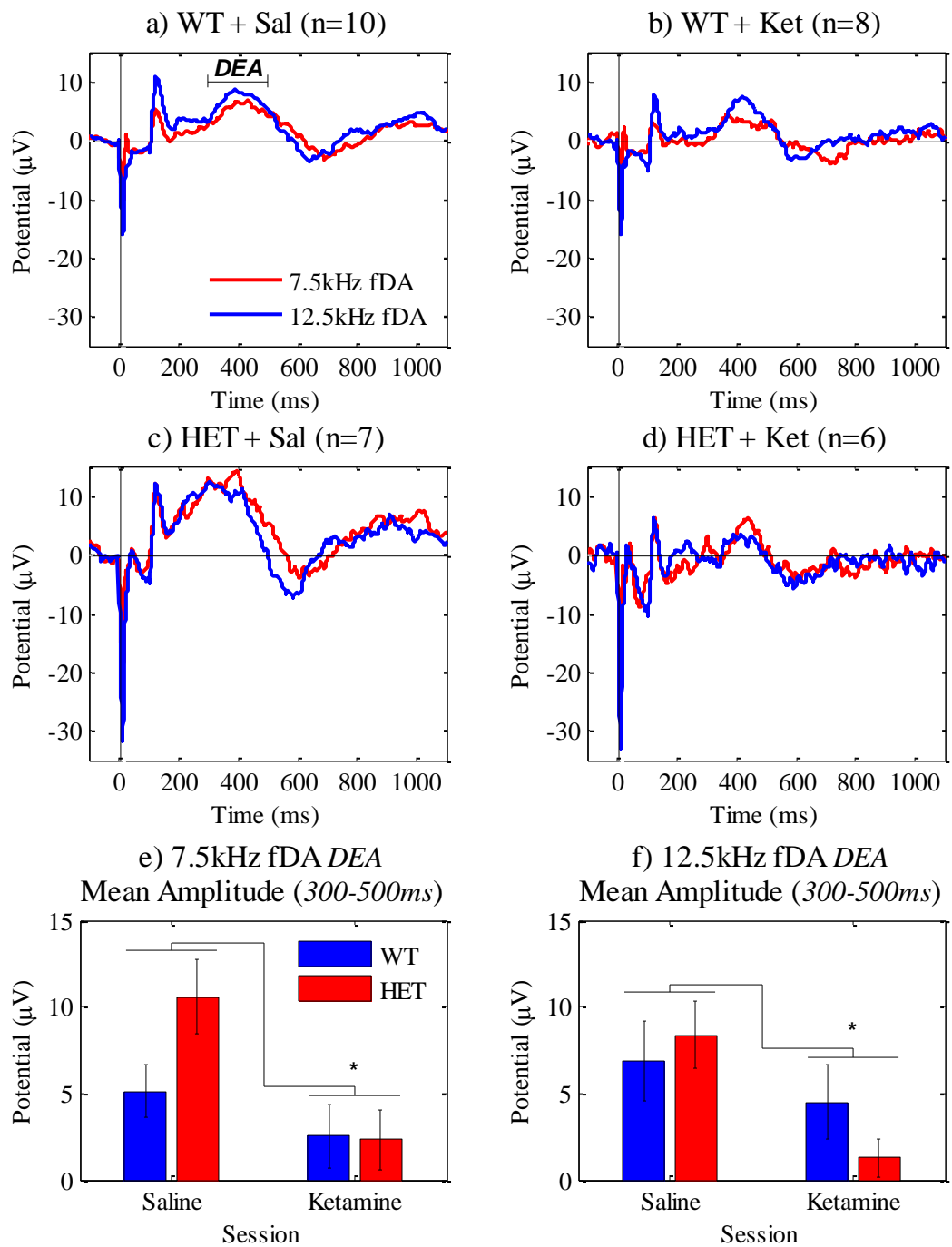


Figure 3.18 - Extended latency auditory evoked potentials to frequency deviant-alone paradigm stimuli in urethane-anaesthetised mice The 7.5 kHz (red) and 12.5 kHz (blue) stimuli evoked waveforms are shown for a) control (WT) mice during the saline session (Sal), b) WT mice following a 10 mg/kg i.p. ketamine injection (Ket), c) *Map2k7^{+/-}* (HET) mice during the saline session, and d) HET mice during the ketamine session. Quantification of e) 7.5 kHz, and f) 12.5 kHz stimuli waveform deviant evoked activity (DEA) mean amplitude from 300-500 ms, as annotated in (a), both showing a significant overall difference ($p < .05$) between sessions; hence the response to ketamine was reduced in WT and HET mice as compared to following saline treatment.

Data in Figure 3.19 have been processed with an 8th order low-pass Butterworth response digital filter with a 10 Hz cut-off frequency to isolate slow AEP features. Also, stimulus onset and offset potentials from fDA paradigm waveforms <170 ms which cannot be compared have been removed. Comparing the shape of both pairs of waveforms reveals that fMMR and fDA evoked responses from urethane-anaesthetised mice are closely correlated ($R^2 > .75$), potentially suggesting that they may share the same underlying neuronal mechanisms, which may reflect environmental salience.

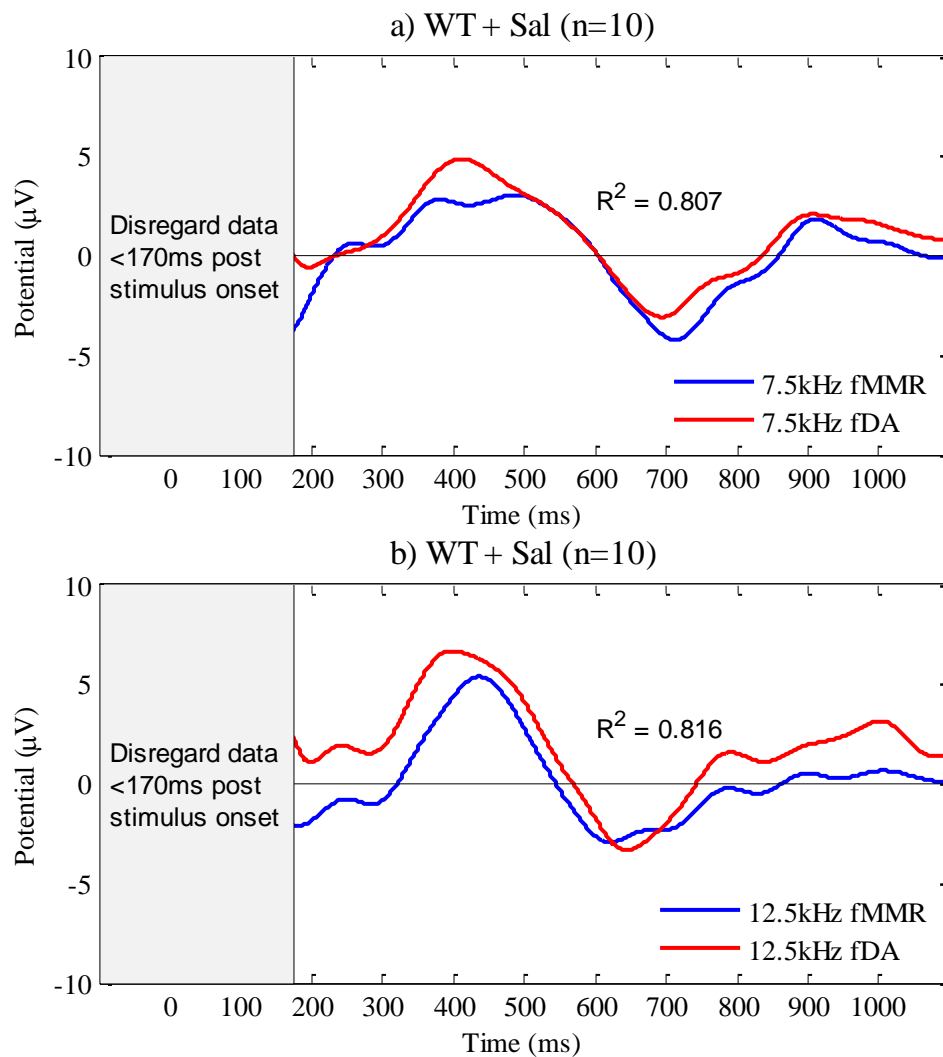


Figure 3.19 - Comparison of frequency mismatch response and deviant-alone paradigm extended latency evoked potentials from urethane-anaesthetised mice These plots from control animals in the saline session (WT + Sal) display the extended epoch frequency mismatch response (fMMR) and deviant-alone (fDA) waveforms elicited by a) 7.5 kHz (-2.5 kHz descending oddball), and b) 12.5 kHz (+2.5 kHz ascending oddball) stimuli. Both fMMR and fDA waveforms following closely correlated trajectories ($R^2 > .75$). Activity <170 ms is omitted because stimulus onset and offset peaks occur during this time. These data have been filtered with a 10 Hz cut-off low-pass filter.

3.3.3 *Intensity paradigms in urethane-anaesthetised mice*

Findings from Experiment I intensity consecutive-repetition (iCR), oddball (iOD), deviant-alone (iDA) and many-standards (iMS) paradigms are presented in this section. The effect of auditory stimuli intensities on resulting AEP features, the intensity mismatch response, intensity oddball and control paradigm analysis, and correlation between deviant-alone waveforms and the intensity mismatch response are described.

3.3.3.1 *Stimulus intensity influences auditory evoked potentials*

Auditory stimulus intensity or sound pressure level (SPL) has a fundamental relationship with AEP onset (N1) and offset (P_{offset}) potentials, somewhat similar to tone frequency dependencies discussed in Section 3.3.2.1.

Figure 3.20 provides an analysis of auditory onset responses generated by ten discrete intensity stimuli presented in the iMS paradigm. Waveforms plotted in Figure 3.20a-b visually demonstrate that higher SPL stimuli tend to generate a larger magnitude response. N1 peak amplitudes plotted across stimuli intensity are shown alongside linear regression equations and correlation coefficients in Figure 3.20c-d, which both clearly demonstrate strong inverse linearity ($R^2 < -.9$).

The equivalent analysis for iMS paradigm stimuli offset responses is provided in Figure 3.21. The relationship between SPL and P_{offset} magnitude is apparent from the waveforms displayed in Figure 3.21a-b. These AEPs have had 10 ms pre-offset baseline correction applied (as discussed in Section 3.2.8.3). P_{offset} peak amplitude measurements plotted across stimuli intensities in Figure 3.21c-d illustrate a direct linear relationship ($R^2 > .9$).

Together these data clearly indicate that stimulus intensity/SPL has a direct effect on auditory N1 and P_{offset} potentials measured from the mouse primary auditory cortex EEG.

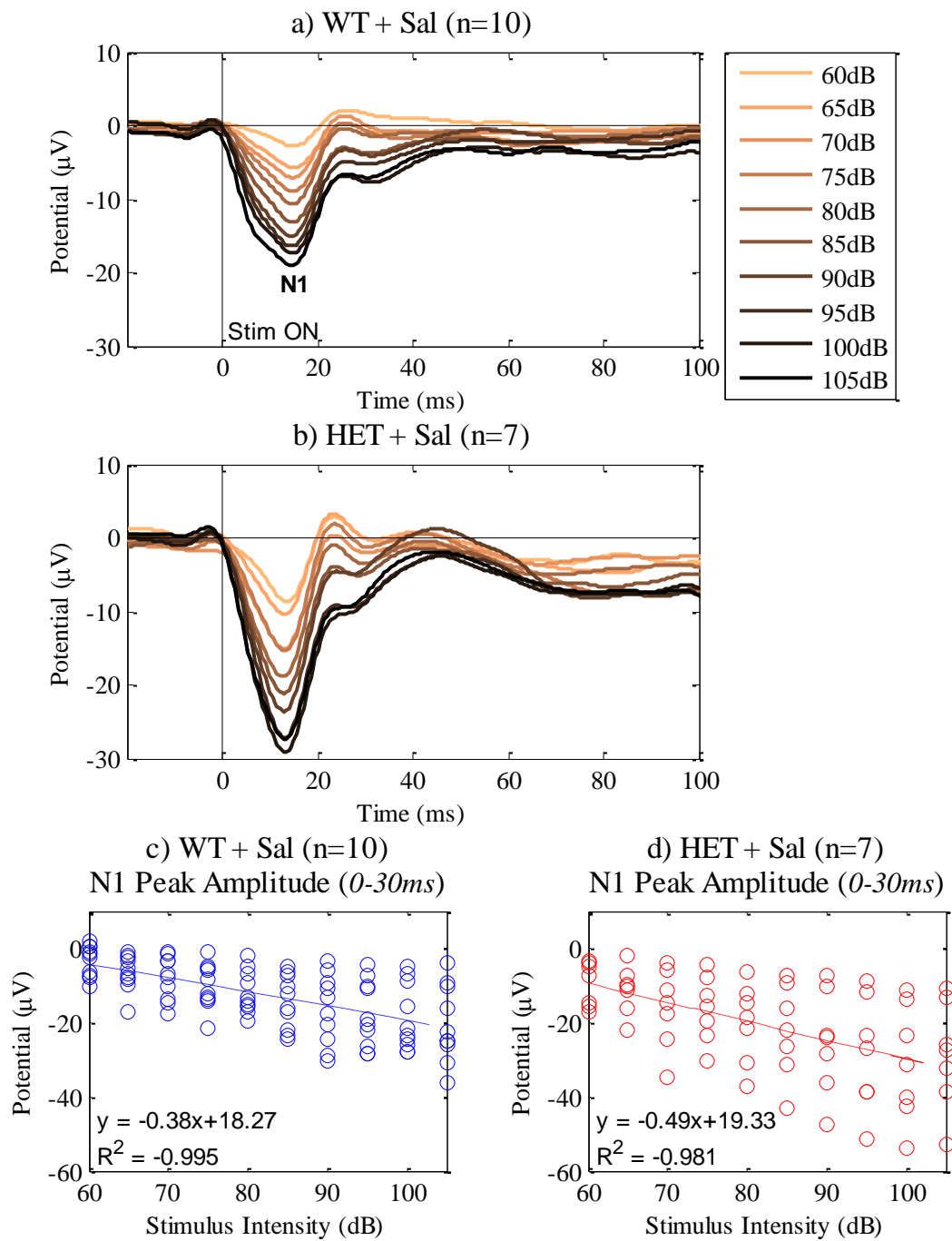


Figure 3.20 - Effect of sound pressure level on auditory onset response in urethane-anaesthetised mice This data was obtained from the intensity many-standards (iMS) paradigm after administration of saline (Sal). a) Control (WT), and b) *Map2k7*^{+/-} (HET) group grand-average auditory evoked potential onset responses from ten iMS stimuli. c) WT, and d) HET subject-wise quantification of onset response (N1) peak amplitude from different intensity (sound pressure level) stimuli with linear regression and correlation coefficients showing strong inverted linear relationships ($R^2 < -.9$). Measurement windows are shown *in brackets*.

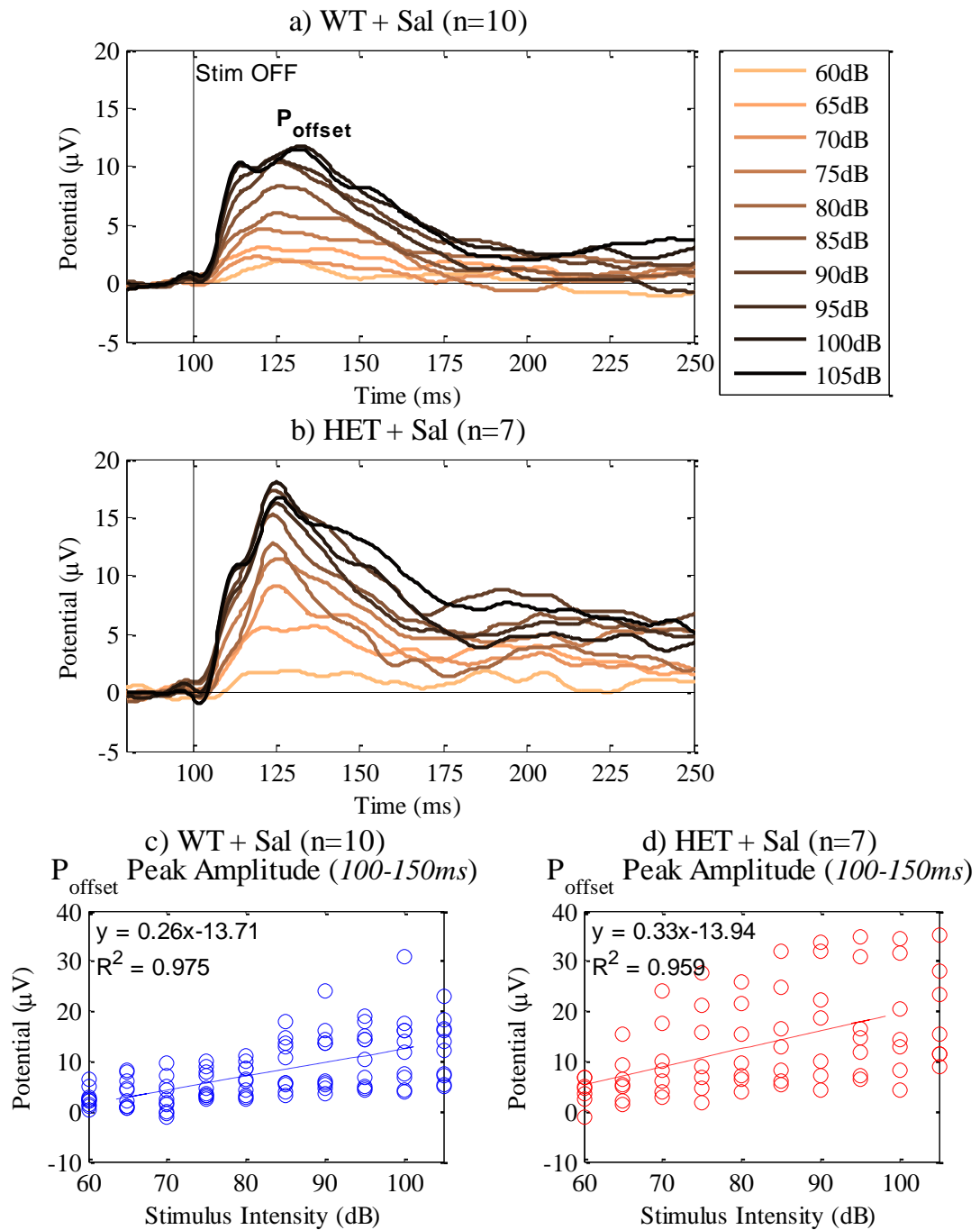


Figure 3.21 - Effect of sound pressure level on auditory offset response in urethane-anaesthetised mice This data was obtained from the intensity many-standards (iMS) paradigm during the saline session (Sal). a) Control (WT), and b) *Map2k7^{+/-}* (HET) group grand-average auditory evoked potential offset responses with 10 ms pre-offset baseline correction applied (e.g. see Figure 3.2). c) WT, and d) HET subject-wise quantification of offset response (P_{offset}) peak amplitudes to different intensity stimuli with linear regression and correlation coefficients, both showing highly linear relationships ($R^2 > .9$). Measurement windows are shown *in brackets*.

3.3.3.2 *Increasing intensity oddball elicits a mismatch response*

Results from the iOD paradigm are presented here. This paradigm was designed to investigate the intensity mismatch response (iMMR) of urethane-anaesthetised mice to oddball stimuli which varied by ± 10 dB from an 80 dB standard. Quieter (70 dB) and louder (90 dB) oddball stimuli evoked waveforms are plotted in Figure 3.22 and Figure 3.23, respectively, alongside the standard (80 dB) AEP and each respective iMMR difference wave.

Firstly, addressing the quieter oddball in Figure 3.22, the resulting iMMR seen in the control group is not the same as those previously observed from the fOD paradigm in Section 3.3.2.2. Early deflections in the 70 dB iMMR occur during stimuli onset and offset potential latencies, which as illustrated in Section 3.3.3.1 are sensitive to stimulus intensity. Thus these deflections are caused by differences in N1 and P_{offset} amplitudes evoked by standard and oddball stimuli. No additional features are apparent from these waveforms, suggesting that the decreasing intensity oddball does not generate an iMMR that reflects sensory memory disruption.

In contrast, louder oddball stimuli (Figure 3.23) are seen to elicit a large positive amplitude extended-latency iMMR in WT mice during the saline recording session, which peaks at 415.1 ms (± 31.4 ms sem), comparable with fMMR waveforms reported in Section 3.3.2.2. In the recording session following 10 mg/kg i.p. ketamine administration this response is entirely abolished and the iMMR amplitude during this latency range remains near to baseline levels. HET mice do not exhibit substantial differences between 80 dB standard and 90 dB oddball stimuli AEPs other than onset and offset response amplitudes, resulting in a less pronounced iMMR, with no apparent effects of ketamine on these waveforms.

Quantification of control and disease model group waveforms from the iOD paradigm are provided in Figure 3.24. Deviant evoked activity mean amplitude from 300-500 ms measured from 80 dB standard stimuli are presented in Figure 3.24a, from both ± 10 dB oddball stimuli in Figure 3.24b, and from both of the resulting iMMR difference waveforms in Figure 3.24c. This approach is consistent with that applied to quantify the fOD paradigm data in Figure 3.15.

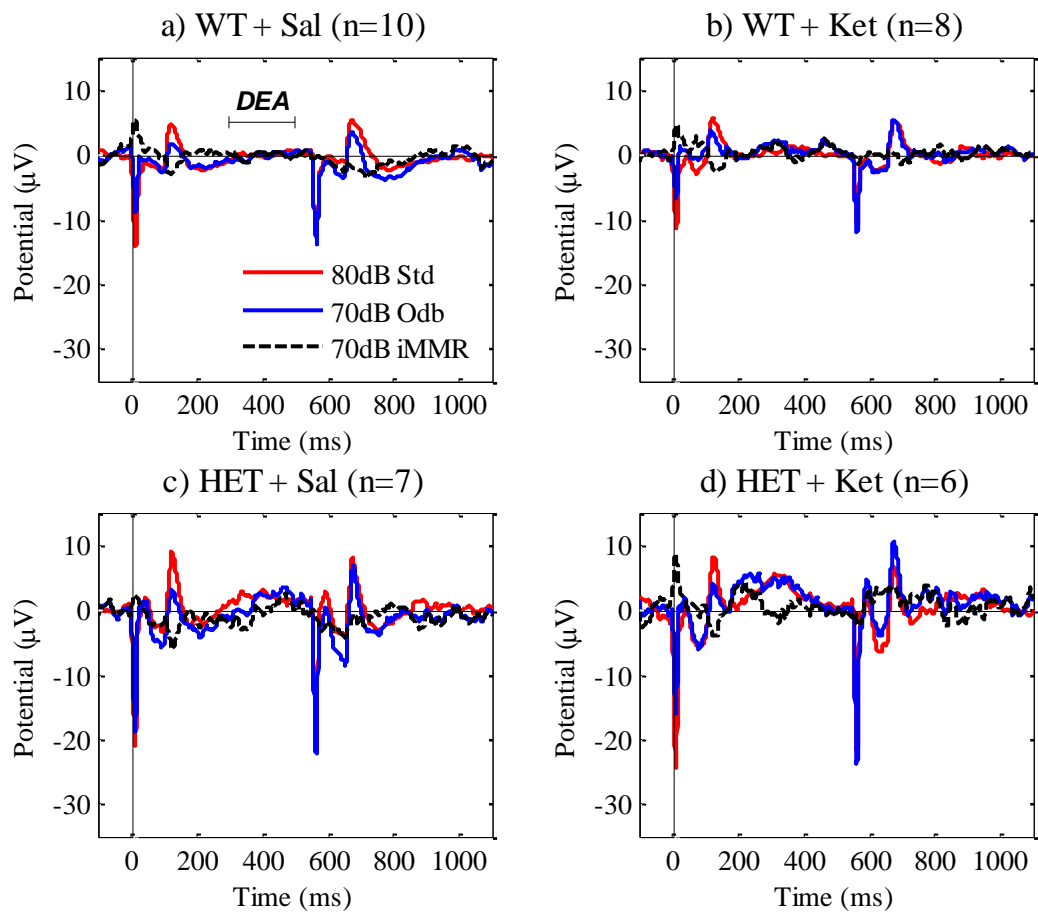


Figure 3.22 - Quieter intensity (-10 dB) oddball mismatch response in urethane-anesthetised mice The 80 dB standard (Std; red), 70 dB oddball (Odb; blue) and resulting intensity mismatch response (iMMR; black dashed) auditory evoked potential waveforms are displayed for a) control (WT) mice during the saline session (Sal), b) WT mice following 10 mg/kg i.p. ketamine injection (Ket), c) *Map2k7*^{+/-} (HET) mice during the saline session, and d) HET mice during the ketamine session. The paired AEP subtraction method (Figure 3.1b) has been applied in this analysis. The deviant evoked activity (DEA) measurement window is annotated on (a), highlighting an absence of response.

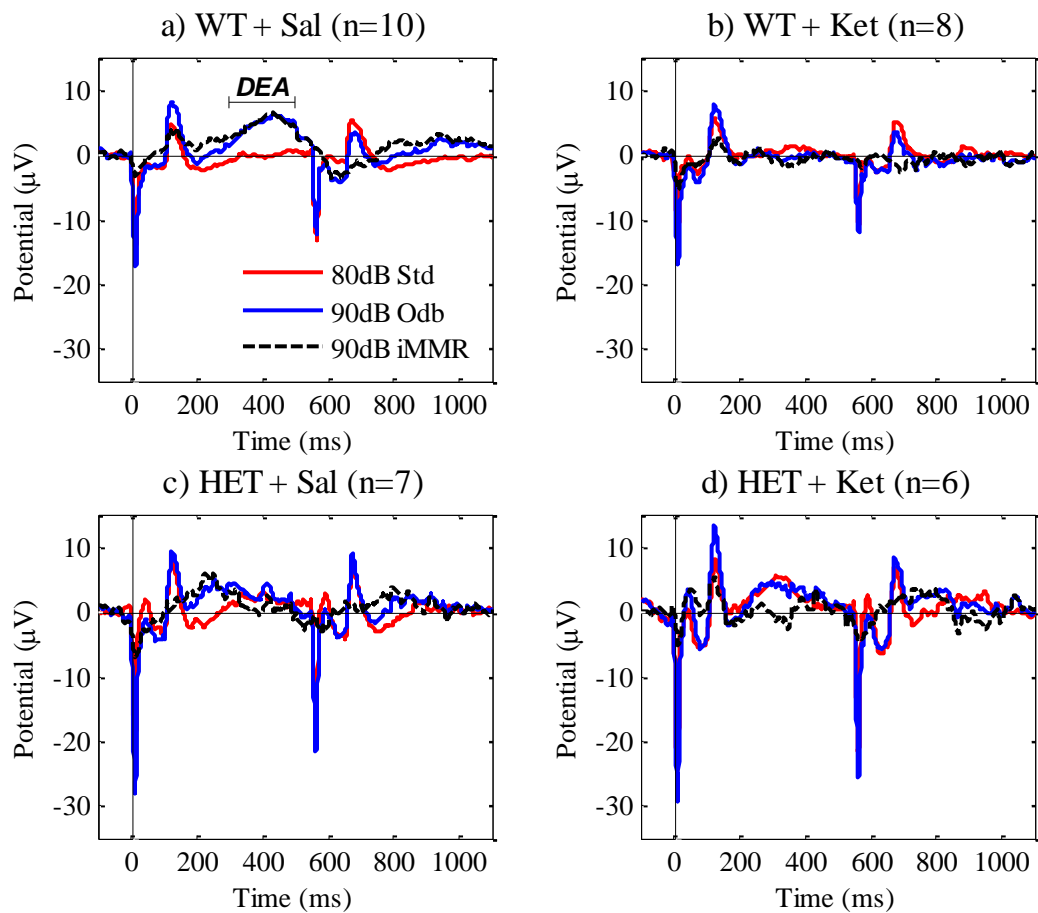


Figure 3.23 - Louder intensity (+10 dB) oddball mismatch response in urethane-anesthetised mice The 80 dB standard (Std; red), 90 dB oddball (Odb; blue) and resulting intensity mismatch response (MMR; black dashed) auditory evoked potential waveforms are displayed for a) control (WT) mice during the saline session (Sal), b) WT mice following 10 mg/kg i.p. ketamine injection (Ket), c) *Map2k7*^{+/-} (HET) mice during the saline session, and d) HET mice during the ketamine session. The paired AEP subtraction method (Figure 3.1b) has been applied in this analysis. Deviant evoked activity (DEA) is annotated on (a).

In Figure 3.24a the 80 dB standard stimulus DEA mean amplitude from 300-500 ms displays a statistically significant effect of genotype, revealed by one-way ANOVA with genotype as a between-subjects factor [$F_{2,12} = 5.416$; $p = .034$]. This data parallels findings from the fOD paradigm shown in Figure 3.15a, reinforcing the suggestion that *Map2k7^{+/-}* mice show more responsivity to standard stimuli.

Data displayed in Figure 3.24b illustrate that 90 dB oddball stimuli evoke higher amplitude DEA than 70 dB oddball in the control group during the saline session (WT+Sal), and additionally that this amplitude is significantly reduced following 10 mg/kg i.p. ketamine administration in the drug model (WT+Ket). This finding was confirmed statistically by performing a repeated measures ANOVA on 90 dB oddball data from WT mice with session as a within-subjects factor, returning a significant effect of ketamine versus saline to reduce DEA mean amplitude from the 90 dB fOD stimulus AEP [$F_{1,7} = 6.654$; $p = .037$].

Figure 3.24c illustrates that when each iMMR is individually compared against zero (no difference condition) by a repeated measures ANOVA with stimuli and zero as within-subjects factors, only the 90 dB iMMR from control animals during the saline recording session (WT+Sal) displays a value significantly greater than zero [$F_{1,9} = 7.715$; $p = .021$]. The same statistical test for genetic (HET+Sal) [$F_{1,6} = .344$; $p = .579$], drug (WT+Ket) [$F_{1,7} = .463$; $p = .518$] and combined drug and genotype model (HET+Ket) [$F_{1,5} = .031$; $p = .868$] groups returned no significant effects. Annotations in the plot are used to emphasise this distinction.

Overall these data from the iOD paradigm suggest that louder intensity oddball stimuli evoke an iMMR with similar characteristics to the fMMR previously observed (Section 3.3.2.2), whereas quieter intensity oddball stimuli did not evoke this response. The *Map2k7^{+/-}* mice displayed an increased response to the standard stimulus which lowers iMMR amplitude. Recordings made from WT mice following 10 mg/kg i.p. ketamine (drug model) demonstrate reduced amplitude in response to the 90 dB oddball stimulus. Therefore enhanced response to the standard and diminished response to the oddball are separate electrophysiological reactions by which iMMR amplitude reduction occurs in the genetic and drug models, respectively.

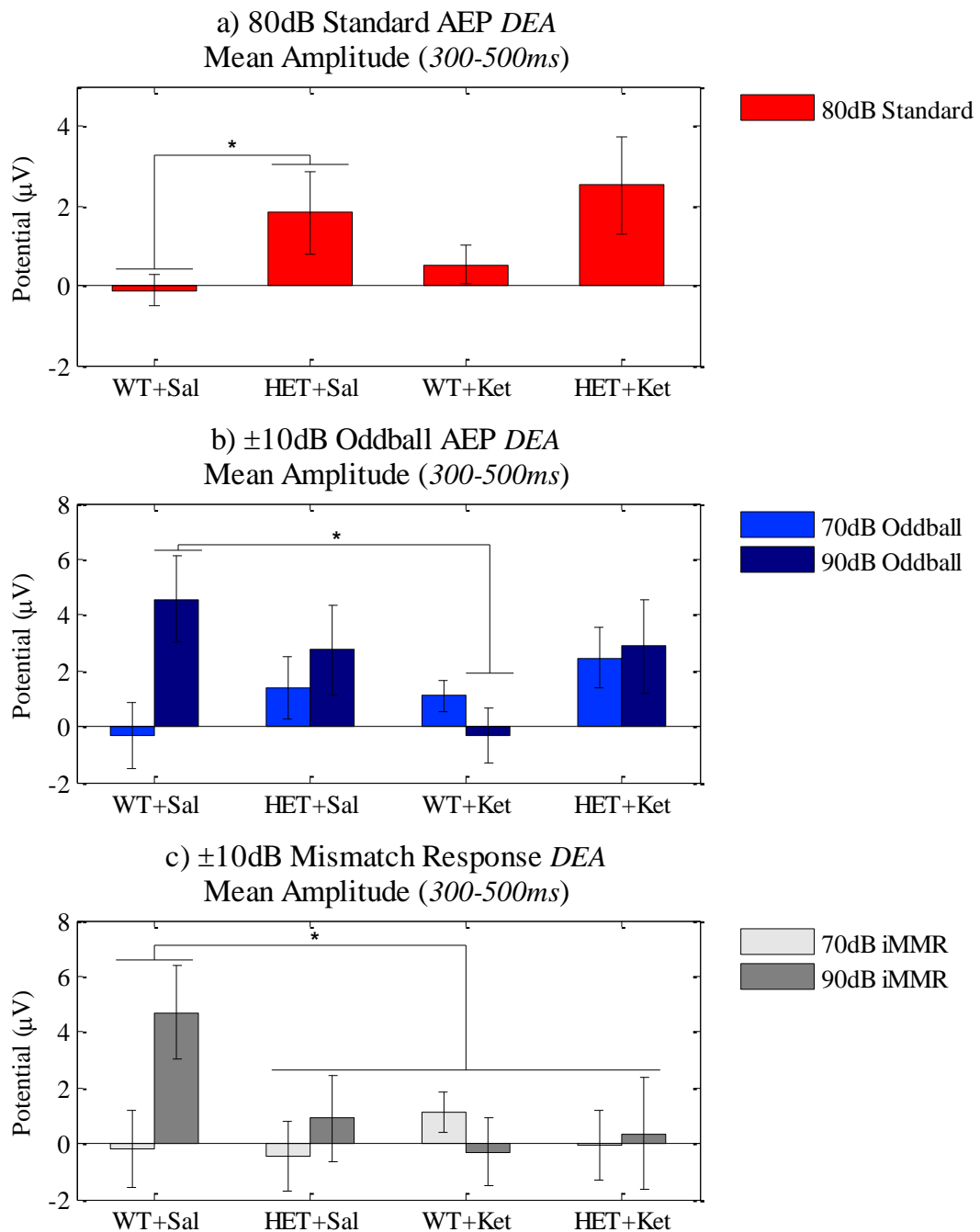


Figure 3.24 - Quantification of intensity mismatch responses in urethane-anaesthetised control, *Map2k7*^{+/-} and NMDA receptor antagonism models Deviant evoked activity, defined as mean amplitude from 300-500 ms, from control (WT) mice following saline injection (WT+Sal; control model; n = 10), *Map2k7*^{+/-} (HET) mice in the saline recording session (HET+Sal; genetic model; n = 7), WT mice following 10 mg/kg i.p. ketamine (WT+Ket; drug model; n = 8), and HET mice in the ketamine session (HET+Ket; combined genetic and drug model; n=6) is provided for a) the 80 dB standard stimulus auditory evoked potential (AEP), which shows a significant effect of the genetic model ($p < .05$); b) louder (90 dB) and quieter (70 dB) oddball stimuli AEPs, showing a significant effect of the 90 dB oddball which is reduced in the drug model ($p < .05$), and c) the resulting intensity mismatch response (iMMR), illustrating that the 90 db–80 dB difference waveform in the control group is the only one which displays amplitude significantly greater than zero (no difference condition). Bars represent group means \pm sem.

3.3.3.3 *Auditory evoked potentials from intensity consecutive-repetition, oddball and many-standards paradigms suggest context-specific response*

Physically identical stimuli AEP waveforms from iCR, iOD and iM) paradigms are plotted together in Figure 3.25. Data from WT and HET groups during the saline recording session are plotted in the left and right hand side of the figure, respectively.

Visual inspection of WT data may suggest that context-specific activity is observed in response to the 90 dB oddball stimulus from the iOD paradigm. 90 dB stimuli AEPs from iCR and iMS paradigms do not elicit the same positive amplitude deflection from ≈ 300 -500 ms observed in the iOD paradigm, suggesting that this feature is specific to the oddball condition. 80 dB and 70 dB stimuli AEPs in WT mice do not exhibit any obvious context-specific response.

From the HET group data it is difficult to distinguish any activity which may be considered context-specific. All of the AEP waveforms shown appear to exhibit a slow biphasic response which goes negative from ≈ 50 -250 ms then positive from ≈ 250 ms onwards; this underlying waveform is described in Section 3.3.1.4. The positive portion of this underlying characteristic appears to follow a similar trajectory to the (90 dB) oddball-specific response observed in WT mice.

To quantify the identified amplitude changes from these waveforms DEA mean amplitude within a specified measurement window of 300-500 ms was compared across stimuli, paradigms, and between groups, as shown in Figure 3.26.

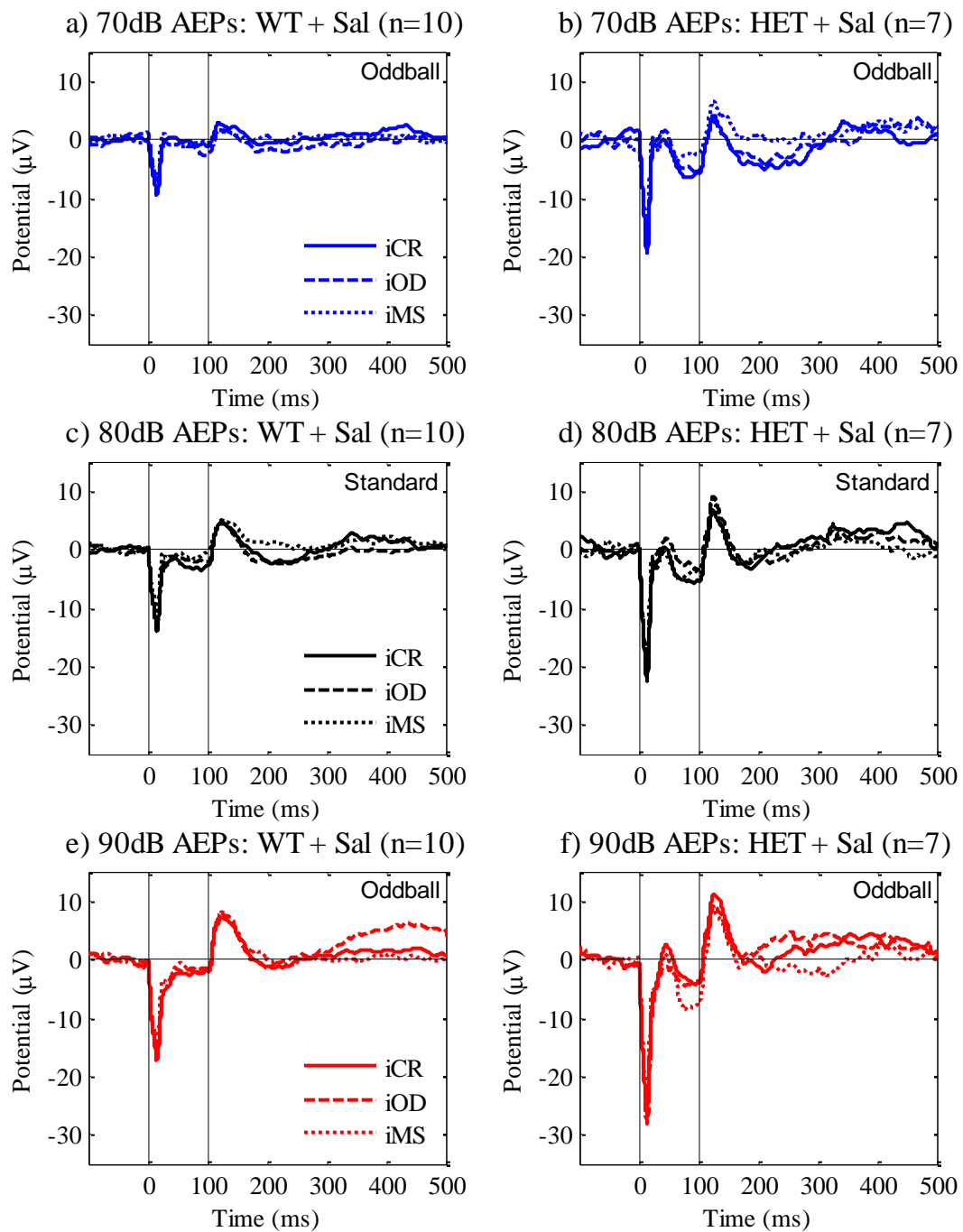


Figure 3.25 - Auditory evoked potentials from urethane-anesthetised mice to different intensity stimuli presented in oddball and control paradigms Control (WT) animal data are on the left and *Map2k7^{+/-}* (HET) data are on the right hand side plots, which each display evoked waveforms to physically identical stimuli in intensity consecutive repetition (iCR), oddball (iOD) and many standards (iMS) paradigms presented sequentially throughout the saline recording session (Sal). Waveforms plotted are 70 dB (-10 dB oddball) auditory evoked potentials (AEPs) from a) WT and b) HET mice, 80 dB (standard) AEPs from c) WT and d) HET mice, and 90 dB (+10 dB oddball) AEPs from e) WT and f) HET mice.

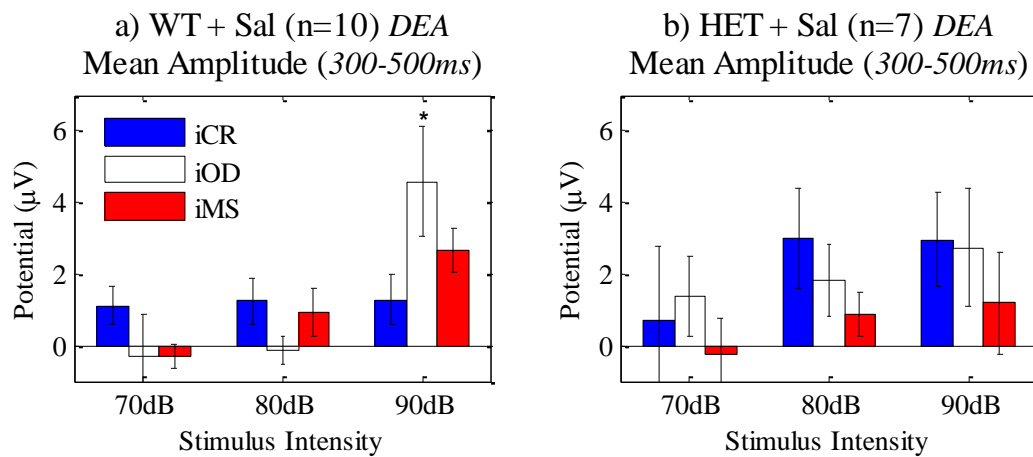


Figure 3.26 - Quantification of deviant evoked activity from urethane-anaesthetised mice to different intensity stimuli presented in oddball and control paradigms These bar graphs of group means \pm sem display deviant evoked activity (DEA) measurements, defined as mean amplitude from 300-500 ms, from 70 dB (-10 dB oddball), 80 dB (standard) and 90 dB (+10 dB oddball) intensity stimuli auditory evoked potentials (AEPs) from intensity oddball (iOD) paradigm and intensity consecutive-repetition (iCR) and many standards (iMS) control paradigms in the saline session (Sal). a) Control (WT) group measurements showing a significant effect of the louder oddball presented in the iOD paradigm ($p < .05$). b) *Map2k7^{+/-}* (HET) group data showing no significant effects.

Repeated measures ANOVA tests were performed on these data similarly to those applied to frequency-varying paradigms in Figure 3.17 to compare DEA from physically identical stimuli presented in iOD, iCR and iMS paradigms. Essentially for each group individual stimuli were compared across three paradigms and for individual paradigms the three stimuli were compared. This analysis revealed a significant effect of the iOD paradigm for the 90 dB stimulus [$F_{2,8} = 13.592$; $p = .006$; lower-bound because Mauchly's test $p < .05$], and a significant effect of the 90 dB stimulus within the iOD paradigm [$F_{2,16} = 7.344$; $p = .005$; Mauchly's test $p > .05$] in the control group, as may be expected. Overall these findings indicate that louder oddball stimuli elicit an iMMR which manifests as a measured increase in amplitude over the 300-500 ms latency range in wild-type mice, similar to which was observed in response to frequency oddball and deviant-alone paradigm stimuli AEPs. Notably the 90 dB stimulus does not evoke this response in *Map2k7^{+/-}* mice.

3.3.3.4 *Intensity deviant-alone paradigm elicits extended latency potentials which correlate with mismatch response of increasing intensity oddball stimuli*

The iDA paradigm evoked responses from WT and HET mice during saline and 10 mg/kg i.p. ketamine recording sessions are analysed in Figure 3.27. These appear very similar to data from dDA and fDA paradigms discussed in Section 3.3.1.5 and Section 3.3.2.4, respectively.

Relatively large amplitude positive deflections occur following stimuli offset responses in waveforms from the saline session. These are typical of DA paradigm AEPs previously addressed. This DEA is reduced in recordings following 10 mg/kg i.p. ketamine administration, consistent with previously presented findings. These observations are quantified in Figure 3.27e-f.

Repeated measures ANOVA using stimuli and session as within-subject factors and gender and genotype as between-subjects factors revealed a significant overall difference between saline and ketamine sessions [$F_{1,10} = 7.058$; $p = .024$]. There were no direct effects of stimulus intensity [$F_{1,10} = .868$; $p = .374$], gender [$F_{1,10} = .814$; $p = .388$] or genotype [$F_{1,10} = .005$; $p = .945$]; however this analysis did suggest a trend for an interaction between genotype and DEA amplitude from different intensity stimuli [$F_{1,10} = 4.459$; $p = .061$]. Based upon this a one-way ANOVA was conducted. This additional test assessed the lower intensity stimulus DEA mean amplitude measured from 300-500 ms across genotypes and returned a non-significant result [$F_{1,13} = 3.932$; $p = .069$].

These iDA paradigm AEPs may be compared against iMMR difference waveforms obtained from the iOD paradigm, as was performed for frequency-varying stimuli in Figure 3.19. This analysis for the control group during the saline recording session is shown in Figure 3.28. The quieter oddball (70 dB) iMMR and equivalent iDA paradigm AEP are plotted in the upper panel. Visual inspection of these waveforms and the accompanying correlation coefficient suggest that they are relatively unlike, suggesting that quieter oddball stimuli may not trigger the same response as the iDA paradigm. The lower panel presents the louder oddball (90 dB) iMMR and its associated iDA paradigm AEP. Here there appears to be a closer relationship, perhaps indicative of common underlying neuronal generators. All of the waveforms in Figure 3.28 have been processed with an 8th order low-pass Butterworth filter with 10 Hz cut-off frequency to isolate slow-wave AEP features.

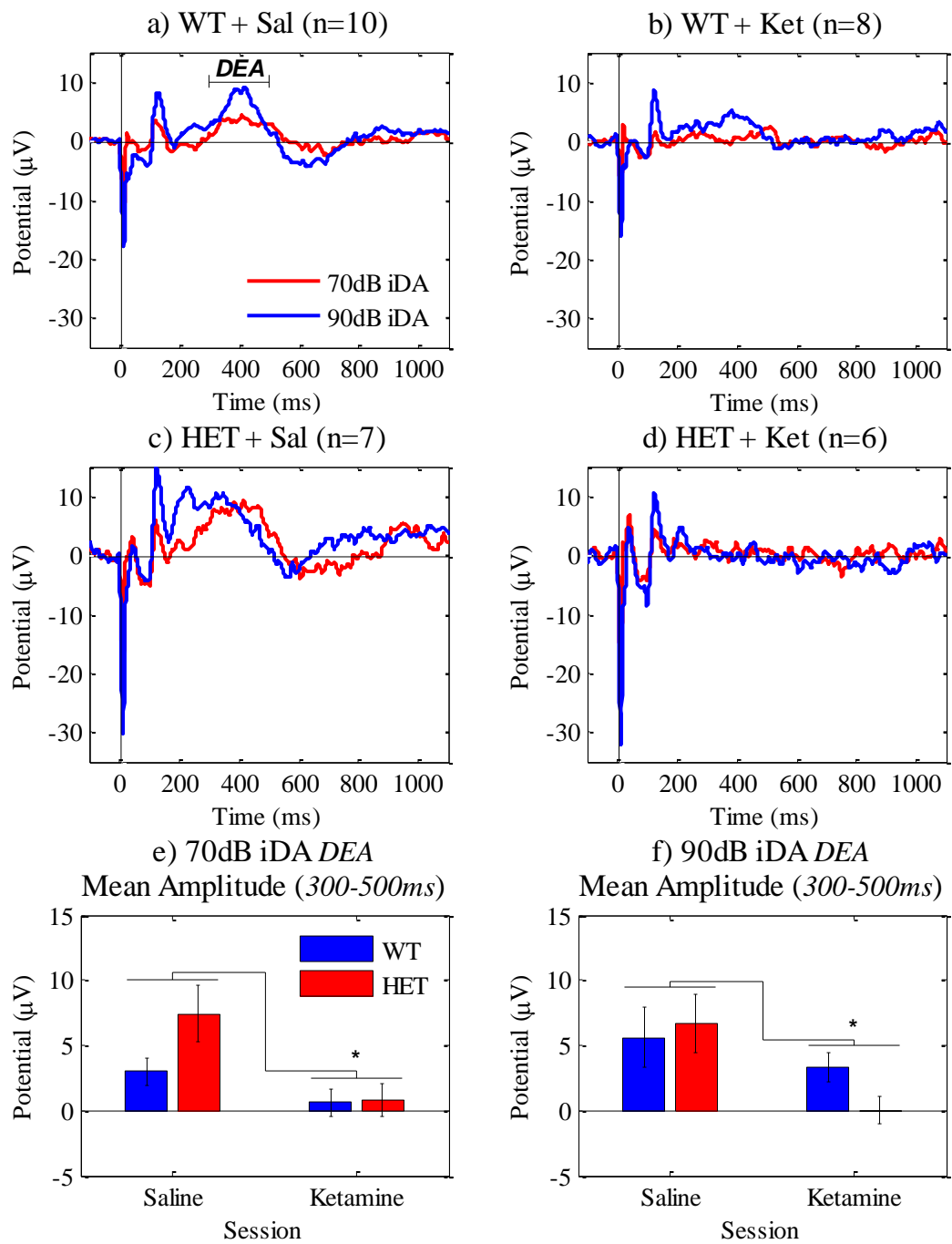


Figure 3.27 - Extended latency auditory evoked potentials to intensity deviant-alone paradigm stimuli in urethane-anaesthetised mice The 70 dB (red) and 90 dB (blue) stimuli evoked waveforms are shown for a) control (WT) mice during the saline session (Sal), b) WT mice following a 10 mg/kg i.p. ketamine injection (Ket), c) *Map2k7^{+/-}* (HET) mice during the saline session, and d) HET mice during the ketamine session. Quantification of e) 70 dB, and f) 90 dB deviant evoked activity (DEA) mean amplitude from 300-500 ms, displayed as group means \pm sem, both showing significant overall difference ($p < .05$) between sessions, with ketamine apparently reducing DEA amplitude from both stimuli. Deviant evoked activity (DEA) is annotated on (a).

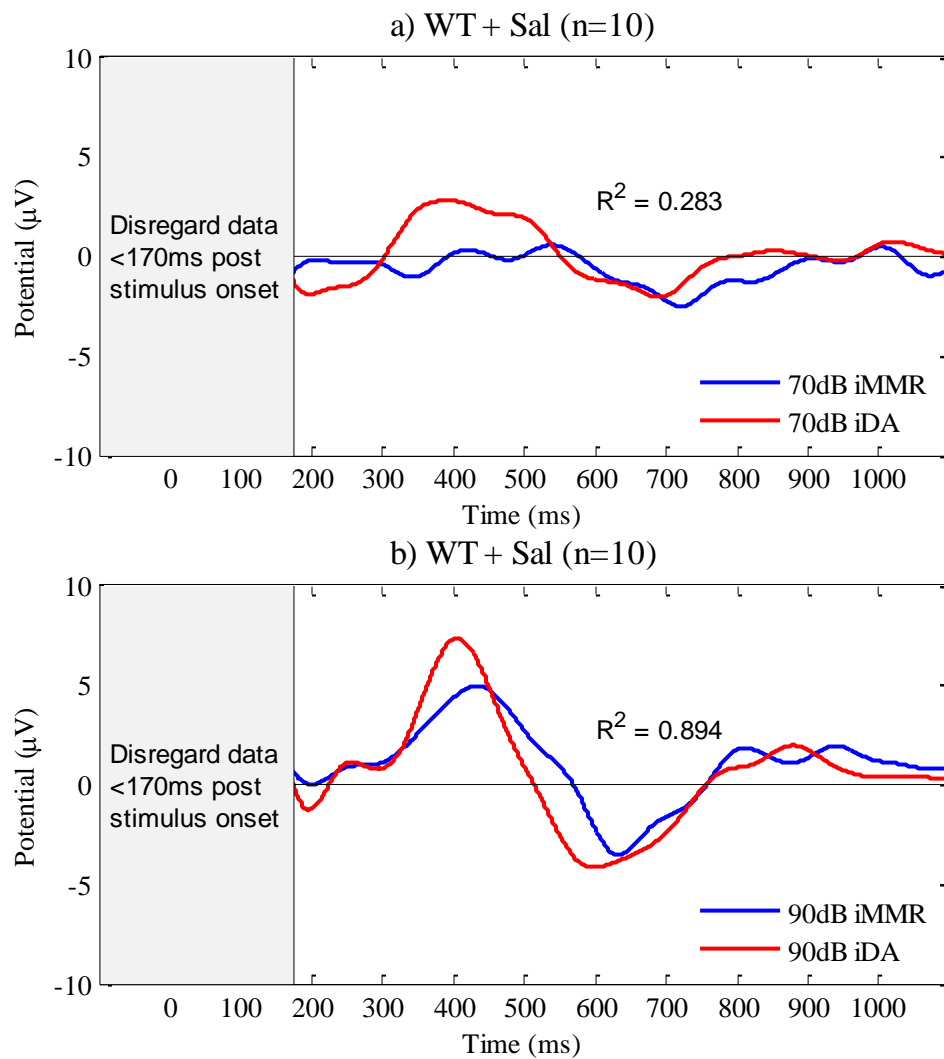


Figure 3.28 - Comparison of intensity mismatch response and deviant-alone paradigm extended latency evoked potentials from urethane-anaesthetised mice These graphs from control mice during the saline recording session (WT+Sal) show the extended epoch intensity mismatch response (iMMR) and deviant-alone (iDA) paradigm waveforms elicited by a) 70 dB (−10 dB quieter oddball), and b) 90 dB (+10 dB louder oddball) stimuli. 90 dB stimuli evoked waveforms are closely correlated, whereas 70 dB stimuli evoked waveforms are not. Activity <170 ms is omitted because stimulus onset and offset peaks occur during this time. These data have been filtered with a 10 Hz cut-off low-pass filter.

3.3.4 Auditory evoked potential changes throughout Experiment I

Mice were anaesthetised with urethane throughout this experiment and were continually presented with auditory stimulation for approximately four hours in total. This somewhat lengthy protocol was required to conduct detailed investigations into auditory stimuli duration, frequency, and intensity variation effects. It is quite possible that auditory cortex activity, and neurological activity overall, may vary during this period, potentially occurring from deepening anaesthesia and/or prolonged relatively high-intensity auditory stimulation.

Ketamine (10 mg/kg i.p.) was administered midway through the protocol (Figure 2.15) to model physiological deficits related to NMDA receptor neuropathology in schizophrenia. Comparisons between saline control and ketamine recording sessions in this study design are therefore inherently confounded by anaesthesia time course and prolonged auditory stimulation. To assist in dissociating these effects, measures of interest may be compared across paradigms presented longitudinally throughout the experiment to gain insight into ongoing trends which may or may not be influenced by ketamine administration.

Auditory paradigms were presented to each subject in the same sequence without counterbalancing. Therefore it is possible to examine AEP features which may change throughout the experiment by comparing the same measure from physically identical stimuli in different auditory paradigms. The obvious choice for these comparisons in the standard stimulus (100 ms, 10 kHz, 80 dB, 450 ms ISI) which was constant in consecutive-repetition (CR), oddball (OD) and many-standards (MS) paradigms.

3.3.4.1 Stimulus onset potential

Onset response (N1) peak amplitude was measured from standard stimuli evoked waveforms from dCR, dOD, dMS, fCR, fOD, fMS, iCR, iOD and iMS paradigms during the saline recording session and following 10 mg/kg i.p. ketamine administration. These data from WT and HET mice are shown in Figure 3.29. Standard stimuli were omitted from deviant-alone (DA) paradigms therefore these are not included in this analysis.

Figure 3.29 clearly illustrates a trend towards decreasing N1 peak amplitude throughout the experiment. This reduction in magnitude is observed in both WT and HET data to a similar extent, although the HET group consistently displays greater negative amplitude than WT. Repeated measures ANOVA with each individual paradigm as within-subjects factors confirmed a significant overall effect of genotype [$F_{1,10} = 4.993$, $p = .049$], with HET mice consistently displaying a greater negative peak amplitude N1 response.

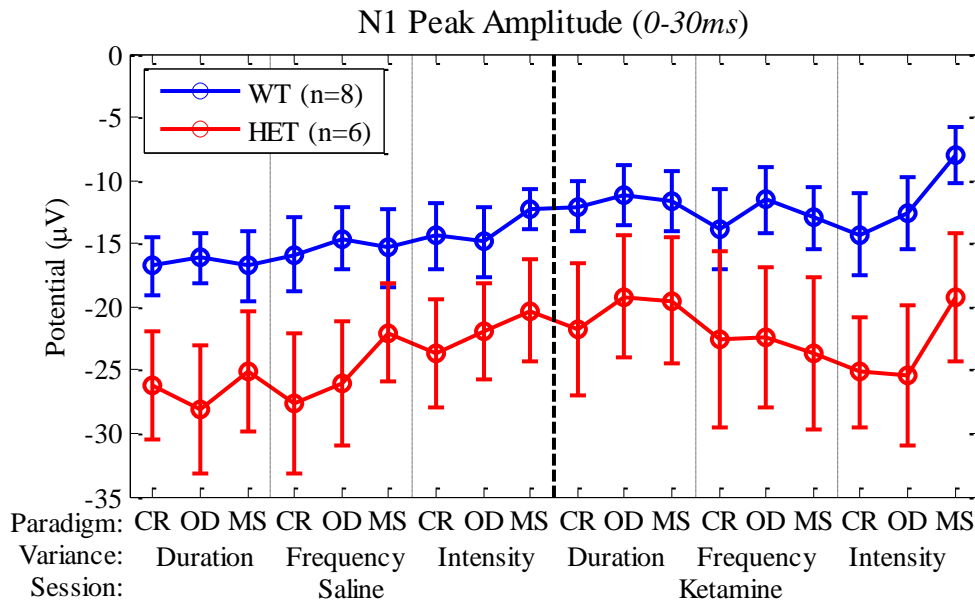


Figure 3.29 - Auditory stimulus onset response peak amplitudes from physically identical stimuli presented throughout Experiment I Data shown from control (WT) and *Map2k7^{+/-}* (HET) animals are onset response (N1) peak amplitude group means \pm sem. These measurements were taken from physically identical standard (100 ms, 10 kHz, 80 dB, 450 ms ISI) stimuli auditory evoked potentials (AEPs) from consecutive-repetition (CR), oddball (OD) and many-standards (MS) paradigms presented sequentially in duration-, frequency-, then intensity-varying paradigms in sessions following physiological saline then 10 mg/kg i.p. ketamine injections (see Section 2.9.1 for a full description of the Experiment I protocol). The measurement window is shown in brackets and a line through each data series illustrates a time dependency from left to right.

3.3.4.2 Stimulus offset potential

Offset response (P_{offset}) peak amplitudes measured from standard stimuli evoked waveforms in dCR, dOD, dMS, fCR, fOD, fMS, iCR, iOD, and iMS paradigms following saline and 10 mg/kg i.p. ketamine injections are compared in Figure 3.30. Deviant-alone paradigms did not utilise standard stimuli with the same parameters as the above, thus DA paradigms could not be included in this analysis.

The WT group appears to exhibit a modest steady reduction in P_{offset} peak amplitude throughout the experiment, whereas HET group data is more erratic, making its interpretation more challenging. This may be due in part to concomitant ongoing activity during the 100 ms standard stimulus offset response measurement window, i.e. the slow biphasic response negative half-cycle from ≈ 50 -250 ms described in Figure 3.8.

Repeated measures ANOVA with each individual paradigm as a repeated measure suggested a trend towards significantly greater P_{offset} peak in the HET group [$F_{1,10} = 4.335$, $p = .064$] compared with WT controls. Again, this observation is possibly influenced by the biphasic response seen in *Map2k7*^{+/-} mice. However, an alternative interpretation may be that the increased offset response is related to an enhanced onset response (Figure 3.29).

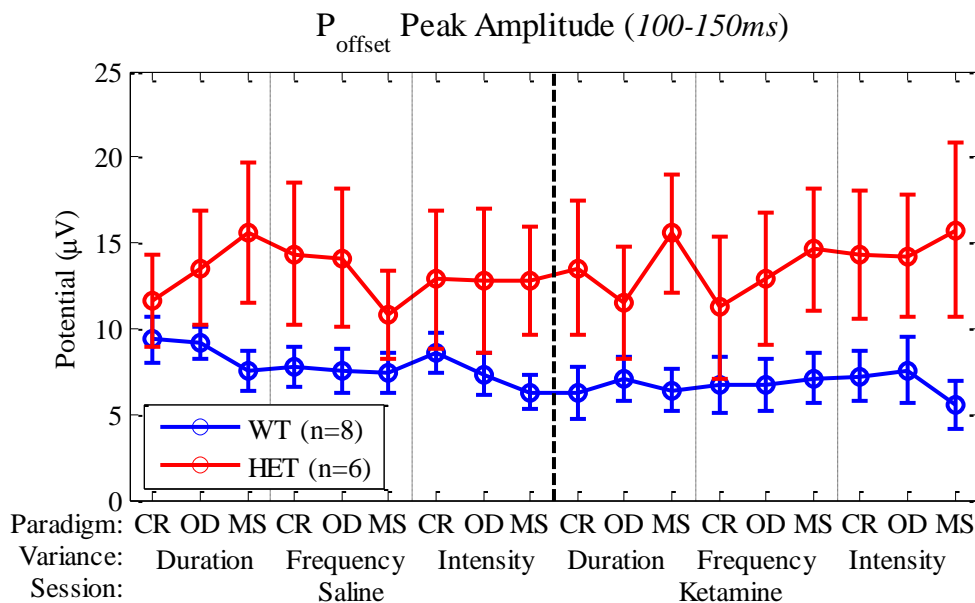


Figure 3.30 - Auditory stimulus offset response peak amplitudes from identical physical stimuli presented throughout Experiment I Data shown from control (WT) and *Map2k7*^{+/-} (HET) mice are offset response (P_{offset}) peak amplitude group means \pm sem taken from physically identical standard (100 ms, 10 kHz, 80 dB, 450 ms ISI; 10 ms pre-offset baseline corrected) stimuli evoked waveforms. The measurement window is written in brackets. These data were recorded sequentially from consecutive-repetition (CR), oddball (OD) and many-standards (MS) paradigms with duration, frequency, then intensity sound variance in sessions following physiological saline and 10 mg/kg i.p. ketamine administration (the entire protocol is explained in Section 2.9.1).

3.3.4.3 Deviant evoked activity

A total of six DA paradigms were presented throughout Experiment I with stimuli varying in duration (dDA), frequency (fDA) and intensity (iDA), firstly following physiological saline then repeated after 10 mg/kg i.p. ketamine injections.

Although stimuli employed in each of these paradigms were not identical, they appeared to elicit a similar extended latency electrophysiological response peaking positively approximately between $\approx 300\text{-}500$ ms (e.g. Figure 3.10), justifying the establishment of a standardised deviant evoked activity (DEA) mean amplitude measurement window which has been applied to quantify all of the DA paradigm waveforms throughout this experiment.

To roughly compare data from separate DA paradigms both of the resulting AEPs may be averaged together, combining physical stimuli changes in both directions. This is an approximate method applied here to examine possible longitudinal effects encountered throughout this experiment.

Figure 3.31 displays DEA mean amplitude from combined AEPs in each DA paradigm. A trend towards reducing amplitude is observed across both saline and ketamine recording sessions, with obvious implications for interpreting effects of session which may potentially be attributed to 10 mg/kg i.p. ketamine.

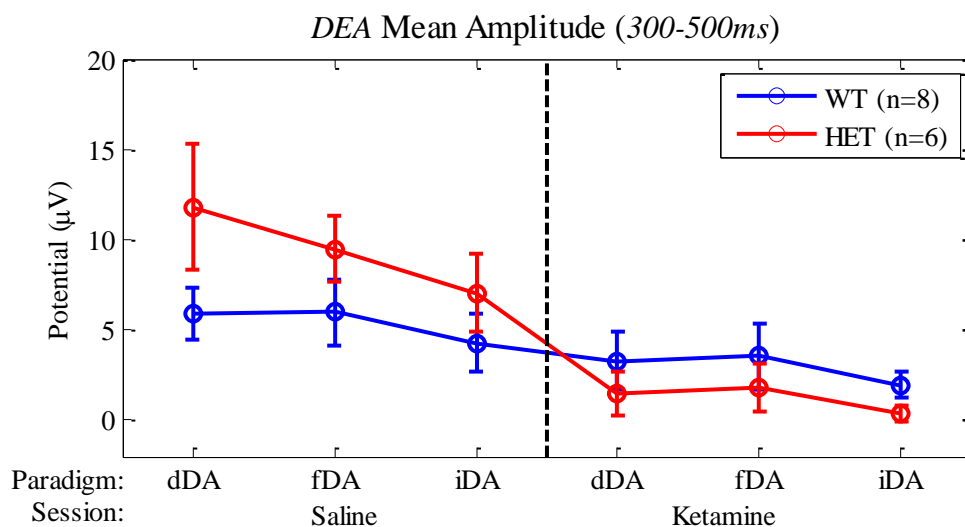


Figure 3.31 - Deviant evoked activity measured from deviant-alone paradigm stimuli presented throughout Experiment I Data shown from control (WT) and *Map2k7^{+/-}* (HET) groups are deviant evoked activity (DEA) mean amplitudes from 300-500 ms, plotted as group means \pm sem, from the deviant-alone (DA) paradigms throughout Experiment I. DEA was measured from the average waveform produced by combining both increasing and decreasing sound variance stimuli auditory evoked potentials from duration, frequency, and intensity deviant-alone paradigms (dDA, fDA, iDA), shown for both saline and 10 mg/kg i.p. ketamine recording sessions. A line through each data series illustrates a time dependency from left to right.

3.3.5 *Spectral analyses*

The spectral analyses methods detailed in Section 2.10.2 were used to examine data from urethane-anaesthetised WT control and HET mice before and after 10 mg/kg i.p. ketamine administration. The EEG power spectrum and event-related spectral perturbation (ERSP) were computed to analyse data in the frequency and time-frequency domains, respectively.

EEG power spectra from dCR and dOD paradigms are plotted in Figure 3.32. The dCR paradigm was played \approx 0-10 min post saline and ketamine injections, while the dOD paradigm was played \approx 10-20 min after injections. Analysis of this data revealed no significant genotype or ketamine effects.

Auditory evoked ERSP examples from urethane-anaesthetised mice following saline and 10 mg/kg i.p. ketamine administration are plotted in Figure 3.33. These display the ERSP response to 150 ms stimuli presented in the dCR paradigm, played \approx 0-10 min post injections. From visual comparison overall power appears to be reduced, however statistical analysis did not return any significant differences following adjustment for multiple comparisons. It should be noted that Bonferroni corrections for multiple comparisons are perhaps overly conservative in the case of this analysis due to the large number of compared data points.

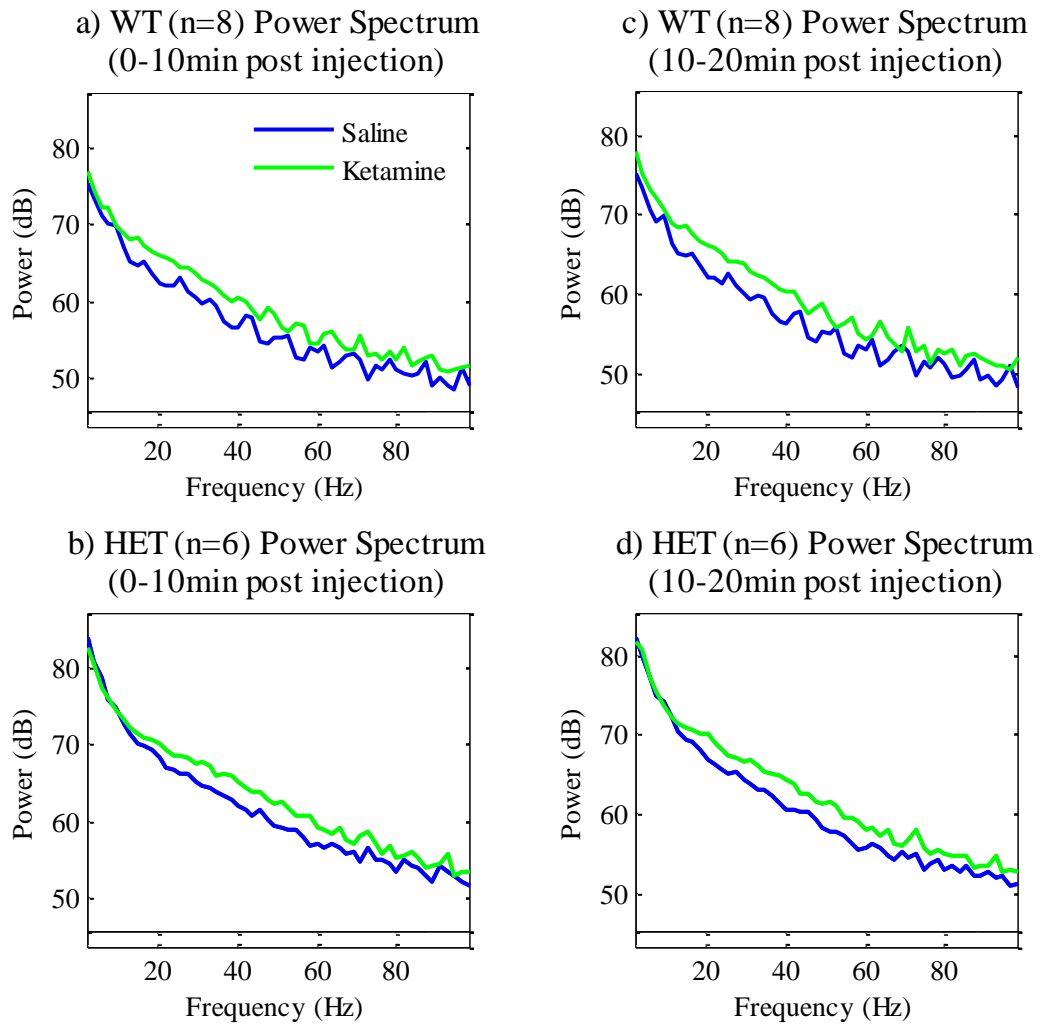


Figure 3.32 - EEG power spectra from urethane-anaesthetised mice exposed to ketamine Group-average power spectra are plotted from a) wild-type (WT) mice over 0-10 min and b) 10-20 min post saline/ketamine (10 mg/kg) i.p. injections, and c) *Map2k7^{+/-}* (HET) mice from 0-10 min, and d) 10-20 min post injections. Statistical analysis of this data revealed no significant effects of genotype or ketamine.

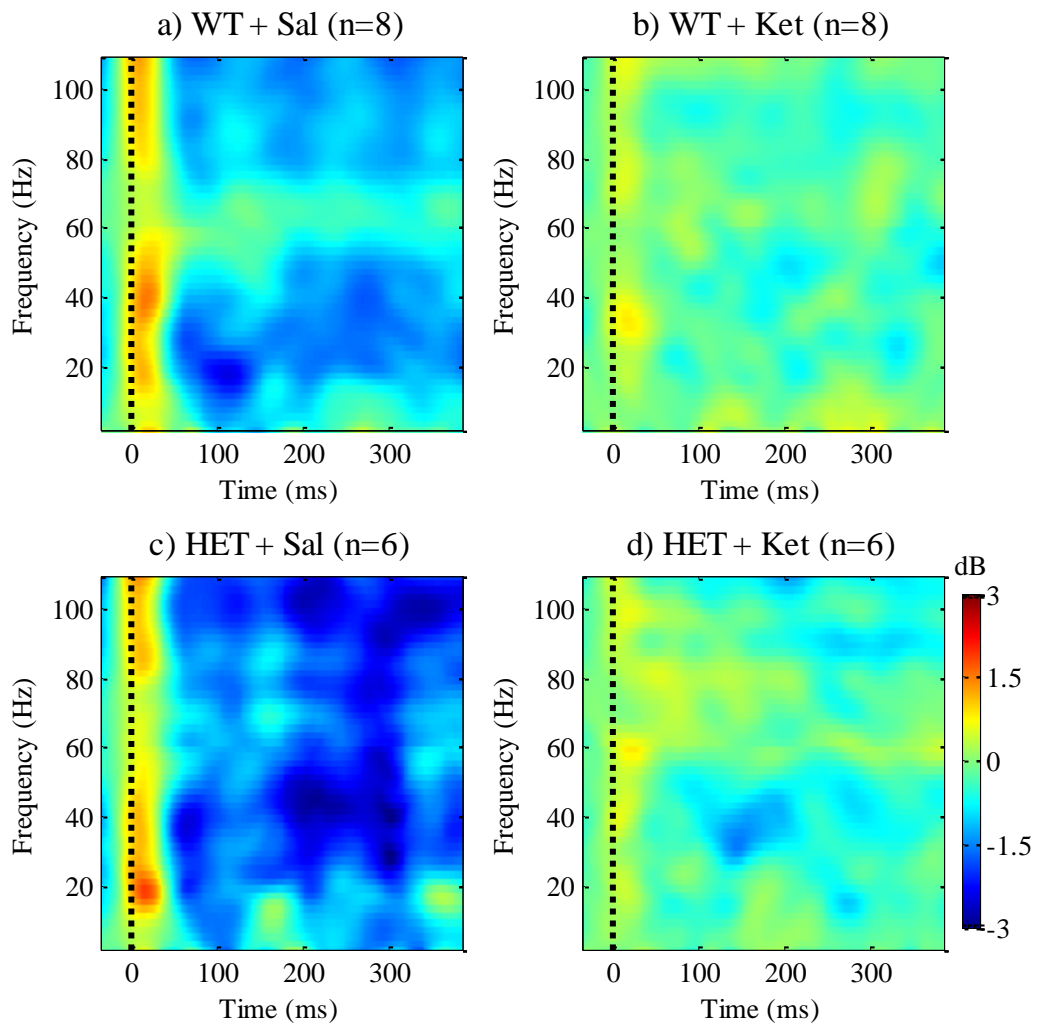


Figure 3.33 - Auditory event-related spectral perturbation (ERSP) from urethane-anaesthetised mice exposed to ketamine Time-frequency plots are displayed for wild-type (WT) mice following a) saline and b) 10 mg/kg i.p. ketamine injections, and *Map2k7^{+/-}* (HET) mice post c) saline and d) ketamine injections. These were evoked by the 150 ms, 10 kHz, 80 dB stimulus presented in the duration consecutive-repetition (dCR) paradigm, played \approx 0-10 min post injections. The Fourier transform method was applied to compute the power at each frequency in 2 Hz increments from 2-110 Hz. The colour scale to the right of (d) applies to all. Overall power across all frequencies from 0-50 ms appears reduced in the ketamine session, although these were not found to be statistically significant following adjustment for multiple comparisons.

3.3.6 Results Summary

Observations from Experiment I are summarised below in tabularised form. Firstly, the AEP features observed from urethane-anaesthetised mice are summarised in Table 3.1. How these varied fundamentally with auditory stimuli duration, frequency and intensity manipulations is outlined in Table 3.2. Although not strictly proportional by the mathematical definition, this term is used here to identify dependencies between AEP features and these physical properties of auditory stimuli.

AEP Feature	Peak Latency	Polarity	Quantification
N1	15.5±1.1 ms sem post stimuli onset	Negative	Peak amplitude from 0-50 ms post onset
P _{offset}	25.2±1.2 ms sem post stimuli offset	Positive	Peak amplitude from 0-50 ms post offset
DEA	394.1±23.3 ms sem post stimuli onset	Positive	Mean amplitude from 300-500 ms post onset

Table 3.1 - Summary of auditory evoked potential features observed from urethane-anaesthetised mice The auditory onset response (N1), offset response (P_{offset}) and deviant evoked activity (DEA) auditory evoked potential features are described in this table. Overall peak latencies, polarity and method of quantifying each AEP feature are provided. Sensitivities of these features to stimuli duration, frequency and intensity manipulations are summarised in Table 3.2.

AEP Feature	Duration	Frequency	Intensity
N1	No effect	Amplitude \propto - stimulus frequency	Amplitude \propto - stimulus intensity
P _{offset}	Latency \propto stimulus duration	Amplitude \propto stimulus frequency	Amplitude \propto stimulus intensity
DEA	No effect	No effect	No effect

Table 3.2 - Summary of urethane-anaesthetised mouse auditory evoked potential sensitivities to stimuli duration, frequency and intensity variations This table summarises onset response (N1), offset response (P_{offset}) and deviant evoked activity (DEA) sensitivities to auditory stimuli duration, frequency and intensity changes. Proportional (\propto) and negatively proportional (\propto -) relationships between physical features of auditory stimuli and the resulting N1, P_{offset} and DEA features are noted. DEA is not sensitive to duration, frequency or intensity variations, therefore is unlikely to reflect physical features of auditory stimuli *per se*. DEA may appear to be an ‘all-or-nothing’ type response to environmentally salient stimuli in the deviant-alone (DA) condition or frequency and increasing intensity oddballs.

Key findings from *Map2k7^{+/-}* and 10 mg/kg i.p. ketamine models are summarised in Table 3.3. Onset responses were consistently greater in HET mice versus WT controls (Figure 3.29), while offset responses were marginally increased (Figure 3.30). Deviant evoked activity, defined as an amplitude increase \approx 300-500 ms, was considered non-specifically increased in the *Map2k7^{+/-}* model, after having been displayed in response to regular/non-deviant stimuli in various auditory paradigms (e.g. Figure 3.15a and Figure 3.24a), whereas in WT controls DEA was only observed in response to frequency and increasing intensity oddball stimuli and deviant-alone paradigm stimuli. Overall these findings suggest that cortical auditory processing is altered in *Map2k7^{+/-}* mice.

Model	N1	P _{offset}	DEA
<i>Map2k7^{+/-}</i>	Enlarged	Marginally Enlarged (non-significant)	Non-specifically Increased
Ketamine*	Reduction	Reduction	Reduction

Table 3.3 - Summary of urethane-anaesthetised *Map2k7^{+/-}* and 10 mg/kg i.p. ketamine model effects on auditory evoked potential features Findings specific to schizophrenia-related *Map2k7^{+/-}* (HET) and ketamine-induced NMDA receptor hypofunction models and their effects on auditory onset (N1), offset (P_{offset}) and deviant evoked activity (DEA) features are summarised here. The HET group consistently displayed an enlarged N1 (Figure 3.29) and trended towards greater P_{offset} peak amplitude (Figure 3.30). * By experimental design the effects of ketamine were inherently confounded with urethane anaesthesia time course and repetitive auditory stimulation therefore these effects cannot be confirmed.

Findings from paradigms incorporating stimuli varying in different physical features of sound are presented in Table 3.4. This table addresses the respective duration, frequency and intensity mismatch responses (dMMR/fMMR/iMMR). The dMMR was clearly caused by offset responses from oddball and standard stimuli which occur at different latencies. An fMMR was observed from \pm 2.5 kHz oddball stimuli, characterised as a slow amplitude increase reaching a maximum at \approx 300-500 ms, correlating with frequency deviant-alone (fDA) paradigm evoked waveforms. An iMMR was evoked by +10 dB but not -10 dB oddball stimuli, similarly correlated with iDA paradigm waveforms and peaking between \approx 300-500 ms. These findings suggest that frequency and increasing intensity oddball stimuli evoke similar electrophysiological responses to DA paradigm stimuli, perhaps reflecting environmental salience. DEA was otherwise specific to the DA paradigm condition. Consecutive-repetition and many-standards paradigms succinctly demonstrated the effects of varying respective physical features of auditory stimuli on resulting N1 and P_{offset} responses.

Paradigm	Duration	Frequency	Intensity
Oddball	dMMR caused by P_{offset} Responses	± 2.5 kHz fMMR ≈ 300 -500 ms (DEA)	+10 dB iMMR ≈ 300 -500 ms (DEA)
Consecutive- repetition	P_{offset} latency sensitivity	N1 and P_{offset} amplitude sensitivity	N1 and P_{offset} amplitude sensitivity
Many-standards	P_{offset} latency sensitivity	N1 and P_{offset} amplitude sensitivity	N1 and P_{offset} amplitude sensitivity
Deviant-alone	DEA ≈ 300 -500 ms	DEA ≈ 300 -500 ms	DEA ≈ 300 -500 ms

Table 3.4 - Paradigm-specific observations from stimuli duration, frequency and intensity manipulations in urethane-anaesthetised mice This table summarises findings from each respective oddball and control paradigm with stimuli varying in three different physical features of sound. Definitions of the onset response (N1), offset response (P_{offset}) and deviant evoked activity (DEA) are assumed from Table 3.1. The deviant-alone paradigm elicited DEA. In addition, frequency and intensity mismatch responses (fMMR/iMMR) also displayed apparent DEA. Consecutive-repetition and many-standards paradigms illustrated the effect of varying different physical features of auditory stimuli.

In the next section, these findings are discussed with relevance to their biological underpinnings, and possible interpretations in relation to current experimental and theoretical models of the mismatch response introduced in Chapter 1.

3.4 Discussion

This chapter has shown clearly that changes in stimuli duration, frequency and intensity fundamentally alter the AEP observed from urethane-anaesthetised mice. Interestingly, the schizophrenia-related *Map2k7*^{+/-} (HET) gene disruption group has consistently displayed an enlarged onset response (N1) compared with wild-type (WT) littermates. Furthermore, a frequency and intensity oddball (OD) paradigm induced mismatch response (fMMR/iMMR) signature has been identified in WT animals which is diminished in HET mice. These fMMR/iMMR difference waveforms display prominent extended-latency amplitude variations that correlate with deviant-alone (DA) paradigm AEPs; potentially suggesting that OD and DA paradigms evoke similar neurophysiological processes, putatively defined here as deviant-evoked activity (DEA), due to the presence of an environmentally salient auditory stimulus. Any effects of ketamine were unfortunately confounded with a deepening state of anaesthesia and repeated auditory stimulation over time. Longitudinal examinations of AEP measurements taken from recordings made at different stages throughout the experimental protocol certainly suggest that the effect of ketamine may have been negligible. These points are discussed in more detail in the following subsections.

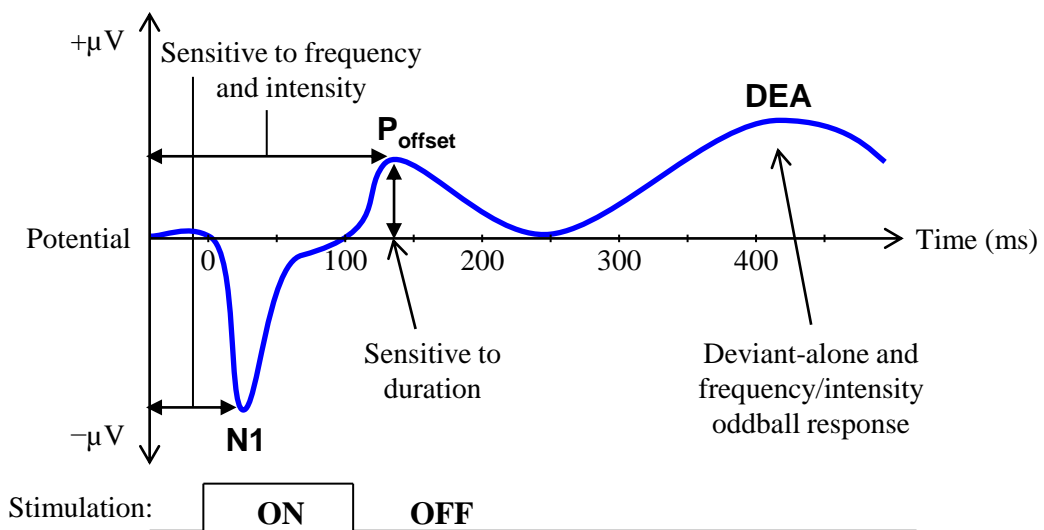


Figure 3.34 - Illustration of auditory evoked potential features observed from urethane-anaesthetised mice Onset (N1), offset (P_{offset}) and deviant-evoked activity (DEA) responses are portrayed in this representation, which were the most robust features observed from auditory cortex AEPs in this experiment. N1 and P_{offset} amplitudes were sensitive to stimulus frequency and intensity; P_{offset} latency was sensitive to stimulus duration; DEA was elicited in deviant-alone paradigms, and frequency and intensity (only to louder stimuli) oddball paradigms. Mismatch response waveforms resulting from N1 or P_{offset} changes can be attributed to physical properties of stimuli, regardless of context, thus not analogous with current popular interpretations of human mismatch negativity. On the other hand, DEA may correspond better with the human MMN because it is present only in conditions where a significant sensory-memory disruption takes place.

3.4.1 *Effects of stimuli duration, frequency and intensity on auditory evoked potentials in urethane-anaesthetised mice*

The duration of auditory stimuli was directly responsible for positive amplitude offset response (P_{offset}) peak latency (e.g. Figure 3.8a-b). This effect was instrumental in shaping the duration mismatch response (dMMR) difference waveforms from 50 ms (-50 ms) and 150 ms ($+50$ ms) oddball stimuli when the 100 ms standard AEP was subtracted (Figure 3.4 and Figure 3.5, respectively); the only significant difference between increasing and decreasing duration oddball dMMR waves being position of the positive peak, which correlated with oddball latency (Figure 3.6). Additionally, there were no significant differences between AEP waveforms elicited by identical duration stimuli presented in oddball and different control paradigms that could not be explained by a process of adaptation (Figure 3.7).

As mentioned in the introduction to this chapter, Nakamura et al.(2011) reported finding offset potentials in anaesthetised rats but did not associate this with a dMMR. In the present study, however, the P_{offset} response was far more explicit. This may be due to differences in experimental setup such as background acoustics, or other conditions resulting in reduced quality data, which the authors highlight themselves as an issue. Furthermore, the use of instantaneous rise/fall times in the present study may have played an important role in generating such a pronounced P_{offset} deflection. A previous study investigating off responses in primary auditory cortex of rats suggested that stimuli duration, intensity and fall time all influence cortical offset activity (Takahashi et al., 2004). Indeed, stimuli offset responses are known to occur at the level of the brainstem (Henry, 1985), inferior colliculus (Brand et al., 2000), thalamus (He, 2002) and auditory cortex (Qin et al., 2007) in animals/rodents under anaesthesia, and have an inverse relationship with stimuli fall times.

An offset response is also seen in EEG recordings from conscious human subjects (Hillyard and Picton, 1978, Hari et al., 1987, Pantev et al., 1996, Yamashiro et al., 2009). Authors suggest that both stimuli onset and offset responses are reactions to abrupt changes in the auditory environment (Yamashiro et al., 2009), although their physiological underpinnings remain to be fully elucidated. Currently there does not appear to be an established link in the literature connecting stimuli offset potentials and the duration mismatch response. The findings of this study directly implicate the offset response as a key determinant of dMMR waveform characteristics in urethane-anaesthetised mice. Understanding more about the physiology behind this phenomenon may be beneficial for understanding dMMR deficits seen in patients with schizophrenia and genetically susceptible individuals (Section 1.2.1).

Both stimulus frequency and intensity manipulations similarly influenced N1 and P_{offset} features of the AEP (Figure 3.11 and Figure 3.12 for frequency, Figure 3.20 and Figure 3.21 for intensity). These in effect caused deflections in each respective mismatch response (fMMR/iMMR) difference waveform in the latency range of these AEP features. Opposite polarity deflections were observed from decreasing versus increasing oddball changes in both frequency (Figure 3.13 and Figure 3.14) and intensity (Figure 3.22 and Figure 3.23). However, these effects may be ascribed to the physical characteristics of stimuli themselves and implicit differences in the resulting magnitudes of evoked electrophysiological activity. Mouse hearing is considerably poorer at the lowest frequencies applied (<2.5 kHz) and becomes increasingly more sensitive towards the higher frequencies employed, without surpassing the range of lowest audible threshold of the typical mouse audiogram (Heffner and Heffner, 2007). The findings here may therefore indicate that AEP amplitudes increase with frequency sensitivity. To examine whether this is true, stimuli frequencies exceeding the range of greatest hearing sensitivity (\approx 14-18 kHz) may be applied to test whether a comparable decay in amplitude occurs with increasing tone frequencies; however, the equipment used in this experiment is incapable of performing such a feat.

The effect of intensity, sound pressure level (SPL), or loudness has been studied extensively in both humans and animals. Loudness dependence of the auditory evoked potential (LDAEP), as observed from this study, has been proposed to reflect serotonergic (5-hydroxytryptamine, 5-HT) neurotransmission in the primary auditory cortex, with low levels of 5-HT associated with a greater degree of intensity dependence (Hegerl and Juckel, 1993). Despite promising early studies in animals (Juckel et al., 1997, Juckel et al., 1999) and clinical groups including migraine (Wang et al., 1996), major depressive (Gallinat et al., 2000, Linka et al., 2004) and schizophrenia patients (Juckel et al., 2003) suggesting central 5-HT levels can be approximated with LDAEP, this hypothesis remains controversial. This controversy arises mainly due to the finding that other neurotransmitter systems including dopamine and glutamate influence LDAEP, suggesting that it may not relate specifically to serotonin function (Nathan et al., 2005, O'Neill et al., 2008, Oliva et al., 2010). Nevertheless, altered LDAEP is associated with a range of neuropsychiatric diseases (Park et al., 2010), and specifically in schizophrenia (Juckel, 2015), which is suggested to arise from altered 5-HT signalling. Although there are evident differences in N1 amplitudes between WT and HET mice (discussed in Section 3.4.3 below), the relative LDAEP of each group was not substantially different, perhaps suggesting that 5-HT function is not impaired in the *Map2k*^{+/-} gene disruption model.

3.4.2 Mismatch responses in urethane-anaesthetised mice

As mentioned already, the physical properties of stimuli (duration, frequency and intensity) themselves altered the respective mismatch responses by having effects on AEP N1 and P_{offset} responses. These differences are not ‘true’ oddball induced effects comparable with the human MMN because they are not context-specific; i.e. they do not reflect an auditory change-detection mechanism in response to presentation of oddball stimuli, as there are little differences between N1 and P_{offset} features in oddball versus control paradigms (Figure 3.7, Figure 3.16 and Figure 3.25). How these features vary with changes in the physical properties of stimuli examined are illustrated in Figure 3.34.

Frequency and increasing intensity oddball stimuli did evoke additional AEP features in control animals, putatively named deviant-evoked activity (DEA), in the respective fMMR (Figure 3.13, Figure 3.14 and Figure 3.15) and iMMR waveforms (Figure 3.22, Figure 3.23 and Figure 3.24). These fMMR and iMMR difference waves, computed with the double-epoch subtraction method described in Section 3.2.8.1, were highly correlated with frequency and intensity deviant-alone (fDA/iDA) paradigm AEPs (Figure 3.18 and Figure 3.27). The apparent effects of *Map2k7*^{+/-} gene disruption and ketamine hypofunction models (discussed below) on these fMMR and iMMR waveforms are intriguing; the former with enhanced DEA to the standard and the latter with reduced DEA to the oddball, each decreasing the difference waveform DEA by different means (Figure 3.15 and Figure 3.24).

The DEA feature observed in AEPs to deviant-alone paradigm stimuli, ascending/descending frequency and increasing intensity oddball stimuli is characterised by a positive rise in amplitude, peaking approximately between 300-500 ms, followed by a slow negative deflection peaking approximately between 500-700 ms post stimuli onset. Hitherto deviant-alone control paradigms have been employed to control for different presentation rates of standard and oddball stimuli. However, these results and common sense may lead one to think of the DA paradigm as a positive control for sensory-memory disruption; wherein stimuli presented against a background of relative silence are more likely to violate an auditory sensory-memory trace than if preceded by a train of comparably similar auditory stimuli. This logically follows on from the repeated finding that degree of difference (for example, in frequency) between standard and oddball stimuli has a significant effect on the magnitude of the observed MMN (Näätänen et al., 2012).

In initial work by Ruusuvirta et al. (1998), urethane-anaesthetised rats exhibited a slow positive amplitude deflection peaking at ≈ 300 ms in response to a fDA control paradigm. This may reflect the initial portion of DEA observed in the present study. However, the authors do not address this response in their paper, presumably because the oddball condition did not evoke a similar response. Furthermore, waveforms are only plotted up to 350 ms post stimuli onset. One possible reason why this extended latency feature was not seen in response to oddball stimuli may be the closeness of frequencies used as standards and oddballs, which were separated by 500 Hz. In contrast, the present study used greater frequency separation of 2.5 kHz. Currently there are little records of extended latency AEP components in urethane-anaesthetised mice to be found in the literature, thus the current study may provide a foundation for examining these phenomena in closer detail.

The fact that decreasing sound intensity (-10 dB) oddball stimuli failed to elicit DEA in the same manner as DA, frequency and increasing intensity oddball stimuli may be useful for conceptualising the physiological significance of this response. It may be speculated that the processes responsible for eliciting DEA are triggered by environmental salience of auditory stimuli; thus offering a plausible explanation why a transient decrease in acoustic level fails to elicit this response. Interpreting these waveforms within this framework may suggest a role of involuntary switching of attention in response to stimuli, consistent with models of MMN (Garrido et al., 2009). Additionally, the latency of DEA is indicative of higher order processing, perhaps involving downstream communication, feedback, and integration of signals from such structures as the hippocampus, which has been implicated in generation of MMN in urethane-anaesthetised rats (Ruusuvirta et al., 2013, Ruusuvirta et al., 2015).

3.4.3 *Map2k7^{+/-} gene disruption in urethane-anaesthetised mice*

The present study found significant differences between the auditory evoked potential from HET mice compared with WT controls, both related to normal auditory processing and in the context of mismatch responses. Consistently throughout this experiment, the N1 response was significantly enlarged in the HET group (Figure 3.3). Moreover, a slow biphasic response became apparent in the HET group following initial auditory stimulation, characterised by a negative potential from ≈ 100 -200 ms then a positive deflection from ≈ 300 -400 ms (Figure 3.8). The positive half-cycle of this biphasic response may reflect the DEA element of mismatch responses discussed above, thus indicating how fMMR/iMMR difference waveforms are diminished in the HET group through an increased DEA in response to non-novel/standard stimuli.

The N1 observed here in mice may be comparable with the N100 seen in humans (see Figure 1.3), specifically because it is influenced in the same manner by frequency, intensity and inter-stimulus interval (as seen in DA paradigms), it is the first relatively large negative amplitude deflection post stimuli onset, and is present during an anaesthetised state (Butler, 1968, Fischer et al., 2000, Woods, 1995). This feature measured from the primary auditory cortex reflects afferent thalamo-cortical signalling from the medial geniculate body of the thalamus exciting densely populated large LIII/IV pyramidal neurons (Winer and Schreiner, 2011). It is thought to be modulated by glutamate (Watson et al., 2009), γ -aminobutyric acid (GABA; Kruglikov and Rudy, 2008) and/or serotonin (Golimbet et al., 2008) neurotransmitter systems.

Schizophrenia patients consistently show reduced N100 amplitudes (Rosburg et al., 2008, Turetsky et al., 2009). It is unclear exactly how a deleted copy of the *Map2k7*^{+/-} gene alters N1. It may be speculated that this mutation provides functional compensation to restore decreased N100 in patients, whereas in an isolated genetic model this results in N1 enlargement. Further research is required to determine at which point in the auditory system enhanced auditory-evoked electrophysiological activity emerges in *Map2k7*^{+/-} mice and which neuronal mechanisms may be responsible. Firstly, however, the next chapter will seek to determine whether this response is present in conscious animals.

The slow biphasic response in urethane-anaesthetised HET mice is more challenging to describe in neurophysiological terms because of the limited research in this niche. The findings of this experiment considered in isolation may suggest that *Map2k7*^{+/-} gene disruption increases sensitivity of slow wave activity in the AEP, specifically the defined DEA observed here in response to environmentally salient stimuli. If this DEA reflects involuntary switching of attention, indicative of a sensory-memory disruption, it may be postulated that HET mice display impaired attentional filtering compared with WT controls, which also occurs in patients with schizophrenia (Weinberger and Harrison, 2010).

Whether these electrophysiological deficits manifest as observable behavioural dysfunctions of attention cannot be confirmed from this study alone. Interestingly, Openshaw et al. (2015) has recently shown that *Map2k7*^{+/-} mice display attentional deficits in a 5-choice serial reaction time task (5-CSRTT) which were restored with minocycline, a drug known to alleviate symptoms relating to attention in schizophrenia patients (Liu et al., 2014). Although its precise mechanism of action in the brain is unknown, its beneficial effects are thought to be related to neuroprotection of grey matter pathology associated with schizophrenia (Chaves et al., 2015). It is important to note that this was not a large-scale study hence these

results are not definitive. How these electrophysiological observations relate to *Map2k7* function remains to be elucidated, but possible explanations are offered in the general discussion (Section 6.1.3).

3.4.4 *Ketamine, confounds and longitudinal analyses*

In this experiment ketamine (10 mg/kg) was administered by the intraperitoneal route approximately 1.5 hours into the recording protocol. By this point, animals had been under the effects of urethane for more than 3 hours. Thus any effects of ketamine are confounded with extended periods of repeated auditory stimulation, known to cause habituation (Budd et al., 1998, Butler, 1968, Recasens et al., 2015), and urethane anaesthesia, which also alters auditory evoked activity (Capsius and Leppelsack, 1996, Devonshire et al., 2010, Shirasaka and Wasterlain, 1995).

Inspection of AEP measurements made from identical physical stimuli (standard 100 ms, 10 kHz, 80 dB, 450 ms ISI) may suggest that N1 (Figure 3.29) and P_{offset} (Figure 3.30) amplitudes are steadily attenuated throughout the protocol, with no discriminable effect of ketamine. DEA elicited by deviant-alone paradigm stimuli, which was significantly diminished following ketamine (Figure 3.10, Figure 3.17 and Figure 3.26), also appears to begin decaying in amplitude before drug administration (Figure 3.31). Furthermore, spectral analysis suggested no significant effect of ketamine on the EEG power spectrum (Figure 3.32), and uniformly diminished event-related spectral dynamics (Figure 3.33), potentially reflecting habituation. Overall, these findings indicate that ketamine does not have a significant effect on auditory evoked activity in urethane-anaesthetised mice. This does not agree with previous findings that NMDA receptor antagonists diminish the MMR in urethane-anaesthetised rats (Tikhonravov et al., 2008, Tikhonravov et al., 2010, Shiramatsu et al., 2013). Although the waveforms observed from these earlier studies differ substantially and lack a coherent explanation of the underlying AEP feature(s) supposedly diminished by NMDA receptor antagonism, instead relying on interpretations from the human MMN literature.

Nevertheless, NMDA receptor blockade with ketamine may alter the AEP from conscious mice, as other studies suggest (Maxwell et al., 2006, Ehrlichman et al., 2008, Featherstone et al., 2013). In the next chapter the confound of urethane anaesthesia is removed, and the effects of ketamine on auditory evoked activity in conscious *Map2k7*^{+/-} and wild-type control mice are assessed.

3.4.5 *Recommendations for Experiment II*

Following the data analyses presented in this chapter, several revisions to the experimental protocol were implemented for Experiment II (discussed fully in the next chapter). These recommendations and their rationale are summarised here:

1. Stimuli duration in frequency- and intensity-varying paradigms was changed from 100 ms to 50 ms. The reason for this adjustment is that DEA observed from fOD/iOD and fDA/iDA paradigms may have been partially obscured by the P_{offset} response. Figure 3.9 illustrates this principle. Thus decreasing stimuli duration to 50 ms aims to reduce overlapping of these AEP components.
2. In duration-varying paradigms a constant stimulus onset asynchrony (SOA)/variable inter-stimulus interval (ISI) condition was applied. This would enable a double-epoch subtraction to be performed on dOD data, comparable with fOD and iOD paradigms in this chapter, where the standards may effectively cancel each other out. However, a variable ISI condition may also alter the AEP. This resulted in two versions of duration-varying paradigms being implemented; one with a variable ISI and another with a constant ISI, as explained in the next chapter.

Chapter 4. Experiment II: evaluation of multivariate auditory paradigms in conscious wild-type and *Map2k7*^{+/-} mice exposed to ketamine

4.1 Introduction

Experiment II is driven by the hypothesis that conscious mice display a mismatch response (MMR) to different physical features of sound (duration, frequency and intensity) comparable with those observed from urethane-anaesthetised mice, in-keeping with the overarching hypotheses of this thesis set out in Section 1.5. The following experiment aims to characterise this MMR and investigate the effects of schizophrenia-related genetic (*Map2k7^{+/-}*) and pharmacological (ketamine) models. This is designed to confirm and expand upon findings presented in Chapter 3, in particular the observation that *Map2k7^{+/-}* mice display altered auditory-evoked electrophysiological activity, and examine any fundamental differences between urethane-anaesthetised and conscious mouse auditory responses. Relevant published studies of oddball paradigms in conscious rodents are briefly reviewed below, providing a snapshot of current knowledge in the field of preclinical MMR research, and setting the scene for understanding the contributions of this study.

4.1.1 Previous studies in conscious rodents

The following subsections provide some background information about relevant studies in conscious rodents. Overall findings are discussed with less emphasis given to methodological details. It may be assumed that electrode configurations, animal numbers, genotypes and auditory evoked potential (AEP)/MMR profiles typically vary from publication to publication, unless stated specifically.

4.1.1.1 Duration

The first published research article addressing mouse MMN-like responses to duration oddballs asked the question “is there mismatch negativity in mice?” (Umbricht et al., 2005). This particular study investigated both frequency and duration deviance in various oddball paradigms, concluding in summary that only duration-varying oddball paradigms evoked deviance-related and context-specific activity comparable with the human MMN. This finding highlights the mouse duration MMR (dMMR) as a potential translatable biomarker. Additionally, this mouse dMMR varied depending on the degree and direction of difference between standard and oddball stimuli durations, congruent with the human MMN response (Colin et al., 2009, Takegata et al., 2008). This also corresponds with findings from guinea pigs which demonstrated asymmetry between duration increment and decrement oddball paradigms (Okazaki et al., 2006). Further applications of duration-varying oddball paradigms in conscious mice have reported an increase in positive amplitude of the AEP, suggested by the authors to reflect selective attention in a fear-conditioned paradigm (Bickel et al., 2007). In this study, fear-conditioning mice received foot shocks during presentation of long

duration oddball stimuli. Post-conditioning EEG recordings made without foot shocks displayed significantly greater AEP positive peak amplitudes in fear-conditioned mice but not in controls, considered to arise from selective attention towards the conditioned stimulus (Bickel et al., 2007). The same study found that mice deficient in GluN1 (formerly notated NR1) subunits of the NMDA receptor displayed a comparatively diminished response, therefore suggested to reflect the human MMN, in which reduced amplitude in schizophrenia patients is attributed to dysfunctional NMDA receptors (Bickel et al., 2007).

However, none of these studies manages to pinpoint the mechanism by which this dMMR is generated. Conclusions are presented in terms of sensory-cognitive change/difference detection without eliminating alternative explanations for the mismatch in observed electrophysiological activity, such as stimulus specific adaptation (SSA; see Section 1.2.2.6) or more fundamental aspects of neurophysiological processing. It may be challenging to interpret the mouse MMR outside of the established framework of human MMN, although it is necessary to verify whether an analogous signal exists in mice that appropriate controls are incorporated into experimental designs to avoid reaching false conclusions. These should rule out other possible causes of a mismatch between electrophysiological responses, considering the physical properties of stimuli themselves, context(s) in which they are presented and the potential for SSA to occur (as discussed by Harms et al., 2015).

Often a constant stimulus onset asynchrony (SOA) is employed, which is the time between initiations of consecutive auditory stimuli. In stimulus duration-varying paradigms this will inherently alter the period between offset of one stimulus and onset of the next, referred to as the inter-stimulus interval (ISI), potentially influencing the auditory response. This situation is illustrated in Figure 2.12. Depending upon how the sequence of auditory stimuli and ISI gaps are structured there may be an observable effect on the resulting oddball or standard AEP. ISI is in fact capable of inducing an MMN response in humans (Martin et al., 2009, Näätänen et al., 1993). In this chapter the effects of ISI duration on auditory evoked activity in mice are explored, in addition to stimuli duration changes, in oddball and control conditions.

4.1.1.2 Frequency

Several studies of mouse AEP and mismatch responses to frequency-varying oddball paradigms and their reliance on intact NMDA receptor signalling have been published by the Siegel Lab at University of Pennsylvania. These have investigated acute (Siegel et al., 2003, Connolly et al., 2004, Ehrlichman et al., 2008, Featherstone et al., 2013) and chronic (Amann et al., 2009, Featherstone et al., 2014, Nagy et al., 2015) NMDA receptor antagonism with ketamine, and acute MK-801 (Saunders et al., 2012). Doses of ketamine administered in acute experiments ranged from 10 to 50 mg/kg i.p., while chronic designs used 5-20 mg/kg i.p. over 14-28 days.

Initial studies in conscious mice did not reveal a significant effect of acute 10 mg/kg i.p. ketamine on the AEP (Siegel et al., 2003, Connolly et al., 2004), although recordings reportedly commenced 15 min after drug administration. Following characterisation of the acute ketamine dose response on auditory evoked activity in mice (Maxwell et al., 2006), it was found that 10 mg/kg i.p. ketamine significantly reduces peak amplitude measured between 25-50 ms post stimuli onset in recordings made up to 15 minutes after intraperitoneal drug delivery (Ehrlichman et al., 2008). Thus previous studies were likely to have missed the main window of effect. A frequency mismatch response (fMMR) was found to occur over the latency range which was diminished by acute 10 mg/kg i.p. ketamine (Ehrlichman et al., 2008), contradictory to previous work (Umbricht et al., 2005). In a paired-click paradigm experiment 50 mg/kg i.p. ketamine was also found to significantly reduce amplitude of a 40 ms AEP feature (Featherstone et al., 2013).

Studies of fMMR in mice have also examined genetic risk factors in schizophrenia-related models. GluN1 deficient mice were found to display generally greater amplitude AEP and visually evoked potential (VEP) waveforms (Bodarky et al., 2009, Halene et al., 2009). Models of hetero- and homozygous disruption of the Akt1 gene linked with schizophrenia (Schwab et al., 2005) produced an altered response to ketamine compared with wild-type control animals (Featherstone et al., 2013). This thesis seeks to expand upon the existing literature addressing genetic risk factors relevant to schizophrenia in mouse models by investigating AEP and MMR waveforms in the *Map2k7*^{+/-} heterozygous gene disruption model (Winchester et al., 2012). This HET model has not previously been characterised using electrophysiological techniques, thus these are completely novel data. Furthermore, the potential role of NMDA receptors in these responses will be addressed with a pharmacological challenge of 10 mg/kg i.p. ketamine.

One consideration to be aware of regarding the above published electrophysiological studies is that recordings are made from a three-electrode arrangement, with the active electrode implanted into the CA3 region of the hippocampus (3 mm), reference in the ipsilateral frontal cortex (1 mm) and ground electrode in between (1 mm); electrode lengths are noted in brackets. These findings do not therefore directly represent activity of auditory cortices, where the origins of the MMR are partly thought to reside in humans (for review see Garrido et al., 2009, Rinne et al., 2000). Hence in this study, the primary auditory cortex was selected to examine the acute effect of 10 mg/kg i.p. ketamine on AEP and MMR waveforms in conscious mice in response to frequency, as well as duration and intensity manipulations.

In addition to the aforementioned studies in mice, there is a large body of research concerning the fMMR in conscious rats (Eriksson and Villa, 2005, Roger et al., 2009, Nakamura et al., 2011, Jung et al., 2013, Harms et al., 2014, Sivarao et al., 2014, Witten et al., 2014). However, the relationship between the so-called MMN-*like* response in rodents and the human MMN remains controversial due methodological inconsistencies and variable findings (e.g. polarity, latency range, negative results), as described in Section 1.3 (Escera and Malmierca, 2014, Grimm et al., 2016, Nagai et al., 2013, Nelken and Ulanovsky, 2007, Todd et al., 2013). This thesis takes a systematic approach, examining the independent manipulation of basic physical features of auditory stimuli on evoked electrophysiological activity in the primary auditory cortex of mice; in doing so contributing towards the characterisation of MMN biomarker signatures in rodent models relevant to schizophrenia.

4.1.1.3 Intensity

A couple of studies have investigated electrophysiological responses of conscious mice to intensity variations in oddball paradigms, although these were combined with frequency changes (Ehlers and Somes, 2002, Slawewski et al., 2003). Having found AEPs potentially useful for studying genetic effects on central auditory processing in mice, these studies fall short in dissociating frequency and intensity oddball effects which are inherently confounded in their experimental design. Thus throughout this thesis intensity, frequency and duration are each manipulated individually in oddball and control paradigms to dissociate their relative effects on the resulting AEP and MMR waveforms.

4.1.2 *Challenges and opportunities of using conscious rodents*

Using conscious mice in this experiment posed several technical challenges. Free movement of animals during electrophysiological recordings typically increases movement artifacts, deteriorating the quality of data. Additionally, in a study of auditory evoked activity, accurate control over the relative sound source location is difficult to achieve if animals are continuously moving around changing their position in relation to the speaker. To overcome or limit these factors animal movement was restricted using a holding tube (described in Section 2.6.1.2). This may have altered stress hormone levels such as cortisol, potentially altering the mouse AEP response (Al-Mana et al., 2008). Connecting the EEG acquisition system to animal head-mounts and taking continuous recordings may also induce stress. Elimination of stress induced physiological changes in this type of *in-vivo* experiment is infeasible, therefore psychophysiological stress may be considered as a covariate. This is presumed to effect animals equally. However, it cannot be dismissed that perhaps wild-type (WT) control and *Map2k7*^{+/-} (HET) mice undergo different stress responses which may differentially alter their electrophysiology.

The use of conscious subjects allowed recordings to be made over multiple days, as opposed to the situation in Experiment I where mice were exterminated following a single session under urethane-anaesthesia. This enabled a systematic investigation of stimulus duration, frequency, intensity and ISI duration variations which would not have been practical with a fully anaesthetised design. Furthermore, the within-subjects repeated measures design adopted throughout this thesis addresses the 3Rs in animal research.

4.1.3 *Experiment II aims*

The hypothesis tested in this chapter is that an MMR can be elicited from the auditory cortex of conscious mice to manipulations in stimulus duration, frequency, intensity and ISI duration. This is probed systematically with a series of oddball and control paradigms. In addition, the proposition that schizophrenia-related *Map2k7*^{+/-} gene disruption and ketamine-induced NMDA receptor antagonism models display altered auditory activity and MMR waveforms is explored. Furthermore, to examine whether *Map2k7* may be involved in modifying NMDA receptor function, ketamine is administered to HET mice and the resulting auditory electrophysiological responses are measured.

Thus the six key aims of Experiment II are to:

1. Determine the effects of ISI duration on the AEP from conscious mice and characterise the associated duration mismatch response (dMMR).
2. Determine the effects of auditory stimulus duration on the AEP from conscious mice and characterise the associated duration mismatch response (dMMR).
3. Determine the effects of auditory stimulus frequency on the AEP from conscious mice and characterise the frequency mismatch response (fMMR).
4. Determine the effects of auditory stimulus intensity on the AEP from conscious mice and characterise the intensity mismatch response (iMMR).
5. Examine any differences in respective AEP and MMR waveforms from conscious wild-type control (WT) and *Map2k7*^{+/-} (HET) mice.
6. Investigate the effects of 10 mg/kg i.p. ketamine on the AEP in conscious mice and whether this is altered in HET mice.

4.2 Methods

Materials and methods applied in Experiment II are summarised in this section. Full details are provided in Chapter 2 and cross-references are provided within the text to allow the reader to easily navigate towards elaborated descriptions.

4.2.1 *Animal details*

Wild-type (WT; n=10) control and *Map2k7*^{+/-} (HET; n=10) schizophrenia-related gene disruption model mouse groups were used in this experiment. For full details see Section 2.4.4 and Appendix B.

4.2.2 *Surgery*

Aseptic stereotactic surgery was performed to implant cortical EEG recording electrodes bilaterally above the primary auditory cortices of each animal, after which they fully recovered for five days before making electrophysiological recordings. This surgical procedure is described in Section 2.5.2.

4.2.3 *Electrophysiological recordings*

During auditory stimulation cortical EEG was recorded from the primary auditory cortices of animals within a soundproof recording chamber (Figure 2.5) using an Intan Technologies data acquisition system. Data was acquired at 1 kS/s with a bandwidth of 1-500 Hz. Details of the equipment used and recording parameters are provided in Section 2.6.1.

4.2.4 *Auditory paradigms*

Experiment II incorporated a paradigm presentation sequence consisting of consecutive-repetition (CR), oddball (OD), deviant-alone (DA) and many-standards (MS) paradigms. These were employed with stimuli varying in duration (dCR/dOD/dDA/dMS), frequency (fCR/fOD/fDA/fMS) and intensity (iCR/iOD/iDA/iMS). For each feature of sound under investigation this sequence was presented once after physiological saline and again following 10 mg/kg i.p. ketamine injections. Descriptions of these auditory paradigms are provided in Section 2.7.

4.2.5 *Stimuli properties*

Standard stimuli in duration-varying paradigms were 100 ms, 10 kHz, and 80 dB, and duration oddballs varied by ± 50 ms. Standard stimuli in frequency and intensity varying paradigms were 50 ms, 10 kHz, and 80 dB; with frequency oddball stimuli varying by ± 2 kHz, and intensity oddball stimuli varying by ± 10 dB. All auditory stimuli were monophonic pure tone sinusoids with instantaneous rise/fall times. In the duration many-standards (dMS)

paradigm stimuli durations varied from 50-275 ms in 25 ms increments, fMS paradigm stimuli frequencies varied from 8-12.5 kHz in 500 Hz increments, and iMS paradigm stimuli intensities varied from 70-92.5 dB in 2.5 dB increments. Levels of stimuli responsible for inducing waveforms presented in the results are clearly labelled in figure legends. Details of auditory stimuli parameters are provided in Section 2.8.2.

4.2.6 Experimental protocol

The experimental protocol and paradigm presentation sequence for Experiment II is outlined in Section 2.9.2. In summary, after recovering from surgery and habituation to test equipment (Section 2.6.1.2) mice underwent testing over several days with alternate resting days. Auditory paradigms with stimuli varying either in duration, frequency or intensity were each presented in the presence and absence of ketamine on a single test day. Two versions of duration-varying paradigms were included; one using constant stimulus onset asynchrony (SOA) and another with constant inter-stimulus interval (ISI), as discussed in Section 2.8.2.

4.2.7 Artifact rejection

Threshold artifact rejection ($\pm 500 \mu\text{V}$) was applied to datasets from Experiment II, as described in Section 2.10.1, to prevent extraneous noise sources from distorting individual subjects' AEP. Overall mean rejection rates of 0.87% (sd 0.054%) were considered suitably low to suggest sufficient data quality, and there were no significant effects of genotype, gender, session or paradigm.

However, upon computing the AEP from each animal it was apparent that the quality of recordings was not entirely consistent. A decision was made to exclude three subjects (details provided in Section 2.4.4) from electrophysiological analyses on the basis of absent auditory evoked responses and excessive noise. Examples of rejected and accepted datasets are shown in Figure 4.1. This may have been due to incorrect surgical/implantation technique, technical faults and/or increased movement artifacts.

Additionally, individual recording channels were rejected for either being incessantly noisy or for containing no signal (tied to ground). This was the case for four subjects where instead of averaging bilateral electrode channels only reliable channel data was selected for computing their AEP. These occurrences were most likely caused by imperfect surgical technique. There were no significant differences between reliable channels recorded in the remainder of subjects so here it is considered permissible to include unilateral AEPs for analyses. Details of unreliable channels are provided in Appendix B.

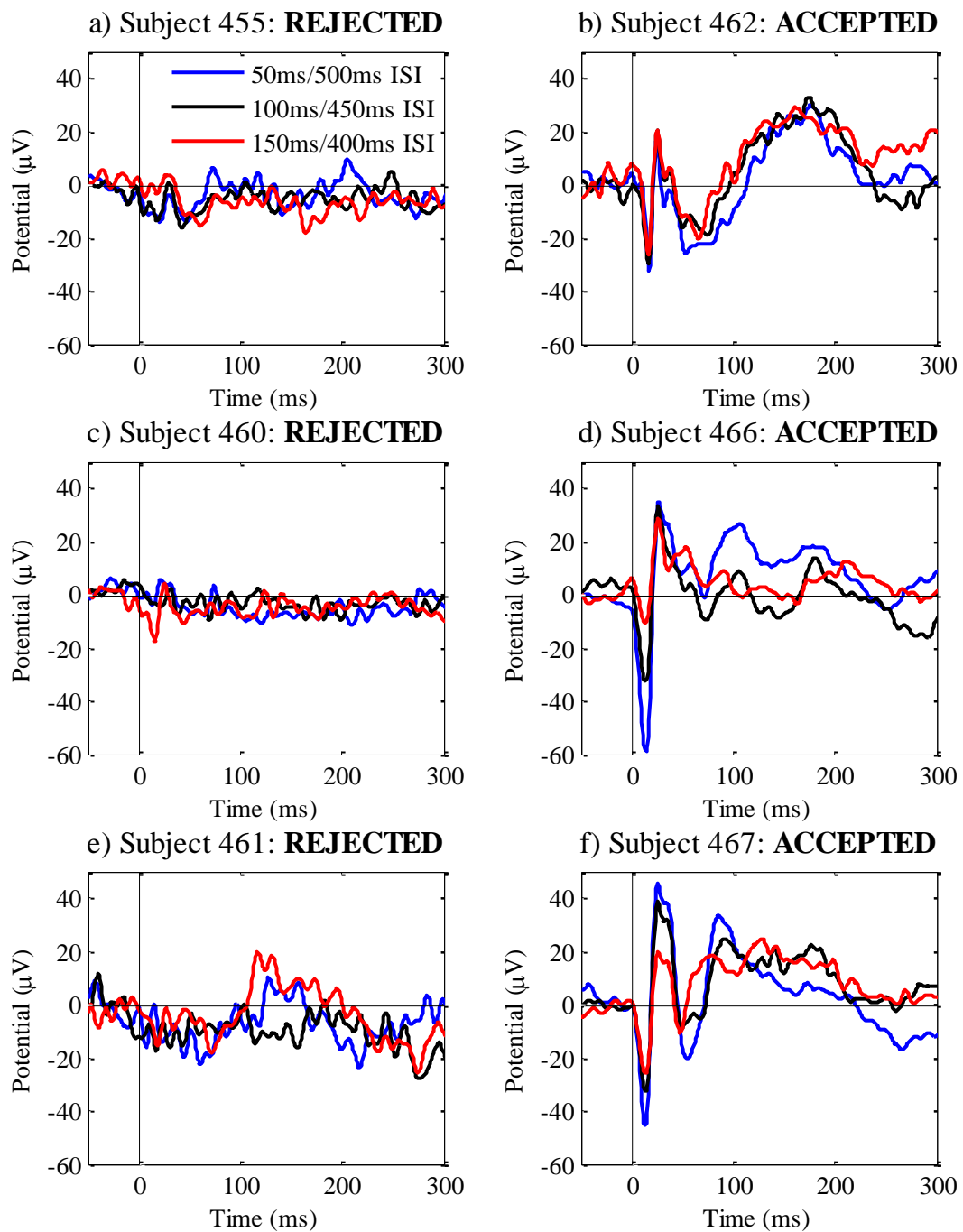


Figure 4.1 - Examples of accepted and rejected data for auditory evoked potential analyses These waveforms were generated from the duration consecutive-repetition (dCR) paradigm with variable inter-stimulus interval (ISI). Panels a), c), and e) on the left hand side display data from subjects which were excluded from analysis because of the limited quality of recordings, which resulted in AEP waveforms without clearly defined peaks that were present in cleaner datasets. Examples of acceptable data are given on the right hand side panels b), d), and f), in which the effects of varying ISI may be observed (discussed fully in 4.3.1.2).

4.2.8 *Auditory evoked potential computations*

The traditional approach to calculating the mismatch response (Figure 3.1a) was taken in Experiment II. Additional event-related potential (ERP) computations included calculating the mean AEP from ten duration many-standards (dMS) paradigm stimuli, incorporating addition and division operations (also applied in Experiment I; see Section 3.2.8.2). This was then subtracted from each individual dMS stimulus' AEP to isolate offset responses from conscious mice data; this analysis is provided in Section 4.3.1.3.

4.2.9 *Auditory evoked potential measurements*

Auditory evoked potential waveforms from conscious mice displayed some characteristic features which are quantified from various paradigms throughout this chapter. The two foremost AEP features are introduced below, whereas ad hoc measurements are described in relevant results sections which follow.

4.2.9.1 *Primary onset potential (N1)*

The primary onset potential (N1) is a relatively large initial deflection, measured as peak negative amplitude over five samples (5 ms) from a 0-30 ms post stimulus onset measurement window. This is equivalent to N1 response from Experiment I (Section 3.2.9.1).

4.2.9.2 *Secondary potential (P2)*

The secondary potential (P2) is a large positive amplitude response immediately following N1, measured as positive peak amplitude over 5 ms from 20-60 ms post stimulus onset. This feature was not present in urethane-anaesthetised mice and therefore may be considered an indication of conscious auditory processing.

4.2.9.3 *Subsequent peaks (N3, P4, N5 and P6)*

Subsequent deflections in the auditory evoked potential following on from N1 and P2 features were identified, as shown in Figure 4.11, Figure 4.12 and Figure 4.17, as N3 (50-80 ms), P4 (60-100 ms), N5 (100-150 ms) and P6 (150-250 ms); latency ranges *in brackets* provide their respective measurement windows. These alternating polarity peaks are quantified in Figure 4.26 and Figure 4.27. Compared with N1 and P2 these subsequent deflections were lower in amplitude and more temporally variable, possibly reflecting secondary, tertiary, or higher order sensory processing.

4.2.9.4 Offset response (P_{offset} and N_{offset})

Positive (P_{offset}) and negative (N_{offset}) stimuli offset potential deflections were observed from different duration stimuli in the dMS paradigm (see Figure 4.5 and Figure 4.6). These features were quantified by measuring the relative positive and negative polarity peaks from 0-50 ms and 50-100 ms post stimuli offset measurement windows, respectively.

4.2.10 Video footage analysis

The block-matching algorithm described in Section 2.10.3 was applied to video footage of conscious mice within the recording chamber. Mean optical flow from a 160 x 120 pixel optical flow matrix plotted across time was used as a proxy measure of animal movement during the experiment, and time-binned statistical analysis was performed. This analysis is detailed in Section 4.3.5.

4.3 Results

Key findings from conscious mice in Experiment II are presented here. This section preserves the same general layout and structure as for Experiment I (Section 3.3), beginning with results from paradigms with stimuli varying in duration, frequency then intensity. These are followed by a motion estimation analysis of video footage recorded during test sessions. It may be emphasised here that the electrophysiological response observed from conscious animals is different from their anaesthetised counterparts, however there are some consistencies which will become apparent as the results are presented.

4.3.1 *Duration paradigms in conscious mice*

Two versions of duration-varying paradigms were used in this experiment, the first with variable ISI and the second with constant ISI, discussed in Section 2.8.2. Findings from both are reported in this subsection which illustrates the effects of varying stimuli duration and the ISI delay. Evidence provided below demonstrates that both of these temporal variations induce profound changes in the electrophysiological responses observed, thereby potentially impacting the mismatch response obtained by manipulating either of these features of sound in an oddball paradigm.

4.3.1.1 *Map2k7^{+/-} mice display increased stimulus onset response*

Representative AEP waveforms from conscious wild-type control (WT) and *Map2k7^{+/-}* (HET) mice are analysed in Figure 4.2, similar to the analysis of urethane-anaesthetised animal responses presented in Figure 3.3. The grand-average AEP from both groups in saline and 10 mg/kg i.p. ketamine recording sessions are provided in Figure 4.2a and Figure 4.2b, respectively. These waveforms reflect the electrophysiological response to standard 100 ms, 10 kHz, 80 dB, 450 ms ISI stimuli in the duration many-standards (dMS) paradigm with variable ISI, which was presented \approx 30-40 min after injecting ketamine. The absence of any outstanding differences between the responses from the two treatment sessions is perhaps therefore unsurprising as these recordings were possibly made after the main drug effects had subsided. The acute effects of ketamine are addressed later on in this chapter, in Section 4.3.2.4 and Section 4.3.3.3.

In conscious subjects the most prominent AEP features are the primary negative onset response (N1) which is followed by a rapid secondary positive response (P2) and a series of lower amplitude, alternating polarity deflections from \approx 50-250 ms before returning to baseline. These relatively smaller potentials are less well defined than the first two peaks and tended to vary more throughout recordings (e.g. see Section 4.3.1.7 and Section 4.3.3.4), perhaps indicative of adaptive processes. Nevertheless, these are not quantified here and

focus is placed on the larger, more temporally precise N1 and P2 potentials. Offset responses cannot be isolated from these waveforms and are therefore addressed separately in Section 4.3.1.3.

Consistent with findings from Experiment I in urethane-anaesthetised mice, conscious HET subjects are seen to exhibit significantly greater N1 peak amplitudes than wild-type WT controls [$F_{1,16} = 4.786$, $p = .044$], quantified in Figure 4.2c. This was computed by performing a repeated measures ANOVA with genotype (WT/HET) and gender (male/female) as between-subjects factors and treatment session (saline/ketamine) as a within-subjects factor. There were no significant effects of gender [$F_{1,16} = .078$, $p = .784$] or ketamine [$F_{1,16} = .205$, $p = .657$] on this N1 peak amplitude data. This finding reinforces the suggestion that *Map2k7^{+/-}* mice may have abnormal N1 response generators compared with control animals.

Similar statistical analysis for N1 peak latency (Figure 4.2d) revealed that it does not differ significantly between genotypes [$F_{1,16} = .351$, $p = .562$], genders [$F_{1,16} = .210$, $p = .653$] or treatment sessions [$F_{1,16} = .342$, $p = .567$]. Overall the N1 potential reaches a peak at 14.3 ms (± 0.5 ms sem) post stimulus onset, which is comparable with urethane-anaesthetised mice (15.5 ± 1.1 ms sem) data presented in Section 3.3.1.1.

In contrast to the N1 response, the same statistical test applied to P2 peak amplitude measurements graphed in Figure 4.2e returned no significant effects of genotype [$F_{1,16} = .014$, $p = .908$], gender [$F_{1,16} = 1.794$, $p = .199$], or ketamine [$F_{1,16} = .148$, $p = .706$]. Although this feature appears to be unaffected by ketamine in these recordings, made ≈ 30 -40 min after drug administration, it was found to vary considerable under its acute effects. This observation was most evident in consecutive-repetition (CR) paradigm recordings made ≈ 0 -10 min post 10 mg/kg i.p. ketamine administration (e.g. Figure 4.17).

P2 peak latency (Figure 4.2f) showed no significant differences between genotypes [$F_{1,16} = .046$, $p = .833$], genders [$F_{1,16} = .896$, $p = .358$], or treatment sessions [$F_{1,16} = 1.242$, $p = .281$]. Overall P2 peak latency was found to occur at 28.8 ms (± 1.2 ms sem) post stimulus onset. The P2 potential was not present in urethane-anaesthetised mice.

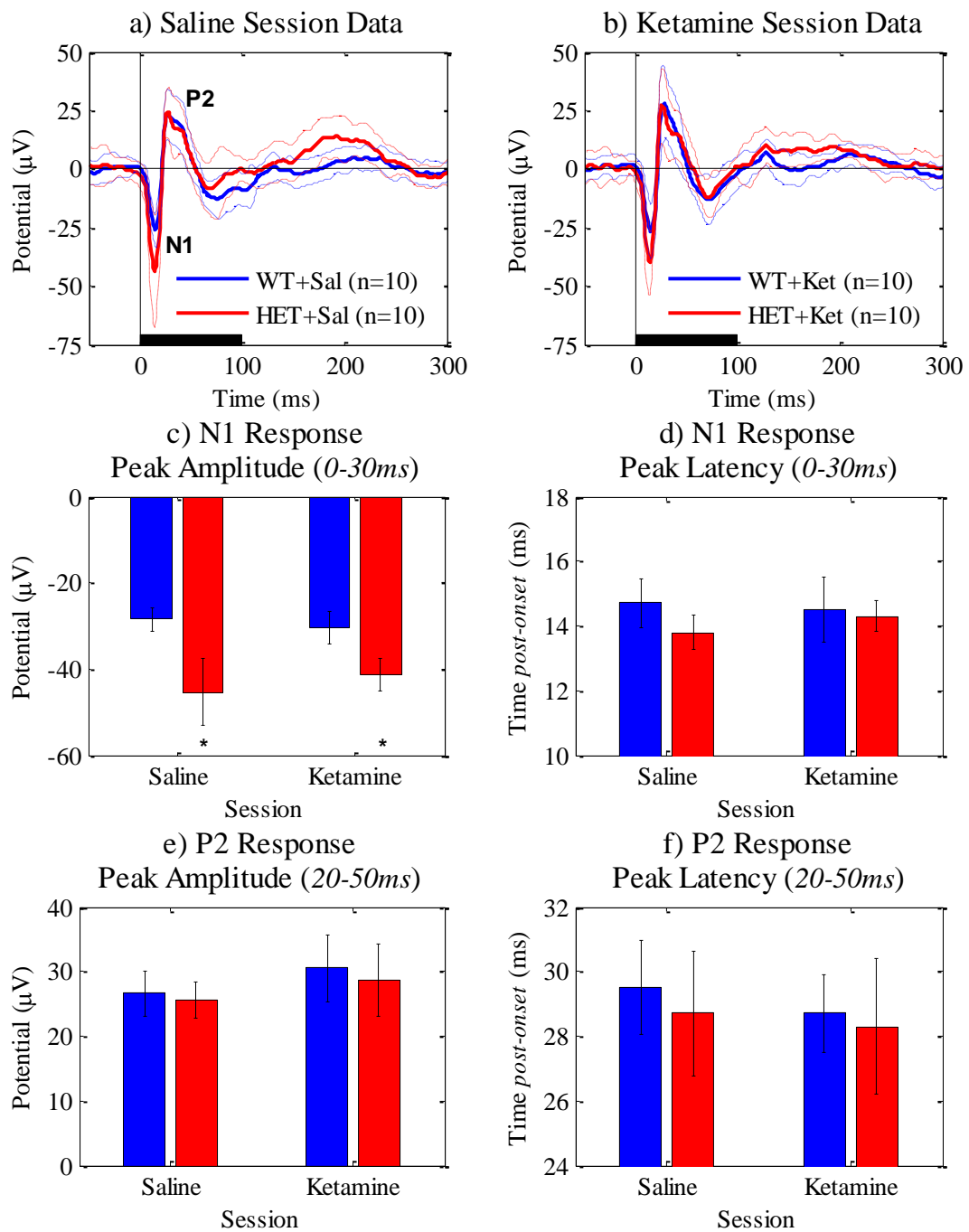


Figure 4.2 - Comparison of conscious wild-type and *Map2k7*^{+/-} grand-average auditory evoked potential waveforms This representative data analysis from conscious subjects is similar to that provided in Figure 3.3 for urethane-anaesthetised mice. Standard (100 ms, 10 kHz, 80 dB, 450 ms ISI) stimuli AEP responses from the duration many-standards (dMS) paradigm are shown for wild-type control (WT; bold blue \pm sem in dotted blue) and *Map2k7*^{+/-} (HET; bold red \pm sem in dotted red) mice following a) an injection of physiological saline (Sal), and b) 10 mg/kg i.p. ketamine (Ket). Auditory stimulation is illustrated by a solid black rectangle. Defined primary (N1) and secondary (P2) potentials are followed by a series of less pronounced deflections which are not addressed here. The presence of an offset response in these waveforms is difficult to distinguish (see Figure 4.5). AEP features quantified are: c) N1 peak amplitude measured from 0-30 ms, showing a statistically significant effect of genotype ($p < .05$); d) N1 peak latency; e) P2 peak amplitude measured from 20-60 ms, and; f) P2 peak latency. Data are represented as means \pm sem. There were no ketamine effects in this analysis of data recorded \approx 30-40 minutes following drug administration.

4.3.1.2 Inter-stimulus interval influences auditory evoked potentials

Data from the dMS paradigm with variable ISI are presented here. In effect, this analysis may be interpreted as an examination of ISI effects because within the measurement window being assessed (0-50 ms post stimulus onset) all stimuli are ‘on’ so to speak, with the only difference between them being the ISI which preceded their onset.

Waveforms from this dMS paradigm are plotted in Figure 4.3, labelled in the legend with ISI delay opposed to stimulus duration. Visual inspection of these AEPs suggests that longer silence between a preceding stimulus offset and following stimulus onset induces greater N1 and P2 potentials in the resulting AEP. Varying ISI did not appear to have any recognisable effect on other less well defined features of the AEP waveform in conscious mice.

These AEP features are quantified in Figure 4.4, with correlation coefficients highlighting strong linear relationships between ISI delay and N1 ($R^2 < -.9$) and P2 ($R^2 > .9$) peak amplitude measurements from both genotype groups. A discussion of how ISI, stimulus frequency and intensity variations each influence these measures is provided in Section 4.4.1.

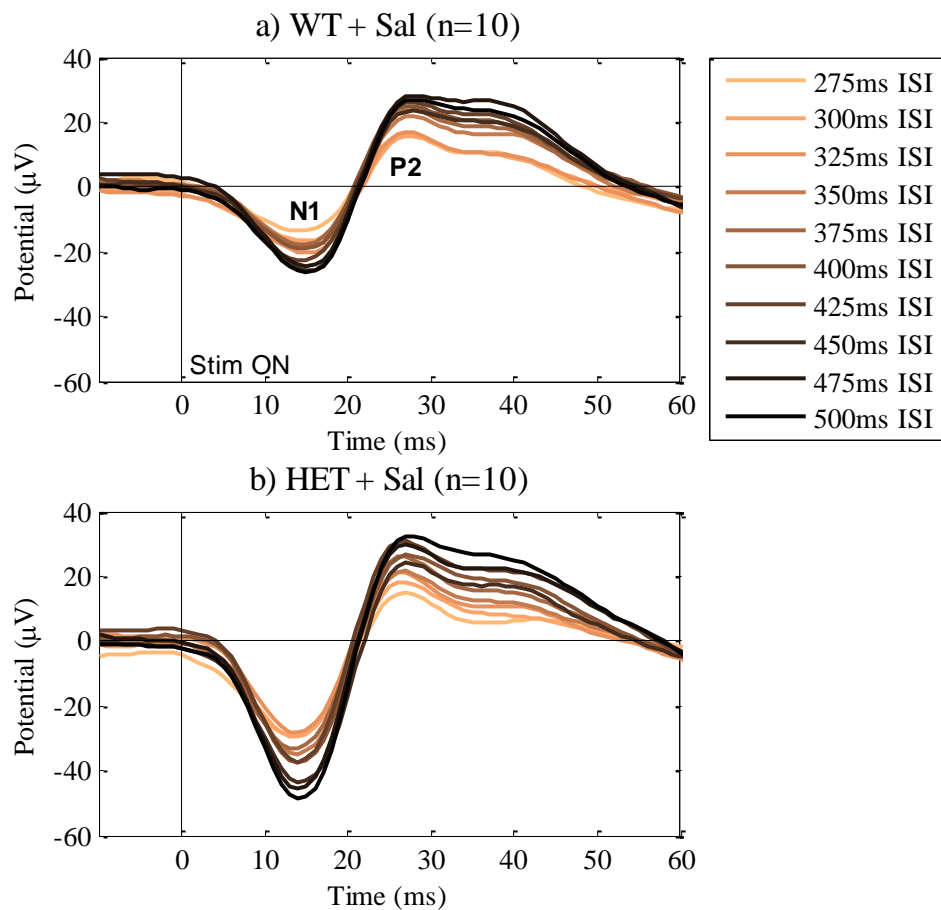


Figure 4.3 - Effect of inter-stimulus interval on primary and secondary auditory responses in conscious wild-type and *Map2k7*^{+/-} mice These auditory evoked potentials were obtained from duration many-standards (dMS) paradigm stimuli with variable inter-stimulus interval (ISI) recorded during the saline session (Sal). a) Control (WT), and b) *Map2k7*^{+/-} (HET) grand-average primary onset (N1) and secondary (P2) responses to ten dMS stimuli with varying ISI presented in the saline recording session (Sal). N1 and P2 peak amplitudes measured from both groups are analysed in Figure 4.4.

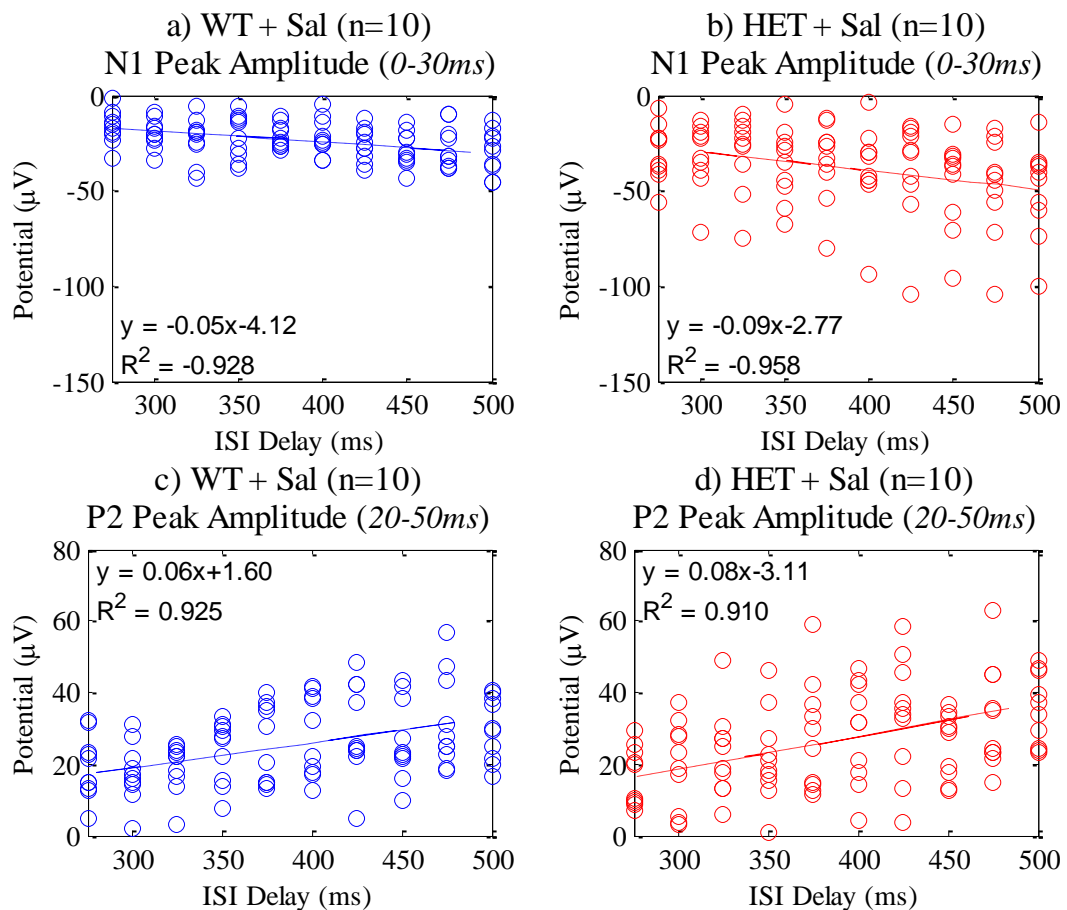


Figure 4.4 - Quantification of inter-stimulus interval effect on auditory evoked potentials in conscious wild-type and *Map2k7*^{+/-} mice Primary negative onset response (N1) peak amplitude measured from 0-30 ms is shown for a) control (WT), and b) *Map2k7*^{+/-} (HET) mice. Secondary positive response (P2) peak amplitude from 20-50 ms is shown for c) WT, and d) HET mice. Measurement windows are provided *in brackets*. These data were recorded from the duration many-standards (dMS) paradigm with varying inter-stimulus interval (ISI) delay, presented in the first session following a physiological saline (Sal) injection.

4.3.1.3 Stimuli offset responses are observed in conscious mice

Findings from the dMS paradigm with constant ISI are presented here. Hence this is an examination of auditory stimulation duration effects and the resulting offset response.

Figure 4.5 displays representative AEPs from ten dMS paradigm stimuli with constant ISI and illustrates the process of isolating stimuli offset responses from the much larger amplitude underlying waveform. Study-average waveforms from combined WT and HET group data are used in this analysis to provide the clearest possible view of these relatively low amplitude stimuli offset potentials. This was performed to effectively demonstrate that offset responses occur in conscious mice, whereas potential genotype or ketamine effects are analysed in Figure 4.6.

Each individual AEP from ten different duration stimuli are shown in Figure 4.5a, each of which exhibit a small positive amplitude deflection emerging from the common waveform

shape, that peaks approximately 25 ms post offset. Stimuli offset times are indicated by vertical dashed lines. The mean AEP calculated by averaging together all of these waveforms is plotted in red on Figure 4.5b, superimposed on top of greyed-out individual AEPs from dMS stimuli. By subtracting the mean AEP from each individual AEP, stimuli offset responses are isolated (Figure 4.5c).

It appears as though stimuli offset responses from 50 ms and 75 ms stimuli are typically lower in amplitude than those generated by ≥ 100 ms duration stimuli. This may be due to much larger amplitude deflections which occur during the immediate period following stimuli onset potentially obscuring their measurement. Another interpretation may be that the duration of auditory stimulation is related to offset response peak magnitude, with shorter duration stimuli eliciting a lesser response than longer duration stimuli.

The overall offset response is characterised as illustrated in Figure 4.6. Firstly, the difference waveforms from Figure 4.5c are synchronised at stimuli offset times, as shown in Figure 4.6a. For each group these synchronised offset response waveforms are averaged together for comparison in Figure 4.6b. These highlight the general offset response trajectory which comprises of sharp positive (P_{offset}) and extended negative (N_{offset}) deflections with peak latencies of 23.4 ms (± 1.4 ms sem; Figure 4.6c) and 74.6 ms (± 2.1 ms sem; Figure 4.6d) post stimulus offset, respectively. To quantify these, peak-to-peak amplitude between P_{offset} and N_{offset} was measured, presented in Figure 4.6e, revealing no significant effects of genotype [$F_{1,16} = .188$, $p = .671$], gender [$F_{1,16} = .043$, $p = .839$] or ketamine [$F_{1,16} = .833$, $p = .375$].

Overall these findings demonstrate that stimuli offset responses occur in conscious mice, which may potentially impact the duration mismatch response (dMMR) generated by using duration oddball stimuli, addressed next in Section 4.3.1.4.

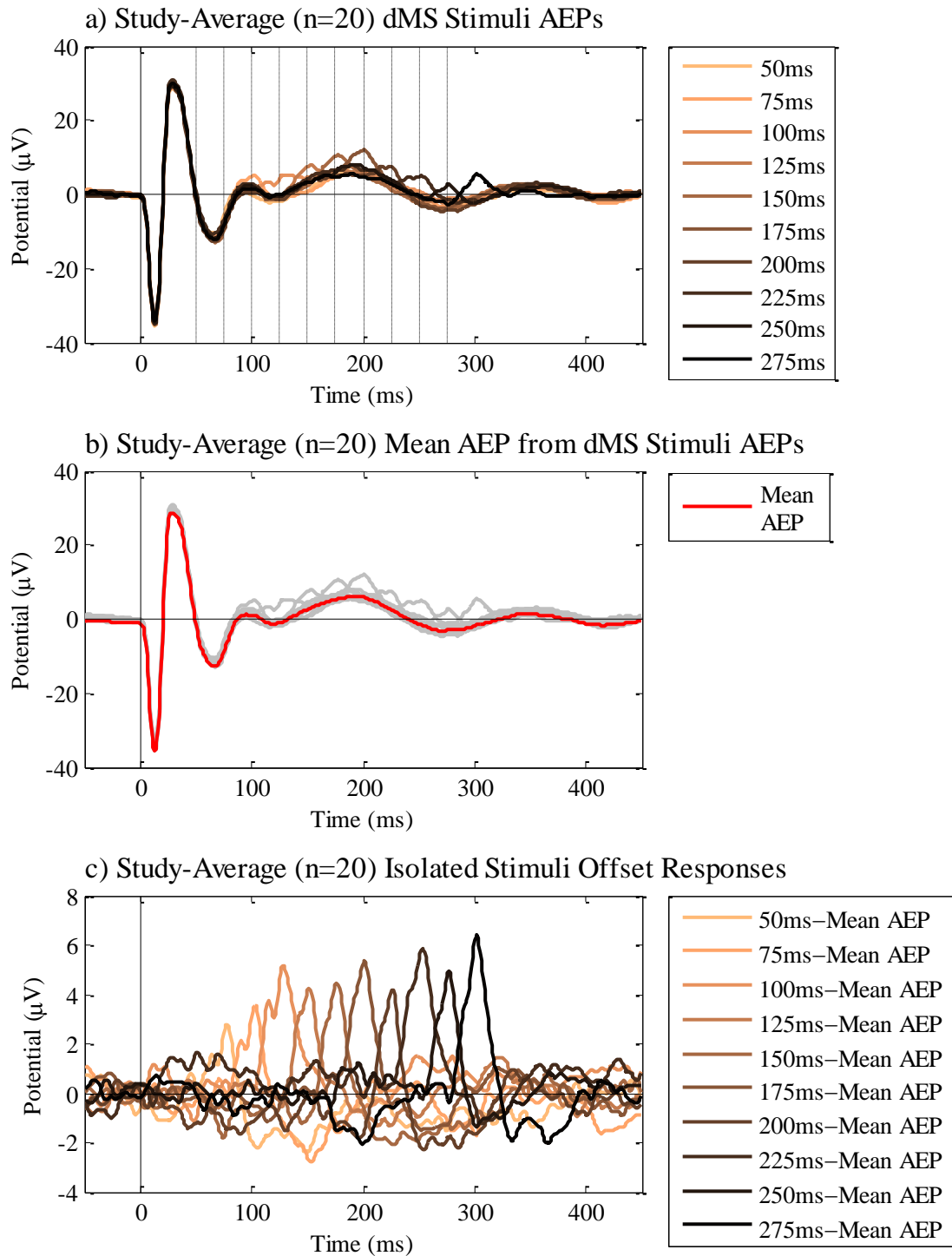


Figure 4.5 - Effect of stimulus duration on auditory offset response in conscious mice
 Control (WT; n = 10) and *Map2k7^{+/-}* (HET; n = 10) group data from the duration many-standards (dMS) paradigm with constant inter-stimulus interval (ISI) are combined in this analysis. a) Study-average auditory evoked potentials (AEPs) to ten dMS stimuli from 50-275 ms in duration, with 25 ms spaced vertical dashed lines indicating stimuli offset times. b) Mean AEP produced by averaging together the waveforms in (a). c) Offset potentials are isolated from the ongoing waveform by subtracting the mean AEP shown in (b) from each individual AEP in (a). The stimulus offset response is analysed further in Figure 4.6.

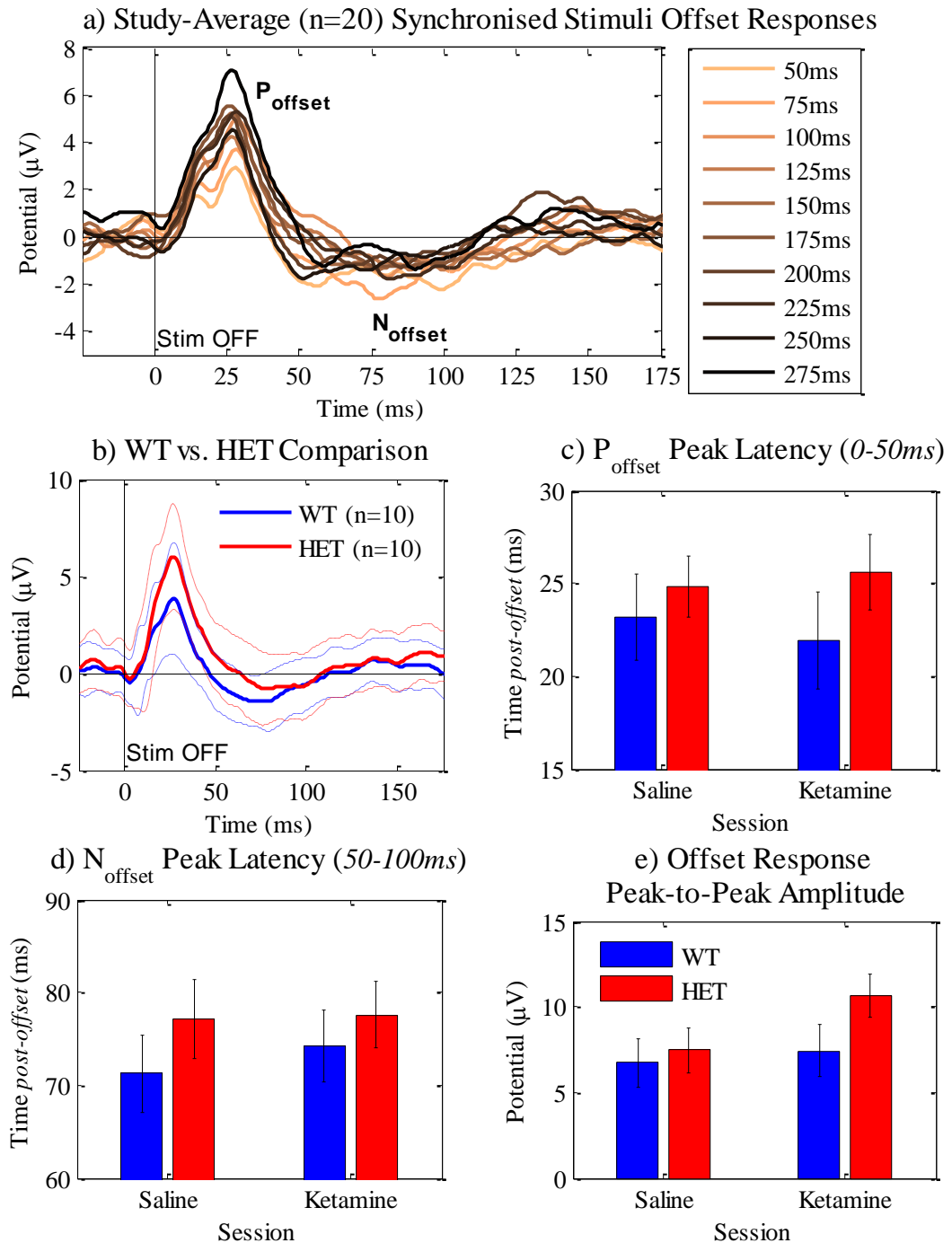


Figure 4.6 - Characterising the auditory stimulus offset response in conscious mice a) Following offset potential isolation described in Figure 4.5 waveforms are aligned at stimuli offset times (0 ms), revealing distinct positive (P_{offset}) and negative (N_{offset}) amplitude deflections. b) Comparison of control (WT; bold blue \pm sem in dotted blue) and *Map2k7^{+/-}* (HET; bold red \pm sem in dotted red) group grand-average offset potential waveforms. Quantification of c) P_{offset} peak latency, d) N_{offset} peak latency, and e) offset response peak-to-peak amplitude displayed as group means \pm sem, with neither showing any significant effects of genotype or ketamine. Measurement windows post stimuli offset are provided *in brackets*.

4.3.1.4 *Duration mismatch response in conscious mice is influenced by stimuli offset potentials*

Duration mismatch response waveforms from study-average WT and HET data combined are shown in Figure 4.7. Whole-study data is used here to enhance the clarity of relatively low amplitude responses from within EEG recordings of conscious subjects. The upper panel (Figure 4.7a) provides findings from the duration oddball (dOD) paradigm with variable ISI, whereas the lower panel (Figure 4.7b) shows waveforms from the dOD paradigm with constant ISI. These plots illustrate how both ISI and stimulus duration may influence the resulting dMMR.

Firstly, addressing the variable ISI condition in Figure 4.7a, prominent deflections occur <50 ms post stimuli onset, before offset of any oddball stimuli. This is attributed to differences between N1 and P2 peak amplitudes generated by the 450 ms ISI standard stimulus and either longer (500 ms) or shorter (400 ms) ISI oddball stimuli, thus resulting in opposite polarity deflections in the 400 ms ISI and 500 ms ISI dMMR waveforms <50 ms post stimuli onset. This may be termed an ISI oddball response. Constant ISI waveforms in Figure 4.7b do not display any prominent deflections <50 ms, reinforcing the observation that this is an ISI effect.

Secondly, more pertinent to the analysis of stimuli duration oddballs, both variable and constant ISI dOD paradigm data in Figure 4.7 demonstrate the influence of stimuli offset responses in shaping the resulting dMMR difference waveforms. To clarify, dMMR waveforms were generated by subtracting the 100 ms standard stimulus AEP from the 50 ms (-50 ms) and the 150 ms (+50 ms) oddball AEP. The negative deflection in both 50 ms and 150 ms dMMR waveforms that peak at ≈ 125 ms are caused by the offset response (P_{offset}) of the 100 ms standard AEP, whereas positive deflections in each dMMR are caused by the P_{offset} feature from each respective oddball AEP, which occur at ≈ 75 ms and ≈ 175 ms for 50 ms and 150 ms dMMR waveforms, respectively.

These waveforms from the dOD paradigm with constant ISI are quantified in Figure 4.8. Positive peak latency from 50 ms and 150 ms dMMR waveforms are displayed in the top two panels. There is a clear difference between them, attributed to the respective P_{offset} response of each oddball AEP. Negative peak latencies from each dMMR plotted in the middle panels are comparable, effectively due to the P_{offset} response of the standard AEP. Peak-to-peak amplitudes are shown in the bottom two panels. These metrics were not significantly affected by genotype or ketamine.

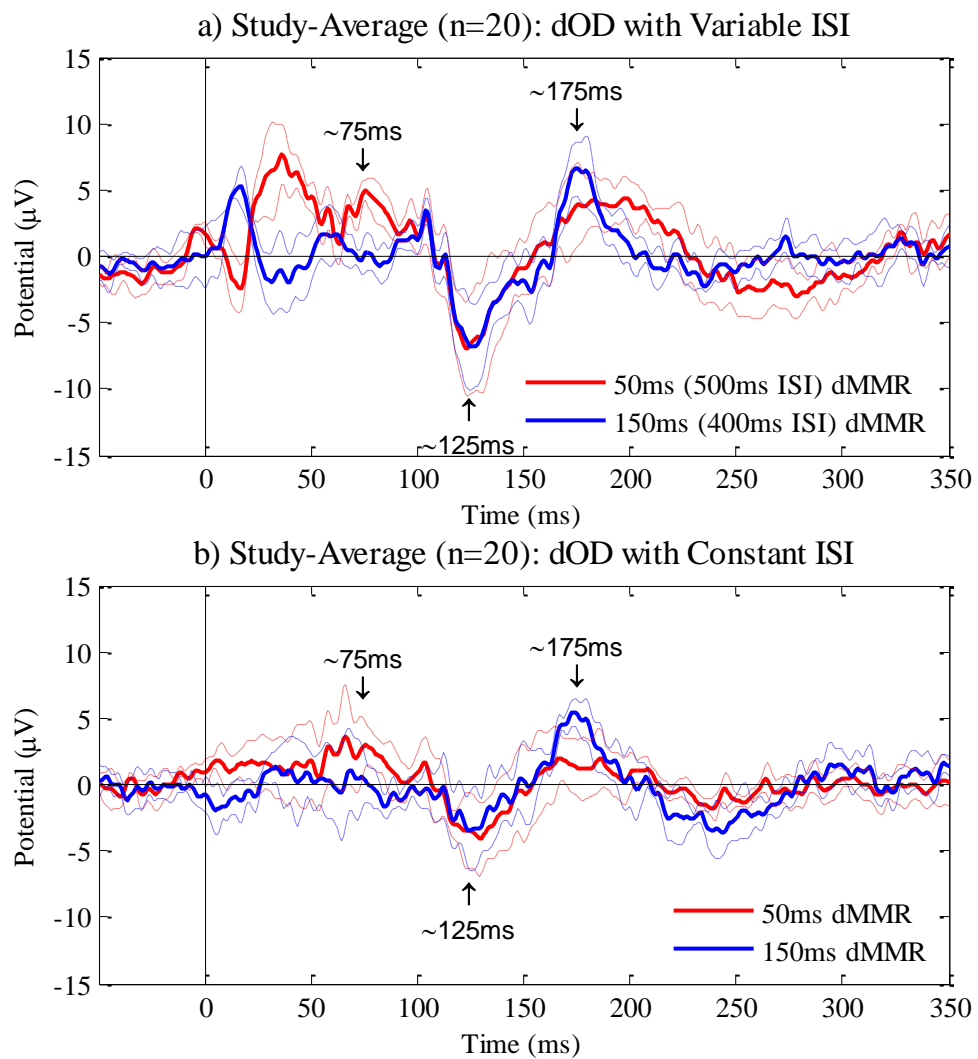


Figure 4.7 - Increasing (+50 ms) and decreasing (-50 ms) duration oddball mismatch responses in conscious mice Control (WT; n = 10) and *Map2k7^{+/-}* (HET; n = 10) recordings from saline and 10 mg/kg i.p. ketamine recordings are combined here to view the relatively small effect. Study-average 50 ms (bold red \pm sem in dotted red) and 150 ms (bold blue \pm sem in dotted blue) duration mismatch response (dMMR) waveforms are plotted from the duration oddball (dOD) paradigms with a) variable inter-stimulus interval (ISI), and b) constant ISI. Approximate offset response (P_{offset}) times for 50 ms (-50 ms oddball), 100 ms (standard) and 150 ms (+50 ms oddball) duration stimuli are annotated on both plots.

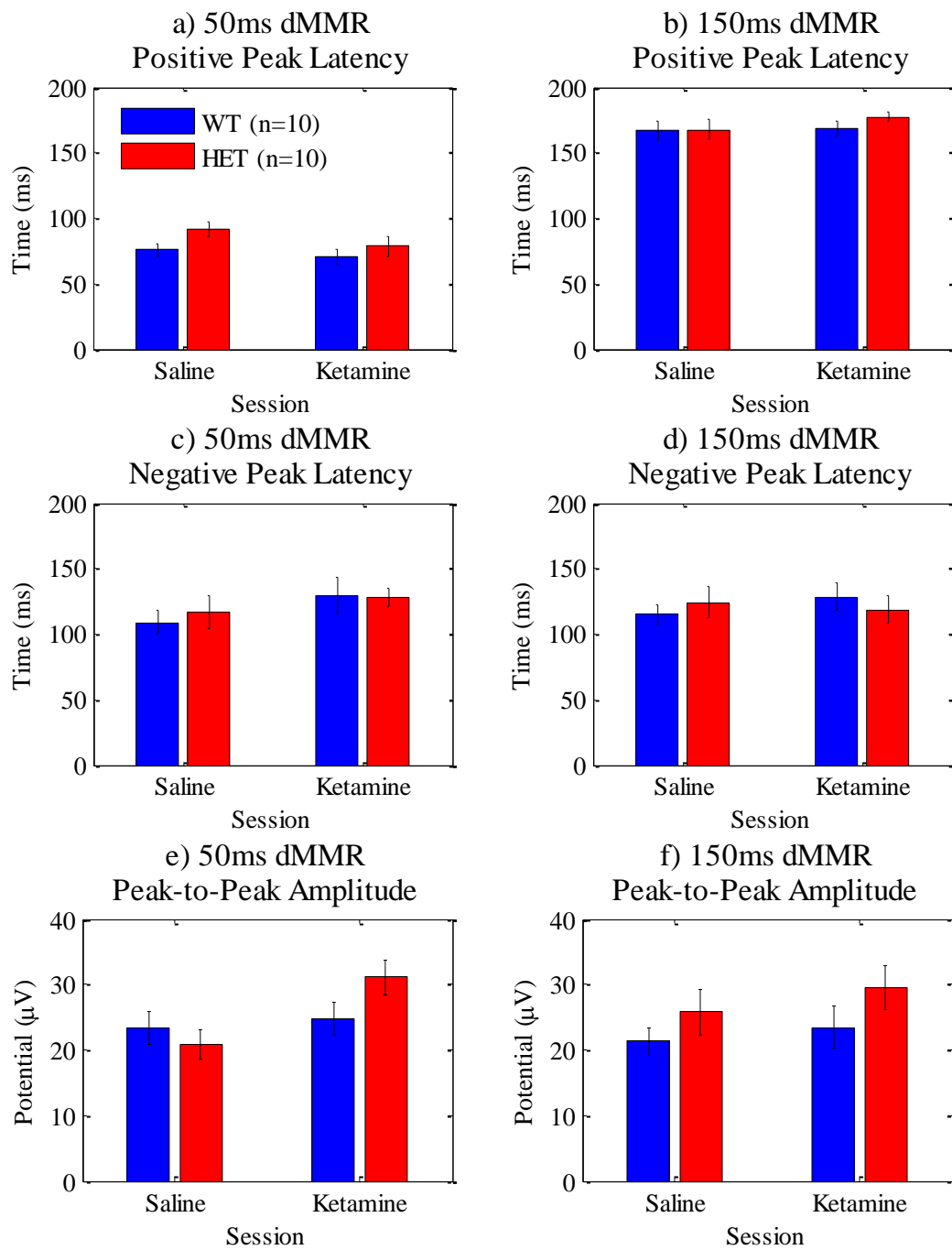


Figure 4.8 - Quantification of decreased (-50 ms) and increased ($+50$ ms) duration oddball mismatch responses in conscious mice Data are shown from control (WT) and *Map2k7^{+/-}* (HET) mice in the duration oddball paradigm (dOD) with constant inter-stimulus interval (ISI) following saline and 10 mg/kg i.p. ketamine administrations. Mean positive peak latency from a) 50 ms (-50 ms oddball) and b) 150 ms ($+50$ ms oddball) duration mismatch response (dMMR), negative peak latency from c) 50 ms and d) 150 ms dMMR, and; peak-to-peak amplitude from e) the 50 ms and f) the 150 ms dMMR are presented in bar charts \pm sem error bars. It is apparent that 50 ms and 150 ms dMMR waveforms exhibit positive peak latencies defined by their respective oddball stimuli, whereas there are no other significant differences.

4.3.1.5 *Inter-stimulus interval mismatch response in conscious mice*

As mentioned in Section 4.3.1.4, ISI oddball stimuli induce a dMMR characterised by two deflections peaking approximately in the regions of primary (N1) and secondary (P2) AEP peaks. This may reasonably be considered an effect of ISI variations on N1 and P2 potential amplitudes (Section 4.3.1.2). Nevertheless, this reflects an electrophysiological difference between standard and oddball stimuli processing which warrants further analysis.

Difference waveforms from the dOD paradigm with variable ISI are plotted in Figure 4.9a-d. From visual inspection it is apparent that 400 ms (-50 ms) and 500 ms (+50 ms) ISI dMMR waveforms exhibit initial ≈ 15 ms and secondary ≈ 35 ms peaks of opposite polarity. For comparison the rectified area (RA), or 'area under the curve', may be computed, which effectively provides a rectified measure for quantifying the magnitude of waveforms with alternating polarities. SA of 400 ms and 500 ms ISI dMMR waveforms from 0-60 ms are shown in Figure 4.9c and Figure 4.9d, respectively. There were no significant differences between genotypes [$F_{1,16} = .396$, $p = .538$], saline and ketamine treatment sessions [$F_{1,16} = .569$, $p = .462$] or different direction ISI duration changes [$F_{1,16} = .371$, $p = .551$].

4.3.1.6 *Context-specific effects of varying inter-stimulus interval stimuli in oddball and control paradigms*

To investigate whether N1 and P2 peak amplitudes evoked by physically identical stimulus/ISI combinations differed according to the paradigm being presented, these peaks were measured from stimuli presented in duration consecutive-repetition (dCR), oddball (dOD) and many-standards (dMS) paradigms with variable ISI, reported in Figure 4.10. These data were recorded from the saline recording session.

Repeated measures ANOVA with stimuli and paradigm as within-subjects factors and genotype and gender as between-subjects factors highlighted a significant effect of stimulus/ISI on N1 [$F_{2,15} = 15.251$, $p < .001$] and P2 [$F_{2,15} = 17.149$, $p < .001$] peak amplitudes, as may be expected. When the dCR paradigm data were omitted from this test a significant effect of genotype on N1 peak amplitude was found [$F_{1,16} = 4.479$, $p = .050$], perhaps indirectly suggesting that the dCR paradigm (presented first) effected the N1 response; visual observation of WT data also supports the theory that paradigm order had an influence over N1 peak amplitude. Unexpectedly, gender significantly affected P2 peak amplitude [$F_{1,16} = 5.670$, $p = .030$], with females showing lower peak amplitude than males.

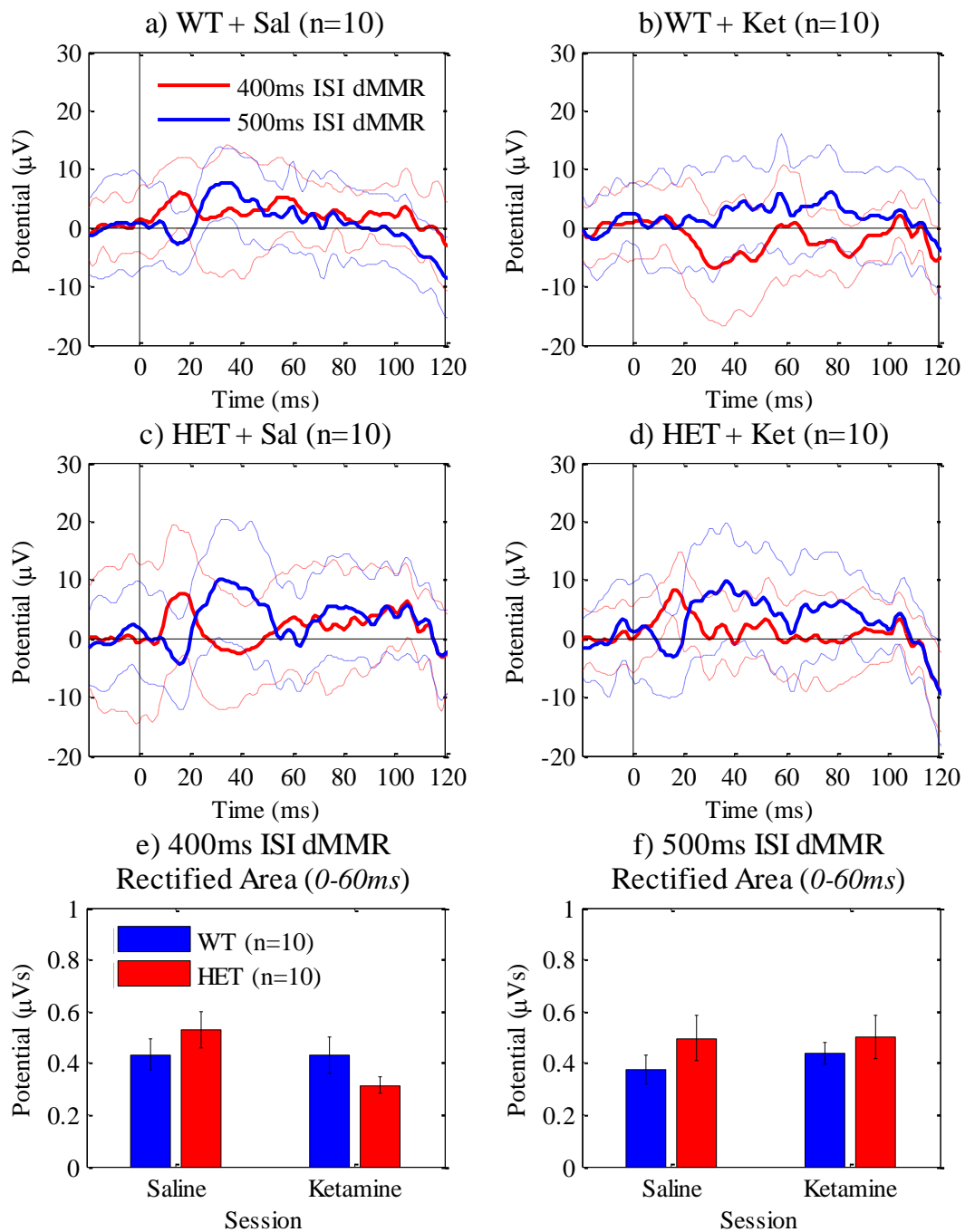


Figure 4.9 - Inter-stimulus interval oddball mismatch responses in conscious wild-type and *Map2k7*^{+/-} mice receiving ketamine These data were produced from the duration oddball paradigm (dOD) with variable inter-stimulus interval (ISI) and are interpreted here in terms of ISI. 400 ms ISI (-50 ms oddball; bold red ± sem in dotted red) and 500 ms ISI (+50 ms oddball; bold blue ± sem in dotted blue) duration mismatch response (dMMR) are plotted for a) control (WT) mice during the saline session (Sal), b) WT mice following 10 mg/kg i.p. ketamine (Ket), c) *Map2k7*^{+/-} (HET) mice in the saline session, and d) HET mice post ketamine administration. It can be seen that increasing and decreasing duration oddballs produce opposite polarity deflections in the regions of N1 and P2 deflections, presumably due to their sensitivity to ISI described in Section 4.3.1.2. Signed area from 0-60 ms are reported as the mean ± sem for e) the 400 ms and f) the 500 ms ISI dMMR, effectively rectifying and quantifying each dMMR. Here there are no statistically significant differences between increasing and decreasing duration oddballs, genotypes or treatment conditions.

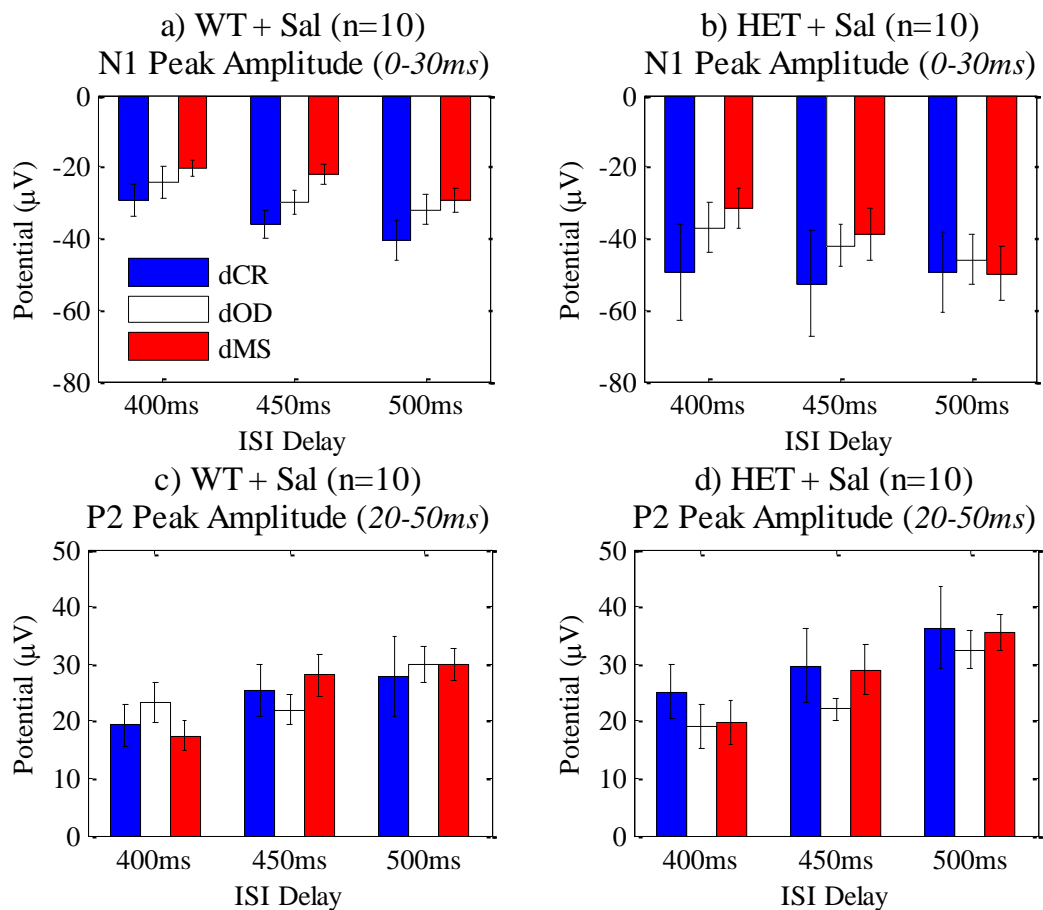


Figure 4.10 - Context-specific analysis of primary and secondary auditory evoked features from inter-stimulus interval oddball and control paradigms Measurements were taken from 500 ms (+50 ms oddball), 450 ms (standard) and 400 ms (-50 ms oddball) inter-stimulus interval (ISI) delay stimuli evoked waveforms from duration consecutive-repetition (dCR, oddball (dOD) and many-standards (dMS) paradigms with varying ISI. Primary auditory onset feature (N1) peak amplitude is shown for a) control (WT), and b) *Map2k7^{+/-}* (HET) mice following an injection of physiological saline (Sal). Secondary evoked feature (P2) peak amplitudes are also given for c) WT and d) HET mice during the saline session. Data presented are means \pm sem error bars, with measurement windows displayed in brackets.

4.3.1.7 Comparison of auditory-evoked potential waveforms from identical stimuli presented in duration paradigms throughout Experiment II

Representative grand-average AEPs from stimuli with identical physical properties presented in different paradigms throughout Experiment II are provided in Figure 4.11 and Figure 4.12 for WT and HET groups, respectively. Duration consecutive-repetition (dCR), oddball (dOD) and many-standards (dMS) paradigms with variable ISI following physiological saline (Sal) then 10 mg/kg i.p. ketamine (Ket) injections were presented sequentially as displayed in the figure legends. 50 ms (500 ms ISI), 100 ms (450 ms ISI) and 150 ms (400 ms ISI) AEPs are plotted in top, middle and bottom panels, respectively.

Any differences between waveforms in the same plot evoked by identical stimuli may be interpreted as context-specific, suggesting that a particular paradigm/sequence of auditory stimuli is responsible for evoking or altering a particular AEP feature. Another interpretation may be that AEP differences are drug-induced, illustrating the effects of 10 mg/kg i.p. ketamine administration. Equally, observed waveform changes may be considered the visualisation of adaptive processes in response to prolonged auditory stimulation, thereby effected progressively throughout the experiment. Each of these interpretations is addressed separately below.

The idea that a stimulus may induce context-specific activity when presented in a particular sequence is the founding principle of the oddball paradigm and mismatch response, thus if a stimulus physically identical to the oddball were presented in a different condition it should elicit a different response. However, identifying a context-specific response from these waveforms proves very difficult because they generally display the same features.

The effects of acute ketamine administration are demonstrated here in waveforms from the dCR (Ket) played \approx 0-10 min, dOD (Ket) played \approx 10-20 min and dMS (Ket) played \approx 30-40 min post drug delivery. Duration deviant-alone (dDA) paradigm data is omitted from this analysis because it effectively incorporating a much larger ISI; representative analyses of DA and CR paradigms with extended ISI are provided in Section 4.3.3.3. Visual inspection of the waveforms in Figure 4.11 and Figure 4.12 indicates that during the initial phase following 10 mg/kg i.p. ketamine administration, reflected by dCR (Ket) data, the secondary evoked potential feature (P2) is greatly diminished; this reduction in amplitude appears to recover in dOD (Ket) and dMS (Ket) paradigms. Representative quantitative analysis of the acute ketamine effects on frequency consecutive-repetition (fCR) paradigm AEP features, provided in Section 4.3.2.4, substantiates these observations.

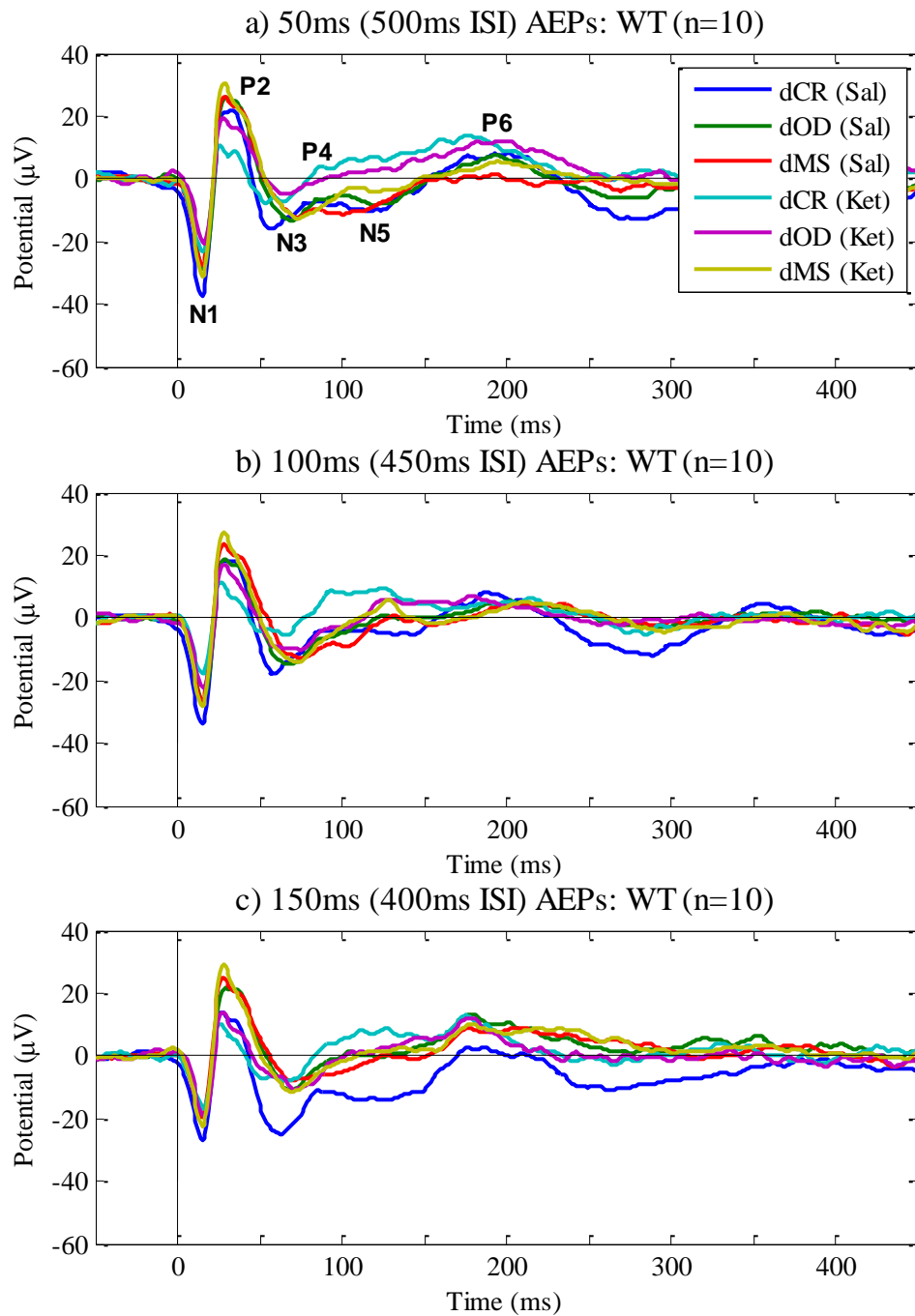


Figure 4.11 - Auditory evoked potentials from conscious control animals throughout an Experiment II test session Data are shown from wild-type control (WT) mice in duration consecutive-repetition (dCR), oddball (dOD) and many-standards (dMS) paradigms with variable inter-stimulus interval (ISI), following saline (Sal) and 10 mg/kg i.p. ketamine (Ket); displayed in the legend by order of recording throughout the experiment. Auditory evoked potentials (AEPs) are plotted for a) 50 ms stimuli with 500 ms ISI, b) 100 ms stimuli with 450 ms ISI, and c) 150 ms stimuli with 400 ms ISI. Pronounced N1 and P2 peaks and subsequent lower amplitude deflections N3, P4, N5 and P6 are labelled in (a). These AEPs can be compared against *Map2k7*^{+/-} (HET) group waveforms displayed in Figure 4.12.

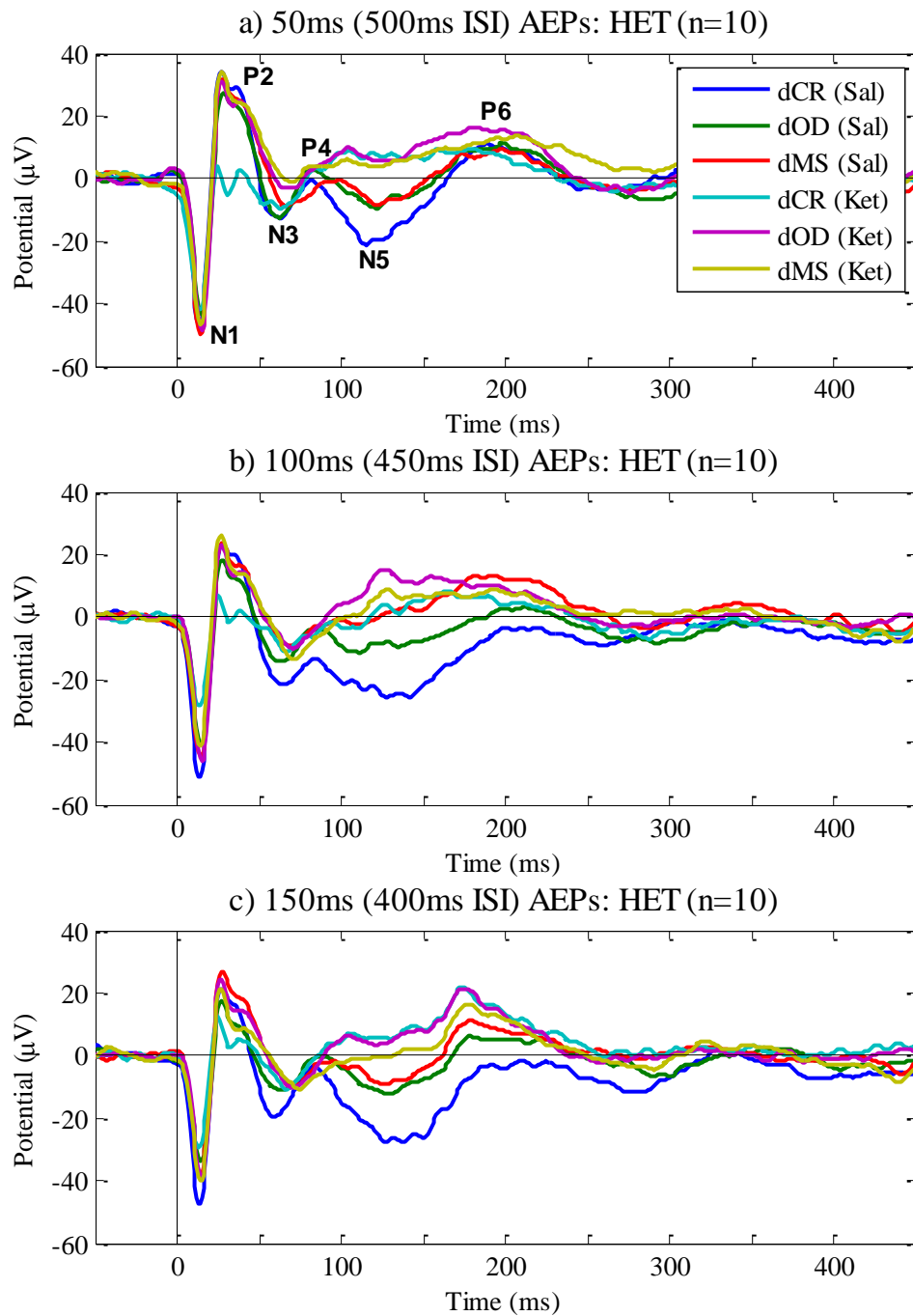


Figure 4.12 - Auditory evoked potentials from conscious *Map2k7^{+/-}* animals throughout an Experiment II test session Data shown are *Map2k7^{+/-}* (HET) group responses to duration consecutive-repetition (dCR), oddball (dOD) and many-standards (dMS) paradigms with variable inter-stimulus interval (ISI), following saline (Sal) and 10 mg/kg i.p. ketamine (Ket). Data series in the legend are in order of recording during the experiment. Auditory evoked potentials (AEPs) are plotted for a) 50 ms stimuli with 500 ms ISI, b) 100 ms stimuli with 450 ms ISI, and c) 150 ms stimuli with 400 ms ISI. N1, P2, N3, P4, N5 and P6 peaks are labelled in (a). These AEPs may be visually compared with equivocal control (WT) group waveforms in Figure 4.11.

To potentially analyse adaptations in auditory processing which may occur in response to extended periods of auditory stimulation each data series should be considered in terms of its order of presentation during the experiment. As illustrated in the general methods (Figure 2.14), the dCR paradigm was presented firstly, followed by dOD, dDA (omitted from this analysis), then dMS in the saline recording session (Sal), then this sequence was repeated in the ketamine session (Ket).

Remaining conscious of this order of presentation and visually inspecting the waveforms in Figure 4.11 and Figure 4.12 may suggest, generally, that stimuli presented in earlier paradigms induce greater negative amplitude in the region of ≈ 50 -200 ms and a more pronounced series of deflections. This tempering may be considered indicative of an adaptive change to prolonged auditory stimulation (with rates of 2 Hz). It should be noted that between dOD and dMS paradigms there was a period of relatively lower auditory stimulation, with dDA paradigms which had an average stimulation rate of 0.4 Hz. This may account for the apparent recovery of negative potential during this latency range between AEPs evoked by dOD and dMS paradigm stimuli. Additionally, N1 peak amplitudes evoked by dCR (Sal) stimuli appear more negative, possibly because this was the first bout of auditory stimulation applied, consistent with observations from Figure 4.10a-b.

In summary, Figure 4.11 and Figure 4.12 demonstrate that *Map2k7^{+/-}* mice generally display a larger amplitude N1 potential, while the P2 response appears reduced by ketamine. Subsequent deflections from ≈ 50 -200 ms are seen to vary throughout test sessions, particularly from 100-150 ms, possibly suggesting an adaptive electrophysiological response.

These AEPs from conscious mice evoked by physically identical stimuli presented in different contexts are representative of Experiment II tests investigating duration, frequency and intensity manipulations. Thus the same general observations mentioned above were found in test sessions assessing each physical feature of sound variance. A representative quantification of N1 peak amplitude, P2 peak amplitude and mean amplitude from 100-150 ms provided in the intensity-varying paradigms Section 4.3.3.4 is also relevant to the findings described above.

4.3.2 Frequency paradigms in conscious mice

This section covers the effects of tone frequency on auditory evoked potentials and describes the frequency mismatch response in conscious mice. The acute effects of 10 mg/kg i.p. ketamine are explored in the frequency consecutive-repetition (fCR) paradigm, representative of observations from other CR paradigms in Experiment II.

4.3.2.1 Stimulus frequency influences auditory evoked potentials

Group grand-average AEP waveforms (<60 ms) from the frequency many-standards (fMS) paradigm are plotted in Figure 4.13. Amplitude of N1 and P2 potential deflections are seen to vary with stimulus frequency. Generally, increasing frequency produces greater magnitude N1 and P2 features, similar to observations made for ISI variations in Section 4.3.1.2.

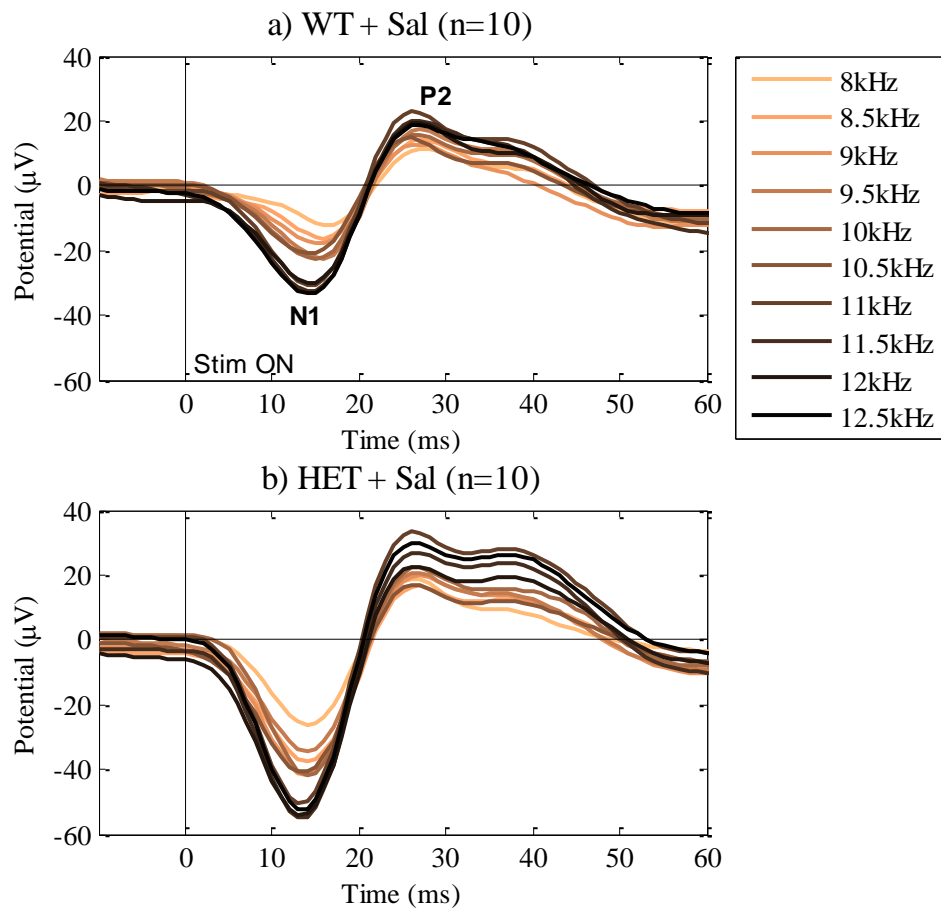


Figure 4.13 - Effect of tone frequency on primary and secondary auditory responses in conscious wild-type and *Map2k7*^{+/-} mice These waveforms were generated by frequency many-standards (fMS) paradigm stimuli. a) Control (WT), and b) *Map2k7*^{+/-} (HET) group grand-average primary onset (N1) and secondary (P2) responses to ten fMS stimuli presented following an injection of physiological saline (Sal). N1 and P2 peak amplitude measurements from both groups are reported in Figure 4.14.

N1 and P2 peak amplitude measurements from ten fMS paradigm stimuli of different tone frequency are analysed in Figure 4.13, with linear regression equations and correlation coefficients provided in each plot. Both N1 and P2 peak amplitudes are linearly correlated with stimulus frequency, although the N1 response may be marginally more so than the P2 response. These findings are discussed along with ISI and stimulus intensity/sound pressure level (SPL) effects in Section 4.4.1.

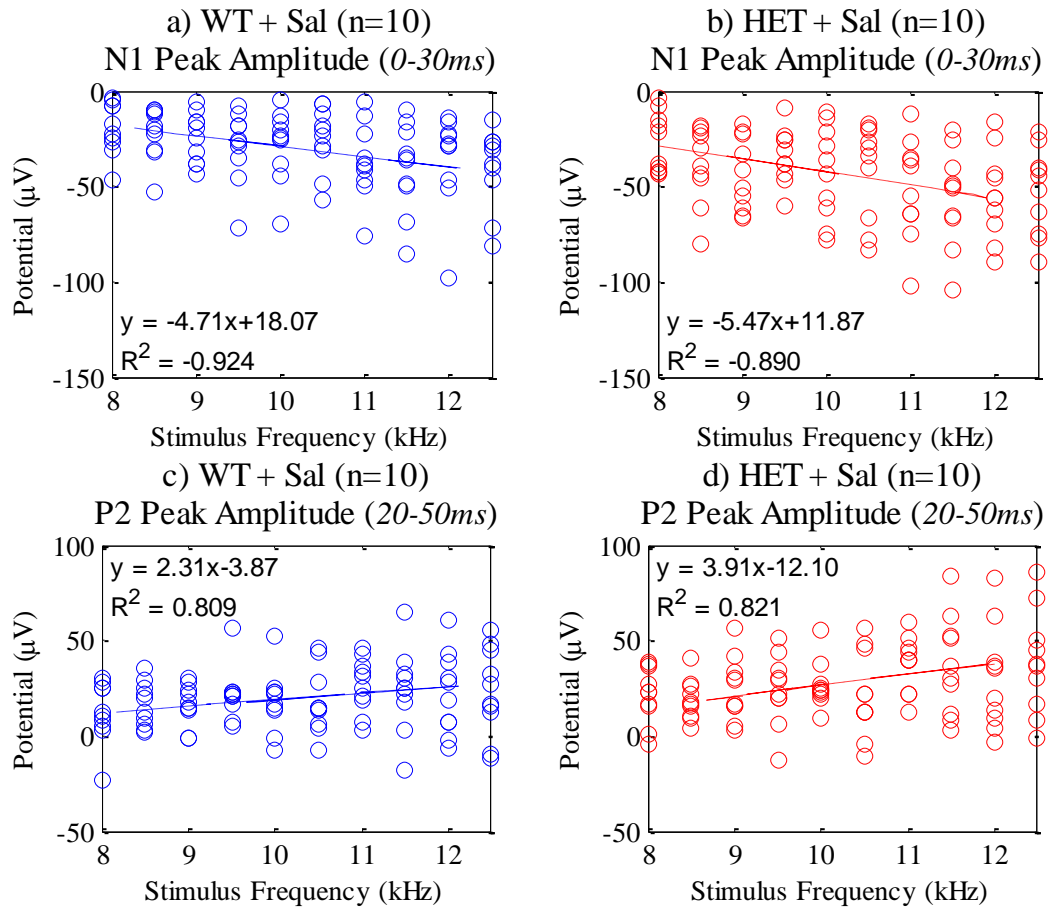


Figure 4.14 - Quantification of tone frequency effects on auditory evoked potentials in conscious wild-type and *Map2k7*^{+/-} mice Primary negative onset response (N1) peak amplitudes measured from 0-30 ms are shown for a) control (WT), and b) *Map2k7*^{+/-} (HET) mice. Secondary positive response (P2) peak amplitudes measured from 20-50 ms are shown for c) WT, and d) HET mice. These data are from the frequency many-standards (fMS) paradigm presented following administration of physiological saline (Sal) corresponding to the grand-average waveforms shown in Figure 4.13.

4.3.2.2 Frequency mismatch response in conscious mice

Frequency mismatch response (fMMR) difference waveforms from the frequency oddball (fOD) paradigm in conscious mice are shown in Figure 4.15. These were generated by the traditional method of computing the mismatch response, where the 10 kHz standard frequency stimuli AEP was subtracted from the 8 kHz (−2 kHz descending) and 12 kHz (+2 kHz ascending) frequency oddball stimuli AEP individually to produce 8 kHz and 12 kHz fMMR difference waveforms.

Ascending and descending frequency oddball stimuli evoke alternate polarity deflections in the region of N1 and P2 AEP features. These therefore appear to reflect frequency sensitivity as opposed to deviance detection *per se*. The N1 peak is particularly strongly correlated with tone frequency, evident in initial fMMR deflections at ≈ 15 ms which are opposite polarity for ascending and descending oddballs. The second waveform deflection peaking at ≈ 35 ms is more pronounced in the ascending oddball fMMR than the descending, perhaps indicative of the P2 response being less strongly linearly correlated with stimulus frequency (Figure 4.14).

Rectified area (RA) of both fMMR waveforms from 0-60 ms are quantified in the two lower panels of Figure 4.15. This reflects the overall magnitude of N1 and P2 potential differences between each frequency oddball and standard stimuli AEPs. In this analysis there were no statistically significant effects of genotype [$F_{1,16} = 1.121$, $p = .305$] or ketamine [$F_{1,16} = 3.299$, $p = .088$]. There was however a significant effect of ascending versus descending fMMR waveforms [$F_{1,16} = 10.793$, $p = .005$], with higher frequency oddball stimuli eliciting a greater magnitude fMMR than the lower frequency oddball. This suggests that higher frequency oddball stimuli elicit a more pronounced mismatch response, possibly representing mouse hearing sensitivity to higher frequencies.

No significant effects of 10 mg/kg i.p. ketamine are observed in these waveforms. This may be because the fOD paradigm was played ≈ 10 -20 min following drug administration. Data presented later in this chapter from the fCR paradigm, presented ≈ 0 -10 min after injecting ketamine, suggests this dose significantly alters the AEP waveform P2 feature.

Speculatively, this may potentially have implications for the fMMR response if the fOD paradigm were presented immediately following drug delivery (e.g. see Figure 4.17e-f).

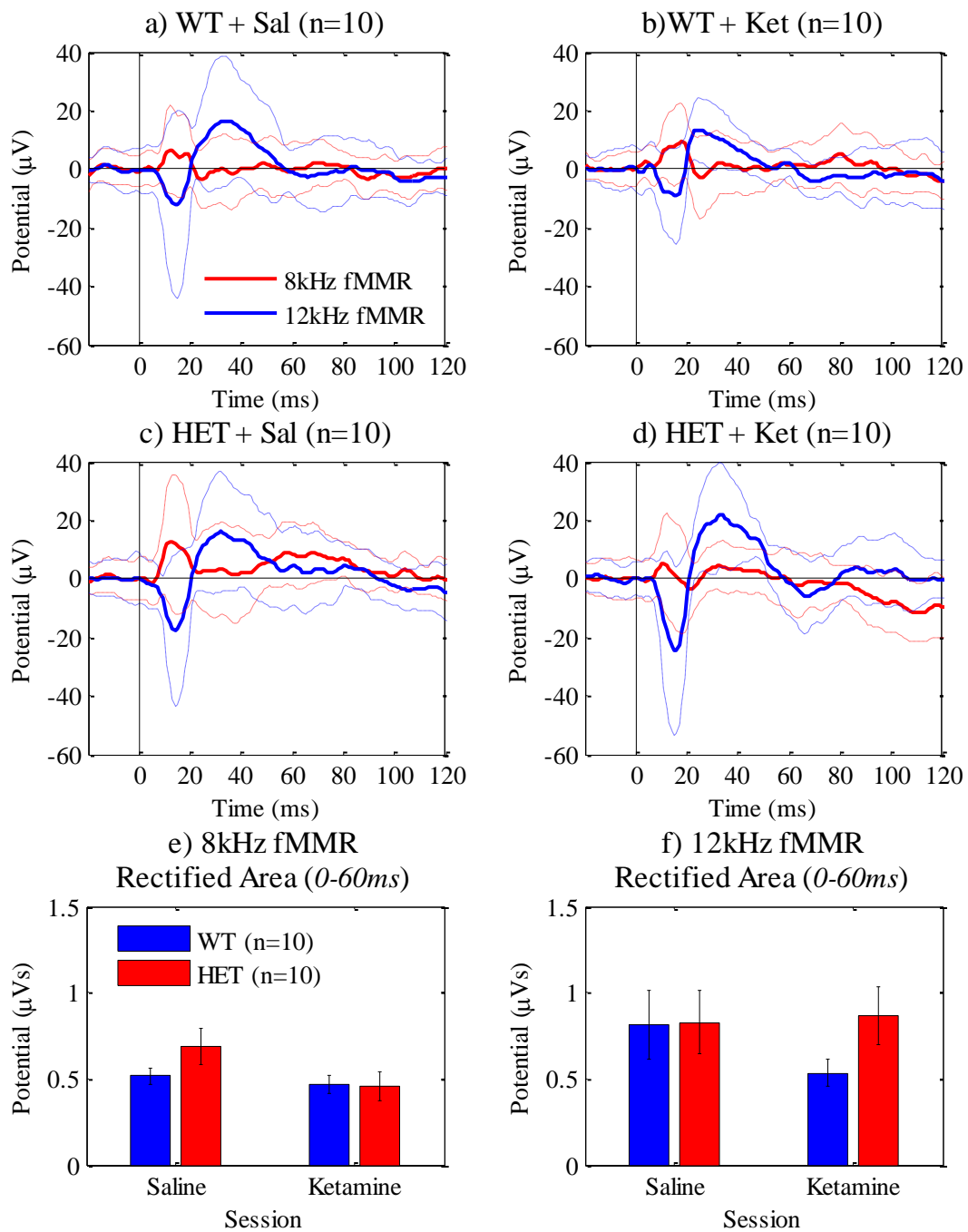


Figure 4.15 - Frequency mismatch responses in conscious wild-type and *Map2k7*^{+/-} mice receiving ketamine This data is from the frequency oddball (fOD) paradigm. The 8 kHz (-2 kHz oddball) frequency mismatch response (fMMR; bold red ± sem in dotted red) and 12 kHz (+2 kHz oddball) fMMR (bold blue ± sem in dotted blue) waveforms are displayed for a) control (WT) mice during the saline session (Sal), b) WT mice following 10 mg/kg i.p. ketamine (Ket), c) *Map2k7*^{+/-} (HET) mice in the saline control session, and d) HET mice in the session after ketamine administration. Ascending and descending oddball fMMR waveforms clearly display opposite polarity deflections in the regions of N1 and P2 deflections, indicative of their respective frequency sensitivities (Section 4.3.2.1). The fMMR waveforms are quantified with signed area from 0-60 ms, which effectively rectifies both signals, plotted as group means ± sem for e) the 8 kHz and f) the 12 kHz fMMR. There are no significant differences between genotypes or treatment conditions, however higher frequency oddballs generated a significantly greater response overall ($p < .05$) compared with lower frequency oddballs.

4.3.2.3 *Context-specific effects of varying frequency stimuli in oddball and control paradigms*

To assess any specific paradigm induced changes to primary or secondary evoked features, peak amplitude measurements were taken from frequency consecutive-repetition (fCR), oddball (fOD) and many-standards (fMS) paradigm stimuli AEPs, displayed in Figure 4.16. These data were recorded during the saline recording session. Repeated measures ANOVA with stimuli (8 kHz/10 kHz/12 kHz) and paradigm (fCR/fOD/fMS) as within-subjects factors and gender and genotype as between-subjects were performed on both N1 and P2 peak amplitude measurements.

The N1 response (Figure 4.16a-b) is significantly altered by stimulus frequency [$F_{1,16} = 13.989$, $p = .002$; lower-bound because Mauchly's test $p < .05$], as expected from findings described in Section 4.3.2.1. When 10 kHz standard stimuli data were removed from this analysis, leaving only the two oddball stimuli, a significant effect of paradigm [$F_{2,32} = 4.611$, $p = .017$; Mauchly's test $p > .05$] was found, caused by the fOD paradigm which evoked greater negative peak amplitudes than fCR and fMS paradigms. This may reflect frequency desensitisation in the auditory cortex, also known as stimulus specific adaptation (SSA; introduced in Section 1.2.2.6); i.e. when a specific frequency is presented repeatedly neurons initially very responsive to that tone gradually become desensitised and therefore less active during its presentation. This theory is addressed in Section 4.4.2.

When fCR paradigm data were omitted from N1 analysis a significant effect of genotype was revealed [$F_{1,16} = 4.534$, $p = .049$], with the HET group displaying a greater negative onset response. This may support the suggestion that the CR paradigm (presented first) temporarily enhances N1 peak amplitudes in the WT group (as observed from AEP waveforms in Figure 4.11). This finding may also relate biologically to the physiological mechanisms of SSA, as discussed in Section 4.4.3.

P2 peak amplitude is also sensitive to stimulus frequency [$F_{2,32} = 9.197$, $p = .001$; sphericity assumed because Mauchly's test $p > .05$]. There is also a significant effect of paradigm [$F_{2,32} = 3.536$, $p = .041$; sphericity assumed] (actually caused by the fMS which shows generally lower amplitudes) and an underlying interaction effect between stimulus frequency and paradigm [$F_{1,16} = 4.645$, $p = .047$; lower-bound]. A significant overall effect of gender was also observed [$F_{1,16} = 5.773$, $p = .029$], with females showing lower amplitude compared with males.

In Figure 4.16c-d comparing the ascending oddball (12 kHz) stimulus P2 peak amplitude with paradigm as the within-subjects factor reveals a significant effect of paradigm [$F_{2,32} = 4.849$, $p = .014$; sphericity assumed because Mauchly's test $p > .05$], caused by the fOD paradigm which evoked significantly greater peak amplitude than fCR of fMS control paradigms. This suggests that the ascending fOD condition produces an fMMR in the region of P2 in conscious mice, whereas the descending oddball does not. Interestingly, there is a highly significant effect of gender in this analysis [$F_{1,16} = 16.579$, $p = .001$] as well as a gender-paradigm interaction [$F_{2,32} = 4.318$, $p = .022$; Mauchly's test $p > .05$], suggesting the P2 response may be affected differently in each gender.

In summary, N1 peak amplitudes are increased in response to both ascending and descending frequency oddball stimuli in the fOD paradigm compared with fCR and fMS control paradigms. Standard stimuli N1 responses are not significantly different across these auditory paradigms. This may reflect frequency desensitisation, referred to as SSA. The P2 peak amplitude appears to be increased specifically in response to the *ascending* frequency oddball in the fOD paradigm, whereas the descending frequency oddball does not elicit this context-specific P2 effect.

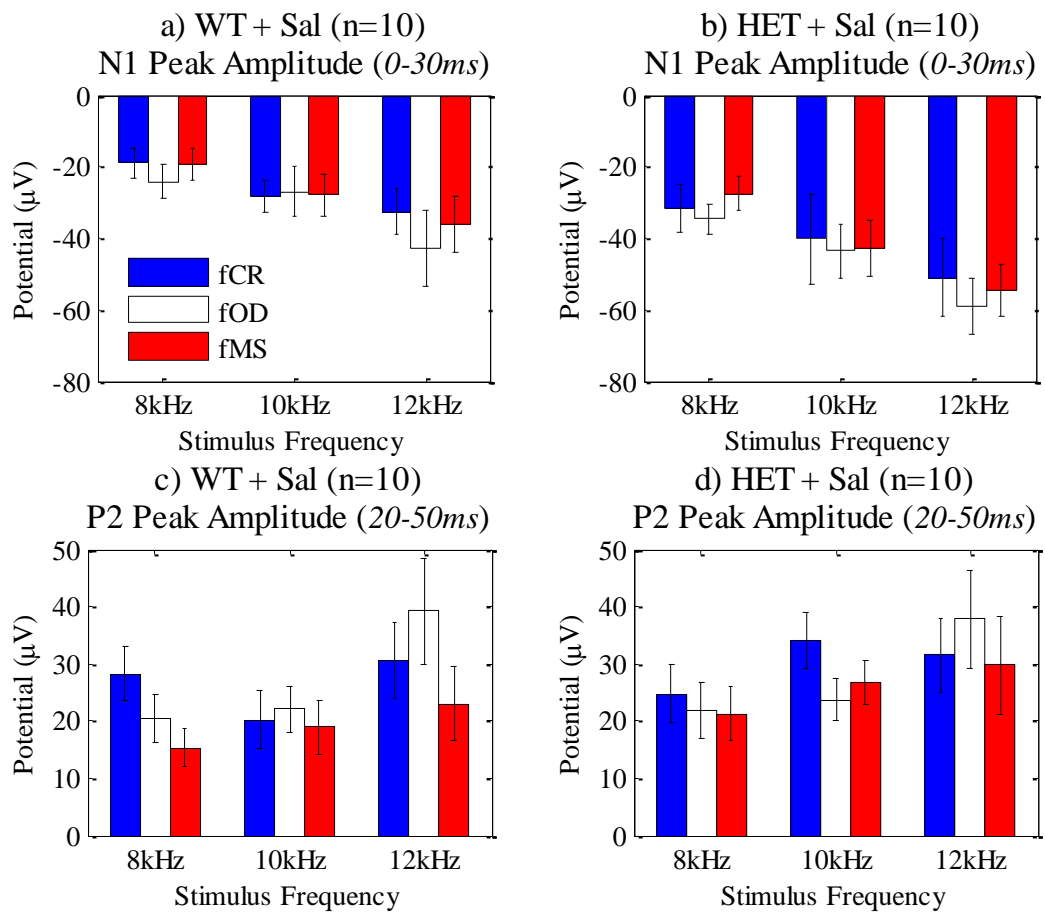


Figure 4.16 - Context-specific analysis of primary and secondary auditory evoked features from frequency oddball and control paradigms in conscious wild-type and *Map2k7*^{+/-} mice Measurements were taken from the 8 kHz (-2 kHz oddball), 10 kHz (standard) and 12 kHz (+2 kHz oddball) stimuli auditory evoked potential (AEP) waveforms from frequency consecutive-repetition (fCR), oddball (fOD) and many-standards (fMS) paradigms. The primary onset response (N1) peak amplitude is shown for a) control (WT) and b) *Map2k7*^{+/-} (HET) mice following an injection of physiological saline (Sal). The secondary evoked feature (P2) peak amplitude is also given for c) WT and d) HET mice during the saline session. Bar charts display means ± sem and measurement windows are shown *in brackets*.

4.3.2.4 Acute effect of ketamine on conscious mouse auditory evoked potentials

As introduced in Section 4.3.1.7, the acute effects of 10 mg/kg i.p. ketamine on AEPs in conscious mice are most evident in consecutive-repetition (CR) paradigms which were presented \approx 0-10 min post drug administration. Findings from the frequency CR (fCR) paradigm provided here are representative of results from other CR paradigms in Experiment II (e.g. waveforms discussed in Section 4.3.1.7) and illustrate the acute effects of ketamine on AEPs from conscious mice.

AEP waveforms from fCR paradigm stimuli in saline (Sal) and ketamine (Ket) recording sessions are displayed in Figure 4.17a-d. There are dramatic differences between sessions, particularly the secondary (P2) feature which appears to be entirely abolished by the effects of ketamine. Moreover, this reduced P2 potential is comparable between all three frequency stimuli post drug administration, possibly suggesting that it disrupts frequency-sensitive generators.

The lower two plots (Figure 4.17e-f) display fMMR-like difference waveforms produced by subtracting the 10 kHz stimulus AEP from the 8 kHz and 12 kHz AEP from the fCR paradigm during the ketamine session (recorded 0-10 min post administration). These reflect how the fMMR may appear if the fOD paradigm was presented immediately following drug injection. From visual inspection it is clear that the initial fMMR deflection is still present, due to the differences in N1 potential, whereas the secondary deflection caused by the P2 response is far less apparent than in waveforms from the fOD paradigm (Figure 4.15). This suggests that non-specific reductions in the P2 response induced by ketamine may be responsible for decreasing fMMR amplitudes from 20-60 ms.

N1, P2 and N5 features from fCR paradigm waveforms are quantified in Figure 4.18. Repeated measures ANOVA revealed no effect of ketamine on N1 peak amplitude [$F_{1,16} = .372$, $p = .550$], although it had a highly significant effect on P2 peak amplitude [$F_{1,16} = 25.930$, $p < .001$] and N5 peak amplitude [$F_{1,16} = 17.928$, $p = .001$]. N3, P4 and P6 peaks did not display any significant effects and are omitted from this analysis. How these three representative observations change throughout Experiment II saline and 10 mg/kg i.p. ketamine test sessions are further assessed in Section 4.3.3.4. No significant genotype, gender or drug interaction effects were observed from these analyses.

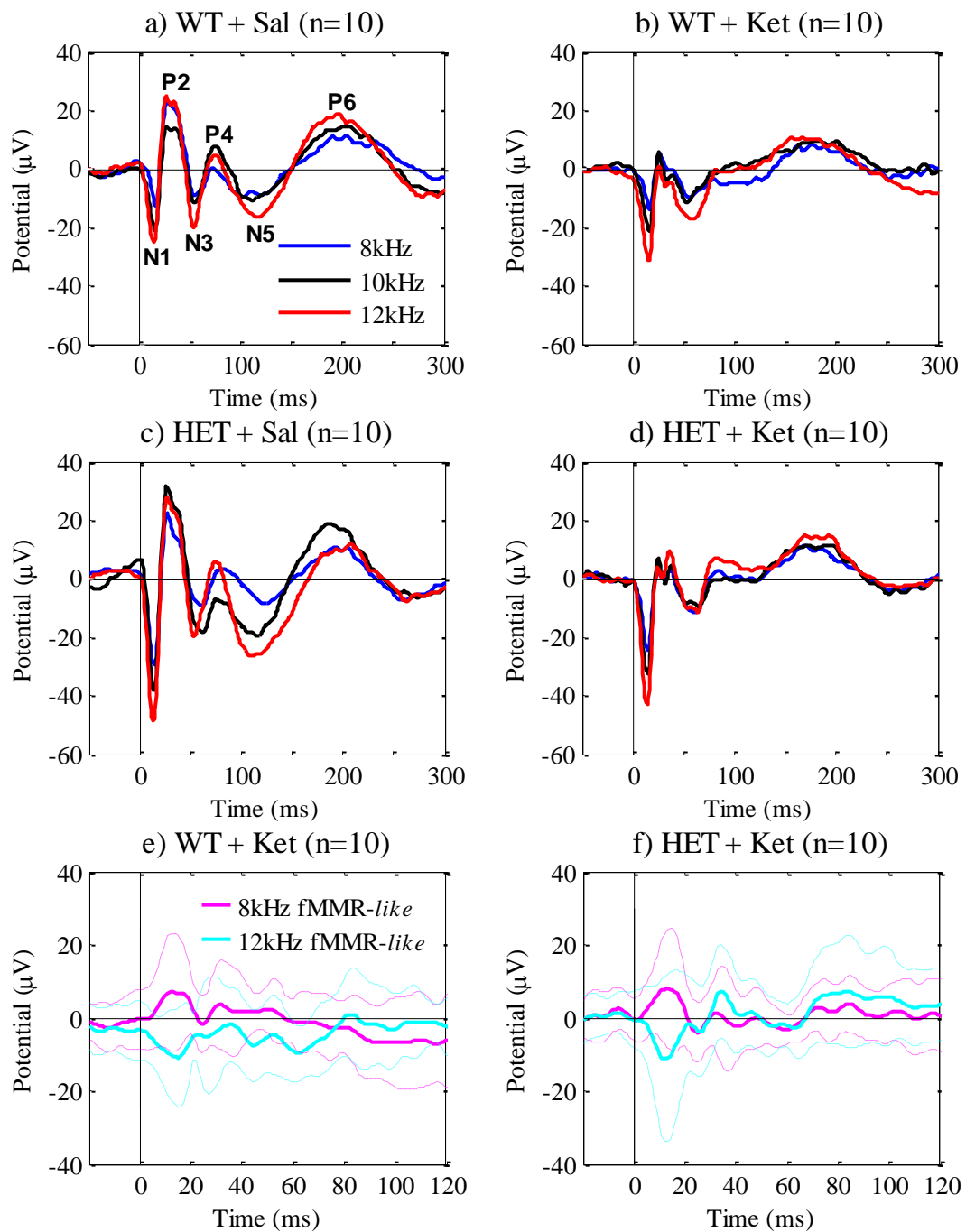


Figure 4.17 - Acute effects of 10 mg/kg i.p. ketamine on auditory evoked potentials in conscious wild-type and *Map2k7*^{+/-} mice These grand-average waveforms were generated from frequency consecutive-repetition (fCR) paradigm data recorded ≈0-10 min post saline (Sal) and 10 mg/kg i.p. ketamine (Ket) injections. The 8 kHz (blue), 10 kHz (black) and 12 kHz (red) stimuli AEP are shown for a) control (WT) mice following the saline injection, b) WT mice following ketamine administration, c) *Map2k7*^{+/-} (HET) mice during the saline session, and d) HET mice during the ketamine session. N1, P2, N3, P4, N5 and P6 peaks are labelled in (a); however only N1, P2 and N5 are quantified in Figure 4.18. 8 kHz – 10 kHz (bold magenta ± sem in dotted magenta) and 12 kHz – 10 kHz (bold cyan ± sem in dotted cyan) difference waveforms comparable to frequency mismatch responses (fMMR-like) are shown for e) WT, and f) HET mice following the ketamine injection; these may be visually compared with fMMR waveforms in Figure 4.15.

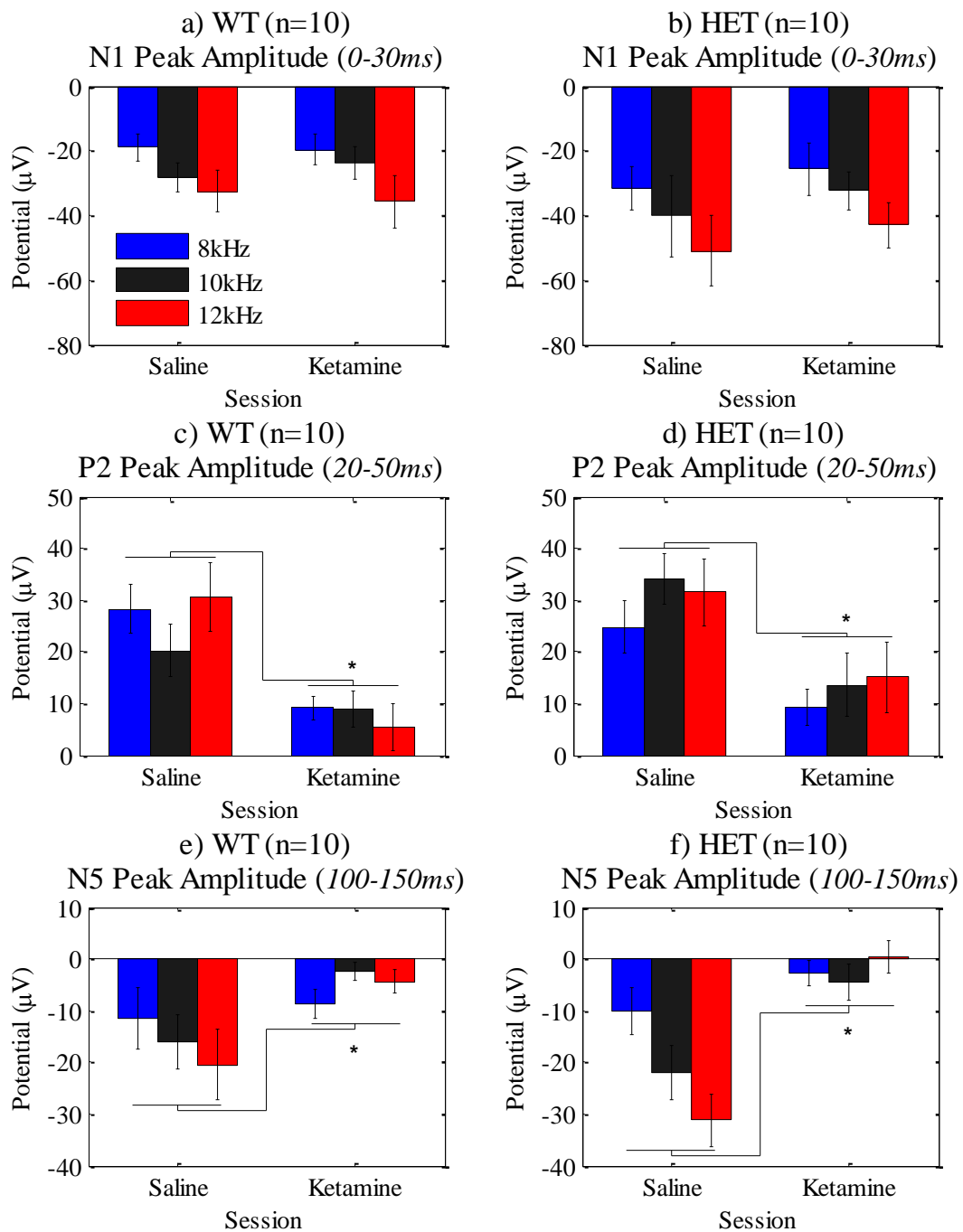


Figure 4.18 - Quantification of the acute effects of 10 mg/kg i.p. ketamine on auditory evoked potential features in conscious wild-type and *Map2k7*^{+/-} mice This is an analysis of frequency consecutive-repetition (fCR) paradigm waveforms introduced in Figure 4.17. Measurements were taken from 8 kHz (blue), 10 kHz (black) and 12 kHz (red) evoked waveforms from each subject in sessions following a physiological saline and 10 mg/kg i.p. ketamine injections. N1, P2 and N5 features labelled in Figure 4.17 are quantified here; N3, P4 and P6 peaks did not display any significant effects and are omitted from this analysis. Primary onset response (N1) peak amplitude is displayed for a) control (WT), and b) *Map2k7*^{+/-} (HET); secondary response (P2) peak amplitude is displayed for c) WT, and d) HET, both showing a significant effect of ketamine ($p < .05$); and N5 peak amplitude is also plotted for e) WT, and f) HET mice, with both showing a significant effect of ketamine ($p < .05$). Bar graphs are means \pm sem, with relevant measurement windows displayed *in brackets*. This analysis is representative of other Experiment II consecutive-repetition (CR) paradigms played \approx 0-10 min after delivering ketamine.

4.3.3 Intensity paradigms in conscious mice

Findings presented in this section include the effects of stimulus intensity/sound pressure level (SPL) on AEP features, the intensity mismatch response in conscious mice, a comparison between deviant-alone and extended ISI consecutive-repetition paradigm waveforms, and a longitudinal examination of AEP features throughout Experiment II.

4.3.3.1 Stimulus intensity influences auditory evoked potentials

Group grand-average AEPs from the intensity many-standards (iMS) paradigm presented in the saline recording session are plotted in Figure 4.19. Similarly to ISI and tone frequency variations, altering SPL of auditory stimuli in the iMS paradigm appears to have a direct effect on N1 and P2 evoked potentials, which displayed greater magnitude with increasing stimulus intensity.

Group-wise analysis of N1 and P2 peak amplitudes measured from each subject with linear regression and correlation coefficient of the line of best fit are provided in Figure 4.20. Both N1 and P2 peak amplitudes from each group are highly correlated with stimulus intensity ($R^2 > .9$).

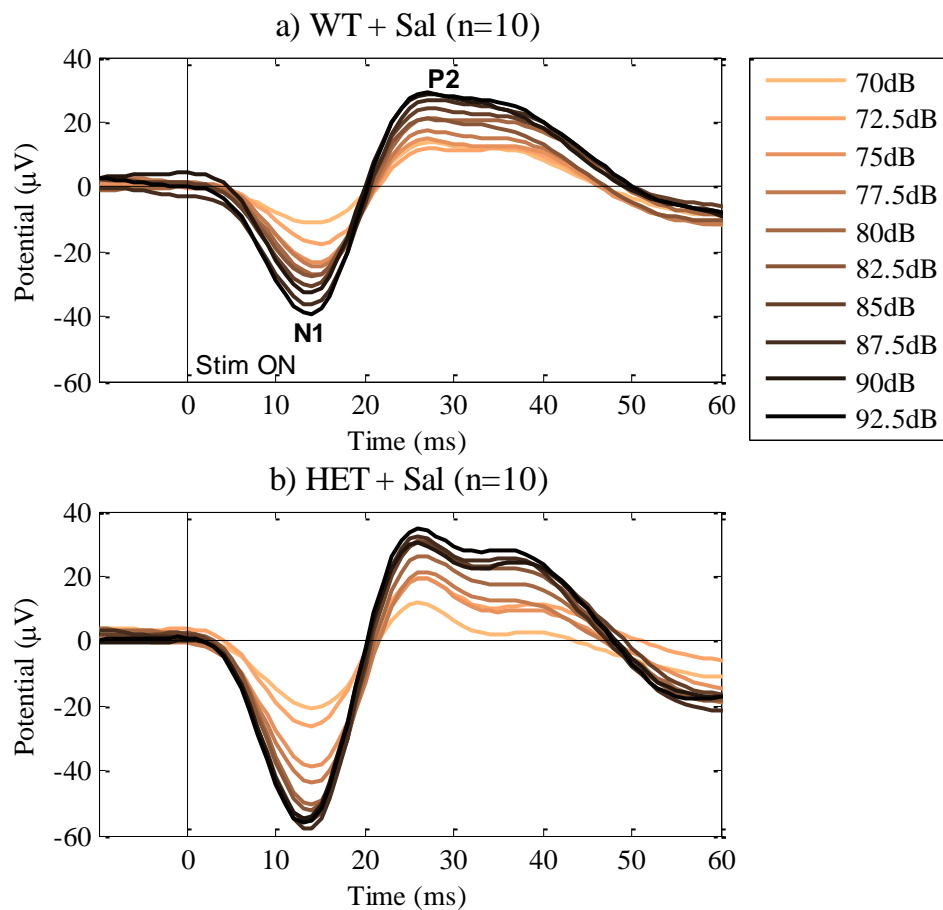


Figure 4.19 - Effect of sound pressure level on primary and secondary auditory responses in conscious wild-type and *Map2k7*^{+/-} mice These waveform plots were produced from intensity many-standards (iMS) paradigm recordings made following i.p. administration of physiological saline (Sal). a) Control (WT), and b) *Map2k7*^{+/-} (HET) group grand-average primary (N1) and secondary (P2) evoked responses to ten iMS stimuli of different sound intensity. Corresponding N1 and P2 peak amplitudes measured from each subject are reported in Figure 4.20.

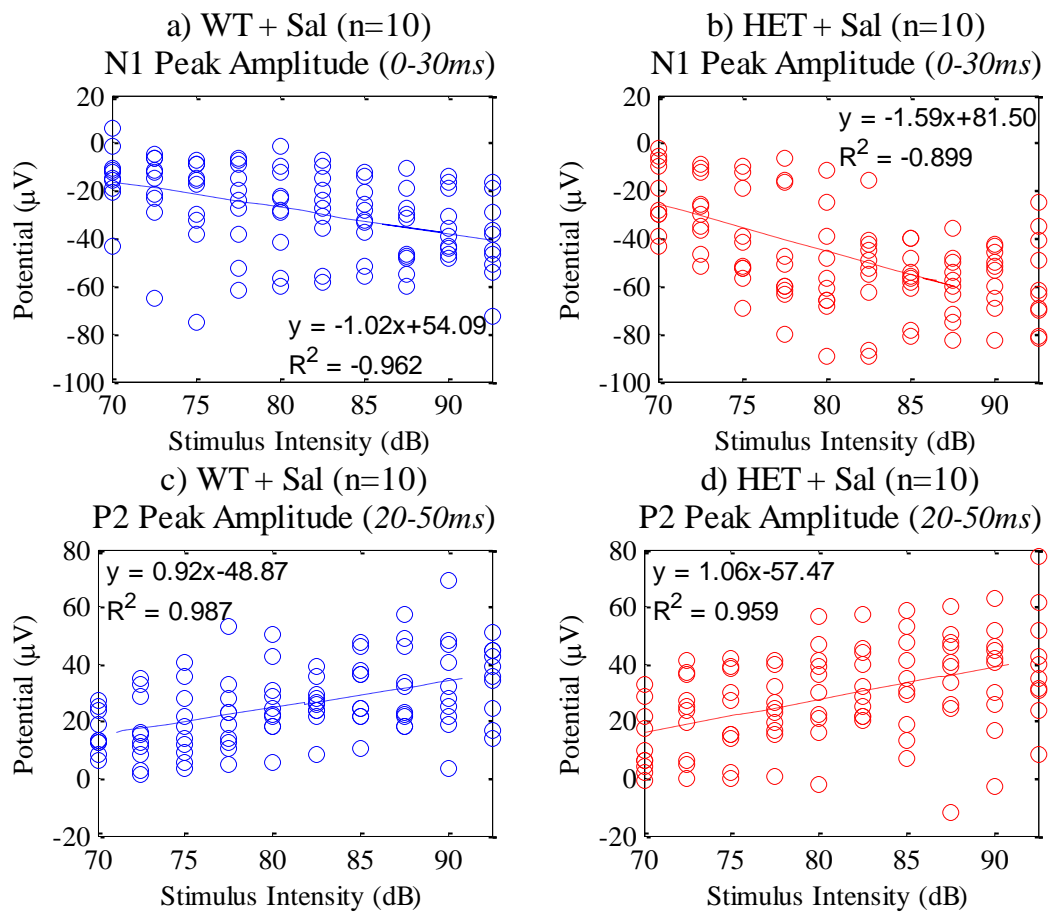


Figure 4.20 - Quantification of sound pressure level effects on auditory evoked potentials in conscious wild-type and *Map2k7*^{+/-} mice Primary negative onset response (N1) peak amplitude measured from 0-30 ms is shown for a) control (WT), and b) *Map2k7*^{+/-} (HET) mice. Secondary positive response (P2) peak amplitude measured from 20-50 ms is shown for c) WT, and d) HET mice. This is a quantification of intensity many-standards (iMS) paradigm auditory evoked potentials from the saline control (Sal) session, group-wise grand-average waveforms of which are plotted in Figure 4.19.

4.3.3.2 Intensity mismatch response in conscious mice

The intensity/SPL mismatch response (iMMR) difference waveforms obtained by subtracting the 80 dB standard AEP from 70 dB (−10 dB) and 90 dB (+10 dB) oddball AEPs from the intensity oddball (iOD) paradigm are plotted in Figure 4.21a-d. Differences arise within regions sensitive to stimulus intensity, particularly N1 and P2 responses at ≈15 ms and ≈35 ms, therefore oddball stimuli of increasing and decreasing intensity generate opposite polarity deflections in their respective iMMR waveforms. This observation is comparable with inter-stimulus interval and tone frequency mismatch responses presented in Section 4.3.1.5 and Section 4.3.2.2, respectively.

Quantification of rectified area from quieter (−10 dB) and louder (+10 dB) oddball iMMR difference waveforms measured from 0-60 ms are shown in the left and right lower panels of Figure 4.21, respectively. Deflections across this region reflect overall differences in the N1 and P2 responses between oddballs and the standard AEP. There were no significant effects of 10 mg/kg i.p. ketamine in this analysis [$F_{1,16} = .236$, $p = .634$], although bear in mind that the iOD paradigm was presented ≈10-20 min post drug delivery. Neither were there any effects of genotype [$F_{1,16} < .001$, $p = .986$] or differences between louder and quieter oddball iMMR magnitudes [$F_{1,16} = .142$, $p = .712$].

Figure 4.22 displays intensity consecutive-repetition (iCR) paradigm difference waveforms following ketamine administration, plotted here to visually compare how acute NMDA receptor disruption with ketamine (≈0-10 min post drug delivery) may influence the iMMR if the iOD paradigm were presented during this period. Here the iMMR-like waveform deflections are suppressed over the 20-40 ms post stimulus onset latency, associated with reduced P2 amplitude caused by ketamine.

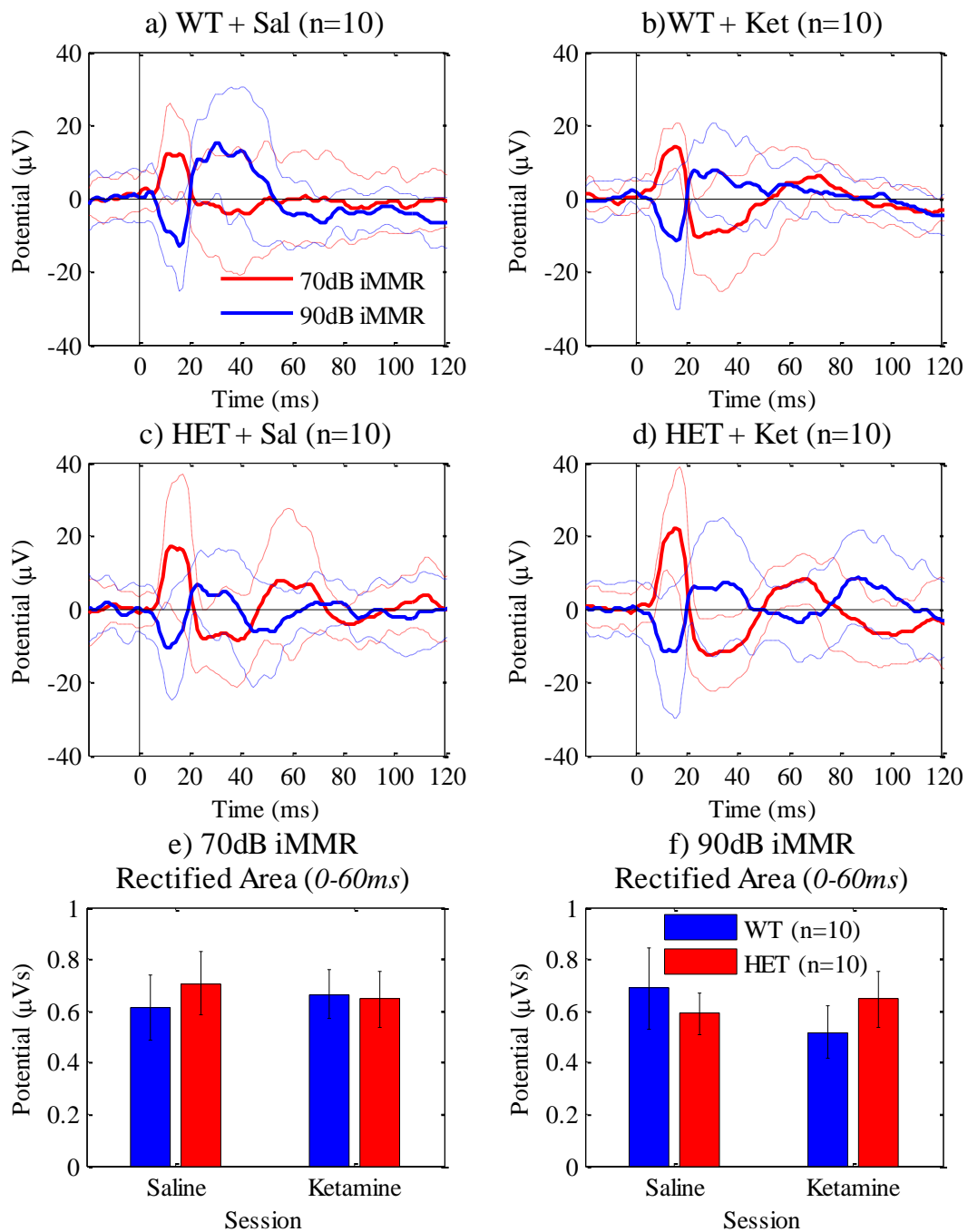


Figure 4.21 - Intensity mismatch responses in conscious wild-type and *Map2k7*^{+/-} mice receiving ketamine This data was generated from the intensity oddball (iOD) paradigm. The 70 dB (-10 dB oddball) intensity mismatch response (iMMR; bold red ± sem in dotted red) and 90 dB (+10 dB oddball) iMMR (bold blue ± sem in dotted blue) waveforms ± sem are displayed for a) control (WT) mice during the saline (Sal) session, b) WT mice following a 10 mg/kg i.p. ketamine (Ket) injection, c) *Map2k7*^{+/-} (HET) mice during the saline session, and d) HET mice during the ketamine session. Increasing and decreasing intensity oddball iMMR waveforms evidently display opposite polarity deflections in the region of N1 and P2 features, which as discussed in Section 4.3.3.1 are sensitive to stimulus sound pressure level. Signed area from 0-60 ms is quantified from e) the 70 dB and f) the 90 dB iMMR, plotted as means ± sem. This analysis revealed no significant genotype or ketamine effects, or any significant difference between louder and quieter iMMR response magnitudes.

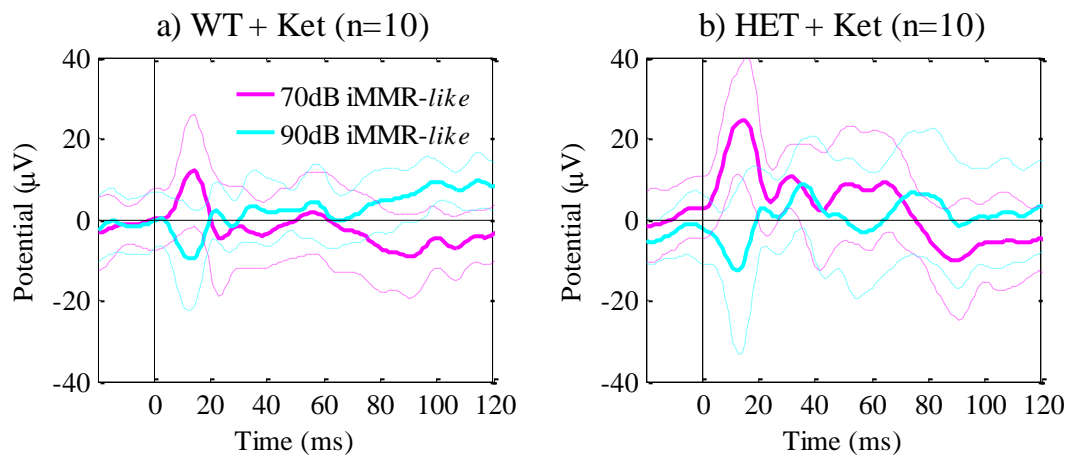


Figure 4.22 - Intensity mismatch response-like waveforms from intensity consecutive-repetition paradigm in conscious wild-type and *Map2k7*^{+/-} mice following 10 mg/kg i.p. ketamine These intensity mismatch response-like (iMMR-like) difference waveforms were produced by subtracting 80 dB (standard equivalent) from 70 dB and 90 dB (oddball equivalent) AEPs from the intensity consecutive-repetition (iCR) paradigm, played \approx 0-10 min after injecting 10 mg/kg i.p. ketamine (Ket). Resulting 70 dB– 80 dB (bold magenta \pm sem in dotted magenta) and 90 dB– 80 dB (bold cyan \pm sem in dotted cyan) iMMR-like difference waveforms are plotted for a) control (WT) and b) *Map2k7*^{+/-} (HET) groups. The purpose of this analysis is to examine how the acute effects of ketamine may influence difference waveforms in conscious mice. Compared with intensity mismatch responses in Figure 4.21a-d, large areas of difference from 20-60 ms are greatly diminished, corresponding to secondary evoked feature (P2) amplitude reduction from ketamine (e.g. Figure 4.18).

4.3.3.3 Comparison of deviant-alone vs. consecutive-repetition paradigm auditory evoked potentials with extended inter-stimulus interval

Two additional sequences of oddball stimuli presentations with an extended ISI of 2s were included in Experiment II consecutive repetition paradigms, as discussed in Section 2.8.2. This was designed to control for the deviant-alone (DA) paradigm condition which also effectively had an extended ISI, deemed appropriate from Experiment I findings (Section 3.4.5). Data presented here from intensity CR (iCR) and DA (iDA) paradigms with extended ISI are representative of findings from these paradigms using stimuli varying in duration and frequency in Experiment II.

Firstly, inspecting iDA waveforms in Figure 4.23, it is apparent that N1 and P2 deflections are greatly enlarged compared with those evoked from previously addressed paradigms, however this may be expected considering the influence of ISI over these features (Section 4.3.1.2). There does not appear to be any pronounced effects of 10 mg/kg i.p. ketamine on these AEPs, although the iDA paradigm was played \approx 20-30 min post administration, likely after the acute drug effects have subsided.

Secondly, addressing waveforms from the iCR paradigm with a 2s ISI plotted in Figure 4.24, it may be noted that N1 and P2 potentials from recordings made after injecting physiological saline are somewhat comparable to iDA AEPs from the saline session. There are however notable differences in the ketamine session waveforms. Specifically, following 10 mg/kg i.p. ketamine both N1 and P2 amplitudes appear diminished in both WT and *Map2k7^{+/-}* mice. A visual difference still exists between these diminished N1 peaks evoked by 70 dB and 90 dB stimuli, suggesting this reduction in amplitude is equal for both louder and quieter stimuli. Conversely, following ketamine the P2 responses from 70 dB and 90 dB AEPs are almost identical, and any effect of SPL on these features is apparently abolished.

N1 and P2 peak amplitudes from iDA and iCR (2s ISI) paradigms in saline (Sal) and 10 mg/kg i.p. ketamine (Ket) test sessions are quantified in Figure 4.25. Repeated measures ANOVA considering each paradigm-session combination separately (i.e. iCR-Sal vs. iCR-Ket vs. iDA-Sal vs. iDA-Ket) as within-subjects factors and genotype and gender as between-subjects factors revealed a significant effect of iCR-Ket on N1 [$F_{3,48} = 12.716$, $p < .001$] and P2 peak amplitudes [$F_{3,48} = 19.557$, $p < .001$]. A significant effect of gender to reduce P2 amplitude was also found [$F_{1,16} = 8.931$, $p = .009$].

One-way ANOVA of iCR-Ket N1 peak amplitude data showed that a significant effect of stimulus [$F_{1,16} = 8.532$, $p = .010$] remains under the effects of ketamine. In contrast, the same test applied to P2 peak data returned a non-significant result [$F_{1,16} = .546$, $p = .470$], suggesting that that ketamine nullifies the relationship between stimulus SPL and P2 peak amplitude but not N1.

In summary, there appears to be little difference between iDA and iCR with 2s ISI paradigm evoked waveforms following injection of physiological saline. However both vary substantially from those observed in response to DA paradigms in urethane-anaesthetised mice (e.g. Figure 3.9). Following 10 mg/kg ketamine changes are observed in the iCR data (recorded ≈ 0 -10 min post drug delivery), which show decreased N1 and P2 peak amplitudes. The reduction in N1 amplitude appears equal for both 70 dB and 90 dB stimuli AEPs, which retain a significant effect of stimulus intensity, whereas their P2 responses are blunted to the same level. This indicates that ketamine can acutely abolish P2 peak amplitude differences caused by stimuli with different physical properties, in this case intensity or SPL. The same was also true for tone frequency differences in DA and CR paradigms with extended ISI, of which these results are representative. These findings have implications for interpreting observed reductions in MMR difference waveforms following ketamine administration, such that resultant potential changes are likely to occur more so in the region of P2 than N1.

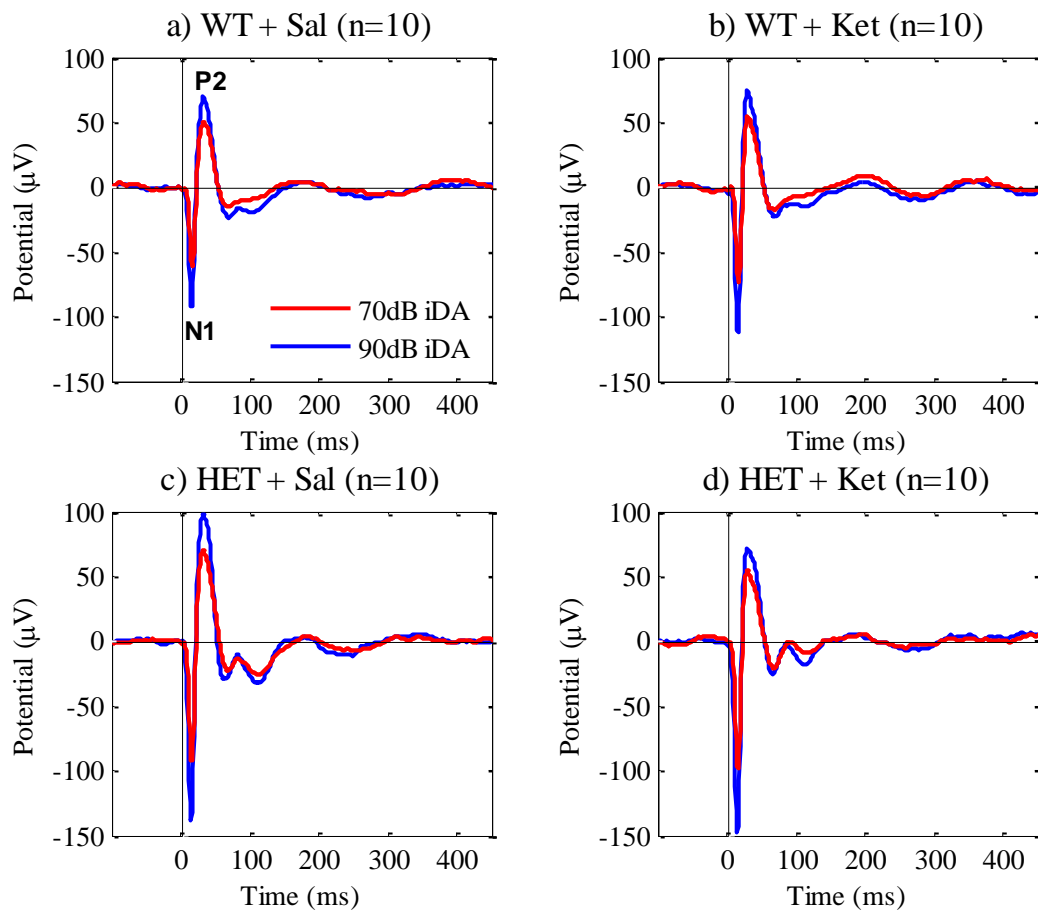


Figure 4.23 - Auditory evoked potentials from deviant-alone paradigm stimuli in conscious wild-type and *Map2k7*^{+/-} mice receiving ketamine These plots were produced from intensity deviant-alone (iDA) paradigm data and are typical of auditory evoked potentials from other DA paradigms in conscious mice. 70 dB (red) and 90 dB (blue) iDA stimuli evoked waveforms are plotted for a) control (WT) mice after an i.p. saline (Sal) injection, b) WT mice following administration of 10 mg/kg i.p. ketamine (Ket), c) *Map2k7*^{+/-} (HET) mice during the saline session, and d) HET mice during the ketamine session. No notable effect of ketamine is observed in this data which was acquired \approx 30-40 min after injecting the drug; see Figure 4.24 to compare these waveforms with those from the intensity consecutive-repetition (iCR) paradigm with extended inter-stimulus interval (ISI), presented \approx 0-10 min post ketamine administration.

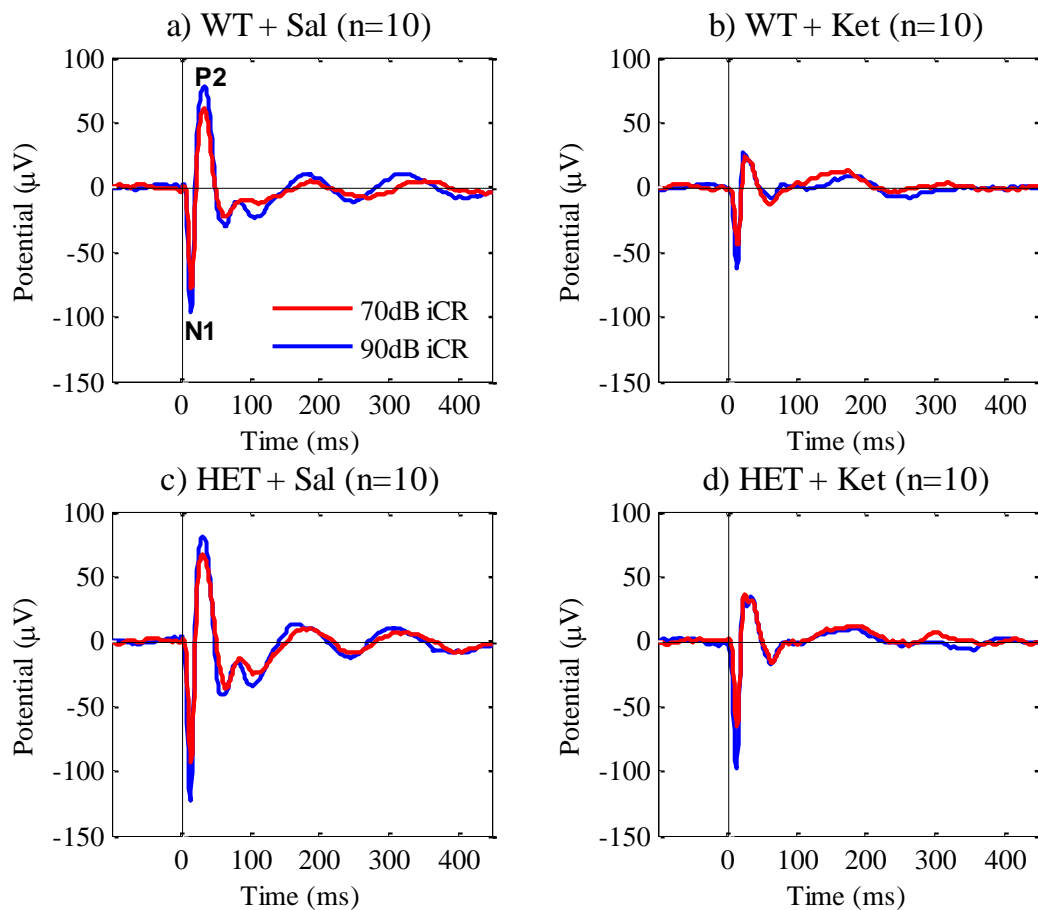


Figure 4.24 - Auditory evoked potentials from consecutive-repetition paradigm with extended inter-stimulus interval in conscious wild-type and *Map2k7*^{+/-} mice receiving ketamine These auditory evoked waveforms were generated by intensity consecutive-repetition (iCR) paradigm stimuli with an inter-stimulus interval of 2s. 70 dB (red) and 90 dB (blue) iCR waveforms are plotted for a) control (WT) mice during the saline session (Sal), b) WT mice following 10 mg/kg i.p. ketamine injection (Ket), c) *Map2k7*^{+/-} (HET) mice during the saline session, and d) HET mice during the ketamine session. The saline session waveforms in a) and c) appear qualitatively similar to intensity deviant-alone (iDA) paradigm evoked potentials shown in Figure 4.23; however amplitude reductions are apparent in ketamine session data recorded ≈0-10 min post drug administration.

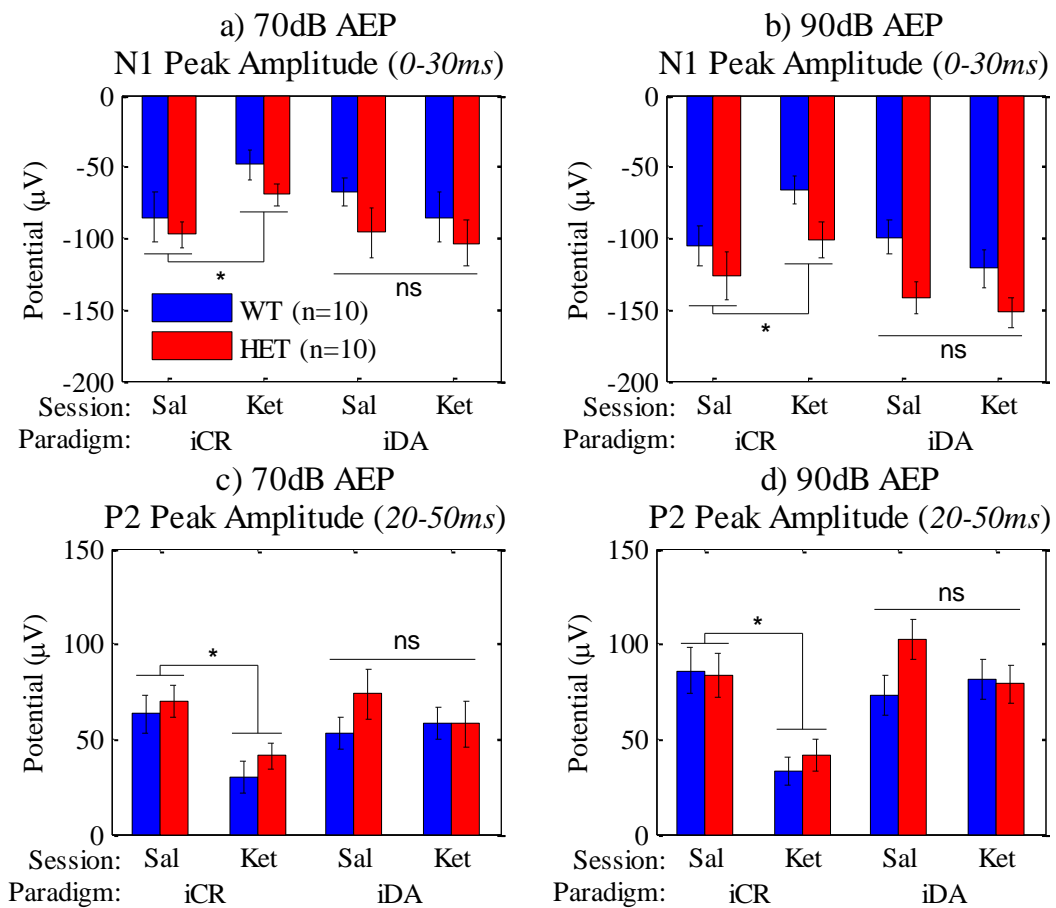


Figure 4.25 - Quantification of deviant-alone and consecutive-repetition paradigms with extended inter-stimulus interval in conscious wild-type and *Map2k7^{+/-}* mice receiving ketamine These plots display data from control (WT; n = 10) and *Map2k7^{+/-}* (HET; n = 10) mice in intensity consecutive-repetition (iCR) and deviant-alone (iDA) paradigms presented following physiological saline control (Sal) and 10 mg/kg i.p. ketamine (Ket) injections (group grand-average waveforms shown in Figure 4.23 and Figure 4.24). These iCR data were acquired with a 2s inter-stimulus interval condition. Primary auditory onset (N1) peak amplitude is shown for a) 70 dB, and b) 90 dB stimuli. Secondary response (P2) peak amplitude is also displayed for c) 70 dB, and d) 90 dB stimuli. Data presented are means \pm sem, measurement windows are shown *in brackets*, and asterisks are used to denote a significant effect ($p < .05$) of the iCR paradigm in the ketamine recording session.

4.3.3.4 Auditory evoked potential changes throughout Experiment II

It is important to understand how AEP waveforms may change throughout an experiment to avoid reaching false conclusions about the effects of a particular paradigm or pharmacological manipulation which may in reality be due to other processes tied to the experimental protocol. This issue was introduced in Section 4.3.1.7 when describing representative waveforms acquired throughout an entire test session in Experiment II.

To investigate this further, peak amplitude measurements were taken from AEPs to physically identical ‘standard’ stimuli (50 ms, 10 kHz, 80 dB with 450 ms ISI) presented throughout intensity-varying auditory paradigms. Analysis of N1, P2, N3, P4 and N5 peak amplitude data are provided in Figure 4.26. Data from intensity consecutive-repetition (iCR), oddball (iOD) and many-standards (iMS) paradigms played in order following physiological saline (Sal) and then 10 mg/kg i.p. ketamine (Ket) injections are plotted linearly along the y-axis, giving an approximation of time during each session. The intensity deviant-alone (iDA) paradigm presented in between iOD and iMS paradigms is omitted here because it did not employ physically identical stimulus properties. Relevant timings are therefore iCR \approx 0-10 min, iOD \approx 10-20 min and iMS \approx 30-40 min after respective saline and ketamine injections, with gaps from either session at \approx 20-30 min where iDA paradigms were presented.

Statistical analysis of N1 peak amplitude data in Figure 4.26a by repeated measures ANOVA with session and paradigm as within-subjects factors and genotype and gender as between-subjects factors revealed a statistically significant overall effect of genotype [$F_{1,16} = 6.802$, $p = .019$], with *Map2k7^{+/-}* (HET) mice displaying greater negative peak amplitudes than controls (WT). Pairwise comparisons of genotype data from each individual paradigm returned significant difference between WT and HET groups in the iMS-Sal [$F_{1,16} = 6.695$, $p = .020$], iOD-Ket [$F_{1,16} = 9.015$, $p = .008$] and iMS-Ket [$F_{1,16} = 6.315$, $p = .023$] paradigms, while all excluding the iCR-Sal paradigm were approaching the set criterion for statistical significance ($\alpha = .05$).

P2 peak amplitude data shown in Figure 4.26b was assessed with repeated measures ANOVA considering all six paradigm conditions as within-subjects factors, and genotype and gender as between-subjects factors. This test confirmed a statistically significant effect caused by ketamine in the CR paradigm (iCR-Ket) [$F_{1,16} = 8.749$, $p = .009$; lower-bound adjustment], suggesting that 10 mg/kg i.p. ketamine acutely reduces P2 peak amplitude in conscious mice. There were no significant effects of genotype [$F_{1,16} = .778$, $p = .391$] or gender [$F_{1,16} = 3.129$, $p = .096$].

It can be seen from visual inspection of Figure 4.26e that N5 peak amplitude is initially negative and begins to shift positive from the first paradigm onwards, perhaps suggesting that this reflects an adaptive change to continual auditory stimulation and not a specific effect of paradigm or session *per se*. This was highlighted in Figure 4.18e-f. Interestingly, in the WT group the negative amplitude is seen to recover slightly between iOD and iMS paradigms in both sessions; it may be postulated that this could result from relatively lower auditory stimulation rates in iDA (0.4 Hz) compared with other paradigms (2 Hz), effectively giving the auditory processing system a rest period to recover. Statistical analysis of N5 returned a significant effect of genotype during the iCR-Sal [$F_{1,16} = 6.368$, $p = .023$] and iOD-Sal [$F_{1,16} = 4.596$, $p = .048$] paradigms, with HET mice displaying more negative amplitudes.

Otherwise N3, P4 and P6 peak amplitudes did not exhibit any evidence of significant paradigm-, ketamine-, or genotype-specific effects. Likewise, analysis of N1, P2, N3, P4, N5 and P6 peak latencies in Figure 4.27 did not reveal any significant interpretable effects.

In summary, the N1 response consistently displays greater negative peak amplitude in *Map2k7^{+/-}* mice compared with wild-type controls. The P2 response is significantly attenuated ≈ 0 -10 min following 10 mg/kg i.p. ketamine administration, which subsequently appears to recover >10 min following drug delivery. Later deflections in the AEP waveform were more challenging to interpret, however N5 peak amplitude may reflect an adaptive change throughout the experiment to continual repetitive auditory stimulation.

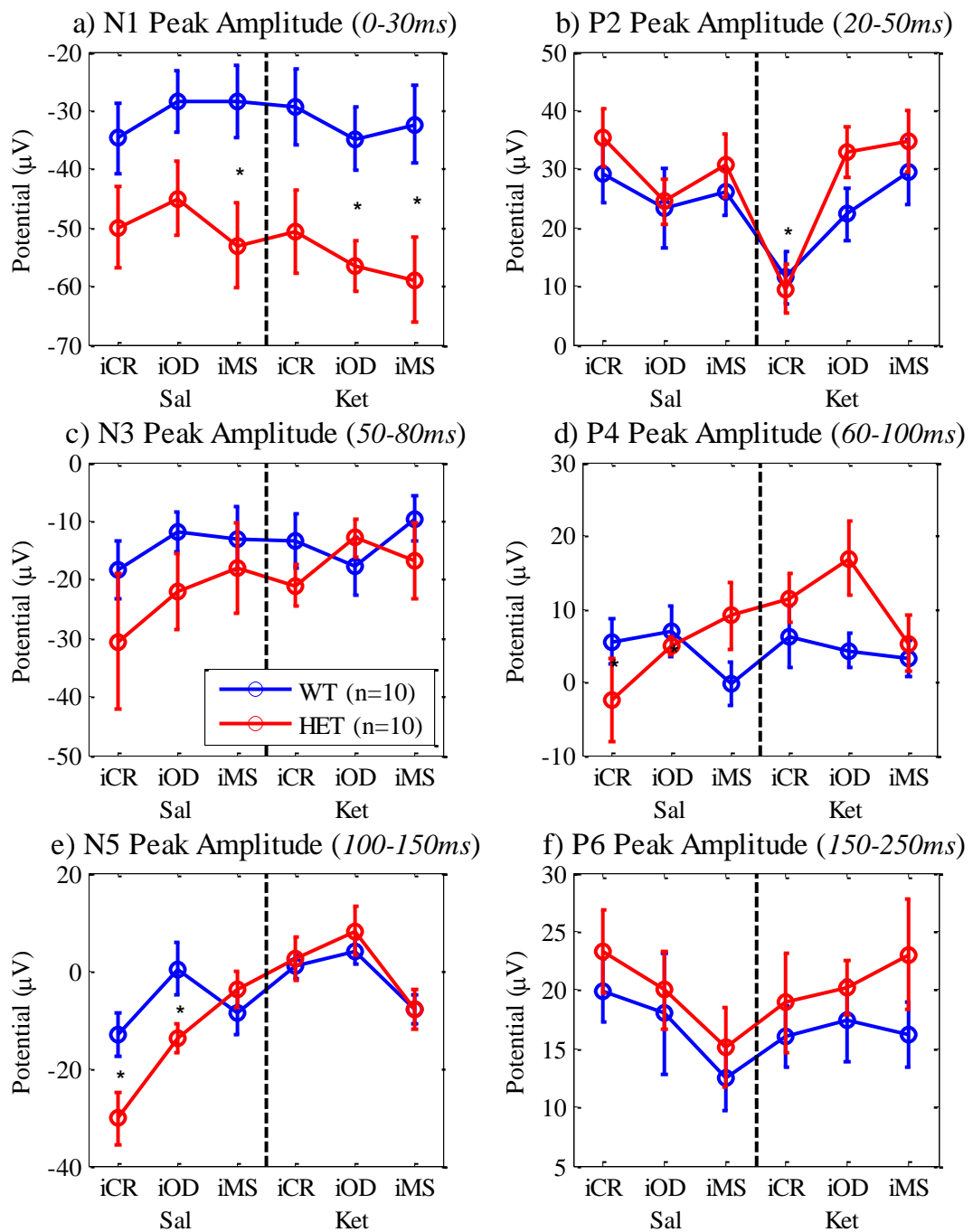


Figure 4.26 - Longitudinal examination of six peak amplitudes from conscious mice throughout Experiment II These data from control (WT) and *Map2k7^{+/-}* (HET) groups were acquired from physically identical standard 50 ms, 10 kHz, 80 dB, 450 ms ISI stimuli auditory evoked potentials from intensity consecutive-repetition (iCR), oddball (iOD), and many-standards (iMS) paradigms presented consecutively throughout the experiment in sessions following physiological saline (Sal) and 10 mg/kg i.p. ketamine (Ket) administration. a) Primary onset response (N1) peak amplitude measurements showing significant effects of genotype ($p < .05$). b) Secondary response (P2) peak amplitudes exhibiting a significant effect of ketamine ($p < .001$) in the iCR paradigm recorded $\approx 0-10$ min post drug delivery. c) N3 peak amplitudes. d) P4 peak amplitudes. e) N5 peak amplitude showing a general shift towards positivity throughout the experiment. f) P6 peak latency. These observations are representative of Experiment II findings, hence are comparable between test sessions with stimuli varying in duration and frequency that have not been included for brevity. Data are presented as group means \pm sem, and measurement windows are shown *in brackets*.

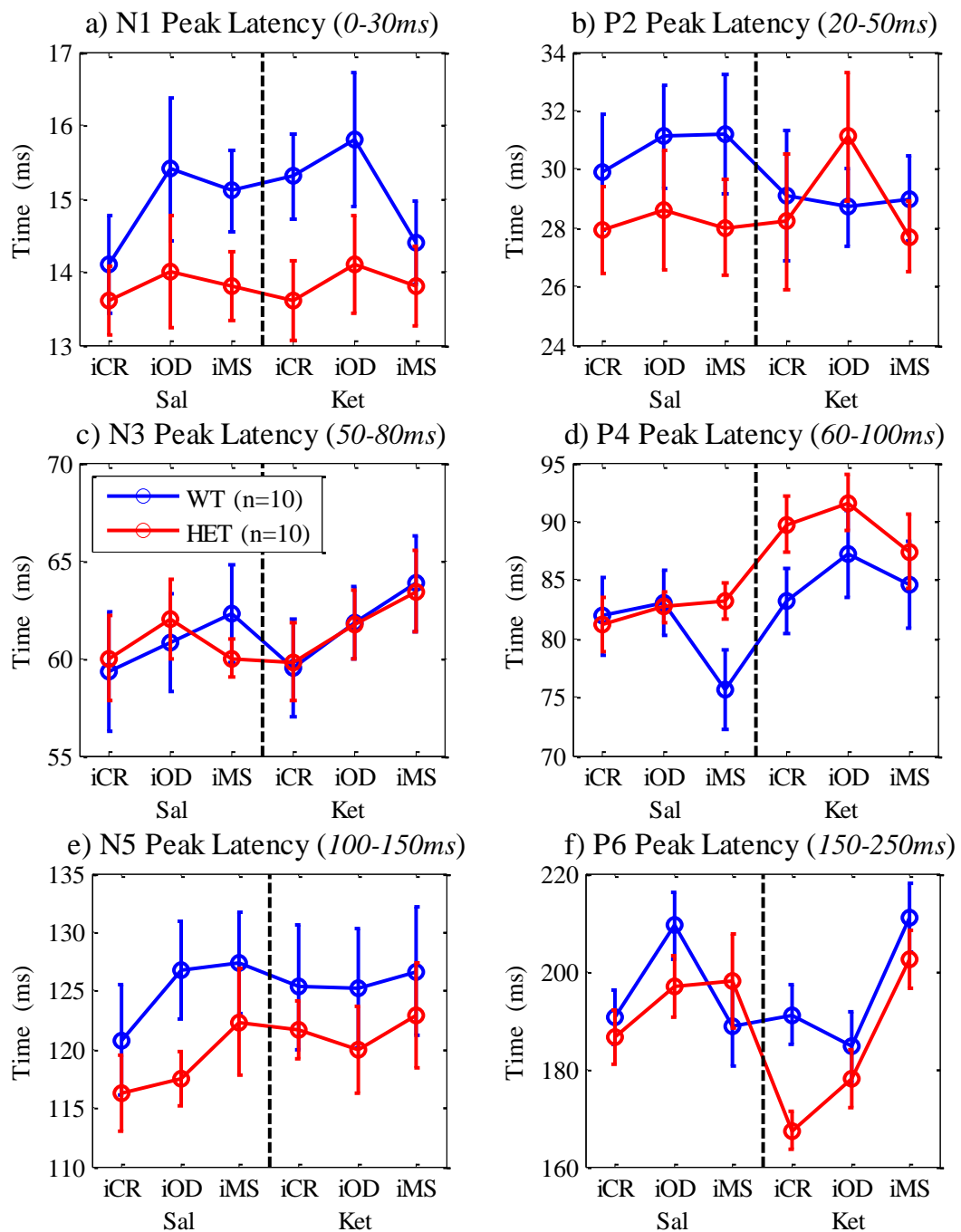


Figure 4.27 - Longitudinal examination of six peak latencies from conscious mice throughout Experiment II These data from control (WT) and *Map2k7^{+/-}* (HET) groups were acquired from physically identical standard 50 ms, 10 kHz, 80 dB, 450 ms ISI stimuli auditory evoked potentials from intensity consecutive-repetition (iCR), oddball (iOD), and many-standards (iMS) paradigms presented consecutively throughout the experiment in sessions following physiological saline (Sal) and 10 mg/kg i.p. ketamine (Ket) administration. a) N1 peak latency. b) P2 peak latency. c) N3 peak latency. d) P4 peak latency. e) N5 peak latency. f) P6 peak latency. There are no significant effects of genotype or ketamine observed in this analysis. Data are presented as group means \pm sem, with measurement windows shown *in brackets*.

4.3.4 Spectral analyses

Spectral analyses as described in Section 2.10.2 were applied to data from conscious wild-type (WT) control and *Map2k7^{+/-}* (HET) mice before and after ketamine administration to examine any effects in the frequency (EEG power spectrum) and time-frequency (event-related spectral perturbation; ERSP) domains.

EEG power spectra from the frequency consecutive-repetition (fCR) and oddball (fOD) paradigms are plotted in Figure 4.28. In fCR paradigm data recorded \approx 0-10 min after delivering saline and 10 mg/kg i.p. ketamine injections, a statistically significant ($p < .05$) increase in gamma band power (\approx 50-70 Hz) is observed following ketamine compared with the saline session. In contrast, fOD paradigm data recorded \approx 10-20 min post injections does not display the same level of significance, which may be due to ketamine effects wearing off. No significant differences were found between the EEG power spectrum of WT and HET mice.

An auditory evoked ERSP time-frequency analysis is provided in Figure 4.29. These plots compare the 12 kHz stimulus evoked spectral dynamics from fCR paradigms post saline and 10 mg/kg i.p. ketamine administrations. There are clearly differences between saline session ERSP plots on the left hand side panels and ketamine session ERSP plots on the right hand side panels. However, it cannot be ascertained whether this difference is due to ketamine or adaptive change to continued auditory stimulation. Regardless of which caused the overall decrease in spectral power, these were found to be statistically non-significant when Bonferroni corrections for multiple comparisons were applied.

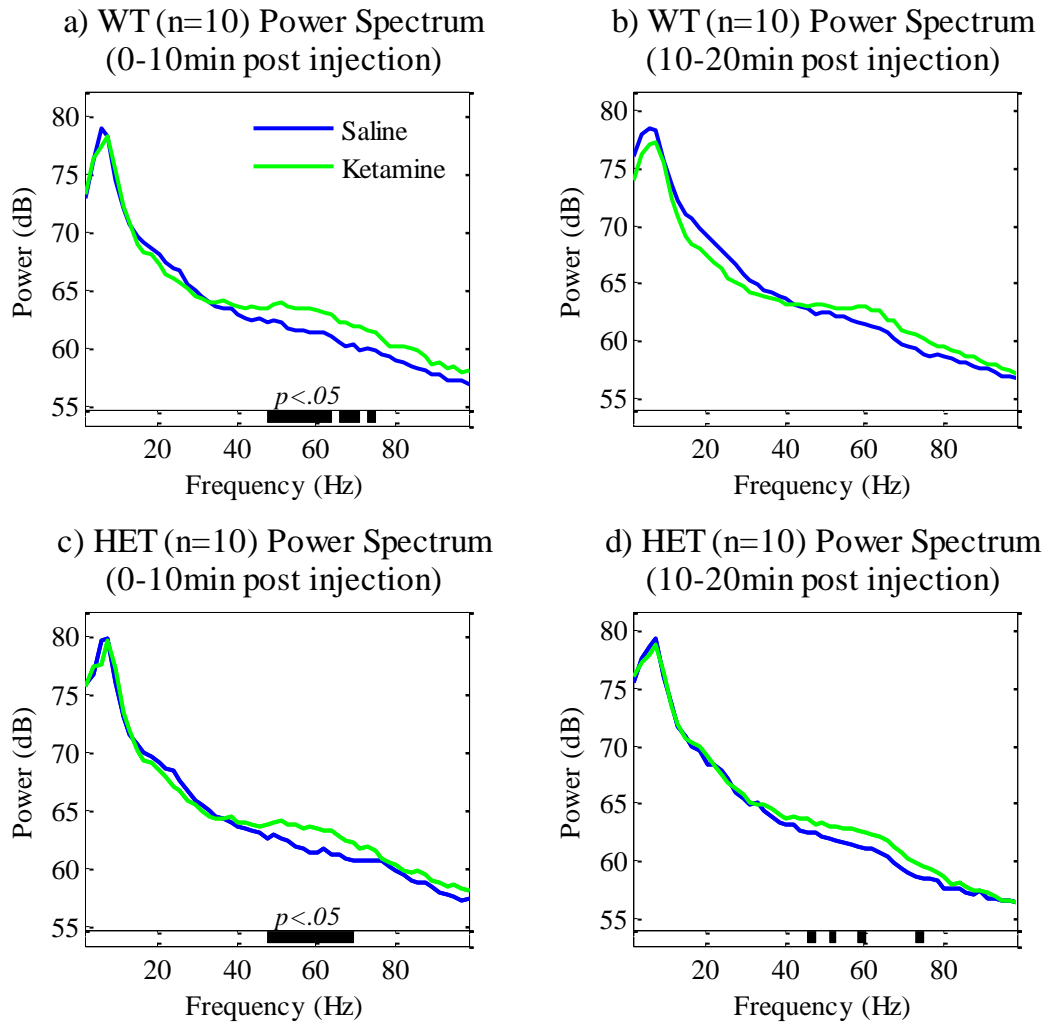


Figure 4.28 - EEG power spectra from conscious mice exposed to ketamine Group-average power spectra are plotted from a) wild-type (WT) mice over 0-10 min and b) 10-20 min post saline/ketamine (10 mg/kg) i.p. injections, and c) *Map2k7^{+/-}* (HET) mice from 0-10 min, and d) 10-20 min post injections. Statistical panels at the bottom of each plot use solid black shading to illustrate statistically significant ($p < .05$) differences between saline and ketamine session power at each frequency, determined by paired t-tests at each frequency, with Bonferroni corrections for multiple comparisons. There appears to be a significant increase in signal power across frequencies ≈ 50 -70 Hz caused by ketamine from 0-10 min which largely dissipates by 10-20 min post administration. This frequency range corresponds to the gamma band cited throughout the literature. There were no significant effects of genotype on these power spectra.

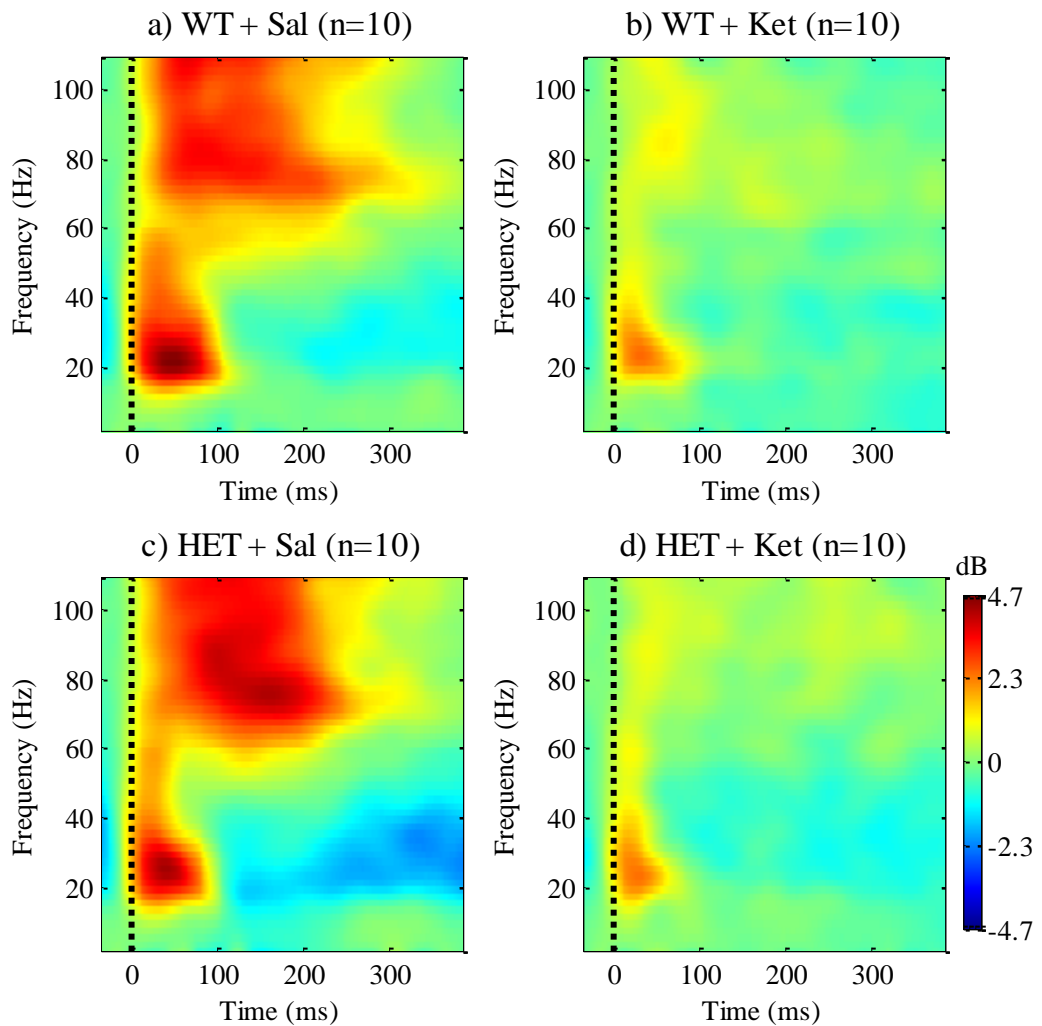


Figure 4.29 - Auditory event-related spectral perturbation (ERSP) from conscious mice exposed to ketamine Time-frequency plots are displayed for wild-type (WT) mice following a) saline and b) 10 mg/kg i.p. ketamine injections, and *Map2k7*^{+/-} (HET) mice post c) saline and d) ketamine injections. These were evoked by the 12 kHz, 50 ms, 80 dB stimulus presented in the frequency consecutive-repetition (fCR) paradigm, played ≈0-10 min post injections. The Fourier transform method was applied to compute the power at each frequency from 2-110 Hz in 2 Hz increments. The colour scale to the right of (d) applies to all. Overall power in the ERSP following ketamine is evidently reduced, primarily from ≈70-100 Hz across ≈10-250 ms. However, statistical analysis with corrections for multiple comparisons revealed no statistically significant effects.

4.3.5 *Video footage analysis*

The block-matching algorithm method described in Section 2.10.3 was applied to video footage of conscious mice within Recording Chamber A in Experiment II (Figure 2.5) in an attempt to quantify animal movement. Video film from 21 subjects undergoing saline and 10 mg/kg i.p. ketamine test sessions was gathered for this analysis. The pilot (male WT) and another WT female mouse were not filmed during their test sessions, whereas film from two female HET subjects were used in this analysis while their electrophysiology data were considered too poor for inclusion in AEP analyses (e.g. see Figure 4.1).

Figure 4.30 displays example video clips from subject 484 which are representative of footage which provided data input for the block-matching algorithm. This situation is not ideal, as annotated in the figure, for one because animal orientation within the holding tube changed throughout the course of filming, and also because the EEG cable moved around with the animal. These uncontrolled factors most probably influenced the block-matching algorithm output by altering relative proportions of the animal and apparatus movement contained within the footage. However, these proportion changes may be considered a co-variant, assumed to contribute equally to each experiment, therefore making data comparisons between sessions, genotypes and genders valid.

Averaged 160 x 120 pixel optical flow matrices, referred to as mean optical flow, output from the block-matching algorithm are graphed over time for both sessions (upper panels), genotypes (middle panels) and genders (lower panels) in Figure 4.31. This mean optical flow measure gives an approximation of movement between consecutive frames in the video, for which the conscious animal under test is considered responsible for generating. It can be seen from visual inspection of the raw data in this figure that movement is greater during the early part of each session when subjects are first inserted into the recording chamber.

To perform statistical analysis mean optical flow data were pooled into five minute bins and comparisons of session (Saline vs. Ketamine), genotype (WT vs. HET) and gender (Female vs. Male) were performed to test for any statistically significant effects (Figure 4.32). Repeated measures ANOVA with eight bins and session as within-subjects factors, genotype and gender as between-subjects factors suggested an underlying overall effect of session [$F_{1,17} = 3.894$, $p = .065$]. Pairwise comparisons between sessions at each bin revealed statistically significant higher gross movement at 0-5 min [$F_{1,17} = 12.642$, $p = .002$] and 5-10 min [$F_{1,17} = 9.371$, $p = .007$] after delivering 10 mg/kg i.p. ketamine, suggesting the drug increased animal locomotion over this time.

There is no recognisable pattern of difference between WT and HET groups. When comparing binned data from both genders it appears as though males consistently display slightly more gross motion than females, although not statistically significant, possibly due to their typically larger body mass.

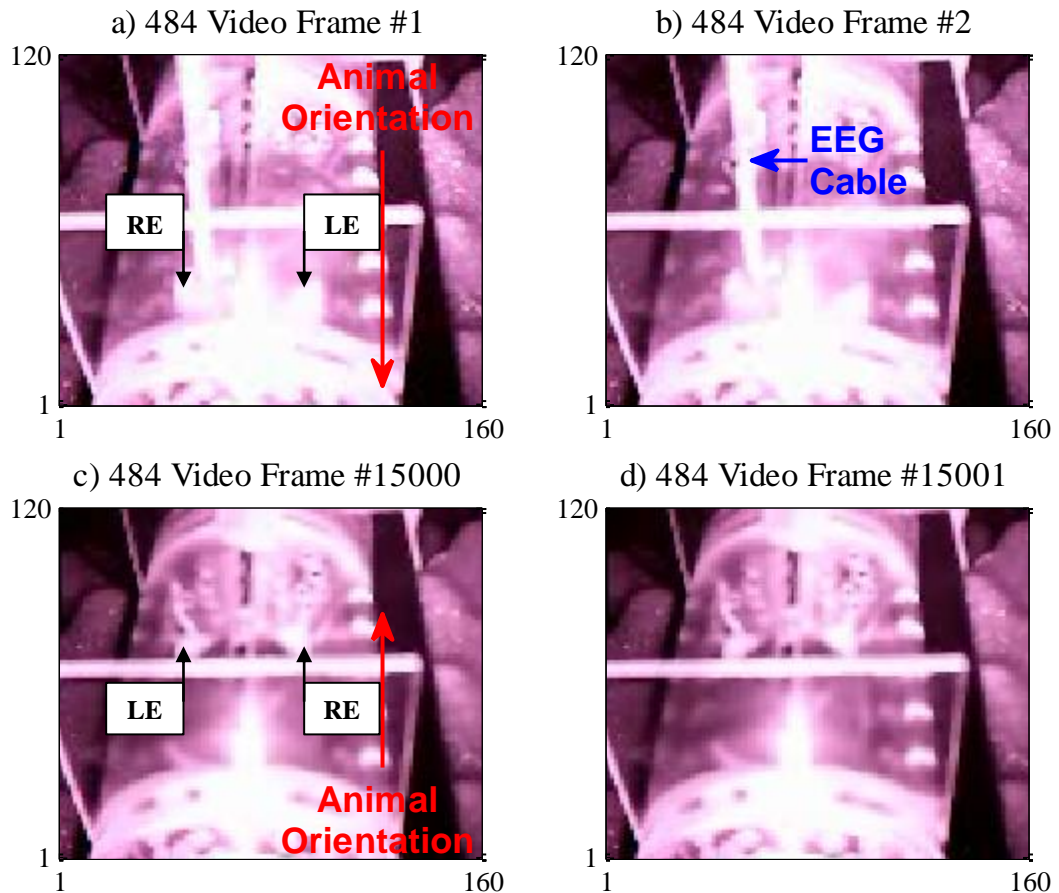


Figure 4.30 - Example of video frames used in a block-matching algorithm to estimate motion of conscious mice in Experiment II These images were extracted from film of subject 484 during the experiment. Optical flow output from the algorithm provided a surrogate measure of animal movement within the chamber. Each frame is a 160 x 120 pixel greyscale image. The upper panels a) and b) and lower panels c) and d) show separate consecutive pairs of frames from distant time points during the experiment. Animal orientation is reversed in c) and d) compared with a) and b), changing its relative proportions within the recorded frames; the recording system cable is also moved. The mouse's right-ear (RE) and left-ear (LE) are labelled in (a) and (c) which indicate animal orientation. Results from video analysis of all animals are shown in Figure 4.31 and Figure 4.32.

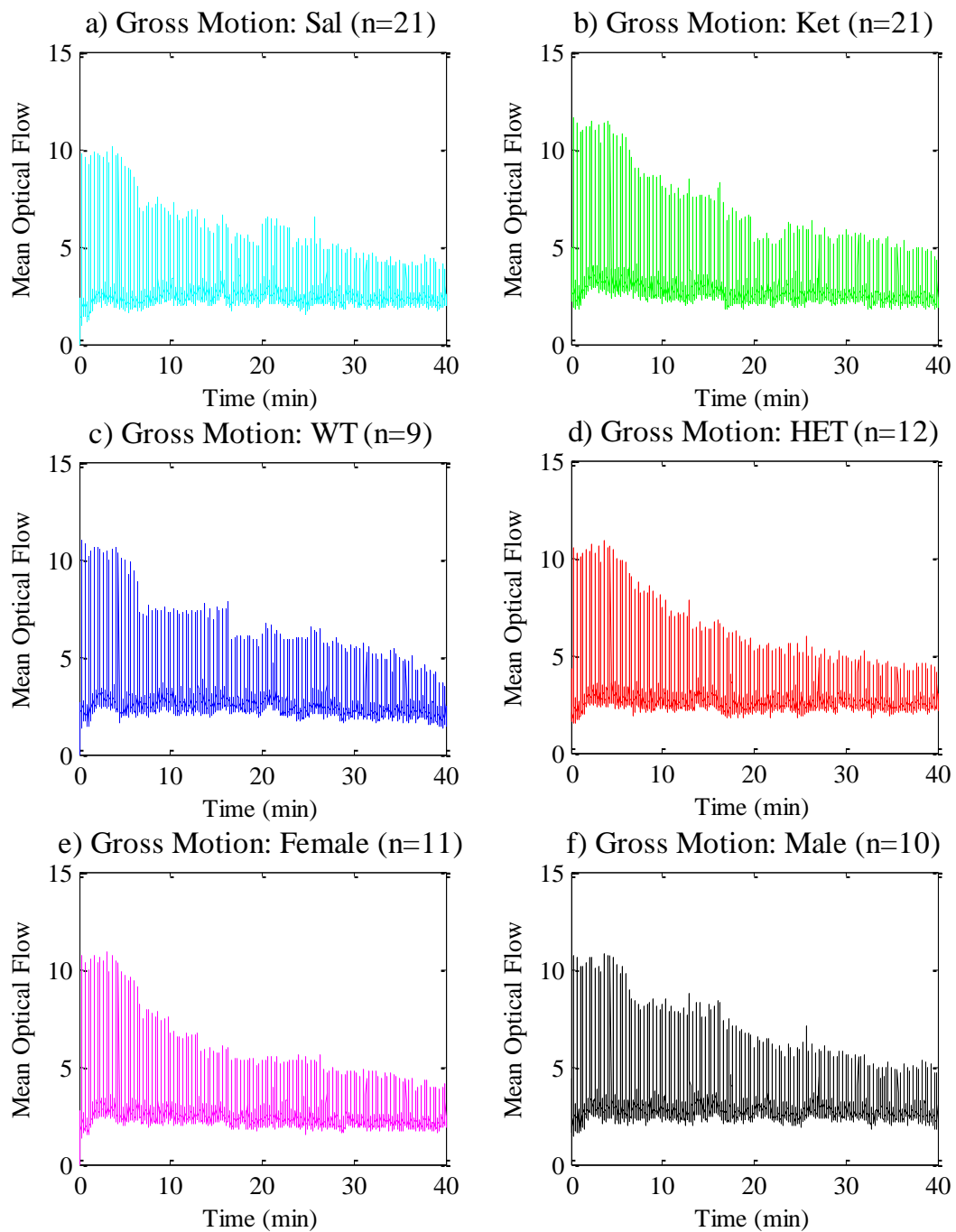


Figure 4.31 - Gross motion data output from the block-matching algorithm Two-dimensional optical flow matrices calculated between each consecutive pair of frames were averaged to produce mean optical flow, reflecting gross motion between consecutive images, and plotted over time during each recording session. Data is displayed for a) all subjects following a saline i.p. control injection (Sal), b) all subjects after a 10 mg/kg i.p. ketamine administration (Ket), c) control (WT), d) *Map2k7^{+/-}* (HET), e) female, and f) male mice. Group sizes here differ from electrophysiological analyses because i) two WT animals were not filmed (pilot plus one), and ii) video footage from two HET subjects was permitted for this analysis although their electrophysiology data were excluded from auditory evoked potential analyses.

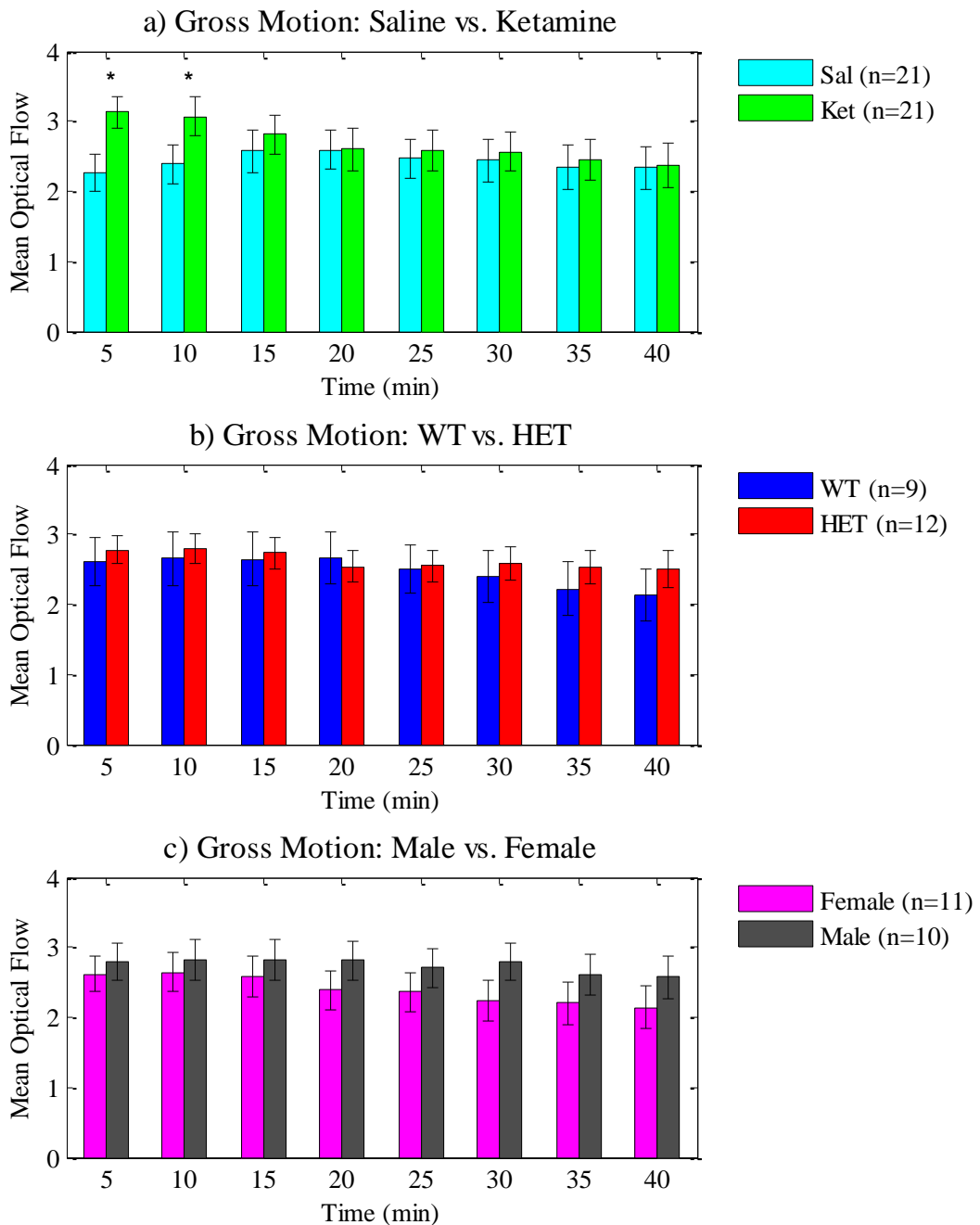


Figure 4.32 - Time-binned comparisons of gross motion from conscious mice in Experiment II These plots display data from Figure 4.31 averaged over five minute time bins \pm sem; a) saline vs. 10 mg/kg i.p. ketamine session, b) control (WT) vs. *Map2k7^{+/-}* (HET) genotype, and c) male vs. female gender. Ketamine produced a significant increase in mean optical flow from 0-10 min post drug administration ($p < .05$). Males appear to display consistent marginally greater movement than females, potentially due to their typically larger body mass, however this was not statistically significant.

4.3.6 Results Summary

Findings from Experiment II are summarised in the tables below. AEP features observed from conscious mice are outlined in Table 3.1. How some of these features were seen to vary with ISI delay and stimulus duration, frequency and intensity/SPL manipulations are outlined in Table 3.2. Although not strictly proportional by the mathematical definition, the \propto symbol is used here to label direct relationships between AEP features and physical properties of auditory stimuli. Key findings from schizophrenia-related *Map2k7^{+/-}* and ketamine models are also covered in Table 3.3. These findings and the various mismatch responses are discussed below in Section 4.4.

AEP Feature	Peak Latency	Polarity	Quantification
N1	14.3±0.5 ms post stimuli onset	Negative	Peak amplitude from 0-30 ms post onset
P2	28.8±1.2 ms post stimuli onset	Positive	Peak amplitude from 20-50 ms post onset
N3	59.4±1.4 ms post stimuli onset	Negative	Peak amplitude from 50-80 ms post onset
P4	84.2±1.4 ms post stimuli onset	Positive	Peak amplitude from 60-100 ms post onset
N5	121.3±2.1 ms post stimuli onset	Negative	Peak amplitude from 100-150 ms post onset
P6	183.7±2.5 ms post stimuli onset	Positive	Peak amplitude from 150-250 ms post onset
P _{offset}	23.4±1.4 ms post stimuli offset	Positive	Peak amplitude from 0-50 ms post offset
N _{offset}	74.6±2.1 ms post stimuli offset	Negative	Peak amplitude from 50-100 ms post offset

Table 4.1 - Summary of auditory evoked potential features observed from conscious mice Prominent deflections observed in the auditory evoked potential (AEP) of conscious mice are outlined including N1, P2, N3, P4, N5 and P6 peaks, as well as offset response deflections P_{offset} and N_{offset}. Overall peak latency (mean ± standard error of the mean), polarity and method of quantifying each feature are detailed. How N1, P2 and offset potential responses vary with duration, frequency and intensity manipulations are summarised in Table 3.2. Effects of the *Map2k7^{+/-}* disruption and 10 mg/kg i.p. ketamine models, including additional observations are summarised in Table 3.3.

AEP Feature	Duration	Frequency	Intensity
N1	Amplitude \propto - ISI delay	Amplitude \propto - stimulus frequency	Amplitude \propto - stimulus intensity
P2	Amplitude \propto ISI delay	Amplitude \propto stimulus frequency	Amplitude \propto stimulus intensity
P _{offset} /N _{offset}	Latency \propto stimulus duration	Uncertain	Uncertain

Table 4.2 - Summary of conscious mouse auditory evoked potential sensitivities to stimuli duration, frequency and intensity variations This table summarises N1, P2 and offset response (P_{offset}/N_{offset}) sensitivities to inter-stimulus interval (ISI) duration, and auditory stimuli duration, frequency and intensity manipulations. Positive and negative dependencies are denoted by \propto and \propto -, respectively. ISI, stimulus frequency and intensity had comparable effects on N1 and P2 peak amplitudes, whereas stimulus duration itself was linearly related to stimuli offset response latency. Due to the processes involved in isolating stimuli offset responses from conscious mice (Figure 4.5 and Figure 4.6) it was not possible to ascertain the relationship between P_{offset}/N_{offset} and stimulus frequency or intensity variations.

AEP Feature	<i>Map2k7</i> ^{+/-}	Ketamine	Comments
N1	Enlarged	Marginally Reduced	Initially enlarged (e.g. in CR paradigms)
P2	No effect	Reduced 0-10 min (CR paradigms)	Ketamine may diminish MMR from 20-60 ms by non-specific P2 reduction
N5	Initially enlarged then comparable	Reduction*	*May reflect gradual adaptation to auditory stimulation
Video Analysis	No effect	Increased movement 0-10 mins	Ketamine effect coincides with observations of P2 reductions (0-10 min)

Table 4.3 - Summary of conscious *Map2k7*^{+/-} and 10 mg/kg i.p. ketamine model effects on auditory evoked potential features and video analysis Significant findings from *Map2k7*^{+/-} (HET) and ketamine models are outlined here. The HET group consistently displayed an enlarged N1 response which is consistent with Experiment I findings from urethane-anaesthetised mice. The most pronounced effect of ketamine was on the P2 feature, which was non-specifically reduced in recordings made 0-10 min post drug delivery, meaning that the P2 peak amplitude became insensitive to physical properties of sound such as frequency or intensity. The N5 feature also appeared diminished following ketamine injection, however analysis of data recorded throughout an entire test session suggested this may reflect an adaptive process as opposed to a drug-induced response. Analysis of video footage also suggested a significant effect of 10 mg/kg i.p. ketamine from 0-10 min after administration to increase movement of animals within the recording chamber.

4.4 Discussion

This chapter described the first study to explicitly demonstrate the similarities and differences between AEP waveforms from conscious and urethane-anaesthetised mice. Stimuli duration, frequency and intensity, as well as ISI delay, have been shown to exert profound influence over AEP features. Consistent with previous findings from Chapter 3/Experiment I, the *Map2k7^{+/-}* (HET) gene disruption model appears to cause an enlargement of the initial onset (N1) response compared with wild-type (WT) controls. Mismatches of electrophysiological activity have been analysed, although there is no evidence that this compares with previous observations of deviant-evoked activity (DEA) in Experiment I; moreover, these mismatch responses may be explained by the physical properties of stimuli themselves regardless of their context. Ketamine had a significant effect for approximately 10 minutes, acting to abolish the P2 response, enhance spectral power in the low-gamma frequency range (50-70 Hz) and increase animal movement. However, processes of auditory adaptation may have been observed from the AEP measured at different points in the recording procedure due to repeated auditory stimulation, potentially confounding some of the interpretation of the effects of ketamine. These findings are discussed in the following subsections.

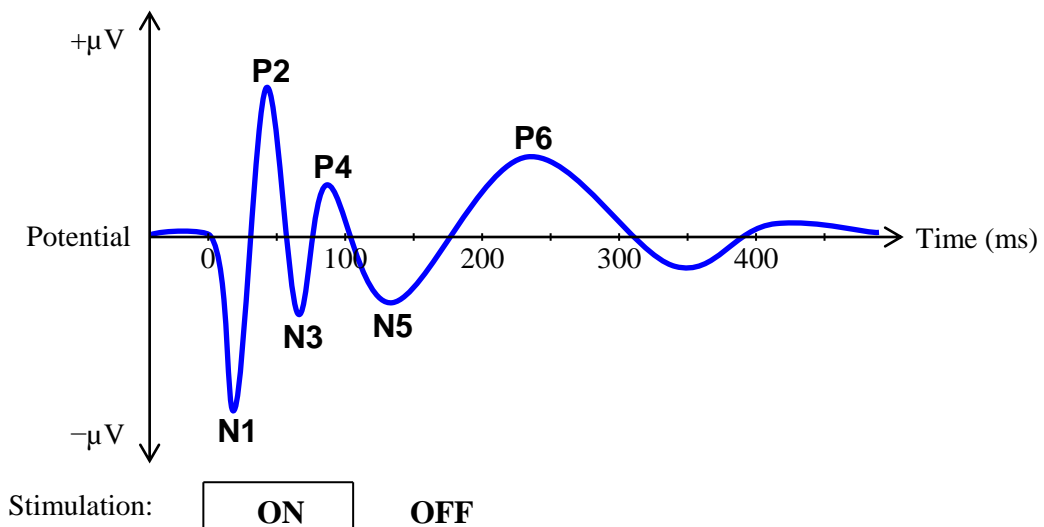


Figure 4.33 - Illustration of auditory evoked potential features observed from conscious mice This example waveform illustrates the prominent AEP deflections observed from conscious mice, named according to polarity and ordinal number as N1, P2, N3, P4, N5 and P6. N1 and P2 were both sensitive to ISI, stimulus frequency and intensity variations. N5 appeared to be sensitive to extended periods of auditory stimulation throughout the recording sessions. In addition, N1 was enlarged in *Map2k7^{+/-}* mice compared with wild-type controls; and P2 was acutely abolished by 10 mg/kg i.p. ketamine administration compared with a saline control injection. This may be compared with the example waveform in Figure 3.34.

4.4.1 Effects of inter-stimulus interval, duration, frequency and intensity on auditory evoked potentials in conscious mice

Offset potentials with peak latencies directly correlated with stimulus duration were most evident from duration many-standards (dMS) control paradigm waveforms (Figure 4.5 and Figure 4.6). The amplitude of these offset responses appeared to vary with stimuli duration, with longer stimuli generating higher amplitudes. This agrees with previous reports that auditory off responses are influenced by the duration of stimulation preceding offset (He, 2002, Takahashi et al., 2004, Jung et al., 2013). It was not effective to apply the same method of isolating these features from frequency- and intensity-varying many-standards (fMS/iMS) paradigms. However, considering the results from urethane-anaesthetised mice in Chapter 3 and findings from other studies (He, 2002, Takahashi et al., 2004, Jung et al., 2013), it is reasonable to predict that these properties may similarly influence offset response amplitudes. It has been suggested that the offset response reflects an underlying inhibitory process which acts in response to an excitatory onset response (Takahashi et al., 2004); therefore anything that increases the onset response may cause a reactive increase in the offset response. There are no previous reports in the literature of offset responses in conscious mice, which crucially may play a role in the duration mismatch response (dMMR) difference waveform, discussed further below.

An illustration of the AEP from conscious mice is provided in Figure 4.33. Inter-stimulus interval, frequency and intensity had similar effects on N1 and P2 deflections (Figure 4.3, Figure 4.13 and Figure 4.19, respectively). Each of these physical properties of auditory stimulation had a direct relationship with evoked potential amplitudes. For example, greater ISI, stimuli frequency or intensity results in larger magnitude N1 and P2 responses. This is equally true for the human N100 and P200 responses (Picton et al., 1977), potentially suggesting that these features reflect comparable underlying electrophysiological processes. These phenomena were instrumental in forming the respective MMR to each of these properties of sound manipulation in oddball paradigms, as discussed below. Although loudness dependency of the auditory evoked potential (LDAEP) is purported to reflect brain serotonin levels (Juckel, 2015), as discussed in Section 3.4.1, to the author's knowledge no neurotransmitter systems have been linked with ISI or frequency dependency of the AEP.

4.4.2 *Mismatch responses in conscious mice*

Mismatch responses resulting from ISI delay (Figure 4.9), frequency (Figure 4.15) and intensity (Figure 4.21) manipulations in oddball paradigms shared similar profiles, predominantly reflecting sensitivity of N1 and P2 deflections to each respective physical feature of sound, as described above. Due to these sensitivities, opposite direction oddball changes (+ISI/frequency/intensity vs. -ISI/frequency/intensity) generated opposite polarity deflections in difference waveforms relative to the standard. For example, a 500 ms (+50 ms) ISI oddball MMR displayed a negative deflections in the N1 latency range and a positive deflection in the P2 latency range, whereas a 400 ms (-50 ms) ISI oddball produces the opposite; a positive deflection in the region of N1 and negative deflection in the region of P2. This example equally applies if ISI is replaced with frequency or intensity. The magnitude of these MMR waveforms will inherently vary with oddball distance from the standard, which is also true for the human mismatch negativity (Pakarinen et al., 2007). However, the differences observed here between responses to oddball and standard stimuli may be fully attributed to their physical properties, which does not agree with the mechanisms thought to underlie the human MMN (Näätänen et al., 2005).

Somewhat similar to data from urethane-anaesthetised mice presented in Chapter 3, the duration mismatch response (dMMR) in conscious mice appears to reflect differences in stimuli offset response ($P_{\text{offset}}/N_{\text{offset}}$; Figure 4.6) and latency (Figure 4.7 and Figure 4.8). This may explain prior findings in conscious mice which found a dMMR which varied depending on the duration of standard and oddball stimuli (Umbricht et al., 2005). However, the present study indicates that this is a mechanistic aspect of auditory processing, not involving cognitive or memory processes as was suggested previously (Umbricht et al., 2005, Bickel et al., 2007, Bickel et al., 2008), due to the fact that it occurs automatically in response to auditory stimulation regardless of context. It has been proposed that auditory offset responses reflect a post-inhibitory rebound following auditory stimulation, suggesting that one process drives the other (Kuwada and Batra, 1999); however, another study argues that both onset and offset responses in the auditory cortex are underpinned by distinct afferent neural pathways with non-overlapping sets of synapses, suggesting that they are independently driven processes (Scholl et al., 2010). Ultimately, the origins of offset responses are not completely understood. Further research aiming to pinpoint the neurophysiological mechanisms of offset responses may be helpful for interpreting dMMR in rodents and other species. Moreover, this may prompt further examination of the processes underlying human duration MMN and corresponding deficits in schizophrenia patients and 'at-risk' individuals (discussed in Section 1.2.1).

Increasing and decreasing oddball mismatch responses from ISI delay- and intensity-varying oddball paradigms were not significantly different in rectified area analysis (Figure 4.9e-f and Figure 4.21e-f, respectively). In contrast, fMMR waveforms in response to ascending frequency oddballs were significantly larger overall compared with descending frequency oddballs (Figure 4.15e-f). This may reflect non-linearity of the mouse auditory system, which is preferentially tuned towards ≈ 14 -18 kHz sound frequencies (Heffner and Heffner, 2007).

The findings presented here suggest that the MMR to duration, ISI, frequency and intensity oddball paradigms recorded from the mouse auditory cortex reflect differences induced by the physical properties of auditory stimuli themselves, regardless of context, as determined through the application of stringent control conditions. Recent publication of data from rats supports this suggestion that physical properties of stimuli are instrumental in the resulting MMN-like responses from a frequency oddball paradigm (Ruusuvirta et al., 2015). This questions the utility of rodents for modelling the human mismatch negativity. Furthermore, clarification of the mechanisms underlying human MMN is also required to verify its interpretation and exclude this possibility. This discussion is expanded in Chapter 6.

4.4.3 *Map2k7^{+/-} gene disruption in conscious mice*

The HET gene deletion group displayed a significantly enlarged onset response compared with the WT control group (Figure 4.2), consistent with the observation of increased N1 magnitude in urethane-anaesthetised mice in Chapter 3 (discussed in Section 3.4.3). This statistical significance emerged following initial bouts of auditory stimulation (Figure 4.26a), perhaps indicative that abhorrent sensory gating or adaptation (introduced in Section 1.2.2.6 and discussed below) may be responsible. However, relative reductions in N1 amplitude with successive auditory paradigms appear similar (Figure 4.10), leaving uncertainty as to the specific processes underlying the larger peak amplitude N1 in HET mice.

Repetition suppression, or sensory gating, of AEP amplitudes in humans is considered to reflect refractory periods of neural generators as opposed to gradual habituation (Budd et al., 1998). This refers specifically to the human P50 and N100 responses (Figure 1.3) which decreases in peak amplitude with repeated presentation of auditory stimuli. Deficits in sensory gating of the P50/N100 are seen in patients with schizophrenia (Budnick and Braff, 1992, Brockhaus-Dumke et al., 2008), associated with dysfunctional neural inhibition underlying decreased measures of attention (Potter et al., 2006). Therefore the increased N1 observed from HET mice in the present study may relate to abnormal neural refractory/inhibitory mechanisms seen in patients with schizophrenia.

Cholinergic neurotransmission has been found to regulate sensory gating deficits in schizophrenia patients via α -7 nicotinic receptors (Adler et al., 1998), leading to recent development of multiple drugs targeting this signalling mechanism (agonists and positive allosteric modulators) for treating neuropsychiatric disease, with varying success (Hashimoto, 2015). How this relates to *Map2k7* function is uncertain, however, feedback following activation of NMDA receptors in the rat auditory cortex *in vitro* has been suggested to decrease acetylcholine (ACh) release (Metherate and Ashe, 1995). Reduced ACh may result in lower downstream stimulation of α -7 nicotinic receptors, thus impairing normal sensory gating. Furthermore, ablating the gene coding for α -7 nicotinic receptors disrupts extracellular cortical (Lin et al., 2014) and striatal (Beggiato et al., 2013) release of γ -aminobutyric acid (GABA), the key inhibitory neurotransmitter. It may be hypothesised that *Map2k7* participates in a post-synaptic NMDA receptor activated feedback mechanism. Missing one copy of this gene in the mouse auditory cortex may infer reduced local ACh, in turn decreasing α -7 nicotinic receptor stimulation, lowering extracellular GABA release, and impairing sensory adaptation. This is one possible explanation for the enlarged N1 response observed in both anaesthetised and conscious HET mice; however, further biochemical and electrophysiological research is necessary to clarify these interactions. The effects of ketamine (discussed below) were not significantly different between genotypes, perhaps suggesting NMDA receptor-mediated signalling is unimpaired in this genetic model.

These findings do not necessarily replicate those from any other studies in genetically altered mouse models relevant to the glutamatergic hypothesis of schizophrenia. Mice with complete deletion of the NR1 (now notated GluN1) gene (*NR1*^{-/-}) display significantly greater overall AEP amplitudes not restricted to a specific latency range (Bodarky et al., 2009, Halene et al., 2009), whereas heterozygous gene disruption (*NR1*^{+/-}) is found to cause a deficit in mismatch responses without significantly altering typical AEP amplitudes (Featherstone et al., 2015). Similarly, mice with reduced expression of neuregulin 1 (*Nrg1*^{+/-}) have also been reported to show diminished mismatch responses without having substantially atypical AEPs relative to controls (Ehrlichman et al., 2009). In addition, mice with altered Akt1 gene expression (both *Akt1*^{-/-} and *Akt1*^{+/-}) have apparently shown greater reductions in AEP amplitudes following 50 mg/kg i.p. ketamine relative to wild-type controls; although pre-ketamine AEP waveforms were not significantly different (Featherstone et al., 2013). Therefore the *Map2k7*^{+/-} model stands apart in its relative specificity to produce enlarged AEP peak amplitudes specifically within the latency range of 0-30 ms. This indicates that a specific early-stage process in central auditory processing is altered in this model. The fact that this occurs in both urethane-anaesthetised and conscious

mice suggests this is a robust finding which may be amenable to further examination, as discussed in Section 6.1.3.

4.4.4 *Ketamine effects in conscious mice*

Ketamine (10 mg/kg) was administered by the intraperitoneal route approximately 40 minutes into the recording protocol (Figure 2.14). Its significant effects were apparent for up to 10 minutes, during presentation of the consecutive-repetition (CR) paradigm. During this window of effect the secondary onset response (P2; which occurred ≈ 20 -50 ms post stimuli onset) was abolished (Figure 4.17a-d and Figure 4.18), but then recovered in subsequent paradigms (Figure 4.26b).

This is somewhat similar to the findings of Ehrlichman et al. (2008) and others (Maxwell et al., 2006, Featherstone et al., 2013) who have shown that NMDA receptor antagonism diminishes hippocampal auditory evoked potential amplitudes ≈ 25 -50 ms post stimuli onset. Although these studies report opposite polarity peaks recorded from a different brain region, their latencies are comparable with those in the present study. It may be tentatively assumed that these reflect common underlying neural generators; polarity and morphology of these waveform peaks could easily be inverted by the different respective positioning of ground, reference and recording electrodes. As discussed above, by non-specifically reducing P2 magnitude, acute ketamine may transiently abolish MMR amplitudes from ≈ 20 -50 ms post stimuli onset in conscious mice. This would be in some way comparable with the temporary reduction in human MMN caused by ketamine or reductions in chronic schizophrenia patients (Rosburg and Kreitschmann-Andermahr, 2016), as discussed in Section 1.2.1. The finding that P2, which appears to rely on intact NMDA receptor function, is observed from conscious but not urethane-anaesthetised mice (Chapter 3) may suggest that it reflects an element of conscious sensory awareness which is acutely perturbed by ketamine.

In addition to the robust effect on P2, when stimuli were presented with a greater ISI of 2s (versus 450 ms), the N1 response amplitude was also diminished following ketamine administration (Figure 4.24 and Figure 4.25). This is somewhat similar to findings that phencyclidine (PCP) inhibits early AEP components in monkeys at long but not short inter-stimulus intervals (Javitt et al., 2000). This may indicate that the generators of N1 and P2 observed here from conscious mice have different refractory periods. Furthermore, this may suggest that N1 may be partly dependent on intact NMDA receptor mediated signalling, although to a lesser extent than P2.

Ketamine significantly increased EEG spectral power in the low gamma range (≈ 50 -70 Hz) that recovered after approximately 10 minutes (Figure 4.28). This parallels previous findings

that ketamine induced NMDA receptor antagonism enhances evoked and spontaneous gamma power in mice (Lazarewicz et al., 2010). Conversely, untreated and first-episode schizophrenia patients exhibit decreased gamma synchrony relative to healthy controls (Gallinat et al., 2004, Symond et al., 2005), which is proposed to reflect abhorrent glutamatergic signalling. However, this response in HET mice is not significantly different from WT controls, indicating that *Map2k7* is unlikely to be involved in the processes underpinning gamma-band oscillations (described in Section 0).

Motion estimation of video data recorded during the experiment suggests that animal movement was significantly increased for the first 10 minutes after injecting ketamine (Figure 4.32). This is consistent with repeated findings that NMDA receptor antagonism, induced for example by ketamine or PCP, produces hyperlocomotion in animal models (Jentsch and Roth, 1999). The precise cause of this increase in motor activity has not been fully elucidated, although may involve indirect effects of NMDA antagonism throughout neural circuits involving multiple neurotransmitter systems. Nevertheless, analysis of video footage here corresponds well with previous studies using different methodologies, and in combination with AEP and gamma synchrony illustrates a significant effect of 10 mg/kg i.p. ketamine lasting approximately 10 minutes.

The fact that the P2 response was observed in conscious but not urethane-anaesthetised mice may suggest that it is associated with conscious perception. Moreover, the observation that it is acutely diminished following ketamine administration may reflect distortion of conscious perception by this psychomimetic substance. As illustrated in Figure 4.17e-f and Figure 4.22, if administered immediately prior to the oddball paradigm this effect of ketamine may have altered the resulting MMR from ≈ 20 -50 ms. This window of effect is somewhat limiting, particularly in this type of electrophysiological investigation where constancy of effect throughout oddball and control paradigms is desirable; highlighting genetically altered animals as the preferred option for neuropsychiatric disease modelling in this situation.

Event-related spectral power variations were evidently attenuated following administration of ketamine (Figure 4.29), although this may also reflect sensory adaptation to repeated auditory stimulation, as seen in some AEP features (Figure 4.11 and Figure 4.12). Adaptation was particularly apparent in potentials between 100-150 ms post stimuli onset (Figure 4.18e-f and Figure 4.26e). In this respect the effects of ketamine are confounded by prolonged repetitive auditory stimulation; which may have been mitigated somewhat if saline and ketamine recording sessions were conducted on different days.

4.4.5 Summary of findings from Experiment II

In summary, this chapter has shown for the first time that the mismatch responses observed from the auditory cortex of conscious mice may be explained by the physical properties of stimuli themselves. These are due either to offset responses of duration-varying stimuli, or inherent N1 and P2 amplitude changes with variation in stimuli frequency, intensity or ISI. Considering the prevailing theories of human MMN (Section 1.2.3), this mouse MMR is not analogous, which conflicts with the original hypothesis of this research. However, further clarification may be required to determine whether the human MMN can also be described in terms of the physical properties of stimuli, as has been argued previously (Ruusuvirta et al., 2015). If translational relevance can be confirmed, understanding how these different components (P_{offset} , N1 and P2) are generated may therefore be useful for interpreting reductions in the human MMN caused by these properties of sound; in which case both genetic and pharmacological mouse models will have their relative merits, discussed further in Chapter 6.

The *Map2k7*^{+/-} model displays a significantly greater N1 component, whereas other features of the AEP are comparable. This is suggestive of altered early-stage auditory processing neurophysiology, with possible thalamo-cortical origins, discussed further in Section 6.1.3. Ketamine produced significant decreases in the P2 amplitude of the mouse AEP, increases in gamma-band power and animal movement over a 10 minute period; furthermore, these effects of ketamine did not differ significantly between wild-type controls and *Map2k7*^{+/-} mice. This final point is also supported by findings from 2-deoxyglucose (2-DG) imaging which did not find a differential response to PCP between control and *Map2k7*^{+/-} mice (Dawson et al., *unpublished data*), suggesting that *Map2k7* may not be involved in NMDA receptor-mediated responses.

It is feasible that ketamine, by non-specifically abolishing AEP amplitudes between ≈ 25 -50 ms, may decrease MMR amplitudes from frequency, intensity or ISI oddball paradigms. This may translate to reductions in human MMN caused by NMDA receptor antagonists, if, as mentioned above, the human MMN does indeed correspond with the mouse MMR in its dependency on the physical properties of stimuli.

4.4.6 Recommendations for Experiment III

Although Experiment III differs more substantially from both Experiment I and Experiment II, there were a couple of protocol adjustments recommended following analyses of these data listed below:

1. Tones are to be generated with a 5 ms cosine ramp function at their beginning and end, effectively implementing 5 ms rise/fall times on auditory stimuli. This is in contrast to instantaneous rise/fall times of auditory stimuli in Experiment I and Experiment II; designed to examine how this may influence onset (N1) and offset (P_{offset}) responses.
2. Due to potential confounds of an extended period of urethane anaesthesia the protocol should be shortened. Focus should be placed upon the frequency mismatch response, with abbreviated examinations of stimuli duration and intensity variations.
3. The oddball paradigm should be presented immediately following ketamine administration to investigate the drug effect on resulting MMR waveforms.

Chapter 5. Experiment III: laminar auditory cortex mismatch response investigation in urethane-anaesthetised wild-type and *Map2k7*^{+/-} mice exposed to ketamine

5.1 Introduction

Experiment III applied a technically demanding electrophysiology recording technique which aimed to provide a greater level of resolution than the approach taken in the two preceding chapters. Multichannel silicon probes with a linear two-shank electrode arrangement were used to record laminar cortical responses during various sequences of auditory stimulation, with emphasis placed on investigating the frequency mismatch response (fMMR). This technique is applied to test the hypothesis that the MMR in mice exhibits a laminar-specific profile. Genetic (*Map2k7^{+/-}*) and pharmacological (ketamine) models relevant to schizophrenia were investigated, consistent with the two prior experiments, and mice were anaesthetised with urethane as in Experiment I.

Although this protocol focussed on presenting frequency oddball and control paradigms, additional sequences with stimuli varying in duration and intensity were included to study their effects on laminar auditory evoked activity. To introduce this experiment and give context to appreciate its contributions to the field, a review of current literature surrounding laminar auditory cortex activity, neural responses to different physical features of sound and suggested neural correlates of the mismatch response are provided below.

5.1.1 Laminar investigations of the auditory cortex

The layered structure of the auditory cortex (Figure 1.8) is anatomically and functionally specialised to process sensory information from upstream in the auditory pathway (Figure 1.5). Its precise function remains to be fully elucidated, thus this is an active area of research using multichannel silicon probe technology designed to record neural activity across cortical laminae (O'Connell et al., 2014, Schneider et al., 2014, Sloas et al., 2016).

Flow of bioelectric information through the cortex varies greatly depending on the auditory environment. For example, without any active stimulation, the auditory cortex exhibits a spontaneous laminar activation profile consisting of gradual upward signal propagation from deep to superficial layers, and laterally between columns. In contrast, auditory stimulation induces an initial cortical response predominantly in LIII/IV via afferent thalamic projections, from which signals are immediately transmitted laterally between columns. This difference in signal flow throughout cortical lamina is suggested to reflect activation of separate neural circuits (Sakata and Harris, 2009).

Considering that there are separate proposed neural circuits underlying spontaneous and evoked auditory processing, it may be postulated that multiple circuits exist for dealing with more complex auditory scenarios. For example, there may be one neural circuit specialised for processing regular (*standard*) stimuli and another one which processes irregular (*oddball*)

stimuli. It may be possible in this example that the alternative neural circuits would exhibit different electrophysiological signatures, potentially resulting in a measurable mismatch response. Similar concepts of specific neural circuits being involved in processing different classes of stimuli have already been proposed (Nelken, 2004, Mizrahi et al., 2014), although experimental techniques have not yet been capable of proving these hypotheses. The experiment described in this chapter does not claim to test this “alternative circuits” hypothesis of mouse MMR; as it is feasible such circuits involve multiple cortical and subcortical structures. As discussed in Section 1.2.2.3, cortical MMN generators are suggested to reside in the supragranular layers (LII/III) of the auditory cortex and rely on intact NMDA receptor function (Javitt et al., 1996), which is hypothesised to reflect predictive error coding (Section 1.2.3 and Figure 1.9) (Baldeweg and Hirsch, 2015). This question can be probed by analysing laminar responses from urethane-anaesthetised mice in the experiment discussed herein.

5.1.2 *Duration-tuned neurons*

Duration tuning refers to the finding that certain neurons respond preferentially to auditory stimuli of specific durations. For instance, recordings of neurons in the auditory cortex of brown bats display short-, long- and band-duration specificity (Galazyuk and Feng, 1997), meaning that some neurons respond to short duration stimuli, some to long duration stimuli and some to stimuli of durations within a narrow band. This has also been shown in the auditory cortex of the cat, in addition to neurons which respond at tone offsets (He et al., 1997). In the mouse inferior colliculus these duration-tuning properties and offset-triggered neurons have also been demonstrated (Brand et al., 2000). In the primary auditory cortex of cats offset-specific neurons have been classified and compared with onset neurons; it was found that both are actively triggered (Qin et al., 2007), rather than offset responses arising from an inhibition-rebound effect as suggested by Phillips et al. (2002).

This prior work provides some basis for investigating the origins of the offset response observed in Experiment I (e.g. Figure 3.8) and Experiment II (Figure 4.5 and Figure 4.6). By incorporating duration-varying stimuli in modified consecutive-repetition (_{mod}CR) and duration many-standards (dMS) paradigms, Experiment III aims to investigate duration tuning in the auditory cortex of mice and examine any laminar-specific activity in relation to the stimuli offset response.

5.1.3 *Frequency-tuned neurons*

Frequency tuning refers to the behaviour of auditory neurons to respond preferentially to specific frequencies. This is a well-known feature of auditory neurons in all mammals (Merzenich et al., 1975, Reale and Imig, 1980). The sound frequency which evokes the maximum response from a neuron is called the characteristic frequency (CF), or where a limited range of frequencies are used the one which elicits the maximum neural response may be called the best frequency (BF). The BF is typically determined by plotting the frequency response area (FRA; Section 2.10.7) and determining the frequency which most effectively elicits neural activity. This relates to topographic frequency sensitivity introduced in Section 1.2.2.

To state that neurons in the primary auditory cortex are ‘frequency-tuned’ is perhaps slightly misleading. More accurately, as explained in Section 1.2.2.1, the auditory organs are anatomically and functionally specialised (tuned) to resolve sound frequencies over the range of hearing, from which a topographical representation, or map, of frequency information is preserved throughout the ascending auditory pathway up to the level of the primary auditory cortex (Schreiner and Winer, 2007). This topographical frequency sensitivity, or tonotopy, in mice is observed over cortical columns with separation distances of $>100\ \mu\text{m}$ (Rothschild et al., 2010).

Tonotopy presents a quandary when recording neural activity at the single-unit, multi-unit and local field potential scales in response to frequency-varying oddball experiments. Once implanted, the first seemingly logical step may be to determine the BF of neural tissue being recorded by the implanted electrode(s); however, there is a question of which stimulus (oddball or standard) should the BF be applied to, and what the optimal frequency separation between standards and oddballs should be? These decisions may inherently result in a mismatch of measured electrophysiology which is unrelated to the oddball/novel-stimulus condition. Additionally, although stimulation onset responses display tonotopic organisation in the cortex, it is unknown whether the fMMR at these scales also follows some tonotopic structure. As a pragmatic approach, in the present experiment BF was determined by calculating the FRA and this frequency was applied as the standard, with increasing and decreasing oddballs varying by a pre-determined $\pm 3\ \text{kHz}$.

5.1.4 *Intensity tuned neurons*

Similar to concepts of duration and frequency encoding, some neurons are reported to display responses which correlate with sound intensity or loudness. Some are referred to as *non-monotonic* because their firing patterns increase with intensity up to a point then cease

to respond with louder stimuli; others increase firing rates with sound level up to a point then remain constant, and these are labelled *monotonic* (Phillips and Irvine, 1981). The difference between these two intensity-tuning profiles is thought to reflect differences in excitatory and inhibitory synaptic inputs to these cells (Wu et al., 2006), which are also apparently arranged in a topographic structure in areas of auditory cortex (Sutter and Schreiner, 1995). It is unclear how these intensity-tuning properties of neurons correspond with loudness dependency of auditory evoked potentials (LDAEP) discussed in Section 3.4.1. By including stimuli of varying sound pressure level (SPL), the present experiment aims to provide evidence of correlation between global and cellular level neural activity, which when combined with findings from the previous two chapters may direct us towards the potential mechanisms of the intensity mismatch response (iMMR).

5.1.5 *Stimulus specific adaptation and mismatch responses*

As described in Section 1.2.2.6, SSA is suggested to reflect a single-neuron correlate of mismatch negativity. Although SSA is a consistent finding in response to repeated versus sporadic presented frequency stimuli, it is still unclear whether the same occurs in response to stimuli duration and intensity/SPL parameters. To the author's knowledge there is one published study which examines duration- and intensity-selective habituation in auditory cortex multi-unit activity (MUA) (Farley et al., 2010). This study investigating SSA in response to a duration oddball paradigm reported to find an effect of adaptation on MUA; however this was observed in the stimuli onset response, and there was an opposite direction 'adaptation' for shorter and longer duration stimuli. On close inspection of this data (Figure 3e-h of Farley et al., 2010) it appears as though an inter-stimulus interval (ISI) effect may have been causing the observed changes in MUA; a longer ISI is employed in the oddball sequence with shorter duration stimuli as the standard and longer duration stimuli as the oddball, and a shorter ISI in the reverse condition.

By administering MK-801, Farley et al. (2010) showed that NMDA receptor antagonists suppress activity in the auditory cortex evoked by standard and oddball frequency stimuli equally, although relative SSA was unaffected. This provides some basis for interpreting the effects of ketamine in the present chapter. Farley et al. (2010) also used a many-standards control paradigm, which previous studies of SSA neglected. They concluded that SSA may encode rarity, but not novelty, because there was no difference in response to frequency-deviant stimuli presented in oddball and equally-probable (many-standards control) conditions. Experiment III seeks to explore this relationship between SSA and the fMMR further, in attempt to resolve some of these inconsistencies in the literature.

5.1.6 *Experiment III aims*

This experiment tests the hypothesis that auditory evoked potentials and mismatch responses in the auditory cortex of urethane-anaesthetised mice display a laminar-specific profile, consistent with the existence of an intra-cortical generator. To achieve this, this experiment aims to characterise laminar auditory evoked responses of the auditory cortex to duration, frequency and intensity manipulations, both at local field potential and cellular resolutions. The frequency mismatch response (fMMR) is explored more closely with oddball and control paradigms in wild-type control (WT) and *Map2k7^{+/-}* (HET) mice, to inspect whether abnormal electrophysiology in HET mice is lamina-specific. Moreover, the suggestion that ketamine-induced NMDA receptor antagonism perturbs laminar electrophysiological activity in the auditory cortex of urethane-anaesthetised mice is assessed.

Henceforth the five primary objectives of Experiment III are to:

1. Employ multichannel silicon probe technology to investigate laminar auditory evoked activity and frequency mismatch responses in urethane-anaesthetised WT and HET mice.
2. Investigate laminar activity in response to duration, frequency and intensity variations on auditory evoked potential (AEP), multi- and single-unit activity (MUA and SUA) measurements in urethane-anaesthetised WT and HET mice.
3. Characterise the laminar fMMR in urethane-anaesthetised WT and HET mice.
4. Examine any differences in respective evoked laminar activity from urethane-anaesthetised WT and HET mice and determine whether these correspond with previous findings from Chapter 3 and Chapter 4.
5. Investigate the effects of 10 mg/kg i.p. ketamine on laminar activity in urethane-anaesthetised mice.

5.2 Methods

Materials and methods applied in Experiment III are summarised in this section. Full details are provided in Chapter 2 therefore only a brief description of the important information is provided here.

5.2.1 *Animal details*

Wild-type control (WT; $n = 9$) and *Map2k7*^{+/-} (HET; $n = 12$) mice were used in this experiment, full details of which are provided in Section 2.4.5 and Appendix C. From the entire cohort five subjects exhibited an identifiable auditory evoked potential (AEP): two WT (one female) and three HET (one female). Possible reasons for this relatively low success rate are discussed in Section 5.4.4.

5.2.2 *Surgery*

Animals were anaesthetised with urethane before undergoing surgery and remained unconscious throughout the experiment. Grounding electrode and a head-holding fixture were attached to the skull and a craniotomy was performed to expose the left auditory cortex in preparation for multichannel probe implantation. This surgical procedure is described in Section 2.5.3.

5.2.3 *Multichannel probe implantation*

The 32 channel two-shank silicon probe (Figure 2.6) was implanted into the exposed auditory cortex tissue while anaesthetised animals were head-fixed inside Recording Chamber B (Figure 2.7), as described in Section 2.6.2. This procedure was conducted delicately to avoid damaging the fragile probes.

A motorised stereotactic manipulator offered fine control (0.5 μm) movement in x-, y- and z-axes, illustrated in Figure 5.1a; these correspond respectively to rostrocaudal (R-C), dorsoventral (D-V) and mediolateral (M-L) planes relative to the mouse brain schematic in Figure 5.1b. Probe implantation followed the D-V plane, or y-axis, at an angle about the x-axis ($\angle x$) of 40°, manually set using a protractor built into the manipulator. This configuration was designed to insert the probe approximately perpendicular to the curved surface of the auditory cortex.

Figure 5.1c portrays a situation where the angle about the z-axis ($\angle z$) is not equal to the ideal 0° set manually. This may cause the two probe shanks to be uneven, possibly penetrating cortical tissue at different depths. Viewed under a stereomicroscope it was difficult to achieve perfectly level probe alignment, which perhaps caused Shank A and Shank B to be

implanted at slightly different depths, as suggested by Figure 5.4. Additionally, the angle about the implantation axis ($\angle y$), if not equal to 0° , could have potentially contributed towards variability of probe shank locations as illustrated in Figure 5.1d.

No post-experiment histology was performed to confirm probe placement. However, electrophysiological responses to auditory stimulation and probe geometry were used to estimate probe depth and verify its general location within the auditory cortex, as discussed in Section 5.2.6.

Two identical probes were alternated between each run of the experiment. Following each run using a separate animal the probe used was soaked for >12 hr in contact lens solution to remove residual protein, as per standard *in-vivo* probe care guidelines from the manufacturer.

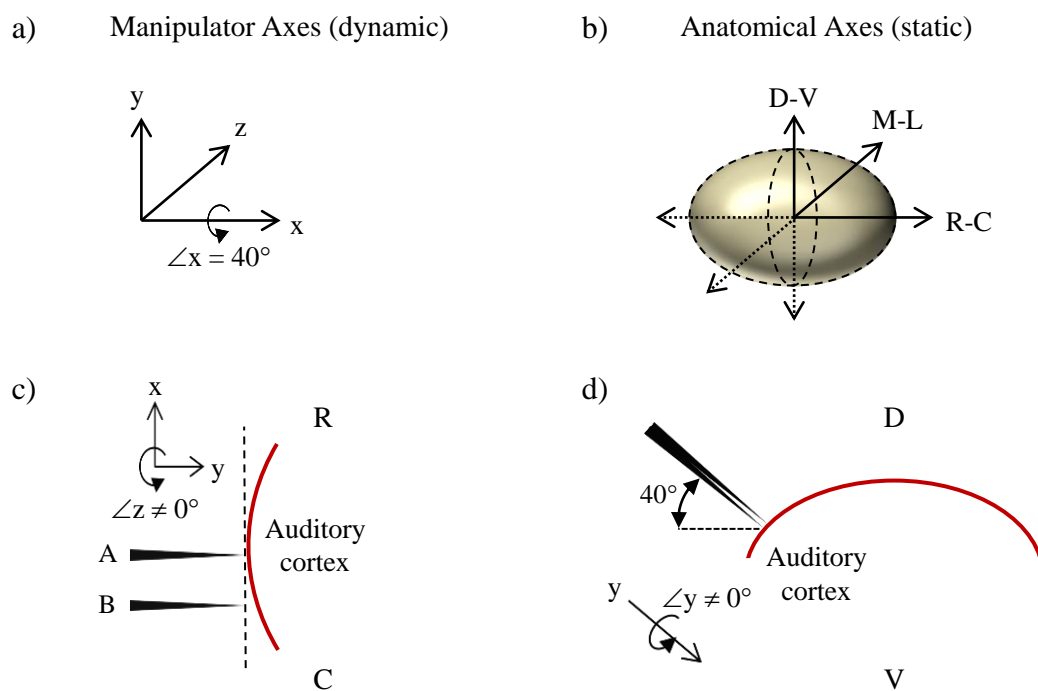


Figure 5.1 – Illustration of multichannel probe implantation axes and potential misalignments a) The manipulator axis system which was flexible, with an angle about the x-axis ($\angle x$) set to 40° to account for the laterally sloping cortical surface, and all other angles ideally set to 0° . b) Anatomical axis of the mouse brain representing rostral-caudal (R-C), dorsoventral (D-V), and mediolateral (M-L) planes which translate to the x, y and z-axes of the manipulator, respectively. c) Demonstrates an issue faced when implanting two shanks into the R-C curved surface of the cortex with a non-ideal angle about the z-axis ($\angle z \neq 0^\circ$). At the point of contact shanks are uneven, potentially leading to one shank (A) being implanted deeper than the other (B) in the example. d) A non-ideal angle about the y-axis ($\angle y \neq 0^\circ$) may also lead to shank misalignment.

5.2.4 *Electrophysiological recordings*

Local field potential (LFP) and neuron spiking (SUA and MUA) data were recorded from the 32 channel multichannel probe implanted into the auditory cortex. Wide-band signals sampled at 20 kS/s were stored using a custom data acquisition system (National Instruments, TX, USA). Details of the recording setup are provided in Section 2.6.2. These recordings were band-pass filtered between 0-300 Hz and 500-9500 Hz to isolate LFP and spiking data, respectively.

The AEP was extracted from LFP recordings down-sampled to 1 kS/s with the same general processing steps applied to Experiment I and Experiment II data, described in Section 2.10.1, except that threshold artifact rejection was not performed. These invasive recordings were much larger in amplitude than epidural EEG acquired in Experiment I and Experiment II. Thus when combined with a head-fixed condition, which limited interference from cardiorespiratory movements, artifact rejection was considered unnecessary.

Channel averaging was also performed as illustrated by Figure 5.2. This provided a visualisation of AEP waveforms from both shanks at different implantation depths/distances along each respective shank, simplifying visual comparisons of data as opposed to viewing waveforms from each channel (Ch1-32) in individual plots. In some instances whole-probe average data analysis are also presented.

Channel-specific artifacts were identified in some of the datasets. Firstly, crosstalk was observed between the synchronisation pulse (Ch0) and the first electrode channel (Ch1) of the recording system, characterised by an inverted square pulse from 0-50 ms occurring as each auditory stimulus was played. Energy output through the sync channel was evidently too high, however unfortunately this remained unnoticed for the majority of test sessions. Secondly, in some experiments middle channels Ch7 and Ch24 were contaminated with recurrent high-frequency noise from an unknown source. This interference was present during some test sessions but not others. Nevertheless for consistency these three channels were removed from all quantitative analysis.

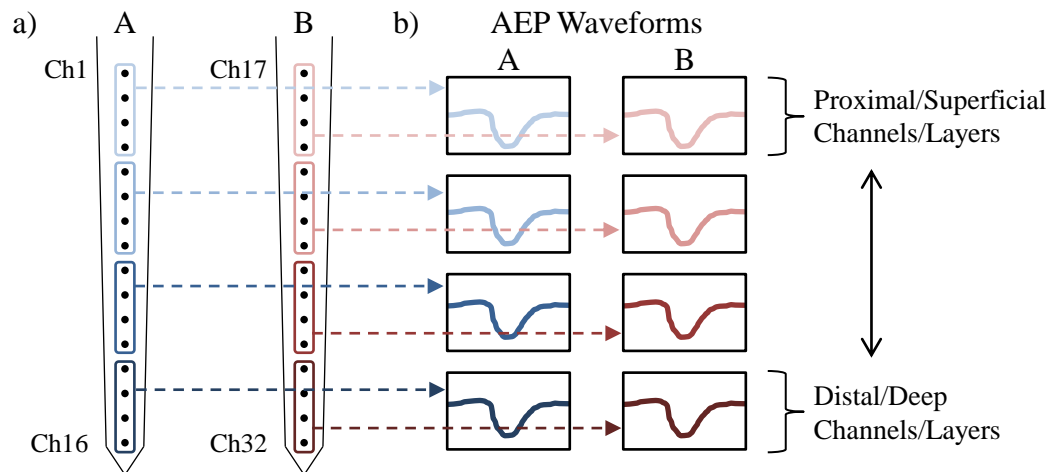


Figure 5.2 - Channel averaging used to analyse laminar auditory evoked responses This figure illustrates how channels are averaged together in groups of four to visualise auditory evoked potential (AEP) waveforms from proximal/superficial to distal/deep channels/layers. a) Schematic diagram of multichannel probe with 32 channels (Ch1-32) spaced over two 16 channel shanks (A and B). Channels are averaged together in groups of four as indicated. b) Example of AEP waveform plots produced by averaging channels illustrated with coloured annotations. This method allows a visualisation of AEPs in larger plots than would be possible if all 32 channels were presented in the same figure. While simplifying the data this approach retains differences between shanks and approximate channel depths; see Figure 5.7 for an example.

5.2.5 Auditory paradigms

Experiment III focussed on investigating stimulus frequency variations, although the protocol did incorporate a modified consecutive-repetition ($_{\text{mod}}\text{CR}$) paradigm which additionally examined duration and intensity effects. This was followed with a duration many-standards (dMS) paradigm with constant inter-stimulus interval (ISI) identical to Experiment I and Experiment II dMS paradigms. Frequency oddball (fOD), deviant-alone (fDA) and many-standards (fMS) paradigms were then presented before and after a 10 mg/kg i.p. ketamine administration. The rationale for each of these paradigms is provided in Section 2.7.

5.2.6 Stimuli properties

After probe implantation described in Section 2.5.3 and outlined in Section 5.2.3 above, a frequency response (FR) screening procedure was carried out. This is described in Section 2.8.3 and summarised here. Different frequency stimuli (2-32 kHz) were played at different sound intensities (40, 50, 60 and 70 dB) while recording local tissue electrophysiology. This aimed to 1) confirm probe placement within the auditory cortex, and 2) quickly acquire data for on-line analysis of the best frequency (BF) of locally recorded neurons.

This was important for selecting frequencies for subsequent auditory stimuli that would successfully evoke an auditory response due to the frequency sensitivity or tonotopic

behaviour of the auditory cortex (Section 1.2.2.3). Frequency response area (FRA) from each shank and the whole-probe of each subject were computed as described in Section 2.10.7. The FRA from the five ‘successful’ experiments are plotted in Figure 5.3. Possible reasons why this procedure did not achieve its first aim listed above for all subjects are discussed in Section 5.4.4. Table 5.1 provides stimulus frequencies for the fOD paradigm for each of these animals, determined by FR screening.

The BF was applied as the frequency for all stimuli other than ascending (BF+3 kHz) and descending (BF−3 kHz) frequency oddballs, and fMS paradigm stimuli. Standard stimuli were therefore 50 ms duration, *BF* frequency and 70 dB intensity with a common 450 ms ISI. In the _{mod}CR paradigm 50 ms, 100 ms and 150 ms duration, BF+3 kHz and BF−3 kHz frequency, 60 dB and 80 dB intensity stimuli were presented to explore these physical dimensions of sound variance (specified in Table 2.6). In the fMS paradigm ten stimuli varying only in frequency ranged from BF−4 kHz to BF+5 kHz in 1 kHz increments. All stimuli were monophonic pure tones with 5 ms rise/fall times (in contrast to instantaneous rise/fall times used in Experiment I and Experiment II). Full details of auditory stimuli parameters in Experiment III are provided in Section 2.8.3.

Subject	Descending Oddball	Standard (BF)	Ascending Oddball
36 (WT, female)	9 kHz	12 kHz	15 kHz
74 (HET, male)	9 kHz	12 kHz	15 kHz
75 (HET, male)	11 kHz	14 kHz	17 kHz
76 (WT, male)	13 kHz	16 kHz	19 kHz
77 (HET, female)	9 kHz	12 kHz	15 kHz

Table 5.1 - Auditory stimuli frequencies determined for Experiment III subjects Details of standard, ascending and descending oddball stimuli frequencies calculated for the five successful experiment animals are provided. The best frequency (BF) computed from the frequency response (FR) screening procedure was selected as the standard; oddball frequencies varied by ± 3 kHz from the BF.

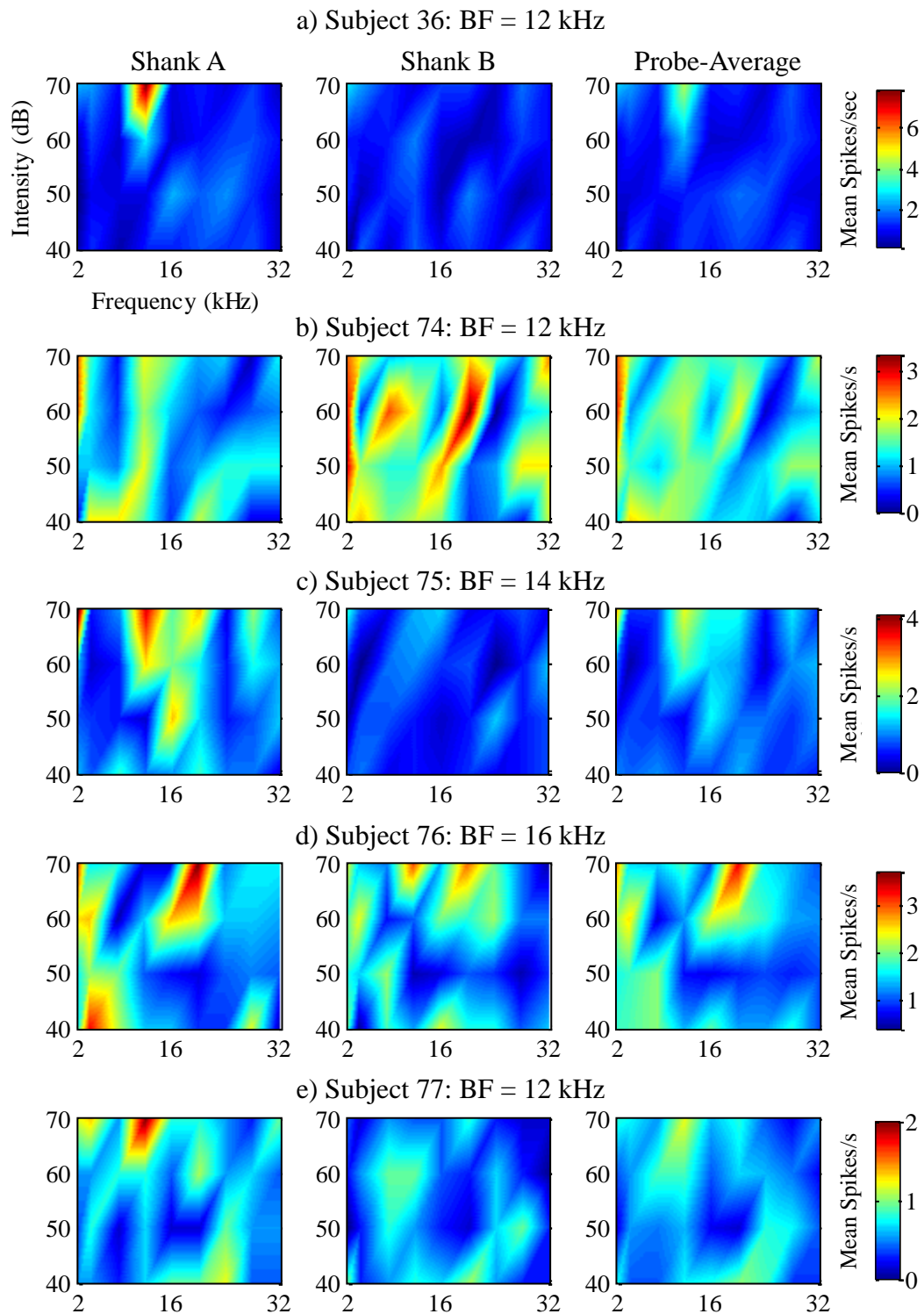


Figure 5.3 - Frequency Response Area plots from Experiment III subjects The frequency response (FR) screening procedure led to these plots being produced ‘on-line’ during the experiment to determine the best frequency (BF) of neural tissue located nearby Shank A (Ch1-16), Shank B (Ch17-32) and the Probe-Average (Ch1-32). These data are shown from subjects a) 36, b) 74, c) 75, d) 76, and e) 77. Colour scales on the right hand side indicate multi-unit activity (MUA) as mean number of spikes per second during auditory stimulation. The frequency evoking greater overall MUA was determined to be the BF for each animal, which was used in subsequent auditory paradigms (see Table 5.1).

5.2.7 Experimental protocol

After surgery the 32-channel two-shank linear electrode arrangement probe was slowly implanted, described in Section 2.6.2 and addressed above. Once in place, the FR screening procedure was performed (Section 2.8.3) to determine the BF of local neurons. This BF was applied as the central frequency in the auditory paradigms which followed FR screening, with all other stimuli frequencies determined by set variances from the BF. The _{mod}CR, dMS, fOD, fDA and fMS paradigms were presented before injecting 10 mg/kg i.p. ketamine via an implanted drug delivery system, after which fOD, fDA and fMS paradigms were repeated. This experimental protocol and paradigm presentation sequence is outlined in Section 2.9.3.

5.2.8 Current source density analysis

Current source density (CSD) analysis described in Section 2.10.5 was applied to multichannel LFP recordings from the five animals in Experiment III which displayed clear auditory evoked potentials. The main sink and source channels from Shank A and Shank B were computed for each subject, with the results presented in Table 5.2. However, there were some discrepancies in these results which are noted, perhaps indicative of methodological issues, that prevented alignment of datasets.

Subject	Shank A Sink	Shank A Source	Shank B Sink	Shank B Source
36 (WT, female)	Ch10	Ch12	Ch28 (12)	Ch19 (3)
74 (HET, male)	Ch9	Ch7	Ch18 (2)	Ch19 (3)
75 (HET, male)	Ch3	Ch7	Ch21 (5)	Ch25 (9)
76 (WT, male)	Ch5	Ch8	Ch30 (14)	Ch21 (5)
77 (HET, female)	Ch4	Ch7	Ch18 (2)	Ch20 (4)

Table 5.2 - Main current sink and source channels from current source density analysis of urethane-anaesthetised mice in Experiment III Current source density (CSD) analysis, as illustrated in Figure 5.4, was performed on data from each subject and the resulting main sink and source channels from Shank A and Shank B are detailed in this table (relative channels for Shank B to compare with Shank A are shown *in brackets*; lower channel number suggests shanks are implanted more deeply). It is expected that the main sink channel should appear in a more superficial layer than the source, as shown in Figure 5.4. Three instances where this assumption was false are labelled in red; these may indicate methodological discrepancies, e.g. incorrect probe placement.

An example of CSD analysis from Subject 75 data is provided in Figure 5.4. This displays the main sink (0 μm relative depth to LIII/IV) and source channels in red and blue horizontal dashed lines, respectively, in Figure 5.4a for Shank A and Figure 5.4b for Shank B. Each shank had a working electrode distance of 800 μm . Average waveforms from combined sink channels and combined source channels from Shank A and Shank B are plotted in Figure 5.4c, displaying opposite polarity peaks at approximately 25 ms post stimuli onset, characteristic of auditory cortex input from the thalamic recipient layers LIII/IV. Essentially this data suggests that shanks may have been positioned in the auditory cortex at different relative depths, perhaps due to the condition illustrated in Figure 5.1c, and this should be considered when interpreting the results which follow.

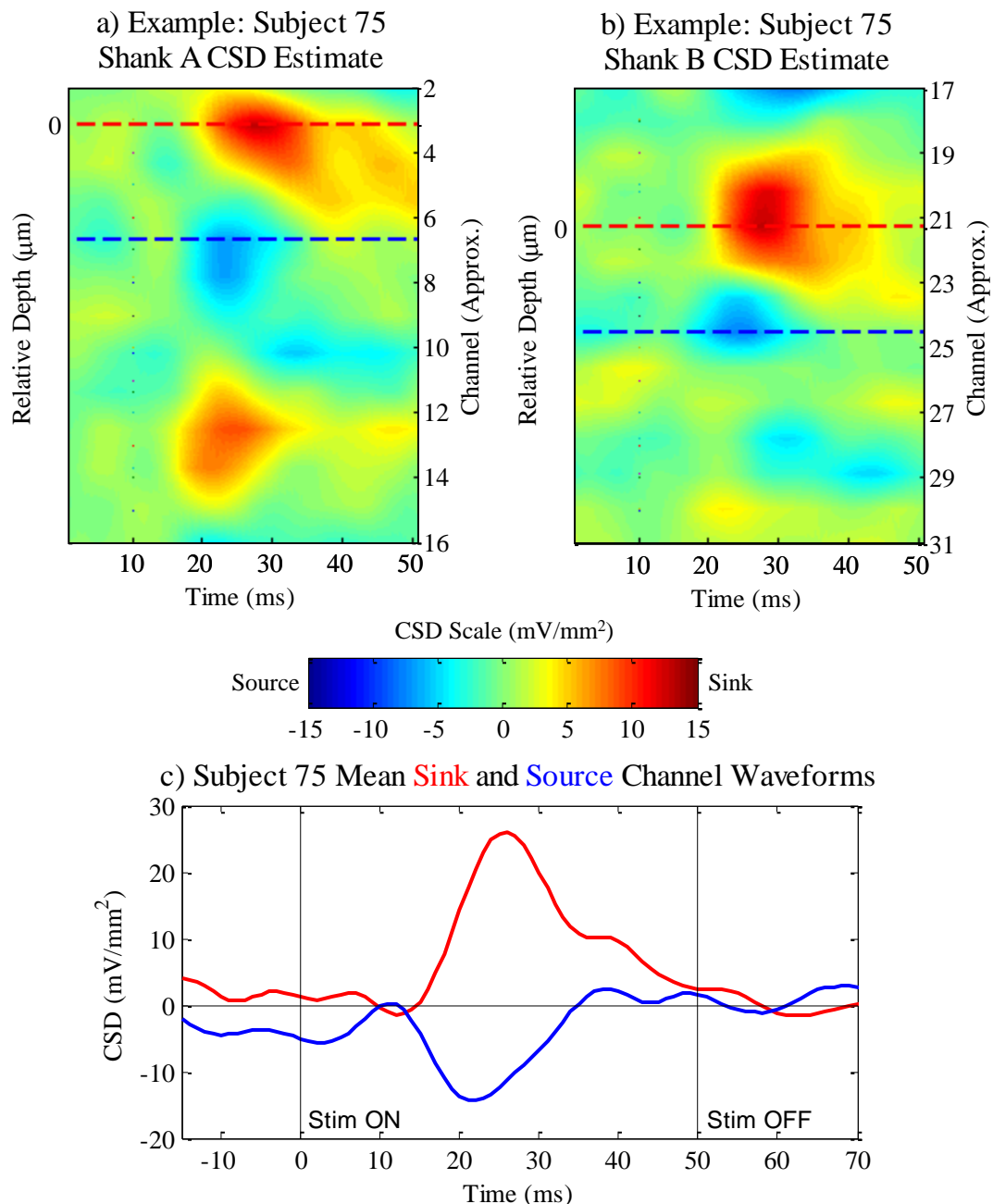


Figure 5.4 - Example of current source density estimate of electrode depth from Subject 75 (HET, male) Data from subject 75 was used to generate this current source density (CSD) estimate for a) Shank A (Ch2-16*) and b) Shank B (Ch17-32) from the two-shank multichannel probe. These plots are an average of the first hundred stimuli presented in the modified consecutive-repetition paradigm, employing the best frequency (BF), plotted across the time during which stimulation is applied. Sink regions (red) display net positive CSD and source regions (blue) display net negative CSD. The maximum sink channel, thought to reflect the main thalamic input layer to the cortex (III/IV), on each probe is marked with a horizontal red dashed line labelled 0 μm relative depth; the counterpart source channel is shown with a blue dashed line. Approximate electrode channel numbers are provided on the second y-axis of each plot; not exact because of the mathematical operators required to compute the CSD (Section 2.10.5). However, this analysis suggests Shank A is implanted further than Shank B. c) Mean sink and source channel waveforms from the whole probe. *Ch1 from Shank A was removed from analysis because of a crosstalk artifact from the synchronisation pulse.

5.3 Results

Experiment III focussed on investigating the frequency mismatch response (fMMR) and the effects of frequency variation on auditory evoked activity in the primary auditory cortex of urethane-anaesthetised mice. Nevertheless, the effects of stimuli duration and intensity variations were also studied using a modified consecutive-repetition ($_{\text{mod}}\text{CR}$) paradigm (Section 2.8.3). This results section is therefore presented following the same general order as Experiment I and Experiment II for consistency, with findings from stimuli duration, frequency, then intensity effects presented in separate subsections below. These are followed by an examination of spiking activating before and after administration of 10 mg/kg i.p. ketamine.

5.3.1 *Duration paradigms and laminar responses in urethane-anaesthetised mice*

In the $_{\text{mod}}\text{CR}$ paradigm the first three sequences of 100 stimuli each used the BF (determined individually for each subject), 70 dB intensity, a 450 ms ISI and 5 ms rise/fall times; the only difference between them being duration. The first 100 stimuli were 100 ms, the second were 150 ms and the third were 50 ms in duration. Results from these stimuli are reported in Section 5.3.1.1. Additionally, re-referencing was performed to examine differences between superficial and deep channel AEP waveforms in Section 5.3.1.2, offering a different perspective of the stimuli offset response. Findings from the duration many-standards (dMS) paradigm, including analysis of multi-unit activity correlates of stimuli onset and offset responses, are presented in Section 5.3.1.3.

5.3.1.1 *Offset responses vary with channel depth*

The 32 channel silicon probes used to record electrophysiological data in Experiment III had two 16-channel shanks, labelled Shank A (Ch1-16) and Shank B (Ch17-32). Auditory evoked potentials in response to duration-varying stimuli in the $_{\text{mod}}\text{CR}$ paradigm from Shank A are shown in Figure 5.5, with corresponding waveforms from Shank B shown in Figure 5.6. Stimuli onset (N1) and offset responses (P_{offset}) are observed in the AEP from both shanks, although interestingly the morphology of P_{offset} appears to change with channel depth. For example, the P_{offset} response at Ch2 (proximal/superficial channel) of Shank A displays a positive amplitude peak, in contrast with Ch16 (distal/deep channel) which does not reach overall positive amplitude, only a gradation of negative amplitude and return to baseline.

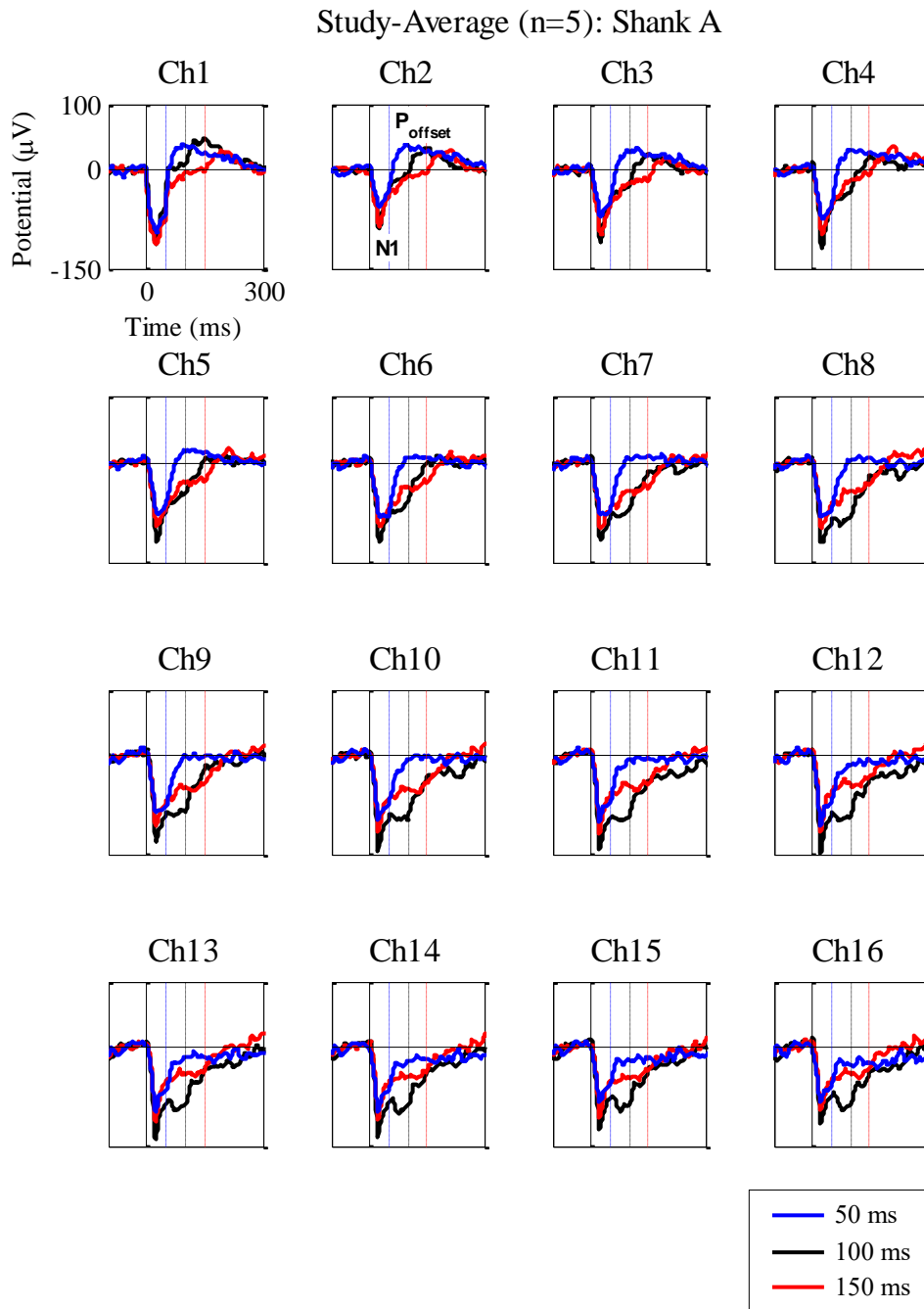


Figure 5.5 - Grand-average auditory evoked potentials to different duration stimuli across multichannel probe electrodes Ch1-16 (Shank A) Three different duration stimuli presented first in the modified consecutive-repetition paradigm in the order: 100 ms, 150 ms, then 50 ms, are seen to generate onset (N1) and offset (P_{offset}) responses. P_{offset} deflections appear more pronounced in superficial channels (e.g. Ch1-4) than deeper channels (e.g. Ch13-16). Stimulus order may play a role in modulating the N1 peak, with the first (100 ms) eliciting the greatest negative potential, followed by the second (150 ms) then the third (50 ms). Crosstalk from the sync pulse induced a negative square-wave artifact in Ch1 from 0-50 ms; therefore this channel is removed from any quantitative analysis. Coloured vertical lines are used to indicate respective offset latencies for each duration stimulus. Comparable waveforms from Shank B are plotted in Figure 5.7.

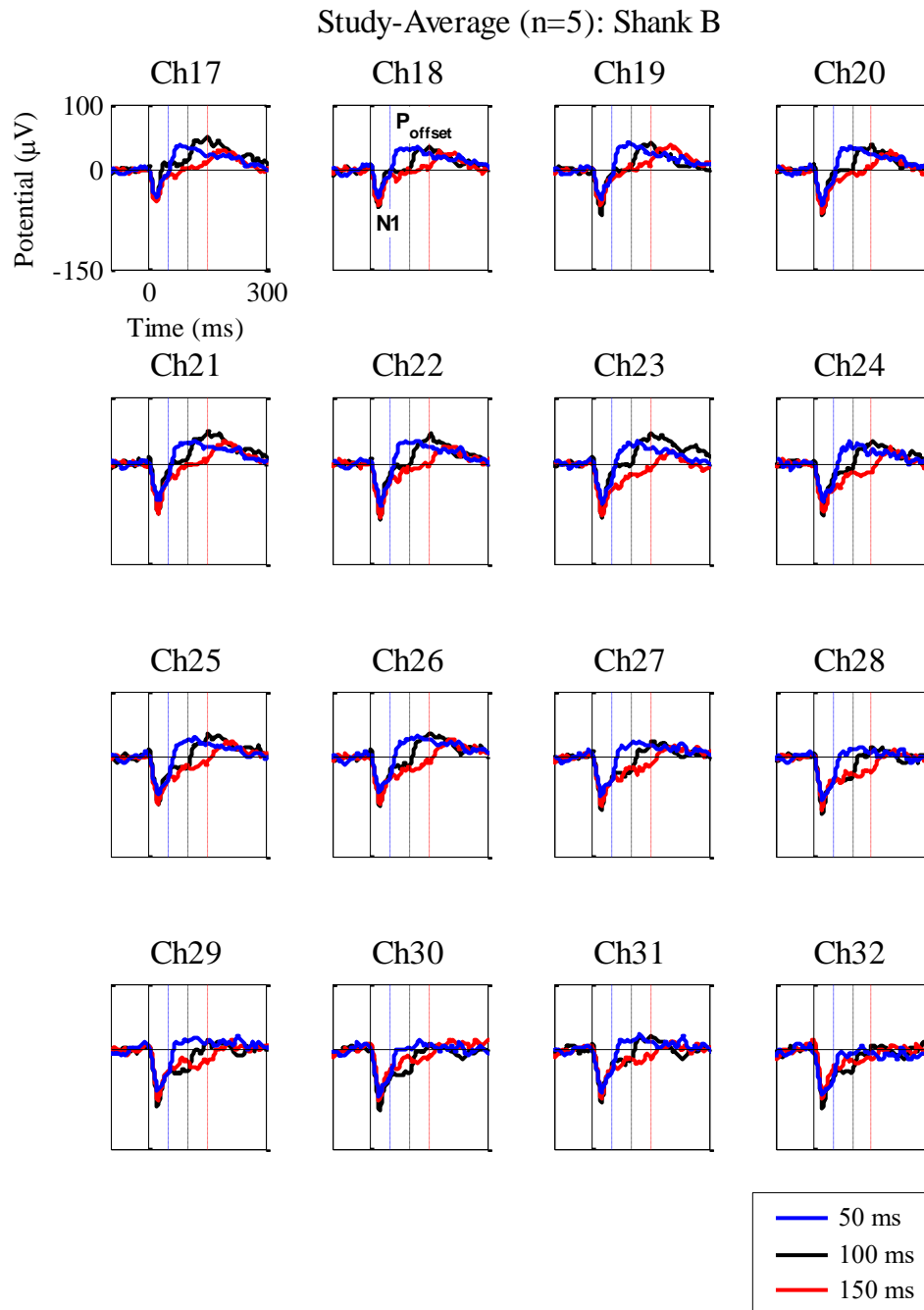


Figure 5.6 - Grand-average auditory evoked potentials to different duration stimuli across multichannel probe electrodes Ch17-32 (Shank B) These waveforms correspond with Shank A auditory evoked potentials to different duration stimuli plotted in Figure 5.5. Onset (N1) and offset (P_{offset}) responses are labelled on the CH18 plot. The morphology of P_{offset} appears to change in deep layers (e.g. Ch29-32); in comparison with Figure 5.5 this morphology change occurs in ‘deeper’ channels and is less extensive. This may be indicative of uneven shank implantation. Coloured vertical lines indicate stimuli offset times.

Waveforms produced by averaging channels together in groups of four (apart from Ch1 which was contaminated with crosstalk, Ch7 and Ch24 which suffered from interference) as illustrated by Figure 5.2 are plotted in Figure 5.7. These plots provide an easier visual comparison of AEP waveforms evoked by different duration stimuli at different distances along Shank A and Shank B. Proximal channels were relatively superficial whereas distal channels were implanted deeper in the auditory cortex. Although no histology was performed to verify probe placement, the presence of an auditory response may be combined with the known probe geometry to reasonably assert the approximate channel locations within the cortex.

The N1 and P_{offset} waveform features from 50 ms, 100 ms and 150 ms duration stimuli in the modified CR paradigm are quantified in Figure 5.8. Whole-probe averaged control (WT) and *Map2k7^{+/-}* (HET) group AEPs are plotted in Figure 5.8a and Figure 5.8b, respectively. Repeated measures ANOVA tests were applied to this data with stimulus duration as a within-subjects factor and genotype and gender as between-subjects factors.

This analysis revealed no significant effects of genotype [$F_{1,1} = .531$, $p = .599$], gender [$F_{1,1} = .031$, $p = .888$] or stimulus duration [$F_{1,1} = .014$, $p = .924$] on N1 peak latency shown in Figure 5.8c. Although it appears that N1 peak amplitude decreases with stimulus order (Figure 5.8d), this was not statistically significant [$F_{1,1} = 1.064$, $p = .490$]. There were also no significant differences between genotypes [$F_{1,1} = .170$, $p = .751$] or genders [$F_{1,1} = .713$, $p = .554$] on N1 peak amplitude. Close inspection of this data may suggest WT mice display greater reduction of N1 peak amplitude with repeated stimulation, potentially underlying the enlarged N1 found in HET mice.

P_{offset} peak latency measurements graphed in Figure 5.8e displayed no significant effects of genotype [$F_{1,1} = 12.751$, $p = .174$], gender [$F_{1,1} = 7.435$, $p = .224$] or stimulus duration [$F_{1,1} = 8.247$, $p = .213$]. Also, P_{offset} peak amplitudes in Figure 5.8e were not significantly influenced by stimulus duration [$F_{1,1} = 8.969$, $p = .205$], genotype [$F_{1,1} = 3.132$, $p = .327$], gender [$F_{1,1} = .010$, $p = .935$], although it appears as though shorter duration stimuli evoke greater P_{offset} peaks. This analysis lacks statistical power due to low sample numbers.

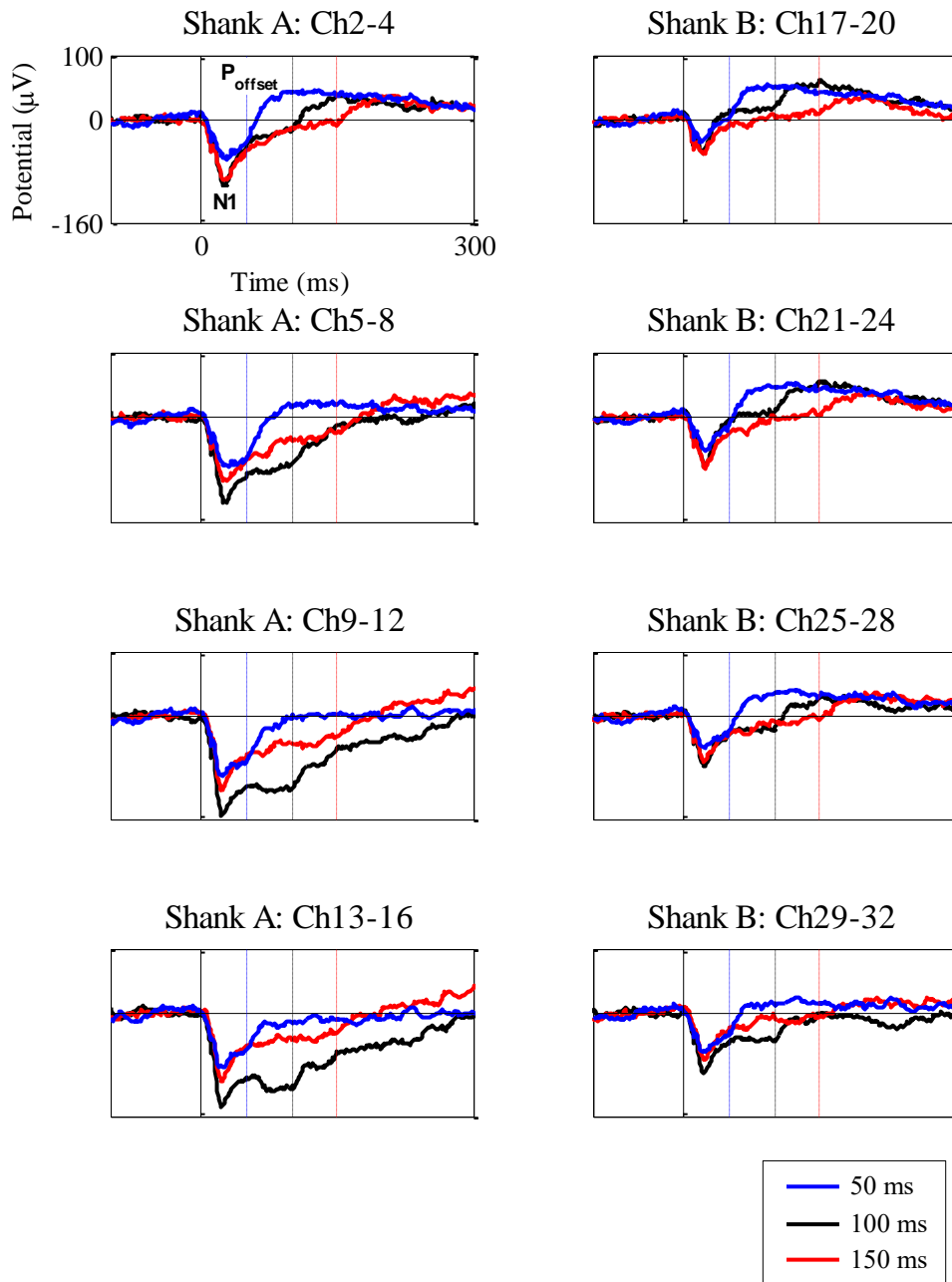


Figure 5.7 - Channel-averaged grand-average auditory evoked potentials to different duration stimuli in Experiment III Channels from each shank are averaged in groups of four as illustrated in Figure 5.2 (except from Ch1, Ch7 and Ch24 which were removed because of noise artifacts). Ch2-4 from Shank A and Ch17-20 from Shank B reflect the most superficial channels, and Ch13-16 from Shank A and Ch29-32 from Shank B reflect the deepest channels, from each shank of the multichannel probe. The morphology of offset potentials is seen to vary more dramatically from superficial to deep channels of Shank A compared with Shank B, perhaps indicative of uneven probe placement (e.g. Figure 5.1c) as suggested by CSD analysis (Figure 5.4 and Table 5.2).

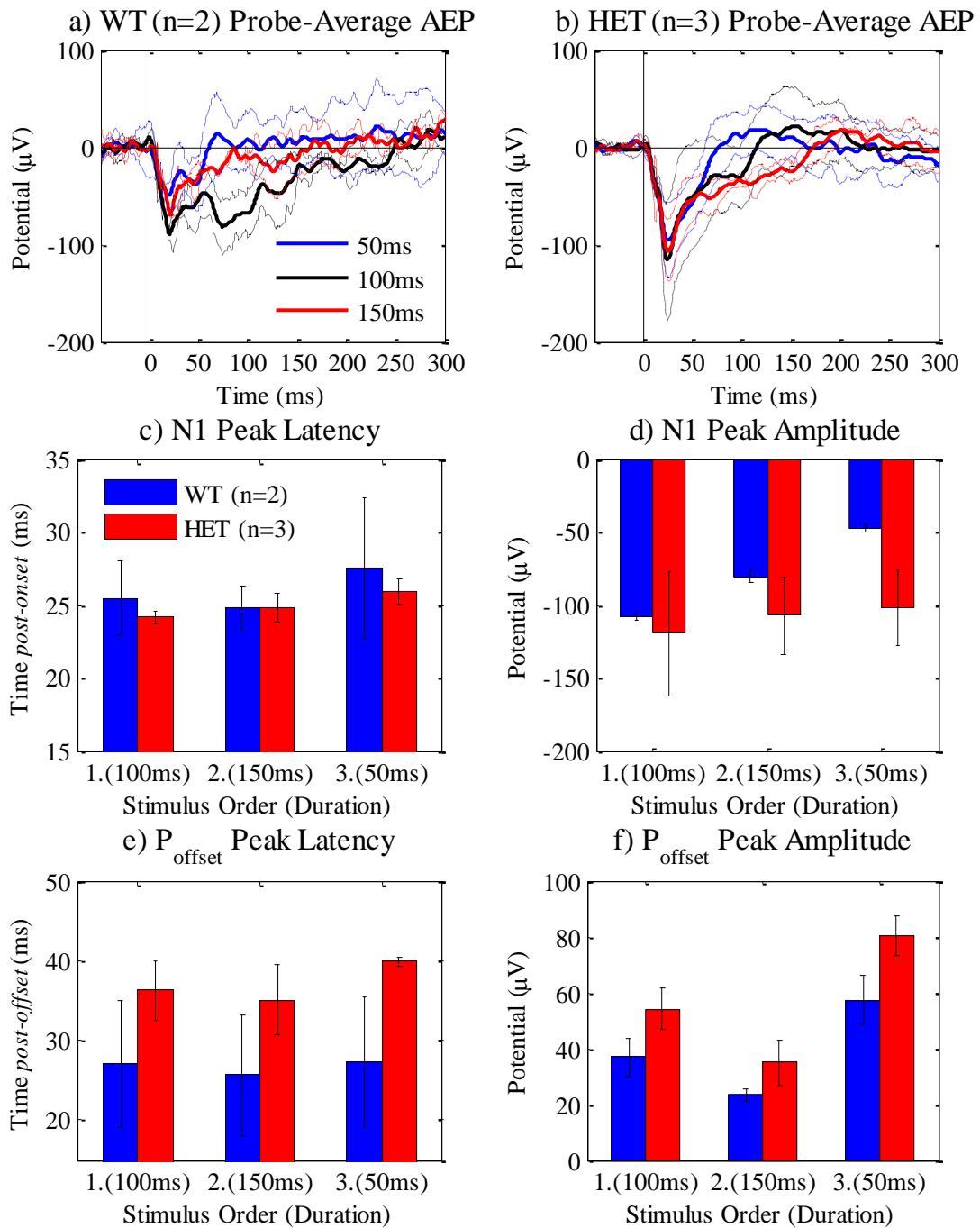


Figure 5.8 - Quantification of onset and offset responses to different duration stimuli from wild-type and *Map2k7*^{+/-} mice in Experiment III Whole-probe average (Ch1-32; with Ch1, Ch7 and Ch24 omitted due to noise/artifacts) auditory evoked potential (AEP) waveforms are plotted with \pm sem displayed as dashed lines for a) wild-type control (WT) and b) *Map2k7*^{+/-} (HET) groups. The following measures were quantified from these waveforms from each subject. c) Onset response (N1) peak latency measured from 0-50 ms post stimuli onset, displaying no effects of genotype, stimuli duration or order. d) N1 peak amplitude which displays an apparent reduction in amplitude with increasing stimulus order. e) Offset response (P_{offset}) peak latency measured from 0-50 ms post stimuli offset, showing no significant differences. f) P_{offset} peak amplitudes showing a trend towards greater amplitudes in response to shorter duration stimuli. Quantification of P_{offset} was performed on waveforms with 10 ms pre-offset baseline correction (e.g. Figure 3.2) and bar charts display group mean \pm sem.

5.3.1.2 *Re-referencing to deep channels reveals slow positive amplitude response in superficial channels underlying the offset response*

Assessing waveforms from different duration stimuli in Figure 5.5, Figure 5.6 and Figure 5.7, it is apparent that the AEP in superficial channel recordings are different from those observed in deep channels. Morphology of the offset response (P_{offset}) changes from a positive amplitude peak in proximal/superficial channels to predominantly negative potential in distal/deep electrode recordings. To visualise this difference in evoked electrophysiology re-referencing was performed, removing signals common to deep channels. Shank A electrodes were re-referenced to Ch16 and Shank B electrodes were re-referenced to Ch32 to isolate superficial activity which may cause this positive amplitude P_{offset} deflection.

Figure 5.9 displays AEP waveforms from superficial, deep, and re-referenced recordings from Shank A and Shank B to 50 ms, 100 ms and 150 ms duration stimuli. These waveforms illustrate the difference between superficial and deep cortical responses to auditory stimulation. In superficial channels there appears to be a mechanism which counteracts the negative potential induced by stimulation onset, restoring the measured activity to baseline before offset. When auditory stimulation is then removed this counteracting response is observed as a positive amplitude P_{offset} deflection, although its origins precede stimuli offset latency. Additionally, deeper channels tend to display greater N1 peak amplitudes.

Statistical comparison of superficial and deep channel AEP data using two-sample t-tests suggested regions of significant difference ($p < .05$) between superficial and deep channels were present. Time points where these differences were found are indicated in Figure 5.9 using solid black lines.

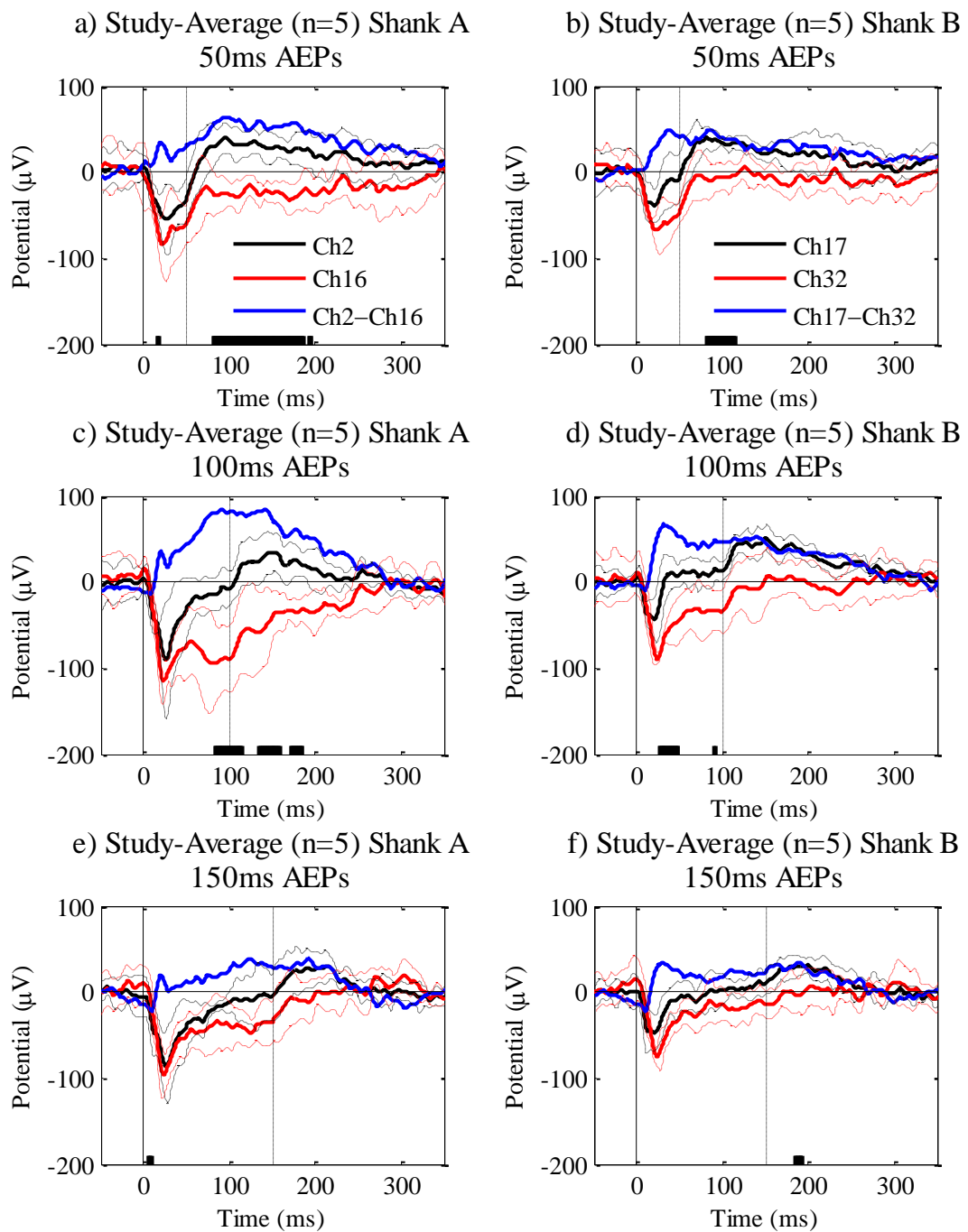


Figure 5.9 - Difference between proximal/superficial and distal/deep channel auditory evoked potentials to different duration stimuli The superficial-most channel (black) of Shank A (Ch2; Ch1 omitted) and Shank B (Ch17), deepest channel (red) of Shank A (Ch16) and Shank B (Ch32), and superficial re-referenced to deep channel (blue) from Shank A (Ch2-Ch16) and Shank B (Ch17-Ch32) auditory evoked potential (AEP) waveforms are plotted. AEPs to 50 ms stimuli are shown for a) Shank A, and b) Shank B; 100 ms AEPs are shown for c) Shank A, and d) Shank B; and 150 ms AEPs are shown for e) Shank A, and f) Shank B. These waveforms suggest that the positive peak amplitude offset response (P_{offset}) observed in superficial channels but not in deep channels may actually be caused by an early response which returns potential to baseline in superficial channels before stimuli offset occurs. T-tests revealed statistically significant ($p < .05$) difference between superficial and deep channels, shown in plots with black bars.

5.3.1.3 Group analysis reveals little evidence of multi-unit activity correlates of stimuli onset and offset responses

Results from the dMS paradigm are analysed in Figure 5.10. The waveforms in Figure 5.10a display N1 and P_{offset} responses, although P_{offset} peaks are comparably more difficult to distinguish than in Experiment I (e.g. Figure 3.8), perhaps due to the lower number of subjects and the observed effect of channel depth. The mean AEP shown in Figure 5.10b was subtracted from each individual AEP in Figure 5.10a to isolate the characteristic offset response plotted in Figure 5.10c. This method was applied to data from conscious subjects in Section 4.3.1.3.

Overall multi-unit activity (MUA) from all subjects from -20 ms to 100 ms about stimuli onset is plotted in Figure 5.10d, showing no discriminable effect of auditory stimulation onset. The same analysis performed from -20 ms to 100 ms about stimuli offsets are plotted in Figure 5.10e, also displaying no apparent effects of stimuli offsets on MUA. The absence of overall MUA correlates of N1 or P_{offset} responses may be due to methodological considerations discussed in Section 5.4.4.

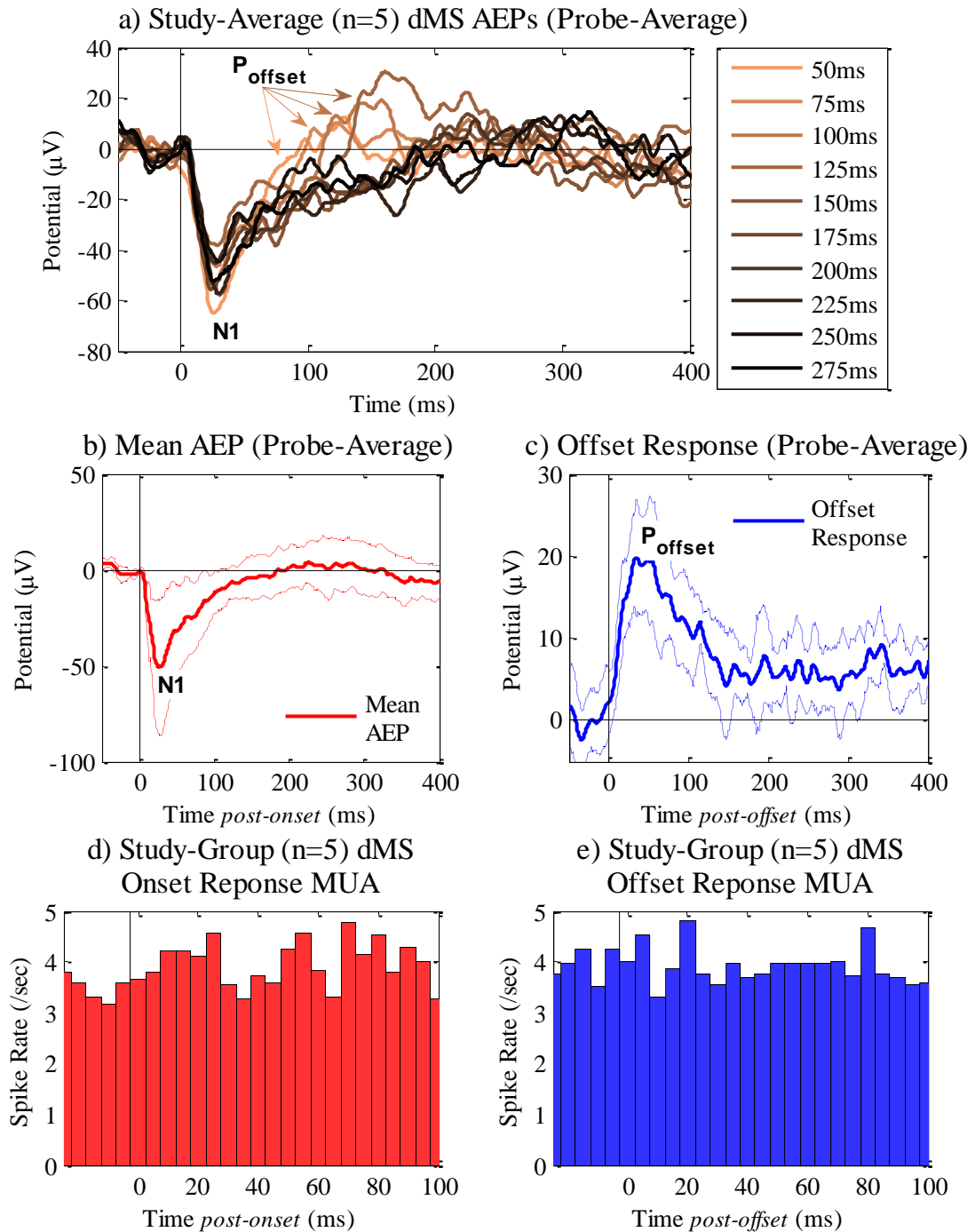


Figure 5.10 - The effects of stimulus duration on auditory evoked potentials and multi-unit activity in Experiment III These data are from the duration many-standards (dMS) paradigm where ten stimuli of different duration were played 100 times each in random order. All channels in the multichannel probe apart from noted exceptions (Section 5.2.4) are used here. a) Grand average auditory evoked potential (AEP) waveforms to 10 dMS stimuli. These are not as easily interpreted as Experiment I data (e.g. Figure 3.8), however some offset responses (P_{offset}) may be observed protruding from the underlying waveform. b) The mean AEP produced by averaging together those plotted in (a). c) The offset response characterised by subtracting the mean AEP in (b) from each individual AEP in (a), synchronising each waveform to stimuli offset times and averaging together, as illustrated in Figure 4.5 and Figure 4.6. d) Overall mean onset response multi-unit activity (MUA), showing no evidence of correlation with the N1 peak. e) Overall mean offset response MUA, also showing no evidence of correlation with the AEP waveform.

5.3.2 Frequency paradigms and laminar response in urethane-anaesthetised mice

Experiment III included frequency oddball (fOD), deviant-alone (fDA), and many-standards (fMS) paradigms, the results of which are presented below. Firstly, findings from the modified consecutive-repetition (_{mod}CR) using three different frequency stimuli are reported, as for stimuli duration (Section 5.3.1.1) and intensity (Section 5.3.3.1) manipulations. Data analyses from the fMS paradigm are then reported, followed by an assessment of the frequency mismatch response (fMMR) evoked by fOD and fDA paradigms. A single-subject analysis of multi-unit activity (MUA) evoked during the fDA paradigm is then provided.

5.3.2.1 Frequency effect in modified consecutive-repetition paradigm

In the _{mod}CR paradigm the best frequency (BF) determined for each individual subject (see Table 5.1), BF+3 kHz and BF-3 kHz frequency stimuli were presented 100 times each. These were all 50 ms in duration, 70 dB sound intensity, had 5 ms rise/fall times and a 450 ms inter-stimulus interval. Overall grand-average AEP waveforms from these three frequency stimuli are plotted in Figure 5.11 for Shank A and Figure 5.12 for Shank B. These waveforms appear to suggest that BF stimuli evoke greater magnitude onset (N1) and offset (P_{offset}) responses than the other two non-BF stimuli.

N1 and P_{offset} responses evoked by BF, BF+3 kHz and BF-3 kHz frequency stimuli AEPs from the _{mod}CR paradigm are quantified in Figure 5.13. These were measured from the whole-probe averages; omitting specific channels corrupted with noise artifacts (see Section 5.2.4). Grand-average AEP waveforms from the WT control group are plotted in Figure 5.13a and those from the *Map2k7*^{+/-} (HET) group are plotted in Figure 5.13b. N1 peak latency quantified in Figure 5.13c shows no statistically significant difference between stimulus frequencies [$F_{1,1} = .533$, $p = .598$], genotypes [$F_{1,1} = .053$, $p = .856$] or genders [$F_{1,1} = .227$, $p = .692$]. Figure 5.13d appears to display that larger N1 peak amplitudes are elicited by BF stimuli compared with BF+3 kHz or BF-3 kHz stimuli; however this is not statistically significant [$F_{1,1} = .690$, $p = .559$]. There are also no significant differences in N1 peak amplitude between genotypes [$F_{1,1} = 3.453$, $p = .314$] or genders [$F_{1,1} = 13.428$, $p = .170$]. Likewise there are no significant effects of stimulus frequency [$F_{1,1} = 1.263$, $p = .463$], genotype [$F_{1,1} = 22.523$, $p = .132$] or gender [$F_{1,1} = 5.173$, $p = .264$] on P_{offset} peak latency as shown in Figure 5.13e. There are also no significant effects of frequency [$F_{1,1} = 0.82$, $p = .822$], genotype [$F_{1,1} = .146$, $p = .768$] or gender [$F_{1,1} = 1.350$, $p = .452$] on P_{offset} peak amplitude in Figure 5.13f. Again, the absence of statistical significance is symptomatic of very low sample numbers.

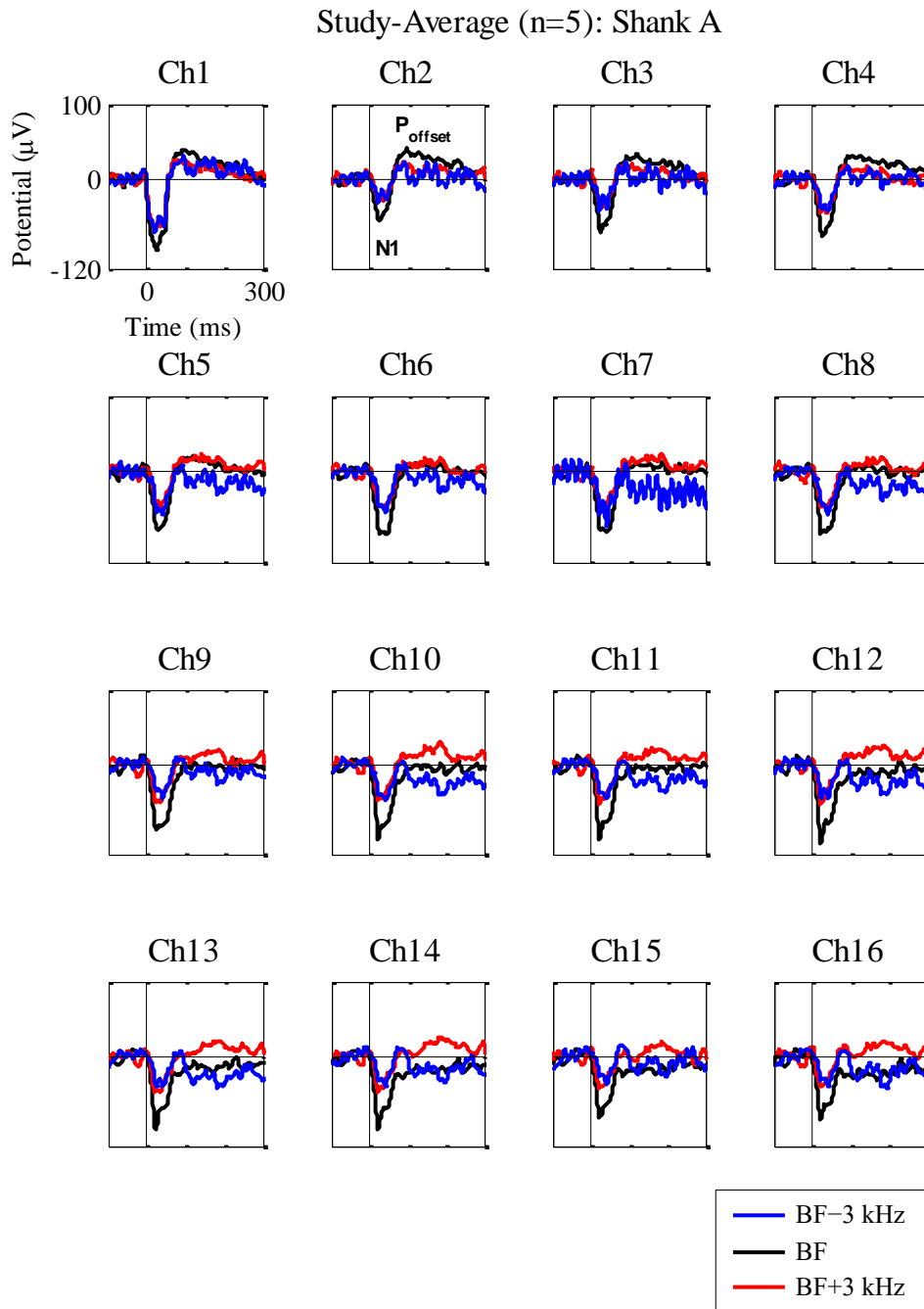


Figure 5.11 - Grand-average auditory evoked potentials to different frequency stimuli across multichannel probe electrodes Ch1-16 (Shank A) These plots display the auditory evoked potential (AEP) response to three different frequency stimuli; the best frequency (BF; black), BF+3 kHz (red) and BF-3 kHz (blue). By visual inspection it appears as though BF stimuli evoke greater onset (N1) and offset (P_{offset}) features of the AEP. This may suggest that the frequency response screening procedure was reasonably successful, and tonotopy is observed in these recordings. Artifacts are observed in Ch1 and Ch7, as discussed in Section 5.2.4, which are therefore removed from further quantitative analysis presented in Figure 5.13. Equivalent AEPs from Shank B are plotted in Figure 5.12.

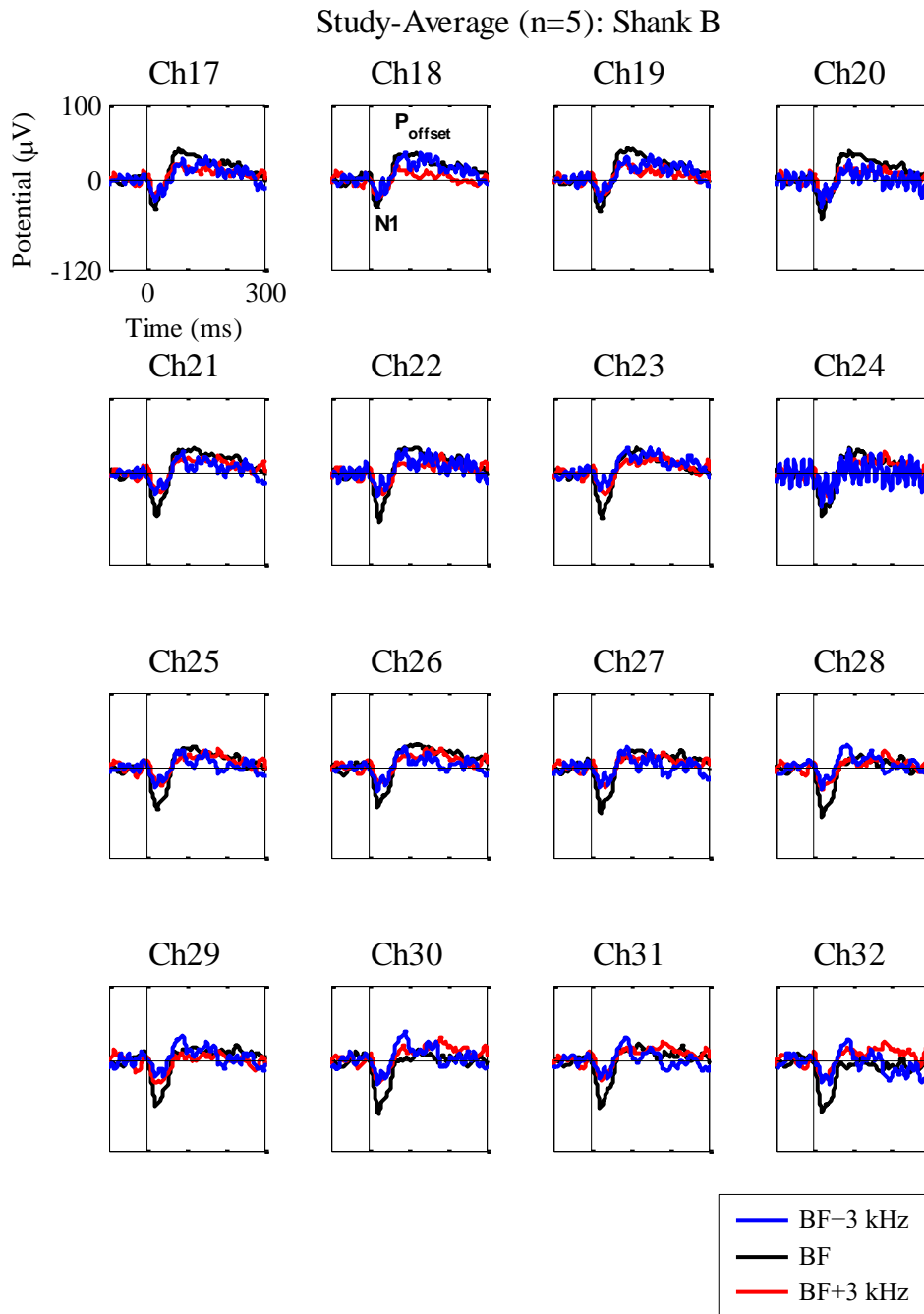


Figure 5.12 - Grand-average auditory evoked potentials to different frequency stimuli across multichannel probe electrodes Ch17-32 (Shank B) Here the evoked waveforms from best frequency (BF; black), BF+3 kHz (red) and BF-3 kHz (blue) stimuli presented in the modified consecutive-repetition ($_{mod}CR$) paradigm are plotted. It may be noted from visual inspection that BF stimuli tend to elicit a larger amplitude response than non-BF stimuli. This may reflect frequency sensitivity or tonotopy of the auditory cortex observed in these local field potential measurements from micro-electrodes. Interference is present in Ch24 which was therefore removed from quantitative analysis presented in Figure 5.13.

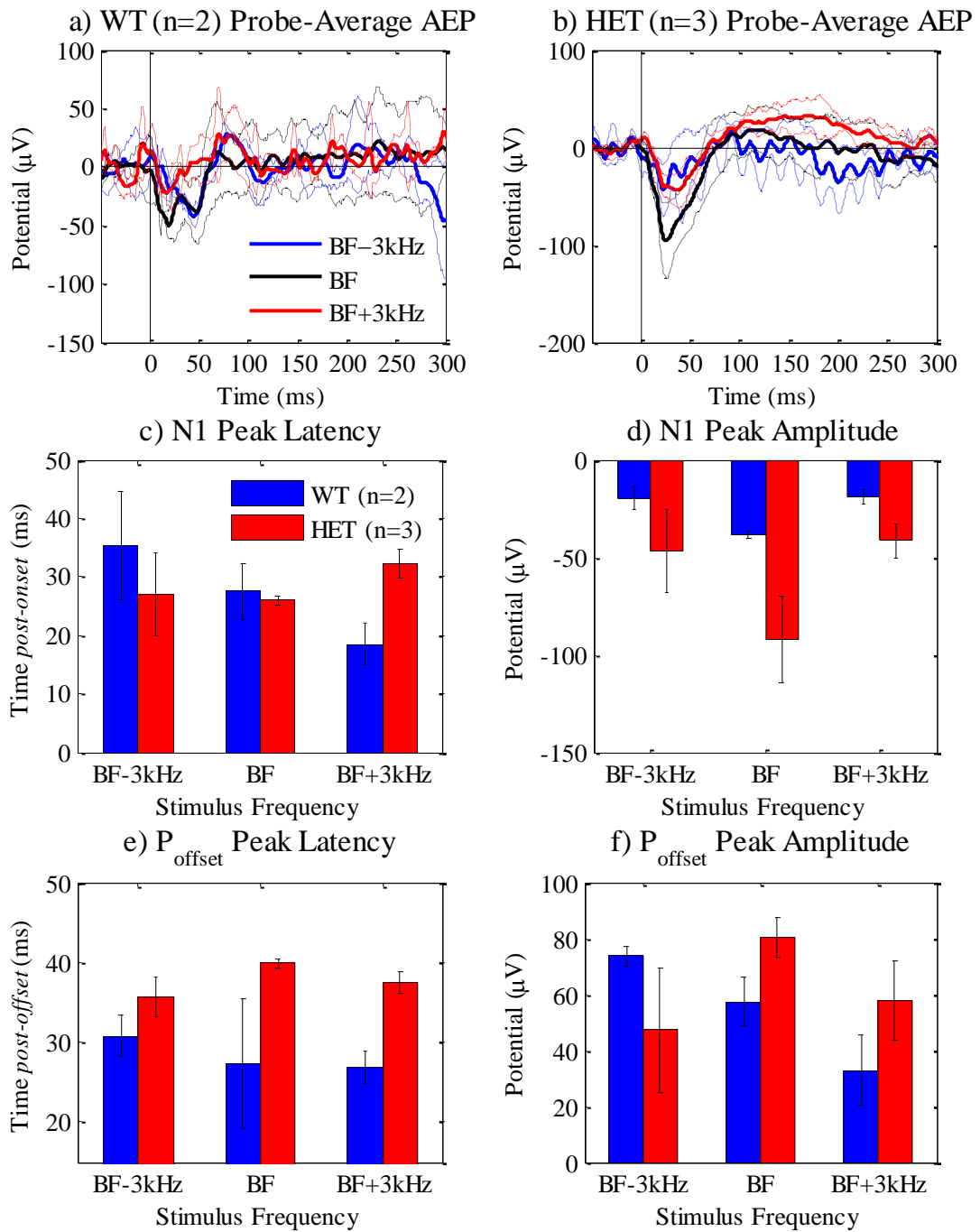


Figure 5.13 - Quantification of onset and offset responses to different frequency stimuli from wild-type and *Map2k7*^{+/-} mice in Experiment III This analysis compares responses to best frequency (BF) and BF±3 kHz stimuli (50 ms, 70 dB) presented in the modified consecutive-repetition paradigm. Probe-average auditory evoked potential (AEP) waveforms are plotted for a) wild-type control (WT) and b) *Map2k7*^{+/-} (HET) groups, with ±sem plotted in dashed lines. The following measurements were quantified: c) Onset response (N1) peak latency; d) N1 peak amplitude displaying a larger amplitude response to the optimum responding frequency (BF), determined for each subject individually during the frequency response pre-screening procedure; e) Offset response (P_{offset}) peak latency, and; f) P_{offset} peak amplitudes showing somewhat less specificity for the BF. P_{offset} measurements were taken from 10 ms pre-offset baseline corrected waveforms (Figure 3.2). Data are presented as group means ±sem.

5.3.2.2 *Frequency effect in the many-standards paradigm*

Importance of the BF is analysed further now from fMS paradigm data. Auditory evoked potential waveforms from ten different frequency stimuli presented in the fMS paradigm are plotted in Figure 5.14a. These are grand-averages of the whole-probe average AEP from each subject. It appears as though BF and BF+2 kHz frequency stimuli generate greater amplitude onset response peaks than other frequency stimuli. Bar charts of N1 peak amplitudes (Figure 5.14b) measured from the AEP evoked by each separate frequency also suggest this may be the case, although BF+2 kHz AEP measurements have a respectively large error bar. Boxplots plotted in Figure 5.14c illustrate that a single outlier is responsible for this enlarged N1 peak in response to BF+2 kHz frequency stimuli. Before removing this outlier results of a one-way ANOVA did not achieve the threshold for statistical analysis [$F_{1,8} = 4.937$, $p = .057$]. However, when this outlier is removed from the analysis a significantly greater [$F_{1,7} = 19.893$, $p = .003$] N1 peak amplitude is observed in response to BF stimuli compared with non-BF stimuli, as illustrated in Figure 5.14d. This suggests at least partially that the FR screening procedure has achieved its aim of determining the most effective auditory stimulus frequency for eliciting an electrophysiological response from local neurons detected by the multichannel probe.

Analysing the responses of individual subjects to different frequency stimuli in the fMS paradigm reveals some degree of variability, illustrated by Figure 5.15. These plots represent absolute potential changes in the AEP to different frequency stimuli in each shank of the multichannel probe for each subject separately. These data are shank-averages; excluding contaminated channels Ch1, Ch7 and Ch24. It is apparent from visual inspection that although responses are generally tuned towards the BF, variation is observed between different shanks (e.g. Subject 36 in Figure 5.15a), narrow and broadly tuned responses (e.g. Subject 36 in Figure 5.15a vs. Subject 74 in Figure 5.15b, respectively), and response latency (e.g. dominant early latency activity from Subject 75 in Figure 5.15c vs. mid-latency dominant activity of Subject 76 in Figure 5.15d). While these findings highlight that BF stimuli preferentially elicit an auditory response measured from LFP recordings of microelectrodes, they also indicate a degree of variability in these responses between subjects, probe shanks and across the range of frequencies used.

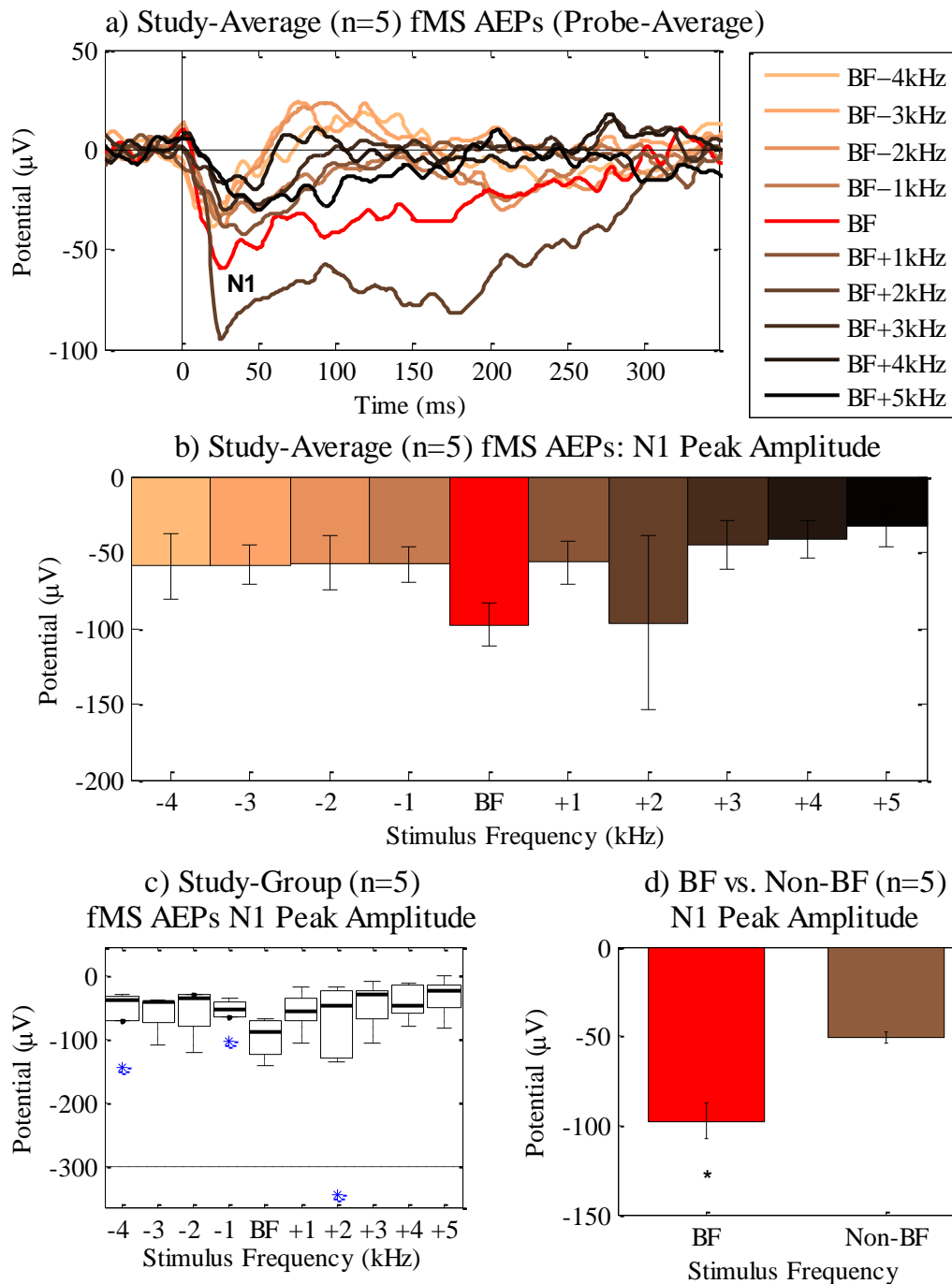


Figure 5.14 - Grand-average auditory evoked potential analysis from frequency many-standards paradigm stimuli a) Grand-average auditory evoked potential (AEP) waveforms from the frequency many-standards (fMS) paradigm stimuli which centred on the best frequency (BF; computed separately for each subject). Besides the BF stimuli, only the BF+2 kHz AEP displays greater onset response (N1) peak amplitude. b) N1 peak amplitude measurements from each frequency stimuli AEP, plotted as group mean \pm sem. This also suggests BF stimuli evoke greater N1 amplitude; however the BF+2 kHz result appears to conflict with this finding. c) Boxplots of N1 peak amplitude for each stimulus frequency, displaying the median as a bold black line and outliers as blue asterisks. A prominent outlier is present in BF+2 kHz data. d) Comparison of BF and non-BF stimuli evoked N1 peak amplitude, with the outlier exceeding $-300 \mu\text{V}$ in (c) removed. BF stimuli evoked significantly greater ($p < .05$) N1 peak amplitude than non-BF stimuli, suggesting frequency-specificity towards the BF.

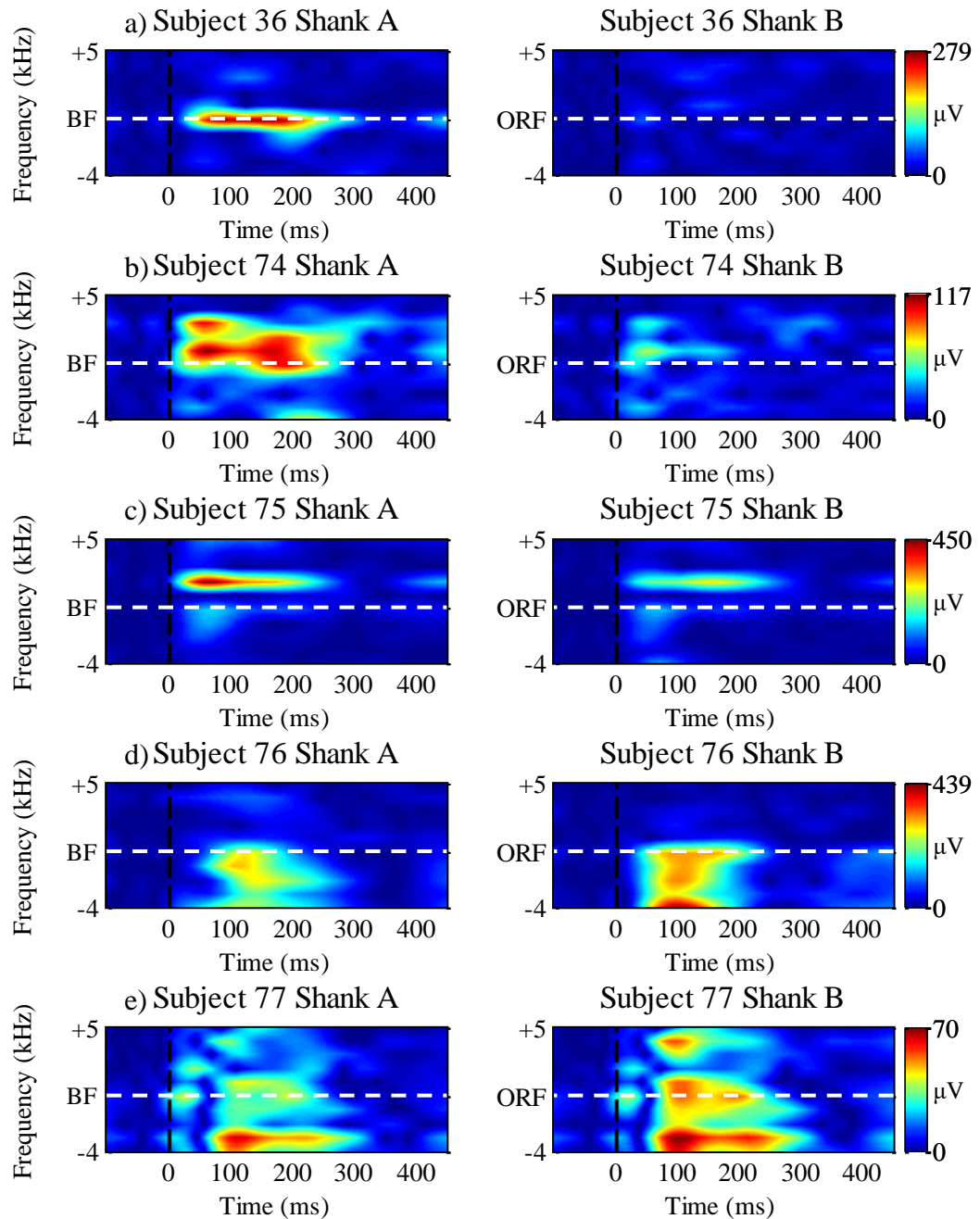


Figure 5.15 - Individual subjects' absolute auditory evoked potential responses to stimuli from the frequency many-standards paradigm Absolute changes in the shank-average auditory evoked potential (AEP) to ten different frequency many-standard (fMS) paradigm stimuli are plotted in a 3D. This gives a sense of the frequency sensitivity of tissue recorded at both shanks from each subject whose data are aggregated together in Figure 5.14. a) Subject 36 exhibits a defined preference towards best frequency (BF) stimuli on Shank A which is not apparent in Shank B. b) Subject 74 displays more diffuse spectral turning towards the BF and higher frequencies which are more prominent in Shank A. c) Subject 75 shows a very high magnitude response to BF+2 kHz stimuli; this outlier is highlighted in Figure 5.14c. d) Subject 76 displays larger magnitude responses to BF and lower frequency stimuli, also later (≈ 100 ms) and more apparent in Shank B. e) Subject 77 also exhibits diffuse spectral tuning generally towards lower frequency stimuli with higher magnitude responses visible in Shank B. This figure illustrates the diversity of responses observed from different subjects towards different frequency stimuli.

5.3.2.3 *Frequency mismatch responses observed in multichannel electrodes*

Data from the fOD paradigm varied considerably between subjects, thus the following findings presented are not statistically significant. Nevertheless, the fMMR evoked from five animals which exhibited AEP waveforms are presented here for completeness. These are presented separately because each are relatively different, although efforts are made to group together responses with shared features.

Firstly, Subject 36 fOD waveforms recorded before administering ketamine are shown in Figure 5.16. These AEPs are plotted over a double epoch, similar to the method described in Section 3.2.8.1. The fMMR evoked by both increasing and decreasing frequency ($BF \pm 3$ kHz) oddball stimuli is comparable with that observed from wild-type mice in Experiment I (e.g. Figure 3.13 and Figure 3.14). This fMMR is characterised by an extended biphasic response to oddball stimuli which goes positive from ≈ 200 -600 ms then negative from ≈ 600 -900 ms before stabilising towards baseline; in contrast, standard stimuli do not evoke this response and only exhibit stimuli onset and offset responses. Interestingly this fMMR is only observed in Shank A, displaying largest amplitude at more superficial channels and being diminished in deeper channels. Therefore this fMMR may not be observed from Shank B if it is implanted more deeply, which CSD analysis from Subject 36 may appear to suggest (Table 5.2), although this cannot be verified without histological analysis. In comparable waveforms from Subject 36 evoked following 10 mg/kg i.p. ketamine administration (Figure 5.17) these biphasic fMMR responses are abolished, similarly to findings from Experiment I (e.g. Figure 3.13 and Figure 3.14) in which the fMMR was diminished following pharmacological challenge with ketamine.

Responses to fOD paradigm stimuli from Subjects 74 (Figure 5.18 and Figure 5.19), 76 (Figure 5.20 and Figure 5.21) and 77 (Figure 5.22 and Figure 5.23) may be grouped together because they share similar characteristics. These animals each display a prominent deflection in response to $BF - 3$ kHz frequency oddball stimuli which is not present in AEP waveforms to BF standard or $BF + 3$ kHz oddball stimuli. This relatively large amplitude response peaks broadly over ≈ 100 -200 ms and changes in polarity generally from positive in superficial channels to negative in deep channels. This change in polarity may indicate that the origins of this response are within the cortex itself, as discussed in Section 5.4.2. Following 10 mg/kg i.p. ketamine administration these responses are not greatly diminished, as shown in Figure 5.19 for Subject 74, Figure 5.21 for Subject 76 and Figure 5.23 for Subject 77, suggesting they do not rely on NMDA receptor function.

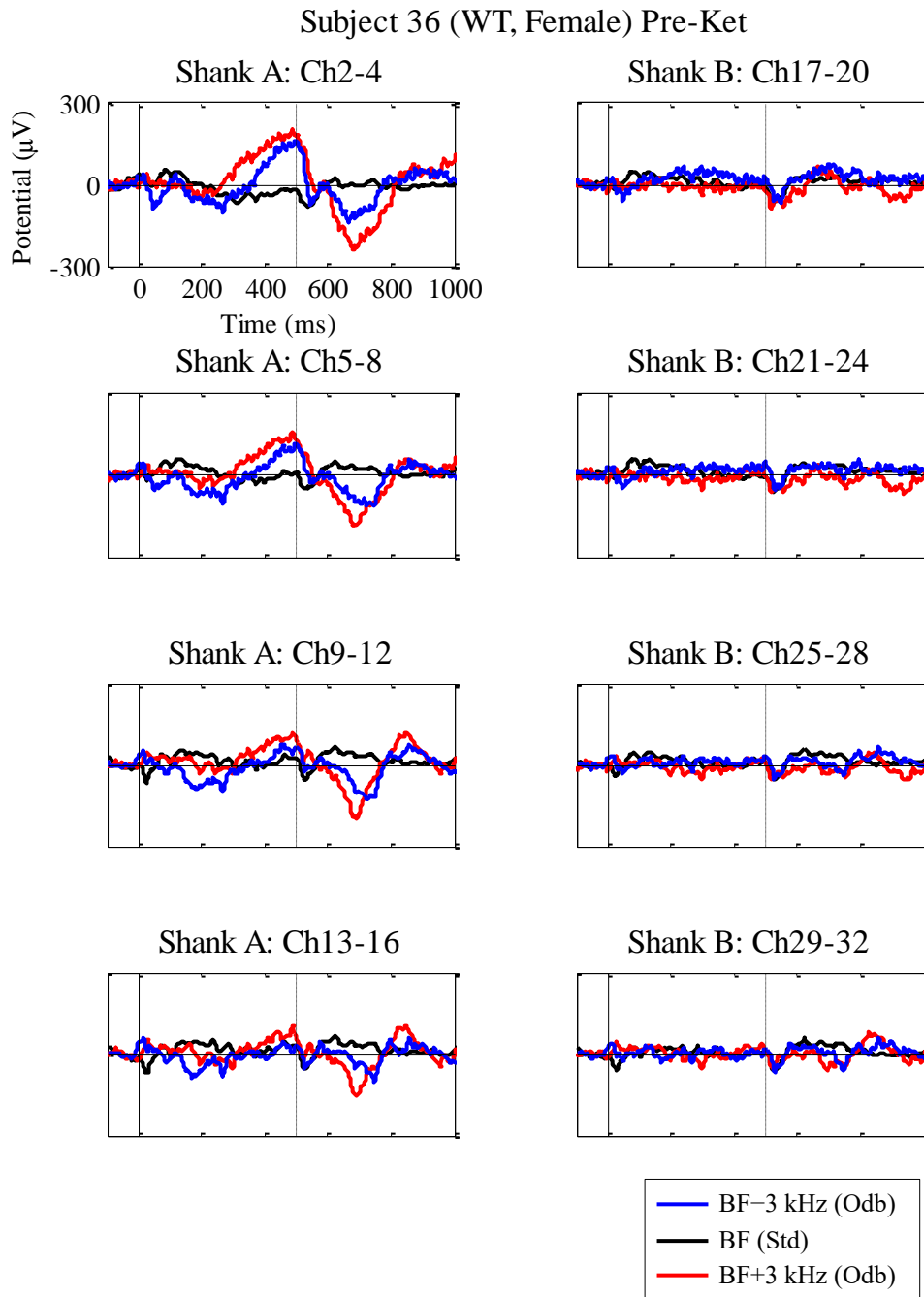


Figure 5.16 - Frequency mismatch response in Subject 36 (WT, female) before ketamine These waveforms are channel-averaged in groups of four from Shank A (Ch1-16) and Shank B (Ch17-32), as shown in Figure 5.2, omitting those contaminated with electromagnetic interference (Ch1, Ch7 and Ch24). Best frequency (BF) standard (Std) and BF \pm 3 kHz oddball (Odb) stimuli evoked waveforms are plotted over a double-epoch, with the second stimuli onset time (500 ms) marked with a vertical dashed line. Both increasing and decreasing frequency oddballs generate a relatively large amplitude biphasic response in Shank A which is greater in more superficial channels and diminishes in deeper channels. This response is not apparent in Shank B recordings. Equivalent waveforms following 10 mg/kg i.p. ketamine administration are plotted in Figure 5.17.

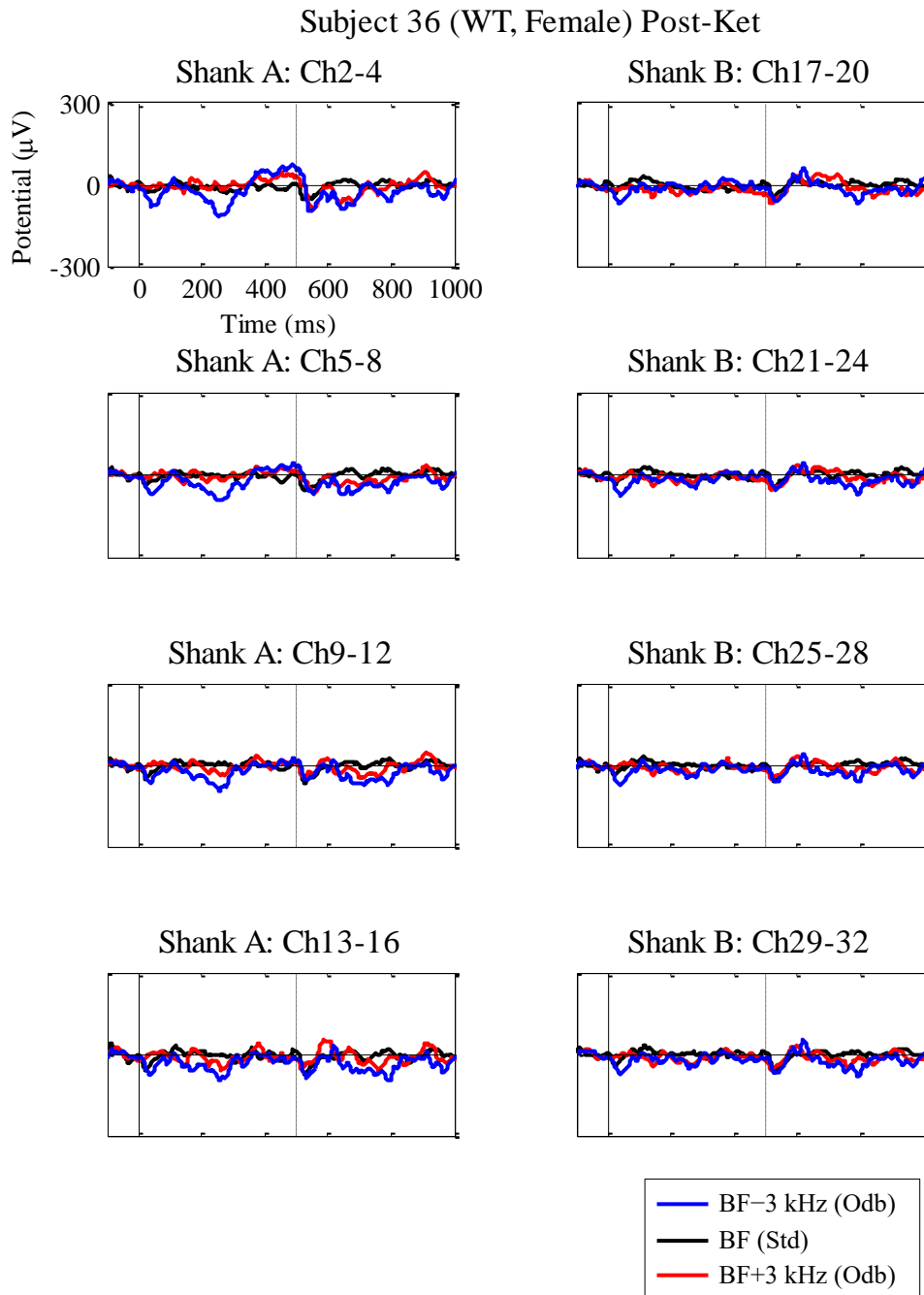


Figure 5.17 - Frequency mismatch response in Subject 36 (WT, female) following 10 mg/kg i.p. ketamine Auditory evoked potential (AEP) waveforms from best frequency (BF) standard (Std) and BF \pm 3 kHz oddball (Odb) stimuli presented in the frequency oddball (fOD) paradigm. These were recorded following 10 mg/kg i.p. ketamine and are plotted over a double-epoch, comparable with plots in Figure 5.16 acquired before delivering ketamine. It appears as though ketamine has greatly diminished the biphasic frequency mismatch response (fMMR) in Shank A observed from pre-ketamine waveforms.

Subject 74 (HET, Male) Pre-Ket

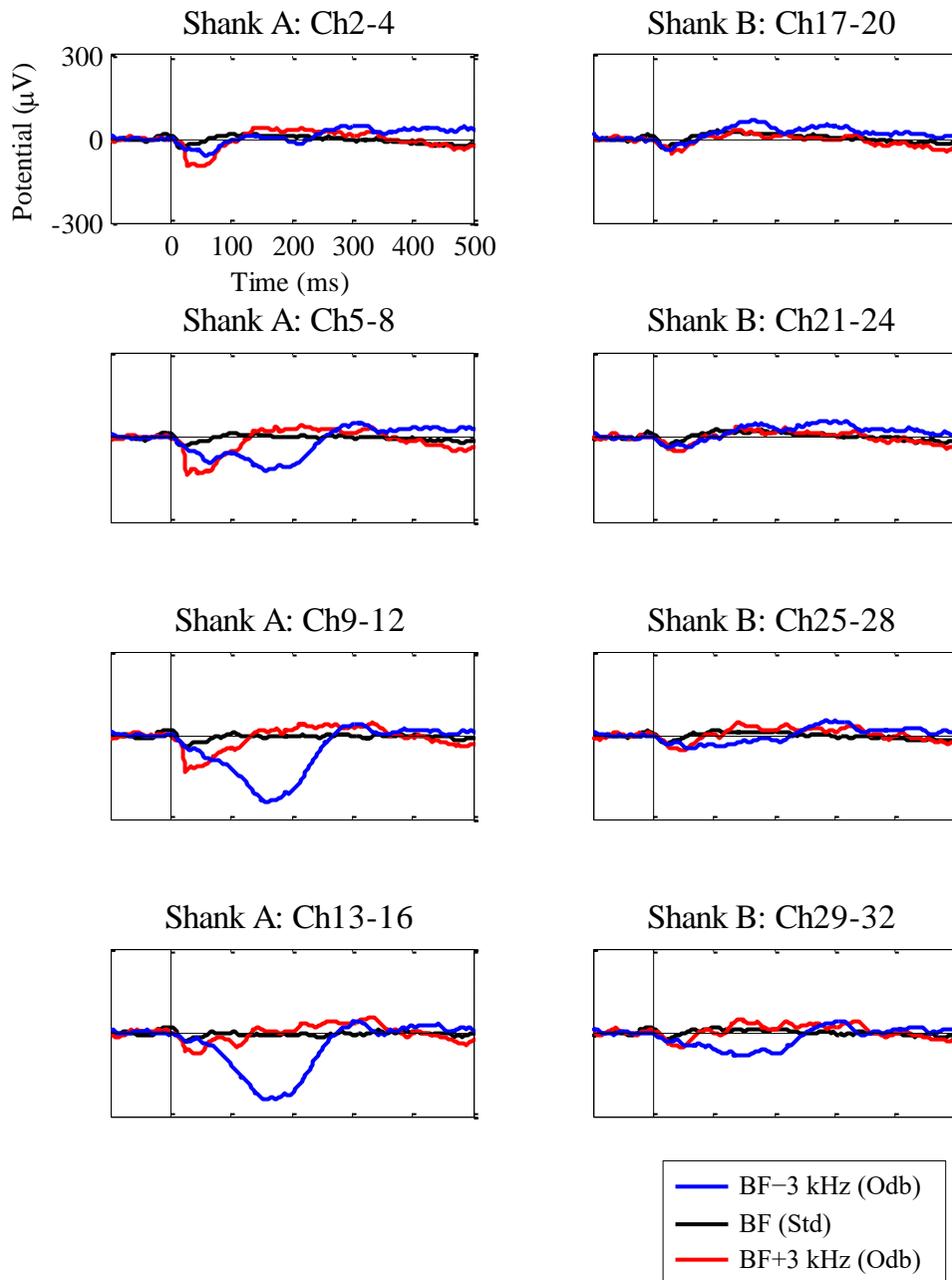


Figure 5.18 - Frequency mismatch response in Subject 74 (HET, male) before ketamine

These waveforms are averaged as illustrated in Figure 5.2, with corrupted channels Ch1, Ch7 and Ch24 omitted. Auditory evoked potential (AEP) waveforms from best frequency (BF) standard (Std) and BF \pm 3 kHz oddball (Odb) stimuli in the frequency oddball (fOD) paradigm are plotted. A relatively large amplitude response is observed in the AEP to BF-3 kHz oddball stimuli. In Shank A this is almost absent in superficial-most channels and increasingly becomes negative in deeper channels. In Shank B this response is of lower amplitude, however, is positive in the most superficial channels and becomes negative in deepest channels. Equivalent waveforms from the fOD paradigm played following ketamine administration are plotted in Figure 5.19.

Subject 74 (HET, Male) Post-Ket

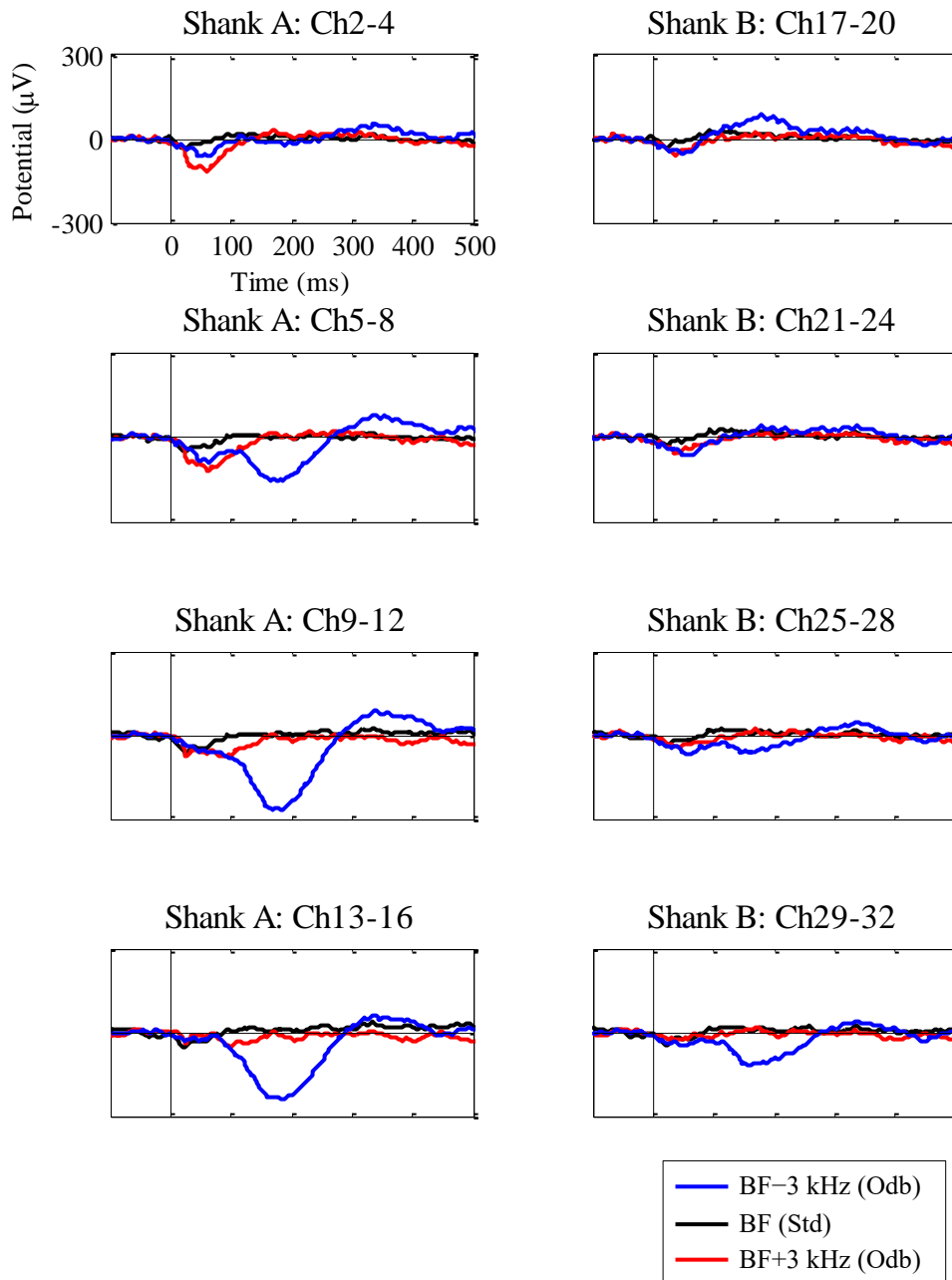


Figure 5.19 - Frequency mismatch response in Subject 74 (HET, male) following 10 mg/kg i.p. ketamine These auditory evoked potential (AEP) waveforms were generated from recordings to the frequency oddball (fOD) paradigm following 10 mg/kg i.p. ketamine. The AEP from best frequency (BF) standard (Std) and BF \pm 3 kHz oddball (Odb) stimuli are plotted. Compared with waveforms evoked by the fOD paradigm presented before administering ketamine in Figure 5.18 these display very similar morphology, thus suggesting that ketamine does not have an effect on the observed AEP features, specifically referring to the large amplitude response to BF-3 kHz oddball stimuli.

Subject 76 (WT, Male) Pre-Ket

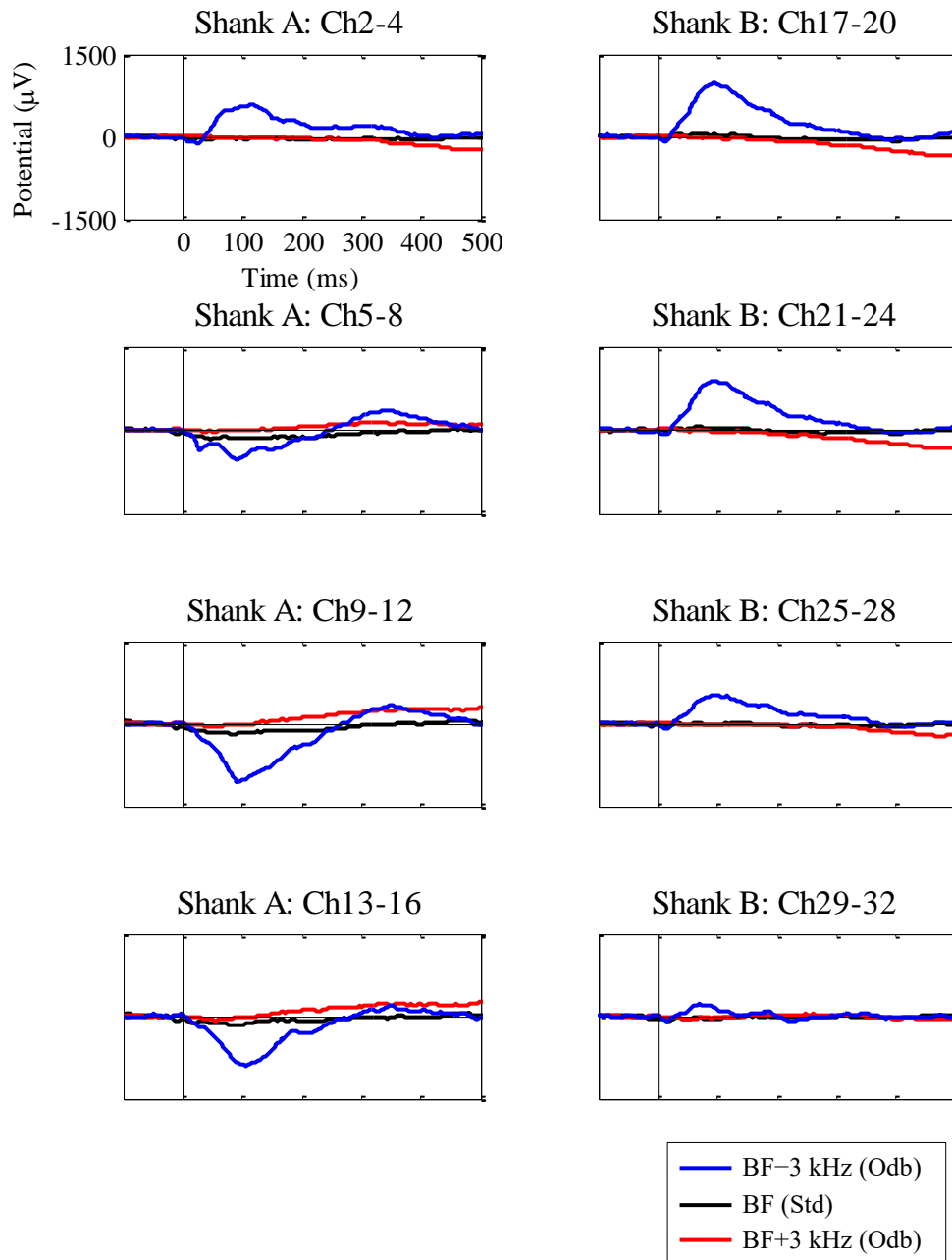


Figure 5.20 - Frequency mismatch response in Subject 76 (WT, male) before ketamine

These plots display auditory evoked potential (AEP) waveforms in response to frequency oddball (fOD) paradigm best frequency (BF) standard (Std) and BF \pm 3 kHz oddball (Odb) stimuli. A large amplitude response to the BF-3 kHz oddball is observed which in Shank A is positive in the most superficial channels then quickly becomes negative in deeper channels. In Shank B this large amplitude response is most positive in superficial channels then decreases in amplitude towards deeper channel recordings. This increased responsiveness of Subject 76 recordings to lower frequency stimuli is perhaps indicated by Figure 5.15d. These AEPs may be compared with those elicited following ketamine administration in Figure 5.21.

Subject 76 (WT, Male) Post-Ket

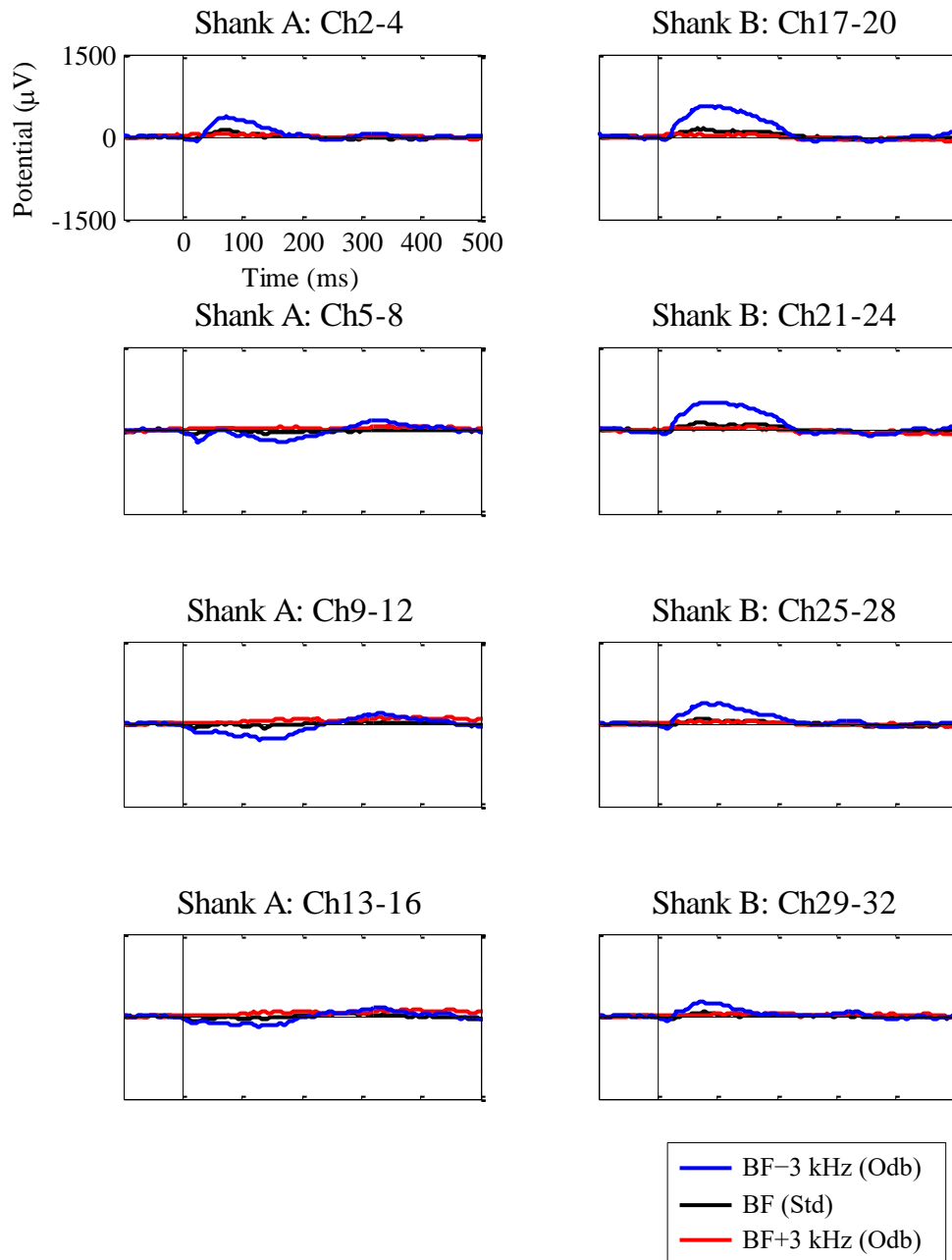


Figure 5.21 - Frequency mismatch response in Subject 76 (WT, male) following 10 mg/kg i.p. ketamine The auditory evoked potential (AEP) in response to best frequency (BF) standard (Std) and BF \pm 3 kHz oddball (Odb) stimuli presented in the frequency oddball paradigm (fOD) following 10 mg/kg i.p. ketamine injection are plotted. These waveforms are somewhat similar with those from the fOD paradigm before administering ketamine shown in Figure 5.20. However, the response to BF-3 kHz Odb stimuli appears reduced in magnitude, while retaining the same general shape and trajectory in both shanks.

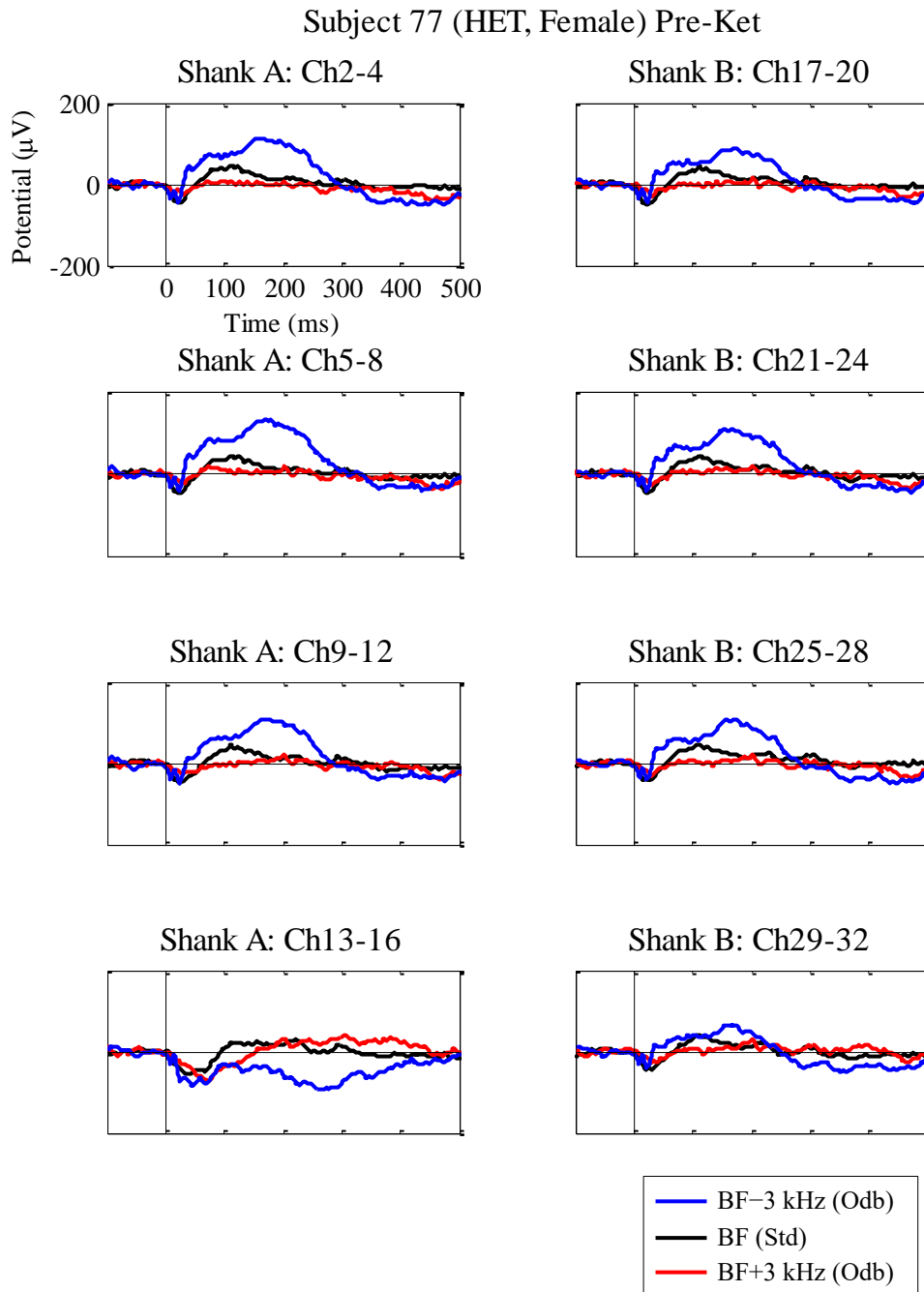


Figure 5.22 - Frequency mismatch response in Subject 77 (HET, female) before ketamine Auditory evoked potential (AEP) waveforms in response to the frequency oddball (fOD) paradigm are plotted here in channel-average format illustrated by Figure 5.2. The best frequency (BF) standard (Std) and BF \pm 3 kHz oddball (Odb) stimuli AEPs are shown. A relatively large amplitude response to the BF-3 kHz Odb stimuli is observed which is positive in superficial channels and appears to decrease slightly in amplitude towards deeper channels, becoming negative in the deepest channels of Shank A. This greater magnitude response to <BF versus >BF stimuli is perhaps indicated by Figure 5.15e. These may be compared with AEPs from the fOD paradigm presented following injection with ketamine plotted in Figure 5.23.

Subject 77 (HET, Female) Post-Ket

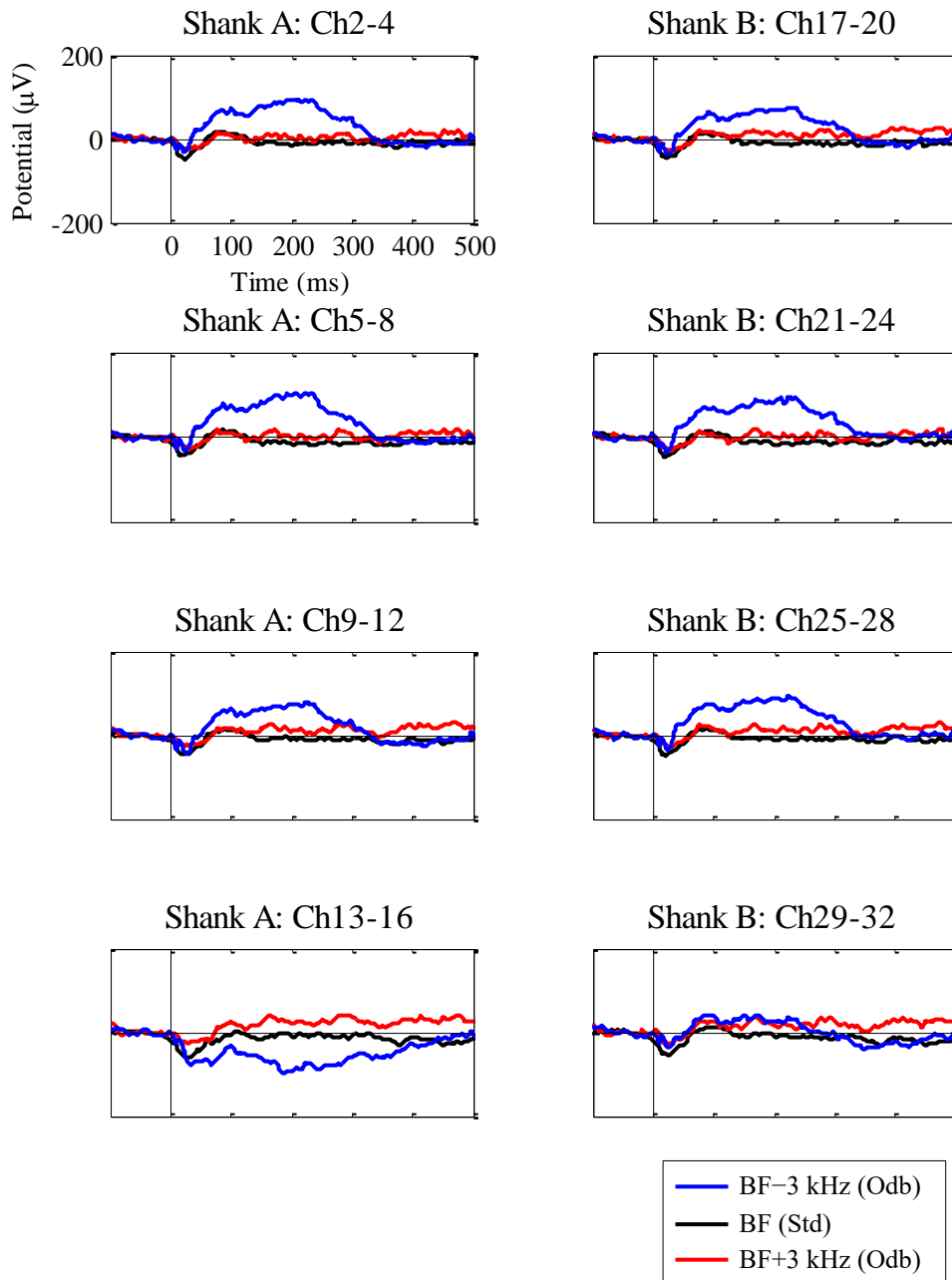


Figure 5.23 - Frequency mismatch response in Subject 77 (HET, female) following 10 mg/kg i.p. ketamine These waveforms are from the frequency oddball (fOD) paradigm following 10 mg/kg i.p. ketamine administration. Best frequency (BF) standard (Std) and BF \pm 3 kHz oddball (Odb) auditory evoked potentials (AEPs) are plotted, comparable with waveforms in Figure 5.22. The relatively large amplitude response to BF-3 kHz stimuli does not appear to be influenced by ketamine.

Frequency oddball paradigm data from Subject 75 is presented in Figure 5.24 over a double epoch, similar to Subject 36 in Figure 5.16. An increase in amplitude from ≈ 300 -500 ms is observed in response to BF-3 kHz oddball stimuli which do not appear to elicit a negative onset response. The second stimulus presentation (BF/Std) indicated by a vertical dashed line elicits an onset response which is greater in magnitude when preceded by non-BF oddball stimuli (BF \pm 3 kHz/Odb).

This may occur due to responsiveness of frequency-tuned neurons progressively increasing over time which they are not stimulated (as discussed in Section 1.2.2.6). Essentially the response to standards preceded by oddballs may not have been tempered or 'adapted' to the same degree as the response to consecutive identical stimuli, particularly apparent here because the BF is the standard and therefore local tissue responds preferentially towards this frequency as opposed to non-BF (oddball) stimuli. Subject 75 died shortly after administering ketamine therefore there are no data to analyse the effects of NMDA receptor disruption on this response.

5.3.2.4 *Frequency deviant-alone paradigm control waveforms*

The fDA paradigm was included in Experiment III as a positive control for sensory-memory disruption. In Experiment I the fDA paradigm appeared to evoke very similar responses to the fOD paradigm, potentially suggestive of a true sensory memory disruption effect. The AEP from BF \pm 3 kHz stimuli presented in the fDA paradigm from each subject are plotted individually, and these may be compared with respective fOD paradigm waveforms already presented to visually assess whether these auditory paradigms evoke comparable neurophysiological mechanisms.

Frequency deviant-alone paradigm waveforms from Subject 36 are plotted in Figure 5.25, from Subject 74 in Figure 5.26, Subject 75 in Figure 5.27, Subject 76 in Figure 5.28 and from Subject 77 in Figure 5.29. These may be visually compared with their counterpart fOD paradigm waveforms reported in Section 5.3.2.3 above. Overall this evidence suggests that BF \pm 3 kHz stimuli presented in fOD and fDA paradigm contexts evoke similar electrophysiological responses, in some ways comparable with findings from Experiment I (Figure 3.19 and Figure 3.28), suggesting the oddball and deviant-alone conditions invoke similar neurophysiological processes in urethane-anaesthetised mice. These findings also suggest that tonotopy plays a role in this response to fOD and fDA stimuli, not necessarily in line with the optimum frequency for eliciting an onset response. However, over interpretation of these results should be avoided due to the very low number of viable subjects, which also display considerable variability.

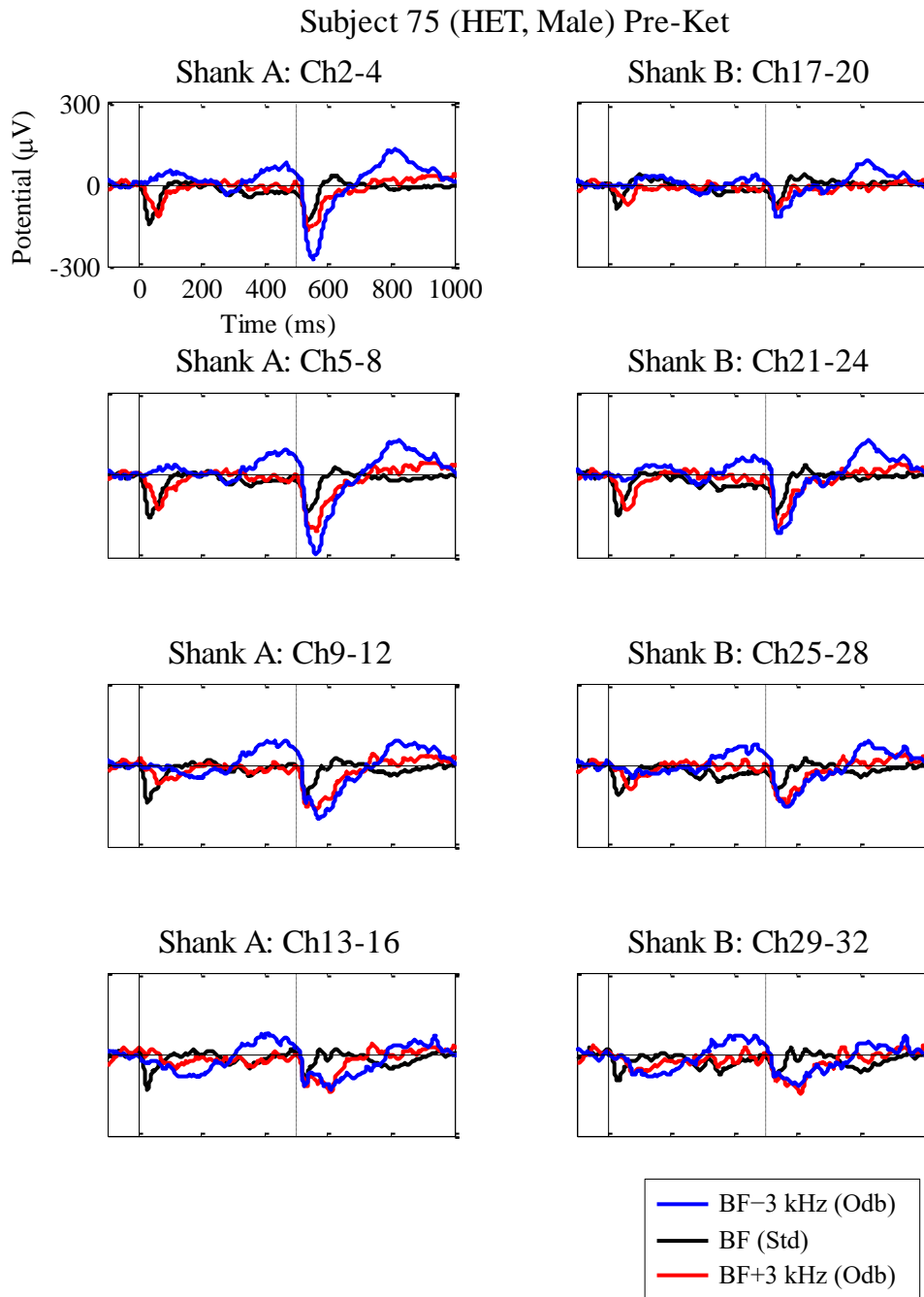


Figure 5.24 - Frequency mismatch response in Subject 75 (HET, male) Here the auditory evoked potential (AEP) waveforms from the frequency oddball (fOD) paradigm are plotted over an extended duration epoch spanning two stimuli presentations. Channel averaging described in Figure 5.2 was performed. Best frequency (BF) standard (Std) and BF \pm 3 kHz oddball (Odb) stimuli are each followed by an BF Std stimuli with onset time 500 ms indicated by a vertical dashed line. The first onset response in the epoch displays greatest peak amplitude to BF Std stimuli, with a slightly lower amplitude peak to BF+3 kHz and almost no apparent onset response to BF-3 kHz stimuli. There is an increasing positive potential from \approx 300-500 ms in response to BF-3 kHz oddball stimuli. However, when the second stimulus in the epoch is presented (all BF), that preceded by BF-3 kHz becomes the greatest in magnitude, the one preceded by BF+3 kHz is the second greatest and that following another BF stimulus appears the smallest. This observation may reflect differential adaptation of local neural tissue which preferentially responds to BF stimuli.

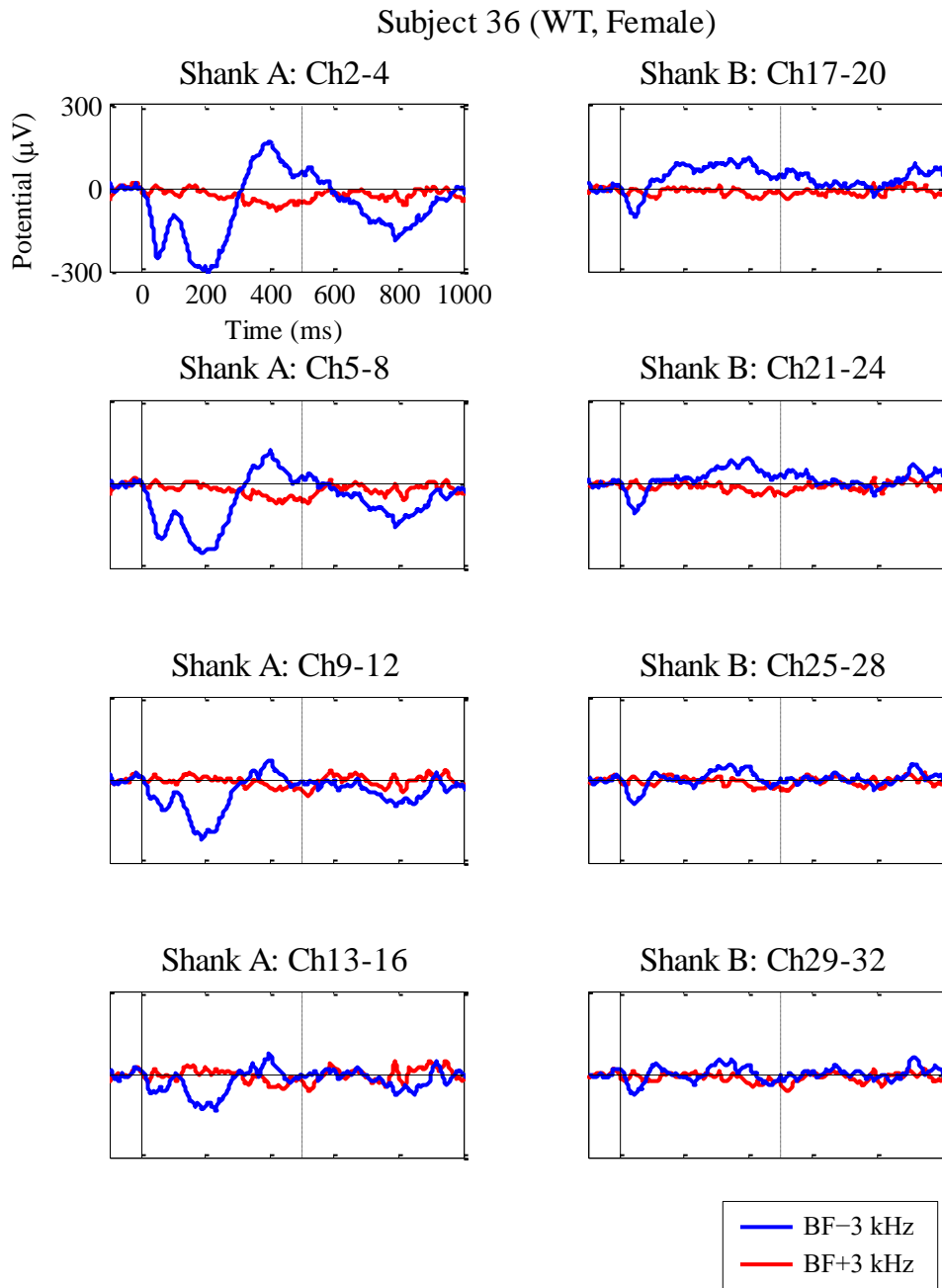


Figure 5.25 - Frequency deviant-alone control waveforms in Subject 36 (WT, female)
 These auditory evoked potential (AEP) waveforms generated from the frequency deviant-alone (fDA) paradigm are plotted over 1s post stimuli onset, comparable with frequency oddball (fOD) paradigm AEPs from Subject 36 shown in Figure 5.16. There appears to be a large biphasic response to best frequency (BF)-3 kHz stimuli which reaches a peak positive amplitude at ≈ 400 ms and negative at ≈ 800 ms. This may be similar to the frequency mismatch response (fMMR) to BF-3 kHz observed from Subject 36. However, in contrast to fOD paradigm results this feature is not seen in response to BF+3 kHz stimuli. The BF-3 kHz AEP also displays a negative amplitude response which peaks at ≈ 200 ms in Shank A, in some ways similar to fOD paradigm data from Subject 74 in Figure 5.18.

Subject 74 (HET, Male)

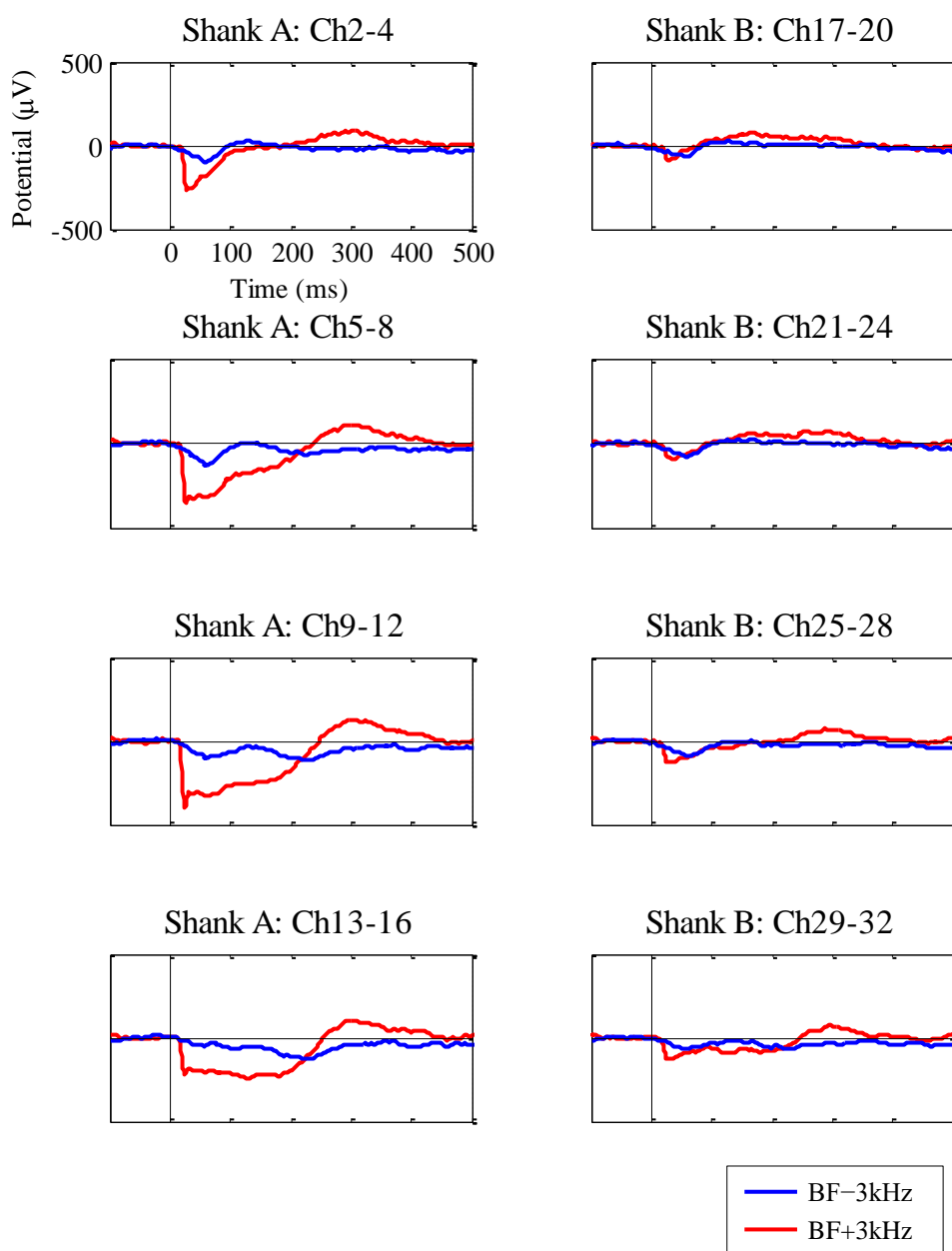


Figure 5.26 - Frequency deviant-alone control waveforms in Subject 74 (HET, male)

These waveforms from the frequency deviant-alone (fDA) paradigm may be compared with those from the frequency oddball (fOD) paradigm in Figure 5.19. The best frequency (BF)+3 kHz stimuli auditory evoked potential (AEP) is considerably different from that in Figure 5.19, mainly due to greatly increased magnitude. The BF-3 kHz stimuli AEP may be similar to that from the fOD paradigm, although displaying a larger magnitude onset response and reduced magnitude subsequent negative potential peaking ≈ 200 ms post stimulus onset. Similarly to fOD waveforms, those observed from Shank A display greater amplitudes than those from Shank B.

Subject 75 (HET, Male)

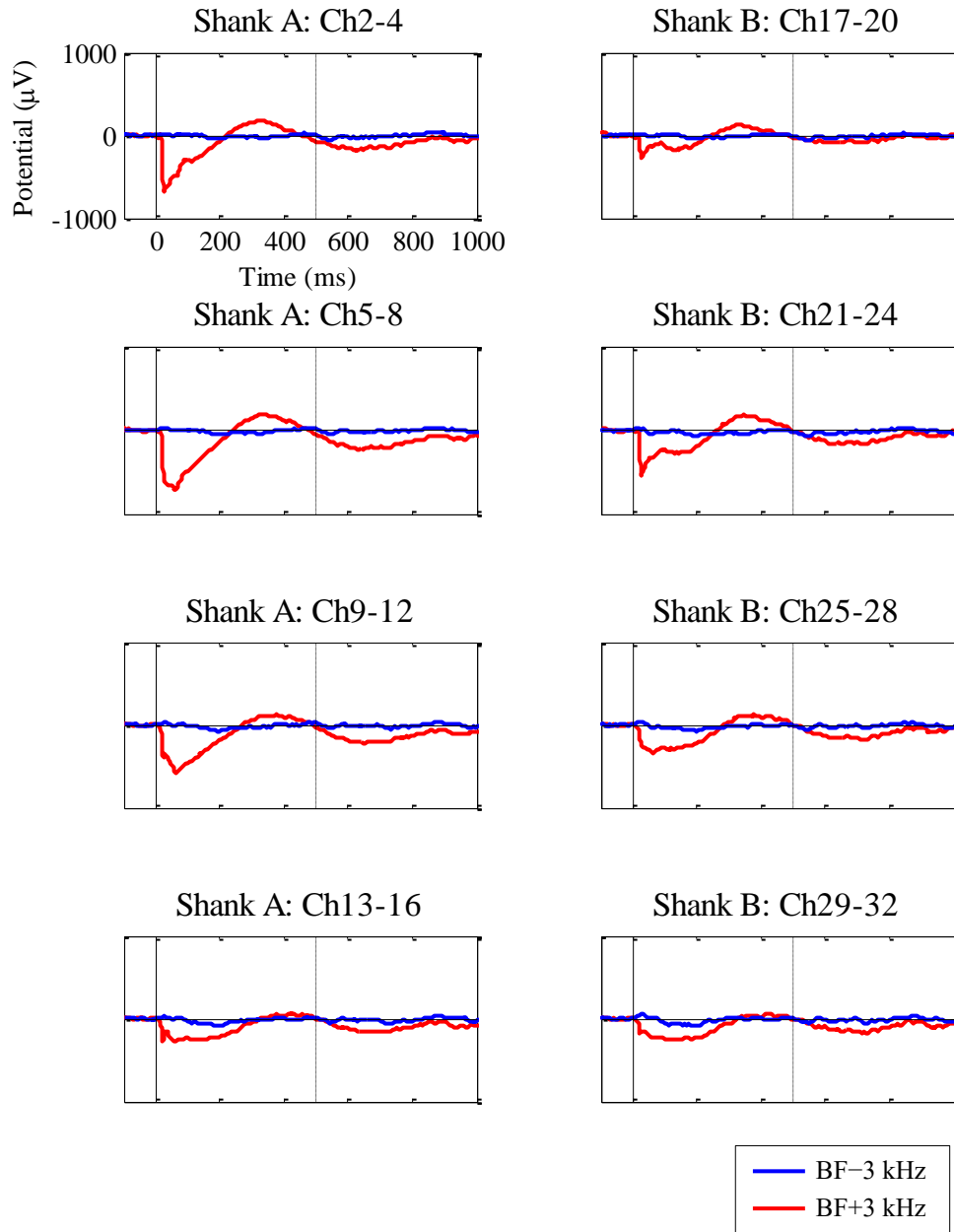


Figure 5.27 - Frequency deviant-alone control waveforms in Subject 75 (HET, male)

These frequency deviant-alone (fDA) control paradigm waveforms may be compared with frequency oddball (fOD) paradigm data from Subject 75 in Figure 5.24. These auditory evoked potentials (AEPs) are quite different from those evoked by the fOD paradigm. There is clearly a far larger response to best frequency (BF)+3 kHz than BF-3 kHz stimuli. This is suggested by frequency many-standards (fMS) paradigm data from Subject 75 plotted in Figure 5.15c. The BF+3 kHz stimuli also evoke a biphasic response which goes positive from ≈ 300 -500 ms and negative from ≈ 600 -800 ms.

Subject 76 (WT, Male)

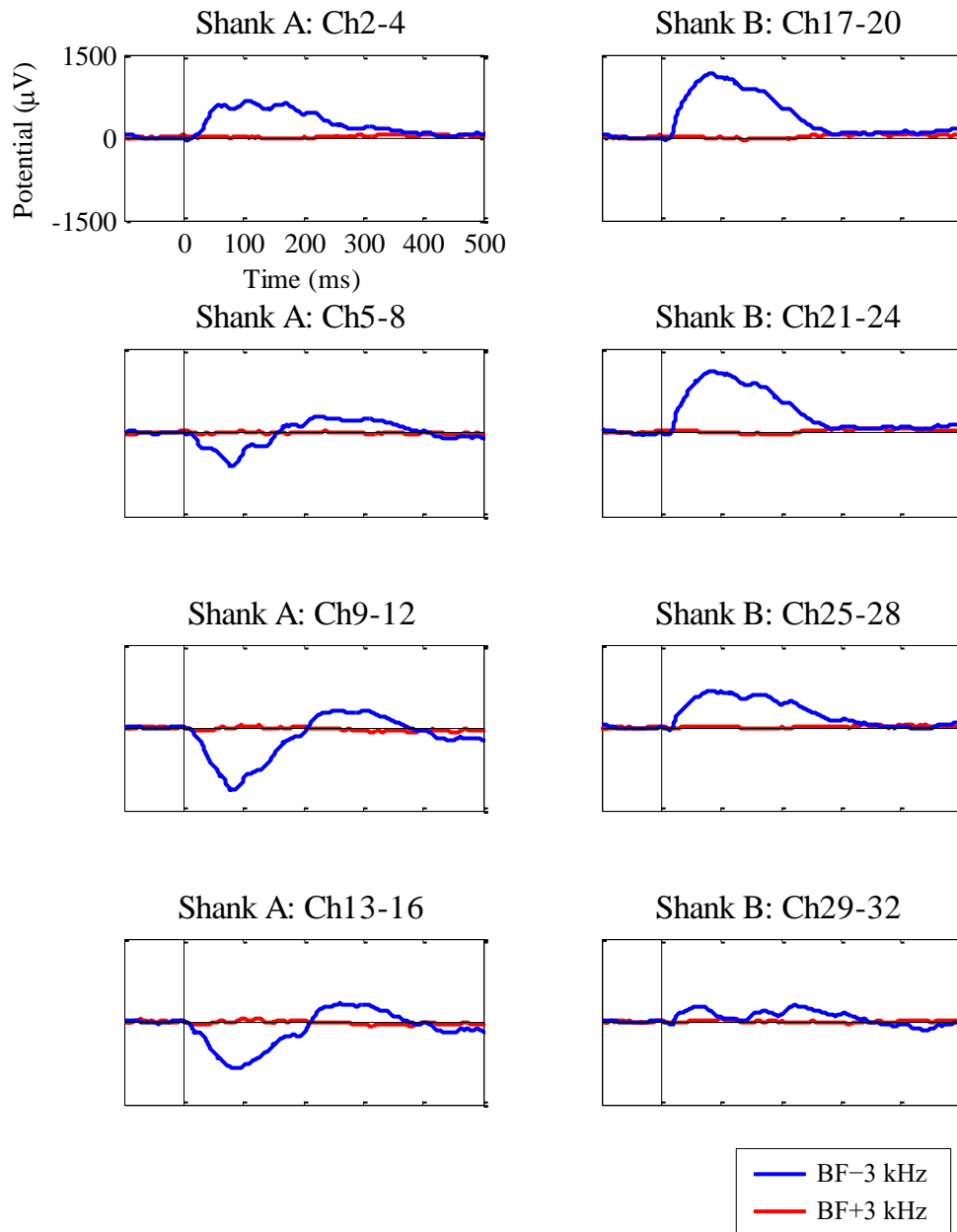


Figure 5.28 - Frequency deviant-alone control waveforms in Subject 76 (WT, male)

These are auditory evoked potentials (AEPs) from the frequency deviant-alone (fDA) control paradigm which may be compared with frequency oddball (fOD) paradigm waveforms from Subject 76 plotted in Figure 5.20. The relatively large amplitude feature observed in response to best frequency (BF)–3 kHz stimuli displays almost identical morphology with the AEP evoked by same frequency stimuli presented in an oddball condition. This strongly suggests the BF–3 kHz stimulus in both fOD and fDA paradigms elicit the same neural response from Subject 76. Increased responsiveness to <BF stimuli versus >BF may also be predicted from data in Figure 5.15d.

Subject 77 (HET, Female)

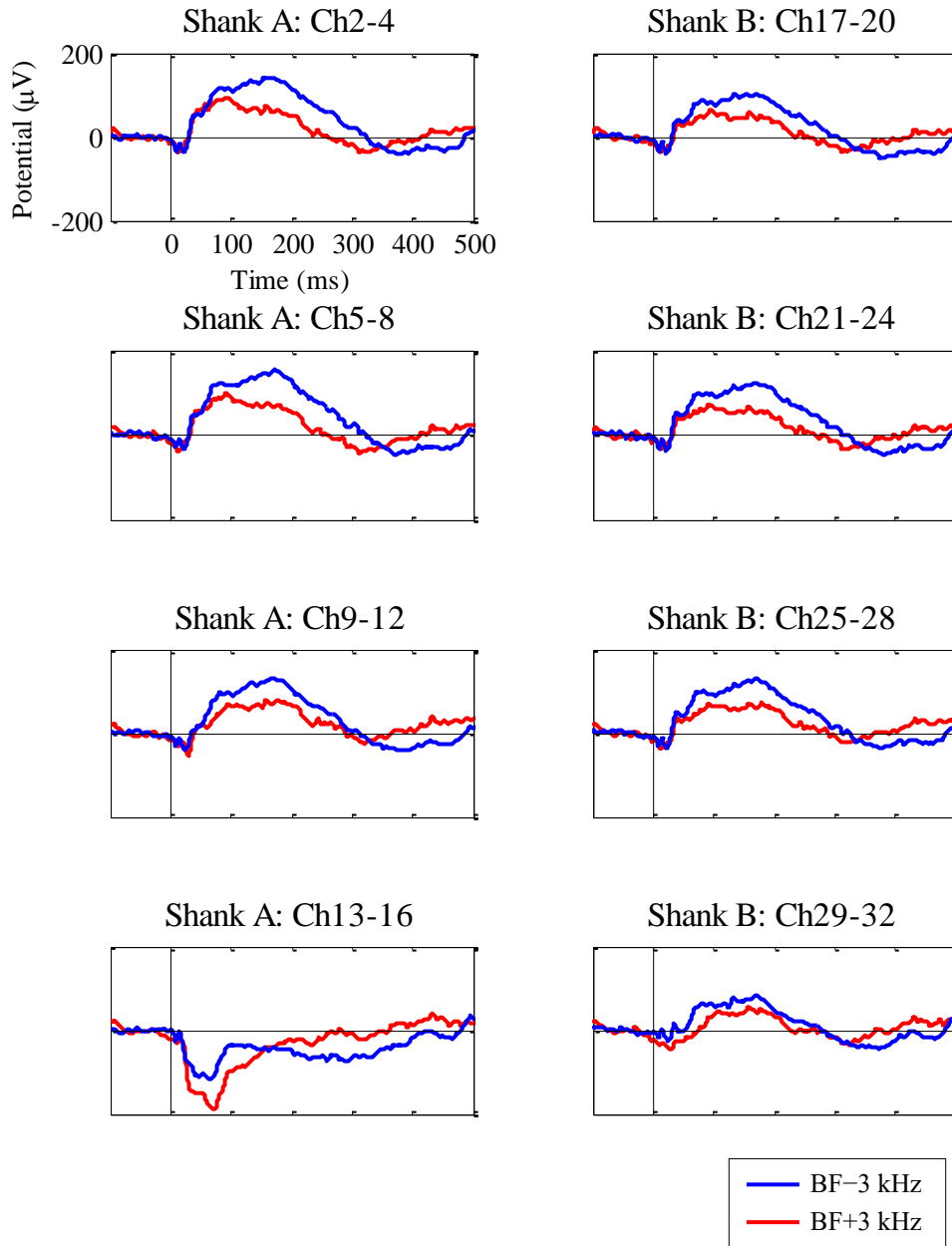


Figure 5.29 - Frequency deviant-alone control waveforms in Subject 77 (HET, female)

These waveforms from the frequency deviant-alone (fDA) control paradigm may be compared with auditory evoked potentials (AEPs) evoked by the same stimuli in a frequency oddball (fOD) paradigm in Figure 5.22. The response to best frequency (BF)-3 kHz stimuli is comparable to that observed from the fOD paradigm. However, the BF+3 kHz stimuli in this fDA paradigm appear to evoke a similar response which peaks in positive amplitude from ≈ 100 -200 ms in superficial channels, then decreases in amplitude and becomes negative in deeper channels. This data suggests fDA stimuli AEP features are similar to that of the fOD paradigm.

5.3.2.5 *Comparison of auditory evoked potentials and multi-unit activity from frequency deviant-alone stimuli*

Single-subject (Subject 75; HET, male) analysis of MUA and AEP waveforms in response to fDA stimuli is provided in Figure 5.30. Here there is clearly a far greater magnitude AEP to BF+3 kHz stimuli. This may be expected considering the fMS paradigm data presented in Figure 5.15c, which suggests that electrophysiology measured from this animal is greater in response to the higher frequencies employed.

Interestingly, bursts of concentrated activity occur in response to BF−3 kHz stimuli, shown by the MUA raster plot in Figure 5.30c. This has a marked influence on the peri-stimulus time histogram (PSTH) in Figure 5.30e. However, it is challenging to draw any correlations from this activity or to understand anything physiologically relevant about this observation due to its irregular nature.

MUA in response to BF+3 kHz stimuli appears to demonstrate a degree of synchronisation with stimuli onset (Figure 5.30d), which correlate with the relatively large amplitude N1 peak observed in Figure 5.30b. This increased firing rate immediately following stimuli onset is also reflected in the PSTH plotted in Figure 5.30f. This data suggests auditory neuron(s) were being detected in multichannel probe recordings; however, the spike-sorting algorithm was unable to separate this from MUA (discussed in Section 5.4.4).

Only data from Subject 75 (HET, male) is presented here because its spiking activity and AEP waveforms demonstrated some correlation. Analysis of multichannel recordings from other animals did not display any interesting correlations between the AEP and spiking activity and are therefore omitted.

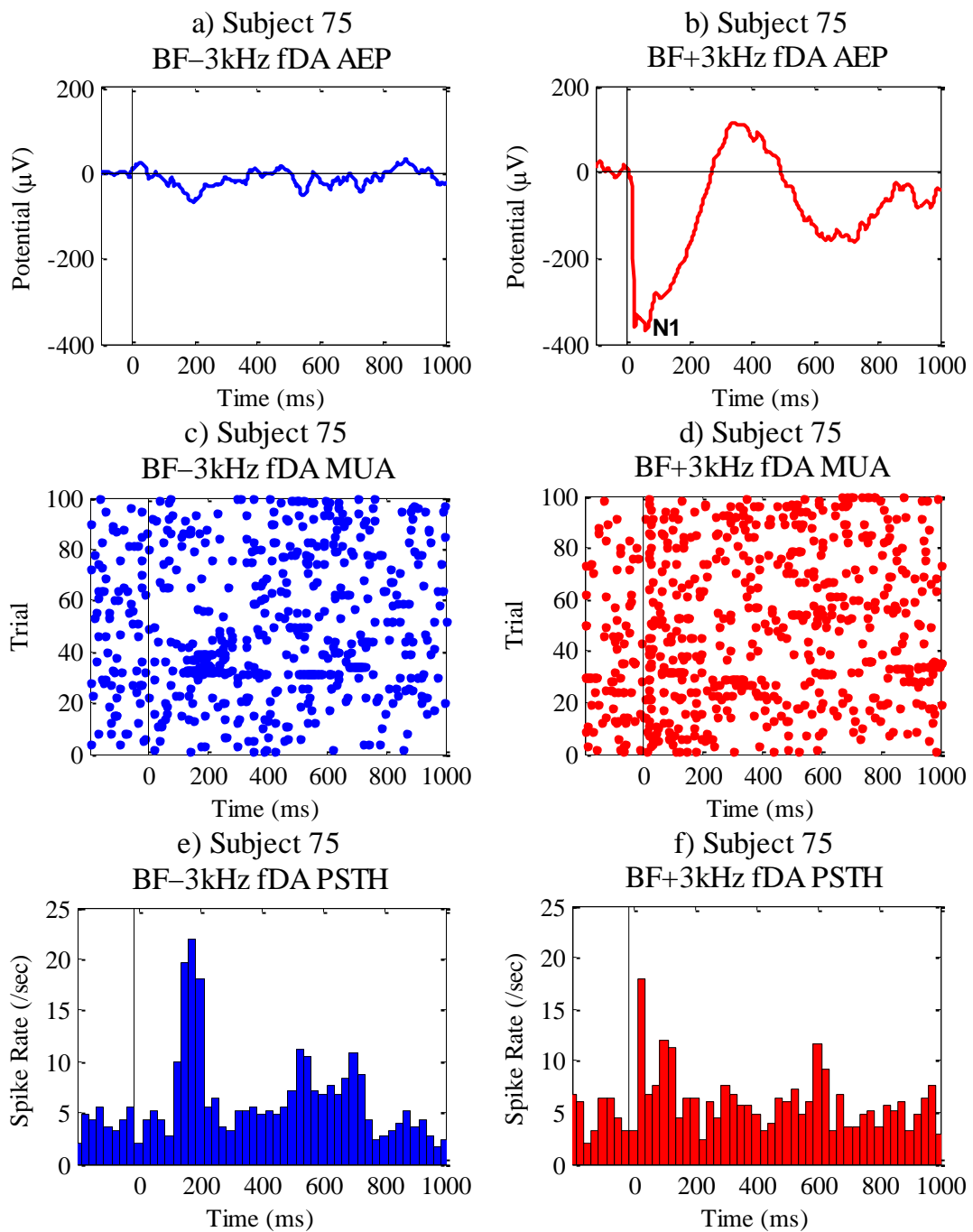


Figure 5.30 - Comparison of frequency deviant-alone auditory evoked potentials and multi-unit activity from Subject 75 (HET, male) Frequency deviant-alone (fDA) paradigm data from Subject 75 is analysed here. Resulting probe-average auditory evoked potential (AEP) waveforms are shown for a) best frequency (BF)-3 kHz, and b) BF+3 kHz stimuli. There is a greater amplitude onset (N1) response to the higher frequency stimuli, followed by a biphasic response which reaches a positive peak at ≈ 400 ms and a negative peak at ≈ 700 ms. Raster plots displaying all identified spikes or multi-unit activity (MUA) recorded during each presentation (trial) of c) BF-3 kHz and d) BF+3 kHz stimuli are plotted. There appears to be a condensed region of activity in response to BF-3 kHz stimuli between trials 30-40 across a latency range of ≈ 100 -300 ms. The BF+3 kHz MUA plot also displays spots of condensed activity, however most notably there is synchronised firing following stimulus onset, perhaps reflecting the large N1 peak in (b). The peri-stimulus time histogram (PSTH) of this MUA is shown for e) BF-3 kHz and f) BF+3 kHz stimuli, reflecting overall firing rates in (c) and (d), respectively.

5.3.3 *Intensity paradigms and laminar response in urethane-anaesthetised mice*

Results from the modified consecutive-repetition ($_{\text{mod}}\text{CR}$) paradigm intensity-varying stimuli are presented here. In this paradigm there were 100 consecutive repetitions of 60 dB, 70 dB and 80 dB stimuli (and others detailed in Table 2.6), each 50 ms in duration, the best frequency (BF) for each individual subject, played with a 450 ms ISI and 5 ms rise/fall times. It should be noted that the $_{\text{mod}}\text{CR}$ paradigm included seven physically distinct auditory stimuli in total, each of which were presented 100 times consecutively. Analyses in this section were performed on responses to the seventh (60 dB), third (70 dB) and sixth (80 dB) unique stimuli in this sequence.

5.3.3.1 *Effect of stimulus intensity on grand-average auditory evoked potential across electrodes of multichannel probe*

The study-average ($n=5$) AEP response to 60 dB, 70 dB and 80 dB stimuli extracted from LFP recordings at different electrode sites along the multichannel silicon probe are plotted in Figure 5.31 (Shank A) and Figure 5.32 (Shank B). A clear pattern is apparent, consistent with previous findings, where increasing stimuli intensity evokes greater negative amplitude onset (N1) and positive offset (P_{offset}) responses. The probe-average AEP from control (WT) and *Map2k7^{+/-}* (HET) groups are plotted in Figure 5.33a and Figure 5.33b, respectively. Repeated measures ANOVA tests were performed on N1 and P_{offset} measurements with stimulus intensity as a within-subjects factor, genotype and gender as between-subjects factors.

N1 peak latency graphed in Figure 5.33c displays no significant effects of genotype [$F_{1,1} = .375$, $p = .650$], gender [$F_{1,1} = .002$, $p = .971$], or stimulus intensity [$F_{1,1} = .458$, $p = .621$]. In Figure 5.33d it appears as though there is a trend towards greater N1 peak amplitude caused by increasing stimulus intensity. However, this was not statistically significant [$F_{1,1} = 1.329$, $p = .455$]. Also there were no significant effects of genotype [$F_{1,1} = 1.116$, $p = .483$] or gender [$F_{1,1} = 3.644$, $p = .307$] on N1 peak amplitude.

There were no significant findings for P_{offset} peak latency (Figure 5.33e) in relation to genotype [$F_{1,1} = 14.169$, $p = .165$], gender [$F_{1,1} = 2.428$, $p = .363$] or stimulus intensity [$F_{1,1} = .165$, $p = .754$]. Neither were there any significant effect of genotype [$F_{1,1} = .819$, $p = .532$], gender [$F_{1,1} = .335$, $p = .665$] or stimulus intensity [$F_{1,1} = 15.179$, $p = .160$] to influence P_{offset} peak amplitude, displayed in Figure 5.33f, although it appears as though increasing intensity evokes greater amplitude responses.

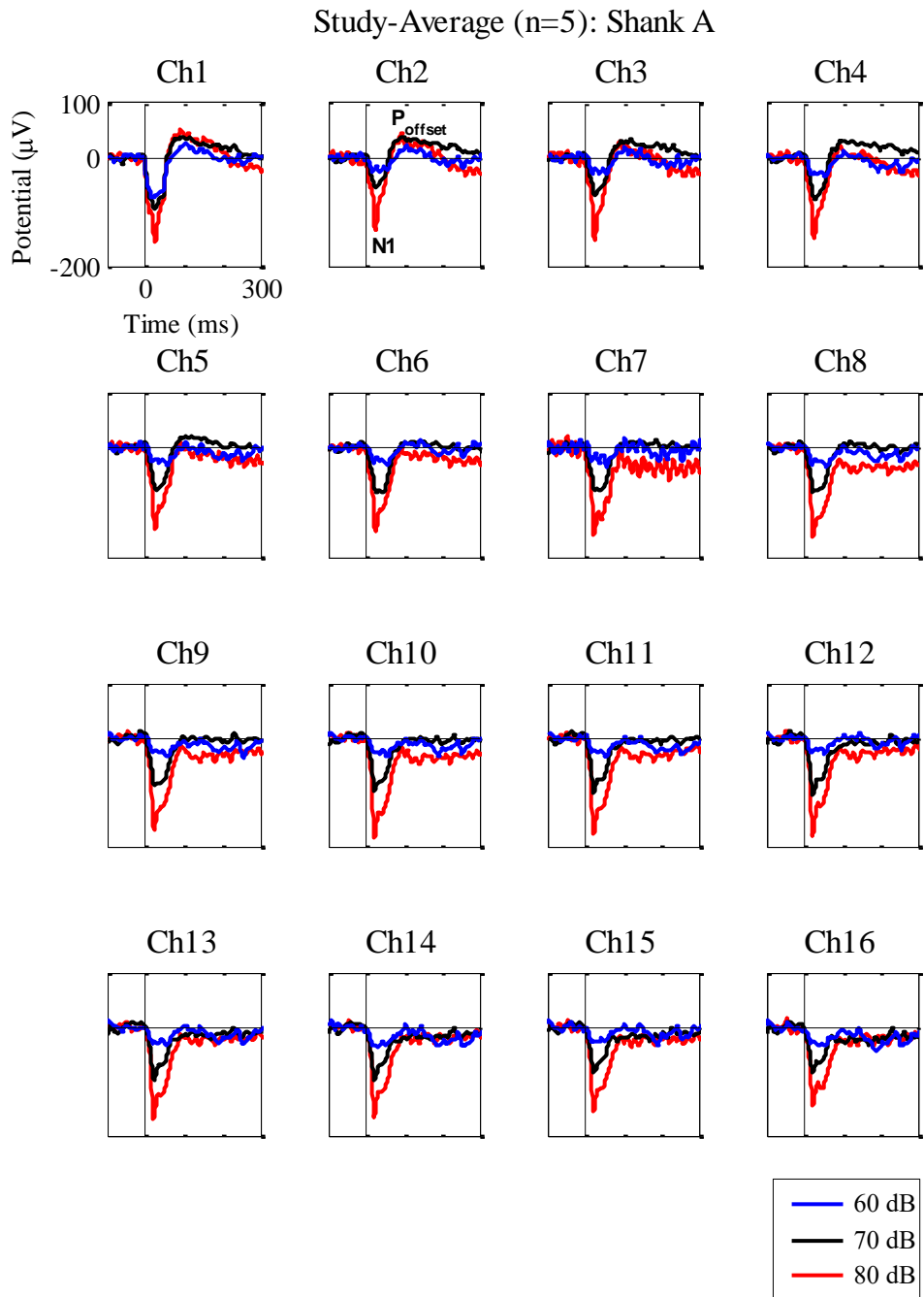


Figure 5.31 - Grand-average auditory evoked potentials to different intensity stimuli across multichannel probe electrodes Ch1-16 (Shank A) Three different intensity stimuli were presented in the modified consecutive-repetition paradigm; 60 dB (blue), 70 dB (black) and 80 dB (red), which were all 50 ms in duration, the best frequency (BF; calculated for each individual subject) and 450 ms inter-stimulus interval. Stimuli onset (N1) and offset (P_{offset}) responses appear to increase in magnitude with intensity. An inverted square-wave crosstalk artifact is apparent in Ch1 and interference is also seen in Ch7; these were removed from quantification in Figure 5.33. Intensity-varying stimuli auditory evoked potentials from Shank B are plotted in Figure 5.32.

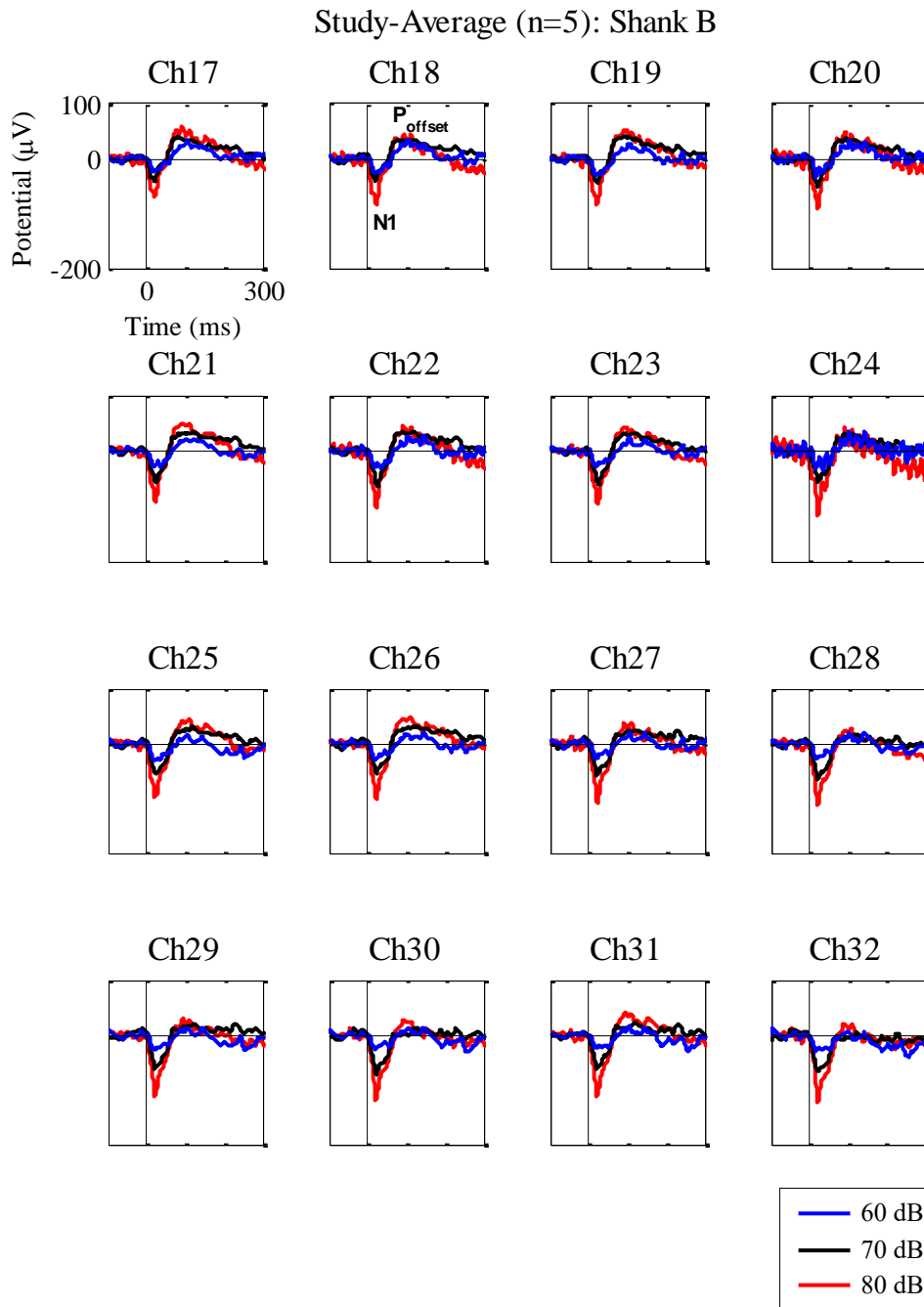


Figure 5.32 - Grand-average auditory evoked potentials to different intensity stimuli across multichannel probe electrodes Ch17-32 (Shank B) Similarly to Shank A waveforms plotted in Figure 5.31, the auditory evoked potentials to 60 dB (blue), 70 dB (black) and 80 dB (red) stimuli presented in the modified consecutive-repetition paradigm are plotted here. These stimuli were each 50 ms in duration, the best frequency (BF) for each subject and had an inter-stimulus interval (ISI) of 450 ms. Higher intensity stimuli elicit greater onset (N1) and offset (P_{offset}) response magnitudes, as observed from Shank A as well. Interference is present in Ch24 which is removed from the quantitative analysis in Figure 5.33.

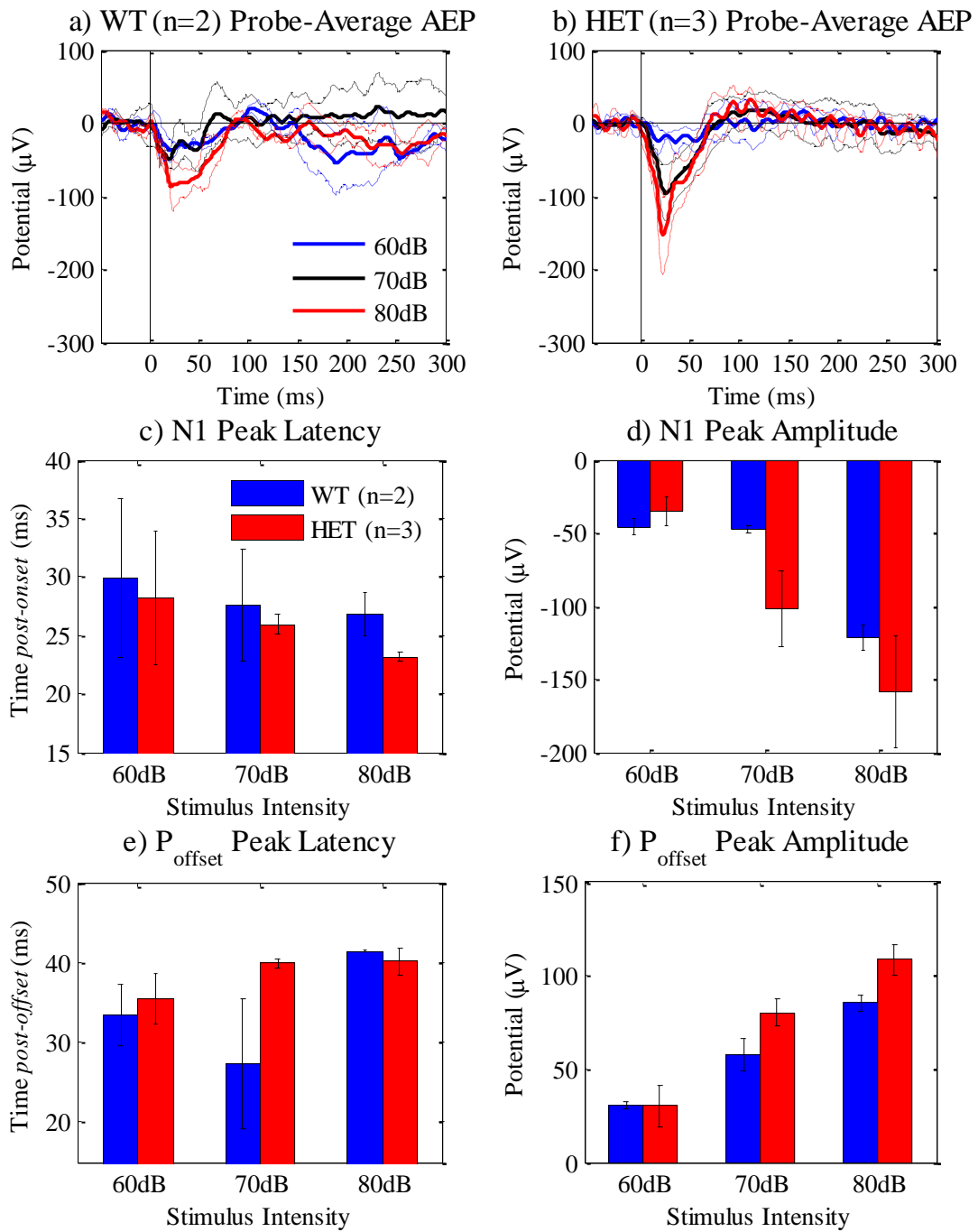


Figure 5.33 - Quantification of onset and offset responses to different intensity stimuli from wild-type and *Map2k7*^{+/-} mice in Experiment III Probe-average auditory evoked potential (AEP) waveforms from different intensity stimuli presented in the modified consecutive-repetition paradigm are plotted for a) wild-type control (WT) and b) *Map2k7*^{+/-} (HET) groups, \pm sem displayed by dashed lines. The following measures were quantified from the probe-average AEP extracted from each subject, displayed as group means \pm sem. c) Onset response (N1) peak latency. d) N1 peak amplitude displaying a trend towards greater negative amplitude with increasing stimulus intensity. e) Offset response (P_{offset}) peak latency measured from 0-50 ms post stimuli offset. f) P_{offset} peak amplitudes, also showing a trend towards greater magnitude responses with increasing stimuli intensity. 10 ms pre-offset baseline correction was used to quantify P_{offset} peak latency and amplitude, as illustrated by Figure 3.2.

5.3.3.2 *Comparison of auditory evoked potentials and multi-unit activity in response to different intensity stimuli*

Effects of stimulus intensity on multi-unit activity are analysed here with a comparison of AEP and MUA responses from Subject 75 presented in Figure 5.34. Although this analysis was performed on each subject individually, Subject 75 was the only one which displayed evidence of stimulus intensity effects on the resulting MUA and is therefore the only one reported. This may be suggested to arise from methodological considerations discussed in Section 5.4.4.

The AEP from 60 dB, 70 dB and 80 dB stimuli presented in the _{mod}CR paradigm are plotted in Figure 5.34a, Figure 5.34b and Figure 5.34c, respectively. The onset response (N1) is evidently larger for higher intensity auditory stimuli, as illustrated by the findings presented in Section 5.3.3.1 above. The purpose of this analysis is therefore to assess the MUA which may correlate with this increase in AEP amplitude caused by higher intensity stimuli. MUA detected during presentation of 60 dB, 70 dB and 80 dB stimuli in the _{mod}CR paradigm are shown as raster plots in Figure 5.34d, Figure 5.34e and Figure 5.34f, respectively. These are plotted with time post stimuli onset on the x-axis and trial (100 stimuli presentations each) on the y-axis, with each point illustrating a single-unit spike. Spikes were computed by the method described in Section 2.10.6. MUA was time-averaged over 25 ms time bins and plotted as the peri-stimulus time histogram (PSTH) for 60 dB, 70 dB and 80 dB stimuli in Figure 5.34g, Figure 5.34h and Figure 5.34i, respectively.

Visual comparison suggests early (≈ 0 -50 ms) MUA spike rates increase in response to higher intensity stimuli, corresponding with larger N1 amplitudes observed in the AEP. This analysis suggests MUA from the auditory cortex increases with sound intensity; however, this is single-subject data and therefore not statistically significant.

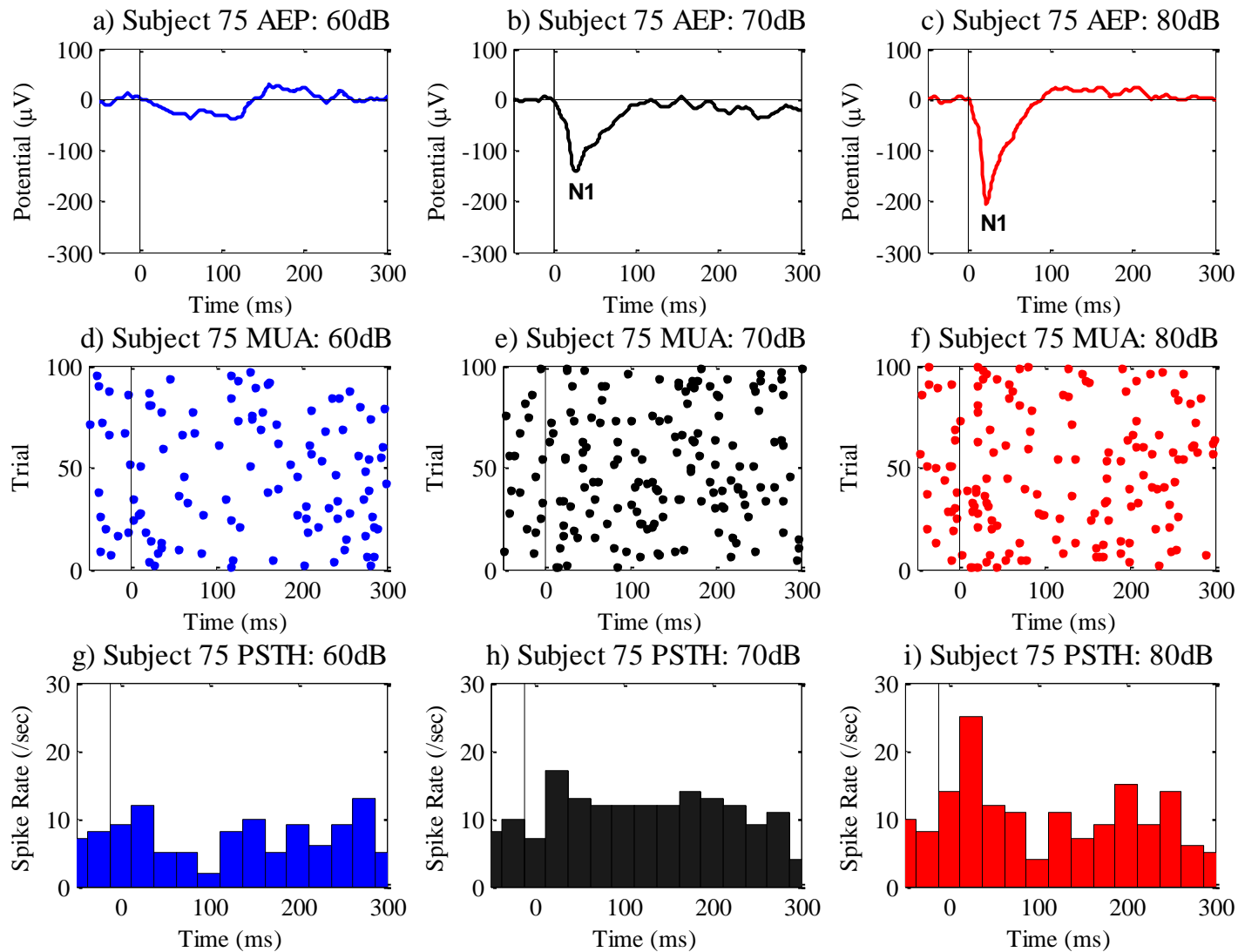


Figure 5.34 - Analysis of auditory evoked potential and multi-unit activity responses to different intensity stimuli in Subject 75 (HET, male)

This data was recorded in response to 60 dB, 70 dB and 80 dB stimuli, each presented 100 times in the modified consecutive-repetition paradigm. The auditory evoked potential (AEP) to a) 60 dB, b) 70 dB and c) 80 dB are plotted. Raster plots of multi-unit activity (MUA) are shown for d) 60 dB, e) 70 dB and f) 80 dB stimuli. Peri-stimulus time histograms (PSTH) are also shown for d) 60 dB, e) 70 dB and f) 80 dB stimuli. This data demonstrates some evidence of correlation between the AEP, MUA and PSTH, with greater N1 peak amplitude evoking greater MUA, shown in the PSTH.

5.3.4 Spike analyses

An overview of MUA recorded from all subjects (n=21) during pre- and post- 10 mg/kg i.p. ketamine administrations are reported (Figure 5.35), followed by a more detailed analysis of data from subjects which appear to offer contrasting responses to ketamine (Figure 5.36). In Figure 5.35 the total number of spikes recorded during each run of the experiment (Experiment #; each using separate animals) decreases markedly after the first couple then remains constantly below 20×10^3 . This reduction in total spikes recorded may indicate declining quality of recordings with multiple probe uses. The issue of recording quality is addressed in discussion Section 5.4.4. Five animals appear to display effects of ketamine on MUA; experiment #'s 1, 2, 13, 15 and 16, corresponding to Subjects 33, 43, 82, 71 and 77, respectively (Appendix C).

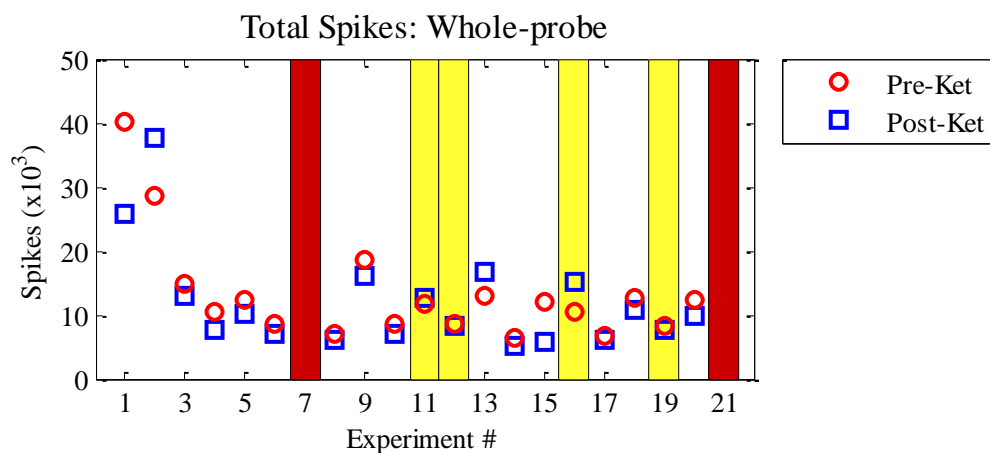


Figure 5.35 - Overview of multi-unit activity from all subjects in Experiment III a) The total number of spikes recorded from each subject arranged by experiment order during frequency oddball (fOD), deviant-alone (fDA) and many-standards (fMS) paradigms presented before delivering ketamine. Two probes were alternated between each consecutive subject and cleaned using procedures described in Section 5.2.3. Nevertheless, an early reduction in the total number of spikes recorded may be attributed to probe wear. Subjects in which an auditory evoked response was observed are highlighted with a yellow background. b) Equivalent to (a) post 10 mg/kg i.p. ketamine injection. Subjects which died prematurely following drug administration are blanked out with burgundy. Subjects which appear to exhibit differences between pre- and post-ketamine recordings are analysed further in Figure 5.36.

Apparent changes in the total number spikes observed in experiment #'s 2 and 15 were determined by visual inspection to arise from extraneous artifacts. Experiment # 2 recordings in the post-ketamine session were terminated prematurely due to a coupling issue with the sync channel, causing a reduction in the total MUA. In experiment # 15 a transient increase in spike activity was found immediately preceding 40 min (approximate drug delivery point), potentially caused by interference induced during ketamine administration. Thus experiment #'s 1, 13 and 16 MUA data are analysed further in Figure 5.36.

In Figure 5.36a it appears as though ketamine decreases the overall MUA detected from Subject 33. In these plots the approximate time at which ketamine was administered is labelled with a vertical dashed line. In contrast, Figure 5.36b and Figure 5.36c suggests ketamine causes a temporary increase in MUA observed from Subjects 82 and 77, respectively which lasts approximately 10 minutes before returning to pre-ketamine levels. Possible explanations for these contrasting observations are offered in Section 5.4.3.

5.3.4.1 Examples of spike waveforms

It should be noted that a quantitative analysis of single-unit activity (SUA) is not provided here. Rather, a brief summary of output from the spike sorting algorithm (Section 2.10.6) is provided with some example waveforms. After applying the klusta-kwik algorithm spike waveforms were classified from each shank separately and were typically located on individual channels. Example spike waveforms from the first three runs of Experiment III are plotted in Figure 5.37. These illustrate a greater diversity of classified spike waveforms were observed from the first two runs (experiment #'s 1 and 2) compared with following recordings.

The spike waveforms from experiment #3 (Figure 5.37e and Figure 5.37f) may represent noise which has incorrectly been classified as neuronal activity because its peak amplitude exceeds the threshold level. Similar waveforms were observed from experiment #'s 1 and 2. However, larger amplitude neuronal spikes (Figure 5.37a, Figure 5.37b, Figure 5.37c and Figure 5.37d) were only clearly observed from the first two runs. This is an issue regarding recording quality which may relate to probe condition. Possible explanations for this are offered in Section 5.4.4. Unreliable spike categorisation in addition to the absence of auditory evoked potentials in LFP recordings impairs the possibility of correlating SUA with specific paradigm events, which is highly unfortunate considering the resources spent to perform Experiment III. Suggestions for protocol improvement are also provided in Section 5.4.4.

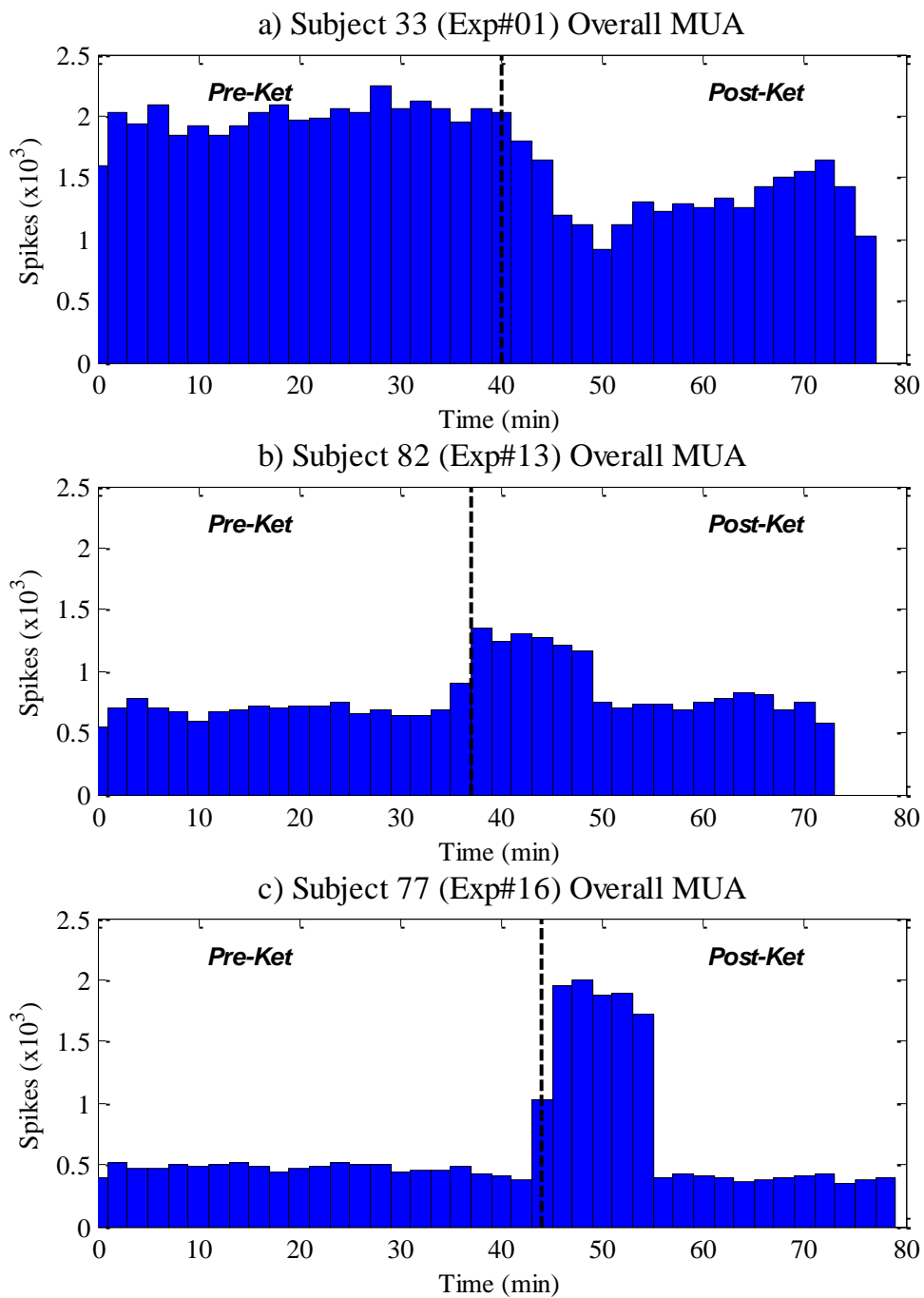


Figure 5.36 - Contrasting effects of 10 mg/kg i.p. ketamine on multi-unit activity in different subjects Multi-unit activity (MUA) is quantified here over 2 min time bins throughout pre-ketamine and post-ketamine periods (≈ 40 min) of Experiment III. a) In Subject 33 (HET, female; Exp#1) 10 mg/kg i.p. ketamine appears to have a depressive effect on MUA. b) Subject 82 (WT, female; Exp#13) displays an increase in activity at the approximate time of ketamine administration. It should be noted that the vertical dashed line displays an estimate of when ketamine was delivered, however this response may suggest it was slightly earlier in this subject. c) In Subject 77 (HET, female; Exp#16) ketamine causes a sharp increase in MUA which lasts approximately 10 min. These variable observations may result from different neuron types being recorded from each subject, addressed in Section 5.4.4.

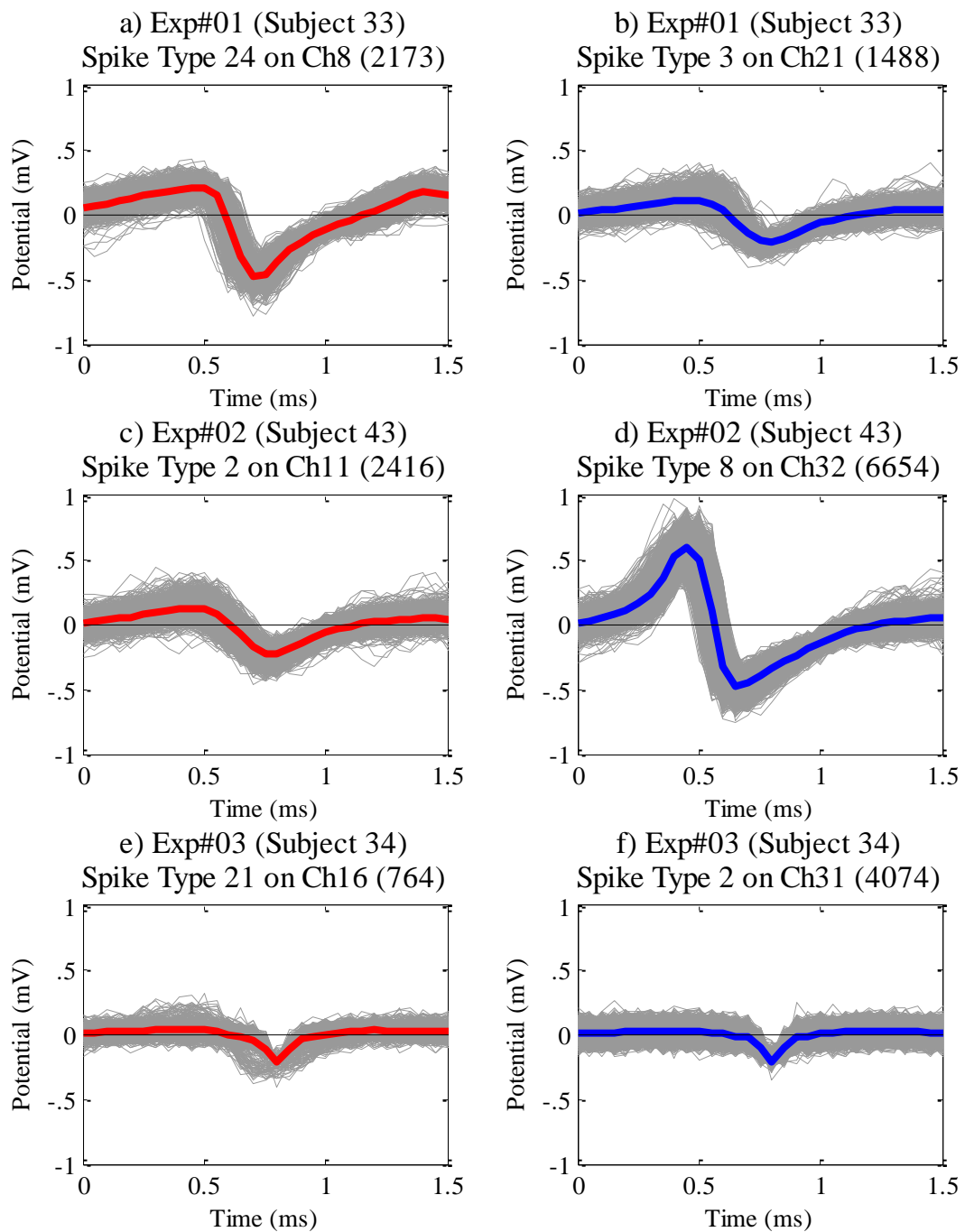


Figure 5.37 - Example spike waveforms These plots demonstrate some of the different waveform shapes observed from the first three runs of Experiment III. Shank A spike recordings are plotted on the left hand side in red those from Shank B are plotted on the right hand side in blue; mean in colour and individual waveforms in grey. Subject 33/Exp#1 (HET, female); a) spike type 24 on Ch8, and b) spike type 2 on Ch21. Subject 43/Exp#2 (WT, female); c) spike type 2 on Ch11, and d) spike type 8 on Ch32. Subject 34/Exp#3 (HET, female); e) spike type 21 on Ch16, and f) spike type 2 on Ch31. A more diverse range of neurons were classified from Exp#1 and Exp#2 data, after which many of the waveforms observed were very similar to those portrayed here from Exp#3 which may partly reflect noise exceeding the spike detection threshold. Comments on recording quality are given in Section 5.4.4.

5.3.5 Results summary

Key findings from Experiment III are outlined below in terms of stimuli duration, frequency and intensity effects, followed by a brief summary of spiking observations. Data from two WT and three HET mice were pooled together for analysis, unless otherwise stated.

5.3.5.1 Stimuli duration effects

Stimuli offset responses (P_{offset}) were observed from different duration stimuli (e.g. Figure 5.5 and Figure 5.6). These manifested as positive amplitude peaks in superficial-most channels, comparable with Experiment I findings, whereas in deepest channels potential remained negative and returned to baseline following stimuli offset. Re-referencing to remove signals common to deep channels (Figure 5.9) revealed that this positive deflection in superficial channel recordings occurs shortly after stimuli onset, driving the potential towards baseline. Offset of auditory stimulation un masks this response, revealing the P_{offset} deflection. Thus multi-unit activity (MUA) which contributes to P_{offset} is likely to precede stimuli offset latency, complicating efforts to identify MUA correlations with this response.

5.3.5.2 Stimuli frequency effects

Auditory evoked potential (AEP) waveforms from different frequency stimuli suggested that the frequency response (FR) screening procedure was at least partially successful. The best frequency (BF) appeared to elicit the largest auditory response overall (Figure 5.11, Figure 5.12 and Figure 5.13). The onset response (N1) peak amplitude was found to be significantly greater for BF stimuli versus non-BF stimuli in the frequency many-standards (fMS) paradigm (Figure 5.14). Analysing the response of each individual animal to ten fMS paradigm stimuli (Figure 5.15) provided an indication of frequency sensitivity of the local neural tissue at the probe implantation site. There were some interesting correlations between these frequency sensitivities and subsequent responses to the frequency oddball (fOD) and deviant-alone (fDA) paradigm evoked waveforms.

The frequency mismatch response (fMMR) observed from five animals which displayed auditory responses varied considerably. Subject 36 (WT, female) displayed a fMMR comparable with those observed from Experiment I (Figure 5.16) which was apparently reduced by 10 mg/kg i.p. ketamine (Figure 5.17). In three cases (Subjects 74, 76 and 77) these fMMR waveforms were similar, specifically a relatively large amplitude response to BF-3 kHz oddball stimuli, peaking at ≈ 100 -200 ms which exhibited a change in polarity from superficial to deep channel recordings (Figure 5.18, Figure 5.20 and Figure 5.22); ketamine did not appear to diminish these responses (Figure 5.19, Figure 5.21 and Figure

5.23). However, the considerable level of variation between individual subjects was obstructive in quantifying the overall fMMR.

The fDA paradigm auditory evoked potentials generally correlated well with fMMR waveforms, similar to Experiment I. In Subject 75 (HET, male), MUA appeared to underlie a large N1 peak in response to BF+3 kHz stimuli in the fDA paradigm (Figure 5.30), suggesting that auditory neurons were detected in recordings from this subject. Otherwise no rational correlations were found between MUA and AEP features.

5.3.5.3 *Stimuli intensity effects*

Increasing stimuli intensity generated larger AEP N1 and P_{offset} features (Figure 5.31, Figure 5.32 and Figure 5.33), in agreement with previous findings. This increased responsiveness was also apparent in MUA observed from Subject 75 (HET, male; Figure 5.34).

5.3.5.4 *Ketamine and spiking activity*

Recordings made from successive animals revealed the total number of spikes decreased initially then remained similar (Figure 5.35). Further examination of MUA from three different subjects during pre- and post-ketamine periods appeared to indicate contrasting effects; with one displaying reduced MUA (Figure 5.36a) and the other two displaying increases in MUA (Figure 5.36b and Figure 5.36c) in response to 10 mg/kg i.p. ketamine. These results are discussed in detail below.

5.3.5.5 *Map2k7^{+/-} gene disruption*

As found in previous chapters the *Map2k7^{+/-}* (HET) model appears to influence the early onset (N1) feature of the auditory evoked potential, which tends to be larger in the HET group versus wild-type (WT) control animals. Although there are insufficient sample sizes here to obtain a statistically significant result, this trend is observed in Figure 5.8, Figure 5.13 and Figure 5.33, which corroborate findings from Experiment I and Experiment II. Multi-unit activity recorded from Subject 75 (HET, male) may suggest that increasing N1 magnitude coincides with increased spiking activity detected in the auditory cortex (Figure 5.30 and Figure 5.34). However, reliable evoked MUA was not observed from the other two HET animals that displayed an auditory response in LFP recordings; thus there is not enough evidence to determine whether HET mice have greater levels of evoked MUA compared with WT controls that could explain the enlarged onset response.

5.4 Discussion

This chapter has provided some preliminary evidence to suggest that the frequency mismatch response recorded from the auditory cortex in urethane-anaesthetised mice displays a laminar-specific profile. Additionally, AEP waveforms extracted from LFP recordings made at different depths in the auditory cortex have been examined, indicating that the offset response (P_{offset}) is underpinned by an earlier response in superficial cortical layers. Multi-unit activity (MUA) correlated with the stimulus onset response (N1) has been observed. Furthermore, there appears to have been contrasting effects of ketamine on cortical spike activity detected. These findings, along with a discussion of the relatively low success rate of this experiment and suggestions for improvement, are addressed in the following subsections.

5.4.1 *Effects of stimuli duration, frequency and intensity on laminar auditory evoked potentials in urethane-anaesthetised mice*

Offset responses were observed from different duration stimuli with 5 ms rise/fall times (Figure 5.10). As seen in superficial channels these correspond with P_{offset} potentials observed in EEG recordings from urethane-anaesthetised mice in Chapter 3. Relative to deep channel recordings these reflect an early electrophysiological change in response to stimulation onset, inducing different waveform morphologies (Figure 5.9). This difference between superficial and deep channel responses may support the hypothesis that offset responses, at least in superficial layers, results from an inhibitory rebound effect, as suggested previously (Kuwada and Batra, 1999). Although the underlying neurochemical processes cannot be ascertained from this data, the observation that potential returns towards baseline immediately following peak onset response may intuitively suggest the action of homeostatic control, of which inhibitory feedback regulation is the proposed mechanism as superficial layers have higher levels of GABAergic signalling (Figure 1.8). This is, however, in contrast with previous observations at the single- and multi-unit (SUA/MUA) level that auditory offset responses are active processes driven by stimuli offset and not by inhibitory rebound (Scholl et al., 2010). Perhaps this is true for intermediate or deep layer recordings, although no MUA or SUA correlates of offset responses were observed from the present study.

There is evidence of adaptation in onset response peak amplitudes following successive presentations of best-frequency (BF), 70 dB stimuli with an ISI of 450 ms. The first, second and third 100 stimuli were 100 ms, 150 ms and 50 ms duration, respectively. Comparing the resulting AEP waveforms <50 ms post stimuli onset indicate N1 peak amplitude reductions

with repeated presentations (Figure 5.8). This potentially reflects fatigue or increased refractory periods of neural generators underlying the N1 response (Budd et al., 1998). Interestingly, the degree of N1 suppression appears to be greater for wild-type (WT) control mice than *Map2k7*^{+/-} heterozygotes (HET). Little difference between WT and HET groups is found in onset response from the first 100 stimuli, whereas separation arises and becomes greater in the second and third sequences of 100 stimuli (Figure 5.8d). Combined with findings from Chapter 3 and Chapter 4, this may indicate that *Map2k7*^{+/-} mice have deficient neural refractory systems which underlie an enlarged N1 peak amplitude over extended periods of auditory stimulation.

Frequency sensitivity of the auditory cortex, or tonotopy (introduced in Section 1.2.2), was observed from LFP recordings (Figure 5.14 and Figure 5.15). This more localised tissue response differs from epidural EEG recorded from animals in Chapter 3 and Chapter 4. This is presumably because tonotopy becomes apparent in higher spatial resolution recordings (LFP $\approx 1 \text{ mm}^2$), using smaller electrodes, whereas epidural EEG measured from skull screws ($\approx 3 \text{ mm}^2$) reflects broader electrophysiological activity (Nelken and Ulanovsky, 2007). Additionally, MUA from Subject 75 (HET, male) in the frequency deviant-alone paradigm was increased in response to higher frequency (BF+3 kHz) but not lower frequency (BF-3 kHz) stimuli (Figure 5.30). This is an indication of cellular resolution frequency tuning (MUA $\approx 100 \mu\text{m}^2$), which correlated with an enlarged stimulus onset response. However, SUA responsible for this response, thought to arise from afferent projections, could not be isolated from spike recordings; discussed in Section 5.4.4 below.

Sound pressure level (SPL), or intensity, increased N1 and P_{offset} responses (e.g. Figure 5.33), as found in previous chapters. Moreover, putative auditory neurons recorded from Subject 75 (HET, male) appeared to vary monotonically with stimulus intensity, corresponding with onset response peak amplitude (Figure 5.34). This interpretation of observed MUA is reasonable considering that the majority of intensity tuned neurons in the auditory cortex are monotonic (Winer and Schreiner, 2011). In an intensity oddball paradigm experiment Farley et al. (2010) showed that loud oddball stimuli generate a significant increase in MUA compared with loud standard stimuli; in contrast, MUA evoked by soft oddball and standard stimuli did not differ significantly. This may suggest that monotonicity, or intensity tuning, is subject to prior auditory inputs, reflecting a form of auditory sensory-memory. However, further investigations concentrating on the intensity mismatch response would be required to establish the true nature of neural spiking variations with SPL, relative to the context of auditory stimulation. Furthermore, the use of broad spectrum 'white noise' stimuli may be preferred for such studies to limit tonotopic effects.

5.4.2 *Frequency mismatch response laminar profile in urethane-anaesthetised mice*

It is not possible to fully characterise the fMMR laminar profile using these results. However they do provide a several insights which may be useful for guiding further research in this area. It should be noted that this discussion relates to the response of urethane-anaesthetised mice only, as seen previously this varies considerably from conscious mice. Firstly, frequency oddball stimuli typically generate long-latency AEP feature(s) peaking >100 ms post stimuli onset. Secondly, these display some degree of tonotopy, but not necessarily in line with the best frequency. Thirdly, this potential generally displays positive polarity in superficial layers, decreasing and becoming negative with increasing cortical depth. In consideration of current dipole models (Kiebel et al., 2008, Schimpf et al., 2002) this suggests that the underlying neural generators involve a prominent cortical component, perhaps comparable with the supragranular (LII/III) generators observed in monkeys by Javitt et al. (1996). Fourthly, this fMMR tends to correlate with deviant-alone paradigm evoked waveforms, indicative of a pronounced contrast between current and preceding auditory inputs. Finally, 10 mg/kg i.p. ketamine did not appear to consistently diminish these long-latency features, suggesting that they are not reliant on intact NMDA receptor signalling.

In order to quantify the laminar profile of this fMMR in urethane-anaesthetised mice the first step requires adequate data alignment, such that channel recordings from different subjects are aligned with regards to cortical depth. This was attempted here with current source density analysis (see example in Figure 5.4 and summary of results in Table 5.2), although the results were not clear enough to confidently unify datasets, as discussed in Section 5.4.4 below. After aligning recordings according to depth they would also have to be normalised based on frequency sensitivity. The usual AEP group-averaging method may then be applied to compare differences between *Map2k7*^{+/-} and wild-type control animals. Furthermore, with better quality recordings quantification of MUA and SUA correlated with these long-latency fMMR potentials may provide information about the cellular sources of this response.

Although firm conclusions cannot be reached from these data, they may tentatively suggest an agreement with the assignment of intracortical sources (LII/III) of prediction error generation (Section 1.2.3 and Figure 1.9) which is observed as an MMR (Baldeweg and Hirsch, 2015). Replication of this experiment with improved technique and cleaner data will assist in confirming this account. An additional step that may be advantageous for dissecting the neural circuitry involved in MMR generation in mice is the implantation of recording

electrodes into subcortical structures such as the auditory thalamus and hippocampus, which are speculated to play a role in generating MMN (Näätänen et al., 2007). It should be reiterated, however, that these data were obtained from urethane-anaesthetised mice and may not necessarily reflect the response of conscious animals.

5.4.3 The effect of ketamine on spike activity in urethane-anaesthetised mice

Ketamine did not significantly affect overall spiking activity. However, three individual animals (Subject 33, HET, female; Subject 82, WT female; Subject 77, HET, female) did appear to show an effect of the drug on MUA (Figure 5.36). Two demonstrated transiently enhanced spike rates immediately following ketamine administration (Subjects 82 and 77), whereas the other displayed a more steady suppression of firing rates (Subject 33). This may reflect the suggested dual excitatory/inhibitory role of NMDA receptors illustrated in Figure 1.2, where inhibition is influenced by γ -aminobutyric acid (GABA) interneurons expressing NMDA receptors (Javitt et al., 2005). Ketamine administration, which can thereby block inhibitory GABAergic interneurons, may furthermore increase circulating extracellular glutamate concentrations resulting in higher levels of glutamatergic excitation via AMPA or kainite receptors (Homayoun and Moghaddam, 2007).

The contrasting observations in the present study may therefore indicate a situation where different types of neurons were being recorded from different subjects. For example, perhaps a higher proportion of ‘quietened’ GABAergic interneurons were recorded from one subject, and more excited glutamatergic pyramidal cells were recorded from the other two subjects. Unfortunately, reliable single-units could not be isolated from these recordings, with many of the spike waveforms displaying similar characteristics (e.g. Figure 5.37e-f). This limits the possibility of investigating these differential responses to NMDA receptor antagonism further; reasons for this are addressed in Section 5.4.4 below.

5.4.4 Success rate/recording issues and suggestions for improvement

Five from 21 animals used in this experiment displayed an auditory evoked response in LFP recordings. This success rate is below acceptable and measures need to be implemented to prevent this from reoccurring in future studies. The obvious reason why auditory responses were not present in 16 runs of the experiment is incorrect probe placement. Furthermore, this indicates a failure of the frequency-response (FR) screening procedure which should have confirmed electrode locations within the auditory cortex frequency representation. Perhaps this happened because spontaneous spiking activity was detected and mistakenly assigned as being auditory-evoked. To mitigate this in future, statistical methods should be applied to

compare evoked and spontaneous (baseline versus stimulation-on) MUA to confirm statistically significant responses to auditory stimulation during FR screening. Moreover, the N1 peak amplitude may also be used to determine the BF (e.g. as illustrated in Figure 5.15) and generally confirm electrode implantation within the auditory cortex.

Among the five animals which did exhibit an auditory response, it proved challenging to correlate overall spiking activity with auditory onset or offset (Figure 5.10d-e). Subject 75 (HET, male) displayed MUA correlated with N1, as discussed above. The reason for this observation may be the sheer diversity of neurons within the cortex and lack of control over which types of neurons are detected in recordings. This also explains the apparently contrasting effects of ketamine on MUA discussed above which may reflect the activity of different neuron types. This lack of control from current *in-vivo* electrophysiology recording techniques is a severely limiting factor. Spike sorting algorithms such as that implemented here (see Section 2.10.6) aim to categorise different spike waveforms according to their recorded properties. However, how these ‘clusters’ correspond with distinct neurobiological entities is unclear. Optogenetic technologies used for controlling specific targeted cell types with light-activated ion channels (Boyden et al., 2005) may partially overcome this limitation when combined with *in-vivo* electrophysiology recordings; however, the number of different neuron types which can be labelled in this way is still practically restricted.

Current source density analysis was somewhat inconclusive (Table 5.2), preventing reliable alignment of data. This may have distorted study-average laminar analysis, although relative proximal to distal channel comparisons may still be generally accepted based on probe geometry. This non-ideal situation is considered to result from poor recording quality. As seen from spike recordings (Figure 5.35), following initial probe uses there was a decline in the total number of spikes recorded, a typical indicator of spike recording quality.

Furthermore, there was a reduction in the diversity of spike waveforms observed (Figure 5.37). This is considered to have resulted from probe wear. Although the prescribed cleaning and care guidelines to extend the usage of these acute probes were followed this reduction in recording quality is still apparent. This highlights probe use and care as key technical considerations for future experiments with repeated use of acutely implanted probes.

Overall these issues and the general unsatisfactory success rate of this experiment indicate that further development of this challenging and novel technological approach and protocols is required. However, the findings do present some interesting insights which are discussed in relation to previous findings from Chapter 3/Experiment I and Chapter 4/Experiment II in Chapter 6.

Chapter 6. General discussion

6.1 Discussion of main findings

The preceding chapters have presented original findings from experiments that explore mismatch responses to different physical features of sound in genetic (*Map2k7^{+/-}*) and NMDA receptor antagonist (ketamine) mouse models relevant to schizophrenia. Stimulus duration, frequency, intensity and inter-stimulus interval manipulations have been examined systematically, and the implications of these findings will now be discussed in relation to the broader fields of animal MMR and human MMN research. Firstly, the effects of state are addressed, after having implemented experiments using urethane-anaesthetised (Chapter 3: Experiment I and Chapter 5: Experiment III) and conscious animals (Chapter 4: Experiment I). Next the mismatch response findings from each of these experiments are summed up with a discussion of their potential impact on the wider field. The unpredicted but robust observations in the auditory evoked potential (AEP) from *Map2k7^{+/-}* (HET) mice are then discussed, with tentatively proposed mechanisms and potential avenues worthy of further exploration. Findings attained from administering the NMDA receptor antagonist ketamine are then discussed, with implications for understanding the neurochemistry of the mouse AEP. Suggestions for further work and comments on the translational relevance of the mouse MMR followed by concluding remarks then bring this discussion to a close.

6.1.1 Anaesthetised and conscious states

Similarities and differences were found between the AEP waveforms elicited from urethane-anaesthetised (Figure 3.34) and conscious mice (Figure 4.33). Onset (N1) and offset (P_{offset}) features were common to both states. Urethane-anaesthetised mice displayed an additional-extended latency feature that was not present in conscious animals, defined here as deviant evoked activity (DEA). DEA was observed in response to deviant-alone paradigms and also frequency and increasing-intensity oddball paradigms. In contrast, conscious subjects displayed a series of five alternating polarity deflections (P2, N3, P4, N5 and P6) following N1, which were not observed in the AEP from urethane-anaesthetised mice.

One interpretation of these differences is that the neurophysiological mechanisms responsible for generating P2, N3, P4, N5 and P6 deflections are blocked by urethane. These components may signify aspects of consciousness; and/or are underpinned by neurotransmitter systems perturbed by urethane (e.g. GABA, glycine, NMDA, AMPA, or ACh receptors), but perhaps remain intact under different anaesthetics. Future studies may employ different anaesthetic agents to investigate this.

These state-differences in AEP morphology fundamentally influence mismatch responses resulting from auditory oddball paradigms; apart from early deflections ($\approx 0-20$ ms) caused

by differences in N1 amplitudes, or in the case of duration MMR, offset potential (P_{offset}) effects (see Section 6.1.2 below). The similarity between urethane-anaesthetised and conscious mice is not entirely inconsistent with the human MMN, which is purportedly observed in anaesthetised and comatose states (Fischer et al., 1999, Fischer et al., 2000, Heinke et al., 2004, Kane et al., 1996). However, peak latencies, polarities and overall AEP morphologies differ substantially between humans and mice.

6.1.2 *Mismatch responses in mice*

When characterising the auditory cortex MMR to duration, frequency, intensity and inter-stimulus interval (ISI) manipulations in conscious and urethane-anaesthetised (minus ISI) mice, a pattern emerged in which difference waveforms could be explained by the physical properties of stimuli used. The only exception to this is the extended latency feature, DEA, elicited from urethane-anaesthetised mice in response to deviant-alone control paradigms as well as frequency and increasing intensity oddball paradigms.

The duration mismatch response was predominantly shaped by stimulus offset responses, which varied in peak latency between stimuli of different durations. This then influenced peak latencies in the difference waveform, perhaps relevant to the human duration MMN which varies depending on the duration of oddball and standard stimuli (Colin et al., 2009, Shelley et al., 1991, Takegata et al., 2008). Offset responses were observed from urethane-anaesthetised and conscious mice using stimuli with instantaneous rise/fall times, and from urethane-anaesthetised mice using 5 ms rise/fall times. Furthermore, laminar analysis (Chapter 5: Experiment III) indicates that the offset potential source is located in superficial layers of the auditory cortex. Determining the nature of this response may be beneficial for understanding reductions in duration MMN seen in patients with schizophrenia (see Section 1.2.1.1).

Frequency, intensity and ISI levels inherently influence AEP amplitudes. In epidural EEG recordings from the auditory cortex of conscious mice (Chapter 4: Experiment II) these physical parameters correlated with N1 and P2 deflections; whereas in urethane-anaesthetised mice (Chapter 3: Experiment I) they correlate with N1 and P_{offset} deflections (effects on P_{offset} were not quantified in conscious animals). These differences were sufficient to explain deflections in mismatch response waveforms produced by physically distinct standard and oddball stimuli. The AEP generated by identical stimuli presented in oddball and control (consecutive-repetition and many-standards) paradigms did not differ significantly. This may therefore be summed up by saying that the physical properties of stimuli are sufficient to explain these mismatch responses in mice. Thus these results do not

support the sensory-memory disruption or stimulus specific adaptation (SSA) hypotheses of MMN.

In conscious animals, the P2 deflection (≈ 25 -50 ms post stimulus onset) in AEPs was acutely abolished by 10 mg/kg i.p. ketamine for up to 10 min post injection. This may feasibly attenuate the MMR reflecting changes in P2 induced by frequency, intensity or ISI differences. In a sense this is comparable with human MMN which is diminished by ketamine in healthy volunteers (Umbricht et al., 2002). However, these findings do not necessarily agree with the interpretation of MMN as reflecting a sensory-memory trace disruption or adaptation effect; rather, this appears to be an obligatory AEP component that relies on NMDA receptors and is modulated by different physical properties of stimuli.

Extended-latency DEA observed from urethane-anaesthetised mice fulfilled some of the criteria set forth by Harms et al. (2015) to establish whether an animal MMR analogous to the human MMN exists in rodents. This feature was elicited by deviant-alone, frequency and increasing intensity oddball paradigms, and may be interpreted to reflect a sensory-memory disruption. Preliminary laminar analysis (Chapter 5: Experiment III) suggests neural generators of DEA may reside intra-cortically, somewhat similar to previous MMR studies in monkeys (Javitt et al., 1996), although NMDA receptor blockade by ketamine did not acutely abolish this response. The fact that this component peaks at approximately ≈ 300 -500 ms disagrees with the principle that mouse AEP features should occur at shorter latencies than humans due to the smaller brain size; whereas the human MMN reportedly peaks at ≈ 150 -250 ms. In addition, it should be reiterated that this response was seen in urethane-anaesthetised but not in conscious mice. It therefore cannot be said with confidence that this DEA represents an MMR analogous to the human MMN, but nevertheless provides an interesting finding that may be worth examining further.

Both MMN and SSA are interpreted in the literature using high-level, generalised theories of sensory-memory disruption and adaptation, respectively. Theoretical models have been devised which seek to explain findings from human EEG and single-neuron recordings in animals using these abstract terms (e.g. Figure 1.9), neglecting to recognise the fundamental role that physical properties of sound play in central auditory processing. This may be an unfortunate shortcoming, as this thesis has found the mouse MMR to be predominantly influenced by physical parameters of auditory stimuli employed in oddball paradigms. SSA may occur in response to frequency changes, as different populations of neurons are stimulated by different sound frequencies; however, there are no clear indications in the literature this occurs in response to stimulus duration or intensity changes, for example.

Overall, this highlights the need to systematically control for the potential effects of physical properties of stimuli in both animal MMR and human MMN experiments.

6.1.3 *The Map2k7^{+/-} model*

Urethane-anaesthetised and conscious *Map2k7^{+/-}* (HET) mice displayed a significantly increased amplitude onset response (N1) compared with wild-type controls, whereas other AEP features were comparable in amplitude and latency. This was observed from two separate cohorts, suggesting this is replicable effect of *Map2k7* gene disruption. It may be proposed that this N1 response could be a mouse analogue of the human N100 which is diminished in schizophrenia patients (Rosburg et al., 2008, Turetsky et al., 2009). One possible hypothesis is that *Map2k7* acts to restore these deficits in humans against other neuropathological factors driving its amplitude down; although this is purely speculation. Although the N1 seen from mice in this study is the same polarity as N100 in humans this does not necessarily mean that they reflect the same neurophysiological processes. Potentially the N1 is more akin to the human P50 (Figure 1.3), which is actually the first large deflection observed in the human AEP. It has also been suggested in Section 4.4.3 that enlarged N1 in HET mice could reflect abhorrent sensory gating, which is disturbed in schizophrenia patients; potentially reflecting a complex interaction of glutamatergic, GABAergic, nicotinic, cholinergic and serotonergic systems. To examine this further will involve performing studies with a range of pharmacological challenges to dissect the potential role of these different neurotransmitters in mouse N1 generation. Investigations using ketamine in these mice did not reveal a genotype-ketamine interaction, suggesting that NMDA receptors are unlikely to be involved in the altered N1 response in *Map2k7^{+/-}* mice. Considering that ketamine did not observably have a differential effect on HET versus WT mice with regards to AEP amplitudes, EEG spectral power or animal movement, indications are that NMDA receptor-mediated signalling is not impaired by *Map2k7* gene disruption. It is possible that AMPA receptors in the auditory system (reviewed by Parks, 2000), being the fastest transmitters of synaptic excitation, may play a pivotal role in the mouse N1 response. Stimulation of AMPA receptors activate intracellular MAPK signalling cascades (Perkinton et al., 1999, Sweatt, 2001), and there is evidence of JNK pathways being involved in regulating AMPA receptors (Thomas et al., 2008, Zhu et al., 2005). To examine the relationship between auditory cortex neurophysiology, AMPA receptors and *Map2k7*, further studies using *in-vivo* and *in-vitro* electrophysiological techniques with AMPA receptor antagonists (such as talmpanel or perampanel, for example) may be conducted.

6.1.4 *The NMDA antagonist model*

Ketamine (10 mg/kg i.p.) had negligible effect on auditory cortex electrophysiology measured from urethane-anaesthetised mice. On the other hand, in conscious animals it specifically and acutely ablated the P2 deflection of the AEP, measured between ≈ 25 -50 ms; this effect lasted for ≈ 10 min, and coincided with heightened locomotion and gamma band synchrony. This is somewhat similar to findings from Ehrlichman et al. (2008) that showed ketamine diminished the mouse MMR, evoked by a frequency oddball paradigm, from ≈ 25 -75 ms. The P2 peak was not present in the AEP from urethane-anaesthetised mice, thus explaining the apparent lack of ketamine effect; this may be because the dose of urethane administered was sufficient to block this response, as this anaesthetic is found to inhibit NMDA receptors (Hara and Harris, 2002). This thesis has demonstrated (Chapter 4: Experiment II) how ketamine may diminish the mouse MMR induced by physical properties of stimuli (frequency, intensity or ISI), by abolishing both standard and oddball stimuli P2 deflections, reducing the difference between them.

From these findings it may tentatively be proposed that P2 in conscious mice reflects the human N100 (Figure 1.3), both of which are modified by physical parameters of stimuli and are attenuated by ketamine; thus inferring that the human MMN is a modification of the N100 caused by physical differences between stimuli. Unfortunately the time window of effect observed in these studies was rather brief, with ketamine inducing observable neurophysiological changes for up to 10 min. This transient response is a limiting factor for lengthy electrophysiology recording protocols involving multiple control paradigms. Perhaps a continuous drug infusion approach may be taken in order to compensate, although this would pose additional technical challenges. The preferred route suggested for exploring neurophysiology of auditory evoked potentials and mismatch responses in mice may be to use techniques for genetic manipulation, e.g. using genetic mouse models as described in this thesis, which are not temporally restricted in this manner. Although pharmacological studies will be valuable moving forward in this area of research, their time-course of action should be considered in the design of future experiments.

6.2 Suggestions for further work

A few recommendations are presented below.

6.2.1 *Technical improvements*

The potential for movement artifacts to contaminate AEP waveforms from conscious mice should be rigorously controlled in future studies. This could be in the form of an accelerometer attached to the amplifier head-stage, or electromyography (EMG) data, sampled synchronously with EEG recordings, enabling the production and analysis of an auditory-evoked movement signal. Furthermore, video footage analysis performed as part of Experiment II demonstrated that ketamine enhanced animal movement within the recording chamber for a period following injection; an improvement upon this technique may be simultaneously recording video and audio, which will enable an analysis of any sound-locked video motion.

In both Experiment I and Experiment II, AEP waveform features were seen to vary over time (minutes to hours) as multiple auditory paradigms were presented, which may be interpreted as a form of adaptation. Experiment design must be carefully considered in light of these findings, and appropriate counterbalancing of auditory paradigms selected for future studies.

In view of the 3Rs initiative (replacement, reduction and refinement of animals in research), a key recommendation for future studies is that the same animals are used in conscious and anaesthetised experiments. This would aim to maximise data output from animals, thereby reducing the total number required. Taking this approach it may be possible to conduct multiple experiments using a single cohort of mice.

6.2.2 *Component characterisation*

In order to characterise the biochemical and neurophysiological basis of AEP components (e.g. N1, P2, N3, P4, N5, P6, $P_{\text{offset}}/N_{\text{offset}}$, and DEA), different pharmacological agents may be employed. Disrupting neurotransmitter systems suspected to play a role in generating these features may be applied quite straightforwardly, for example using AMPA or GABA receptor modulators (such as talampanel or bamaluzole, respectively). Additionally, genetic contributions may also be explored, which may be more desirable. Further characterisation of physical features that influence AEP components may also be performed. One pertinent feature is stimulus rise and fall time, which may be examined using a variation of the many-standards paradigm. It may be hypothesised that rise/fall time is instrumental in determining onset and offset response peak amplitude and latency, therefore particularly relevant for the duration mismatch response.

6.2.3 *Translational validity*

This thesis has shown that AEP waveforms may be elicited from urethane-anaesthetised and conscious mice, somewhat similar to humans. Importantly, the influence that physical properties of auditory stimuli have on this AEP in mice leads to the suggestion that the human AEP may be sensitive to physical parameters in a similar manner. This should be considered when assessing human MMN studies, and provides an alternative view to the traditional hypotheses.

Two separate mouse models representing neurobiological risk factors for schizophrenia have been found to display separate effects on the AEP; with *Map2k7*^{+/-} mice showing an enlarged onset response (N1) during anaesthetised and conscious states, while 10 mg/kg i.p. ketamine specifically abolished the secondary response (P2) in conscious mice. These findings indicate that mouse models of the AEP can be used for visualising the effects of different neurobiological manipulations. As such, this may provide a resource for testing drugs designed to act on these disease mechanisms. Parallel studies in humans would be beneficial for determining cross-species validity and ascertaining the degree of translational relevance.

Overall, the mouse is a useful model for exploring central auditory processing, with tools available to probe the underlying mechanisms more deeply than is possible in humans. This work may be expanded to characterise different genetic risk factors relevant to schizophrenia, and begin exploring the effects of different pharmacological agents on the resulting AEP and MMR waveforms.

6.3 Conclusions

The mismatch response in mice is predominantly influenced by physical properties of stimuli, not necessarily reflecting sensory-memory disruption or adaptation mechanisms hypothesised to underlie human mismatch negativity. One component appeared to exemplify some characteristics of the human MMN: deviant-evoked activity (DEA), although this was only observed from urethane-anaesthetised mice and occurred significantly later than the human MMN (300-500 ms vs. 150-250 ms), raising questions about what this response may represent. NMDA receptor antagonism with 10 mg/kg i.p. ketamine acutely abolishes the second AEP deflection (P2, \approx 25-50 ms), increases gamma band EEG oscillations (\approx 50-70 Hz) and increases movement in conscious mice over a ten minute period; although none of these effects were observed in urethane-anaesthetised animals. In a difference waveform produced by AEPs from two physically distinct stimuli (e.g. differing in frequency, intensity or inter-stimulus interval), abolition of P2 caused by NMDA receptor antagonism may be interpreted as a decrease in MMR amplitude; illustrating a potential link with the human MMN, which is also diminished by ketamine. Schizophrenia-related *Map2k7*^{+/-} heterozygous gene disruption mice display an enlarged AEP onset response (N1, \approx 0-20 ms) in both urethane-anaesthetised and conscious states, the mechanisms of which require further examination. Overall these findings provide thought-provoking insight into the potential underlying mechanisms of mismatch negativity and auditory evoked potentials in mice.

References

- ADAMS, J. C. & MUGNAINI, E. 1984. Dorsal nucleus of the lateral lemniscus: a nucleus of GABAergic projection neurons. *Brain research bulletin*, 13, 585-590.
- ADLER, L. E., OLINCY, A., WALDO, M., HARRIS, J. G., GRIFFITH, J., STEVENS, K., FLACH, K., NAGAMOTO, H., BICKFORD, P. & LEONARD, S. 1998. Schizophrenia, sensory gating, and nicotinic receptors. *Schizophrenia Bulletin*, 24, 189.
- AHMED, M., MÄLLO, T., LEPPÄNEN, P. H., HÄMÄLÄINEN, J., ÄYRÄVÄINEN, L., RUUSUVIRTA, T. & ASTIKAINEN, P. 2011. Mismatch brain response to speech sound changes in rats. *Frontiers in psychology*, 2.
- AKATSUKA, K., WASAKA, T., NAKATA, H., INUI, K., HOSHIYAMA, M. & KAKIGI, R. 2005. Mismatch responses related to temporal discrimination of somatosensory stimulation. *Clinical Neurophysiology*, 116, 1930-1937.
- AL-MANA, D., CERANIC, B., DJAHANBAKHCH, O. & LUXON, L. 2008. Hormones and the auditory system: a review of physiology and pathophysiology. *Neuroscience*, 153, 881-900.
- ALHO, K. 1995. Cerebral generators of mismatch negativity (MMN) and its magnetic counterpart (MMNm) elicited by sound changes. *Ear and hearing*, 16, 38-51.
- AMANN, L. C., HALENE, T. B., EHRLICHMAN, R. S., LUMINAIS, S. N., MA, N., ABEL, T. & SIEGEL, S. J. 2009. Chronic ketamine impairs fear conditioning and produces long-lasting reductions in auditory evoked potentials. *Neurobiology of Disease*, 35, 311-317.
- ANDERSON, L. A., CHRISTIANSON, G. B. & LINDEN, J. F. 2009. Stimulus-specific adaptation occurs in the auditory thalamus. *The Journal of neuroscience*, 29, 7359-7363.
- ANDREOU, C., NOLTE, G., LEICHT, G., POLOMAC, N., HANGANU-OPATZ, I. L., LAMBERT, M., ENGEL, A. K. & MULERT, C. 2015. Increased resting-state gamma-band connectivity in first-episode schizophrenia. *Schizophrenia Bulletin*, 41, 930-939.
- ANTUNES, F. M., NELKEN, I., COVEY, E. & MALMIERCA, M. S. 2010. Stimulus-specific adaptation in the auditory thalamus of the anesthetized rat. *Plos One*, 5, e14071.
- ARGUELLO, P. A. & GOGOS, J. A. 2011. Psychiatric Genetics and the Generation of Mutant Animal Models. *Animal Models of Schizophrenia and Related Disorders*, 189-209.
- ASSOCIATION, A. P. 2000. *Diagnostic and statistical manual of mental disorders DSM-IV-TR fourth edition (text revision)*.
- ASSOCIATION, A. P. 2013. *Diagnostic and statistical manual of mental disorders (DSM-5®)*, American Psychiatric Pub.
- ASTIKAINEN, P., RUUSUVIRTA, T. & KORHONEN, T. 2001. Somatosensory event-related potentials in the rabbit cerebral and cerebellar cortices: a correspondence with mismatch responses in humans. *Neuroscience Letters*, 298, 222-224.
- ASTIKAINEN, P., RUUSUVIRTA, T. & NÄÄTÄNEN, R. 2014. Rapid categorization of sound objects in anesthetized rats as indexed by the electrophysiological mismatch response. *Psychophysiology*, 51, 1195-1199.

- ASTIKAINEN, P., RUUSUVIRTA, T., WIKGREN, J. & PENTTONEN, M. 2006. Memory-based detection of rare sound feature combinations in anesthetized rats. *Neuroreport*, 17, 1561-1564.
- ASTIKAINEN, P., STEFANICS, G., NOKIA, M., LIPPONEN, A., CONG, F. Y., PENTTONEN, M. & RUUSUVIRTA, T. 2011. Memory-Based Mismatch Response to Frequency Changes in Rats. *Plos One*, 6.
- ATAGÜN, M., ŞİKOĞLU, E., CAN, S., KARAKAŞ-UĞURLU, G., ULUSOY-KAYMAK, S., ÇAYKÖYLÜ, A., ALGİN, O., PHILLIPS, M., MOORE, C. & ÖNGÜR, D. 2015. Investigation of Heschl's gyrus and planum temporale in patients with schizophrenia and bipolar disorder: A proton magnetic resonance spectroscopy study. *Schizophrenia Research*, 161, 202-209.
- ATKINSON, R. J., MICHIE, P. T. & SCHALL, U. 2012. Duration mismatch negativity and P3a in first-episode psychosis and individuals at ultra-high risk of psychosis. *Biological Psychiatry*, 71, 98-104.
- BALDEWEG, T. 2007. ERP repetition effects and mismatch negativity generation: a predictive coding perspective. *Journal of Psychophysiology*, 21, 204-213.
- BALDEWEG, T. & HIRSCH, S. R. 2015. Mismatch negativity indexes illness-specific impairments of cortical plasticity in schizophrenia: a comparison with bipolar disorder and Alzheimer's disease. *International Journal of Psychophysiology*, 95, 145-155.
- BALDEWEG, T., KLUGMAN, A., GRUZELIER, J. & HIRSCH, S. R. 2004. Mismatch negativity potentials and cognitive impairment in schizophrenia. *Schizophrenia Research*, 69, 203-217.
- BALDEWEG, T., KLUGMAN, A., GRUZELIER, J. H. & HIRSCH, S. R. 2002. Impairment in frontal but not temporal components of mismatch negativity in schizophrenia. *International Journal of Psychophysiology*, 43, 111-122.
- BARHAM, R. M. & BOERSMA, F. J. 1975. *Orienting Responses in a Selection of Cognitive Tasks*, Rotterdam University Press.
- BARTA, P. E., PEARLSON, G. D., BRILL, L. B., ROYALL, R., MCGILCHRIST, I. K., PULVER, A. E., POWERS, R. E., CASANOVA, M. F., TIEN, A. Y. & FRANGOU, S. 1997. Planum temporale asymmetry reversal in schizophrenia: replication and relationship to gray matter abnormalities. *American Journal of Psychiatry*, 154, 661-667.
- BASTOS, A. M., USREY, W. M., ADAMS, R. A., MANGUN, G. R., FRIES, P. & FRISTON, K. J. 2012. Canonical microcircuits for predictive coding. *Neuron*, 76, 695-711.
- BEAGLEY, H. & KNIGHT, J. 1967. Changes in auditory evoked response with intensity. *The Journal of Laryngology & Otology*, 81, 861-873.
- BEGGIATO, S., ANTONELLI, T., TOMASINI, M. C., TANGANELLI, S., FUXE, K., SCHWARCZ, R. & FERRARO, L. 2013. Kynurenic acid, by targeting $\alpha 7$ nicotinic acetylcholine receptors, modulates extracellular GABA levels in the rat striatum in vivo. *European Journal of Neuroscience*, 37, 1470-1477.
- BICKEL, S. & JAVITT, D. C. 2009. Neurophysiological and neurochemical animal models of schizophrenia: Focus on glutamate. *Behavioural Brain Research*, 204, 352-362.

- BICKEL, S., LIPP, H.-P. & UMBRICH, D. 2008. Early auditory sensory processing deficits in mouse mutants with reduced NMDA receptor function. *Neuropsychopharmacology*, 33, 1680-1689.
- BICKEL, S., LIPP, H. & UMBRICH, D. 2007. Impaired attentional modulation of auditory evoked potentials in N-methyl-D-aspartate NR1 hypomorphic mice. *Genes, Brain and Behavior*, 6, 558-568.
- BODARKY, C. L., HALENE, T. B., EHRLICHMAN, R. S., BANERJEE, A., RAY, R., HAHN, C.-G., JONAK, G. & SIEGEL, S. J. 2009. Novel environment and GABA agonists alter event-related potentials in N-methyl-D-aspartate NR1 hypomorphic and wild-type mice. *Journal of Pharmacology and Experimental Therapeutics*, 331, 308-318.
- BOISON, D., SINGER, P., SHEN, H.-Y., FELDON, J. & YEE, B. K. 2012. Adenosine hypothesis of schizophrenia—opportunities for pharmacotherapy. *Neuropharmacology*, 62, 1527-1543.
- BOTTCHER-GANDOR, C. & ULLSPERGER, P. 1992. Mismatch Negativity in Event-Related Potentials to Auditory Stimuli as a Function of Varying Interstimulus Interval. *Psychophysiology*, 29, 546-550.
- BOWERS JR, M., BANNON, M. & HOFFMAN JR, F. 1987. Activation of forebrain dopamine systems by phencyclidine and footshock stress: evidence for distinct mechanisms. *Psychopharmacology*, 93, 133-135.
- BOYDEN, E. S., ZHANG, F., BAMBERG, E., NAGEL, G. & DEISSEROTH, K. 2005. Millisecond-timescale, genetically targeted optical control of neural activity. *Nature Neuroscience*, 8, 1263-1268.
- BRAND, A., URBAN, R. & GROTHE, B. 2000. Duration tuning in the mouse auditory midbrain. *Journal of Neurophysiology*, 84, 1790-1799.
- BRENNER, C. A., KRISHNAN, G. P., VOHS, J. L., AHN, W.-Y., HETRICK, W. P., MORZORATI, S. L. & O'DONNELL, B. F. 2009. Steady state responses: electrophysiological assessment of sensory function in schizophrenia. *Schizophrenia Bulletin*, 35, 1065-1077.
- BROCKHAUS-DUMKE, A., SCHULTZE-LUTTER, F., MUELLER, R., TENDOLKAR, I., BECHDOLF, A., PUKROP, R., KLOSTERKOETTER, J. & RUHRMANN, S. 2008. Sensory gating in schizophrenia: P50 and N100 gating in antipsychotic-free subjects at risk, first-episode, and chronic patients. *Biological Psychiatry*, 64, 376-384.
- BRODMANN, K. 2007. *Brodman's: Localisation in the cerebral cortex*, Springer Science & Business Media.
- BRUNIA, C., VAN BOXTEL, G. & BÖCKER, K. 2012. Negative slow waves as indices of anticipation: the Bereitschaftspotential, the contingent negative variation, and the stimulus-preceding negativity. *The Oxford handbook of event-related potential components*, 189-207.
- BUCHANAN, R. W., JAVITT, D. C., MARDER, S. R., SCHOOLER, N. R., GOLD, J. M., MCMAHON, R. P., URIEL HERESCO-LEVY, M. & CARPENTER, W. T. 2007. The Cognitive and Negative Symptoms in Schizophrenia Trial (CONSIST): the efficacy of glutamatergic agents for negative symptoms and cognitive impairments. *American Journal of Psychiatry*.

- BUDD, T., BARRY, R. J., GORDON, E., RENNIE, C. & MICHIE, P. 1998. Decrement of the N1 auditory event-related potential with stimulus repetition: habituation vs. refractoriness. *International Journal of Psychophysiology*, 31, 51-68.
- BUDNICK, B. & BRAFF, D. L. 1992. Sensory gating deficits in schizophrenia: new results. *Am J Psychiatry*, 149, 488-493.
- BUTLER, R. A. 1968. Effect of changes in stimulus frequency and intensity on habituation of the human vertex potential. *The Journal of the Acoustical Society of America*, 44, 945-950.
- BUZSÁKI, G., ANASTASSIOU, C. A. & KOCH, C. 2012. The origin of extracellular fields and currents—EEG, ECoG, LFP and spikes. *Nature Reviews Neuroscience*, 13, 407-420.
- CAPSIUS, B. & LEPPELSACK, H.-J. 1996. Influence of urethane anesthesia on neural processing in the auditory cortex analogue of a songbird. *Hearing research*, 96, 59-70.
- CARLEN, M., MELETIS, K., SIEGLE, J., CARDIN, J., FUTAI, K., VIERLING-CLAASSEN, D., RUEHLMANN, C., JONES, S. R., DEISSEROTH, K. & SHENG, M. 2012. A critical role for NMDA receptors in parvalbumin interneurons for gamma rhythm induction and behavior. *Molecular psychiatry*, 17, 537-548.
- CEDERHOLM, J. M. E., FROUD, K. E., WONG, A. C. Y., KO, M., RYAN, A. F. & HOUSLEY, G. D. 2012. Differential actions of isoflurane and ketamine-based anaesthetics on cochlear function in the mouse. *Hearing research*, 292, 71-79.
- CELSIS, P., BOULANOUAR, K., DOYON, B., RANJEVA, J., BERRY, I., NESPOULOUS, J. & CHOLLET, F. 1999. Differential fMRI responses in the left posterior superior temporal gyrus and left supramarginal gyrus to habituation and change detection in syllables and tones. *NeuroImage*, 9, 135-144.
- CHAVES, C., MARQUE, C. R., MAIA-DE-OLIVEIRA, J. P., WICHERT-ANA, L., FERRARI, T. B., SANTOS, A. C., ARAÚJO, D., MACHADO-DE-SOUSA, J. P., BRESSAN, R. A. & ELKIS, H. 2015. Effects of minocycline add-on treatment on brain morphometry and cerebral perfusion in recent-onset schizophrenia. *Schizophrenia Research*, 161, 439-445.
- CHERLYN, S. Y. T., SAN WOON, P., LIU, J. J., ONG, W. Y., TSAI, G. C. & SIM, K. 2010. Genetic association studies of glutamate, GABA and related genes in schizophrenia and bipolar disorder: a decade of advance. *Neuroscience & Biobehavioral Reviews*, 34, 958-977.
- CHRISTIANSON, G. B., CHAIT, M., DE CHEVEIGNÉ, A. & LINDEN, J. F. 2014. Auditory evoked fields measured noninvasively with small-animal MEG reveal rapid repetition suppression in the guinea pig. *Journal of neurophysiology*, 112, 3053-3065.
- CITRI, A. & MALENKA, R. C. 2008. Synaptic plasticity: multiple forms, functions, and mechanisms. *Neuropsychopharmacology*, 33, 18-41.
- COHEN, S. M., TSIEN, R. W., GOFF, D. C. & HALASSA, M. M. 2015. The impact of NMDA receptor hypofunction on GABAergic neurons in the pathophysiology of schizophrenia. *Schizophrenia Research*, 167, 98-107.
- COLIN, C., HOONHORST, I., MARKESSIS, E., RADEAU, M., DE TOURCHANINOFF, M., FOUCHER, A., COLLET, G. & DELTENRE, P. 2009. Mismatch Negativity (MMN) evoked by sound duration contrasts: An unexpected

- major effect of deviance direction on amplitudes. *Clinical Neurophysiology*, 120, 51-59.
- COMMISSION, S. 2012. The abandoned illness: a report from the Schizophrenia Commission. In: COMMISSION, S. (ed.) *London: Rethink Mental Illness*.
- CONNOLLY, P. M., MAXWELL, C., LIANG, Y. L., KAHN, J. B., KANES, S. J., ABEL, T., GUR, R. E., TURETSKY, B. I. & SIEGEL, S. J. 2004. The effects of ketamine vary among inbred mouse strains and mimic schizophrenia for the P80, but not P20 or N40 auditory ERP components. *Neurochemical research*, 29, 1179-1188.
- CRADDOCK, N. & OWEN, M. J. 2010. The Kraepelinian dichotomy—going, going... but still not gone. *The British Journal of Psychiatry*, 196, 92-95.
- CSÉPE, V. 1995. On the origin and development of the mismatch negativity. *Ear and hearing*, 16, 91-104.
- CSÉPE, V., KARMOS, G. & MOLNAR, M. 1987. Evoked potential correlates of stimulus deviance during wakefulness and sleep in cat—animal model of mismatch negativity. *Electroencephalography and Clinical Neurophysiology*, 66, 571-578.
- CUTHBERT, B. N. & INSEL, T. R. 2013. Toward the future of psychiatric diagnosis: the seven pillars of RDoC. *BMC medicine*, 11, 1.
- DE MARTINO, F., MOEREL, M., VAN DE MOORTELE, P.-F., UGURBIL, K., GOEBEL, R., YACOB, E. & FORMISANO, E. 2013. Spatial organization of frequency preference and selectivity in the human inferior colliculus. *Nature communications*, 4, 1386.
- DELORME, A. & MAKEIG, S. 2004. EEGLAB: an open source toolbox for analysis of single-trial EEG dynamics including independent component analysis. *Journal of Neuroscience Methods*, 134, 9-21.
- DEOUELL, L. Y. 2007. The frontal generator of the mismatch negativity revisited. *Journal of Psychophysiology*, 21, 188-203.
- DEOUELL, L. Y., BENTIN, S. & GIARD, M.-H. 1998. Mismatch negativity in dichotic listening: evidence for interhemispheric differences and multiple generators. *Psychophysiology*, 35, 355-365.
- DEUTCH, A. Y., TAM, S.-Y., FREEMAN, A. S., BOWERS, M. B. & ROTH, R. H. 1987. Mesolimbic and mesocortical dopamine activation induced by phencyclidine: contrasting pattern to striatal response. *European journal of pharmacology*, 134, 257-264.
- DEVONSHIRE, I. M., GRANDY, T. H., DOMMETT, E. J. & GREENFIELD, S. A. 2010. Effects of urethane anaesthesia on sensory processing in the rat barrel cortex revealed by combined optical imaging and electrophysiology. *European Journal of Neuroscience*, 32, 786-797.
- DOHERTY, J. L., O'DONOVAN, M. C. & OWEN, M. J. 2012. Recent genomic advances in schizophrenia. *Clinical genetics*, 81, 103-109.
- DUNCAN, C. C., BARRY, R. J., CONNOLLY, J. F., FISCHER, C., MICHIE, P. T., NÄÄTÄNEN, R., POLICH, J., REINVANG, I. & VAN PETTEN, C. 2009. Event-related potentials in clinical research: guidelines for eliciting, recording, and quantifying mismatch negativity, P300, and N400. *Clinical Neurophysiology*, 120, 1883-1908.

- DUQUE, D., PÉREZ-GONZÁLEZ, D., AYALA, Y. A., PALMER, A. R. & MALMIERCA, M. S. 2012. Topographic distribution, frequency, and intensity dependence of stimulus-specific adaptation in the inferior colliculus of the rat. *The Journal of neuroscience*, 32, 17762-17774.
- EGERTON, A. & STONE, J. M. 2012. The Glutamate Hypothesis of Schizophrenia: Neuroimaging and Drug Development. *Current Pharmaceutical Biotechnology*, 13, 1500-1512.
- EHLERS, C. L. & SOMES, C. 2002. Long latency event-related potentials in mice: effects of stimulus characteristics and strain. *Brain Research*, 957, 117-128.
- EHRlichman, R. S., LUMINAIS, S. N., WHITE, S. L., RUDNICK, N. D., MA, N., DOW, H. C., KREIBICH, A. S., ABEL, T., BRODKIN, E. S. & HAHN, C.-G. 2009. Neuregulin 1 transgenic mice display reduced mismatch negativity, contextual fear conditioning and social interactions. *Brain Research*, 1294, 116-127.
- EHRlichman, R. S., MAXWELL, C. R., MAJUMDAR, S. & SIEGEL, S. J. 2008. Deviance-elicited changes in event-related potentials are attenuated by ketamine in mice. *Journal of cognitive neuroscience*, 20, 1403-1414.
- EINEVOLL, G. T., KAYSER, C., LOGOTHETIS, N. K. & PANZERI, S. 2013. Modelling and analysis of local field potentials for studying the function of cortical circuits. *Nature Reviews Neuroscience*, 14, 770-785.
- ELLISON, G. 1995. The N-methyl-D-aspartate antagonists phencyclidine, ketamine and dizocilpine as both behavioral and anatomical models of the dementias. *Brain Research Reviews*, 20, 250-267.
- ERIKSSON, J. & VILLA, A. E. 2005. Event-related potentials in an auditory oddball situation in the rat. *Biosystems*, 79, 207-212.
- ESCERA, C. & MALMIERCA, M. S. 2014. The auditory novelty system: An attempt to integrate human and animal research. *Psychophysiology*, 51, 111-123.
- FALKAI, P., BOGERTS, B., SCHNEIDER, T., GREVE, B., PFEIFFER, U., PILZ, K., GONSIORZCYK, C., MAJTENYI, C. & OVARY, I. 1995. Disturbed planum temporale asymmetry in schizophrenia. A quantitative post-mortem study. *Schizophrenia Research*, 14, 161-176.
- FARLEY, B. J., QUIRK, M. C., DOHERTY, J. J. & CHRISTIAN, E. P. 2010. Stimulus-specific adaptation in auditory cortex is an NMDA-independent process distinct from the sensory novelty encoded by the mismatch negativity. *The Journal of neuroscience*, 30, 16475-16484.
- FEATHERSTONE, R., NAGY, L., HAHN, C. & SIEGEL, S. 2014. Juvenile exposure to ketamine causes delayed emergence of EEG abnormalities during adulthood in mice. *Drug and alcohol dependence*, 134, 123-127.
- FEATHERSTONE, R. E., SHIN, R., KOGAN, J. H., LIANG, Y., MATSUMOTO, M. & SIEGEL, S. J. 2015. Mice with subtle reduction of NMDA NR1 receptor subunit expression have a selective decrease in mismatch negativity: implications for schizophrenia prodromal population. *Neurobiology of Disease*, 73, 289-295.
- FEATHERSTONE, R. E., TATARD-LEITMAN, V. M., SUH, J. D., LIN, R., LUCKI, I. & SIEGEL, S. J. 2013. Electrophysiological and behavioral responses to ketamine in mice with reduced Akt1 expression. *Psychopharmacology*, 227, 639-649.
- FIELD, K. J., WHITE, W. J. & LANG, C. M. 1993. Anaesthetic effects of chloral hydrate, pentobarbitone and urethane in adult male rats. *Laboratory Animals*, 27, 258-269.

- FISCHER, C., MORLET, D., BOUCHET, P., LUAUTE, J., JOURDAN, C. & SALORD, F. 1999. Mismatch negativity and late auditory evoked potentials in comatose patients. *Clinical Neurophysiology*, 110, 1601-1610.
- FISCHER, C., MORLET, D. & GIARD, M.-H. 2000. Mismatch negativity and N100 in comatose patients. *Audiology and Neurotology*, 5, 192-197.
- FISHMAN, Y. I. & STEINSCHNEIDER, M. 2012. Searching for the mismatch negativity in primary auditory cortex of the awake monkey: deviance detection or stimulus specific adaptation? *The Journal of neuroscience*, 32, 15747-15758.
- FRODL-BAUCH, T., KATHMANN, N., MÖLLER, H.-J. & HEGERL, U. 1997. Dipole localization and test-retest reliability of frequency and duration mismatch negativity generator processes. *Brain Topography*, 10, 3-8.
- GALABURDA, A. M., CORSIGLIA, J., ROSEN, G. D. & SHERMAN, G. F. 1987. Planum temporale asymmetry, reappraisal since Geschwind and Levitsky. *Neuropsychologia*, 25, 853-868.
- GALAZYUK, A. V. & FENG, A. S. 1997. Encoding of sound duration by neurons in the auditory cortex of the little brown bat, *Myotis lucifugus*. *Journal of Comparative Physiology A*, 180, 301-311.
- GALLINAT, J., BOTTLENDER, R., JUCKEL, G., MUNKE-PUCHNER, A., STOTZ, G., KUSS, H.-J., MAVROGIORGOU, P. & HEGERL, U. 2000. The loudness dependency of the auditory evoked N1/P2-component as a predictor of the acute SSRI response in depression. *Psychopharmacology*, 148, 404-411.
- GALLINAT, J., WINTERER, G., HERRMANN, C. S. & SENKOWSKI, D. 2004. Reduced oscillatory gamma-band responses in unmedicated schizophrenic patients indicate impaired frontal network processing. *Clinical Neurophysiology*, 115, 1863-1874.
- GANDAL, M. J., EDGAR, J. C., KLOOK, K. & SIEGEL, S. J. 2012. Gamma synchrony: towards a translational biomarker for the treatment-resistant symptoms of schizophrenia. *Neuropharmacology*, 62, 1504-1518.
- GAREY, L. J., ONG, W., PATEL, T., KANANI, M., DAVIS, A., MORTIMER, A., BARNES, T. & HIRSCH, S. 1998. Reduced dendritic spine density on cerebral cortical pyramidal neurons in schizophrenia. *Journal of Neurology, Neurosurgery & Psychiatry*, 65, 446-453.
- GARRIDO, M. I., KILNER, J. M., STEPHAN, K. E. & FRISTON, K. J. 2009. The mismatch negativity: A review of underlying mechanisms. *Clinical Neurophysiology*, 120, 453-463.
- GEREAU, R. W. & SWANSON, G. 2008. *The glutamate receptors*, Springer Science & Business Media.
- GEYER, M. A., KREBS-THOMSON, K., BRAFF, D. L. & SWERDLOW, N. R. 2001. Pharmacological studies of prepulse inhibition models of sensorimotor gating deficits in schizophrenia: a decade in review. *Psychopharmacology*, 156, 117-154.
- GIARD, M. H., PERRIN, F., PERNIER, J. & BOUCHET, P. 1990. Brain Generators Implicated in the Processing of Auditory Stimulus Deviance: A Topographic Event-Related Potential Study. *Psychophysiology*, 27, 627-640.
- GLANTZ, L. A. & LEWIS, D. A. 2000. Decreased dendritic spine density on prefrontal cortical pyramidal neurons in schizophrenia. *Archives of general psychiatry*, 57, 65-73.

- GODEY, B., SCHWARTZ, D., DE GRAAF, J., CHAUVEL, P. & LIEGEOIS-CHAUVEL, C. 2001. Neuromagnetic source localization of auditory evoked fields and intracerebral evoked potentials: a comparison of data in the same patients. *Clinical neurophysiology*, 112, 1850-1859.
- GOFF, D. C. & COYLE, J. T. 2001. The emerging role of glutamate in the pathophysiology and treatment of schizophrenia. *American Journal of Psychiatry*.
- GOLIMBET, V., LEBEDEVA, I., KOROVAITSEVA, G., LEZHEIKO, T. & YUMATOVA, P. 2008. Association of 5-HTTLPR serotonin transporter gene polymorphism and Val66Met brain-derived neurotrophic factor gene polymorphism with auditory N100 evoked potential amplitude in patients with endogenous psychoses. *Bulletin of experimental biology and medicine*, 146, 605-608.
- GONZALEZ-BURGOS, G. & LEWIS, D. A. 2012. NMDA receptor hypofunction, parvalbumin-positive neurons, and cortical gamma oscillations in schizophrenia. *Schizophrenia Bulletin*, 38, 950-957.
- GRILL-SPECTOR, K., HENSON, R. & MARTIN, A. 2006. Repetition and the brain: neural models of stimulus-specific effects. *Trends in Cognitive Sciences*, 10, 14-23.
- GRIMM, S. & ESCERA, C. 2012. Auditory deviance detection revisited: evidence for a hierarchical novelty system. *International Journal of Psychophysiology*, 85, 88-92.
- GRIMM, S., ESCERA, C. & NELKEN, I. 2016. Early indices of deviance detection in humans and animal models. *Biological psychology*, 116, 23-27.
- HALENE, T. B., EHRLICHMAN, R. S., LIANG, Y., CHRISTIAN, E. P., JONAK, G. J., GUR, T. L., BLENDY, J. A., DOW, H. C., BRODKIN, E. S. & SCHNEIDER, F. 2009. Assessment of NMDA receptor NR1 subunit hypofunction in mice as a model for schizophrenia. *Genes, Brain and Behavior*, 8, 661-675.
- HALGREN, E., BAUDENA, P., CLARKE, J. M., HEIT, G., LIÉGEOIS, C., CHAUVEL, P. & MUSOLINO, A. 1995. Intracerebral potentials to rare target and distractor auditory and visual stimuli. I. Superior temporal plane and parietal lobe. *Electroencephalography and Clinical Neurophysiology*, 94, 191-220.
- HARA, K. & HARRIS, R. A. 2002. The anesthetic mechanism of urethane: the effects on neurotransmitter-gated ion channels.
- HARI, R., HÄMÄLÄINEN, M., ILMONIEMI, R., KAUKORANTA, E., REINIKAINEN, K., SALMINEN, J., ALHO, K., NÄÄTÄNEN, R. & SAMS, M. 1984. Responses of the primary auditory cortex to pitch changes in a sequence of tone pips: neuromagnetic recordings in man. *Neuroscience Letters*, 50, 127-132.
- HARI, R., KAILA, K., KATILA, T., TUOMISTO, T. & VARPULA, T. 1982. Interstimulus interval dependence of the auditory vertex response and its magnetic counterpart: implications for their neural generation. *Electroencephalography and Clinical Neurophysiology*, 54, 561-569.
- HARI, R., PELIZZONE, M., MÄKELÄ, J., HÄLLSTRÖM, J., LEINONEN, L. & LOUNASMAA, O. 1987. Neuromagnetic responses of the human auditory cortex to on-and offsets of noise bursts. *Audiology*, 26, 31-43.
- HARMS, L. 2016. Mismatch responses and deviance detection in N-methyl-D-aspartate (NMDA) receptor hypofunction and developmental models of schizophrenia. *Biological psychology*, 116, 75-81.
- HARMS, L., FULHAM, W. R., TODD, J., BUDD, T. W., HUNTER, M., MEEHAN, C., PENTTONEN, M., SCHALL, U., ZAVITSANOU, K. & HODGSON, D. M. 2014.

Mismatch negativity (MMN) in freely-moving rats with several experimental controls.

- HARMS, L., MICHIE, P. T. & NÄÄTÄNEN, R. 2015. Criteria for determining whether mismatch responses exist in animal models: Focus on rodents. *Biological psychology*.
- HARRISON, P. J. & EASTWOOD, S. L. 1998. Preferential involvement of excitatory neurons in medial temporal lobe in schizophrenia. *The Lancet*, 352, 1669-1673.
- HASHIMOTO, K. 2015. Targeting of $\alpha 7$ nicotinic acetylcholine receptors in the treatment of schizophrenia and the use of auditory sensory gating as a translational biomarker. *Current pharmaceutical design*, 21, 3797-3806.
- HAYASHI-TAKAGI, A. & SAWA, A. 2010. Disturbed synaptic connectivity in schizophrenia: convergence of genetic risk factors during neurodevelopment. *Brain research bulletin*, 83, 140-146.
- HE, J. 2002. OFF responses in the auditory thalamus of the guinea pig. *Journal of neurophysiology*, 88, 2377-2386.
- HE, J., HASHIKAWA, T., OJIMA, H. & KINOUCI, Y. 1997. Temporal integration and duration tuning in the dorsal zone of cat auditory cortex. *The Journal of neuroscience*, 17, 2615-2625.
- HEFFNER, H. E. & HEFFNER, R. S. 2007. Hearing ranges of laboratory animals. *Journal of the American Association for Laboratory Animal Science*, 46, 20-22.
- HEFFNER, H. E., HEFFNER, R. S., CONTOS, C. & OTT, T. 1994. Audiogram of the hooded Norway rat. *Hearing research*, 73, 244-247.
- HEGERL, U. & JUCKEL, G. 1993. Intensity dependence of auditory evoked potentials as an indicator of central serotonergic neurotransmission: a new hypothesis. *Biological Psychiatry*, 33, 173-187.
- HEINKE, W., KENNTNER, R., GUNTER, T. C., SAMMLER, D., OLTHOFF, D. & KOELSCH, S. 2004. Sequential effects of increasing propofol sedation on frontal and temporal cortices as indexed by auditory event-related potentials. *Anesthesiology*, 100, 617-625.
- HENRY, K. R. 1985. ON and OFF components of the auditory brainstem response have different frequency-and intensity-specific properties. *Hearing research*, 18, 245-251.
- HILLYARD, S. A., HINK, R. F., SCHWENT, V. L. & PICTON, T. W. 1973. Electrical signs of selective attention in the human brain. *Science*, 182, 177-180.
- HILLYARD, S. A. & PICTON, T. W. 1978. On and off components in the auditory evoked potential. *Perception & Psychophysics*, 24, 391-398.
- HOFFMAN, D. C. & DONOVAN, H. 1994. D1 and D2 dopamine receptor antagonists reverse prepulse inhibition deficits in an animal model of schizophrenia. *Psychopharmacology*, 115, 447-453.
- HOMAYOUN, H. & MOGHADDAM, B. 2007. NMDA receptor hypofunction produces opposite effects on prefrontal cortex interneurons and pyramidal neurons. *The Journal of neuroscience*, 27, 11496-11500.
- HONG, L. E., SUMMERFELT, A., BUCHANAN, R. W., O'DONNELL, P., THAKER, G. K., WEILER, M. A. & LAHTI, A. C. 2009. Gamma and delta neural oscillations and association with clinical symptoms under subanesthetic ketamine. *Neuropsychopharmacology*, 35, 632-640.

- HOWES, O. D. & KAPUR, S. 2009. The dopamine hypothesis of schizophrenia: version III—the final common pathway. *Schizophrenia Bulletin*, 35, 549-562.
- HUSI, H., WARD, M. A., CHOUDHARY, J. S., BLACKSTOCK, W. P. & GRANT, S. G. 2000. Proteomic analysis of NMDA receptor–adhesion protein signaling complexes. *Nature Neuroscience*, 3, 661-669.
- INSEL, T., CUTHBERT, B., GARVEY, M., HEINSSSEN, R., PINE, D. S., QUINN, K., SANISLOW, C. & WANG, P. 2010. Research domain criteria (RDoC): toward a new classification framework for research on mental disorders. *American Journal of Psychiatry*, 167, 748-751.
- JÄÄSKELÄINEN, I. P., AHVENINEN, J., BONMASSAR, G., DALE, A. M., ILMONIEMI, R. J., LEVÄNEN, S., LIN, F.-H., MAY, P., MELCHER, J. & STUFFLEBEAM, S. 2004. Human posterior auditory cortex gates novel sounds to consciousness. *Proceedings of the National Academy of Sciences of the United States of America*, 101, 6809-6814.
- JACOBSEN, T., HORENKAMP, T. & SCHRÖGER, E. 2003. Preattentive memory-based comparison of sound intensity. *Audiology and Neurotology*, 8, 338-346.
- JACOBSEN, T. & SCHRÖGER, E. 2001. Is there pre-attentive memory-based comparison of pitch? *Psychophysiology*, 38, 723-727.
- JAVITT, D., JAYACHANDRA, M., LINDSLEY, R., SPECHT, C. & SCHROEDER, C. 2000. Schizophrenia-like deficits in auditory P1 and N1 refractoriness induced by the psychomimetic agent phencyclidine (PCP). *Clinical Neurophysiology*, 111, 833-836.
- JAVITT, D. C., DONESHKA, P., GROCHOWSKI, S. & RITTER, W. 1995. Impaired mismatch negativity generation reflects widespread dysfunction of working memory in schizophrenia. *Archives of general psychiatry*, 52, 550-558.
- JAVITT, D. C., HASHIM, A. & SERSHEN, H. 2005. Modulation of striatal dopamine release by glycine transport inhibitors. *Neuropsychopharmacology*, 30, 649-656.
- JAVITT, D. C., SCHROEDER, C. E., STEINSCHNEIDER, M., AREZZO, J. C. & VAUGHAN JR, H. G. 1992. Demonstration of mismatch negativity in the monkey. *Electroencephalography and Clinical Neurophysiology*, 83, 87-90.
- JAVITT, D. C., STEINSCHNEIDER, M., SCHROEDER, C. E. & AREZZO, J. C. 1996. Role of cortical N-methyl-D-aspartate receptors in auditory sensory memory and mismatch negativity generation: implications for schizophrenia. *Proceedings of the National Academy of Sciences*, 93, 11962-11967.
- JEMEL, B., ACHENBACH, C., MÜLLER, B. W., RÖPCKE, B. & OADES, R. D. 2002. Mismatch negativity results from bilateral asymmetric dipole sources in the frontal and temporal lobes. *Brain Topography*, 15, 13-27.
- JENTSCH, J. D. & ROTH, R. H. 1999. The neuropsychopharmacology of phencyclidine: from NMDA receptor hypofunction to the dopamine hypothesis of schizophrenia. *Neuropsychopharmacology*, 20, 201-225.
- JESSEN, F., FRIES, T., KUCHARSKI, C., NISHIMURA, T., HOENIG, K., MAIER, W., FALKAI, P. & HEUN, R. 2001. Amplitude reduction of the mismatch negativity in first-degree relatives of patients with schizophrenia. *Neuroscience Letters*, 309, 185-188.
- JUCKEL, G. 2015. Serotonin: from sensory processing to schizophrenia using an electrophysiological method. *Behavioural brain research*, 277, 121-124.

- JUCKEL, G., GALLINAT, J., RIEDEL, M., SOKULLU, S., SCHULZ, C., MÖLLER, H.-J., MÜLLER, N. & HEGERL, U. 2003. Serotonergic dysfunction in schizophrenia assessed by the loudness dependence measure of primary auditory cortex evoked activity. *Schizophrenia Research*, 64, 115-124.
- JUCKEL, G., HEGERL, U., MOLNÁR, M., CSÉPE, V. & KARMOS, G. 1999. Auditory evoked potentials reflect serotonergic neuronal activity—a study in behaving cats administered drugs acting on 5-HT_{1A} autoreceptors in the dorsal raphe nucleus. *Neuropsychopharmacology*, 21, 710-716.
- JUCKEL, G., MOLNÁR, M., HEGERL, U., CSÉPE, V. & KARMOS, G. 1997. Auditory-evoked potentials as indicator of brain serotonergic activity first evidence in behaving cats. *Biological psychiatry*, 41, 1181-1195.
- JUNG, F., STEPHAN, K. E., BACKES, H., MORAN, R., GRAMER, M., KUMAGAI, T., GRAF, R., ENDEPOLS, H. & TITTEMEYER, M. 2013. Mismatch Responses in the Awake Rat: Evidence from Epidural Recordings of Auditory Cortical Fields. *Plos One*, 8.
- KANE, N., CURRY, S., ROWLANDS, C., MANARA, A., LEWIS, T., MOSS, T., CUMMINS, B. & BUTLER, S. 1996. Event-related potentials—neurophysiological tools for predicting emergence and early outcome from traumatic coma. *Intensive care medicine*, 22, 39-46.
- KAUR, S., ROSE, H., LAZAR, R., LIANG, K. & METHERATE, R. 2005. Spectral integration in primary auditory cortex: laminar processing of afferent input, in vivo and in vitro. *Neuroscience*, 134, 1033-1045.
- KETZ, N. A., JENSEN, O. & O'REILLY, R. C. 2015. Thalamic pathways underlying prefrontal cortex–medial temporal lobe oscillatory interactions. *Trends in Neurosciences*, 38, 3-12.
- KHODAI, T. J. 2014. *Functional laminar architecture of rat primary auditory cortex following acoustic trauma*. PhD, University of Strathclyde.
- KIEBEL, S. J., DAUNIZEAU, J., PHILLIPS, C. & FRISTON, K. J. 2008. Variational Bayesian inversion of the equivalent current dipole model in EEG/MEG. *NeuroImage*, 39, 728-741.
- KISHIMOTO, H., NAKAGAWA, K., WATANABE, T., KITAGAWA, D., MOMOSE, H., SEO, J., NISHITAI, G., SHIMIZU, N., OHATA, S. & TANEMURA, S. 2003. Different properties of SEK1 and MKK7 in dual phosphorylation of stress-induced activated protein kinase SAPK/JNK in embryonic stem cells. *Journal of Biological Chemistry*, 278, 16595-16601.
- KLEIN, C., VON DER BEHRENS, W. & GAESE, B. H. 2014. Stimulus-specific adaptation in field potentials and neuronal responses to frequency-modulated tones in the primary auditory cortex. *Brain Topography*, 27, 599-610.
- KOBLIN, D. D. 2002. Urethane: help or hindrance? *Anesthesia & Analgesia*, 94, 241-242.
- KOLLURI, N., SUN, Z., SAMPSON, A. R. & LEWIS, D. A. 2005. Lamina-specific reductions in dendritic spine density in the prefrontal cortex of subjects with schizophrenia. *American Journal of Psychiatry*, 162, 1200-1202.
- KORZYUKOV, O., PFLIEGER, M. E., WAGNER, M., BOWYER, S. M., ROSBURG, T., SUNDARESAN, K., ELGER, C. E. & BOUTROS, N. N. 2007. Generators of the intracranial P50 response in auditory sensory gating. *Neuroimage*, 35, 814-826.

- KRAUS, N., MCGEE, T., LITTMAN, T., NICOL, T. & KING, C. 1994. Nonprimary auditory thalamic representation of acoustic change. *Journal of Neurophysiology*, 72, 1270-1277.
- KROPOTOV, J. D., ALHO, K., NÄÄTÄNEN, R., PONOMAREV, V. A., KROPOTOVA, O. V., ANICHKOV, A. D. & NECHAEV, V. B. 2000. Human auditory-cortex mechanisms of preattentive sound discrimination. *Neuroscience Letters*, 280, 87-90.
- KRUGLIKOV, I. & RUDY, B. 2008. Perisomatic GABA release and thalamocortical integration onto neocortical excitatory cells are regulated by neuromodulators. *Neuron*, 58, 911-924.
- KUMARI, V. & POSTMA, P. 2005. Nicotine use in schizophrenia: the self medication hypotheses. *Neuroscience & Biobehavioral Reviews*, 29, 1021-1034.
- KUWADA, S. & BATRA, R. 1999. Coding of sound envelopes by inhibitory rebound in neurons of the superior olivary complex in the unanesthetized rabbit. *The Journal of neuroscience*, 19, 2273-2287.
- LAKE, C. R. 2012. *Schizophrenia is a Misdiagnosis: Implications for the DSM-5 and the ICD-11*, Springer Science & Business Media.
- LARA, D. R., DALL'IGNA, O. P., GHISOLFI, E. S. & BRUNSTEIN, M. G. 2006. Involvement of adenosine in the neurobiology of schizophrenia and its therapeutic implications. *Progress in Neuro-Psychopharmacology and Biological Psychiatry*, 30, 617-629.
- LAU, C.-I., WANG, H.-C., HSU, J.-L. & LIU, M.-E. 2013. Does the dopamine hypothesis explain schizophrenia? *Reviews in the Neurosciences*, 24, 389-400.
- LAZAR, R. & METHERATE, R. 2003. Spectral interactions, but no mismatch negativity, in auditory cortex of anesthetized rat. *Hearing research*, 181, 51-56.
- LAZAREWICZ, M. T., EHRLICHMAN, R. S., MAXWELL, C. R., GANDAL, M. J., FINKEL, L. H. & SIEGEL, S. J. 2010. Ketamine modulates theta and gamma oscillations. *Journal of cognitive neuroscience*, 22, 1452-1464.
- LEE, C., SCHREINER, C., IMAIZUMI, K. & WINER, J. 2004a. Tonotopic and heterotopic projection systems in physiologically defined auditory cortex. *Neuroscience*, 128, 871-887.
- LEE, C. C., IMAIZUMI, K., SCHREINER, C. E. & WINER, J. A. 2004b. Concurrent tonotopic processing streams in auditory cortex. *Cerebral Cortex*, 14, 441-451.
- LIEBERMAN, J., KANE, J. & ALVIR, J. 1987. Provocative tests with psychostimulant drugs in schizophrenia. *Psychopharmacology*, 91, 415-433.
- LIGHT, G. A. & BRAFF, D. L. 2005. Mismatch negativity deficits are associated with poor functioning in schizophrenia patients. *Archives of general psychiatry*, 62, 127-136.
- LIN, H., HSU, F.-C., BAUMANN, B. H., COULTER, D. A., ANDERSON, S. A. & LYNCH, D. R. 2014. Cortical parvalbumin GABAergic deficits with $\alpha 7$ nicotinic acetylcholine receptor deletion: implications for schizophrenia. *Molecular and Cellular Neuroscience*, 61, 163-175.
- LINDEN, J. F., LIU, R. C., SAHANI, M., SCHREINER, C. E. & MERZENICH, M. M. 2003. Spectrotemporal structure of receptive fields in areas AI and AAF of mouse auditory cortex. *Journal of Neurophysiology*, 90, 2660-2675.
- LINKA, T., MÜLLER, B. W., BENDER, S. & SARTORY, G. 2004. The intensity dependence of the auditory evoked N1 component as a predictor of response to

- Citalopram treatment in patients with major depression. *Neuroscience Letters*, 367, 375-378.
- LIPSKA, B. K. 2004. Using animal models to test a neurodevelopmental hypothesis of schizophrenia. *Journal of psychiatry & neuroscience: JPN*, 29, 282.
- LIU, F., GUO, X., WU, R., OU, J., ZHENG, Y., ZHANG, B., XIE, L., ZHANG, L., YANG, L. & YANG, S. 2014. Minocycline supplementation for treatment of negative symptoms in early-phase schizophrenia: a double blind, randomized, controlled trial. *Schizophrenia Research*, 153, 169-176.
- LOPEZ-CALDERON, J. & LUCK, S. J. 2014. ERPLAB: an open-source toolbox for the analysis of event-related potentials. *Frontiers in Human Neuroscience*, 8.
- LUCK, S. J. 2014. *An introduction to the event-related potential technique*, MIT press.
- LUCK, S. J., MATHALON, D. H., O'DONNELL, B. F., HÄMÄLÄINEN, M. S., SPENCER, K. M., JAVITT, D. C. & UHLHAAS, P. J. 2011. A roadmap for the development and validation of event-related potential biomarkers in schizophrenia research. *Biological Psychiatry*, 70, 28-34.
- MAESTRONI, G., CONTI, A. & PIERPAOLI, W. 1988. Role of the pineal gland in immunity. III. Melatonin antagonizes the immunosuppressive effect of acute stress via an opiate mechanism. *Immunology*, 63, 465.
- MAGGI, C. & MELI, A. 1986. Suitability of urethane anesthesia for physiopharmacological investigations in various systems Part 1: General considerations. *Experientia*, 42, 109-114.
- MAKEIG, S. 1993. Auditory event-related dynamics of the EEG spectrum and effects of exposure to tones. *Electroencephalography and Clinical Neurophysiology*, 86, 283-293.
- MARCOTTE, E. R., PEARSON, D. M. & SRIVASTAVA, L. K. 2001. Animal models of schizophrenia: a critical review. *Journal of psychiatry & neuroscience: JPN*, 26, 395.
- MARKRAM, H., MULLER, E., RAMASWAMY, S., REIMANN, M. W., ABDELLAH, M., SANCHEZ, C. A., AILAMAKI, A., ALONSO-NANCLARES, L., ANTILLE, N. & ARSEVER, S. 2015. Reconstruction and simulation of neocortical microcircuitry. *Cell*, 163, 456-492.
- MARTIN, L. F., DAVALOS, D. B. & KISLEY, M. A. 2009. Nicotine enhances automatic temporal processing as measured by the mismatch negativity waveform. *Nicotine & Tobacco Research*, 11, 698-706.
- MAXWELL, C. R., EHRLICHMAN, R. S., LIANG, Y., TRIEF, D., KANES, S. J., KARP, J. & SIEGEL, S. J. 2006. Ketamine produces lasting disruptions in encoding of sensory stimuli. *Journal of Pharmacology and Experimental Therapeutics*, 316, 315-324.
- MAY, P., TIITINEN, H., ILMONIEMI, R. J., NYMAN, G., TAYLOR, J. G. & NÄÄTÄNEN, R. 1999. Frequency change detection in human auditory cortex. *Journal of computational neuroscience*, 6, 99-120.
- MAY, P. J. & TIITINEN, H. 2010. Mismatch negativity (MMN), the deviance-elicited auditory deflection, explained. *Psychophysiology*, 47, 66-122.
- MEADOR-WOODRUFF, J. H. & HEALY, D. J. 2000. Glutamate receptor expression in schizophrenic brain. *Brain research reviews*, 31, 288-294.

- MERZENICH, M. M., KNIGHT, P. L. & ROTH, G. L. 1975. Representation of cochlea within primary auditory cortex in the cat. *Journal of Neurophysiology*, 38, 231-249.
- METHERATE, R. & ASHE, J. H. 1995. Synaptic interactions involving acetylcholine, glutamate, and GABA in rat auditory cortex. *Experimental brain research*, 107, 59-72.
- MICHIE, P., BUDD, T., TODD, J., ROCK, D., WICHMANN, H., BOX, J. & JABLENSKY, A. 2000. Duration and frequency mismatch negativity in schizophrenia. *Clinical Neurophysiology*, 111, 1054-1065.
- MICHIE, P. T., MALMIERCA, M. S., HARMS, L. & TODD, J. 2016. Understanding the neurobiology of MMN and its reduction in schizophrenia. *Biological psychology*, 116, 1-3.
- MINZENBERG, M. J., FIRL, A. J., YOON, J. H., GOMES, G. C., REINKING, C. & CARTER, C. S. 2010. Gamma oscillatory power is impaired during cognitive control independent of medication status in first-episode schizophrenia. *Neuropsychopharmacology*, 35, 2590-2599.
- MIZRAHI, A., SHALEV, A. & NELKEN, I. 2014. Single neuron and population coding of natural sounds in auditory cortex. *Current Opinion in Neurobiology*, 24, 103-110.
- MOEREL, M., DE MARTINO, F. & FORMISANO, E. 2014. An anatomical and functional topography of human auditory cortical areas. *Frontiers in neuroscience*, 8, 225.
- MOHANTY, S. 2011. *Development of EEG test for psychiatric disorder - 'Schizophrenia'*. MSc, University of Strathclyde.
- MOLHOLM, S., MARTINEZ, A., RITTER, W., JAVITT, D. C. & FOXE, J. J. 2005. The neural circuitry of pre-attentive auditory change-detection: an fMRI study of pitch and duration mismatch negativity generators. *Cerebral Cortex*, 15, 545-551.
- MORRIS, B. J. & PRATT, J. A. 2014. Novel treatment strategies for schizophrenia from improved understanding of genetic risk. *Clinical genetics*, 86, 401-411.
- MÜLLER, B., JÜPTNER, M., JENTZEN, W. & MÜLLER, S. 2002. Cortical activation to auditory mismatch elicited by frequency deviant and complex novel sounds: a PET study. *NeuroImage*, 17, 231-239.
- NÄÄTÄNEN, R. 1992. *Attention and brain function*, Psychology Press.
- NÄÄTÄNEN, R., GAILLARD, A. W. & MÄNTYSALO, S. 1978. Early selective-attention effect on evoked potential reinterpreted. *Acta psychologica*, 42, 313-329.
- NÄÄTÄNEN, R., JACOBSEN, T. & WINKLER, I. 2005. Memory-based or afferent processes in mismatch negativity (MMN): A review of the evidence. *Psychophysiology*, 42, 25-32.
- NÄÄTÄNEN, R., JIANG, D., LAVIKAINEN, J., REINIKAINEN, K. & PAAVILAINEN, P. 1993. Event-related potentials reveal a memory trace for temporal features. *Neuroreport*, 5, 310-312.
- NÄÄTÄNEN, R. & KREEGIPUU, K. 2012. The Mismatch Negativity (MMN). *The Oxford handbook of event-related potential components*, 143-158.
- NÄÄTÄNEN, R., KUJALA, T., ESCERA, C., BALDEWEG, T., KREEGIPUU, K., CARLSON, S. & PONTON, C. 2012. The mismatch negativity (MMN)—a unique window to disturbed central auditory processing in ageing and different clinical conditions. *Clinical Neurophysiology*, 123, 424-458.

- NÄÄTÄNEN, R., PAAVILAINEN, P., ALHO, K., REINIKAINEN, K. & SAMS, M. 1989. Do event-related potentials reveal the mechanism of the auditory sensory memory in the human brain? *Neuroscience Letters*, 98, 217-221.
- NÄÄTÄNEN, R., PAAVILAINEN, P., RINNE, T. & ALHO, K. 2007. The mismatch negativity (MMN) in basic research of central auditory processing: a review. *Clinical Neurophysiology*, 118, 2544-2590.
- NÄÄTÄNEN, R., PAKARINEN, S., RINNE, T. & TAKEGATA, R. 2004. The mismatch negativity (MMN): towards the optimal paradigm. *Clinical Neurophysiology*, 115, 140-144.
- NAGAI, T., TADA, M., KIRIHARA, K., ARAKI, T., JINDE, S. & KASAI, K. 2013. Mismatch negativity as a “translatable” brain marker toward early intervention for psychosis: a review. *Frontiers in psychiatry*, 4.
- NAGY, L., FEATHERSTONE, R., HAHN, C. & SIEGEL, S. 2015. Delayed emergence of behavioral and electrophysiological effects following juvenile ketamine exposure in mice. *Translational psychiatry*, 5, e635.
- NAKAMURA, T., MICHIE, P. T., FULHAM, W. R., TODD, J., BUDD, T. W., SCHALL, U., HUNTER, M. & HODGSON, D. M. 2011. Epidural auditory event-related potentials in the rat to frequency and duration deviants: evidence of mismatch negativity? *Frontiers in psychology*, 2, 367.
- NAKAZAWA, K., ZSIROS, V., JIANG, Z., NAKAO, K., KOLATA, S., ZHANG, S. & BELFORTE, J. E. 2012. GABAergic interneuron origin of schizophrenia pathophysiology. *Neuropharmacology*, 62, 1574-1583.
- NATHAN, P. J., O'NEILL, B. & CROFT, R. J. 2005. Is the loudness dependence of the auditory evoked potential a sensitive and selective in vivo marker of central serotonergic function? *Neuropsychopharmacology*, 30, 1584-1585.
- NEILL, J. C., BARNES, S., COOK, S., GRAYSON, B., IDRIS, N. F., MCLEAN, S. L., SNIGDHA, S., RAJAGOPAL, L. & HARTE, M. K. 2010. Animal models of cognitive dysfunction and negative symptoms of schizophrenia: focus on NMDA receptor antagonism. *Pharmacology & therapeutics*, 128, 419-432.
- NELKEN, I. 2004. Processing of complex stimuli and natural scenes in the auditory cortex. *Current Opinion in Neurobiology*, 14, 474-480.
- NELKEN, I. 2014. Stimulus-specific adaptation and deviance detection in the auditory system: experiments and models. *Biological Cybernetics*, 108, 655-663.
- NELKEN, I. & ULANOVSKY, N. 2007. Mismatch negativity and stimulus-specific adaptation in animal models. *Journal of Psychophysiology*, 21, 214.
- NELKEN, I., YARON, A., POLTEROVICH, A. & HERSHENHOREN, I. 2013. Stimulus-specific adaptation beyond pure tones. *Basic Aspects of Hearing*. Springer.
- NICHOLSON, C. & FREEMAN, J. A. 1975. Theory of current source-density analysis and determination of conductivity tensor for anuran cerebellum. *Journal of Neurophysiology*, 38, 356-368.
- O'CONNELL, M. N., BARCZAK, A., SCHROEDER, C. E. & LAKATOS, P. 2014. Layer specific sharpening of frequency tuning by selective attention in primary auditory cortex. *The Journal of neuroscience*, 34, 16496-16508.
- O'NEILL, B. V., CROFT, R. J. & NATHAN, P. J. 2008. The loudness dependence of the auditory evoked potential (LDAEP) as an in vivo biomarker of central serotonergic

- function in humans: rationale, evaluation and review of findings. *Human psychopharmacology*, 23, 355.
- OERTEL-KNÖCHEL, V., KNÖCHEL, C., MATURA, S., PRVULOVIC, D., LINDEN, D. E. & VAN DE VEN, V. 2013. Reduced functional connectivity and asymmetry of the planum temporale in patients with schizophrenia and first-degree relatives. *Schizophrenia Research*, 147, 331-338.
- OESTREICHER, E., ARNOLD, W. & FELIX, D. 2002. Neurotransmission of the cochlear inner hair cell synapse-implications for inner ear therapy. *Rational Pharmacotherapy of the Inner Ear*. Karger Publishers.
- OKAZAKI, S., KANO, S. I., TAKAURA, K., TSUKADA, M. & OKA, K. 2006. Change detection and difference detection of tone duration discrimination. *Neuroreport*, 17, 395-399.
- OLIVA, J., LEUNG, S., CROFT, R. J., O'NEILL, B. V., O'KANE, J., STOUT, J., PHAN, K. L. & NATHAN, P. J. 2010. The loudness dependence auditory evoked potential is insensitive to acute changes in serotonergic and noradrenergic neurotransmission. *Human Psychopharmacology: Clinical and Experimental*, 25, 423-427.
- OPENSHAW, R., THOMSON, D., PENNINGER, J., PRATT, J. & MORRIS, B. 2016. Mice haploinsufficient for Map2k7, a gene involved in neurodevelopment and risk for schizophrenia, show impaired attention, a vigilance decrement deficit and unstable cognitive processing in an attentional task: impact of minocycline. *Psychopharmacology*, 1-13.
- OPENSHAW, R., THOMSON, D., PRATT, J. & MORRIS, B. 2015. Mice haploinsufficient for Map2k7, a schizophrenia risk gene, show impaired associative learning and attentional deficits: Impact of minocycline. *European Neuropsychopharmacology*, S293.
- OPITZ, B., RINNE, T., MECKLINGER, A., VON CRAMON, D. Y. & SCHRÖGER, E. 2002. Differential contribution of frontal and temporal cortices to auditory change detection: fMRI and ERP results. *NeuroImage*, 15, 167-174.
- PAKARINEN, S., TAKEGATA, R., RINNE, T., HUOTILAINEN, M. & NÄÄTÄNEN, R. 2007. Measurement of extensive auditory discrimination profiles using the mismatch negativity (MMN) of the auditory event-related potential (ERP). *Clinical Neurophysiology*, 118, 177-185.
- PANTEV, C., EULITZ, C., HAMPSON, S., ROSS, B. & ROBERTS, L. 1996. The auditory evoked "off" response: sources and comparison with the "on" and the "sustained" responses. *Ear and hearing*, 17, 255-265.
- PAOLETTI, P., BELLONE, C. & ZHOU, Q. 2013. NMDA receptor subunit diversity: impact on receptor properties, synaptic plasticity and disease. *Nature Reviews Neuroscience*, 14, 383-400.
- PARK, Y.-M., LEE, S.-H., KIM, S. & BAE, S.-M. 2010. The loudness dependence of the auditory evoked potential (LDAEP) in schizophrenia, bipolar disorder, major depressive disorder, anxiety disorder, and healthy controls. *Progress in Neuro-Psychopharmacology and Biological Psychiatry*, 34, 313-316.
- PARKS, T. N. 2000. The AMPA receptors of auditory neurons. *Hearing research*, 147, 77-91.
- PATTERSON, J. V., HETRICK, W. P., BOUTROS, N. N., JIN, Y., SANDMAN, C., STERN, H., POTKIN, S. & BUNNEY, W. E. 2008. P50 sensory gating ratios in

- schizophrenics and controls: a review and data analysis. *Psychiatry research*, 158, 226-247.
- PAUSE, B. M. & KRAUEL, K. 2000. Chemosensory event-related potentials (CSERP) as a key to the psychology of odors. *International Journal of Psychophysiology*, 36, 105-122.
- PAZO-ALVAREZ, P., CADAVEIRA, F. & AMENEDO, E. 2003. MMN in the visual modality: a review. *Biological psychology*, 63, 199-236.
- PERGADIA, M. 2012. Multi-locus genome-wide association analysis supports the role of glutamatergic synaptic transmission in the etiology of major depressive disorder.
- PERKINTON, M. S., SIHRA, T. S. & WILLIAMS, R. J. 1999. Ca²⁺-permeable AMPA receptors induce phosphorylation of cAMP response element-binding protein through a phosphatidylinositol 3-kinase-dependent stimulation of the mitogen-activated protein kinase signaling cascade in neurons. *The Journal of neuroscience*, 19, 5861-5874.
- PHILLIPS, D. & IRVINE, D. 1981. Responses of single neurons in physiologically defined primary auditory cortex (AI) of the cat: frequency tuning and responses to intensity. *Journal of Neurophysiology*, 45, 48-58.
- PHILLIPS, D. P., HALL, S. & BOEHNKE, S. 2002. Central auditory onset responses, and temporal asymmetries in auditory perception. *Hearing research*, 167, 192-205.
- PICTON, T. W., HILLYARD, S. A., GALAMBOS, R. & SCHIFF, M. 1971. Human auditory attention: a central or peripheral process? *Science*, 173, 351-353.
- PICTON, T. W., WOODS, D. L., BARIBEAU-BRAUN, J. & HEALEY, T. M. 1977. Evoked potential audiometry. *J Otolaryngol*, 6, 90-119.
- PILOWSKY, L., BRESSAN, R., STONE, J., ERLANDSSON, K., MULLIGAN, R., KRISTAL, J. & ELL, P. 2006. First in vivo evidence of an NMDA receptor deficit in medication-free schizophrenic patients. *Molecular psychiatry*, 11, 118-119.
- PINAULT, D. 2008. N-methyl d-aspartate receptor antagonists ketamine and MK-801 induce wake-related aberrant γ oscillations in the rat neocortex. *Biological Psychiatry*, 63, 730-735.
- PINCZE, Z., LAKATOS, P., RAJKAI, C., ULBERT, I. & KARMOS, G. 2001. Separation of mismatch negativity and the N1 wave in the auditory cortex of the cat: a topographic study. *Clinical Neurophysiology*, 112, 778-784.
- PINCZE, Z., LAKATOS, P., RAJKAI, C., ULBERT, I. & KARMOS, G. 2002. Effect of deviant probability and interstimulus/interdeviant interval on the auditory N1 and mismatch negativity in the cat auditory cortex. *Cognitive Brain Research*, 13, 249-253.
- PLACK, C. J. 2013. *The sense of hearing*, Psychology Press.
- POLESZAK, E., WLAZ, P., KÊDZIERSKA, E., NIEOCZYM, D., WYSKA, E., SZYMURA-OLEKSIK, J., FIDECKA, S., RADZIWON-ZALESKA, M. & NOWAK, G. 2006. Immobility stress induces depression-like behavior in the forced swim test in mice: effect of magnesium and imipramine. *Pharmacological reports*, 58, 746.
- POLLEY, D. B., READ, H. L., STORACE, D. A. & MERZENICH, M. M. 2007. Multiparametric auditory receptive field organization across five cortical fields in the albino rat. *Journal of Neurophysiology*, 97, 3621-3638.

- POLYAKOV, A. & PRATT, H. 1994. Three-channel Lissajous' trajectory of the binaural interaction components in human auditory brain-stem evoked potentials. *Electroencephalography and Clinical Neurophysiology/Evoked Potentials Section*, 92, 396-404.
- POLYAKOV, A. & PRATT, H. 1995. Three-channel Lissajous' trajectory of the binaural interaction components of human auditory middle-latency evoked potentials. *Hearing research*, 82, 205-215.
- POTTER, D., SUMMERFELT, A., GOLD, J. & BUCHANAN, R. W. 2006. Review of clinical correlates of P50 sensory gating abnormalities in patients with schizophrenia. *Schizophrenia Bulletin*, 32, 692-700.
- PRATT, H., LUCK, S. & KAPPENMAN, E. 2011. Sensory ERP components. *The Oxford handbook of event-related potential components*, 89-114.
- PRATT, J., DAWSON, N., MORRIS, B. J., GRENT, T., ROUX, F. & UHLHAAS, P. J. 2016. Thalamo-cortical communication, glutamatergic neurotransmission and neural oscillations: A unique window into the origins of ScZ? *Schizophrenia Research*.
- PRATT, J., WINCHESTER, C., DAWSON, N. & MORRIS, B. 2012. Advancing schizophrenia drug discovery: optimizing rodent models to bridge the translational gap. *Nat Rev Drug Discov*, 11, 560-579.
- PRIETO, J. J. & WINER, J. A. 1999. Layer VI in cat primary auditory cortex: Golgi study and sublamina origins of projection neurons. *Journal of Comparative Neurology*, 404, 332-358.
- QIN, L., CHIMOTO, S., SAKAI, M., WANG, J. & SATO, Y. 2007. Comparison between offset and onset responses of primary auditory cortex ON-OFF neurons in awake cats. *Journal of neurophysiology*, 97, 3421-3431.
- RASK-ANDERSEN, H., LIU, W., ERIXON, E., KINNEFORS, A., PFALLER, K., SCHROTT-FISCHER, A. & GLUECKERT, R. 2012. Human cochlea: anatomical characteristics and their relevance for cochlear implantation. *The Anatomical Record*, 295, 1791-1811.
- RATNANATHER, J. T., POYNTON, C. B., PISANO, D. V., CROCKER, B., POSTELL, E., CEBRON, S., CEYHAN, E., HONEYCUTT, N. A., MAHON, P. B. & BARTA, P. E. 2013. Morphometry of superior temporal gyrus and planum temporale in schizophrenia and psychotic bipolar disorder. *Schizophrenia Research*, 150, 476-483.
- REALE, R. A. & IMIG, T. J. 1980. Tonotopic organization in auditory cortex of the cat. *Journal of Comparative Neurology*, 192, 265-291.
- RECASENS, M., LEUNG, S., GRIMM, S., NOWAK, R. & ESCERA, C. 2015. Repetition suppression and repetition enhancement underlie auditory memory-trace formation in the human brain: an MEG study. *NeuroImage*, 108, 75-86.
- RINNE, T., ALHO, K., ILMONIEMI, R., VIRTANEN, J. & NÄÄTÄNEN, R. 2000. Separate time behaviors of the temporal and frontal mismatch negativity sources. *NeuroImage*, 12, 14-19.
- RINNE, T., GRATTON, G., FABIANI, M., COWAN, N., MACLIN, E., STINARD, A., SINKKONEN, J., ALHO, K. & NÄÄTÄNEN, R. 1999. Scalp-Recorded Optical Signals Make Sound Processing in the Auditory Cortex Visible? *NeuroImage*, 10, 620-624.

- RIPKE, S., NEALE, B. M., CORVIN, A., WALTERS, J. T., FARH, K.-H., HOLMANS, P. A., LEE, P., BULIK-SULLIVAN, B., COLLIER, D. A. & HUANG, H. 2014. Biological insights from 108 schizophrenia-associated genetic loci. *Nature*, 511, 421.
- ROBBINS, T. 2002. The 5-choice serial reaction time task: behavioural pharmacology and functional neurochemistry. *Psychopharmacology*, 163, 362-380.
- ROGER, C., HASBROUCQ, T., RABAT, A., VIDAL, F. & BURLE, B. 2009. Neurophysics of temporal discrimination in the rat: a mismatch negativity study. *Psychophysiology*, 46, 1028-1032.
- ROJAS, M. J., NAVAS, J. A. & RECTOR, D. M. 2006. Evoked response potential markers for anesthetic and behavioral states. *American Journal of Physiology-Regulatory, Integrative and Comparative Physiology*, 291, R189-R196.
- ROSBURG, T. 2003. Left hemispheric dipole locations of the neuromagnetic mismatch negativity to frequency, intensity and duration deviants. *Cognitive Brain Research*, 16, 83-90.
- ROSBURG, T., BOUTROS, N. N. & FORD, J. M. 2008. Reduced auditory evoked potential component N100 in schizophrenia—a critical review. *Psychiatry research*, 161, 259-274.
- ROSBURG, T. & KREITSCHMANN-ANDERMAHR, I. 2016. The effects of ketamine on the mismatch negativity (MMN) in humans—A meta-analysis. *Clinical Neurophysiology*, 127, 1387-1394.
- ROSSANT, C., KADIR, S. N., GOODMAN, D. F., SCHULMAN, J., HUNTER, M. L., SALEEM, A. B., GROSMARK, A., BELLUSCIO, M., DENFIELD, G. H. & ECKER, A. S. 2016. Spike sorting for large, dense electrode arrays. *Nature Neuroscience*.
- ROSSI, A., SERIO, A., STRATTA, P., PETRUZZI, C., SCHIAZZA, G., MANCINI, F. & CASACCHIA, M. 1994. Planum temporale asymmetry and thought disorder in schizophrenia. *Schizophrenia Research*, 12, 1-7.
- ROTHSCHILD, G., NELKEN, I. & MIZRAHI, A. 2010. Functional organization and population dynamics in the mouse primary auditory cortex. *Nature Neuroscience*, 13, 353-360.
- ROWLAND, L. M., KONTSON, K., WEST, J., EDDEN, R. A., ZHU, H., WIJTENBURG, S. A., HOLCOMB, H. H. & BARKER, P. B. 2012. In vivo measurements of glutamate, GABA, and NAAG in schizophrenia. *Schizophrenia Bulletin*, sbs092.
- RUUSUVIRTA, T., KOIVISTO, K., WIKGREN, J. & ASTIKAINEN, P. 2007. Processing of melodic contours in urethane-anaesthetized rats. *European Journal of Neuroscience*, 26, 701-703.
- RUUSUVIRTA, T., KORHONEN, T., PENTTONEN, M. & ARIKOSKI, J. 1995. Hippocampal evoked potentials to pitch deviances in an auditory oddball situation in the rabbit: no human mismatch-like dependence on standard stimuli. *Neuroscience Letters*, 185, 123-126.
- RUUSUVIRTA, T., LIPPONEN, A., PELLINEN, E.-K., PENTTONEN, M. & ASTIKAINEN, P. 2015. Auditory cortical and hippocampal local-field potentials to frequency deviant tones in urethane-anesthetized rats: An unexpected role of the sound frequencies themselves. *International Journal of Psychophysiology*, 96, 134-140.

- RUUSUVIRTA, T., LIPPONEN, A., PELLINEN, E., PENTTONEN, M. & ASTIKAINEN, P. 2013. Auditory Cortical and Hippocampal-System Mismatch Responses to Duration Deviants in Urethane-Anesthetized Rats. *Plos One*, 8.
- RUUSUVIRTA, T., PENTTONEN, M. & KORHONEN, T. 1998. Auditory cortical event-related potentials to pitch deviances in rats. *Neuroscience Letters*, 248, 45-48.
- RYUGO, D. K., FAY, R. R. & POPPER, A. N. 2010. *Auditory and vestibular efferents*, Springer Science & Business Media.
- SAALMANN, Y. B. & KASTNER, S. 2011. Cognitive and perceptual functions of the visual thalamus. *Neuron*, 71, 209-223.
- SABRI, M. & CAMPBELL, K. B. 2001. Effects of sequential and temporal probability of deviant occurrence on mismatch negativity. *Cognitive Brain Research*, 12, 171-180.
- SAKATA, S. 2016. State-dependent and cell type-specific temporal processing in auditory thalamocortical circuit. *Scientific reports*, 6.
- SAKATA, S. & HARRIS, K. D. 2009. Laminar structure of spontaneous and sensory-evoked population activity in auditory cortex. *Neuron*, 64, 404-418.
- SAKATA, S. & HARRIS, K. D. 2012. Laminar-dependent effects of cortical state on auditory cortical spontaneous activity. *Frontiers in neural circuits*, 6, 109.
- SALA, C. & SEGAL, M. 2014. Dendritic spines: the locus of structural and functional plasticity. *Physiological reviews*, 94, 141-188.
- SALAMAN, M. & ROE, F. 1953. Incomplete carcinogens: ethyl carbamate (urethane) as an initiator of skin tumour formation in the mouse. *British journal of cancer*, 7, 472.
- SALISBURY, D. F., SHENTON, M. E., GRIGGS, C. B., BONNER-JACKSON, A. & MCCARLEY, R. W. 2002. Mismatch negativity in chronic schizophrenia and first-episode schizophrenia. *Archives of general psychiatry*, 59, 686-694.
- SANDNER, G. & CANAL, N. M. 2007. Relationship between PPI and baseline startle response. *Cognitive neurodynamics*, 1, 27-37.
- SASAKI, T., WADA, T., KISHIMOTO, H., IRIE-SASAKI, J., MATSUMOTO, G., GOTO, T., YAO, Z., WAKEHAM, A., MAK, T. W. & SUZUKI, A. 2001. The Stress Kinase Mitogen-activated Protein Kinase Kinase (MKK) 7 Is a Negative Regulator of Antigen Receptor and Growth Factor Receptor-induced Proliferation in Hematopoietic Cells. *The Journal of experimental medicine*, 194, 757-768.
- SAUNDERS, J. A., GANDAL, M. J., ROBERTS, T. P. & SIEGEL, S. J. 2012. NMDA antagonist MK801 recreates auditory electrophysiology disruption present in autism and other neurodevelopmental disorders. *Behavioural Brain Research*, 234, 233-237.
- SCHALL, U., JOHNSTON, P., TODD, J., WARD, P. B. & MICHIE, P. T. 2003. Functional neuroanatomy of auditory mismatch processing: an event-related fMRI study of duration-deviant oddballs. *NeuroImage*, 20, 729-736.
- SCHALL, U., MÜLLER, B. W., KÄRGEL, C. & GÜNTÜRKÜN, O. 2015. Electrophysiological mismatch response recorded in awake pigeons from the avian functional equivalent of the primary auditory cortex. *Neuroreport*, 26, 239-244.
- SCHERG, M., VAJSAR, J. & PICTON, T. W. 1989. A source analysis of the late human auditory evoked potentials. *Journal of cognitive neuroscience*, 1, 336-355.
- SCHIMPF, P. H., RAMON, C. & HAUEISEN, J. 2002. Dipole models for the EEG and MEG. *IEEE Transactions on Biomedical Engineering*, 49, 409-418.

- SCHMID, M. C., SINGER, W. & FRIES, P. 2012. Thalamic coordination of cortical communication. *Neuron*, 75, 551-552.
- SCHNEIDER, D. M., NELSON, A. & MOONEY, R. 2014. A synaptic and circuit basis for corollary discharge in the auditory cortex. *Nature*, 513, 189-194.
- SCHOLL, B., GAO, X. & WEHR, M. 2010. Nonoverlapping sets of synapses drive on responses and off responses in auditory cortex. *Neuron*, 65, 412-421.
- SCHREINER, C. E. & WINER, J. A. 2007. Auditory cortex mapmaking: principles, projections, and plasticity. *Neuron*, 56, 356-365.
- SCHRÖGER, E. 1996. The influence of stimulus intensity and inter-stimulus interval on the detection of pitch and loudness changes. *Electroencephalography and Clinical Neurophysiology/Evoked Potentials Section*, 100, 517-526.
- SCHRÖGER, E., TERVANIEMI, M., WOLFF, C. & NÄÄTÄNEN, R. N. 1996. Preattentive periodicity detection in auditory patterns as governed by time and intensity information. *Cognitive brain research*, 4, 145-148.
- SCHUMACHER, J. W., SCHNEIDER, D. M. & WOOLLEY, S. M. 2011. Anesthetic state modulates excitability but not spectral tuning or neural discrimination in single auditory midbrain neurons. *Journal of Neurophysiology*, 106, 500-514.
- SCHWAB, S. G., HOEFGEN, B., HANSES, C., HASSENBACH, M. B., ALBUS, M., LERER, B., TRIXLER, M., MAIER, W. & WILDENAUER, D. B. 2005. Further evidence for association of variants in the AKT1 gene with schizophrenia in a sample of European sib-pair families. *Biological Psychiatry*, 58, 446-450.
- SEEMAN, P. 1987. Dopamine receptors and the dopamine hypothesis of schizophrenia. *Synapse*, 1, 133-152.
- SEEMAN, P. 2011. All roads to schizophrenia lead to dopamine supersensitivity and elevated dopamine D2High receptors. *CNS neuroscience & therapeutics*, 17, 118-132.
- SHELLEY, A. M., WARD, P., CATTS, S., MICHIE, P. T., ANDREWS, S. & MCCONAGHY, N. 1991. Mismatch negativity: an index of a preattentive processing deficit in schizophrenia. *Biological Psychiatry*, 30, 1059-1062.
- SHERMAN, S. M. 2005. Thalamic relays and cortical functioning. *Progress in Brain Research*, 149, 107-126.
- SHERMAN, S. M. 2007. The thalamus is more than just a relay. *Current Opinion in Neurobiology*, 17, 417-422.
- SHIRAMATSU, T. I., KANZAKI, R. & TAKAHASHI, H. 2013. Cortical Mapping of Mismatch Negativity with Deviance Detection Property in Rat. *Plos One*, 8.
- SHIRASAKA, Y. & WASTERLAIN, C. G. 1995. The effect of urethane anesthesia on evoked potentials in dentate gyrus. *European journal of pharmacology*, 282, 11-17.
- SIEGEL, S., CONNOLLY, P., LIANG, Y. L., LENOX, R. H., GUR, R. E., BILKER, W. B., KANES, S. J. & TURETSKY, B. I. 2003. Effects of strain, novelty, and NMDA blockade on auditory-evoked potentials in mice. *Neuropsychopharmacology*, 28, 675-682.
- SIVARAO, D. V., CHEN, P., YANG, Y., LI, Y.-W., PIESCHL, R. & AHLJANIAN, M. K. 2014. NR2B antagonist CP-101,606 abolishes pitch-mediated deviance detection in awake rats. *Frontiers in psychiatry*, 5.

- SLAWECKI, C. J., GRAHAME, N. J., ROTH, J., KATNER, S. N. & EHLERS, C. L. 2003. EEG and ERP profiles in the high alcohol preferring (HAP) and low alcohol preferring (LAP) mice: relationship to ethanol preference. *Brain Research*, 961, 243-254.
- SLOAS, D. C., ZHUO, R., XUE, H., CHAMBERS, A. R., KOLACZYK, E., POLLEY, D. B. & SEN, K. 2016. Interactions across Multiple Stimulus Dimensions in Primary Auditory Cortex. *eneuro*, ENEURO. 0124-16.2016.
- SNELL, R. S. 2001. *Clinical neuroanatomy: A review with questions and explanations*, Lippincott Williams & Wilkins.
- SOBOTKA, S. & RINGO, J. L. 1994. Stimulus specific adaptation in excited but not in inhibited cells in inferotemporal cortex of macaque. *Brain Research*, 646, 95-99.
- SPENCER, K. M., NIZNIKIEWICZ, M. A., SHENTON, M. E. & MCCARLEY, R. W. 2008. Sensory-evoked gamma oscillations in chronic schizophrenia. *Biological Psychiatry*, 63, 744-747.
- STEINSCHNEIDER, M., TENKE, C. E., SCHROEDER, C. E., JAVITT, D. C., SIMPSON, G. V., AREZZO, J. C. & VAUGHAN, H. G. 1992. Cellular generators of the cortical auditory evoked potential initial component. *Electroencephalography and Clinical Neurophysiology/Evoked Potentials Section*, 84, 196-200.
- STIEBLER, I., NEULIST, R., FICHTEL, I. & EHRET, G. 1997. The auditory cortex of the house mouse: left-right differences, tonotopic organization and quantitative analysis of frequency representation. *Journal of Comparative Physiology A*, 181, 559-571.
- SUGIMOTO, K., OHMOMO, H., SHUTOH, F., NOGAMI, H. & HISANO, S. 2015. Presentation of noise during acute restraint stress attenuates expression of immediate early genes and arginine vasopressin in the hypothalamic paraventricular nucleus but not corticosterone secretion in rats. *Neuroscience research*, 96, 20-29.
- SUN, T. & HEVNER, R. F. 2014. Growth and folding of the mammalian cerebral cortex: from molecules to malformations. *Nature Reviews Neuroscience*, 15, 217-232.
- SUN, Y., FARZAN, F., BARR, M. S., KIRIHARA, K., FITZGERALD, P. B., LIGHT, G. A. & DASKALAKIS, Z. J. 2011. Gamma oscillations in schizophrenia: Mechanisms and clinical significance. *Brain Research*, 1413, 98-114.
- SUTTER, M. & SCHREINER, C. 1995. Topography of intensity tuning in cat primary auditory cortex: single-neuron versus multiple-neuron recordings. *Journal of Neurophysiology*, 73, 190-204.
- SWEATT, J. D. 2001. The neuronal MAP kinase cascade: a biochemical signal integration system subserving synaptic plasticity and memory. *Journal of Neurochemistry*, 76, 1-10.
- SYMOND, M. B., HARRIS, A. W., GORDON, E. & WILLIAMS, L. M. 2005. "Gamma synchrony" in first-episode schizophrenia: a disorder of temporal connectivity? *American Journal of Psychiatry*, 162, 459-465.
- SZYMANSKI, F. D., GARCIA-LAZARO, J. A. & SCHNUPP, J. W. 2009. Current source density profiles of stimulus-specific adaptation in rat auditory cortex. *Journal of Neurophysiology*, 102, 1483-1490.
- SZYMANSKI, M. D., YUND, E. W. & WOODS, D. L. 1999. Phonemes, intensity and attention: differential effects on the mismatch negativity (MMN). *The Journal of the Acoustical Society of America*, 106, 3492-3505.

- TAASEH, N., YARON, A. & NELKEN, I. 2011. Stimulus-specific adaptation and deviance detection in the rat auditory cortex. *Plos One*, 6, e23369.
- TAKAHASHI, H., NAKAO, M. & KAGA, K. 2004. Cortical mapping of auditory-evoked offset responses in rats. *Neuroreport*, 15, 1565-1569.
- TAKEGATA, R., TERVANIEMI, M., ALKU, P., YLINEN, S. & NÄÄTÄNEN, R. 2008. Parameter-specific modulation of the mismatch negativity to duration decrement and increment: Evidence for asymmetric processes. *Clinical Neurophysiology*, 119, 1515-1523.
- TERVANIEMI, M. & BRATTICO, E. 2004. From sounds to music towards understanding the neurocognition of musical sound perception. *Journal of Consciousness Studies*, 11, 9-27.
- TERVANIEMI, M., LEHTOKOSKI, A., SINKKONEN, J., VIRTANEN, J., ILMONIEMI, R. & NÄÄTÄNEN, R. 1999. Test-retest reliability of mismatch negativity for duration, frequency and intensity changes. *Clinical Neurophysiology*, 110, 1388-1393.
- TERVANIEMI, M., MEDVEDEV, S., ALHO, K., PAKHOMOV, S., ROUDAS, M., VAN ZUIJEN, T. & NÄÄTÄNEN, R. 2000. Lateralized automatic auditory processing of phonetic versus musical information: a PET study. *Human brain mapping*, 10, 74-79.
- THOMAS, G. M., LIN, D. T., NURIYA, M. & HUGANIR, R. L. 2008. Rapid and bi-directional regulation of AMPA receptor phosphorylation and trafficking by JNK. *The EMBO journal*, 27, 361-372.
- THOMAS, H. & LÓPEZ, V. 2003. Comparative study of inter-and intrahemispheric cortico-cortical connections in gerbil auditory cortex. *Biological research*, 36, 155-169.
- THOMPSON, R. 2013. *Genetic and functional investigation of FXYD6 and MAP2K7 as risk factors in schizophrenia*. University of Glasgow.
- THOMSON, D. M., MCVIE, A., MORRIS, B. J. & PRATT, J. A. 2011. Dissociation of acute and chronic intermittent phencyclidine-induced performance deficits in the 5-choice serial reaction time task: influence of clozapine. *Psychopharmacology*, 213, 681-695.
- THUNÉ, H., RECASENS, M. & UHLHAAS, P. J. 2016. The 40-Hz Auditory Steady-State Response in Patients With Schizophrenia: A Meta-analysis. *JAMA psychiatry*.
- TIKHONRAVOV, D., NEUVONEN, T., PERTOVAARA, A., SAVIOJA, K., RUUSUVIRTA, T., NÄÄTÄNEN, R. & CARLSON, S. 2008. Effects of an NMDA-receptor antagonist MK-801 on an MMN-like response recorded in anesthetized rats. *Brain Research*, 1203, 97-102.
- TIKHONRAVOV, D., NEUVONEN, T., PERTOVAARA, A., SAVIOJA, K., RUUSUVIRTA, T., NÄÄTÄNEN, R. & CARLSON, S. 2010. Dose-related effects of memantine on a mismatch negativity-like response in anesthetized rats. *Neuroscience*, 167, 1175-1182.
- TODD, J., HARMS, L., MICHIE, P. & SCHALL, U. 2013. Mismatch negativity (MMN): Translating the potential. *Frontiers in psychiatry*, 4.
- TODD, J., MICHIE, P. T., SCHALL, U., KARAYANIDIS, F., YABE, H. & NÄÄTÄNEN, R. 2008. Deviant matters: duration, frequency, and intensity deviants reveal different patterns of mismatch negativity reduction in early and late schizophrenia. *Biological Psychiatry*, 63, 58-64.

- TSE, C.-Y., TIEN, K.-R. & PENNEY, T. B. 2006. Event-related optical imaging reveals the temporal dynamics of right temporal and frontal cortex activation in pre-attentive change detection. *NeuroImage*, 29, 314-320.
- TSUCHIMOTO, R., KANBA, S., HIRANO, S., ORIBE, N., UENO, T., HIRANO, Y., NAKAMURA, I., ODA, Y., MIURA, T. & ONITSUKA, T. 2011. Reduced high and low frequency gamma synchronization in patients with chronic schizophrenia. *Schizophrenia Research*, 133, 99-105.
- TURETSKY, B. I., BILKER, W. B., SIEGEL, S. J., KOHLER, C. G. & GUR, R. E. 2009. Profile of auditory information-processing deficits in schizophrenia. *Psychiatry research*, 165, 27-37.
- TURETSKY, B. I., DRESS, E. M., BRAFF, D. L., CALKINS, M. E., GREEN, M. F., GREENWOOD, T. A., GUR, R. E., GUR, R. C., LAZZERONI, L. C. & NUECHTERLEIN, K. H. 2015. The utility of P300 as a schizophrenia endophenotype and predictive biomarker: clinical and socio-demographic modulators in COGS-2. *Schizophrenia Research*, 163, 53-62.
- TURNER, J. G., HUGHES, L. F. & CASPARY, D. M. 2005. Divergent response properties of layer-V neurons in rat primary auditory cortex. *Hearing research*, 202, 129-140.
- ULANOVSKY, N., LAS, L., FARKAS, D. & NELKEN, I. 2004. Multiple time scales of adaptation in auditory cortex neurons. *The Journal of neuroscience*, 24, 10440-10453.
- ULANOVSKY, N., LAS, L. & NELKEN, I. 2003. Processing of low-probability sounds by cortical neurons. *Nature Neuroscience*, 6, 391-398.
- UMBRICHT, D., KOLLER, R., VOLLENWEIDER, F. X. & SCHMID, L. 2002. Mismatch negativity predicts psychotic experiences induced by NMDA receptor antagonist in healthy volunteers. *Biological Psychiatry*, 51, 400-406.
- UMBRICHT, D. & KRLJES, S. 2005. Mismatch negativity in schizophrenia: a meta-analysis. *Schizophrenia Research*, 76, 1-23.
- UMBRICHT, D., VYSSOTKI, D., LATANOV, A., NITSCH, R. & LIPP, H.-P. 2005. Deviance-related electrophysiological activity in mice: is there mismatch negativity in mice? *Clinical Neurophysiology*, 116, 353-363.
- VAN DEN BUUSE, M. 2010. Modeling the positive symptoms of schizophrenia in genetically modified mice: pharmacology and methodology aspects. *Schizophrenia bulletin*, 36, 246-270.
- VAN DER WERF, M., HANSEN, M., KÖHLER, S., VERKAAIK, M., VERHEY, F., VAN WINKEL, R., VAN OS, J. & ALLARDYCE, J. 2014. Systematic review and collaborative recalculation of 133 693 incident cases of schizophrenia. *Psychological medicine*, 44, 9-16.
- VAN OPSTAL, J. 2016. Chapter 7 - Acoustic Localization Cues. *The Auditory System and Human Sound-Localization Behavior*. San Diego: Academic Press.
- VAN ROSSUM, J. 1966. The significance of dopamine-receptor blockade for the mechanism of action of neuroleptic drugs. *Archives internationales de pharmacodynamie et de thérapie*, 160, 492.
- VERMA, A. & MOGHADDAM, B. 1996. NMDA receptor antagonists impair prefrontal cortex function as assessed via spatial delayed alternation performance in rats: modulation by dopamine. *The Journal of neuroscience*, 16, 373-379.

- WANG, W., TIMSIT-BERTHIER, M. & SCHOENEN, J. 1996. Intensity dependence of auditory evoked potentials is pronounced in migraine An indication of cortical potentiation and low serotonergic neurotransmission? *Neurology*, 46, 1404-1404.
- WARD, L. M. 2003. Synchronous neural oscillations and cognitive processes. *Trends in Cognitive Sciences*, 7, 553-559.
- WATSON, C., KIRKCALDIE, M. & PAXINOS, G. 2010. Chapter 7 - The human cerebral cortex. *The Brain*. San Diego: Academic Press.
- WATSON, T. D., PETRAKIS, I. L., EDGEcombe, J., PERRINO, A., KRYSTAL, J. H. & MATHALON, D. H. 2009. Modulation of the cortical processing of novel and target stimuli by drugs affecting glutamate and GABA neurotransmission. *International Journal of Neuropsychopharmacology*, 12, 357-370.
- WEINBERGER, D. R. & HARRISON, P. J. (eds.) 2010. *Schizophrenia*: Wiley-Blackwell.
- WELCH, P. D. 1967. The use of fast Fourier transform for the estimation of power spectra: A method based on time averaging over short, modified periodograms. *IEEE Transactions on audio and electroacoustics*, 15, 70-73.
- WINCHESTER, C. L., OHZEKI, H., VOUYIOUKLIS, D. A., THOMPSON, R., PENNINGER, J. M., YAMAGAMI, K., NORRIE, J. D., HUNTER, R., PRATT, J. A. & MORRIS, B. J. 2012. Converging evidence that sequence variations in the novel candidate gene MAP2K7 (MKK7) are functionally associated with schizophrenia. *Human molecular genetics*, 21, 4910-4921.
- WINCHESTER, C. L., PRATT, J. A. & MORRIS, B. J. 2014. Risk genes for schizophrenia: Translational opportunities for drug discovery. *Pharmacology & therapeutics*, 143, 34-50.
- WINER, J. & LARUE, D. 1989. Populations of GABAergic neurons and axons in layer I of rat auditory cortex. *Neuroscience*, 33, 499-515.
- WINER, J. A. & SCHREINER, C. 2011. *The auditory cortex*, New York, New York : Springer.
- WINKLER, I., KARMOS, G. & NÄÄTÄNEN, R. 1996. Adaptive modeling of the unattended acoustic environment reflected in the mismatch negativity event-related potential. *Brain Research*, 742, 239-252.
- WITTEN, L., ORANJE, B., MORK, A., STEINIGER-BRACH, B., GLENTHOJ, B. Y. & BASTLUND, J. F. 2014. Auditory sensory processing deficits in sensory gating and mismatch negativity-like responses in the social isolation rat model of schizophrenia. *Behavioural Brain Research*, 266, 85-93.
- WOODS, D. L. 1995. The component structure of the N1 wave of the human auditory evoked potential. *Electroencephalography and Clinical Neurophysiology-Supplements Only*, 44, 102-109.
- WU, G. K., LI, P., TAO, H. W. & ZHANG, L. I. 2006. Nonmonotonic synaptic excitation and imbalanced inhibition underlying cortical intensity tuning. *Neuron*, 52, 705-715.
- YAMASHIRO, K., INUI, K., OTSURU, N., KIDA, T. & KAKIGI, R. 2009. Automatic auditory off-response in humans: an MEG study. *European Journal of Neuroscience*, 30, 125-131.
- ZHAO, L., LIU, Y., SHEN, L., FENG, L. & HONG, B. 2011. Stimulus-specific adaptation and its dynamics in the inferior colliculus of rat. *Neuroscience*, 181, 163-174.
- ZHU, Y., PAK, D., QIN, Y., MCCORMACK, S. G., KIM, M. J., BAUMGART, J. P., VELAMOOR, V., AUBERSON, Y. P., OSTEN, P. & VAN AELST, L. 2005. Rap2-JNK removes synaptic AMPA receptors during depotentiation. *Neuron*, 46, 905-916.

Appendices

Appendix A - Experiment I animal details

ID no.	DOB	SEX	Genotype	Date Used	Age (weeks)	Weight	Comments
408	16/04/2014	M	WT	04/08/2014	15.71	25.60	d.p.k
409	16/04/2014	F	WT	13/08/2014	17.00	20.10	d.d.s.
410	16/04/2014	F	WT	07/08/2014	16.14	20.00	d.d.s.
413	16/04/2014	M	HET	05/08/2014	15.86	26.00	
415	16/04/2014	M	HET	06/08/2014	16.00	26.80	
416	16/04/2014	F	HET	11/08/2014	16.71	20.80	d.p.k
417	16/04/2014	F	WT	12/08/2014	16.86	20.70	
418	08/05/2014	M	WT	20/08/2014	14.86	28.20	m.e.
420	08/05/2014	M	HET	19/08/2014	14.71	29.30	m.e.
422	08/05/2014	M	HET	16/08/2014	14.29	32.40	
423	08/05/2014	M	WT	15/08/2014	14.14	28.20	
424	08/05/2014	M	WT	18/08/2014	14.57	24.90	
425	08/05/2014	M	WT	14/08/2014	14.00	28.90	
426	08/05/2014	M	HET	19/08/2014	14.71	29.30	m.e.; d.d.s.
427	08/05/2014	F	HET	20/08/2014	14.86	21.90	
428	08/05/2014	F	HET	21/08/2014	15.00	25.00	d.d.s.
429	08/05/2014	F	WT	02/09/2014	16.71	21.70	d.p.k
430	08/05/2014	F	WT	03/09/2014	16.86	20.60	
431	08/05/2014	F	HET	26/08/2014	15.71	21.20	
432	08/05/2014	F	WT	22/08/2014	15.14	22.20	
433	08/05/2014	F	WT	23/08/2014	15.29	22.40	

m.e. = missing eartag (mice were re-genotyped); d.d.s. = died during surgery; d.p.k. = died post-ketamine.

Appendix B - Experiment II animal details

ID no.	DOB	SEX	Genotype	Surgery Date	Age (weeks)	Weight (g)	Comments
453	18/06/2014	F	WT	26/01/2015	31.71	25.9	No 2nd duration
454	18/06/2014	F	WT	26/01/2015	31.71	23.8	
455	25/06/2014	M	WT	13/01/2015	31.00	23.5	Pilot; r.f.a.
458	25/06/2014	F	WT	28/01/2015	31.00	22.6	
459	25/06/2014	M	WT	27/01/2015	31.14	23.0	
460	26/06/2014	M	HET	27/01/2015	31.00	23.4	Bad Ch1; r.f.a.
461	25/06/2014	F	HET	28/01/2015	34.14	23.6	Bad Ch2; r.f.a.
462	25/06/2014	F	WT	29/01/2015	34.29	22.7	
463	26/06/2014	F	HET	29/01/2015	36.86	25.6	
464	25/06/2014	M	HET	30/01/2015	32.43	25.4	
465	25/06/2014	M	WT	30/01/2015	32.43	24.2	
466	26/06/2014	M	HET	17/02/2015	34.86	23.8	
467	25/06/2014	M	WT	17/02/2015	28.86	32.9	
468	25/06/2014	M	WT	10/03/2015	30.86	34.9	
469	26/06/2014	F	HET	20/02/2015	30.71	31.2	
470	25/06/2014	F	WT	20/02/2015	31.29	30.2	No 2nd duration
471	25/06/2014	F	HET	10/03/2015	31.29	33.6	No 2nd duration
472	10/07/2014	M	HET	19/02/2015	33.71	32.9	
473	10/07/2014	M	WT	19/02/2015	32.00	30.0	d.d.s.
474	10/07/2014	M	HET	23/02/2015	33.86	32.1	
478	10/07/2014	F	WT	22/02/2015	36.86	29.1	
480	10/07/2014	F	HET	22/02/2015	32.00	27.4	No 2nd duration
482	10/07/2014	F	HET	11/03/2015	32.57	33.9	
484	17/07/2014	M	HET	23/02/2015	31.57	35.0	Bad Ch1

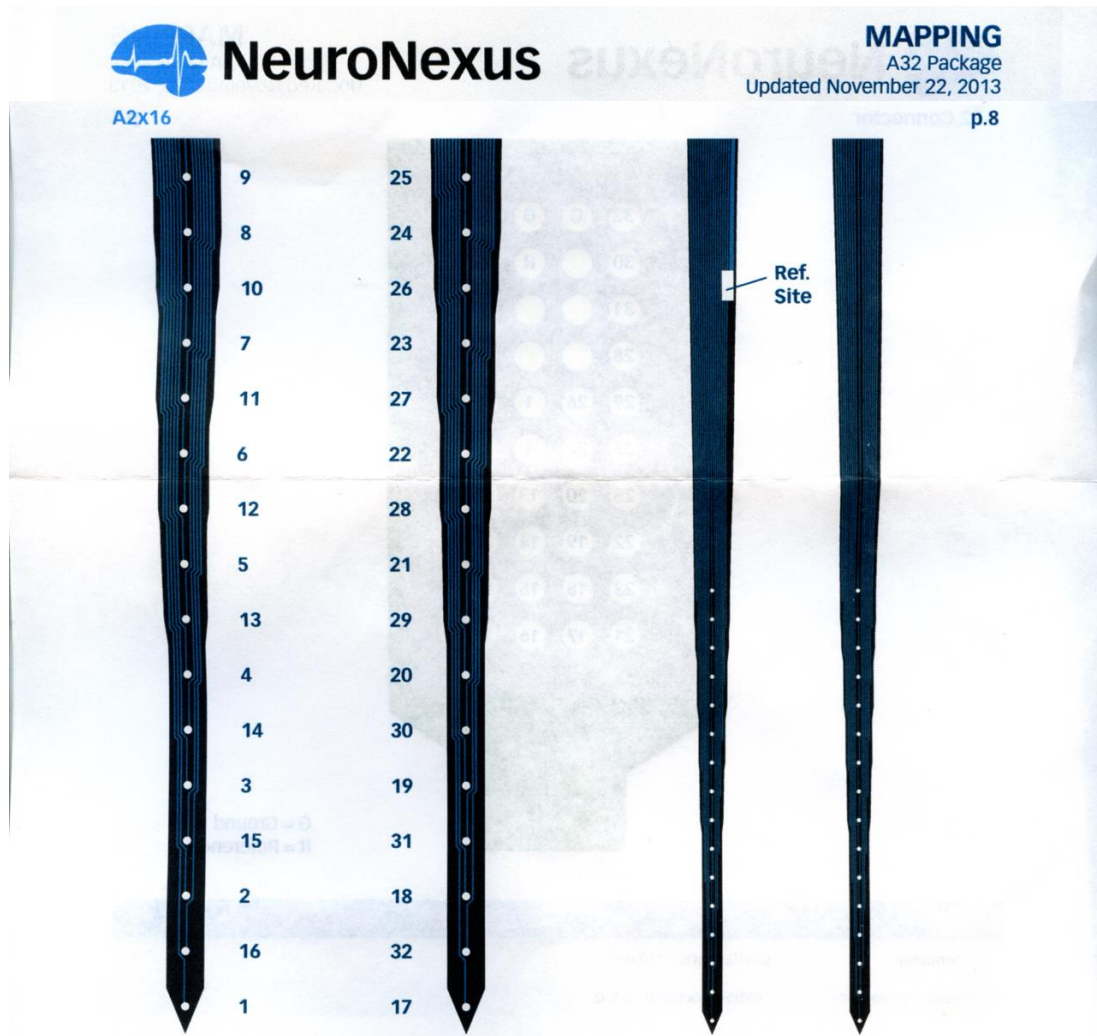
No 2nd duration = no duration-varying paradigms with constant ISI because of technical problems;
r.f.a. = removed from analysis; d.d.s. = died during surgery; Bad Ch1/2 = recording quality issue with specific channel.

Appendix C - Experiment III animal details

Exp	ID no.	DOB	SEX	Genotype	DATE	Age (weeks)	Weight (g)	Notes
01	33	08/02/2015	F	HET	29/05/2015	15.7	22.0	n.a.
02	43	04/02/2015	F	WT	30/05/2015	16.4	24.4	n.a.
03	34	08/02/2015	F	HET	31/05/2015	16.0	21.5	n.a.
04	37	08/02/2015	F	HET	04/06/2015	16.6	22.2	n.a.
05	66	20/02/2015	F	WT	06/06/2015	15.1	24.2	n.a.
06	67	20/02/2015	M	HET	12/06/2015	16.0	29.9	n.a.
07	35	08/02/2015	F	WT	19/06/2015	18.7	25.5	d.d.s
08	49	05/02/2015	F	HET	19/06/2015	19.1	26.6	n.a.
09	57	08/02/2015	F	HET	20/06/2015	18.9	23.6	n.a.
10	51	05/02/2015	F	HET	20/06/2015	19.3	21.6	n.a.
11	36	08/02/2015	F	WT	21/06/2015	19.0	25.6	
12	74	27/02/2015	M	HET	21/06/2015	16.3	28.0	
13	82	01/03/2015	F	WT	22/06/2015	16.1	21.0	n.a.
14	80	01/03/2015	F	WT	22/06/2015	16.1	21.8	n.a.
15	71	27/02/2015	M	WT	26/06/2015	17.0	28.7	n.a.
16	77	27/02/2015	F	HET	27/06/2015	17.1	25.5	
17	78	27/02/2015	F	HET	27/06/2015	17.1	25.9	n.a.
18	79	01/03/2015	M	WT	28/06/2015	17.0	25.8	n.a.
19	76	27/02/2015	M	WT	28/06/2015	17.3	32.5	
20	81	01/03/2015	F	HET	29/06/2015	17.1	23.4	n.a.
21	75	27/02/2015	M	HET	29/06/2015	17.4	31.7	d.p.k
X	72	27/02/2015	M	WT	28/06/2015	17.3		d.d.s
X	58	08/02/2015	F	WT	05/06/2015	16.7		d.d.s

n.a. = no observed auditory evoked potential; d.d.s = died during surgery; d.p.k. = died post-ketamine.

Appendix D - Multichannel probe datasheet



Serial Number: #EDC			
Model: A2x16 : A2x16-10mm-50-500-177-A32			
Thickness (um) : 50			
Defective site #: n/a			
Site 1	1.82	Site 17	1.65
Site 2	1.97	Site 18	1.95
Site 3	1.99	Site 19	1.90
Site 4	1.72	Site 20	1.82
Site 5	1.94	Site 21	1.61
Site 6	1.71	Site 22	1.69
Site 7	1.70	Site 23	1.69
Site 8	1.81	Site 24	1.55
Site 9	1.78	Site 25	1.51
Site 10	1.72	Site 26	1.63
Site 11	1.61	Site 27	1.59
Site 12	1.73	Site 28	1.61
Site 13	1.75	Site 29	1.56
Site 14	1.52	Site 30	1.98
Site 15	1.77	Site 31	2.94
Site 16	1.69	Site 32	1.92

Serial Number: #FC8			
Model: A2x16 : A2x16-10mm-50-500-177-A32			
Thickness (um) : 50			
Defective site #: n/a			
Site 1	1.68	Site 17	1.51
Site 2	1.57	Site 18	1.45
Site 3	1.73	Site 19	1.35
Site 4	1.48	Site 20	1.40
Site 5	1.44	Site 21	1.37
Site 6	1.44	Site 22	1.41
Site 7	1.44	Site 23	1.46
Site 8	1.47	Site 24	1.41
Site 9	1.29	Site 25	1.46
Site 10	1.41	Site 26	1.34
Site 11	1.29	Site 27	1.34
Site 12	1.36	Site 28	1.62
Site 13	1.49	Site 29	1.47
Site 14	1.34	Site 30	1.66
Site 15	1.33	Site 31	1.45
Site 16	1.28	Site 32	1.42

Excerpts from Neuronexus multichannel silicon probe (A2v16-10 mm-50-500-177-A32) datasheet

Appendix E - Matlab scripts

1. Experiment I scripts

```
clear all
daq.reset;
%This script performs Experiment I stimuli presentation

%Check background noise level
SoundTest

%Load calibrated gain values after running SpeakerCalibration.m
load('SpeakerCalibration.mat');
%Load stimulus codes
load('MMNcode.mat')
load('MSCcode.mat')
ISI = 0.45; %inter stimulus interval in seconds

%Initialize NI device
device = daq.getDevices;
vendor=daq.getVendors;
s = daq.createSession('ni');
s1 = daq.createSession('ni');
rate = 30e3;
s.Rate = rate;
s.addAnalogOutputChannel('Dev1',0:1, 'Voltage');
s1.addDigitalChannel('Dev1','Port1/Line0', 'OutputOnly');
outputSingleScan(s1,0);

%Duration Consecutive Repetition control (0.continuous)
durSPT = DurationSPT(rate,StdGain,ISI);
queueOutputData(s, durSPT);
prepare(s);
%Instruct to setup open-ephys
fprintf(1,'\nSet up Ephys and press any key to continue\n');pause
fprintf(1,'\nDuration Stimulus Pulse Train running...');
outputSingleScan(s1,1);
startForeground(s);
stop(s)
outputSingleScan(s1,0);
fprintf(1,' complete!\n');
clear durSPT

%Duration Oddball Paradigm (filename_1.continuous)
durMMN = DurationMMN(rate,StdGain,MMNcode,ISI);
queueOutputData(s, durMMN);
prepare(s);
fprintf(1,'\nDuration Oddball MMN running...');
outputSingleScan(s1,1);
startForeground(s);
stop(s)
outputSingleScan(s1,0);
fprintf(1,' complete!\n');
clear durMMN

%Duration Deviant Alone control (filename_2.continuous)
durDA = DurationDA(rate,StdGain,MMNcode,ISI);
queueOutputData(s, durDA);
prepare(s);
fprintf(1,'\nDuration Deviant Alone running...');
outputSingleScan(s1,1);
startForeground(s);
stop(s)
outputSingleScan(s1,0);
fprintf(1,' complete!\n');
clear durDA

%Duration Many Standards control (filename_3.continuous)
durMSC = DurationMSC(rate,StdGain,MSCcode,ISI);
queueOutputData(s, durMSC);
prepare(s);
fprintf(1,'\nDuration Many Standards running...');
outputSingleScan(s1,1);
startForeground(s);
stop(s)
outputSingleScan(s1,0);
fprintf(1,' complete!\n');
clear durMSC
```

```

%Frequency Consecutive Repetition control (filename_4.continuous)
frqSPT = FrequencySPT(rate,StdGain,UpFrqDevGain,LowFrqDevGain,ISI);
queueOutputData(s, frqSPT);
prepare(s);
fprintf(1,'\nFrequency Stimulus Pulse Train running...');
outputSingleScan(s1,1);
startForeground(s);
stop(s)
outputSingleScan(s1,0);
fprintf(1,' complete!\n');
clear frqSPT

%Frequency Oddball Paradigm (filename_5.continuous)
freqMMN = FrequencyMMN(rate,StdGain,UpFrqDevGain,LowFrqDevGain,MMNcode,ISI);
queueOutputData(s, freqMMN);
prepare(s);
fprintf(1,'\nFrequency Oddball MMN running...');
outputSingleScan(s1,1);
startForeground(s);
stop(s)
outputSingleScan(s1,0);
fprintf(1,' complete!\n');
clear freqMMN

%Frequency Deviant Alone control (filename_6.continuous)
freqDA = FrequencyDA(rate,StdGain,UpFrqDevGain,LowFrqDevGain,MMNcode,ISI);
queueOutputData(s, freqDA);
prepare(s);
fprintf(1,'\nFrequency Deviant Alone running...');
outputSingleScan(s1,1);
startForeground(s);
stop(s)
outputSingleScan(s1,0);
fprintf(1,' complete!\n');
clear freqDA

%Frequency Many Standards control (filename_7.continuous)
freqMSC = FrequencyMSC(rate,fgain0,fgain1,fgain2,fgain3,fgain4,...
    LowFrqDevGain,fgain6,StdGain,fgain8,UpFrqDevGain,MSCcode,ISI);
queueOutputData(s, freqMSC);
prepare(s);
fprintf(1,'\nFrequency Many Standards running...');
outputSingleScan(s1,1);
startForeground(s);
stop(s)
outputSingleScan(s1,0);
fprintf(1,' complete!\n');
clear freqMSC

%Intensity Consecutive Repetition control (filename_8.continuous)
intSPT = IntensitySPT(rate,StdGain,UpIntDevGain,LowIntDevGain,ISI);
queueOutputData(s, intSPT);
prepare(s);
fprintf(1,'\nIntensity Stimulus Pulse Train running...');
outputSingleScan(s1,1);
startForeground(s);
stop(s)
outputSingleScan(s1,0);
fprintf(1,' complete!\n');
clear intSPT

%Intensity Oddball Paradigm (filename_9.continuous)
intMMN = IntensityMMN(rate,StdGain,UpIntDevGain,LowIntDevGain,MMNcode,ISI);
queueOutputData(s, intMMN);
prepare(s);
fprintf(1,'\nIntensity Oddball MMN running...');
outputSingleScan(s1,1);
startForeground(s);
stop(s)
outputSingleScan(s1,0);
fprintf(1,' complete!\n');
clear intMMN

%Intensity Deviant Alone control (filename_10.continuous)
intDA = IntensityDA(rate,StdGain,UpIntDevGain,LowIntDevGain,MMNcode,ISI);
queueOutputData(s, intDA);
prepare(s);
fprintf(1,'\nIntensity Deviant Alone running...');
outputSingleScan(s1,1);
startForeground(s);
stop(s)
outputSingleScan(s1,0);
fprintf(1,' complete!\n');

```

```

clear intDA

%Intensity Many Standards control (filename_11.continuous)
intMSC = IntensityMSC( rate,igain0,igain1,LowIntDevGain,igain3,...
    StdGain,igain5,UpIntDevGain,igain7,igain8,igain9,MSCcode,ISI );
queueOutputData(s, intMSC);
prepare(s);
fprintf(1,'\nIntensity Many Standards running...');
outputSingleScan(s1,1);
startForeground(s);
stop(s);
outputSingleScan(s1,0);
fprintf(1,' complete!\n');
clear intMSC

%Protocol complete message
fprintf(1,'\nDONE!\n');
msgbox('Full MMN Protocol Complete. Press OK','', 'warn');

function [ dataout ] = DurationSPT( rate,StdInt,ISI )
% This function generates data formatted for analogue output via a NI USB
% DAQ device to a loudspeaker for presentation of auditory stimuli

%----- Set auditory stimuli parameters -----%
Frq = 10000;      % stimuli frequency (Hertz)
StdDur = 0.1;    % standard stimuli duration (seconds)
DevDurUp = 0.15; % upper deviant stimuli duration (seconds)
DevDurLow = 0.05; % lower deviant stimuli duration (seconds)

%----- Computations to prepare data output -----%
ISIdelay(1:(rate*ISI),1) = zeros; %set delay for ISIdelay
IBIdelay(1:(rate*5),1) = zeros; %5 second inter-block interval
pulse1(1:(rate*0.05),1) = 3; %set trigger pulse for standard
pulse1((rate*0.05):(rate*StdDur),1) = zeros;
pulse2(1:(rate*0.05),1) = 1.5; %set trigger pulse for upper deviant
pulse2((rate*0.05):(rate*DevDurUp),1) = zeros;
pulse3(1:(rate*0.05),1) = 1.5; %set trigger pulse for lower deviant
pulse3((rate*0.05):(rate*DevDurLow),1) = zeros;
t1 = (1:(StdDur*rate))/rate; % generate standard auditory stimuli
output1 = transpose(StdInt*sin(2*pi*Frq*t1));
t2 = (1:(DevDurUp*rate))/rate; % generate upper deviant auditory stimuli
output2 = transpose(StdInt*sin(2*pi*Frq*t2));
t3 = (1:(DevDurLow*rate))/rate; % generate lower deviant auditory stimuli
output3 = transpose(StdInt*sin(2*pi*Frq*t3));

%combine delays, trigger pulse and standard stimuli into Nx2 array
standard = [cat(1,ISIdelay,pulse1) cat(1,ISIdelay,output1)];
updeviant = [cat(1,ISIdelay,pulse2) cat(1,ISIdelay,output2)];
lowdeviant = [cat(1,ISIdelay,pulse3) cat(1,ISIdelay,output3)];
IBI = [IBIdelay IBI];

%----- Prepare data output -----%
dataout = [];
for i=1:100;dataout = cat(1,dataout,standard);end
for i=101;dataout = cat(1,dataout,IBI);end
for i=102:201; dataout = cat(1,dataout,updeviant);end
for i=202;dataout = cat(1,dataout,IBI);end
for i=203:302;dataout=cat(1,dataout,lowdeviant);end
dataout = cat(1,dataout,IBI);
end

```



```

function [ dataout ] = DurationMMN( rate,StdInt,MMNcode,ISI )
% This function generates data formatted for analogue output via a NI USB
% DAQ device to a loudspeaker for presentation of auditory stimuli

%----- Set auditory stimuli parameters -----%
Frq = 10000;      % stimuli frequency (Hertz)
StdDur = 0.1;    % standard stimuli duration (Seconds)
DevDurUp = 0.15; % upper deviant stimuli duration (Seconds)
DevDurLow = 0.05; % lower deviant stimuli duration (Seconds)

%----- Computations to prepare data output -----%
ISIdelay(1:(rate*ISI),1) = zeros; %set delay for ISIdelay
pulse1(1:(rate*0.05),1) = 3; %set trigger pulse for standard
pulse1((rate*0.05):(rate*StdDur),1) = zeros;
pulse2(1:(rate*0.05),1) = 1.5; %set trigger pulse for upper deviant
pulse2((rate*0.05):(rate*DevDurUp),1) = zeros;
pulse3(1:(rate*0.05),1) = 1.5; %set trigger pulse for upper deviant
pulse3((rate*0.05):(rate*DevDurLow),1) = zeros;
t1 = (1:(StdDur*rate))/rate; % generate standard auditory stimuli time base
output1 = transpose(StdInt*sin(2*pi*Frq*t1));
t2 = (1:(DevDurUp*rate))/rate; % generate upper deviant auditory stimuli
output2 = transpose(StdInt*sin(2*pi*Frq*t2));
t3 = (1:(DevDurLow*rate))/rate; % generate lower deviant auditory stimuli
output3 = transpose(StdInt*sin(2*pi*Frq*t3));

%combine delays, trigger pulse and stimuli into Nx2 array
standard = [cat(1,ISIdelay,pulse1) cat(1,ISIdelay,output1)];
updeviant = [cat(1,ISIdelay,pulse2) cat(1,ISIdelay,output2)];
lowdeviant = [cat(1,ISIdelay,pulse3) cat(1,ISIdelay,output3)];
DELAY = [ISIdelay ISIdelay];

%----- Prepare data output -----%
dataout = [];
for i=1:size(MMNcode,1)
    if MMNcode(i,1)==1; dataout = cat(1,dataout,standard);end
    if MMNcode(i,1)==2; dataout = cat(1,dataout,updeviant);end
    if MMNcode(i,1)==3; dataout = cat(1,dataout,lowdeviant);end
end
dataout=cat(1,dataout,DELAY);
end

```

```

function [ dataout ] = DurationDA( rate,DurInt,MMNcode,ISI )
% This function generates data formatted for analogue output via a NI USB
% DAQ device to a loudspeaker for presentation of auditory stimuli

%----- Set auditory stimuli parameters -----%
Frq = 10000;      % stimuli frequency (Hertz)
StdDur = 0.1;    % standard stimuli duration (Seconds)
StdInt=0;        % standard intensity 0 therefore silent
DevDurUp = 0.15; % upper deviant stimuli duration (Seconds)
DevDurLow = 0.05; % lower deviant stimuli duration (Seconds)

%----- Computations to prepare data output -----%
ISIdelay(1:(rate*ISI),1) = zeros; %set delay for ISI

```

```

pulse1(1:(rate*0.05),1) = 3; %set trigger pulse for standard
pulse1((rate*0.05):(rate*StdDur),1) = zeros;
pulse2(1:(rate*0.05),1) = 1.5; %set trigger pulse for upper deviant
pulse2((rate*0.05):(rate*DevDurUp),1) = zeros;
pulse3(1:(rate*0.05),1) = 1.5; %set trigger pulse for upper deviant
pulse3((rate*0.05):(rate*DevDurLow),1) = zeros;
t1 = (1:(StdDur*rate))/rate; % generate standard auditory stimuli time base
output1 = transpose(StdInt*sin(2*pi*Frq*t1));
t2 = (1:(DevDurUp*rate))/rate; % generate upper deviant auditory stimuli
output2 = transpose(DurInt*sin(2*pi*Frq*t2));
t3 = (1:(DevDurLow*rate))/rate; % generate lower deviant auditory stimuli
output3 = transpose(DurInt*sin(2*pi*Frq*t3));

%combine delays, trigger pulse and stimuli into Nx2 array
standard = [cat(1,ISIdelay,pulse1) cat(1,ISIdelay,output1)];
updeviant = [cat(1,ISIdelay,pulse2) cat(1,ISIdelay,output2)];
lowdeviant = [cat(1,ISIdelay,pulse3) cat(1,ISIdelay,output3)];
DELAY = [ISIdelay ISIdelay];

%----- Prepare data output -----%
dataout = [];
for i=1:size(MMNcode,1)
    if MMNcode(i,1)==1; dataout = cat(1,dataout,standard); end
    if MMNcode(i,1)==2; dataout = cat(1,dataout,updeviant); end
    if MMNcode(i,1)==3; dataout = cat(1,dataout,lowdeviant); end
end
dataout=cat(1,dataout,DELAY);
end

```

```

function [ dataout ] = DurationMSC( rate,StdInt,MSCcode,ISI )
% This function generates data formatted for analogue output via a NI USB
% DAQ device to a loudspeaker for presentation of auditory stimuli

%----- Set auditory stimuli parameters -----%
Frq = 10000; % stimuli frequency (Hertz)

std0 = 0.05; %lower deviant equivalent
std1 = 0.075;
std2 = 0.1; %standard equivalent
std3 = 0.125;
std4 = 0.150; %upper deviant equivalent
std5 = 0.175;
std6 = 0.2;
std7 = 0.225;
std8 = 0.25;
std9 = 0.275;

%----- Computations to prepare data output -----%
ISIdelay(1:(rate*ISI),1) = zeros;
finDelay(1:(rate*1),1) = zeros;
DELAY = [finDelay finDelay];
pulse0(1:(rate*0.05),1) = 1.5; %set trigger pulse for Std0
pulse0((rate*0.05):(rate*std0),1) = zeros;

pulse1(1:(rate*0.05),1) = 1.5; %set trigger pulse for std1
pulse1((rate*0.05):(rate*std1),1) = zeros;

```

```

pulse2(1:(rate*0.05),1) = 1.5; %set trigger pulse for Std2
pulse2((rate*0.05):(rate*std2),1) = zeros;
pulse3(1:(rate*0.05),1) = 1.5; %set trigger pulse for Std3
pulse3((rate*0.05):(rate*std3),1) = zeros;
pulse4(1:(rate*0.05),1) = 1.5; %set trigger pulse for Std4
pulse4((rate*0.05):(rate*std4),1) = zeros;
pulse5(1:(rate*0.05),1) = 1.5; %set trigger pulse for Std5
pulse5((rate*0.05):(rate*std5),1) = zeros;
pulse6(1:(rate*0.05),1) = 1.5; %set trigger pulse for Std6
pulse6((rate*0.05):(rate*std6),1) = zeros;
pulse7(1:(rate*0.05),1) = 1.5; %set trigger pulse for Std7
pulse7((rate*0.05):(rate*std7),1) = zeros;
pulse8(1:(rate*0.05),1) = 1.5; %set trigger pulse for Std8
pulse8((rate*0.05):(rate*std8),1) = zeros;
pulse9(1:(rate*0.05),1) = 1.5; %set trigger pulse for Std9
pulse9((rate*0.05):(round(rate*std9)),1) = zeros;
t0 = (1:(std0*rate))/rate; % generate Std0 stimuli
output0 = transpose(StdInt*sin(2*pi*Frq*t0));
t1 = (1:(std1*rate))/rate; % generate Std1 stimuli
output1 = transpose(StdInt*sin(2*pi*Frq*t1));
t2 = (1:(std2*rate))/rate; % generate Std2 stimuli
output2 = transpose(StdInt*sin(2*pi*Frq*t2));
t3 = (1:(std3*rate))/rate; % generate Std3 stimuli
output3 = transpose(StdInt*sin(2*pi*Frq*t3));
t4 = (1:(std4*rate))/rate; % generate Std4 stimuli
output4 = transpose(StdInt*sin(2*pi*Frq*t4));
t5 = (1:(std5*rate))/rate; % generate Std5 stimuli
output5 = transpose(StdInt*sin(2*pi*Frq*t5));
t6 = (1:(std6*rate))/rate; % generate Std6 stimuli
output6 = transpose(StdInt*sin(2*pi*Frq*t6));
t7 = (1:(std7*rate))/rate; % generate Std7 stimuli
output7 = transpose(StdInt*sin(2*pi*Frq*t7));
t8 = (1:(std8*rate))/rate; % generate Std8 stimuli
output8 = transpose(StdInt*sin(2*pi*Frq*t8));
t9 = (1:(std9*rate))/rate; % generate Std9 stimuli
output9 = transpose(StdInt*sin(2*pi*Frq*t9));

Std0 = [cat(1,ISIdelay,pulse0) cat(1,ISIdelay,output0)];
Std1 = [cat(1,ISIdelay,pulse1) cat(1,ISIdelay,output1)];
Std2 = [cat(1,ISIdelay,pulse2) cat(1,ISIdelay,output2)];
Std3 = [cat(1,ISIdelay,pulse3) cat(1,ISIdelay,output3)];
Std4 = [cat(1,ISIdelay,pulse4) cat(1,ISIdelay,output4)];
Std5 = [cat(1,ISIdelay,pulse5) cat(1,ISIdelay,output5)];
Std6 = [cat(1,ISIdelay,pulse6) cat(1,ISIdelay,output6)];
Std7 = [cat(1,ISIdelay,pulse7) cat(1,ISIdelay,output7)];
Std8 = [cat(1,ISIdelay,pulse8) cat(1,ISIdelay,output8)];
Std9 = [cat(1,ISIdelay,pulse9) cat(1,ISIdelay,output9)];

%----- Prepare data output -----%
dataout = [];
for i=1:size(MSCcode,1)
    if MSCcode(i,1)==0; dataout = cat(1,dataout,Std0); end
    if MSCcode(i,1)==1; dataout = cat(1,dataout,Std1); end
    if MSCcode(i,1)==2; dataout = cat(1,dataout,Std2); end
    if MSCcode(i,1)==3; dataout = cat(1,dataout,Std3); end
    if MSCcode(i,1)==4; dataout = cat(1,dataout,Std4); end

```

```

    if MSCcode(i,1)==5; dataout = cat(1,dataout,Std5); end
    if MSCcode(i,1)==6; dataout = cat(1,dataout,Std6); end
    if MSCcode(i,1)==7; dataout = cat(1,dataout,Std7); end
    if MSCcode(i,1)==8; dataout = cat(1,dataout,Std8); end
    if MSCcode(i,1)==9; dataout = cat(1,dataout,Std9); end
end
dataout=cat(1,dataout,DELAY);
end

```

```

function [ dataout ] = FrequencySPT( rate,StdInt,DevIntUp,DevIntLow,ISI )
% This function generates data formatted for analogue output via a NI USB
% DAQ device to a loudspeaker for presentation of auditory stimuli

%----- Set auditory stimuli parameters -----%
StdFrq = 10000;    % standard stimuli frequency (Hertz)
Dur = 0.05;       % stimuli duration (Seconds)
DevFrqUp = 12000; % upper deviant stimuli frequency (Hertz)
DevFrqLow = 8000; % lower deviant stimuli frequency (Hertz)

%----- Computations to prepare data output -----%
ISIdelay(1:(rate*ISI),1) = zeros; %set delay for ISI
IBIdelay(1:(rate*5),1) = zeros; %5 second inter-block interval
pulse1(1:(rate*0.05),1) = 3; %set trigger pulse for standards
pulse1((rate*0.05):(rate*Dur),1) = zeros;
pulse2(1:(rate*0.05),1) = 1.5; %set trigger pulse for deviants
pulse2((rate*0.05):(rate*Dur),1) = zeros;
t = (1:(Dur*rate))/rate; % generate auditory stimuli
output1 = transpose(StdInt*sin(2*pi*StdFrq*t)); % standard
output2 = transpose(DevIntUp*sin(2*pi*DevFrqUp*t)); % increasing deviant
output3 = transpose(DevIntLow*sin(2*pi*DevFrqLow*t)); % decreasing deviant

%combine delays, trigger pulse and stimuli into Nx2 array
standard = [cat(1,ISIdelay,pulse1) cat(1,ISIdelay,output1)];
updeviant = [cat(1,ISIdelay,pulse2) cat(1,ISIdelay,output2)];
lowdeviant = [cat(1,ISIdelay,pulse2) cat(1,ISIdelay,output3)];
IBI = [IBIdelay IBIdelay];

%----- Prepare data output -----%
dataout = [];
for i=1:100; dataout = cat(1,dataout,standard);end
for i=101; dataout = cat(1,dataout,IBI);end
for i=102:201; dataout = cat(1,dataout,updeviant);end
for i=202; dataout = cat(1,dataout,IBI);end
for i=203:302; dataout=cat(1,dataout,lowdeviant);end
dataout=cat(1,dataout,IBI);
end

```

```

function [ dataout ] = FrequencyMMN( rate,StdInt,DevIntUp,DevIntLow,MMNcode,ISI )
% This function generates data formatted for analogue output via a NI USB
% DAQ device to a loudspeaker for presentation of auditory stimuli

%----- Set auditory stimuli parameters -----%
StdFrq = 10000;    % standard stimuli frequency (Hertz)
Dur = 0.05;       % stimuli duration (Seconds)
DevFrqUp = 12000; % upper deviant stimuli frequency (Hertz)
DevFrqLow = 8000; % lower deviant stimuli frequency (Hertz)

```

```

%----- Computations to prepare data output -----%
ISIdelay(1:(rate*ISI),1) = zeros; %set delay for ISI
pulse1(1:(rate*0.05),1) = 3; %set trigger pulse for standards
pulse1((rate*0.05):(rate*Dur),1) = zeros;
pulse2(1:(rate*0.05),1) = 1.5; %set trigger pulse for deviants
pulse2((rate*0.05):(rate*Dur),1) = zeros;
t = (1:(Dur*rate))/rate; % generate auditory stimuli
output1 = transpose(StdInt*sin(2*pi*StdFrq*t)); % standard
output2 = transpose(DevIntUp*sin(2*pi*DevFrqUp*t)); % increasing deviant
output3 = transpose(DevIntLow*sin(2*pi*DevFrqLow*t)); % decreasing deviant

%combine delays, trigger pulse and stimuli into Nx2 array
standard = [cat(1,ISIdelay,pulse1) cat(1,ISIdelay,output1)];
updeviant = [cat(1,ISIdelay,pulse2) cat(1,ISIdelay,output2)];
lowdeviant = [cat(1,ISIdelay,pulse2) cat(1,ISIdelay,output3)];
DELAY = [ISIdelay ISIdelay];

%----- Prepare data output -----%
dataout = [];
for i=1:size(MMNcode,1)
    if MMNcode(i,1)==1; dataout = cat(1,dataout,standard); end
    if MMNcode(i,1)==2; dataout = cat(1,dataout,updeviant); end
    if MMNcode(i,1)==3; dataout = cat(1,dataout,lowdeviant); end
end
dataout=cat(1,dataout,DELAY);
end

```

```

function [ dataout ] = FrequencyDA( rate,~,DevIntUp,DevIntLow,MMNcode,ISI )
% This function generates data formatted for analogue output via a NI USB
% DAQ device to a loudspeaker for presentation of auditory stimuli

%----- Set auditory stimuli parameters -----%
StdFrq = 10000; % standard stimuli frequency (Hertz)
Dur = 0.05; % stimuli duration (Seconds)
StdInt=0; % Standard intensity is 0 therefore silent
DevFrqUp = 12000; % upper deviant stimuli frequency (Hertz)
DevFrqLow = 8000; % lower deviant stimuli frequency (Hertz)

%----- Computations to prepare data output -----%
ISIdelay(1:(rate*ISI),1) = zeros; %set delay for ISI
pulse1(1:(rate*0.05),1) = 3; %set trigger pulse for standards
pulse1((rate*0.05):(rate*Dur),1) = zeros;
pulse2(1:(rate*0.05),1) = 1.5; %set trigger pulse for deviants
pulse2((rate*0.05):(rate*Dur),1) = zeros;
t = (1:(Dur*rate))/rate; % generate auditory stimuli
output1 = transpose(StdInt*sin(2*pi*StdFrq*t)); % standard
output2 = transpose(DevIntUp*sin(2*pi*DevFrqUp*t)); % increasing deviant
output3 = transpose(DevIntLow*sin(2*pi*DevFrqLow*t)); % decreasing deviant

%combine delays, trigger pulse and stimuli into Nx2 array
standard = [cat(1,ISIdelay,pulse1) cat(1,ISIdelay,output1)];
updeviant = [cat(1,ISIdelay,pulse2) cat(1,ISIdelay,output2)];
lowdeviant = [cat(1,ISIdelay,pulse2) cat(1,ISIdelay,output3)];
DELAY = [ISIdelay ISIdelay];

```

```

%----- Prepare data output -----%
dataout = [];
for i=1:size(MMNcode,1)
    if MMNcode(i,1)==1; dataout = cat(1,dataout,standard); end
    if MMNcode(i,1)==2; dataout = cat(1,dataout,updeviant); end
    if MMNcode(i,1)==3; dataout = cat(1,dataout,lowdeviant); end
end
dataout=cat(1,dataout,DELAY);
end

function [ dataout ] = FrequencyMSC( rate,fgain0,fgain1,fgain2,fgain3,...
    fgain4,fgain5,fgain6,fgain7,fgain8,fgain9,MSCcode,ISI )
% This function generates data formatted for analogue output via a NI USB
% DAQ device to a loudspeaker for presentation of auditory stimuli

%----- Set auditory stimuli parameters -----%
Dur = 0.05;          % stimuli duration (Seconds)

std0 = 8e3;          %lower deviant equivalent
std1 = 8.5e3;
std2 = 9e3;
std3 = 9.5e3;
std4 = 10e3;         %standard equivalent
std5 = 10.5e3;
std6 = 11e3;
std7 = 11.5e3;
std8 = 12e3;         %upper deviant equivalent
std9 = 12.5e3;

%----- Computations to prepare data output -----%
ISIdelay(1:(rate*ISI),1) = zeros; %set delay for ISI
pulse(1:(rate*0.05),1) = 1.5; %set trigger pulse for all stimuli
pulse((rate*0.05):(rate*Dur),1) = zeros;
t = (1:(Dur*rate))/rate; % generate timebase for auditory stimuli

output0 = transpose(fgain0*sin(2*pi*std0*t));
output1 = transpose(fgain1*sin(2*pi*std1*t));
output2 = transpose(fgain2*sin(2*pi*std2*t));
output3 = transpose(fgain3*sin(2*pi*std3*t));
output4 = transpose(fgain4*sin(2*pi*std4*t));
output5 = transpose(fgain5*sin(2*pi*std5*t));
output6 = transpose(fgain6*sin(2*pi*std6*t));
output7 = transpose(fgain7*sin(2*pi*std7*t));
output8 = transpose(fgain8*sin(2*pi*std8*t));
output9 = transpose(fgain9*sin(2*pi*std9*t));

Std0 = [cat(1,ISIdelay,pulse) cat(1,ISIdelay,output0)];
Std1 = [cat(1,ISIdelay,pulse) cat(1,ISIdelay,output1)];
Std2 = [cat(1,ISIdelay,pulse) cat(1,ISIdelay,output2)];
Std3 = [cat(1,ISIdelay,pulse) cat(1,ISIdelay,output3)];
Std4 = [cat(1,ISIdelay,pulse) cat(1,ISIdelay,output4)];
Std5 = [cat(1,ISIdelay,pulse) cat(1,ISIdelay,output5)];
Std6 = [cat(1,ISIdelay,pulse) cat(1,ISIdelay,output6)];
Std7 = [cat(1,ISIdelay,pulse) cat(1,ISIdelay,output7)];
Std8 = [cat(1,ISIdelay,pulse) cat(1,ISIdelay,output8)];
Std9 = [cat(1,ISIdelay,pulse) cat(1,ISIdelay,output9)];

```

```

DELAY = [ISIdelay ISIdelay];

%----- Prepare data output -----%
dataout = [];
for i=1:size(MSCcode,1)
    if MSCcode(i,1)==0; dataout = cat(1,dataout,Std0); end
    if MSCcode(i,1)==1; dataout = cat(1,dataout,Std1); end
    if MSCcode(i,1)==2; dataout = cat(1,dataout,Std2); end
    if MSCcode(i,1)==3; dataout = cat(1,dataout,Std3); end
    if MSCcode(i,1)==4; dataout = cat(1,dataout,Std4); end
    if MSCcode(i,1)==5; dataout = cat(1,dataout,Std5); end
    if MSCcode(i,1)==6; dataout = cat(1,dataout,Std6); end
    if MSCcode(i,1)==7; dataout = cat(1,dataout,Std7); end
    if MSCcode(i,1)==8; dataout = cat(1,dataout,Std8); end
    if MSCcode(i,1)==9; dataout = cat(1,dataout,Std9); end
end
dataout=cat(1,dataout,DELAY);
end

```

```

function [ dataout ] = IntensitySPT( rate,StdInt,DevIntUp,DevIntLow,ISI )
% This function generates data formatted for analogue output via a NI USB
% DAQ device to a loudspeaker for presentation of auditory stimuli

%----- Set auditory stimuli parameters -----%
Frq = 10000;    % stimuli frequency (Hertz)
Dur = 0.05;     % stimuli duration (Seconds)

%----- Computations to prepare data output -----%
ISIdelay(1:(rate*ISI),1) = zeros; %set delay for ISI
IBIdelay(1:(rate*5),1) = zeros; %5 second inter-block interval
pulse1(1:(rate*0.05),1) = 3; %set trigger pulse for standard
pulse1((rate*0.1):(rate*Dur),1) = zeros;
pulse2(1:(rate*0.05),1) = 1.5; %set trigger pulse for upper deviant
pulse2((rate*0.1):(rate*Dur),1) = zeros;
t = (1:(Dur*rate))/rate; % generate auditory stimuli
output1 = transpose(StdInt*sin(2*pi*Frq*t)); % standard
output2 = transpose(DevIntUp*sin(2*pi*Frq*t)); % increasing intensity
output3 = transpose(DevIntLow*sin(2*pi*Frq*t)); % decreasing intensity

%combine delays, trigger pulse and standard stimuli into Nx2 array
standard = [cat(1,ISIdelay,pulse1) cat(1,ISIdelay,output1)];
updeviant = [cat(1,ISIdelay,pulse2) cat(1,ISIdelay,output2)];
lowdeviant = [cat(1,ISIdelay,pulse2) cat(1,ISIdelay,output3)];
IBI = [IBIdelay IBIdelay];

%----- Prepare data output -----%
dataout = [];
for i=1:100; dataout = cat(1,dataout,standard);end
for i=101; dataout = cat(1,dataout,IBI);end
for i=102:201; dataout = cat(1,dataout,updeviant);end
for i=202; dataout = cat(1,dataout,IBI);end
for i=203:302; dataout=cat(1,dataout,lowdeviant);end
dataout = cat(1,dataout,IBI);
end

```

```

function [ dataout ] = IntensityMMN( rate,StdInt,DevIntUp,DevIntLow,MMNcode,ISI )
% This function generates data formatted for analogue output via a NI USB
% DAQ device to a loudspeaker for presentation of auditory stimuli

%----- Set auditory stimuli parameters -----%
Frq = 10000;      % stimuli frequency (Hertz)
Dur = 0.05;      % stimuli duration (Seconds)

%----- Computations to prepare data output -----%
ISIdelay(1:(rate*ISI),1) = zeros; %set delay for ISI
pulse1(1:(rate*0.05),1) = 3; %set trigger pulse for standard
pulse1((rate*0.1):(rate*Dur),1) = zeros;
pulse2(1:(rate*0.05),1) = 1.5; %set trigger pulse deviants
pulse2((rate*0.1):(rate*Dur),1) = zeros;
t = (1:(Dur*rate))/rate; % generate auditory stimuli
output1 = transpose(StdInt*sin(2*pi*Frq*t)); % standard
output2 = transpose(DevIntUp*sin(2*pi*Frq*t)); % increasing intensity
output3 = transpose(DevIntLow*sin(2*pi*Frq*t)); % decreasing intensity

%combine delays, trigger pulse and stimuli into Nx2 array
standard = [cat(1,ISIdelay,pulse1) cat(1,ISIdelay,output1)];
updeviant = [cat(1,ISIdelay,pulse2) cat(1,ISIdelay,output2)];
lowdeviant = [cat(1,ISIdelay,pulse2) cat(1,ISIdelay,output3)];
DELAY = [ISIdelay ISIdelay];

%----- Prepare data output -----%
dataout = [];
for i=1:size(MMNcode,1)
    if MMNcode(i,1)==1; dataout = cat(1,dataout,standard); end
    if MMNcode(i,1)==2; dataout = cat(1,dataout,updeviant); end
    if MMNcode(i,1)==3; dataout = cat(1,dataout,lowdeviant); end
end
dataout=cat(1,dataout,DELAY);
end

```

```

function [ dataout ] = IntensityMMN( rate,StdInt,DevIntUp,DevIntLow,MMNcode,ISI )
% This function generates data formatted for analogue output via a NI USB
% DAQ device to a loudspeaker for presentation of auditory stimuli

%----- Set auditory stimuli parameters -----%
Frq = 10000;      % stimuli frequency (Hertz)
Dur = 0.05;      % stimuli duration (Seconds)

%----- Computations to prepare data output -----%
ISIdelay(1:(rate*ISI),1) = zeros; %set delay for ISI
pulse1(1:(rate*0.05),1) = 3; %set trigger pulse for standard
pulse1((rate*0.1):(rate*Dur),1) = zeros;

pulse2(1:(rate*0.05),1) = 1.5; %set trigger pulse deviants
pulse2((rate*0.1):(rate*Dur),1) = zeros;
t = (1:(Dur*rate))/rate; % generate auditory stimuli
output1 = transpose(StdInt*sin(2*pi*Frq*t)); % standard
output2 = transpose(DevIntUp*sin(2*pi*Frq*t)); % increasing intensity
output3 = transpose(DevIntLow*sin(2*pi*Frq*t)); % decreasing intensity

```



```

%combine delays, trigger pulse and stimuli into Nx2 array
standard = [cat(1,ISIdelay,pulse1) cat(1,ISIdelay,output1)];
updeviant = [cat(1,ISIdelay,pulse2) cat(1,ISIdelay,output2)];
lowdeviant = [cat(1,ISIdelay,pulse2) cat(1,ISIdelay,output3)];
DELAY = [ISIdelay ISIdelay];

%----- Prepare data output -----%
dataout = [];
for i=1:size(MMNcode,1)
    if MMNcode(i,1)==1; dataout = cat(1,dataout,standard); end
    if MMNcode(i,1)==2; dataout = cat(1,dataout,updeviant); end
    if MMNcode(i,1)==3; dataout = cat(1,dataout,lowdeviant); end
end
dataout=cat(1,dataout,DELAY);
end

```

```

function [ dataout ] = IntensityDA( rate,~,DevIntUp,DevIntLow,MMNcode,ISI )
% This function generates data formatted for analogue output via a NI USB
% DAQ device to a loudspeaker for presentation of auditory stimuli

%----- Set auditory stimuli parameters -----%
Frq = 10000;          % stimuli frequency (Hertz)
StdInt=0;            % Standard intensity is 0 therefore silent
Dur = 0.05;          % stimuli duration (Seconds)

%----- Computations to prepare data output -----%
ISIdelay(1:(rate*ISI),1) = zeros; %set delay for ISI
pulse1(1:(rate*0.05),1) = 3; %set trigger pulse for standard
pulse1((rate*0.1):(rate*Dur),1) = zeros;
pulse2(1:(rate*0.05),1) = 1.5; %set trigger pulse for upper deviants
pulse2((rate*0.1):(rate*Dur),1) = zeros;
t = (1:(Dur*rate))/rate; % generate auditory stimuli
output1 = transpose(StdInt*sin(2*pi*Frq*t)); % standard
output2 = transpose(DevIntUp*sin(2*pi*Frq*t)); % increasing intensity
output3 = transpose(DevIntLow*sin(2*pi*Frq*t)); % decreasing intensity

%combine delays, trigger pulse and stimuli into Nx2 array
standard = [cat(1,ISIdelay,pulse1) cat(1,ISIdelay,output1)];
updeviant = [cat(1,ISIdelay,pulse2) cat(1,ISIdelay,output2)];
lowdeviant = [cat(1,ISIdelay,pulse2) cat(1,ISIdelay,output3)];
DELAY = [ISIdelay ISIdelay];

%----- Prepare data output -----%
dataout = [];

for i=1:size(MMNcode,1)
    if MMNcode(i,1)==1; dataout = cat(1,dataout,standard); end
    if MMNcode(i,1)==2; dataout = cat(1,dataout,updeviant); end
    if MMNcode(i,1)==3; dataout = cat(1,dataout,lowdeviant); end
end
dataout=cat(1,dataout,DELAY);
end

```

```

function [ dataout ] = IntensityMSC( rate,igain0,igain1,igain2,igain3,...
    igain4,igain5,igain6,igain7,igain8,igain9,MSCcode,ISI )
% This function generates data formatted for analogue output via a NI USB

```

```

% DAQ device to a loudspeaker for presentation of auditory stimuli

%----- Set auditory stimuli parameters -----%
Frq = 10000;          % stimuli frequency (Hertz)
Dur = 0.05;          % stimuli duration (Seconds)

%----- Computations to prepare data output -----%
ISIdelay(1:(rate*ISI),1) = zeros; %set delay for ISI
pulse(1:(rate*0.05),1) = 1.5; %set trigger pulse
pulse((rate*0.05):(rate*Dur),1) = zeros;
t = (1:(Dur*rate))/rate; % generate timebase for auditory stimuli
output0 = transpose(igain0*sin(2*pi*Frq*t));
output1 = transpose(igain1*sin(2*pi*Frq*t));
output2 = transpose(igain2*sin(2*pi*Frq*t)); %Lower deviant
output3 = transpose(igain3*sin(2*pi*Frq*t));
output4 = transpose(igain4*sin(2*pi*Frq*t)); %Standard
output5 = transpose(igain5*sin(2*pi*Frq*t));
output6 = transpose(igain6*sin(2*pi*Frq*t)); %Upper deviant
output7 = transpose(igain7*sin(2*pi*Frq*t));
output8 = transpose(igain8*sin(2*pi*Frq*t));
output9 = transpose(igain9*sin(2*pi*Frq*t));

Std0 = [cat(1,ISIdelay,pulse) cat(1,ISIdelay,output0)];
Std1 = [cat(1,ISIdelay,pulse) cat(1,ISIdelay,output1)];
Std2 = [cat(1,ISIdelay,pulse) cat(1,ISIdelay,output2)];
Std3 = [cat(1,ISIdelay,pulse) cat(1,ISIdelay,output3)];
Std4 = [cat(1,ISIdelay,pulse) cat(1,ISIdelay,output4)];
Std5 = [cat(1,ISIdelay,pulse) cat(1,ISIdelay,output5)];
Std6 = [cat(1,ISIdelay,pulse) cat(1,ISIdelay,output6)];
Std7 = [cat(1,ISIdelay,pulse) cat(1,ISIdelay,output7)];
Std8 = [cat(1,ISIdelay,pulse) cat(1,ISIdelay,output8)];
Std9 = [cat(1,ISIdelay,pulse) cat(1,ISIdelay,output9)];

DELAY = [ISIdelay ISIdelay];

%----- Prepare data output -----%
dataout = [];

for i=1:size(MSCcode,1);
    if MSCcode(i,1)==0; dataout = cat(1,dataout,Std0); end
    if MSCcode(i,1)==1; dataout = cat(1,dataout,Std1); end
    if MSCcode(i,1)==2; dataout = cat(1,dataout,Std2); end
    if MSCcode(i,1)==3; dataout = cat(1,dataout,Std3); end
    if MSCcode(i,1)==4; dataout = cat(1,dataout,Std4); end
    if MSCcode(i,1)==5; dataout = cat(1,dataout,Std5); end
    if MSCcode(i,1)==6; dataout = cat(1,dataout,Std6); end
    if MSCcode(i,1)==7; dataout = cat(1,dataout,Std7); end
    if MSCcode(i,1)==8; dataout = cat(1,dataout,Std8); end
    if MSCcode(i,1)==9; dataout = cat(1,dataout,Std9); end
end
dataout=cat(1,dataout,DELAY);
end

%Generates stimulus code for oddball paradigm
clear all
%----- set oddball paradigm parameters -----%

```

```

totStim = 1000;      % Total stimuli
Pstd = 0.8;         % Standard probability
Pdev = 0.2;         % Deviant probability

intvStds = 3;      % Minimum number of standards between deviants
preStds = 20;     % Number of preeceeding standards at beginning

%error if parameters are nonsense
if (Pstd+Pdev)~=1
    error('Probaility error: check standard/deviant ratio');
end
if (((totStim-preStds)/(intvStds+1))/totStim)<Pdev
    error('Deviant probability error: check oddball parameters');
end

%----- Generate MMN stimulus code -----%
MMNcode((1:totStim),1)=zeros;

MMNcode((1:preStds),1)=1;
%alternate standard tones with randomly selected deviants
for i=preStds:totStim
    check_rule = i/(intvStds+1); % set rule for stds between devs
    if floor(check_rule)==check_rule
        a=rand; %generate a random number then
        if a<=((totStim*(Pdev/2))/((totStim-preStds)/(intvStds+1)))
            %write upper deviant code
            MMNcode(i,1)=2;
        end
        if a>((totStim*(Pdev/2))/((totStim-preStds)/(intvStds+1)))...
            && a<=((totStim*Pdev)/((totStim-preStds)/(intvStds+1)))
            %write lower deviant code
            MMNcode(i,1)=3;
        end
        if a>((totStim*Pdev)/((totStim-preStds)/(intvStds+1)))
            %write standards
            MMNcode(i,1)=1;
        end
    elseif floor(check_rule)<check_rule
        MMNcode(i,1)=1;
    end
end

save('MMNcode', 'MMNcode');

%Generates stimulus code for many standards control paradigm
clear all
for i=1:1000
    a=rand; %generate a random number
    if a<=0.1; MSCcode(i,1)=1; end
    if a>0.1 && a<=0.2; MSCcode(i,1)=2; end
    if a>0.2 && a<=0.3; MSCcode(i,1)=3; end
    if a>0.3 && a<=0.4; MSCcode(i,1)=4; end
    if a>0.4 && a<=0.5; MSCcode(i,1)=5; end
    if a>0.5 && a<=0.6; MSCcode(i,1)=6; end
    if a>0.6 && a<=0.7; MSCcode(i,1)=7; end
    if a>0.7 && a<=0.8; MSCcode(i,1)=8; end
end

```

```

        if a>0.8 && a<=0.9; MSCcode(i,1)=9; end
        if a>0.9; MSCcode(i,1)=10; end
    end

    for i=1:999                %check to ensure no consecutive repeats
        while MSCcode(i) == MSCcode(i+1)
            MSCcode(i+1) = round(rand*10);
        end
    end

    save('MSCcode','MSCcode');

% Calibrates speaker for Experiment I using a single speaker
s = daq.createSession('ni');
rate = 30e3;
s.Rate = rate;
s.DurationInSeconds = 1;

ai=addAnalogInputChannel(s,'Dev1','ai0','voltage');
ai.TerminalConfig = 'SingleEnded';
ao=addAnalogOutputChannel(s,'Dev1','ao1','voltage');

[StdGain1]=SpeakerCal(s,10e3,80,rate,'standard');
[UpIntDevGain1]=SpeakerCal(s,10e3,90,rate,'upper intensity deviant');
[LowIntDevGain1]=SpeakerCal(s,10e3,70,rate,'lower intensity deviant');
[UpFrqDevGain1]=SpeakerCal(s,12e3,80,rate,'upper frequency deviant');
[LowFrqDevGain1]=SpeakerCal(s,8e3,80,rate,'lower frequency deviant');

[fgain11]=SpeakerCal(s,8.5e3,80,rate,'fgain1');
[fgain21]=SpeakerCal(s,9e3,80,rate,'fgain2');
[fgain31]=SpeakerCal(s,9.5e3,80,rate,'fgain3');
[fgain51]=SpeakerCal(s,10.5e3,80,rate,'fgain5');
[fgain61]=SpeakerCal(s,11e3,80,rate,'fgain6');
[fgain71]=SpeakerCal(s,11.5e3,80,rate,'fgain7');
[fgain91]=SpeakerCal(s,12.5e3,80,rate,'fgain9');

[igain11]=SpeakerCal(s,10e3,72.5,rate,'igain1');
[igain21]=SpeakerCal(s,10e3,75,rate,'igain2');
[igain31]=SpeakerCal(s,10e3,77.5,rate,'igain3');
[igain51]=SpeakerCal(s,10e3,82.5,rate,'igain5');
[igain61]=SpeakerCal(s,10e3,85,rate,'igain6');
[igain71]=SpeakerCal(s,10e3,87.5,rate,'igain7');
[igain91]=SpeakerCal(s,10e3,92.5,rate,'igain9');

save('SpeakerCalibration','StdGain','UpIntDevGain','LowIntDevGain',...
    'UpFrqDevGain','LowFrqDevGain','fgain1','fgain2','fgain3','fgain5',...
    'fgain6','fgain7','fgain9','igain1','igain2','igain3','igain5',...
    'igain6','igain7','igain9');
delete(s)
clear all

function [ gain ] = SpeakerCal ( session, freq, dB, samplerate,name )
% Calibrates speaker with radioshack sound level meter [33-2055]

t = (1:(0.05*samplerate))/samplerate;
gain = 5;                % initial gain in V

```

```

majorcalstep=0.1; % calibration step/resolution in V (10 V dynamic range)
minorcalstep=0.01;
for i=1:1000
    output = transpose(gain*sin(2*pi*freq*t));
    queueOutputData(session, output);
    data = session.startForeground();
    a=mean(abs(data))*1000;
    noise=round((9.0992*log(a))+32.853); % for 80 dB range
%   if stimulus intensity measured is less than desired value increase
%   voltage output
    if noise < (dB-10)
        gain = gain+majorcalstep;
        if gain>10
            error('Gain exceeds NI device output range');
        end
    end
    if noise < (dB-5)
        gain = gain+minorcalstep;
        if gain>10
            error('Gain exceeds NI device output range');
        end
    end
    if noise < (dB-1)
        gain = gain+0.0025;
        if gain>10
            error('Gain exceeds NI device output range');
        end
    end
    if noise < dB
        gain = gain+0.001;
        if gain>10
            error('Gain exceeds NI device output range');
        end
    end
%   if stimulus intensity measured is more than desired value decrease
%   voltage output
    if noise > (dB+10)
        gain = gain-majorcalstep;
        if gain<=0
            error('Gain exceeds NI device output range');
        end
    end
    if noise > (dB+5)
        gain = gain-minorcalstep;
        if gain<=0
            error('Gain exceeds NI device output range');
        end
    end
    if noise > (dB+1)
        gain = gain-0.0025;
        if gain<=0
            error('Gain exceeds NI device output range');
        end
    end
    if noise > dB
        gain = gain-0.001;
    end
end

```

```

        if gain<=0
            error('Gain exceeds NI device output range');
        end
    end
    if noise == dB
        break
    end
end
fprintf(1,'\nSound level for %s is calibrated to %ddb',name,noise);
fprintf(1,' with gain value of %d',gain);
end

%This script performs a background acoustic noise check in recording
%chamber A

s2 = daq.createSession('ni'); % use NI DAQ device
rate_s2 = 50e3;
s2.Rate = rate_s2;
s2.DurationInSeconds = 5;

% connect input from sound meter
ai=addAnalogInputChannel(s2,'Dev1','ai0','voltage');
ai.TerminalConfig = 'SingleEnded';
data_s2 = s2.startForeground();
% average across entire sample
a_s2=mean(abs(data_s2))*1000;
noise_s2=round((9.0992*log(a_s2))+32.853); % calibration for 80 dB range

fprintf(1,'\nBackground noise is %ddb\n',noise_s2);
clear s2 ai noise_s2 data_s2 rate_s2 a_s2

```

2. Experiment II scripts

```

% This script runs the duration-varying auditory paradigms with constant
% stimulus onset asynchrony for Experiment II
clear all
daq.reset;

%Check background noise level
SoundTest

%Load calibrated gain values after running SpeakerCalibration.m
load('SpeakerCalibration.mat');
%Load stimulus codes
load('MMNcode.mat')
load('MSCcode.mat')
ISI = 0.45; %inter stimulus interval in seconds

%Initialize NI device
device = daq.getDevices;
vendor=daq.getVendors;
s = daq.createSession('ni');

```

```

s1 = daq.createSession('ni');
rate = 30e3;
s.Rate = rate;
s.addAnalogOutputChannel('Dev1',0:1, 'Voltage');
s1.addDigitalChannel('Dev1','Port1/Line0', 'OutputOnly');
outputSingleScan(s1,0);

% Duration consecutive repetition control (0.continuous)
durSPT = DurationSPT_SOA(rate,StdGain,ISI);
queueOutputData(s, durSPT);
prepare(s);
% Instruction to set up open-ephys
fprintf(1,'\nSet up Ephys and press any key to continue\n');pause
fprintf(1,'\nDuration Stimulus Pulse Train running...');
outputSingleScan(s1,1);
startForeground(s);
stop(s)
outputSingleScan(s1,0);
fprintf(1,' complete!\n');
clear durSPT

% Duration oddball paradigm (filename_1.continuous)
durMMN = DurationMMN_SOA(rate,StdGain,MMNcode,ISI);
queueOutputData(s, durMMN);
prepare(s);
fprintf(1,'\nDuration Oddball MMN running...');
outputSingleScan(s1,1);
startForeground(s);
stop(s)
outputSingleScan(s1,0);
fprintf(1,' complete!\n');
clear durMMN

% Duration deviant alone control (filename_2.continuous)
durDA = DurationDA_SOA(rate,StdGain,MMNcode,ISI);
queueOutputData(s, durDA);
prepare(s);
fprintf(1,'\nDuration Deviant Alone running...');
outputSingleScan(s1,1);
startForeground(s);
stop(s)
outputSingleScan(s1,0);
fprintf(1,' complete!\n');
clear durDA

% Duration many standards control (filename_3.continuous)
durMSC = DurationMSC_SOA(rate,StdGain,MSCcode,ISI);
queueOutputData(s, durMSC);
prepare(s);
fprintf(1,'\nDuration Many Standards running...');
outputSingleScan(s1,1);
startForeground(s);
stop(s)
outputSingleScan(s1,0);
fprintf(1,' complete!\n');
clear durMSC

```

```

% Protocol complete message
fprintf(1, '\nDONE!\n');
msgbox('Duration Protocol Complete. Press OK', '', 'warn');

function [ dataout ] = DurationSPT_SOA(rate,StdInt,ISI)
% This function generates the audio output array for running the
% duration-varying consecutive repetition paradigm with constant stimulus
% onset asynchrony in Experiment II
%----- Set auditory stimuli parameters -----%
Frq = 10000;      % stimuli frequency (Hertz)
StdDur = 0.1;    % standard stimuli (seconds)
DevDurUp = 0.15; % increased oddball duration (seconds)
DevDurLow = 0.05; % decreased oddball duration (seconds)
%----- Computations to prepare data output -----%
ISIdelay(1:(rate*ISI),1)=zeros; % ISI for standard
ISIdelayUp(1:(rate*(ISI-0.05)),1)=zeros; % ISI for increased oddball
ISIdelayLow(1:(rate*(ISI+0.05)),1)=zeros; % ISI for decreased oddball
LongISIdelayUp(1:(rate*(2-0.05)),1)=zeros; % long ISI for increased oddball
LongISIdelayLow(1:(rate*(2+0.05)),1)=zeros; % long ISI for decreased oddball
IBIdelay(1:(rate*5),1) = zeros; % 5 second inter-block interval

pulse1(1:(rate*0.05),1) = 3; % sync pulse for standard
pulse1((rate*0.05):(rate*StdDur),1) = zeros;
pulse2(1:(rate*0.05),1) = 1.5; % sync pulse for increased oddball
pulse2((rate*0.05):(rate*DevDurUp),1) = zeros;
pulse3(1:(rate*0.05),1) = 1.5; % sync pulse for decreased oddball
pulse3((rate*0.05):(rate*DevDurLow),1) = zeros;

t1 = (1:(StdDur*rate))/rate; % standard stimulus
output1 = transpose(StdInt*sin(2*pi*Frq*t1));
t2 = (1:(DevDurUp*rate))/rate; % increased oddball
output2 = transpose(StdInt*sin(2*pi*Frq*t2));
t3 = (1:(DevDurLow*rate))/rate; % decreased oddball
output3 = transpose(StdInt*sin(2*pi*Frq*t3));

% combine delays, trigger pulses and stimuli into arrays
standard = [cat(1,ISIdelay,pulse1) cat(1,ISIdelay,output1)];
updeviant = [cat(1,ISIdelayUp,pulse2) cat(1,ISIdelayUp,output2)];
lowdeviant = [cat(1,ISIdelayLow,pulse3) cat(1,ISIdelayLow,output3)];
updeviantlongISI = [cat(1,LongISIdelayUp,pulse2) cat(1,LongISIdelayUp,output2)];
lowdeviantlongISI = [cat(1,LongISIdelayLow,pulse3) cat(1,LongISIdelayLow,output3)];
IBI = [IBIdelay IBIdelay];
%----- Prepare data output -----%
dataout = [];
for i=1:100; dataout=cat(1,dataout,standard); end
for i=101; dataout=cat(1,dataout,IBI); end
for i=102:201; dataout=cat(1,dataout,updeviant); end
for i=202; dataout=cat(1,dataout,IBI); end
for i=203:302; dataout=cat(1,dataout,lowdeviant); end
for i=303; dataout=cat(1,dataout,IBI); end
for i=304:403; dataout=cat(1,dataout,updeviantlongISI); end
for i=404; dataout=cat(1,dataout,IBI); end
for i=405:504; dataout=cat(1,dataout,lowdeviantlongISI); end
dataout = cat(1,dataout,IBI);
end

```



```

function [ dataout ] = DurationMMN_SOA(rate,StdInt,MMNcode,ISI)
% This function generates the audio output array for running the
% duration-varying oddball paradigm with constant stimulus onset asynchrony
% in Experiment II
%----- Set auditory stimuli parameters -----%
Frq = 10000;      % stimuli frequency (Hertz)
StdDur = 0.1;    % standard stimuli duration (seconds)
DevDurUp = 0.15; % increased oddball duration (seconds)
DevDurLow = 0.05; % decreased oddball duration (seconds)
%----- Computations to prepare data output -----%
ISIdelay(1:(rate*ISI),1) = zeros; % ISI for standard
ISIdelayUp(1:(rate*(ISI-0.05)),1) = zeros; % ISI for increased oddball
ISIdelayLow(1:(rate*(ISI+0.05)),1) = zeros; % ISI for decreased oddball

pulse1(1:(rate*0.05),1) = 3; % sync pulse for standard
pulse1((rate*0.05):(rate*StdDur),1) = zeros;
pulse2(1:(rate*0.05),1) = 1.5; % sync pulse for increased oddball
pulse2((rate*0.05):(rate*DevDurUp),1) = zeros;
pulse3(1:(rate*0.05),1) = 1.5; % sync pulse for decreased oddball
pulse3((rate*0.05):(rate*DevDurLow),1) = zeros;

t1 = (1:(StdDur*rate))/rate; % standard stimulus
output1 = transpose(StdInt*sin(2*pi*Frq*t1));
t2 = (1:(DevDurUp*rate))/rate; % increased oddball
output2 = transpose(DurInt*sin(2*pi*Frq*t2));
t3 = (1:(DevDurLow*rate))/rate; % decreased oddball
output3 = transpose(DurInt*sin(2*pi*Frq*t3));

% combine delays, trigger pulses and stimuli into arrays
standard = [cat(1,ISIdelay,pulse1) cat(1,ISIdelay,output1)];
updeviant = [cat(1,ISIdelayUp,pulse2) cat(1,ISIdelayUp,output2)];
lowdeviant = [cat(1,ISIdelayLow,pulse3) cat(1,ISIdelayLow,output3)];
DELAY = [ISIdelay ISIdelay];
%----- Prepare data output -----%
dataout = [];
for i=1:size(MMNcode,1)
    if MMNcode(i,1)==1; dataout=cat(1,dataout,standard); end
    if MMNcode(i,1)==2; dataout=cat(1,dataout,updeviant); end
    if MMNcode(i,1)==3; dataout=cat(1,dataout,lowdeviant); end
end
dataout=cat(1,dataout,DELAY);
end

```

```

function [ dataout ] = DurationDA_SOA(rate,DurInt,MMNcode,ISI)
% This function generates the audio output array for running the
% duration-varying consecutive repetition paradigm with constant stimulus
% onset asynchrony in Experiment II
%----- Set auditory stimuli parameters -----%
Frq = 10000;      % stimuli frequency (Hertz)
StdDur = 0.1;    % standard stimulus duration (seconds)
StdInt = 0;      % silent standards
DevDurUp = 0.15; % increased oddball duration (seconds)
DevDurLow = 0.05; % decreased oddball duration (seconds)
%----- Computations to prepare data output -----%
ISIdelay(1:(rate*ISI),1) = zeros; % ISI for standard stimulus

```

```

ISIdelayUp(1:(rate*(ISI-0.05)),1) = zeros; % ISI for increased oddball
ISIdelayLow(1:(rate*(ISI+0.05)),1) = zeros; % ISI for decreased oddball

pulse1(1:(rate*0.05),1) = 3; % sync pulse for standard
pulse1((rate*0.05):(rate*StdDur),1) = zeros;
pulse2(1:(rate*0.05),1) = 1.5; % sync pulse for increased oddball
pulse2((rate*0.05):(rate*DevDurUp),1) = zeros;
pulse3(1:(rate*0.05),1) = 1.5; % sync pulse for decreased oddball
pulse3((rate*0.05):(rate*DevDurLow),1) = zeros;

t1 = (1:(StdDur*rate))/rate; % standard stimulus
output1 = transpose(StdInt*sin(2*pi*Frq*t1));
t2 = (1:(DevDurUp*rate))/rate; % increased oddball
output2 = transpose(DurInt*sin(2*pi*Frq*t2));
t3 = (1:(DevDurLow*rate))/rate; % decreased oddball
output3 = transpose(DurInt*sin(2*pi*Frq*t3));

% combine delays, trigger pulses and stimuli into arrays
standard = [cat(1,ISIdelay,pulse1) cat(1,ISIdelay,output1)];
updeviant = [cat(1,ISIdelayUp,pulse2) cat(1,ISIdelayUp,output2)];
lowdeviant = [cat(1,ISIdelayLow,pulse3) cat(1,ISIdelayLow,output3)];
DELAY = [ISIdelay ISIdelay];
%----- Prepare data output -----%
dataout = [];
for i=1:size(MMNcode,1)
    if MMNcode(i,1)==1; dataout=cat(1,dataout,standard); end
    if MMNcode(i,1)==2; dataout=cat(1,dataout,updeviant); end
    if MMNcode(i,1)==3; dataout=cat(1,dataout,lowdeviant); end
end
dataout=cat(1,dataout,DELAY);
end

function [ dataout ] = DurationMSC_SOA(rate,StdInt,MSCcode,ISI)
% This function generates the audio output array for running the
% duration-varying many standards paradigm with constant stimulus onset
% asynchrony in Experiment II
%----- Set auditory stimuli parameters -----%
Frq = 10000; % stimuli frequency (Hertz)
std0 = 0.05; % decreased oddball
std1 = 0.075;
std2 = 0.1; % standard stimulus
std3 = 0.125;
std4 = 0.150; % increased oddball
std5 = 0.175;
std6 = 0.2;
std7 = 0.225;
std8 = 0.25;
std9 = 0.275;
%----- Computations to prepare data output -----%
ISIdelay0(1:(rate*(ISI+(std2-std0))),1) = zeros; % ISI for std0
ISIdelay1(1:(rate*(ISI+(std2-std1))),1) = zeros; % ISI for std1
ISIdelay2(1:(rate*(ISI+(std2-std2))),1) = zeros; % ISI for std2
ISIdelay3(1:(rate*(ISI+(std2-std3))),1) = zeros; % ISI for std3
ISIdelay4(1:(rate*(ISI+(std2-std4))),1) = zeros; % ISI for std4
ISIdelay5(1:(rate*(ISI+(std2-std5))),1) = zeros; % ISI for std5
ISIdelay6(1:(rate*(ISI+(std2-std6))),1) = zeros; % ISI for std6

```

```

ISIdelay7(1:(rate*(ISI+(std2-std7))),1) = zeros; % ISI for std7
ISIdelay8(1:(rate*(ISI+(std2-std8))),1) = zeros; % ISI for std8
ISIdelay9(1:(rate*(ISI+(std2-std9))),1) = zeros; % ISI for std9
finDelay(1:(rate*1),1) = zeros; %delay at end of paradigm

pulse0(1:(rate*0.05),1) = 1.5; % sync pulse for std0
pulse0((rate*0.05):(rate*std0),1) = zeros;
pulse1(1:(rate*0.05),1) = 1.5; % sync pulse for std1
pulse1((rate*0.05):(rate*std1),1) = zeros;
pulse2(1:(rate*0.05),1) = 1.5; % sync pulse for std2
pulse2((rate*0.05):(rate*std2),1) = zeros;
pulse3(1:(rate*0.05),1) = 1.5; % sync pulse for std3
pulse3((rate*0.05):(rate*std3),1) = zeros;
pulse4(1:(rate*0.05),1) = 1.5; % sync pulse for std4
pulse4((rate*0.05):(rate*std4),1) = zeros;
pulse5(1:(rate*0.05),1) = 1.5; % sync pulse for std5
pulse5((rate*0.05):(rate*std5),1) = zeros;
pulse6(1:(rate*0.05),1) = 1.5; % sync pulse for std6
pulse6((rate*0.05):(rate*std6),1) = zeros;
pulse7(1:(rate*0.05),1) = 1.5; % sync pulse for std7
pulse7((rate*0.05):(rate*std7),1) = zeros;
pulse8(1:(rate*0.05),1) = 1.5; % sync pulse for std8
pulse8((rate*0.05):(rate*std8),1) = zeros;
pulse9(1:(rate*0.05),1) = 1.5; % sync pulse for std9
pulse9((rate*0.05):(round(rate*std9)),1) = zeros;

t0 = (1:(std0*rate))/rate; % std0 stimulus
output0 = transpose(StdInt*sin(2*pi*Frq*t0));
t1 = (1:(std1*rate))/rate; % std1 stimulus
output1 = transpose(StdInt*sin(2*pi*Frq*t1));
t2 = (1:(std2*rate))/rate; % std2 stimulus
output2 = transpose(StdInt*sin(2*pi*Frq*t2));
t3 = (1:(std3*rate))/rate; % std3 stimulus
output3 = transpose(StdInt*sin(2*pi*Frq*t3));
t4 = (1:(std4*rate))/rate; % std4 stimulus
output4 = transpose(StdInt*sin(2*pi*Frq*t4));
t5 = (1:(std5*rate))/rate; % std5 stimulus
output5 = transpose(StdInt*sin(2*pi*Frq*t5));
t6 = (1:(std6*rate))/rate; % std6 stimulus
output6 = transpose(StdInt*sin(2*pi*Frq*t6));
t7 = (1:(std7*rate))/rate; % std7 stimulus
output7 = transpose(StdInt*sin(2*pi*Frq*t7));
t8 = (1:(std8*rate))/rate; % std8 stimulus
output8 = transpose(StdInt*sin(2*pi*Frq*t8));
t9 = (1:(std9*rate))/rate; % std9 stimulus
output9 = transpose(StdInt*sin(2*pi*Frq*t9));

% combine delays, trigger pulses and stimuli into arrays
Std0 = [cat(1,ISIdelay0,pulse0) cat(1,ISIdelay0,output0)];
Std1 = [cat(1,ISIdelay1,pulse1) cat(1,ISIdelay1,output1)];
Std2 = [cat(1,ISIdelay2,pulse2) cat(1,ISIdelay2,output2)];
Std3 = [cat(1,ISIdelay3,pulse3) cat(1,ISIdelay3,output3)];
Std4 = [cat(1,ISIdelay4,pulse4) cat(1,ISIdelay4,output4)];
Std5 = [cat(1,ISIdelay5,pulse5) cat(1,ISIdelay5,output5)];
Std6 = [cat(1,ISIdelay6,pulse6) cat(1,ISIdelay6,output6)];
Std7 = [cat(1,ISIdelay7,pulse7) cat(1,ISIdelay7,output7)];

```

```

Std8 = [cat(1,ISIdelay8,pulse8) cat(1,ISIdelay8,output8)];
Std9 = [cat(1,ISIdelay9,pulse9) cat(1,ISIdelay9,output9)];
DELAY = [finDelay finDelay];
%----- Prepare data output -----%
dataout = [];
for i=1:size(MSCcode,1)
    if MSCcode(i,1)==0; dataout=cat(1,dataout,Std0); end
    if MSCcode(i,1)==1; dataout=cat(1,dataout,Std1); end
    if MSCcode(i,1)==2; dataout=cat(1,dataout,Std2); end
    if MSCcode(i,1)==3; dataout=cat(1,dataout,Std3); end
    if MSCcode(i,1)==4; dataout=cat(1,dataout,Std4); end
    if MSCcode(i,1)==5; dataout=cat(1,dataout,Std5); end
    if MSCcode(i,1)==6; dataout=cat(1,dataout,Std6); end
    if MSCcode(i,1)==7; dataout=cat(1,dataout,Std7); end
    if MSCcode(i,1)==8; dataout=cat(1,dataout,Std8); end
    if MSCcode(i,1)==9; dataout=cat(1,dataout,Std9); end
end
dataout=cat(1,dataout,DELAY);
end

```

```

% This script runs the frequency-varying auditory paradigms for
% Experiment II
clear all
daq.reset;

%Check background noise level
SoundTest

%Load calibrated gain values after running SpeakerCalibration.m
load('SpeakerCalibration.mat');
%Load stimulus codes
load('MMNcode.mat')
load('MSCcode.mat')
ISI = 0.45; %inter stimulus interval in seconds

%Initialize NI device
device = daq.getDevices;
vendor=daq.getVendors;
s = daq.createSession('ni');
s1 = daq.createSession('ni');
rate = 30e3;
s.Rate = rate;
s.addAnalogOutputChannel('Dev1',0:1, 'Voltage');
s1.addDigitalChannel('Dev1','Port1/Line0', 'OutputOnly');
outputSingleScan(s1,0);

%Frequency consecutive repetition control (filename_0.continuous)
frqSPT = FrequencySPT(rate,StdGain,UpFrqDevGain,LowFrqDevGain,ISI);
queueOutputData(s, frqSPT);
prepare(s);
%Instruct to setup open-ephys
fprintf(1,'\nSet up Ephys and press any key to continue\n');pause
fprintf(1,'\nFrequency Stimulus Pulse Train running...');
outputSingleScan(s1,1);
startForeground(s);
stop(s)

```

```

outputSingleScan(s1,0);
fprintf(1,' complete!\n');
clear frqSPT

%Frequency oddball paradigm (filename_1.continuous)
freqMMN = FrequencyMMN(rate,StdGain,UpFrqDevGain,LowFrqDevGain,MMNcode,ISI);
queueOutputData(s, freqMMN);
prepare(s);
fprintf(1,'\nFrequency Oddball MMN running...');
outputSingleScan(s1,1);
startForeground(s);
stop(s)
outputSingleScan(s1,0);
fprintf(1,' complete!\n');
clear freqMMN

%Frequency deviant alone control (filename_2.continuous)
freqDA = FrequencyDA(rate,StdGain,UpFrqDevGain,LowFrqDevGain,MMNcode,ISI);
queueOutputData(s, freqDA);
prepare(s);
fprintf(1,'\nFrequency Deviant Alone running...');
outputSingleScan(s1,1);
startForeground(s);
stop(s)
outputSingleScan(s1,0);
fprintf(1,' complete!\n');
clear freqDA

%Frequency many standards control (filename_3.continuous)
freqMSC = FrequencyMSC(rate,LowFrqDevGain,fgain1,fgain2,fgain3,StdGain,...
    fgain5,fgain6,fgain7,UpFrqDevGain,fgain9,MSCcode,ISI);
queueOutputData(s, freqMSC);
prepare(s);
fprintf(1,'\nFrequency Many Standards running...');
outputSingleScan(s1,1);
startForeground(s);
stop(s)
outputSingleScan(s1,0);
fprintf(1,' complete!\n');
clear freqMSC

%Protocol complete message
fprintf(1,'\nDONE!\n');
msgbox('Frequency Protocol Complete. Press OK','', 'warn');

function [ dataout ] = FrequencySPT(rate,StdInt,DevIntUp,DevIntLow,ISI)
% This function generates the audio output array for running the
% frequency-varying consecutive repetition paradigm in Experiment II
%----- Set auditory stimuli parameters -----%
StdFrq = 10000;    % stimuli frequency (Hertz)
Dur = 0.05;      % stimuli duration (seconds)
DevFrqUp = 12000; % ascending oddball frequency (Hertz)
DevFrqLow = 8000; % descending oddball frequency (Hertz)
%----- Computations to prepare data output -----%
ISIdelay(1:(rate*ISI),1) = zeros; % ISI
LongISIdelay(1:(rate*2),1) = zeros; % lons ISI

```

```

IBIdelay(1:(rate*5),1) = zeros; % 5 second inter-block interval

pulse1(1:(rate*0.05),1) = 3; % sync pulse for standard stimuli
pulse1((rate*0.05):(rate*Dur),1) = zeros;
pulse2(1:(rate*0.05),1) = 1.5; % sync pulse for oddball stimuli
pulse2((rate*0.05):(rate*Dur),1) = zeros;

t = (1:(Dur*rate))/rate;
output1 = transpose(StdInt*sin(2*pi*StdFrq*t)); % standard stimulus
output2 = transpose(DevIntUp*sin(2*pi*DevFrqUp*t)); % ascending oddball
output3 = transpose(DevIntLow*sin(2*pi*DevFrqLow*t)); % descending oddball

% combine delays, trigger pulses and stimuli into arrays
standard = [cat(1,ISIdelay,pulse1) cat(1,ISIdelay,output1)];
updeviant = [cat(1,ISIdelay,pulse2) cat(1,ISIdelay,output2)];
lowdeviant = [cat(1,ISIdelay,pulse2) cat(1,ISIdelay,output3)];
updeviantlongISI = [cat(1,LongISIdelay,pulse2) cat(1,LongISIdelay,output2)];
lowdeviantlongISI = [cat(1,LongISIdelay,pulse2) cat(1,LongISIdelay,output3)];
IBI = [IBIdelay IBIdelay];
%----- Prepare data output -----%
dataout = [];
for i=1:100; dataout=cat(1,dataout,standard); end
for i=101; dataout=cat(1,dataout,IBI); end
for i=102:201; dataout=cat(1,dataout,updeviant); end
for i=202; dataout=cat(1,dataout,IBI); end
for i=203:302; dataout=cat(1,dataout,lowdeviant); end
for i=303; dataout=cat(1,dataout,IBI); end
for i=304:403; dataout=cat(1,dataout,updeviantlongISI); end
for i=404; dataout=cat(1,dataout,IBI); end
for i=405:504; dataout=cat(1,dataout,lowdeviantlongISI); end
dataout=cat(1,dataout,IBI);
end

```

```

function [ dataout ] = FrequencyMMN(rate,StdInt,DevIntUp,DevIntLow,MMNcode,ISI)
% This function generates the audio output array for running the
% frequency-varying oddball paradigm in Experiment II
%----- Set auditory stimuli parameters -----%
StdFrq = 10000; % standard stimulus frequency (Hertz)
Dur = 0.05; % stimuli duration (seconds)
DevFrqUp = 12000; % ascending oddball frequency (Hertz)
DevFrqLow = 8000; % descending oddball frequency (Hertz)
%----- Computations to prepare data output -----%
ISIdelay(1:(rate*ISI),1) = zeros; %set delay for ISI

pulse1(1:(rate*0.05),1) = 3; % sync pulse for standard stimuli
pulse1((rate*0.05):(rate*Dur),1) = zeros;
pulse2(1:(rate*0.05),1) = 1.5; % sync pulse for oddball stimuli
pulse2((rate*0.05):(rate*Dur),1) = zeros;

t = (1:(Dur*rate))/rate;
output1 = transpose(StdInt*sin(2*pi*StdFrq*t)); % standard stimulus
output2 = transpose(DevIntUp*sin(2*pi*DevFrqUp*t)); % ascending oddball
output3 = transpose(DevIntLow*sin(2*pi*DevFrqLow*t)); % descending oddball

% combine delays, trigger pulses and stimuli into arrays
standard = [cat(1,ISIdelay,pulse1) cat(1,ISIdelay,output1)];

```

```

updeviant = [cat(1,ISIdelay,pulse2) cat(1,ISIdelay,output2)];
lowdeviant = [cat(1,ISIdelay,pulse2) cat(1,ISIdelay,output3)];
DELAY = [ISIdelay ISIdelay];
%----- Prepare data output -----%
dataout = [];
for i=1:size(MMNcode,1)
    if MMNcode(i,1)==1; dataout=cat(1,dataout,standard); end
    if MMNcode(i,1)==2; dataout=cat(1,dataout,updeviant); end
    if MMNcode(i,1)==3; dataout=cat(1,dataout,lowdeviant); end
end
dataout=cat(1,dataout,DELAY);
end

```

```

function [ dataout ] = FrequencyDA(rate,~,DevIntUp,DevIntLow,MMNcode,ISI)
% This function generates the audio output array for running the
% frequency-varying deviant alone paradigm in Experiment II
%----- Set auditory stimuli parameters -----%
StdFrq = 10000; % standard stimuli frequency (Hertz)
Dur = 0.05; % stimuli duration (seconds)
StdInt= 0 ; % standard stimuli are silent
DevFrqUp = 12000; % ascending oddball frequency (Hertz)
DevFrqLow = 8000; % descending oddball frequency (Hertz)
%----- Computations to prepare data output -----%
ISIdelay(1:(rate*ISI),1) = zeros; %set delay for ISI

pulse1(1:(rate*0.05),1) = 3; % sync pulse for standard stimuli
pulse1((rate*0.05):(rate*Dur),1) = zeros;
pulse2(1:(rate*0.05),1) = 1.5; % sync pulse for oddball stimuli
pulse2((rate*0.05):(rate*Dur),1) = zeros;

t = (1:(Dur*rate))/rate;
output1 = transpose(StdInt*sin(2*pi*StdFrq*t)); % standard stimulus
output2 = transpose(DevIntUp*sin(2*pi*DevFrqUp*t)); % ascending oddball
output3 = transpose(DevIntLow*sin(2*pi*DevFrqLow*t)); % descending oddball

% combine delays, trigger pulses and stimuli into arrays
standard = [cat(1,ISIdelay,pulse1) cat(1,ISIdelay,output1)];
updeviant = [cat(1,ISIdelay,pulse2) cat(1,ISIdelay,output2)];
lowdeviant = [cat(1,ISIdelay,pulse2) cat(1,ISIdelay,output3)];
DELAY = [ISIdelay ISIdelay];
%----- Prepare data output -----%
dataout = [];
for i=1:size(MMNcode,1)
    if MMNcode(i,1)==1; dataout=cat(1,dataout,standard); end
    if MMNcode(i,1)==2; dataout=cat(1,dataout,updeviant); end
    if MMNcode(i,1)==3; dataout=cat(1,dataout,lowdeviant); end
end
dataout=cat(1,dataout,DELAY);
end

```

```

function [ dataout ] = FrequencyMSC(rate,fgain0,fgain1,fgain2,fgain3,...
    fgain4,fgain5,fgain6,fgain7,fgain8,fgain9,MSCcode,ISI)
% This function generates the audio output array for running the
% frequency-varying many standards paradigm in Experiment II
%----- Set auditory stimuli parameters -----%
Dur = 0.05; % stimuli duration (seconds)

```

```

std0 = 8e3;           % descending oddball frequency (Hertz)
std1 = 8.5e3;
std2 = 9e3;
std3 = 9.5e3;
std4 = 10e3;        % standard stimuli frequency (Hertz)
std5 = 10.5e3;
std6 = 11e3;
std7 = 11.5e3;
std8 = 12e3;        % ascending oddball frequency (Hertz)
std9 = 12.5e3;

%----- Computations to prepare data output -----%
ISIdelay(1:(rate*ISI),1) = zeros; % ISI

pulse(1:(rate*0.05),1) = 1.5; % sync pulse
pulse((rate*0.05):(rate*Dur),1) = zeros;

t = (1:(Dur*rate))/rate;
output0 = transpose(fgain0*sin(2*pi*std0*t)); % std0 stimulus
output1 = transpose(fgain1*sin(2*pi*std1*t)); % std1 stimulus
output2 = transpose(fgain2*sin(2*pi*std2*t)); % std2 stimulus
output3 = transpose(fgain3*sin(2*pi*std3*t)); % std3 stimulus
output4 = transpose(fgain4*sin(2*pi*std4*t)); % std4 stimulus
output5 = transpose(fgain5*sin(2*pi*std5*t)); % std5 stimulus
output6 = transpose(fgain6*sin(2*pi*std6*t)); % std6 stimulus
output7 = transpose(fgain7*sin(2*pi*std7*t)); % std7 stimulus
output8 = transpose(fgain8*sin(2*pi*std8*t)); % std8 stimulus
output9 = transpose(fgain9*sin(2*pi*std9*t)); % std9 stimulus

% combine delays, trigger pulses and stimuli into arrays
Std0 = [cat(1,ISIdelay,pulse) cat(1,ISIdelay,output0)];
Std1 = [cat(1,ISIdelay,pulse) cat(1,ISIdelay,output1)];
Std2 = [cat(1,ISIdelay,pulse) cat(1,ISIdelay,output2)];
Std3 = [cat(1,ISIdelay,pulse) cat(1,ISIdelay,output3)];
Std4 = [cat(1,ISIdelay,pulse) cat(1,ISIdelay,output4)];
Std5 = [cat(1,ISIdelay,pulse) cat(1,ISIdelay,output5)];
Std6 = [cat(1,ISIdelay,pulse) cat(1,ISIdelay,output6)];
Std7 = [cat(1,ISIdelay,pulse) cat(1,ISIdelay,output7)];
Std8 = [cat(1,ISIdelay,pulse) cat(1,ISIdelay,output8)];
Std9 = [cat(1,ISIdelay,pulse) cat(1,ISIdelay,output9)];
DELAY = [ISIdelay ISIdelay];

%----- Prepare data output -----%
dataout = [];
for i=1:size(MSCcode,1)
    if MSCcode(i,1)==0; dataout=cat(1,dataout,Std0); end
    if MSCcode(i,1)==1; dataout=cat(1,dataout,Std1); end
    if MSCcode(i,1)==2; dataout=cat(1,dataout,Std2); end
    if MSCcode(i,1)==3; dataout=cat(1,dataout,Std3); end
    if MSCcode(i,1)==4; dataout=cat(1,dataout,Std4); end
    if MSCcode(i,1)==5; dataout=cat(1,dataout,Std5); end
    if MSCcode(i,1)==6; dataout=cat(1,dataout,Std6); end
    if MSCcode(i,1)==7; dataout=cat(1,dataout,Std7); end
    if MSCcode(i,1)==8; dataout=cat(1,dataout,Std8); end
    if MSCcode(i,1)==9; dataout=cat(1,dataout,Std9); end
end
dataout=cat(1,dataout,DELAY);
end

```



```

% This script runs the intensity-varying auditory paradigms for
% Experiment II
clear all
daq.reset;

%Check background noise level
SoundTest

%Load calibrated gain values after running SpeakerCalibration.m
load('SpeakerCalibration.mat');
%Load stimulus codes
load('MMNcode.mat')
load('MSCcode.mat')
ISI = 0.45; %inter stimulus interval in seconds

%Initialize NI device
device = daq.getDevices;
vendor=daq.getVendors;
s = daq.createSession('ni');
s1 = daq.createSession('ni');
rate = 30e3;
s.Rate = rate;
s.addAnalogOutputChannel('Dev1',0:1, 'Voltage');
s1.addDigitalChannel('Dev1','Port1/Line0', 'OutputOnly');
outputSingleScan(s1,0);

%Intensity consecutive repetition control (filename_0.continuous)
intSPT = IntensitySPT(rate,StdGain,UpIntDevGain,LowIntDevGain,ISI);
queueOutputData(s, intSPT);
prepare(s);
%Instruct to setup open-ephys
fprintf(1,'\nSet up Ephys and press any key to continue\n');pause
fprintf(1,'\nIntensity Stimulus Pulse Train running...');
outputSingleScan(s1,1);
startForeground(s);
stop(s)
outputSingleScan(s1,0);
fprintf(1,' complete!\n');
clear intSPT

%Intensity oddball paradigm (filename_1.continuous)
intMMN = IntensityMMN(rate,StdGain,UpIntDevGain,LowIntDevGain,MMNcode,ISI);
queueOutputData(s, intMMN);
prepare(s);
fprintf(1,'\nIntensity Oddball MMN running...');
outputSingleScan(s1,1);
startForeground(s);
stop(s)
outputSingleScan(s1,0);
fprintf(1,' complete!\n');
clear intMMN

%Intensity deviant alone control (filename_2.continuous)
intDA = IntensityDA(rate,StdGain,UpIntDevGain,LowIntDevGain,MMNcode,ISI);
queueOutputData(s, intDA);

```

```

prepare(s);
fprintf(1,'\nIntensity Deviant Alone running...');
outputSingleScan(s1,1);
startForeground(s);
stop(s)
outputSingleScan(s1,0);
fprintf(1,' complete!\n');
clear intDA

%Intensity many standards control (filename_3.continuous)
intMSC = IntensityMSC( rate,LowIntDevGain,igain1,igain2,igain3,StdGain,...
    igain5,igain6,igain7,UpIntDevGain,igain9,MSCcode,ISI );
queueOutputData(s, intMSC);
prepare(s);
fprintf(1,'\nIntensity Many Standards running...');
outputSingleScan(s1,1);
startForeground(s);
stop(s)
outputSingleScan(s1,0);
fprintf(1,' complete!\n');
clear intMSC

%Protocol complete message
fprintf(1,'\nDONE!\n');
msgbox('Intensity Protocol Complete. Press OK','','warn');

```

```

function [ dataout ] = IntensitySPT(rate,StdInt,DevIntUp,DevIntLow,ISI)
% This function generates the audio output array for running the
% intensity-varying consecutive repetition paradigm in Experiment II
%----- Set auditory stimuli parameters -----%
Frq = 10000;          % stimuli frequency (Hertz)
Dur = 0.05;          % stimuli duration (seconds)
%----- Computations to prepare data output -----%
ISIdelay(1:(rate*ISI),1) = zeros; % ISI
LongISIdelay(1:(rate*2),1) = zeros; % long ISI
IBIdelay(1:(rate*5),1) = zeros; % 5 second inter-block interval

pulse1(1:(rate*0.05),1) = 3; % sync pulse for standard stimuli
pulse1((rate*0.1):(rate*Dur),1) = zeros;
pulse2(1:(rate*0.05),1) = 1.5; % sync pulse for oddball stimuli
pulse2((rate*0.1):(rate*Dur),1) = zeros;

t = (1:(Dur*rate))/rate;
output1 = transpose(StdInt*sin(2*pi*Frq*t)); % standard stimulus
output2 = transpose(DevIntUp*sin(2*pi*Frq*t)); % louder oddball
output3 = transpose(DevIntLow*sin(2*pi*Frq*t)); % quieter oddball

% combine delays, trigger pulses and stimuli into arrays
standard = [cat(1,ISIdelay,pulse1) cat(1,ISIdelay,output1)];
updeviant = [cat(1,ISIdelay,pulse2) cat(1,ISIdelay,output2)];
lowdeviant = [cat(1,ISIdelay,pulse2) cat(1,ISIdelay,output3)];
updeviantlongISI = [cat(1,LongISIdelay,pulse2) cat(1,LongISIdelay,output2)];
lowdeviantlongISI = [cat(1,LongISIdelay,pulse2) cat(1,LongISIdelay,output3)];
IBI = [IBIdelay IBIdelay];
%----- Prepare data output -----%
dataout = [];

```

```

for i=1:100; dataout=cat(1,dataout,standard); end
for i=101; dataout=cat(1,dataout,IBI); end
for i=102:201; dataout=cat(1,dataout,updeviant); end
for i=202; dataout=cat(1,dataout,IBI); end
for i=203:302; dataout=cat(1,dataout,lowdeviant); end
for i=303; dataout=cat(1,dataout,IBI); end
for i=304:403; dataout=cat(1,dataout,updeviantlongISI); end
for i=404; dataout=cat(1,dataout,IBI); end
for i=405:504; dataout=cat(1,dataout,lowdeviantlongISI); end
dataout = cat(1,dataout,IBI);
end

```

```

function [ dataout ] = IntensityMMN(rate,StdInt,DevIntUp,DevIntLow,MMNcode,ISI)
% This function generates the audio output array for running the
% intensity-varying oddball paradigm in Experiment II
%----- Set auditory stimuli parameters -----%
Frq = 10000;          % stimuli frequency (Hertz)
Dur = 0.05;          % stimuli duration (seconds)
%----- Computations to prepare data output -----%
ISIdelay(1:(rate*ISI),1) = zeros; % ISI

pulse1(1:(rate*0.05),1) = 3; % sync pulse for standard stimuli
pulse1((rate*0.1):(rate*Dur),1) = zeros;
pulse2(1:(rate*0.05),1) = 1.5; % sync pulse for oddball stimuli
pulse2((rate*0.1):(rate*Dur),1) = zeros;

t = (1:(Dur*rate))/rate;
output1 = transpose(StdInt*sin(2*pi*Frq*t)); % standard stimulus
output2 = transpose(DevIntUp*sin(2*pi*Frq*t)); % louder oddball
output3 = transpose(DevIntLow*sin(2*pi*Frq*t)); % quieter oddball

% combine delays, trigger pulses and stimuli into arrays
standard = [cat(1,ISIdelay,pulse1) cat(1,ISIdelay,output1)];
updeviant = [cat(1,ISIdelay,pulse2) cat(1,ISIdelay,output2)];
lowdeviant = [cat(1,ISIdelay,pulse2) cat(1,ISIdelay,output3)];
DELAY = [ISIdelay ISIdelay];
%----- Prepare data output -----%
dataout = [];
for i=1:size(MMNcode,1)
    if MMNcode(i,1)==1; dataout=cat(1,dataout,standard); end
    if MMNcode(i,1)==2; dataout=cat(1,dataout,updeviant); end
    if MMNcode(i,1)==3; dataout=cat(1,dataout,lowdeviant); end
end
dataout=cat(1,dataout,DELAY);
end

```

```

function [ dataout ] = IntensityDA(rate,~,DevIntUp,DevIntLow,MMNcode,ISI)
% This function generates the audio output array for running the
% intensity-varying deviant alone paradigm in Experiment II
%----- Set auditory stimuli parameters -----%
Frq = 10000;          % stimuli frequency (Hertz)
StdInt = 0;          % standard stimuli are silent
Dur = 0.05;          % stimuli duration (seconds)
%----- Computations to prepare data output -----%
ISIdelay(1:(rate*ISI),1) = zeros; % ISI

```

```

pulse1(1:(rate*0.05),1) = 3; % sync pulse for standard stimuli
pulse1((rate*0.1):(rate*Dur),1) = zeros;
pulse2(1:(rate*0.05),1) = 1.5; % sync pulse for oddball stimuli
pulse2((rate*0.1):(rate*Dur),1) = zeros;

t = (1:(Dur*rate))/rate;
output1 = transpose(StdInt*sin(2*pi*Frq*t)); % standard stimulus
output2 = transpose(DevIntUp*sin(2*pi*Frq*t)); % louder oddball
output3 = transpose(DevIntLow*sin(2*pi*Frq*t)); % quieter oddball

% combine delays, trigger pulses and stimuli into arrays
standard = [cat(1,ISIdelay,pulse1) cat(1,ISIdelay,output1)];
updeviant = [cat(1,ISIdelay,pulse2) cat(1,ISIdelay,output2)];
lowdeviant = [cat(1,ISIdelay,pulse2) cat(1,ISIdelay,output3)];
DELAY = [ISIdelay ISIdelay];
%----- Prepare data output -----%
dataout = [];
for i=1:size(MMNcode,1)
    if MMNcode(i,1)==1; dataout=cat(1,dataout,standard); end
    if MMNcode(i,1)==2; dataout=cat(1,dataout,updeviant); end
    if MMNcode(i,1)==3; dataout=cat(1,dataout,lowdeviant); end
end
dataout=cat(1,dataout,DELAY);
end

function [ dataout ] = IntensityMSC(rate,igain0,igain1,igain2,igain3,...
    igain4,igain5,igain6,igain7,igain8,igain9,MSCcode,ISI)
% This function generates the audio output for running the
% intensity-varying many standards paradigm in Experiment II
%----- Set auditory stimuli parameters -----%
Frq = 10000; % stimuli frequency (Hertz)
Dur = 0.05; % stimuli duration (seconds)
%----- Computations to prepare data output -----%
ISIdelay(1:(rate*ISI),1) = zeros; % ISI

pulse(1:(rate*0.05),1) = 1.5; % sync pulse
pulse((rate*0.05):(rate*Dur),1) = zeros;

t = (1:(Dur*rate))/rate; % generate auditory stimuli
output0 = transpose(igain0*sin(2*pi*Frq*t));
output1 = transpose(igain1*sin(2*pi*Frq*t));
output2 = transpose(igain2*sin(2*pi*Frq*t)); % quieter oddball
output3 = transpose(igain3*sin(2*pi*Frq*t));
output4 = transpose(igain4*sin(2*pi*Frq*t)); % standard
output5 = transpose(igain5*sin(2*pi*Frq*t));
output6 = transpose(igain6*sin(2*pi*Frq*t)); % louder oddball
output7 = transpose(igain7*sin(2*pi*Frq*t));
output8 = transpose(igain8*sin(2*pi*Frq*t));
output9 = transpose(igain9*sin(2*pi*Frq*t));

% combine delays, trigger pulses and stimuli into arrays
Std0 = [cat(1,ISIdelay,pulse) cat(1,ISIdelay,output0)];
Std1 = [cat(1,ISIdelay,pulse) cat(1,ISIdelay,output1)];
Std2 = [cat(1,ISIdelay,pulse) cat(1,ISIdelay,output2)];
Std3 = [cat(1,ISIdelay,pulse) cat(1,ISIdelay,output3)];
Std4 = [cat(1,ISIdelay,pulse) cat(1,ISIdelay,output4)];

```

```

Std5 = [cat(1,ISIdelay,pulse) cat(1,ISIdelay,output5)];
Std6 = [cat(1,ISIdelay,pulse) cat(1,ISIdelay,output6)];
Std7 = [cat(1,ISIdelay,pulse) cat(1,ISIdelay,output7)];
Std8 = [cat(1,ISIdelay,pulse) cat(1,ISIdelay,output8)];
Std9 = [cat(1,ISIdelay,pulse) cat(1,ISIdelay,output9)];
DELAY = [ISIdelay ISIdelay];
%----- Prepare data output ------%
dataout = [];
for i=1:size(MSCcode,1)
    if MSCcode(i,1)==0; dataout=cat(1,dataout,Std0); end
    if MSCcode(i,1)==1; dataout=cat(1,dataout,Std1); end
    if MSCcode(i,1)==2; dataout=cat(1,dataout,Std2); end
    if MSCcode(i,1)==3; dataout=cat(1,dataout,Std3); end
    if MSCcode(i,1)==4; dataout=cat(1,dataout,Std4); end
    if MSCcode(i,1)==5; dataout=cat(1,dataout,Std5); end
    if MSCcode(i,1)==6; dataout=cat(1,dataout,Std6); end
    if MSCcode(i,1)==7; dataout=cat(1,dataout,Std7); end
    if MSCcode(i,1)==8; dataout=cat(1,dataout,Std8); end
    if MSCcode(i,1)==9; dataout=cat(1,dataout,Std9); end
end
dataout=cat(1,dataout,DELAY);
end

% This script runs the duration-varying auditory paradigms with constant
% inter stimulus interval for Experiment II
clear all
daq.reset;

%Check background noise level
SoundTest

%Load calibrated gain values after running SpeakerCalibration.m
load('SpeakerCalibration.mat');
%Load stimulus codes
load('MMNcode.mat')
load('MSCcode.mat')
ISI = 0.45; %inter stimulus interval in seconds

%Initialize NI device
device = daq.getDevices;
vendor=daq.getVendors;
s = daq.createSession('ni');
s1 = daq.createSession('ni');
rate = 30e3;
s.Rate = rate;
s.addAnalogOutputChannel('Dev1',0:1, 'Voltage');
s1.addDigitalChannel('Dev1','Port1/Line0', 'OutputOnly');
outputSingleScan(s1,0);

% Duration consecutive repetition control (0.continuous)
durSPT = DurationSPT_ISI(rate,StdGain,ISI);
queueOutputData(s, durSPT);
prepare(s);
% Instruction to set up open-ephys
fprintf(1,'\nSet up Ephys and press any key to continue\n');pause
fprintf(1,'\nDuration Stimulus Pulse Train running...');

```

```

outputSingleScan(s1,1);
startForeground(s);
stop(s)
outputSingleScan(s1,0);
fprintf(1,' complete!\n');
clear durSPT

% Duration oddball paradigm (filename_1.continuous)
durMMN = DurationMMN_ISI(rate,StdGain,MMNcode,ISI);
queueOutputData(s, durMMN);
prepare(s);
fprintf(1,'\nDuration Oddball MMN running...');
outputSingleScan(s1,1);
startForeground(s);
stop(s)
outputSingleScan(s1,0);
fprintf(1,' complete!\n');
clear durMMN

% Duration deviant alone control (filename_2.continuous)
durDA = DurationDA_ISI(rate,StdGain,MMNcode,ISI);
queueOutputData(s, durDA);
prepare(s);
fprintf(1,'\nDuration Deviant Alone running...');
outputSingleScan(s1,1);
startForeground(s);
stop(s)
outputSingleScan(s1,0);
fprintf(1,' complete!\n');
clear durDA

% Duration many standards control (filename_3.continuous)
durMSC = DurationMSC_ISI(rate,StdGain,MSCcode,ISI);
queueOutputData(s, durMSC);
prepare(s);
fprintf(1,'\nDuration Many Standards running...');
outputSingleScan(s1,1);
startForeground(s);
stop(s)
outputSingleScan(s1,0);
fprintf(1,' complete!\n');
clear durMSC

% Protocol complete message
fprintf(1,'\nDONE!\n');
msgbox('Duration Protocol Complete. Press OK','','warn');

```

```

function [ dataout ] = DurationSPT_ISI(rate,StdInt,ISI)
% This function generates the audio output array for running the
% duration-varying consecutive repetition paradigm with constant inter
% stimulus interval in Experiment II
%----- Set auditory stimuli parameters -----%
Frq = 10000;      % stimuli frequency (Hertz)
StdDur = 0.1;    % standard stimuli (seconds)
DevDurUp = 0.15; % increased oddball duration (seconds)
DevDurLow = 0.05; % decreased oddball duration (seconds)

```

```

%----- Computations to prepare data output -----%
ISIdelay(1:(rate*ISI),1) = zeros; % ISI
LongISIdelay(1:(rate*2),1) = zeros; % long ISI
IBIdelay(1:(rate*5),1) = zeros; %5 second inter-block interval

pulse1(1:(rate*0.05),1) = 3; % sync pulse for standard stimuli
pulse1((rate*0.05):(rate*StdDur),1) = zeros;
pulse2(1:(rate*0.05),1) = 1.5; % sync pulse for increased oddball
pulse2((rate*0.05):(rate*DevDurUp),1) = zeros;
pulse3(1:(rate*0.05),1) = 1.5; % sync pulse for decreased oddball
pulse3((rate*0.05):(rate*DevDurLow),1) = zeros;

t1 = (1:(StdDur*rate))/rate; % standard stimulus
output1 = transpose(StdInt*sin(2*pi*Frq*t1));
t2 = (1:(DevDurUp*rate))/rate; % increased oddball
output2 = transpose(StdInt*sin(2*pi*Frq*t2));
t3 = (1:(DevDurLow*rate))/rate; % decreased oddball
output3 = transpose(StdInt*sin(2*pi*Frq*t3));

% combine delays, trigger pulses and stimuli into arrays
standard = [cat(1,ISIdelay,pulse1) cat(1,ISIdelay,output1)];
updeviant = [cat(1,ISIdelay,pulse2) cat(1,ISIdelay,output2)];
lowdeviant = [cat(1,ISIdelay,pulse3) cat(1,ISIdelay,output3)];
updeviantlongISI = [cat(1,LongISIdelay,pulse2) cat(1,LongISIdelay,output2)];
lowdeviantlongISI = [cat(1,LongISIdelay,pulse3) cat(1,LongISIdelay,output3)];
IBI = [IBIdelay IBIdelay];
%----- Prepare data output -----%
dataout = [];
for i=1:100; dataout=cat(1,dataout,standard); end
for i=101; dataout=cat(1,dataout,IBI); end
for i=102:201; dataout=cat(1,dataout,updeviant); end
for i=202; dataout=cat(1,dataout,IBI); end
for i=203:302; dataout=cat(1,dataout,lowdeviant); end
for i=303; dataout=cat(1,dataout,IBI); end
for i=304:403; dataout=cat(1,dataout,updeviantlongISI); end
for i=404; dataout=cat(1,dataout,IBI); end
for i=405:504; dataout=cat(1,dataout,lowdeviantlongISI); end
dataout = cat(1,dataout,IBI);
end

function [ dataout ] = DurationMMN_ISI(rate,StdInt,MMNcode,ISI)
% This function generates the audio output array for running the
% duration-varying oddball paradigm with constant inter stimulus interval
% in Experiment II
%----- Set auditory stimuli parameters -----%
Frq = 10000; % stimuli frequency (Hertz)
StdDur = 0.1; % standard stimuli duration (seconds)
DevDurUp = 0.15; % increased oddball duration (seconds)
DevDurLow = 0.05; % decreased oddball duration (seconds)
%----- Computations to prepare data output -----%
ISIdelay(1:(rate*ISI),1) = zeros; % ISI

pulse1(1:(rate*0.05),1) = 3; % sync pulse for standard
pulse1((rate*0.05):(rate*StdDur),1) = zeros;
pulse2(1:(rate*0.05),1) = 1.5; % sync pulse for increased oddball
pulse2((rate*0.05):(rate*DevDurUp),1) = zeros;

```

```

pulse3(1:(rate*0.05),1) = 1.5; % sync pulse for decreased oddball
pulse3((rate*0.05):(rate*DevDurLow),1) = zeros;

t1 = (1:(StdDur*rate))/rate; % standard stimulus
output1 = transpose(StdInt*sin(2*pi*Frq*t1));
t2 = (1:(DevDurUp*rate))/rate; % increased oddball
output2 = transpose(StdInt*sin(2*pi*Frq*t2));
t3 = (1:(DevDurLow*rate))/rate; % decreased oddball
output3 = transpose(StdInt*sin(2*pi*Frq*t3));

% combine delays, trigger pulses and stimuli into arrays
standard = [cat(1,ISIdelay,pulse1) cat(1,ISIdelay,output1)];
updeviant = [cat(1,ISIdelay,pulse2) cat(1,ISIdelay,output2)];
lowdeviant = [cat(1,ISIdelay,pulse3) cat(1,ISIdelay,output3)];
DELAY = [ISIdelay ISIdelay];
%----- Prepare data output -----%
dataout = [];
for i=1:size(MMNcode,1)
    if MMNcode(i,1)==1; dataout=cat(1,dataout,standard); end
    if MMNcode(i,1)==2; dataout=cat(1,dataout,updeviant); end
    if MMNcode(i,1)==3; dataout=cat(1,dataout,lowdeviant); end
end
dataout=cat(1,dataout,DELAY);
end

```

```

function [ dataout ] = DurationDA_ISI(rate,DurInt,MMNcode,ISI)
% This function generates the audio output array for running the
% duration-varying deviant alone paradigm with constant inter stimulus
% interval in Experiment II
%----- Set auditory stimuli parameters -----%
Frq = 10000; % stimuli frequency (Hertz)
StdDur = 0.1; % standard stimulus duration (seconds)
StdInt = 0; % silent standards
DevDurUp = 0.15; % increased oddball duration (seconds)
DevDurLow = 0.05; % decreased oddball duration (seconds)
%----- Computations to prepare data output -----%
ISIdelay(1:(rate*ISI),1) = zeros; % ISI

pulse1(1:(rate*0.05),1) = 3; % sync pulse for standard
pulse1((rate*0.05):(rate*StdDur),1) = zeros;
pulse2(1:(rate*0.05),1) = 1.5; % sync pulse for increased oddball
pulse2((rate*0.05):(rate*DevDurUp),1) = zeros;
pulse3(1:(rate*0.05),1) = 1.5; % sync pulse for decreased oddball
pulse3((rate*0.05):(rate*DevDurLow),1) = zeros;

t1 = (1:(StdDur*rate))/rate; % standard stimulus
output1 = transpose(StdInt*sin(2*pi*Frq*t1));
t2 = (1:(DevDurUp*rate))/rate; % increasing oddball
output2 = transpose(DurInt*sin(2*pi*Frq*t2));
t3 = (1:(DevDurLow*rate))/rate; % decreased oddball
output3 = transpose(DurInt*sin(2*pi*Frq*t3));

% combine delays, trigger pulses and stimuli into arrays
standard = [cat(1,ISIdelay,pulse1) cat(1,ISIdelay,output1)];
updeviant = [cat(1,ISIdelay,pulse2) cat(1,ISIdelay,output2)];
lowdeviant = [cat(1,ISIdelay,pulse3) cat(1,ISIdelay,output3)];

```



```

DELAY = [ISIdelay ISIdelay];
%----- Prepare data output -----%
dataout = [];
for i=1:size(MMNcode,1)
    if MMNcode(i,1)==1; dataout=cat(1,dataout,standard); end
    if MMNcode(i,1)==2; dataout=cat(1,dataout,updeviant); end
    if MMNcode(i,1)==3; dataout=cat(1,dataout,lowdeviant); end
end
dataout=cat(1,dataout,DELAY);
end

```

```

function [ dataout ] = DurationMSC_ISI(rate,StdInt,MSCcode,ISI)
% This function generates the audio output array for running the
% duration-varying many standards paradigm with constant inter stimulus
% interval in Experiment II
%----- Set auditory stimuli parameters -----%
Frq = 10000;      % stimuli frequency (Hertz)
std0 = 0.05;     % decreased oddball
std1 = 0.075;
std2 = 0.1;      % standard stimulus
std3 = 0.125;
std4 = 0.150;    % increased oddball
std5 = 0.175;
std6 = 0.2;
std7 = 0.225;
std8 = 0.25;
std9 = 0.275;
%----- Computations to prepare data output -----%
ISIdelay(1:(rate*ISI),1) = zeros; % ISI
finDelay(1:(rate*1),1) = zeros; %delay at end of paradigm

pulse0(1:(rate*0.05),1) = 1.5; % sync pulse for std0
pulse0((rate*0.05):(rate*std0),1) = zeros;
pulse1(1:(rate*0.05),1) = 1.5; % sync pulse for std1
pulse1((rate*0.05):(rate*std1),1) = zeros;
pulse2(1:(rate*0.05),1) = 1.5; % sync pulse for std2
pulse2((rate*0.05):(rate*std2),1) = zeros;
pulse3(1:(rate*0.05),1) = 1.5; % sync pulse for std3
pulse3((rate*0.05):(rate*std3),1) = zeros;
pulse4(1:(rate*0.05),1) = 1.5; % sync pulse for std4
pulse4((rate*0.05):(rate*std4),1) = zeros;
pulse5(1:(rate*0.05),1) = 1.5; % sync pulse for std5
pulse5((rate*0.05):(rate*std5),1) = zeros;
pulse6(1:(rate*0.05),1) = 1.5; % sync pulse for std6
pulse6((rate*0.05):(rate*std6),1) = zeros;
pulse7(1:(rate*0.05),1) = 1.5; % sync pulse for std7
pulse7((rate*0.05):(rate*std7),1) = zeros;
pulse8(1:(rate*0.05),1) = 1.5; % sync pulse for std8
pulse8((rate*0.05):(rate*std8),1) = zeros;
pulse9(1:(rate*0.05),1) = 1.5; % sync pulse for std9
pulse9((rate*0.05):(round(rate*std9)),1) = zeros;

t0 = (1:(std0*rate))/rate; % std0 stimulus
output0 = transpose(StdInt*sin(2*pi*Frq*t0));
t1 = (1:(std1*rate))/rate; % std1 stimulus
output1 = transpose(StdInt*sin(2*pi*Frq*t1));

```

```

t2 = (1:(std2*rate))/rate; % std2 stimulus
output2 = transpose(StdInt*sin(2*pi*Frq*t2));
t3 = (1:(std3*rate))/rate; % std3 stimulus
output3 = transpose(StdInt*sin(2*pi*Frq*t3));
t4 = (1:(std4*rate))/rate; % std4 stimulus
output4 = transpose(StdInt*sin(2*pi*Frq*t4));
t5 = (1:(std5*rate))/rate; % std5 stimulus
output5 = transpose(StdInt*sin(2*pi*Frq*t5));
t6 = (1:(std6*rate))/rate; % std6 stimulus
output6 = transpose(StdInt*sin(2*pi*Frq*t6));
t7 = (1:(std7*rate))/rate; % std7 stimulus
output7 = transpose(StdInt*sin(2*pi*Frq*t7));
t8 = (1:(std8*rate))/rate; % std8 stimulus
output8 = transpose(StdInt*sin(2*pi*Frq*t8));
t9 = (1:(std9*rate))/rate; % std9 stimulus
output9 = transpose(StdInt*sin(2*pi*Frq*t9));

% combine delays, trigger pulses and stimuli into arrays
Std0 = [cat(1,ISIdelay,pulse0) cat(1,ISIdelay,output0)];
Std1 = [cat(1,ISIdelay,pulse1) cat(1,ISIdelay,output1)];
Std2 = [cat(1,ISIdelay,pulse2) cat(1,ISIdelay,output2)];
Std3 = [cat(1,ISIdelay,pulse3) cat(1,ISIdelay,output3)];
Std4 = [cat(1,ISIdelay,pulse4) cat(1,ISIdelay,output4)];
Std5 = [cat(1,ISIdelay,pulse5) cat(1,ISIdelay,output5)];
Std6 = [cat(1,ISIdelay,pulse6) cat(1,ISIdelay,output6)];
Std7 = [cat(1,ISIdelay,pulse7) cat(1,ISIdelay,output7)];
Std8 = [cat(1,ISIdelay,pulse8) cat(1,ISIdelay,output8)];
Std9 = [cat(1,ISIdelay,pulse9) cat(1,ISIdelay,output9)];
DELAY = [finDelay finDelay];
%----- Prepare data output -----%
dataout = [];
for i=1:size(MSCcode,1)
    if MSCcode(i,1)==0; dataout=cat(1,dataout,Std0); end
    if MSCcode(i,1)==1; dataout=cat(1,dataout,Std1); end
    if MSCcode(i,1)==2; dataout=cat(1,dataout,Std2); end
    if MSCcode(i,1)==3; dataout=cat(1,dataout,Std3); end
    if MSCcode(i,1)==4; dataout=cat(1,dataout,Std4); end
    if MSCcode(i,1)==5; dataout=cat(1,dataout,Std5); end
    if MSCcode(i,1)==6; dataout=cat(1,dataout,Std6); end
    if MSCcode(i,1)==7; dataout=cat(1,dataout,Std7); end
    if MSCcode(i,1)==8; dataout=cat(1,dataout,Std8); end
    if MSCcode(i,1)==9; dataout=cat(1,dataout,Std9); end
end
dataout=cat(1,dataout,DELAY);
end

% Dual speaker calibration for Experiment II
s = daq.createSession('ni');
rate = 30e3;
s.Rate = rate;
s.DurationInSeconds = 1;

ai=addAnalogInputChannel(s,'Dev1','ai0','Voltage');
ai.TerminalConfig = 'SingleEnded';
ao=addAnalogOutputChannel(s,'Dev1','ao1','Voltage');

```

```

[StdGain1]=SpeakerCal(s,10e3,80,rate,'standard');
[UpIntDevGain1]=SpeakerCal(s,10e3,90,rate,'upper intensity deviant');
[LowIntDevGain1]=SpeakerCal(s,10e3,70,rate,'lower intensity deviant');
[UpFrqDevGain1]=SpeakerCal(s,12e3,80,rate,'upper frequency deviant');
[LowFrqDevGain1]=SpeakerCal(s,8e3,80,rate,'lower frequency deviant');

[fgain11]=SpeakerCal(s,8.5e3,80,rate,'fgain1');
[fgain21]=SpeakerCal(s,9e3,80,rate,'fgain2');
[fgain31]=SpeakerCal(s,9.5e3,80,rate,'fgain3');
[fgain51]=SpeakerCal(s,10.5e3,80,rate,'fgain5');
[fgain61]=SpeakerCal(s,11e3,80,rate,'fgain6');
[fgain71]=SpeakerCal(s,11.5e3,80,rate,'fgain7');
[fgain91]=SpeakerCal(s,12.5e3,80,rate,'fgain9');

[igain11]=SpeakerCal(s,10e3,72.5,rate,'igain1');
[igain21]=SpeakerCal(s,10e3,75,rate,'igain2');
[igain31]=SpeakerCal(s,10e3,77.5,rate,'igain3');
[igain51]=SpeakerCal(s,10e3,82.5,rate,'igain5');
[igain61]=SpeakerCal(s,10e3,85,rate,'igain6');
[igain71]=SpeakerCal(s,10e3,87.5,rate,'igain7');
[igain91]=SpeakerCal(s,10e3,92.5,rate,'igain9');

%Instruct to setup open-ephys
fprintf(1,'\nPlease reverse sound meter direction and press any key\n');pause

[StdGain2]=SpeakerCal(s,10e3,80,rate,'standard');
[UpIntDevGain2]=SpeakerCal(s,10e3,90,rate,'upper intensity deviant');
[LowIntDevGain2]=SpeakerCal(s,10e3,70,rate,'lower intensity deviant');
[UpFrqDevGain2]=SpeakerCal(s,12e3,80,rate,'upper frequency deviant');
[LowFrqDevGain2]=SpeakerCal(s,8e3,80,rate,'lower frequency deviant');

[fgain12]=SpeakerCal(s,8.5e3,80,rate,'fgain1');
[fgain22]=SpeakerCal(s,9e3,80,rate,'fgain2');
[fgain32]=SpeakerCal(s,9.5e3,80,rate,'fgain3');
[fgain52]=SpeakerCal(s,10.5e3,80,rate,'fgain5');
[fgain62]=SpeakerCal(s,11e3,80,rate,'fgain6');
[fgain72]=SpeakerCal(s,11.5e3,80,rate,'fgain7');
[fgain92]=SpeakerCal(s,12.5e3,80,rate,'fgain9');

[igain12]=SpeakerCal(s,10e3,72.5,rate,'igain1');
[igain22]=SpeakerCal(s,10e3,75,rate,'igain2');
[igain32]=SpeakerCal(s,10e3,77.5,rate,'igain3');
[igain52]=SpeakerCal(s,10e3,82.5,rate,'igain5');
[igain62]=SpeakerCal(s,10e3,85,rate,'igain6');
[igain72]=SpeakerCal(s,10e3,87.5,rate,'igain7');
[igain92]=SpeakerCal(s,10e3,92.5,rate,'igain9');

StdGain=(StdGain1+StdGain2)/2;
UpIntDevGain=(UpIntDevGain1+UpIntDevGain2)/2;
LowIntDevGain=(LowIntDevGain1+LowIntDevGain2)/2;
UpFrqDevGain=(UpFrqDevGain1+UpFrqDevGain2)/2;
LowFrqDevGain=(LowFrqDevGain1+LowFrqDevGain2)/2;

fgain1=(fgain11+fgain12)/2;

```

```

fgain2=(fgain21+fgain22)/2;
fgain3=(fgain31+fgain32)/2;
fgain5=(fgain51+fgain52)/2;
fgain6=(fgain61+fgain62)/2;
fgain7=(fgain71+fgain72)/2;
fgain9=(fgain91+fgain92)/2;

igain1=(igain11+igain12)/2;
igain2=(igain21+igain22)/2;
igain3=(igain31+igain32)/2;
igain5=(igain51+igain52)/2;
igain6=(igain61+igain62)/2;
igain7=(igain71+igain72)/2;
igain9=(igain91+igain92)/2;

save('SpeakerCalibration','StdGain','UpIntDevGain','LowIntDevGain',...
     'UpFrqDevGain','LowFrqDevGain','fgain1','fgain2','fgain3','fgain5',...
     'fgain6','fgain7','fgain9','igain1','igain2','igain3','igain5',...
     'igain6','igain7','igain9');
delete(s)
clear all

```

3. Experiment III

```

% This script runs the Experiment III auditory stimulation sequence. For
% use with apparatus described for recording chamber B
daq.reset;
subjectNumber = 'Exp21';% inset subject ID
diary(subjectNumber)
fprintf(1,'Subject #s\n',subjectNumber);

StdID      =      13;% insert index from running CF analyzer

% Speaker calibration information
CalFile=importdata('exp21.dbspls');
freqs=importdata('Calibration_linear_2-32 kHz.txt');

% Frequency oddball paradigm and modified consecutive repetition paradigm
% stimuli parameters
StdGain = CalFile(7,StdID);
StdFrq = freqs(StdID);
fprintf(1,sprintf('Standard frequency is %i\n',StdFrq))
UpFrqDevGain = CalFile(7,StdID+3);
UpFrqDevFrq = freqs(StdID+3);
fprintf(1,sprintf('Ascending frequency is %i\n',UpFrqDevFrq))
LowFrqDevGain = CalFile(7,StdID-3);
LowFrqDevFrq = freqs(StdID-3);
fprintf(1,sprintf('Descending frequency is %i\n',LowFrqDevFrq))
UpIntDevGain = CalFile(8,StdID);
LowIntDevGain = CalFile(6,StdID);

% Frequency many standards stimuli parameters

```

```

f0 = freqs(StdID-4);
fprintf(1,sprintf('MSC frequency 1 is %i\n',f0))
fgain0 = CalFile(7,StdID-4);
f1 = freqs(StdID-3);           % descending frequency oddball
fprintf(1,sprintf('MSC frequency 2 is %i\n',f1))
fgain1 = CalFile(7,StdID-3);
f2 = freqs(StdID-2);
fprintf(1,sprintf('MSC frequency 3 is %i\n',f2))
fgain2 = CalFile(7,StdID-2);
f3 = freqs(StdID-1);
fprintf(1,sprintf('MSC frequency 4 is %i\n',f3))
fgain3 = CalFile(7,StdID-1);
f4 = freqs(StdID);           % standard stimulus frequency
fprintf(1,sprintf('MSC frequency 5 is %i\n',f4))
fgain4 = CalFile(7,StdID);
f5 = freqs(StdID+1);
fprintf(1,sprintf('MSC frequency 6 is %i\n',f5))
fgain5 = CalFile(7,StdID+1);
f6 = freqs(StdID+2);
fprintf(1,sprintf('MSC frequency 7 is %i\n',f6))
fgain6 = CalFile(7,StdID+2);
f7 = freqs(StdID+3);           % ascending oddball frequency
fprintf(1,sprintf('MSC frequency 8 is %i\n',f7))
fgain7 = CalFile(7,StdID+3);
f8 = freqs(StdID+4);
fprintf(1,sprintf('MSC frequency 9 is %i\n',f8))
fgain8 = CalFile(7,StdID+4);
f9 = freqs(StdID+5);
fprintf(1,sprintf('MSC frequency 10 is %i\n',f9))
fgain9 = CalFile(7,StdID+5);

% Load stimuli presentation codes
load('MMNcode.mat')
load('MSCcode.mat')
ISI = 0.45; %inter stimulus interval in seconds

% Initialize NI device
device = daq.getDevices;
vendor=daq.getVendors;
s = daq.createSession('ni');
s1 = daq.createSession('ni');
rate = 70e3;
s.Rate = rate;
s.addAnalogOutputChannel('Dev1',0:1, 'Voltage');

% Consecutive repetition control block
SPT = stimulusPulseTrains(rate,StdGain,StdFrq,UpFrqDevGain,UpFrqDevFrq,...
    LowFrqDevGain,LowFrqDevFrq,UpIntDevGain,LowIntDevGain,ISI);
queueOutputData(s, SPT);
prepare(s);
fprintf(1,'Start recording in LabVIEW then press any key to continue\n');pause
c = clock;
fprintf(1,'\nStimuli Pulse Train began at %s',datestr(datenum(c(1),c(2),...
    c(3),c(4),c(5),c(6))));
startForeground(s);
stop(s)

```

```

c = clock;
fprintf(1, '\nStimuli Pulse Train ended at %s', datestr(datenum(c(1), c(2), ...
    c(3), c(4), c(5), c(6))));
clear durSPT

% Duration many standards control block
durMSC = DurationMSC(rate, StdGain, StdFrq, MSCcode, ISI);
queueOutputData(s, durMSC);
prepare(s);
c = clock;
fprintf(1, '\nDuration Many Standards began at %s', datestr(datenum(c(1), ...
    c(2), c(3), c(4), c(5), c(6))));
startForeground(s);
stop(s)
c = clock;
fprintf(1, '\nDuration Many Standards ended at %s', datestr(datenum(c(1), ...
    c(2), c(3), c(4), c(5), c(6))));
clear durMSC

% Frequency oddball paradigm block (saline)
freqMMN = FrequencyMMN(rate, StdGain, StdFrq, UpFrqDevGain, UpFrqDevFrq, ...
    LowFrqDevGain, LowFrqDevFrq, MMNcode, ISI);
queueOutputData(s, freqMMN);
prepare(s);
fprintf(1, '\nFrequency Paradigms about to begin - create new file if required');
fprintf(1, ' and press any key to continue\n'); pause
c = clock;
fprintf(1, '\nFrequency Oddball began at %s', datestr(datenum(c(1), c(2), ...
    c(3), c(4), c(5), c(6))));
startForeground(s);
stop(s)
c = clock;
fprintf(1, '\nFrequency Oddball ended at %s', datestr(datenum(c(1), c(2), ...
    c(3), c(4), c(5), c(6))));
clear freqMMN

% Frequency deviant alone stimuli block (saline)
freqDA = FrequencyDA(rate, StdGain, StdFrq, UpFrqDevGain, UpFrqDevFrq, ...
    LowFrqDevGain, LowFrqDevFrq, MMNcode, ISI);
queueOutputData(s, freqDA);
prepare(s);
c = clock;
fprintf(1, '\nFrequency Deviant-Alone began at %s', datestr(datenum(c(1), ...
    c(2), c(3), c(4), c(5), c(6))));
startForeground(s);
stop(s)
c = clock;
fprintf(1, '\nFrequency Deviant-Alone ended at %s', datestr(datenum(c(1), ...
    c(2), c(3), c(4), c(5), c(6))));
clear freqDA

% Frequency many standards control block (saline)
freqMSC = FrequencyMSC(rate, fgain0, f0, fgain1, f1, fgain2, f2, fgain3, f3, ...
    fgain4, f4, fgain5, f5, fgain6, f6, fgain7, f7, fgain8, f8, fgain9, f9, MSCcode, ISI);
queueOutputData(s, freqMSC);
prepare(s);

```

```

c = clock;
fprintf(1, '\nFrequency Many-Standards began at %s', datestr(datenum(c(1), ...
    c(2), c(3), c(4), c(5), c(6))));
startForeground(s);
stop(s)
c = clock;
fprintf(1, '\nFrequency Many-Standards ended at %s', datestr(datenum(c(1), ...
    c(2), c(3), c(4), c(5), c(6))));
clear freqMSC

% Frequency oddball paradigm block (ketamine)
freqMMN = FrequencyMMN(rate, StdGain, StdFrq, UpFrqDevGain, UpFrqDevFrq, ...
    LowFrqDevGain, LowFrqDevFrq, MMNcode, ISI);
queueOutputData(s, freqMMN);
prepare(s);
fprintf(1, '\nAdminister ketamine, setup new file ');
fprintf(1, 'then press any key to continue\n'); pause
c = clock;
fprintf(1, '\nFrequency Oddball began at %s', datestr(datenum(c(1), c(2), ...
    c(3), c(4), c(5), c(6))));
startForeground(s);
stop(s)
c = clock;
fprintf(1, '\nFrequency Oddball ended at %s', datestr(datenum(c(1), c(2), ...
    c(3), c(4), c(5), c(6))));
clear freqMMN

% Frequency deviant alone stimuli block (ketamine)
freqDA = FrequencyDA(rate, StdGain, StdFrq, UpFrqDevGain, UpFrqDevFrq, ...
    LowFrqDevGain, LowFrqDevFrq, MMNcode, ISI);
queueOutputData(s, freqDA);
prepare(s);
c = clock;
fprintf(1, '\nFrequency Deviant-Alone began at %s', datestr(datenum(c(1), ...
    c(2), c(3), c(4), c(5), c(6))));
startForeground(s);
stop(s)
c = clock;
fprintf(1, '\nFrequency Deviant-Alone ended at %s', datestr(datenum(c(1), ...
    c(2), c(3), c(4), c(5), c(6))));
clear freqDA

% Frequency many standards control block (ketamine)
freqMSC = FrequencyMSC(rate, fgain0, f0, fgain1, f1, fgain2, f2, fgain3, f3, ...
    fgain4, f4, fgain5, f5, fgain6, f6, fgain7, f7, fgain8, f8, fgain9, f9, MSCcode, ISI);
queueOutputData(s, freqMSC);
prepare(s);
c = clock;
fprintf(1, '\nFrequency Many-Standards began at %s', datestr(datenum(c(1), ...
    c(2), c(3), c(4), c(5), c(6))));
startForeground(s);
stop(s)
c = clock;
fprintf(1, '\nFrequency Many-Standards ended at %s', datestr(datenum(c(1), ...
    c(2), c(3), c(4), c(5), c(6))));
clear freqMSC

```

```

% Experiment complete message
c = clock;
fprintf(1, '\nExperiment completed at %s\n', datestr(datetime(c(1),c(2),...
    c(3),c(4),c(5),c(6))));
diary off
msgbox('Experiment Complete. Press OK', '', 'warn');

```

```

function [ output ] = generateStimulus(rate,ISIdelay,dur,frq,int,ramp)
% This function generates auditory stimuli for use in auditory
% paradigms defined by stimulus codes
pulse(1:(rate*0.05),1) = 0.5; % trigger pulse
pulse((rate*0.05):(rate*dur),1) = zeros;
% timebase
t = (1:(dur*rate))/rate;
% create edge-tapering ramp function
ramp = transpose([ramp,ones(1,size(t,2)-size(ramp,2)*2),flip1r(ramp)]);
% generate ramped auditory stimuli
stimulus = transpose(int*sin(2*pi*frq*t)).*ramp;
% combine ISI delay with auditory stimulus for output
output = [cat(1,ISIdelay,stimulus) cat(1,ISIdelay,pulse)];
end

```

```

function [ dataout ] = stimulusPulseTrains(rate,IntDur,Frq,IntFrqUp,...
    FrqFrqUp,IntFrqLow,FrqFrqLow,IntIntUp,IntIntLow,ISI)
% This function generates output array for presenting the modified
% consecutive repetition control paradigm in Experiment III
%----- Set auditory stimuli parameters -----%
StdDur = 0.1; % standard stimuli duration (Seconds)
DevDurUp = 0.15; % increasing duration stimuli (Seconds)
DevDurLow = 0.05; % decreasing duration stimuli (Seconds)
Dur = 0.05;
%----- Computations to prepare data output -----%
ISIdelay(1:(rate*ISI),1) = zeros; %set delays
IBIdelay(1:(rate*5),1) = zeros;
IBI = [IBIdelay IBIdelay];

% 5 ms cosine ramp
durr = 0.005;
nr = floor(rate * durr);
ramp = sin(linspace(0, pi/2, nr));

% Generate auditory stimuli
standard = generateStimulus( rate,ISIdelay, StdDur, Frq, IntDur, ramp );
DurUpDev = generateStimulus( rate,ISIdelay, DevDurUp, Frq, IntDur, ramp );
DurLowDev = generateStimulus( rate,ISIdelay, DevDurLow, Frq, IntDur, ramp );
FrqUp = generateStimulus( rate,ISIdelay, Dur, FrqFrqUp, IntFrqUp, ramp );
FrqLow = generateStimulus( rate,ISIdelay, Dur, FrqFrqLow, IntFrqLow, ramp );
IntUp = generateStimulus( rate,ISIdelay, Dur, Frq, IntIntUp, ramp );
IntLow = generateStimulus( rate,ISIdelay, Dur, Frq, IntIntLow, ramp );

%----- Prepare data output -----%
dataout = [];
for i=1:100; dataout=cat(1,dataout,standard); end
for i=101; dataout=cat(1,dataout,IBI); end
for i=102:201; dataout=cat(1,dataout,DurUpDev); end

```



```

for i=202; dataout=cat(1,dataout,IBI); end
for i=203:302; dataout=cat(1,dataout,DurLowDev); end
for i=303; dataout=cat(1,dataout,IBI); end
for i=304:403; dataout=cat(1,dataout,FrqUp); end
for i=404; dataout=cat(1,dataout,IBI); end
for i=405:504; dataout=cat(1,dataout,FrqLow); end
for i=505; dataout=cat(1,dataout,IBI); end
for i=506:605; dataout=cat(1,dataout,IntUp);end
for i=606; dataout=cat(1,dataout,IBI); end
for i=607:706; dataout=cat(1,dataout,IntLow); end
dataout = cat(1,dataout,IBI);
end

```

```

function [ dataout ] = DurationMSC(rate,StdInt,Frq,MSCcode,ISI)
% This function generates output array for presenting the duration many
% standards paradigm in Experiment III
%----- Set auditory stimuli parameters -----%
std0 = 0.05;
std1 = 0.075;
std2 = 0.1;
std3 = 0.125;
std4 = 0.150;
std5 = 0.175;
std6 = 0.2;
std7 = 0.225;
std8 = 0.25;
std9 = 0.275;

%----- Computations to prepare data output -----%
ISIdelay(1:(rate*ISI),1) = zeros; %set delays
finDelay(1:(rate*1),1) = zeros;
DELAY = [finDelay finDelay];

% 5 ms cosine ramp
durr = 0.005;
nr = floor(rate * durr);
ramp = sin(linspace(0, pi/2, nr));

% Generate auditory stimuli
Std0 = generateStimulus( rate,ISIdelay, std0, Frq, StdInt, ramp );
Std1 = generateStimulus( rate,ISIdelay, std1, Frq, StdInt, ramp );
Std2 = generateStimulus( rate,ISIdelay, std2, Frq, StdInt, ramp );
Std3 = generateStimulus( rate,ISIdelay, std3, Frq, StdInt, ramp );
Std4 = generateStimulus( rate,ISIdelay, std4, Frq, StdInt, ramp );
Std5 = generateStimulus( rate,ISIdelay, std5, Frq, StdInt, ramp );
Std6 = generateStimulus( rate,ISIdelay, std6, Frq, StdInt, ramp );
Std7 = generateStimulus( rate,ISIdelay, std7, Frq, StdInt, ramp );
Std8 = generateStimulus( rate,ISIdelay, std8, Frq, StdInt, ramp );
Std9 = generateStimulus( rate,ISIdelay, std9, Frq, StdInt, ramp );

%----- Prepare data output -----%
dataout = [];
for i=1:size(MSCcode,1)
    if MSCcode(i,1)==0; dataout=cat(1,dataout,Std0); end
    if MSCcode(i,1)==1; dataout=cat(1,dataout,Std1); end
    if MSCcode(i,1)==2; dataout=cat(1,dataout,Std2); end

```

```

    if MSCcode(i,1)==3; dataout=cat(1,dataout,Std3); end
    if MSCcode(i,1)==4; dataout=cat(1,dataout,Std4); end
    if MSCcode(i,1)==5; dataout=cat(1,dataout,Std5); end
    if MSCcode(i,1)==6; dataout=cat(1,dataout,Std6); end
    if MSCcode(i,1)==7; dataout=cat(1,dataout,Std7); end
    if MSCcode(i,1)==8; dataout=cat(1,dataout,Std8); end
    if MSCcode(i,1)==9; dataout=cat(1,dataout,Std9); end
end
dataout=cat(1,dataout,DELAY);
end

```

```

function [ dataout ] = FrequencyMMN( rate,StdInt,Frq,UpDevInt,UpDevFrq,...
    LowDevInt,LowDevFrq,MMNcode,ISI )
% This function generates output array for presenting the frequency oddball
% paradigm in Experiment III
%----- Set auditory stimuli parameters -----%
Dur = 0.05;          % stimuli duration (seconds)

%----- Computations to prepare data output -----%
ISIDelay(1:(rate*ISI),1) = zeros; %set delays
DELAY = [ISIDelay ISIDelay];

% 5 ms cosine ramp
durr = 0.005;
nr = floor(rate * durr);
ramp = sin(linspace(0, pi/2, nr));

% Generate auditory stimuli
standard = generateStimulus(rate,ISIDelay,Dur,Frq,StdInt,ramp);
updeviant = generateStimulus(rate,ISIDelay,Dur,UpDevFrq,UpDevInt,ramp);
lowdeviant = generateStimulus(rate,ISIDelay,Dur,LowDevFrq,LowDevInt,ramp);

%----- Prepare data output -----%
dataout = [];

for i=1:size(MMNcode,1)
    if MMNcode(i,1)==1; dataout=cat(1,dataout,standard); end
    if MMNcode(i,1)==2; dataout=cat(1,dataout,updeviant); end
    if MMNcode(i,1)==3; dataout=cat(1,dataout,lowdeviant); end
end
dataout=cat(1,dataout,DELAY);
end

```

```

function [ dataout ] = FrequencyDA( rate,~,Frq,UpDevInt,UpDevFrq,...
    LowDevInt,LowDevFrq,MMNcode,ISI )
% This function generates output array for presenting the frequency deviant
% alone paradigm in Experiment III
%----- Set auditory stimuli parameters -----%
Dur = 0.05;          % stimuli duration (seconds)
StdInt=0;           % make standard stimuli silent

%----- Computations to prepare data output -----%
ISIDelay(1:(rate*ISI),1) = zeros; %set delays
DELAY = [ISIDelay ISIDelay];

% 5 ms cosine ramp

```

```

durr = 0.005;
nr = floor(rate * durr);
ramp = sin(linspace(0, pi/2, nr));

% Generate auditory stimuli
standard = generateStimulus(rate,ISIdelay,Dur,Frq,StdInt,ramp);
updeviant = generateStimulus(rate,ISIdelay,Dur,UpDevFrq,UpDevInt,ramp);
lowdeviant = generateStimulus(rate,ISIdelay,Dur,LowDevFrq,LowDevInt,ramp);

%----- Prepare data output -----%
dataout = [];

for i=1:size(MMNcode,1)
    if MMNcode(i,1)==1; dataout=cat(1,dataout,standard); end
    if MMNcode(i,1)==2; dataout=cat(1,dataout,updeviant); end
    if MMNcode(i,1)==3; dataout=cat(1,dataout,lowdeviant); end
end
dataout=cat(1,dataout,DELAY);
end

function [ dataout ] = FrequencyMSC(rate,fgain0,f0,fgain1,f1,fgain2,f2,...
    fgain3,f3,fgain4,f4,fgain5,f5,fgain6,f6,fgain7,f7,fgain8,f8,fgain9,...
    f9,MSCcode,ISI )
% This function generates output array for presenting the frequency many
% standards paradigm in Experiment III
%----- Set auditory stimuli parameters -----%
Dur = 0.05;          % stimuli duration (seconds)

%----- Computations to prepare data output -----%
ISIdelay(1:(rate*ISI),1) = zeros; %set delays
DELAY = [ISIdelay ISIdelay];

% 5 ms cosine ramp
durr = 0.005;
nr = floor(rate * durr);
ramp = sin(linspace(0, pi/2, nr));

% Generate auditory stimuli
Std0 = generateStimulus( rate,ISIdelay, Dur, f0, fgain0, ramp );
Std1 = generateStimulus( rate,ISIdelay, Dur, f1, fgain1, ramp );
Std2 = generateStimulus( rate,ISIdelay, Dur, f2, fgain2, ramp );
Std3 = generateStimulus( rate,ISIdelay, Dur, f3, fgain3, ramp );
Std4 = generateStimulus( rate,ISIdelay, Dur, f4, fgain4, ramp );
Std5 = generateStimulus( rate,ISIdelay, Dur, f5, fgain5, ramp );
Std6 = generateStimulus( rate,ISIdelay, Dur, f6, fgain6, ramp );
Std7 = generateStimulus( rate,ISIdelay, Dur, f7, fgain7, ramp );
Std8 = generateStimulus( rate,ISIdelay, Dur, f8, fgain8, ramp );
Std9 = generateStimulus( rate,ISIdelay, Dur, f9, fgain9, ramp );

%----- Prepare data output -----%
dataout = [];
for i=1:size(MSCcode,1)
    if MSCcode(i,1)==0; dataout=cat(1,dataout,Std0); end
    if MSCcode(i,1)==1; dataout=cat(1,dataout,Std1); end
    if MSCcode(i,1)==2; dataout=cat(1,dataout,Std2); end

```

```
    if MSCcode(i,1)==3; dataout=cat(1,dataout,Std3); end
    if MSCcode(i,1)==4; dataout=cat(1,dataout,Std4); end
    if MSCcode(i,1)==5; dataout=cat(1,dataout,Std5); end
    if MSCcode(i,1)==6; dataout=cat(1,dataout,Std6); end
    if MSCcode(i,1)==7; dataout=cat(1,dataout,Std7); end
    if MSCcode(i,1)==8; dataout=cat(1,dataout,Std8); end
    if MSCcode(i,1)==9; dataout=cat(1,dataout,Std9); end
end
dataout=cat(1,dataout,DELAY);
end
```

Research output

12th Scottish Neuroscience Group Annual Meeting (SNG2015), University of St Andrews, UK [conference; oral presentation] “[Characterising mismatch negativity-like responses in mouse models relevant to schizophrenia](#)”

International Brain Research Organisation (IBRO) 2015 9th World Congress, Rio de Janeiro, Brazil [conference abstract; poster] “Mismatch negativity-*like* responses in awake and anaesthetised models relevant to schizophrenia”

British Neuroscience Association (BNA) 2015: Festival of Neuroscience, Edinburgh, UK (ISSN 1345-8301 2015) [conference abstract; poster] “[Investigating auditory event-related potentials and mismatch negativity-*like* responses in the schizophrenia-related *Map2k7* gene disruption model](#)”

Medical Engineering Centres and Bioengineering 2014, Imperial College London, UK (ISBN 978-0-9930390-0-3) [conference abstract; oral presentation] “[Investigating mismatch negativity-*like* activity in the *MAP2k7* schizophrenia model](#)”